アルミノリン酸塩結晶細孔中の一次元分子鎖の構造と物性

(研究課題番号 12440192)

平成１２ー１４年度科学研究費補助金
(基盤研究　(B)(2))
研究成果報告書

平成１５年３月

研究代表者　池　田　龍　一
(筑波大学化学系教授)

アルミノリン酸塩結晶細孔中の一次元分子鎖の構造と物性

(研究課題番号 12440192)

平成１２ー１４年度科学研究費補助金
(基盤研究　(B)(2))
研究成果報告書

平成１５年３月

研究代表者　池　田　龍　一
(筑波大学化学系教授)

はしがき

本研究「アルミノリン酸塩結晶細孔中の一次元分子鎖の構造と物性」は、平成12—14年度において、文部科学省科学研究費補助金、基盤研究(B)(2)、(研究課題番号 12440192)の交付を受けて、下記の研究組織により、筑波大学化学系無機物理化学研究室において実施したものである。

アルミノリン酸塩(AlPO)と総称されるマイクロポーラス結晶は断面がほぼ円形の均一な細孔を持つ分子ふるいで、大きさの異なるテンプレート分子を用いることにより、一定サイズ径の一次元のトンネル構造をもつ結晶を作成することができる。本研究においては、$AlPO_4$-5 (径 7.3 Å)の良質結晶を作成して、その一次元細孔中に水素結合、静電引力などの分子間相互作用を利用して、有機分子などの一次元分子鎖を実現し、得られた包接結晶について、X線回折、ERS, NMRなどの磁気共鳴、赤外ラマン分光などの測定を行うことにより、細孔中の一次元鎖の構造と原子、分子の運動を明らかにすることを目的にしている。一次元的に繋がった分子鎖からなる固相、結晶は、3次元的なバルクの結晶とは異なる構造、相変化、電気的・磁気的物性などを示すことが注目され、一次元固有の物性を追求するためには、孤立した一次元系が必要であるが、通常の3次元結晶中では、分子間の相互作用が無視できず、一次元系中の弱い相互作用の検出には多くの困難が伴う。本研究計画において、孤立した1次元系を最近開発された均一の径を持つトンネル構造体 AlPO 中に実現させ、1次元系固有の現象を検出することを試みた。以下、均一な細孔壁を持つ $AlPO_4$-5 と内壁にブンステッド酸点をランダムに持つ SAPO-5 について、細孔中に吸着させることに成功した水、アセトニトリル、トリエチルアミンについての研究成果を報告する。

研究組織

研究代表者　池田　龍一（筑波大学　化学系　教授）
研究分担者　石丸　臣一（筑波大学　化学系　講師）

交付決定額（配分額）

	直接経費	間接経費	合　　計
平成12年度	6，１００千円	0　円	6，１００千円
平成13年度	4，４００千円	0　円	4，４００千円
平成14年度	2，８００千円	0　円	2，８００千円
総　　計	１３，３００千円	0　円	１３，３００千円

序　論

細孔物質の孔内に吸着した分子は、一般にバルクの状態と比べて異なる環境に置かれているゆえに、その挙動・物性はバルクと大きく異なることが予想されている。炭素材料やポーラスシリカ、層状粘土鉱物など分子を孔内に吸着させることのできる物質は多く報告されているが、古くから着目され、様々な用途に利用されてきているものにアルミノケイ酸塩を骨格とするゼオライトが存在する。ゼオライト系化合物の細孔は結晶骨格の隙間に存在するために、その細孔形状はほぼ完全に決まっており、これに吸着した分子は他の吸着媒に吸着したものに比べてその物性を細孔内での分子配列に関連づけて理解しやすいと期待される。特にこれらの化合物のうち一次元のトンネル状細孔を持つ結晶中においては、分子間相互作用の低減や細孔壁面への吸着による安定化だけでなく、吸着分子の移動・拡散が一次元に制限されるなどの要因も絡み合い、特有な動的挙動や新しい物性を実現する場となる可能性が期待されている。

ゼオライト系化合物の一種に骨格がアルミノリン酸塩($AlPO_4$)からなるアルポと呼ばれる一連の化合物がある。この物質の骨格はゼオライトにみられる「酸点」を持たないため、その細孔内の環境はゼオライトよりも均一であり、また吸着分子との相互作用はゼオライトに比べて小さいと言われている。本研究では、アルポの一種であり結晶の c 軸方向に有効径 7.3 Å の均一な一次元トンネル型細孔を持っている $AlPO_4$-5、および比較のために $AlPO_4$-5 の P 原子の一部が Si に置換され、細孔壁面にブレンステッド酸点を持つ SAPO-5 を取り上げ、それらの細孔中に存在する分子がどのような運動状態にあるかを明らかにすることを第一の目的とし、合成時に細孔中に鋳型（テンプレート）として取り込まれたトリエチルアミンの動的挙動を ^1H, ^2H, ^{14}N NMR 等の測定手段を用いて調べた。また分子のサイズが小さく細孔にも吸着しやすく、細孔環境を探るプローブとして水分子とアセトニトリルをとり上げ、同様の測定を行った。

これらの結果に基づいてこの細孔を利用して異方性および分子間相互作用の大きな分子を細孔中に並べれば、新しい一次元相互作用系が現れることが期待される。このような状態における分子の示す挙動を明らかにし、新奇な低次元物性の可能性を探ることを第二の目的とし、一次元細孔に吸着させることによって細孔内で一次元方向に並び、二次非線形光学（SHG）特性を示すことが報告されている p-ニトロアニリンをとりあげた。この分子を $AlPO_4$-5, SAPO-5 および 4.6×6.5 Å の一次元トンネル細孔を持つ $AlPO_4$-11, SAPO-11 に吸着させ、細孔形状や酸点の分子運動への影響を調べた。

実　験

$AlPO_4$-5 は Al_2O_3：P_2O_5：トリエチルアミン：H_2O = 1：1.03：1.55：600 のモル比、SAPO-5 は $AlPO_4$-5 の比に Si / Al = 0.02, 0.05, 0.1, 0.3 となるよう SiO_2 溶液を加えた 4 種のゾル状混合物を調製し、これらをオートクレーブで 180℃、72 時間放置して水熱合成した。$AlPO_4$-11 は Al_2O_3：P_2O_5：ジ-n-プロピルアミン：HF：H_2O = 1：1.5：2.8：0.9：1500 のモル比の混合物をオートクレーブで 150℃、72 時間おいて水熱合成した。合成した試料を乾燥後、十分に脱水する

ために更に120℃で真空下に72時間おいた。

トリエチルアミンは$AlPO_4$-5, SAPO-5 細孔中に取り込まれているので、これを少量のヘリウムガスと共にガラス製試料管に封入したものを、トリエチルアミンについてのNMR試料とした。水分子およびアセトニトリル分子の$AlPO_4$-5, SAPO-5への吸着は、か焼（calcination：焼いて有機物を除去すること）して細孔中のトリエチルアミンを除去した後、試料を室温で飽和蒸気圧のH_2O またはD_2O、およびCH_3CN またはCD_3CN に曝すことより行い、ヘリウムガスと共にガラス製試料管に封入した。*p*-ニトロアニリンについては、か焼した$AlPO_4$-5, SAPO-5, $AlPO_4$-11 と共にガラス管に封入し、100℃で気相吸着させ、ヘリウムと共に封じてNMR 試料とした。

試料については"$AlPO_4$-5(TEA)"のように"ホスト骨格(ゲスト分子)"と表すこととする。

結果と考察

I. トリエチルアミン（TEA）分子の挙動

$AlPO_4$-5(TEA), SAPO-5(TEA)(Si/Al =0.10)についての^{1}H NMR 吸収線の二次モーメントM_2測定の結果、低温から$AlPO_4$-5(TEA)のM_2はゆるやかに減少し、210 K以上で0.5 G^{2}程度まで減少した。SAPO-5(TEA)は低温で11 G^{2}の値を示し、温度を上げると200 K付近で1.7 G^{2}にまで減少した。これを分子運動のモデルを立てて計算した値と比較すると（表1）、$AlPO_4$-5, SAPO-5 の中で、トリエチルアミンはいずれも90 K からすでにメチル基が回転しており、$AlPO_4$-5 では130 K付近、SAPO-5では150 K付近で一軸（擬C_3軸）回転、室温付近で分子全体の等方回転が励起されていることが分かった。$AlPO_4$-5(TEA) および SAPO-5(TEA)のT_1の温度変化を測定したところそれぞれ2つの極小が観測され、その最適化を行った結果（図1）、高温側の極小（等方回転）はBPP 理論式

表1　トリエチルアミンの分子内M_2の計算値（単位G^2）

motional mode	triethylamine (TEA)
rigid	22.7
methyl rotation	11.9
pseudo C_3 rotation	1.3
overall rotation	0.0

$$T_1^{-1}=\frac{2}{3}\gamma^2\Delta M_2\left(\frac{\tau}{1+\omega^2\tau^2}+\frac{4\tau}{1+4\omega^2\tau^2}\right) \qquad (1)$$

によって最適化できたが、低温側（一軸回転）は運動の相関時間τにCole-Davidson型の分布を仮定した修正式

$$T_1^{-1}=\frac{2}{3}\gamma^2\Delta M_2\left\{\frac{\tau_c\sin\left(\beta\tan^{-1}\omega\tau_c\right)}{\omega\tau_c\left(1+\omega^2\tau_c^{\,2}\right)^{\beta/2}}+\frac{2\tau_c\sin\left(\beta\tan^{-1}2\omega\tau_c\right)}{\omega\tau_c\left(1+4\omega^2\tau_c^{\,2}\right)^{\beta/2}}\right\} \qquad (2)$$

を用いる必要があった。SAPO-5(TEA)について同様な解析を行った結果（図2）、SAPO-5(TEA)の相関時間の分布の大きさは$AlPO_4$-5(TEA)よりも小さいことが

明らかになった。

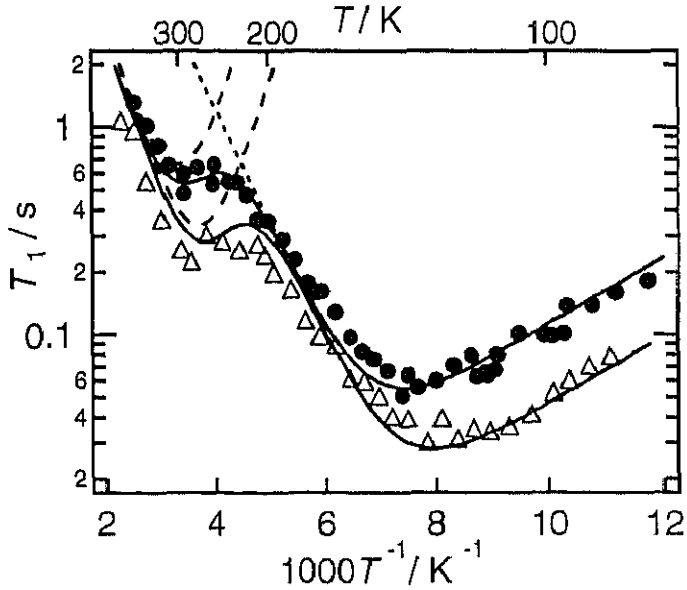

図1　$AlPO_4$-5 中のトリエチルアミンの
^{1}H NMR T_1 の温度依存と最適化曲線

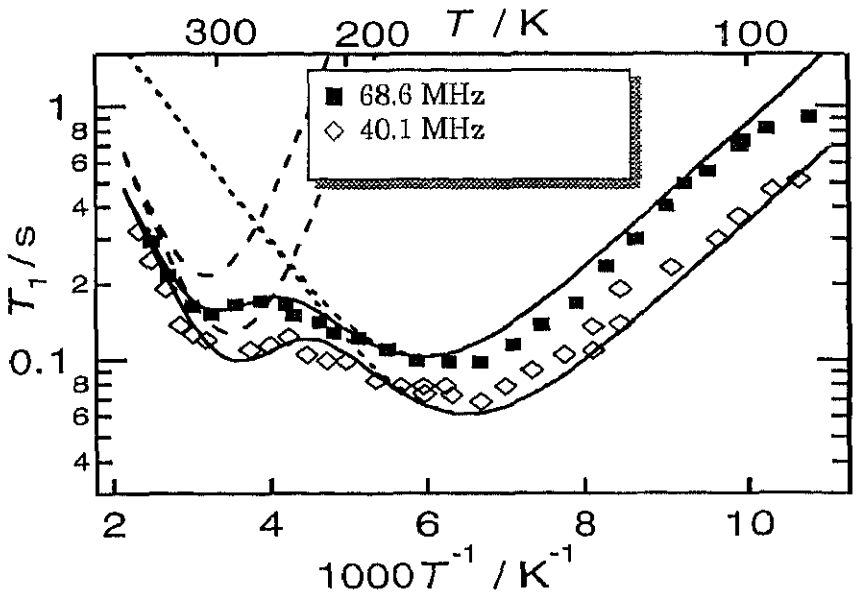

図2　SAPO-5 中のトリエチルアミンの
^{1}H NMR T_1 の温度依存と最適化曲線

を用いる必要があった。SAPO-5(TEA)について同様な解析を行った結果(図2)、SAPO-5(TEA)の相関時間の分布の大きさは $AlPO_4$-5(TEA)よりも小さいことが

明らかになった。そこでさらに酸点の濃度の異なる3種(Si/Al =0.02, 0.05, 0.30)のSAPO-5を合成し、そのT_1を測定、最適化したところ、一軸回転において表2のように分布の大きさを表わすパラメータβ ($0<\beta\leq1$：βが小さいほど分布が大きい) は酸点の濃度の上昇と共に徐々に大きくなり、酸点の数が増えるほど相関時間の分布が小さくなってゆく傾向が確認された。またT_1の極小についてはSAPO-5ではその深さにあまり違いが見られず、$AlPO_4$-5に対し少量の酸点が存在するだけでトリエチルアミンの挙動が変化することが明らかとなった。トリエチルアミンの一軸回転においてSAPO-5中の方が$AlPO_4$-5よりも運動が制限されているのは、ブレンステッド酸点の水素原子がトンネル内部に存在するために運動が阻害されるからであると考えられる。合成時に用いられるテンプレートは細孔内に吸着されたままで、400 K以上の温度でも細孔からの脱着は起こらないにもかかわらず、本研究で$AlPO_4$-5、SAPO-5細孔内ではトリエチルアミンは130-150 Kの低温から自由に運動していること、かつその運動は相関時間の分布を伴う複雑なものであること、相関時間の分布は酸点の濃度が上昇すると小さくなることが明らかとなった。

表2　^{1}H T_1曲線（低温側・一軸回転）の最適化の結果　(Si/Al比は仕込み量)

試料	Si/Al=0 ($AlPO_4$-5)	Si/Al=0.02	Si/Al=0.05	Si/Al=0.1	Si/Al=0.3
極小の深さ ΔM_2 / Gauss^2	13.0±1	8.2±1	7.3±1	7.2±1	6.1±0.8
活性化エネルギー E_a / kJ mol^{-1}	10.5±1	10.0±0.7	9.0±0.7	8.0±0.7	7.5±0.7
温度無限大における運動の相関時間 τ_0 / 10^{-12}s	0.54±0.06	2.2±0.3	3.2±0.4	6.2±0.6	9.1±0.9
β (分布の度合いをあらわすパラメータ)	0.30±0.1	0.40±0.1	0.50±0.1	0.70±0.1	0.80±0.1

II. 水分子の挙動

$AlPO_4$-5(^1H_2O)及び SAPO-5(^1H_2O)のT_1測定の結果、両試料ともT_1は二成分に分けられた。長い成分の温度変化は両試料共ほぼ一致し、それぞれ極小が観測され、この極小を分子全体の等方回転に帰属した。M_2測定においては、SAPO-5(^1H_2O)は100 K付近の低温では固定状態の水分子のM_2の値33.7 G^{2}に近い値 30±5 G^{2}を示した（図3）。$AlPO_4$-5(^1H_2O), SAPO-5(^1H_2O)ともM_2値は温度上昇に伴い連続的に減少し、210 K以上でM_2は2成分に分離、室温で両試料ともM_2は約2.5および0.5 G^{2}になった。^{1}H及び^{2}H NMRスペクトル（図4）では両試料共に150 K以下では固定状態に帰属できる広い線幅の成分が得られ、温度上昇と共に徐々に水分子の等方回転に帰属できる狭い

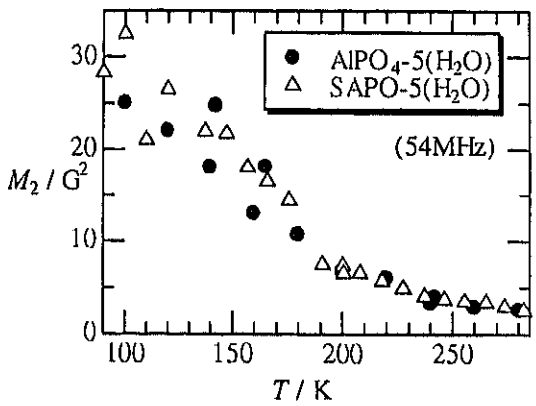

図3　$AlPO_4$-5, SAPO-5に吸着した水分子の^{1}H NMR M_2温度依存

成分が現れた。(図4の355 Kにおける非常に狭い成分は細孔外の水に帰属)
これらの測定結果から、$AlPO_4$-5及びSAPO-5の細孔内において水分子は120 K以下では固定状態にあり、温度上昇に伴って徐々に分子全体の回転運動が励起されてくること、室温においても等方的に回転している分子と壁面に吸着している分子の二種が存在していることが示された。また、$AlPO_4$-5及びSAPO-5のNMR測定の結果には大きな違いは見られず、ブレンステッド酸点の存否による水分子の運動への影響は大きくないことが確認された。

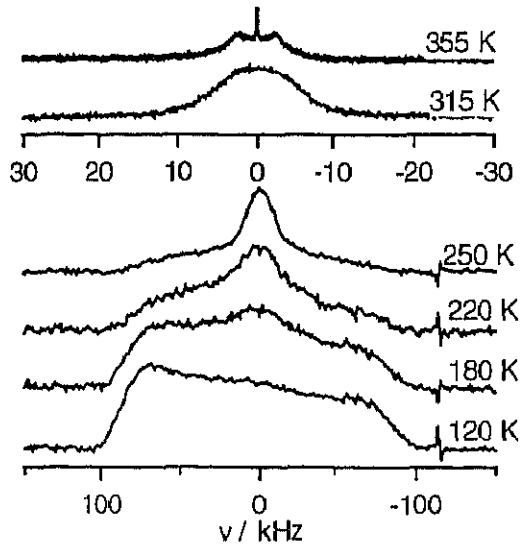

図4　$AlPO_4$-5(D_2O)の ^2H NMR スペクトルの温度変化

Ⅲ. アセトニトリル分子の挙動

$AlPO_4$-5(CD_3CN)の ^2H NMR スペクトル（図5）の130 Kの線形から、核四極子結合定数 e^2Qqh^{-1}=51 kHzと見積もられた。この値はアセトニトリル結晶の一軸回転（53 kHz）と一致しており、130 Kでは分子の一軸回転が励起されていることが分かった。150 K以上では線幅は温度の上昇とともに急激に減少したことから一軸回転に加えて分子全体の回転が励起されていると考えられる。230 K以上では1.6 kHz以下と狭く、アセトニトリルは等方回転していることが分かった。

SAPO-5(CD_3CN)の ^2H NMR スペクトル（図6）では130 K で $AlPO_4$-5(CD_3CN)同様アセトニトリルの一軸回転が励起されていたが、$AlPO_4$-5(CD_3CN)と異なり温度を上昇させても210 Kまでは線幅はほとんど変化せず、それより高温で温度の上昇とともに徐々に減少した。SAPO-5細孔中ではアセトニトリル分子と壁面の水酸基との相互作用が大きく、$AlPO_4$-5に比べて分子が強く束縛されているためと考えられる。

$AlPO_4$-5(CH_3CN)の T_1 では220-250 Kで運動による極小が観測され、最適化から活性化エネルギー＝11.3 kJ mol^{-1}、τの分布β = 0.7が得られた。^2H NMR スペクトルおよび ^1H NMR M_2 の結果との比較により、この運動はアセトニトリルの全体回転に帰属した。SAPO-5(CH_3CN)の T_1 は室温よりやや低い温度と8 K付近に極

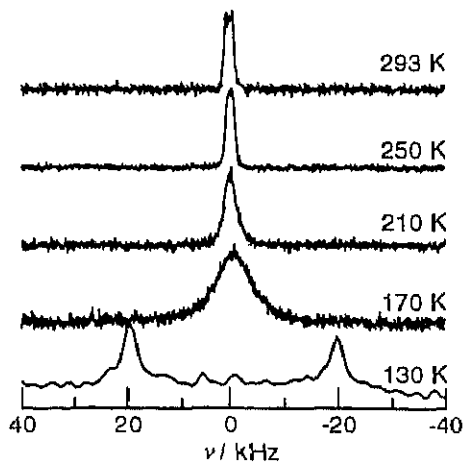

図5　$AlPO_4$-5(CD_3CN)^2H NMR スペクトルの温度変化

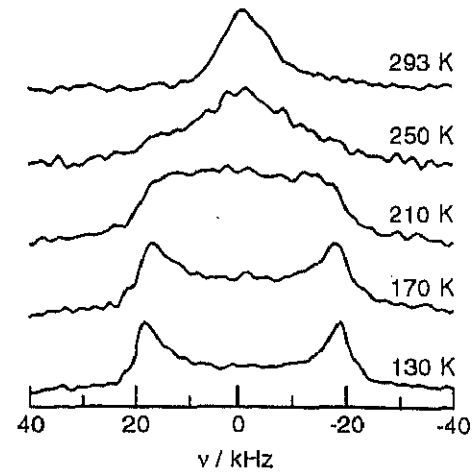

図6 SAPO-5(CD_3CN)^2HNMR スペクトルの温度変化

小を示し、最適化の結果、高温側の極小は分子軸の揺らぎを伴う軸性回転、低温側の極小はアセトニトリルの一軸回転（メチル基回転）に帰属した。活性化エネルギーはそれぞれ 12.1 kJ mol^{-1} および 0.26 kJ mol^{-1}、高温側の曲線の $\beta = 0.3$ となった。トリエチルアミンの場合と異なりSAPO-5中の方が細孔内分子の相関時間の分布は大きいという結果が得られた。

IV. p-ニトロアニリン（pNA）分子の挙動

p-ニトロアニリンを $AlPO_4$-5 に吸着させた試料についての ^1H NMR T_1 測定の結果、室温付近に分子運動による T_1 の極小が見られた。また ^1H NMR スペクトル（図7）の線幅は低温から温度上昇と共に徐々に狭くなり、室温で線幅 2 kHz 程度（半値幅）となった。M_2 の測定からも ^1H スペクトルと同様の結果が得られ、室温において $AlPO_4$-5 細孔内の *p*-ニトロアニリンはかなり大振幅の運動をしていることが示された。

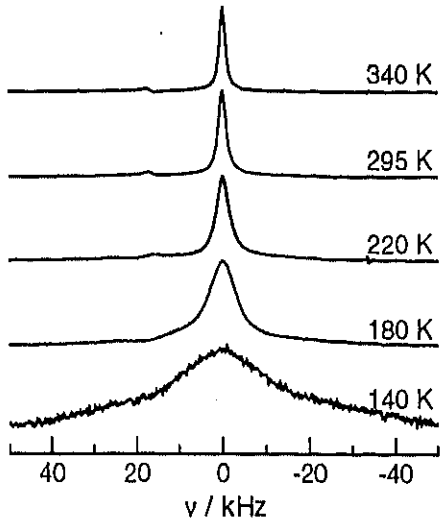

図7 $AlPO_4$-5(pNA)の ^1H NMR スペクトルの温度変化

これに対し SAPO-5(pNA) と $AlPO_4$-11 (pNA)の ^1H NMR スペクトルでは、両試料とも室温において 5±1 kHz および 15±1 kHz の二成分が得られたことから、これらの細孔中では2種類の運動状態にある *p*-ニトロアニリン分子が存在することが示唆された。

結　論

本研究から、$AlPO_4$-5 細孔内での分子の運動のし易さについては、分子サイズの違いがそのまま直結するわけではないことが明らかとなった。細孔内分子の運動性は分子の大きさと細孔径の大きさの兼ね合いのみならず、分子間水素結合や壁面への吸着などの要因が大きな役割を果たしていることが解明された。また、細孔内に存在する酸点が吸着分子に与える影響は様々であり、酸点の量が変化することで分子運動の相関時間の分布が変わることも明らかとなった。適切な細孔径および酸点の量をもつ結晶を用いることにより、吸着分子の配向や運動状態を制御することができることが解明された。

研 究 成 果

（1）学会誌等

1. Cationic Motions and Order-Disorder Phase Transitions in Layer Crystals with a Rotator Phase, $(n\text{-}C_5H_{11}NH_3)_2ZnCl_4$ and $(n\text{-}C_{12}H_{25}NH_3)_2ZnCl_4$, K. Horiuchi, H. Takayama, S. Ishimaru and R. Ikeda, *Bull. Chem. Soc. Jpn.*, 73, 307-314(2000).
2. Studies on ^{133}Cs NMR Spectra and Spin-Lattice Relaxation Times in Incommensurate Cs_2HgCl_4, K. Suzuki, S. Ishimaru and R. Ikeda, *J. Phys. Soc. Jpn.*, 69, 729-733(2000).
3. ^{35}Cl NQR Studies of Hydrogen Transfer in Crystalline p-Chloro- benzoic Acid, T. Nihei, S. Ishimaru and R. Ikeda, *Z. Naturforsch.*, 55a, 355-358(2000).
4. ^{135}Cs NMR Spin-Lattice relaxtion Study in Incommensurate Cs_2CdI_4, K. Suzuki, S. Ishimaru and R. Ikeda, *Z. Naturforsch.*, 55a, 339-342(2000).
5. Dynamic Behaviour of Trimethylamine Molecules Adsorbed in Aluminophosphate($AlPO_4$-5) and Silicoaluminophosphate (SAPO-5), K. Gotoh, S. Ishimaru and R. Ikeda, *Phys. Chem. Chem. Phys.*,2, 1865-1869(2000).
6. Adsorption and Electronic Properties in Tetramethyl- benzidine- Intercalated Tetrasilicicfluormica, S. Ishimaru, H. Sawatari and R. Ikeda, *Mol. Cryst. Liq. Cryst.*, 341, 309-314(2000).
7. Dynamics of n-Octylammonium Ions Intercalated in Saponite, M. Yamauchi, S. Ishimaru and R. Ikeda, *Mol. Cryst. Liq. Cryst.*, 341, 315-320(2000).
8. Ionic Plastic Phases in Trimethylammonium Trifluoroacetate Studied by ^{1}H and ^{19}F NMR Spectroscopy, X-Ray Diffraction and Thermal Measurements, K. Kuchitsu, H. Ono, S. Ishimaru, R. Ikeda and H. Ishida, *Chem. Phys. Phys. Chem.*, 2, 3883-3885(2000).
9. Hydrogen Transfer in Hydrogen-Bonded Chloranilic Acid Studied by ^{35}Cl NQR — A 1:2 Complex with 1,4-Diazine—, T. Nihei, S. Ishimaru, H. Ishida, H. Ishihara and R. Ikeda, *Chem. Phys..Lett.*, 329, 7-14(2000).
10. Hydrogen Transfer in a Hydrogen-Bonded 1:2 Complex of Chloranillic Acid with 1,2-Diazine Studied by ^{35}Cl NQR, T. Nihei, S. Ishimaru, H. Ishida, H. Ishihara and R. Ikeda, *Chem. Lett.*, 2000, 1346-1347.
11. Molecular Motions and Phase Transitions in Halogen-Bridged One-Dimensional Complexes $[Pt(en)_2]$-$[PtX_2(en)_2](ClO_4)_4$ (X: I, Br), N. Kimura, T. Hachisuka, Y. Nakano and R. Ikeda, *Phys. Chem. Chem. Phys.*, 3, 1778-1781(2001).
12. Metal Valence Structures in 1-D Mixed-Metal Complexes $[Ni_{1-x}Pd_xX(chxn)_2]X_2$ Studied by Solid NMR, N. Kimura, M.

Kano, T. Manabe, M. Yamashita and R. Ikeda, *Synth. Metals*, 120, 778-779(2001).

13. Valence Structure and Magnetic Interaction in MMX-type 1D complexes, $A_4[Pt_2I(P_2O_5H_2)_4]nH_2O$, Studied by ^{31}P Solid NMR, N. Kimura, T. Kawashima, S. Miya, T. Manabe, M. Yamashita and R.Ikeda, *Synth. Metals*, 120, 779-780(2001).
14. Magnetic Structure in a Halogen-Bridged 1-D $S = 1/2$ Heisenberg Antiferromagnet $[NiBr(chxn)_2]Br_2$, S. Takaishi, S. Itoh and R. Ikeda, *J. Phys.. Soc. Jpn. Suppl. A*, 70, 103-105 (2001).
15. An Unusual Six-Co-ordinated Platinum(II) Complex Containing a Neutral I_2 Ligand, R. Makiura, I. Nagasawa, N. Kimura, S. Ishimaru, H. Kitagawa and R.Ikeda, *Chem. Commun.*,2001, 1642-1643.
16. Dynamics of Water Molecules in Micropores of $AlPO_4$-5 and SAPO-5 Studied by ^1H NMR, K. Gotoh, S. Ishimaru and R. Ikeda, *Chem. Lett.*, 2001,1250-1251.
17. Dynamic Behavior of Acetonitrile Molecules Adsorbed in $AlPO_4$-5 and SAPO-5 Studied by ^1H and ^2H NMR, S. Ishimaru, K. Gotoh, M. Ichikawa and R. Ikeda, *Microporous and Mesoporous Mater.*, 51, 17-22(2002).
18. Complex-Plane Impedance Study on a Hydrogen-Doped Copper Coordination Polymer: *N,N'*-bis(2-hydroxyethyl) dithiooxamidatecopper (II),Y. Nagao, R. Ikeda, S. Kanda, Y. Kubozono and H. Kitagawa, *Mol. Cryst. Liq. Cryst.*, 379, 89-94(2002).
19. Electronic State of a Hydrogen-Doped Copper Coordination Polymer: *N,N'*-bis(hydroxyethyl)dithiooxamidatocopper(II), $(HOC_2H_4)_2$*datoa*Cu, M. Fujishima, R. Ikeda, S. Kanda, and H. Kitagawa, *Mol. Cryst. Liq. Cryst.*, 379, 223-228(2002).
20. Relaxation process of CT Exciton State in a One-Dimensional MX-Chain Compound $[NiBr(chxn)_2]Br_2$, S. Takaishi, H. Kitagawa and R. Ikeda, *Mol. Cryst. Liq. Cryst.*, 379, 279-284(2002).
21. Electronic State of a Hydrogen-Bridged Mixed-Valence Binuclear Complex, $Ni_2(dta)_4I$, R. Makiura, H. Kitagawa and R. Ikeda,*Mol. Cryst. Liq. Cryst.*, 379, 309-314(2002).
22. Structural and Optical Properties of $Pt_2(dtp)_4Br_2$ (*dtp* = dithio- propionato) and its Halogen-Replacement Effect, A. Kobayashi, H. Kitagawa and R. Ikeda, *Mol. Cryst. Liq. Cryst.*, 379, 315-320(2002).
23. Spin Polarization in Infinite Zigzag Chains of $[Rh_2(HNCOCH_3)_4Cl]_n$, M. Yamauchi, A. B. Koudriavtsev, R. Ikeda, Zhiong Yang and T. Kawamura,*Mol. Cryst. Liq. Cryst.*, 379, 321-326(2002).
24. Spin Structure and Dynamics in a Spin 1/2 One Dimensional Antiferromagnet, $[NiBr(chxn)_2]Br_2$ (chxn: 1*R*,2*R*-cyclohexanediamine), S. Takaishi, K. Kano, H. Kitagawa, Y. Furukawa, K. Kumagai and R. Ikeda, *Chem.*

Lett.,2002, 856-857.

25. Nuclear Quadrupole Resonance Studies on Weak Exchange Interactions between Paramagnetic Ions in $M(II)(H_2O)_6$ $SnCl_6$ (M(II)=Mn, Co, and Ni), H. Miyoshi, R. Ikeda, A. Koshio and K. Horiuchi, *J. Phys. Condens. Matter*, 14, 1085-1090 (2002).
26. Thermochromism in Nickel(II) Complexes: Thermal, Solid State ^1H NMR and Single Crystal X-Ray Analysis of Bis-(N,N-dimetyl- 1,2-ethanediamine)nickel(II) Perchlorate, S. Koner, M. Tsutake, I. Nagasawa, R. Ikeda, .P. K. Saha, A. K. Mukherjee, S. Bernerjee,*J. Mol. Struct.* 608, 63-69(2002).
27. Cationic Motions Studied by ^1H and ^2H Nuclear Magnetic Resonance, X-Ray Diffraction and Thermal Measurements in Solid $CH_3(CH_2)_2NH_3X$, $CH_3(CH_2)_2ND_3X$ and $CD_3(CH_2)_2NH_3X$ (X: F, Cl, Br and I), S. Ishimaru. T. Ishitomi and R. Ikeda, *J. Phys., Condens. Matter*, 14, 6815-6822(2002).
28. A ^{35}Cl NQR Study on Exchange Interactions between Paramagnetic $[IrCl_6]^{2-}$ Ions, H. Miyoshi, K. Horiuchi and R. Ikeda, *Z. Naturforsch.* 57a, 431-434(2002).
29. ^1H, ^2H and ^{13}C NMR Studies of Cation Dynamics in a Layered Perovskite-Type Incommensurate Compound $(n\text{-}C_3H_7NH_3)_2CdCl_4$, K. Suzuki, H. Fujimori, T. Asaji, S. Ishimaru and R. Ikeda, *Z. Naturforch.* 57a, 451-455(2002).
30. ^{133}Cs NMR Spin-Lattice Relaxation Time and Chemical Shift Studies on Cs_2MX_4 Crystals with Sr_2GeS_4 and b-K_2SO_4 Structures Performing no Low Temperature Phase Transition, K. Suzuki, S. Ishimaru and R. Ikeda, *Z. Naturforch.* 57a, 461-464(2002).
31. Molecular Motions in Halogen-Bridged One-Dimensional Pt Complexes, $[Pt^{II}(en)_2][Pt^{IV}X_2(en)_2](ClO_4)_4$ (X=Cl, Br) Studied by ^2H and ^1H NMR, N. Kimura, T. Hachisuka, Y. Nakano and R.Ikeda, *Z. Naturforch.* 57a, 413-418(2002).
32. ^{35}Cl Quadrupole Relaxation Study on $Cs_2[Au(I)Cl_2]$ $[Au(III)Cl_4]$ and $Cs_2[Ag(I)Cl_2][Au(III)Cl_4]$. A. Ishikawa, M. Kurasawa, A. Sasane, R. Ikeda and N. Kojima, *Z. Naturforch.* 57a, 348-352(2002).
33. Substituent Effect on the Magnetic Properties of Copper Coordination Polymers with Dithiooxamide and N,N'-Bis-(hydroxyethyl)dithiooxamide, M. Fujishima, Y. Nagao, R. Ikeda, S. Kanda, H. Kitagawa, *Synth. Metals*, in press.
34. Ab Initio Calculations of Copper Coordination Polymers: H_2dtoaCu and $(HOC_2H_4)_2$dtoaCu (dtoa = dithiooxamide), M. Fujishima, R. Ikeda, T. Kawamura, H. Kitagawa, *Synth. Metals*, in press.
35. A Study on Hydrogen Adsorption of Polymer Protected Pt Nanoparticles, M. Yamauchi, Y. Isobe, R. Ikeda, H. Kitagawa, T. Teranishi, and M. Miyake, *Synthetic Metals*, in press
36. Electron Spin Dynamics in a Spin 1/2 One-Dimensional

Heisenberg Antiferromagnet $[CuX_2(AdH^+)_2]X_2$, S. Takaishi, Y. Furukawa, K. Kumagai and R. Ikeda, *Synth. Metals*, in press.

37. ^{129}I Mossbauer Spectroscopic Study of a One-Dimensional Halogen-Bridged Binuclear Complex, $Pt_2(dtp)_4I$ (*dtp* = $C_2H_5CS_2^-$), A. Kobayashi, H. Kitagawa, R. Ikeda, S. Kitao, M. Seto, M. Mitsumi and K. Toriumi, *Synth. Metals*, in press.
38. A New Semiconducting Organic-Inorganic Nanocomposite, 1,5-Diamino-naphthalene-Saponite Intercalation Compound, S. Ishimaru, M. Yamauchi and R. Ikeda, *Solid State Commun.*, (2002) in press.
39. Dynamic Structure of Molecules Included in Porous Solids Studied by Solid State NMR, S. Ishimaru and R. Ikeda, *Recent Research Developments in Molecular Structure*, ed. A. Gayathri, (2002), Transworld Research Network, in press.
40. Highly Proton-Conductive Copper Coordination Polymers, Y. Nagao, M. Fujishima, R. Ikeda, S. Kanda, and H. Kitagawa, *Synth. Metals*, in press.
41. A new proton-conductive copper coordination polymer, $(HOC_3H_6)_2$ *dtoa*Cu (*dtoa* = dithiooxamide), Y. Nagao, R. Ikeda, T. Kubo, K. Nakasuji, and H. Kitagawa, *Synth. Metals*, in press.
42. Highly Proton-Conductive Copper Coordination Polymer, H_2*dtoa*Cu (H_2*dtoa* = dithiooxamide anion), H. Kitagawa, Y. Nagao, M. Fujishima, R. Ikeda, and S. Kanda, *Inorg. Chem. Commun.*, in press.
43. N. Kimura, H. Aso, K. Takizawa, T. Ishii, H. Miyasaka, K. Sugiura, M. Yamashita and R. Ikeda, ^{13}C NMR Spectra, ^1H NMR Relaxation and ESR Measurements of Br_2 Doped $\{[Pt(en)_2][PtBr_2(en)_2]\}_3(CuBr_4)_4 \cdot 12H_2O$, *Synth. Metals*, in press.
44. Metal Valence Structure in 1-D Mixed-Metal Complexes $[Ni_{1-x}Pd_xX(chxn)_2]X_2$ Studied by Solid NMR, N. Kimura, M. Kano, T. Manabe, M. Yamashita and R. Ikeda, *Synth. Metals*, in press.
45. Electrical Conductivity of a Conductive Mixed-Valence MMX-Chain Pt2(CH3CS2)4I under High Pressure, H. Kitagawa, T. Suto. R. Makiura, R. Ikeda, N. Takeshita and N. Môri, *Synth. Metals*, in press.

（2）口頭発表

1. N. Kimura, S. Ishimaru, R. Ikeda, T. Kawashima, S. Miya, T. Manabe and M. Yamashita, Valence Structure and Magnetic Interaction in MMX-type 1-D Complexes, $A_4[Pt_2I(P_2O_5H_2)_4]\cdot nH_2O$, Studied by ^{31}P Solid NMR, International Conference on Science and Technology of Synthetic Metals, TueC129, July, 2000 (Gastein, Austria).
2. N. Kimura, R. Ikeda, T. Manabe and M. Yamashita, Metal Valence

Structures in 1-D Mixed-Metal Complexes[Ni1-xPdx(chxn)2]Br3 Studied by Solid NMR, International Conference on Science and Technology of Synthetic Metals, TueC128, July, 2000 (Gastein, Austria).

3. 牧浦理恵、長澤五十六、木村憲喜、石丸臣一、北川宏、池田龍一、ヨウ素分子が配位した六配位八面体型白金二価錯体の合成と構造、錯体化学討論会、1A-A16, 2000年9月（草津）。
4. 加納正隆、高石慎也、木村憲喜、真鍋敏夫、北川宏、山下正廣、池田龍一、固体NMR法を用いた擬一次元ハロゲン架橋錯体$[Ni_{1-x}Pd_xBr(chxn)_2]Br_2$におけるスピン構造の研究、、錯体化学討論会、2P1-C04, 2000年9月（草津）。
5. 高石慎也、加納正隆、北川宏、池田龍一、木村憲喜、伊藤晋一、ハロゲン架橋一次元錯体$[NiBr(chxn)_2]Br_2$のスピン構造、錯体化学討論会、1H-F11、2000年9月（草津）。
6. 木村憲喜，加納正隆、石丸臣一、池田龍一、眞鍋敏夫、山下正廣、^{13}C固体NMR法を用いた一次元金属錯体$Ni_{1-x}Pd_x(chxn)_2X_3$における鎖上の原子価構造と電子スピンの磁気相互作用の研究、錯体化学討論会、2P1-C03、2000年9月(草津)。
7. 山内美穂、石丸臣一、池田龍一、フッ化四ケイ素雲母層間におけるグアニジニウムイオンの運動の研究、2000分子構造総合討論会、3c2、2000年9月（東京)。
8. 石丸　臣一、石富　妙、池田　龍一、MD計算によるハロゲン化プロピルアンモニウム最高温相における動的構造の解明、分子構造総合討論会、1p96、2000年9月（東京)。
9. 鈴木　浩一、石丸　臣一、池田　龍一、浅地　哲夫、磁気共鳴法による層状ペロブスカイト型化合物$(n\text{-}C_3H_7NH_3)_2CdCl_4$の不整合相転移の研究、分子構造総合討論会、2p156、2000年9月（東京)。
10. 武石　亮、池田　龍一、石丸　臣一、$[(CH_3)_3CNH_3]_2SO_4$結晶中の陽イオンの動的挙動、分子構造総合討論会、2p160、2000年9月（東京)。
11. 高橋　哲、仁平　貴明、石丸　臣一、石原　秀太、石田　祐之、池田　龍一、^{35}Cl NQR法によるクロラニル酸、1,3-ジアジン系における水素移動の検出、分子構造総合討論会、2p163、2000年9月（東京)。
12. 石丸　臣一、池田　龍一、テトラメチルベンジジン－サポナイト層間化合物の吸着特性、第44回粘土科学討論会、P12、2000年10月（北海道)。
13. 山内美穂、石丸臣一、池田龍一、フッ化四ケイ素雲母層間におけるグアニジニウムイオンの運動、第44回粘土科学討論会、P22、2000年10月（北海道)。
14. 篠原絵美、山内美穂、石丸臣一、池田龍一、雲母及びオクトシリケート層間におけるドデシルトリメチルアンモニウムイオンの構造と運動、粘土化学討論会、P21、2000年10月（北海道)。
15. 篠原絵美、山内美穂、石丸臣一、池田龍一、雲母及びオクトシリケート層間におけるドデシルトリメチルアンモニウムイオンの構造と運動、NMR討論会、P95、2000年11月（東京)。
16. S. Takaishi, S. Itoh, R. Ikeda, Magnetic Structure in a Halogen-Bridged

1-D S=1/2 Heisenberg Antiferromagnet $[NiBr(chxn)_2]Br_2$、The 1st International Symposium on Advanced Science Research (ASR-2000)、P24、2000年10月（日本原子力研究所）。

17. M. Fujishima, S. Kanda, T. Mitani, S. Ishimaru, R. Ikeda, H. Kitagawa, Hydrogen-induced properties of copper coordination polymer: catena-μ-N,N'-bis-(hydroxyethyl) dithiooxamidatocopper(II), 2000 international chemical congress of pacific basin societies, 0884, December, 2000 (Hawaii).
18. 高石慎也、伊藤晋一、池田龍一、ハロゲン架橋一次元錯体[NiBr(chxn)2]Br2の磁気構造、日本物理学会、28pXD-2、２００１年３月（東京）。
19. 石丸　臣一、池田　龍一、BEDO-TTF及び芳香族アミンのフッ化四ケイ素雲母層間化合物の合成と物性、日本化学会第79春季年会、2PB029、2001年3月（東京）。
20. 市川　未央、石丸　臣一、池田　龍一、メソポーラス化合物MCM-41に吸着したアセトニトリル分子の挙動、日本化学会第79春季年会、2PB030、2001年3月（東京）。
21. 後藤　和馬、石丸　臣一、池田　龍一、^{1}H NMRによる$AlPO_4$-5に吸着したp－ニトロアニリンの動的挙動の研究、日本化学会第79春季年会、3PA033、2001年3月（東京）。
22. 石富　妙、石丸　臣一、池田　龍一、ハロゲン化プロピルアンモニウムのRotator相における分子運動、日本化学会第79春季年会、3PA034、2001年3月（東京）。
23. 藤島武蔵、　神田精一、久保園芳博、三谷忠興、石丸臣一、池田龍一、北川宏、ルベアン酸銅配位高分子における水素ドーピング効果、日本化学会第７９春季年会、１Ｅ２－０４，２００１年３月（東京）。
24. E. Shinohara, S. Ishimaru, H. Kitagawa and R. Ikeda, Dynamic Structure of Trimethylalkyl- ammonium Ions Intercalated in Layered Silicates, International Symposium on Magnetic Resonance in Colloid and Interface Science、pp-71、June 2001(Russia).
25. S. Ishimaru, M. Ichikawa, K. Gotoh and R. Ikeda, Dynamic behaviour of acetonitrile molecules adsorbed in $AlPO_4$-5 and SAPO-5 studied by solid NMR method, 13th International Zeolite Conference, 13-P-14, July, 2001, MontPellier.
26. M. Yamauchi, S. Ishimaru, and R. Ikeda, Two-dimensional dynamics of guanidinium ions intercalated in tetrasilicic- fluormica, 14th Conference of the International Society of Magnetic Resonance, PA-56, August 2001 (Greece).
27. N. Kimura, M. Kano, T. Manabe, M. Yamashita and R. Ikeda, Metal Valence Structures in Halogen-Bridged One-Dimensional Mixed Metal Complexes $[Ni_{1-x}Pd_xX(chxn)_2]X_2$ Studied by Solid ^{1}H and ^{13}C NMR, Conference of the International Society of Magnetic Resonance, PA-37, August, 2001 (Rhodes, Greece).
28. S. Takaishi, M. Kanoh and R. Ikeda, ^{1}H NMR Relaxation in an Antiferromagnetically Coupled One-Dimensional S= 1/2 Halogen-Bridged Metal Complex $[NiBr(chxn)_2]Br_2$ (chxn: 1R,2R-cyclohexanediamine), Conference of the International Society of

Magnetic Resonance, PA-44, August, 2001 (Rhodes, Greece).

29. T. Nihei, S. Takahashi, S. Ishimaru, H. Ishihara, H. Ishida and R. Ikeda, Dynamics of H-Bonding in Solid Studied by ^{35}Cl NQR and ^{1}H NMR in Molecular Complexes of Chloranilic Acid and Diazines, Conference of the International Society of Magnetic Resonance, PB-39, August, 2001 (Rhodes, Greece).
30. 石丸　臣一、池田　龍一、ケイ酸化合物層間を利用した二次元伝導材料の開発、日本化学会第 80 秋季年会、2B3-14、2001 年 9 月（千葉）。
31. 藤島武蔵、長尾祐樹、池田龍一、神田精一、北川宏、ルベアン酸系銅配位高分子における物性・構造の水素ドーピング依存性、日本物理学会、20aYG-2, 2001 年 9 月（徳島）。
32. K. Suzuki, H. Fujimori, T. Asaji, S. Ishimaru, R. Ikeda, ^{1}H, ^{2}H and ^{13}C NMR Studies of Cation Dynamics in a Layered Perovskite-Type Incommensurate Compound $(n\text{-}C_3H_7NH_3)_2CdCl_4$, XVI International Symposium on Nuclear Quadrupole Interactions, PB-21, September, 2001 (Hiroshima).
33. K. Suzuki, S. Ishimaru, R. Ikeda, ^{133}Cs NMR Spin-Lattice Relaxation Time and Chemical Shift Studies on Cs_2MX_4 Crystals with Sr_2GeS_4 and $\beta\text{-}K_2SO_4$ Structures Performing no Low Temperature Phase Transition, XVI International Symposium on Nuclear Quadrupole Interactions, PB-22, September, 2001 (Hiroshim).
34. N. Kimura, T. Hachisuka, Y. Nakano and R. Ikeda, Molecular Motions in Halogen-Bridged 1-D Metal Complexes, $[M(en)_2][MX_2(en)_2](ClO_4)_4$ (M: Pt, Pd; X: Cl, Br) Studied by ^{2}H and ^{1}H NMR, International Symposium on Nuclear Quadrupole Interactions, PA-13, September, 2001 (Hiroshima).
35. R. Ikeda(Invited), Detection of Hydrogen Transfer in Hydrogen-Bonds in Solid by ^{35}Cl NQR, International Symposium on Nuclear Quadrupole Interactions, I-1-1, September, 2001 (Hiroshima).
36. H. Miyoshi, K. Horiuchi and R. Ikeda, A ^{35}Cl NQR Study on Exchange Interactions between Paramagnetic $[IrCl_6]^{2-}$ Ions, International Symposium on Nuclear Quadrupole Interactions, PA-19, September, 2001 (Hiroshima).
37. A. Ishikawa, M. Kurasawa, A. sasane, R. Ikeda and N. Kojima, ^{35}Cl Quadrupole Resonance study on $Cs_2(Au(I)Cl_2)[Au(III)Cl_4]$ and $Cs_2(Ag(I)Cl_2)[Au(III)Cl_4]$, , International Symposium on Nuclear Quadrupole Interactions, PB-28, September, 2001 (Hiroshima).
38. S. Takahashi, T. Nihei, H. Ishihara, H. Ishida and R. Ikeda, A ^{35}Cl NQR Study of Hydrogen Transfer in a 1:2 Salt of Chloranilic Acid and 1,3-Diazine, International Symposium on Nuclear Quadrupole Interactions, PB-30, September, 2001 (Hiroshima).
39. Y. Nagao, M. Fujishima, R. Ikeda, S. Kanda, H. Kitagawa, Highly proton-conductive copper coordination polymers, The 56th Yamada Conference, The Fourth International Symposium on Crystalline Organic Metals, Superconductors and Ferromagnets (ISCOM2001), F12Wed, September, 2001 (Hokkaido).
40. M. Fujishima, Y. Nagao, R. Ikeda, S. Kanda, H. Kitagawa, Hydrogen doping effect of copper coordination polymers with dithiooxamide and its derivative, The 4th International Conference on Crystalline Organic

Metals, Superconductors and Ferromagnets, F13Mon, September 2001 (Hokkaido).

41. 篠原絵美、山内美穂、石丸臣一、池田龍一、層状ケイ酸化合物を用いた有機分子の状態制御、日本化学会秋季年会、1B3-04、2001年9月（千葉）。
42. 篠原絵美、山内美穂、石丸臣一、池田龍一、雲母及びオクトシリケート層間にインターカレートした有機分子の構造と挙動、分子構造総合討論会、3p131、2001年9月（北海道）。
43. 高橋哲史、仁平貴明、石原秀太、石田祐之、池田龍一、クロラニル酸 1,3-ジアジン(1:2)塩における水素運動の解明、分子構造総合討論会、2C08、2001年9月（北海道）。
44. 山内美穂、寺西利治、三宅幹生、池田龍一、Pd 金属超微粒子の水素吸蔵と微粒子ないにおける水素及び重水素の挙動、分子構造総合討論会、2C09、2001年9月（北海道）。
45. 北川宏、藤島武蔵、長尾祐樹、池田龍一、神田精一、ルベアン酸銅錯体における電子伝導とプロトン伝導、分子構造総合討論会、2C13、2001年9月（北海道）。
46. 加納正隆、高石慎也、木村憲喜、北川宏、山下正広、池田龍一、固体 NMR 法による擬一次元ハロゲン架橋錯体 $[Ni_{1-x}Pd_xBr(chxn)_2]Br_2$ の電子スピンダイナミクスの研究、分子構造総合討論会、1p103、2001年9月（北海道）。
47. 長澤五十六、川本達也、坂田一矩、北川宏、池田龍一、白金(II)ホスフィン錯体結晶中における I_4^{2-} イオンの存在、錯体化学討論会、2a-A09, 2001年9月（松江）。
48. 長尾祐樹、藤島武蔵、池田龍一、神田精一、北川宏、ルベアン酸系銅錯体のプロトン伝導、錯体化学討論会、3c-C02、2001年9月（松江）。
49. 牧浦理恵、北川宏、池田龍一、ハロゲン架橋混合原子価複核錯体 $Ni_2(dta)_4I$ の電子状態、錯体化学討論会、3c-C04、2001年9月（松江）。
50. 小林厚志、石丸臣一、北川宏、池田龍一、一次元複核金属錯体の合成と物性、錯体化学討論会、3c-C03、2001年9月（松江）。
51. 藤島武蔵、長尾祐樹、池田龍一、神田精一、北川宏、ルベアン酸系銅配位高分子における物性・構造の水素ドーピング依存性、第51回錯体化学討論会、3c-C01、2001年9月（松江）。
52. 木村憲喜、麻生秀光、滝沢孝一、石井知彦、山下正廣、池田龍一、Br_2 ドープした $\{[Pt(en)_2][PtBr_2(en)_2]\}_3(CuBr_4)_4$ 錯体の ESR、^{13}C NMR スペクトルと ^1H 磁気緩和、錯体化学討論会、1P-C29、2001年9月(松江)。
53. 長尾祐樹、藤島武蔵、池田龍一、神田精一、北川宏、ルベアン酸系銅錯体のプロトン伝導性、第56回日本物理学会、20aYG-1, 2001年9月（徳島）。
54. 長尾祐樹、藤島武蔵、石丸臣一、池田龍一、神田精一、北川宏、ルベアン酸銅配位高分子のプロトン伝導性、第27回固体イオニクス討論会、3C11, 2001年11月（東京）。
55. A. Kobayashi, H. Kitagawa, S. Ishimaru and R. Ikeda, Syntheses and

physical properties of one-dimensional metal-dimer systems $Ni_2(dtp)_4$ and $Pd_2(dtp)_4$, International Symposium of Cooperative Phenomena of Assembled Metal Complexes (AMC2001), P-066, Nov. 2001 (Osaka).

56. M. Yamauchi, R. Ikeda, and T. Kawamura, Electronic Spin Structure in Infinite Zigzag Chain of $[Rh_2(HNCOCH_3)_4Cl]_n$, International Symposium on Coorperative Phenomenon of Assembled Metal Complexes, P067, November 2001 (Osaka).
57. Y. Nagao, M. Fujishima, S. Ishimaru, R. Ikeda, S. Kanda, H. Kitagawa, Highly proton-conductive copper coordination polymers, International Symposium on Cooperative Phenomena of Assembled Metal Complexes, P-016, November 2001 (Osaka).
58. S. Takaishi、H. Kitagawa、R. Ikeda、Relaxation Process of CT Exiton State in a One-Dimensional MX-Chain Compound $[NiBr(chxn)_2]Br_2$、International Symposium of Cooperative Phenomena of Assembled Metal Complexes (AMC2001)、C P-055、November 2001 (Osaka).
59. M. Fujishima, I. Ryuichi, S. Kanda, H. Kitagawa, Electrical conductivities and magnetic susceptibilities of copper coordination polymers with dithiooxamide and its substituent, International Symposium on Cooperative Phenomena of Assembled Metal Complexes, P-045, November 2001 (Osaka)
60. S. Takaishi, S. Itoh, R. Ikeda, Antiferromagnetic Structure in a Halogen-Bridged One-Dimensional MX-Chain Compound $[NiBr(chxn)_2]Br_2$, International Symposium of Cooperative Phenomena of Assembled Metal Complexes (AMC2001), C P-057、November 2001 (Osaka).
61. 木村憲喜、加納正隆、高石慎也、池田龍一、１次元反強磁性混合金属錯体$[Ni_{1-x}Pd_xX(chxn)_2]X_2$ (X:Cl Br;chxn:cyclohexanediamine)の ^{13}C と ^{1}H 固体 NMR、NMR 討論会、1L7、2001 年 11 月(京都)。
62. 高石慎也、北川宏、池田龍一、ハロゲン架橋一次元錯体$[Ni_{1-x}Pd_xBr(chxn)_2]Br_2$ の緩和過程、日本物理学会、27pZC-11、2002 年 3 月（滋賀)。
63. 長尾祐樹、池田龍一、久保孝史、中筋一弘、久保園芳博、神田精一、北川宏、ルベアン酸系銅配位高分子のプロトン伝導性の置換基効果、第５７回日本物理学会、27pZC-13、2002 年 3 月（滋賀)。
64. 小林厚志、北川宏、池田龍一、北尾真司、瀬戸誠、ハロゲン架橋一次元複核金属錯体 $Pt_2(dtp)_4I$ (*dtp* = dithiopropionato)の ^{129}I メスバウアー分光学的研究、日本物理学会年次大会、27pZC-4、2002 年 3 月（草津)。
65. 長尾祐樹、池田龍一、久保園芳博、神田精一、北川宏、ルベアン酸系銅配位高分子錯体$(HOC_2H_4)_2dtoa$Cu におけるプロトン伝導性の湿度依存性、日本化学会第８１春季年会、3C7-26, 2002 年 3 月（東京)。
66. 藤島武蔵、池田龍一、延与三知夫、神田精一、北川宏、ルベアン酸銅配位高分子の電解還元反応の機構、日本化学会第８１春季年会、2B3-32, 2002 年 3 月（東京)。
67. 高石慎也、北川宏、池田龍一、ハロゲン架橋一次元錯体$[Ni1-xPdxBr(chxn)_2]Br_2$ の発光、日本化学会春季年会、3 B3-55、

2002年3月（東京）。

67. 垣花　仁、石丸　臣一、池田　龍一、NMRによる固体12-タングストリン酸セシウム中に吸着したアセトニトリル分子の動的挙動の研究、日本化学会第80春季年会、1PC-55、2002年3月（東京）。
68. 小林厚志、北川宏、池田龍一、複核白金(III)錯体 $Pt_2(EtCS_2)_4Br_2$ の合成と物性、日本化学会春季年会、3B3-54、2002年3月（東京）。
69. 山内美穂、池田龍一、寺西利治、三宅幹夫、ポリマー保護金属ナノ粒子中の水素の挙動、日本化学会第81春季年会、3D5-55、2002年3月（東京）。
70. 磯部祐子、山内美穂、池田龍一、寺西利治、三宅幹夫、ポリマー保護Ptナノ粒子における水素吸着、日本化学会第81春季年会、1C6-33、2002年3月（東京）。
71. 星　貴洋、石丸　臣一、池田　龍一、一次元細孔を持つ AlPO4-5 中のp-ベンゾキノンの挙動、日本化学会第81春季年会、1PC-056、2002年3月(東京)。
72. 長澤五十六、黒木知佳、坂田一矩、北川宏、池田龍一、固体でSO2を吸収する白金(II)三級ホスフィン錯体、日本化学会第81春季年会、4B3-41、2002年3月（東京）。
73. 須藤智彦、牧浦理恵、北川宏、池田龍一、ハロゲン架橋一次元錯体の高圧下電気伝導、日本化学会第81春季年会、2B3-039、2002年3月(東京)。
74. 藤島武蔵、池田龍一、延与三知夫、神田精一、北川宏、ルベアン酸銅配位高分子の電解還元反応の機構、日本化学会第81春季年会、2B3-032、2002年3月(東京)。
75. 牧浦理恵、北川宏、池田龍一、MMX型金属錯体 $Ni_2(dta)_4I$ の伝導性と磁性、日本化学会第81春季年会、4D5-035、2002年3月(東京)。
76. 長澤五十六、永島直人、坂田一矩、北川宏、池田龍一、白金(II)三級ホスフィン錯体と臭素分子の固体での反応、日本化学会第81春季年会、1PB-079、2002年3月(東京)。
77. 山内美穂、池田龍一、寺西利治、三宅幹夫、水素を吸着したポリマー保護Pd金属ナノ粒子の構造、日本物理学会第57回年次大会、24aXR-4、2002年3月（京都）。
78. Y. Nagao, R. Ikeda, T. Kubo, K. Nakasuji, S. Kanda, H. Kitagawa, NEW PROTONIC CONDUCTOR OF COORDINATION POLYMER, International Conference on Science and Technology of Synthetic Metals (ICSM2002), ThuB130, June 2002 (Shanghai).
79. A. Kobayashi, H. Kitagawa, R. Ikeda, S. Kitao and M. Seto, ^{129}I Mossbauer spectroscopic study of a one-dimensional halogen-bridged binuclear-metal complex $Pt_2(dtp)_4I$, International Conference on Science and Technology of Synthetic Metals, ThuB137, June 2002 (Shanghai).
80. N. Kimura, K. Kisoda, H. Aso, K. Takizawa, T. Ishii, H. Miyasaka, K. Sugiura, M. Yamashita and R. Ikeda, ^{13}C NMR and ESR Spectra, and ^{1}H Magnetic Relaxations of Br_2 Doped $\{[Pt(en)_2][PtBr_2(en)_2]\}_3(CuBr_4)_4 \cdot 12H_2O$, International Conference on Science and Technology

of Synthetic Metals, MonB164, July, 2002 (Shanghai).

81. M. Fujishima, R. Ikeda, T. Kawamura, H. Kitagawa, Substituent Effect on Electronic State of Copper Coordination Polymers : H_2dtoaCu and $(HOC_2H_4)_2$dtoaCu, International Conference on Science and Technology of Synthetic Metals, ThuB173, July 2002 (Shanghai).
82. S. Takaishi, M. Kano, H. Kitagawa, Y. Furukawa, K. Kumagai and R. Ikeda、Electron Spin Dynamics in a Halogen-Bridged One-Dimensional Antiferromagnet $[NiBr(chxn)_2]Br_2$、ICSM2002、B-136、July 2002 (Shanghai).
83. E. Shinohara, S. Ishimaru, H. Kitagawa, R. Ikeda, H. Yamochi and G. Saito, A Novel Electron Conductive nanocomposite, BEDO-TTF-Tetrasilicicfluormica Intercalation Compound, International Conference on Science and Technology of Synthetic Metals、D129、June 2002 (Shanghai) .
84. Y. Isobe, M. Yamauchi, H. Kitagawa, R. Ikeda, T. Toshiharu, and M. Mikio, A Study on Hydrogen Adsorption of Polymer Protected Pt nanoparticles, International Conference on Science and Technology of Synthetic Metals, F055, June 2002 (Shanghai).
85. A. Ozawa, N. Kimura, H. Kitagawa and R. Ikeda, Spin Dynamics in a Halogen-Bridged 1-D Complex, $[PdBr(chxn)_2]Br_2$, International Conference on Science and Technology of Synthetic Metals, ThuB184, July 2002 (Shanghai).
86. M. Yamauchi, R. Ikeda, and T. Kawamura, Solid State Magnetic Resonance on 1-D Zigzag Chain of $[Rh_2(HNCOCH_3)_4Cl]_n$, 35th International Conference on Coordination Chemistry, P6.094, July 2002 (Heidelberg).
87. H. Kitagawa, Y. Nagao, R. Ikeda, S. Kanda, Highly Proton-Conductive Coordination Polymers, 35th International Conference on Coordination Chemistry (ICCC35), O 6.14, July 2002(Heidelberg).
88. 星　貴洋、石丸　臣一、北川　宏、池田　龍一、一次元細孔性結晶 AlPO4-5 中の p-ベンゾキノン、ヒドロキノンの物性、粘土科学討論会、B20、2002 年 9 月(仙台)。
89. 石丸　臣一、篠原　絵美、北川　宏、池田　龍一、矢持　秀起、齋藤　軍治、フッ化四ケイ素雲母中にインターカレートした BEDO-TTF の伝導性、第 46 回粘土科学討論会、A27、2002 年 9 月 (仙台)。
90. 長尾祐樹、池田龍一、久保孝史、中筋一弘、神田精一、北川宏、銅配位高分子におけるプロトン伝導の温度依存性、第５８回日本物理学会、８ｐSC－１２、２００２年９月 (愛知)。
91. 藤島武蔵、池田龍一、延与三知夫、川村尚、神田精一、北川宏、ルベアン酸銅配位高分子の電解還元機構及び ab initio MO 計算、第５２回錯体化学討論会、１Ｐ－Ｂ１２５、２００２年９月 (東京)。
92. 長尾祐樹、池田龍一、久保孝史、中筋一弘、神田精一、北川宏、高いプロトン伝導性をもつ銅配位高分子の伝導メカニズムに関する研究、第５２回錯体化学討論会、３ｈ－Ｅ０３、２００２年９月 (東京)。
93. 福井章子、田所　誠、長尾祐樹、石丸臣一、北川　宏、池田龍一、

中筋一弘、分子性ナノチャネルに取り込まれた水の構造と性質、第５２回錯体化学討論会、2a－Ａ１０、２００２年９月（東京）。

94. 木村憲喜、木曽田賢治、小澤秋男、池田龍一、^{13}C 固体高分解能NMR法を用いたハロゲン架橋一次元混合原子価錯体$[Pd(chxn)_2][PdX_2(chxn)_2]X_4$ (X: Cl, Br)の研究、第５２回錯体化学討論会、2e-B02、2002年10月(東京)。

95. 長澤五十六、東郷美鈴、坂田一矩、北川宏、白金(II)三級ホスフィン錯体のヨウ素酸化、第５２回錯体化学討論会、1P-A08、2002年９月（東京)。

96. 山内美穂、池田龍一、高崎誉章、揚志勇、川村尚、ハロゲン架橋一次元水車型複核金属錯体の固体核磁気共鳴、第５２回錯体化学討論会、2e-B03、2002年９月（東京)。

97. 北川宏、須藤智彦、池田龍一、辺土正人、上床美也、MMC-Chainの高圧電気伝導度、第５２回錯体化学討論会、2e-B04、2002年９月（東京)。

98. 小林厚志、北川宏、池田龍一、田崎遼子、若林裕助、澤博、ハロゲン架橋一次元混合配位子複核金属錯体の構造と電子状態、第５２回錯体化学討論会、2e-B06、2002年９月（東京)。

99. 高石慎也、北川宏、三谷忠興、池田龍一、S= 1/2 擬一次元銅錯体$CuCl_2$(pid) の磁性、第５２回錯体化学討論会、3d-B02、2002年９月（東京)。

100.小澤秋男、木村憲善、北川宏、池田龍一、一次元臭素架橋パラジウム錯体におけるスピンダイナミクス、第５２回錯体化学討論会、2e-B02、2002年10月(東京)。

101.石丸　臣一、池田　龍一、新奇二次元伝導性物質1,5-ジアミノナフタレン-サポナイト層間化合物の電子挙動、分子構造総合討論会、4B06、2002年10月（神戸)。

102. 藤島武蔵、池田龍一、川村尚、延与三知夫、神田精一、北川宏、ルベアン酸銅配位高分子の電子状態における置換基効果、分子構造総合討論会、４Ｐ０７９、２００２年１０月（神戸)。

103. 星貴洋、石丸臣一、北川宏、池田　龍一、一次元細孔性結晶AlPO4-5中のp-ベンゾキノン、ヒドロキノンの物性、分子構造総合討論会、1P102、2002年10月(神戸)。

104.小林厚志、北川宏、池田龍一、田崎遼子、若林裕助、澤博、混合配位子ハロゲン架橋一次元複核金属錯体の構造と電子状態、分子構造総合討論会、4E-14、2002年10月（神戸)。

105.篠原絵美、石丸臣一、北川宏、池田龍一、矢持秀起、斎藤軍治、層状粘土鉱物層間にインターカレーションしたBEDO-TTFの物性、分子構造総合討論会、2D09、2002年10月（神戸)。

106. 戸田陽子、石丸臣一、池田龍一、三谷洋興、北尾真司、MCM-41孔内におけるフェロセン分子、分子構造総合討論会、1P101、2002年10月（神戸)。

107. 長尾祐樹、池田龍一、久保孝史、中筋一弘、神田精一、北川宏、銅配位高分子錯体のプロトン伝導性とその置換基依存性、分子構造総合討論会、3B-03, 2002年10月（神戸)。

108.高石慎也、北川宏、三谷洋興、池田龍一、S=1/2 擬一次元銅錯体の磁性、日本物理学会、7aWB-3、2002年9月（愛知）。
109.山内美穂、磯部祐子、北川宏、池田龍一、寺西利治、三宅幹夫、Pt族超微粒子における水素の吸着挙動、日本物理学会2002年秋季大会、7pSK-6、2002年9月（愛知）。
110.小林厚志、北川宏、池田龍一、田崎遼子、若林裕助、澤博、ハロゲン架橋一次元混合配位子複核金属錯体の構造と物性、日本物理学会秋期大会、8pSC-10、2002年9月（愛知）。
111.小澤秋男、木村憲善、北川宏、池田龍一、ハロゲン架橋錯体$[Pd(chxn)_2][PdBr_2(chxn)_2]Br_4$における電子スピンダイナミクス、日本物理学会2002年秋季大会、8pSC7、2002年9月(愛知)。
112.山内美穂、磯部祐子、北川宏、池田龍一、寺西利治、三宅幹夫、Pd,Ptナノ粒子に吸蔵された水素の挙動、日本化学会第82秋季年会、3C2-18、2002年9月（大阪）。
113.福井章子、田所　誠、長尾祐樹、石丸臣一、北川　宏、池田龍一、中筋一弘、分子性ナノチャネルに取り込まれた水の構造と性質、第16回基礎有機化学連合討論会、1p098, 2002年10月（東京）。
114.長尾祐樹、池田龍一、久保孝史、中筋一弘、北川宏、新規銅配位高分子の創製とそのプロトン伝導性、第28回固体イオニクス討論会、1C-03, 2002年11月（大阪）。
115.木村憲喜、青木裕史、木曽田賢治、池田龍一、^{13}C固体NMR、Raman、IR測定による一次元混合金属錯体$[Cu(chxn)_2][PtX_2(chxn)_2]X_4$ (X: Cl, Br)の研究，日本化学会春季年会、2003年3月（東京）。
116.高石慎也、北川宏、三谷洋興、鈴木和也、池田龍一、S=1/2 擬一次元Heisenberg反強磁性錯体の$CuCl_2(pid)$スピン構造、日本化学会春季年会、2003年3月（東京）。
117.山内美穂、端健二郎、後藤敦、清水禎、寺西利治、坂東義雄、北川宏、池田龍一、単分散Ｐｄナノ粒子に吸蔵された重水素の固体ＮＭＲ、日本化学会第83春季年会、2003年3月（東京）。
118.戸田陽子、石丸臣一、池田龍一、三谷洋興、北尾真司、MCM-41に吸着したフェロセン分子の酸化と磁性、日本化学会春期年会、2003年3月（東京）。
119.小林厚志、北川宏、池田龍一、若林裕助、澤博、混合配位子型ハロゲン架橋一次元複核金属錯体におけるX線散漫散乱研究、日本化学会春季年会、2003年3月（東京）。
120.小澤秋男、北川宏、池田龍一、ハロゲン架橋一次元複核金属錯体Ni_2dta_4Iの磁気特性、日本化学学会2003年春季大会、2003年3月発表予定（東京）。
121.石丸　臣一、戸川　真紀、篠原　絵美、池田　龍一、川崎　英也、前田　悠、ドデシルジメチルアミンオキシド塩酸塩及びその層間化合物の複素インピーダンス測定、第83回日本化学会春季年会、2003年3月（東京）。
122.長尾祐樹、池田龍一、久保孝史、中筋一弘、北川宏、高いプロトン伝導性を示す錯体ポリマーにおける置換基の役割、日本化学会第83春季年会、２００３年3月（東京）。

123.藤島武蔵、山内美穂、池田龍一、久保孝史、中筋一弘、川村尚、坂東義雄、北川宏、ルベアン酸系高分子で保護された金属微粒子の合成と性質、第８３回日本化学会年春季年会、２００３年３月（東京）。

124.徳永彩、北川宏、池田龍一、辺土正人、上床美也、MMX-Chain 錯体 $Pt_2(C_2H_5CS_2)I$ における高圧下電気伝導度　第８３回日本化学会春季年会、２００３年３月（東京）。

125.徳永彩、北川宏、池田龍一、辺土正人、上床美也
MMX-Chain 錯体 $Pt_2(C_2H_5CS_2)I$ における高圧下電気伝導度　日本物理学会、２００３年３月（仙台）。

126.高石慎也、北川宏、後藤敦、清水禎、池田龍一、ハロゲン架橋一次元 MX 錯体 $[NiBr(chxn)_2]Br_2$ の電子状態、日本物理学会、２００３年３月（仙台）。

127.小林厚志、北川宏、池田龍一、北尾真司、小林康浩、瀬戸誠、混合配位子型ハロゲン架橋一次元複核金属錯体の電子構造、日本物理学会年次大会、2003 年 3 月（仙台）。

128.小澤秋男、北川宏、池田龍一、ハロゲン架橋一次元複核金属錯体 Ni_2dta_4I の磁気特性、日本物理学会 2003 年春季大会、3 月（仙台）。

129.長尾祐樹、池田龍一、久保孝史、中筋一弘、北川宏、ルベアン酸銅配位高分子における重水素効果、第５９回日本物理学会、２００３年３月（仙台）。

130.藤島武蔵、山内美穂、池田龍一、久保孝史、中筋一弘、川村尚、坂東義雄、北川宏、二塩基酸性を有するルベアン酸系高分子で保護された金属微粒子の性質、日本物理学会第５８回年次大会、２００３年３月（仙台）。

Cationic Motions and Order–Disorder Phase Transitions in Layer Crystals with a Rotator Phase, $(n\text{-}C_5H_{11}NH_3)_2ZnCl_4$ and $(n\text{-}C_{12}H_{25}NH_3)_2ZnCl_4$

Keizo Horiuchi,* Himiko Takayama,† Shin'ichi Ishimaru,† and Ryuichi Ikeda†

Faculty of Science, University of the Ryukyus, Nishihara-cho, Okinawa 903-0213

†Department of Chemistry, University of Tsukuba, Tsukuba 305-0006

(Received August 26, 1999)

^{1}H NMR spin-lattice relaxation times T_1 and $T_{1\rho}$ as well as the electrical conductivity were measured as a function of temperature in $(n\text{-}C_5H_{11}NH_3)_2ZnCl_4$ and $(n\text{-}C_{12}H_{25}NH_3)_2ZnCl_4$. The highest-temperature solid phase in both compounds was found to be the rotator phase, where rod-like cations perform uniaxial reorientations about the molecular long axes accompanied by conformational disordering and translational self-diffusion of the cations within the layer perpendicular to c-axis. In the rotator phase, the cations are considered to have a non-intercalated double layer structure. These rotator phases were shown to be quite analogous to those reported in n-alkylammonium chlorides. $(n\text{-}C_5H_{11}NH_3)_2ZnCl_4$ undergoes four structural phase transitions, while $(n\text{-}C_{12}H_{25}NH_3)_2ZnCl_4$ exhibits a single transition above ca. 120 K. All of these transitions were shown to be of order–disorder type.

The rotator phase was first found in solid n-paraffins where the constituent molecules adopt dynamically disordered orientations about their molecular long axes.[1] The molecular motions in this phase, however, could not be fully determined because this phase is formed in a narrow temperature range of less than 10 K. Recently, we discovered a quite analogous phase in n-alkylammonium chlorides $C_nH_{2n+1}NH_3Cl$ (n = 3—10, 12) over a quite wide temperature range of more than 100 K.[2–6] The crystal structure of this rotator phase is tetragonal (space group $P4/nmm$) with a lameller-type double-layered structure. A new characteristic molecular motion found in this phase in addition to the uniaxial rotation of alkylammonium chains, is two-dimensional translational self-diffusion in the lamellar plane perpendicular to the molecular long axis. By comparison with the plastic crystal where the three-dimensional rotation and diffusion of constituent globular molecules or ions take place,[7] we can name the rotator phase "a low-dimensional plastic crystal" because of the restricted motions such as 1D rotation and 2D diffusion. Thermal measurements also suggest that the rotator phase is a highly disordered crystalline state similar to the plastic crystal; the melting entropies ΔS_m observed in the n-alkylammonium chlorides are smaller than 20 J K^{-1} mol^{-1},[2–6] reported as one of the conditions for the formation of the plastic crystal.[7] At the same time, we note that this highly anisotropic cystalline state of lamellar-type double layer structure resembles the smectic liquid crystal, although the centers of gravity of constituent molecules in the layer are disordered in the liquid crystal.

Our present interest is to find rotator phases in systems different from n-alkylammonium chlorides. Recently, we have found the rotator phase in di-n-alkylammonium bromides $(C_nH_{2n+1})_2NH_2Br$ (n = 2—4),[8] which has a crystal structure of $I4/mmm$ analogous to that of $P4/nmm$. Di-n-alkylammonium tetrahalogenozincates $(n\text{-}C_nH_{2n+1}NH_3)_2ZnX_4$ (X = Cl, Br) are known to belong to the A_2BX_4 family with the β-K_2SO_4 structure (space group $Pnma$),[9,10] and we have already studied some short-chain compounds of them with a prime interest in their structural phase transitions.[11–14] The crystal structures in these compounds are characterized by a triple-layered structure that consists of two-dimensional layers made by isolated BX_4 ions being sandwiched by layers of alkylammonium ions. The title compounds, $(n\text{-}C_5H_{11}NH_3)_2ZnCl_4$ and $(n\text{-}C_{12}H_{25}NH_3)_2ZnCl_4$, have been reported to have ΔS_m smaller than 20 J K^{-1} mol^{-1}.[15] From these facts, we may expect the title compounds to have rotator phases. In the present study, the cationic dynamics and structural phase transitions were investigated by the measurements of the temperature dependence of ^{1}H NMR relaxation times and the electrical conductivity.

Experimental

$(n\text{-}C_5H_{11}NH_3)_2ZnCl_4$ and $(n\text{-}C_{12}H_{25}NH_3)_2ZnCl_4$ prepared by the methods described in Ref. 15 were identified by X-ray and thermal measurements as well as by chemical analyses. Anal. Calcd for $(n\text{-}C_5H_{11}NH_3)_2ZnCl_4$: C, 31.31; H, 7.36; N, 7.31%. Found: C, 31.31; H, 7.51; N, 7.19%. Calcd. for $(n\text{-}C_{12}H_{25}NH_3)_2ZnCl_4$: C, 49.70; H, 9.75; N, 4.83%. Found: C, 49.84; H, 9.94; N, 4.83%. X-Ray powder diffraction was measured using Cu $K\alpha$ radiation with a Philips X'Pert-MPD and a Rigaku RINT-1500 diffractometer for $(n\text{-}C_5H_{11}NH_3)_2ZnCl_4$ and $(n\text{-}C_{12}H_{25}NH_3)_2ZnCl_4$, respectively. Differential scanning calorimetry (DSC) was carried out with a DSC120 calorimeter from Seiko Instruments Inc. DTA was also performed on $(n\text{-}C_{12}H_{25}NH_3)_2ZnCl_4$ using a home-made apparatus[16] over the range 300—480 K. The sample temperatures

in DTA and the following measurements were determined using chromel–constantan thermocouples within ±1 K.

The ^{1}H NMR spin-lattice relaxation time, T_1, was measured by a Bruker SXP-100 spectrometer at Larmor frequency of 40 MHz and by a home-made pulsed spectrometer[17] at frequencies of 10—25 MHz. T_1 was determined by a 180°-τ-90° pulse sequence. The ^{1}H NMR spin-lattice relaxation time in the rotating frame, $T_{1\rho}$, and the second moment, M_2, of the resonance linewidth were measured with a Bruker SXP-100 spectrometer at a Larmor frequency of 40 MHz using the spin-locking method[18] applying an r.f. magnetic field of 3.97 G and the solid-echo method[19] with a 90°_x-τ-90°_y pulse sequence, respectively.

The temperature dependence of electrical conductivity was measured at 1 kHz by the two-terminal method with a home-made apparatus using a Yokogawa Hewlett–Packard 4261A LCR meter. The powdered sample was pressed into a disc of 10 mm in diameter and ca. 1 mm thick, and mounted on Cu electrodes using graphite electrodes (Acheson Electrodag 199).

Results and Analysis

$(n$-$C_5H_{11}NH_3)_2ZnCl_4$. In our thermal measurements, $(n$-$C_5H_{11}NH_3)_2ZnCl_4$ showed four first-order structural phase transitions at 141.5, 148, 250, and 349 K, in agreement with the reported results.[20] These five solid phases are named as I, II, III, IV, and V in the order of decreasing temperature. Crystal structures in phases I, II, and III were reported to be all orthorhombic, their space groups being *Pnma* for II and $P2_12_12_1$ for III.[10,20] X-Ray powder diffraction patterns taken at 293±1 K in phase II and at 390±2 K in phase I were well explained using the reported lattice parameters.[10,20]

Temperature dependences of ^{1}H NMR T_1 measured at 40.1 and 10.8 MHz are shown in Fig. 1. A discontinuity in T_1 was observed only at the I–II transition, although four phase transitions are first-order. The observed T_1 curve gave a minimum around 150 K and a Larmor-frequency dependence only on the low-temperature side of T_1 minimum. This temperature depedence is attributable to the magnetic dipolar relaxation caused by thermal molecular motions, and can be analyzed by the BPP equation[21] using the Arrhenius relationship between the motional correlation time, τ_c, and the motional activation energy, E_a, as given by

$$\tau_c = \tau_{c0}\exp\left(\frac{E_a}{RT}\right). \quad (1)$$

The obtained best fit T_1 curves are displayed in Fig. 1 and the determined values of motional parameters are listed in Table 1. The assignment of motional modes was carried out by calculating M_2 values.[22] Since proton positions are unavailable on the crystal structure data, the calculation was performed by assuming proton positions using a standard value for an alkylammonium ion.

The T_1 maximum observed in the high-temperature range of phase II suggests the onset of a new motion other than the NH_3^+ rotation. We assigned it to the 180° flip of the whole cations about the molecular long axes, because in short alkyl chain salts such as n-$C_4H_9NH_3X$ (X = Cl, Br, I)[3,23,24] and n-$C_5H_{11}NH_3Cl$,[4] the 180°-flip or analogous two-site jumps

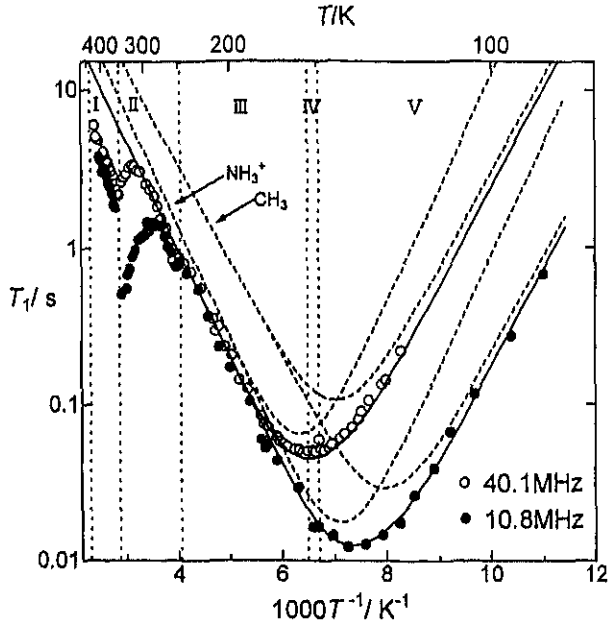

Fig. 1. Temperature dependences of ^{1}H NMR T_1 observed in $(n$-$C_5H_{12}NH_3)_2ZnCl_4$. Solid curves are the best-fitted calculated ones. Broken curves are contributions from respective molecular motions (see text). Dotted lines represent the phase transition temperatures.

Table 1. Activation Energies, E_a, Pre-exponential Factors, τ_{c0}, and Motional Modes of n-Pentylammonium Cations in $(n$-$C_5H_{11}NH_3)_2ZnCl_4$ Determined by ^{1}H NMR T_1 and $T_{1\rho}$

Phase	E_a / kJ mol^{-1}	τ_{c0} / 10^{-12} s	Motional mode
III–V	12±1	14±1	CH_3 rotation
	14±1	0.73±0.07	NH_3^+ rotation
II	34±3		180° flip
I	18±2		Axial rotation + conformational disorder
	72±7		Self-diffusion
	85±9[a)]		Self-diffusion

a) Derived from electrical conductivity.

of the entire alkyl chain were found in the low-temperature phases. We therefore analysed the T_1 variations in phase II by a superimpose of 180°-flip and NH_3^+ rotation, giving the best fitted curves displayed in Fig. 2.

^{1}H NMR $T_{1\rho}$ observed in phase I is shown in Fig. 3 along with T_1 data. The increase in T_1 and the decrease in $T_{1\rho}$ with increasing temperature suggest that two different molecular motions are effective in the relaxation process in this phase: one is rapid and the other is slow. The temperature dependence of M_2 in the range 308—411 K is represented in Fig. 4. M_2 values in phase I were abruptly reduced to less than 2 G^2 from ca. 20 G^2 just below the transition temperature in phase II, implying the onset of a new motion in phase I that averages most of the proton dipolar interactions. It is the rapid motion that is responsibe for this large M_2 reduction, and the motion is considered to be the axial rotation of rigid cations about

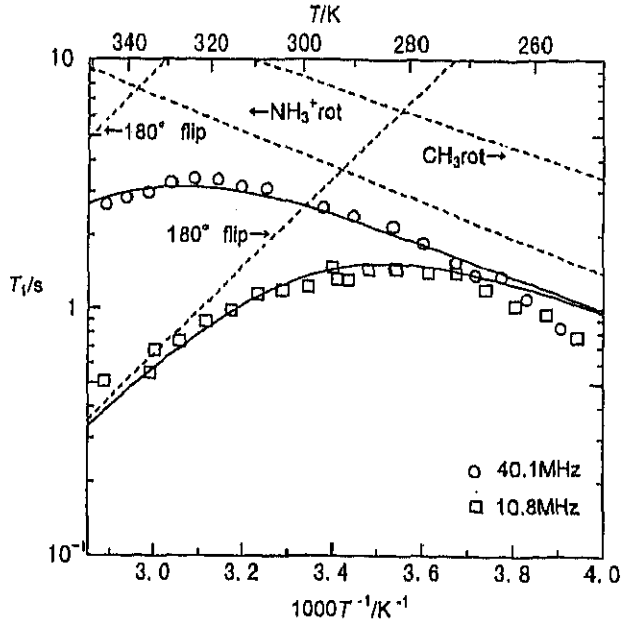

Fig. 2. Temperature dependences of ^{1}H NMR T_1 in phase II of $(n\text{-}C_5H_{12}NH_3)_2ZnCl_4$. Solid curves are the best-fitted calculated ones. Broken curves are contributions from respective molecular motions (see text).

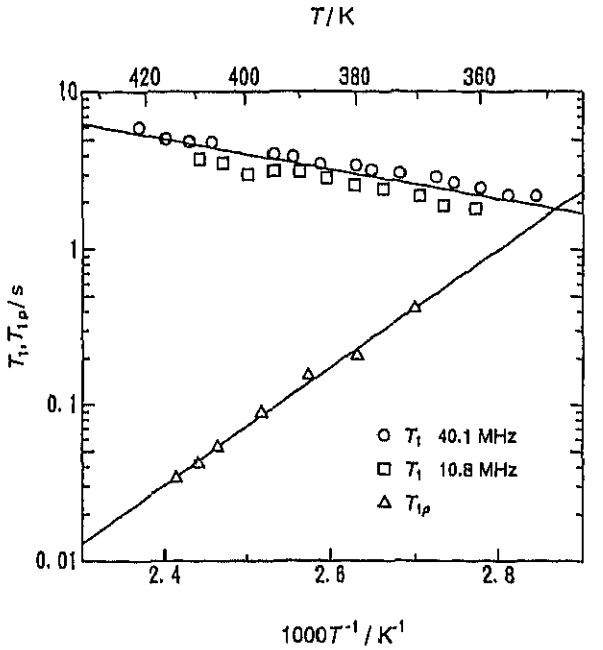

Fig. 3. Temperature dependences of ^{1}H NMR T_1 and $T_{1\rho}$ at an r.f. magnetic field of 3.97 G in phase I of $(n\text{-}C_5H_{12}NH_3)_2ZnCl_4$. Solid lines are the best-fitted calculated ones (see text).

their molecular axes; however, the axial rotation leads to the calculated M_2 value of ca. 8 G^2, which is much larger than the observed value. Hence, the rapid motion is dynamically more disordered than the uniaxial rotation and this disorder can be attributed to the orientational distribution of the cationic long axis about the crystallographic c-axis and/or the conformational disorder of the *trans–gauche* structure in

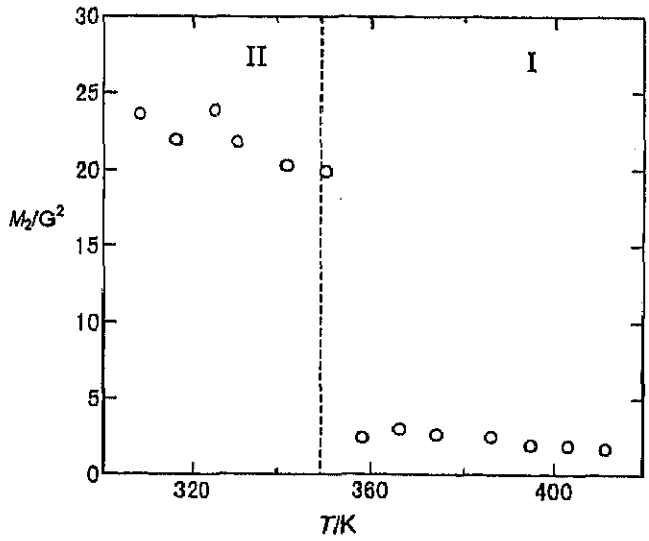

Fig. 4. A temperature dependence of M_2 of ^{1}H NMR linewidth in phases I and II of $(n\text{-}C_5H_{12}NH_3)_2ZnCl_4$. A broken line indicates the phase transition temperature of 349 K.

the alkyl chain. E_a of this composite motion was evaluated from the slope in the log T_1 vs. T^{-1} plot, because in the fast motion limit of the BPP equation T_1^{-1} is proportional to τ_c. The resulting best fit line is represented in Fig. 3 and E_a of the motion was estimated to be 18±2 kJ mol^{-1}.

The slow motion responsible for the temperature dependence of $T_{1\rho}$ was attributed to cationic translational self-diffusion. To confirm this, we measured the ac electrical conductivity σ between 340 and 420 K; this result is shown in Fig. 5. This clearly shows a marked ionic conduction in phase I. In general, the diffusion constant D for moving ions in crystals can be written by the following Nernst–Einstein

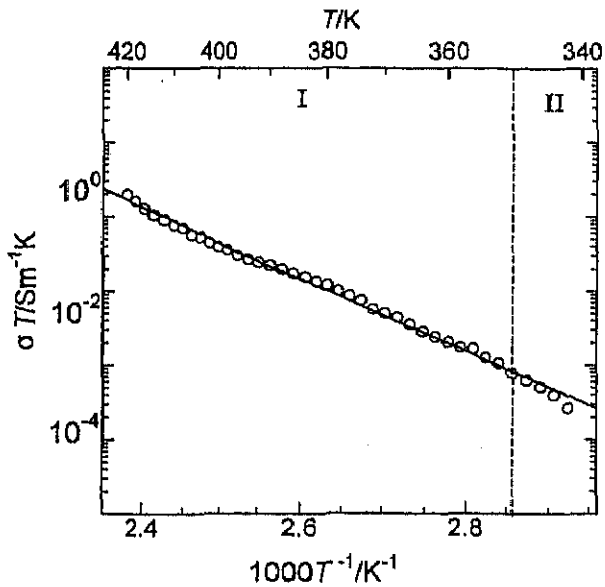

Fig. 5. A temperature dependence of ac electrical conductivity σ in phase I of $(n\text{-}C_5H_{12}NH_3)_2ZnCl_4$. A solid line is the best-fit Arrhenius relation given in text. A broken line denotes the phase transition temperature of 349 K.

equation:

$$D = \frac{kT\sigma}{(Ze)^2 N}, \quad (2)$$

where Ze and N stand for the charge of the diffusing ion and the number of these ions in a unit volume, respectively. By assuming the Arrhenius relationship for the self-diffusion, D can be written as

$$D = D_0 \exp\left(\frac{E_a}{RT}\right). \quad (3)$$

E_a determined from the slope in $\log(\sigma T)$ vs. T^{-1} plots was 85±9 kJ mol^{-1} and the obtained best fit line is depicted in Fig. 5. Since this compound has a layer structure, the ionic diffusion is most likely two-dimensional. If this is the case, $T_{1\rho}$ can no longer be expressed by the usual BPP-type equation. The temperature variation of $T_{1\rho}$ caused by 2D diffusion can be derived from the treatments by MacGillivray and Sholl,[25] who calculated the relaxation rates in a 2D square lattice. In the limit of slow diffusion and very low concentration of vacancies, the $T_{1\rho diff}$ equation approximately applicable to the present system is given by

$$T_{1\rho diff}^{-1} = \left(0.074545 \frac{8}{9} \frac{\gamma^4 \hbar^2 N C_V Z}{a^6 \omega_1^2}\right) \tau_c^{-1}, \quad (4)$$

where ω_1, N, C_V, Z, and a represent the Larmor frequency in the spin-locking r.f. magnetic field, the number of protons taking part in the diffusion, the concentration of lattice vacancies, the number of the nearest cationic sites for the diffusional jumps and the lattice constant corresponding to this jump. E_a of the slow motion was evaluated to be 72±7 kJ mol^{-1} from the slope in $\log T_{1\rho}^{-1}$ vs. T^{-1} plots using Eqs. 4 and 1. Two E_a values derived from $T_{1\rho}$ and σ are nearly the same, which confirms that the temperature variation of $T_{1\rho}$ can be ascribed to the cationic self-diffusion.

$(n$-$C_{12}H_{25}NH_3)_2ZnCl_4$. $(n$-$C_{12}H_{25}NH_3)_2ZnCl_4$ exhibited two heat anomalies, in good agreement with those in the previous report;[15] one was attributed to a structural phase transition and the other to the fusion. The phases above and below the phase transition temperature of 362 K are named high-temperature phase (HTP) and room-temperature phase (RTP), respectively. An X-ray powder diffraction pattern taken at 292±1 K in RTP was well explained by the reported monoclinic structure (space group $P2_1/c$).[26] An X-ray pattern at 389±2 K in HTP with no structural data, showed only a few (00l) peaks.

^{1}H NMR T_1 was measured as a function of temperature at Larmor frequencies of 40.2, 25.5, and 12.8 MHz (89—415 K). The results are shown in Fig. 6. A discontinuity in T_1 was observed at 362 K, consistent with the thermal measurement. The asymmetric T_1 minimum observed in RTP was analyzed by the BPP equation;[21] these results are shown in Fig. 6 and Table 2. We see that three thermal motions are effective in T_1. By calculating M_2 values, the two shallow minima on the low-temperature side were assigned to the threefold reorientations of the two crystallographically non-equivalent CH_3 groups.

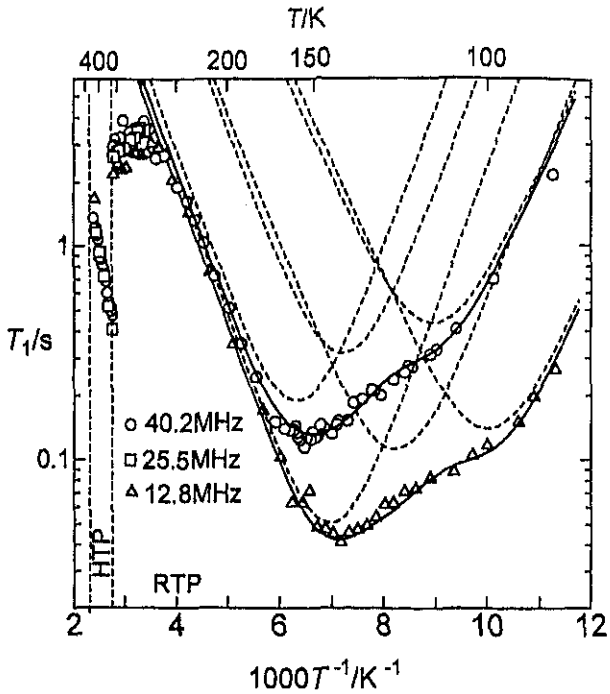

Fig. 6. Temperature dependences of ^{1}H NMR T_1 observed in $(n$-$C_{12}H_{25}NH_3)_2ZnCl_4$. Solid curves are the best-fitted calculated ones. Broken curves are contributions from respective molecular motions (see text). Vertical broken lines stand for the phase transition temperatures.

Table 2. Activation Energies, E_a, Pre-exponential Factors, τ_{c0}, and Motional Modes of n-Dodecylammonium Cations in $(n$-$C_{12}H_{25}NH_3)_2ZnCl_4$ Determined by ^{1}H NMR T_1 and $T_{1\rho}$

Phase	E_a / kJ mol^{-1}	τ_{c0} / 10^{-13} s	Motional mode
RTP	8.8±0.9	2.4±0.2	CH_3 rotation
	11±0.1	2.3±0.2	CH_3 rotation
	13±0.1	1.3±0.1	NH_3^+ rotation
HTP	23±2		Axial rotation + conformational disorder
	76±8		Self-diffusion
	74±7[a)]		Self-diffusion

a) Derived from electrical conductivity.

In the high-temperature region of RTP, T_1 reached a maximum and became short on heating indicating that a new motion is excited just below the transition temperature. The temperature dependence of M_2 of ^{1}H NMR linewidth observed between 294 and 402 K is displayed in Fig. 7. A gradual decrease in M_2 over a wide temperature range upon heating observed in RTP can be attributed to molecular motions in a potential well with unequal minima.[27] With referring to the analysis in $(n$-$C_5H_{11}NH_3)_2ZnCl_4$, this motion can be assigned to the 180° flip of the entire cations about their molecular axes. Since the phase transition at 362 K is of order–disorder type, potential wells for this motion of entire cations are expected to have unequal minima in RTP.

. The temperature variation of ^{1}H NMR $T_{1\rho}$ observed in

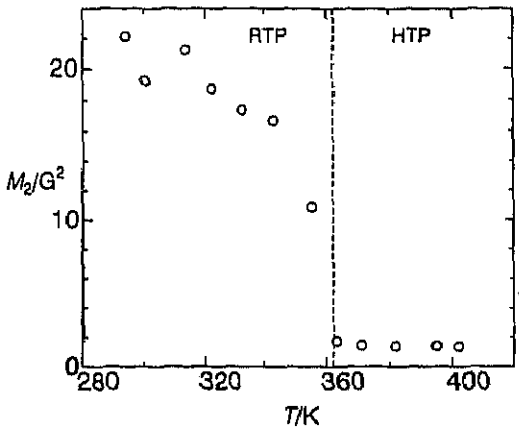

Fig. 7. A temperature dependence of M_2 of ^{1}HNMR linewidth observed in $(n\text{-}C_{12}H_{25}NH_3)_2ZnCl_4$. A broken line indicates the phase transition temperature of 362 K.

HTP is shown in Fig. 8 together with T_1 data. These results are quite similar to those obtained in phase I of $(n\text{-}C_5H_{11}NH_3)_2ZnCl_4$ given in Fig. 3, suggesting the superimposed motions. M_2 of ca. 1.5 G^2 observed in HTP is nearly the same as those observed in phase I of $(n\text{-}C_5H_{11}NH_3)_2ZnCl_4$ shown in Fig. 4. The temperature dependence of the ac electrical conductivity σ observed between 350 and 415 K is shown in Fig. 9. The results of the best fit to the data performed analogously to those in $(n\text{-}C_5H_{11}NH_3)_2ZnCl_4$ are given in Figs. 8 and 9 and Table 2. The temperature variation of T_1 was attributed to the uniaxial

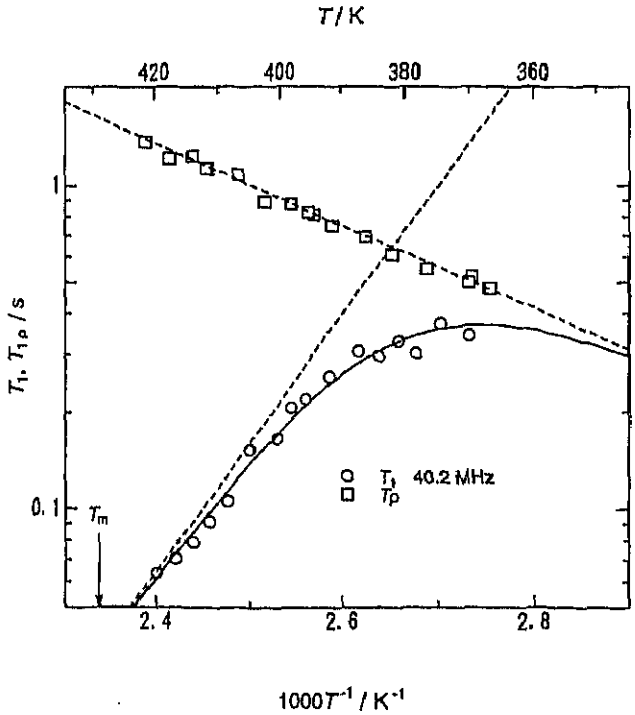

Fig. 8. Temperature dependences of ^{1}HNMR T_1 and $T_{1\rho}$ at an r.f. magnetic field of 3.97 G in HTP of $(n\text{-}C_{12}H_{25}NH_3)_2ZnCl_4$. A solid curve is the best-fitted calculated one. Broken lines are contributions from respective molecular motions (see text).

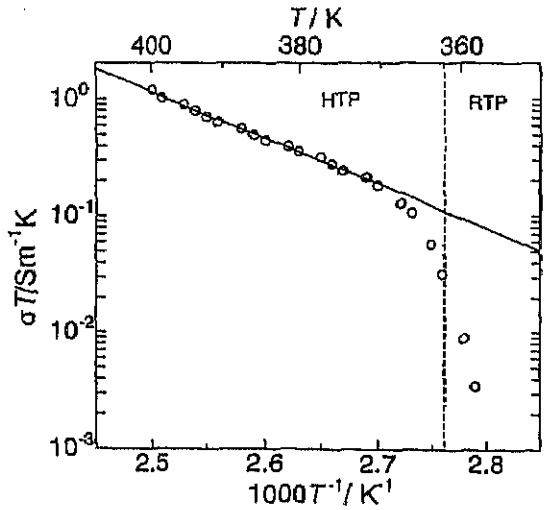

Fig. 9. A temperature dependence of a.c. electrical conductivity σ in HTP of $(n\text{-}C_{12}H_{25}NH_3)_2ZnCl_4$. A solid line is the best-fit Arrhenius relation given in text. A broken line represents the phase transition temperature of 362 K.

rotation of rigid cations about their molecular axes, accompanied by the orientational distribution of the axes and/or conformational disorder. The cationic self-diffusion is responsible for the temperature dependences of $T_{1\rho}$ and σ.

Discussion

Phase Transitions. Small transition entropies ΔS_t of 2—3 J K^{-1} mol^{-1} were observed at V–IV and IV–III transitions in $(n\text{-}C_5H_{11}NH_3)_2ZnCl_4$.[13,20] In phase III, both of the crystallographically nonequivalent N atoms have five neighboring Cl atoms with N···Cl distances of 3.2—3.5 Å, suggesting disordered hydrogen bonds.[10] Gomez Cuevas et al. suggested that these phase transitions could be related with the changes in the N–H···Cl hydrogen bonds scheme that lead to an ordered low-temperature phase.[20] If this is the case, the ordered phase has a potential well with unequal minima for NH_3^+ motion, and a discontinuous change in the potential energy curve occurs in the first-order transitions at 141.5 and 148 K. This should affect the temperature dependence of T_1, as can be expected from our analysis shown in Fig. 1; however, we could not detect any anomaly in T_1 curve observed around transition temperatures and in phase V, suggesting that the NMR result contradicts the above picture.

Thermal and X-ray studies on the structural phase transition at 250 K in $(n\text{-}C_5H_{11}NH_3)_2ZnCl_4$ revealed the onset of an order-disorder transition for the orientation of the rigid pentylammonium chains which take two disordered sites about their molecular axes in phase II.[10] This was confirmed by our analysis that the 180° flip of rigid cations about their molecular long axes is excited in phase II. From the present study, it is shown that this disorder is dynamical. Since the transition is first-order, the potential curve for the flip motion should be discontinuously altered at the transition. However, no discontinuity in T_1 was observed at the III–II transition; this is because, as can be seen from the analysis given in Fig. 2, T_1 around 250 K governed mostly by the NH_3^+ rotation masks

the 180° flip contribution.

Phase I in $(n\text{-}C_5H_{11}NH_3)_2ZnCl_4$ is believed to be in a conformationally highly disordered state.[20] This is consistent with our analysis that the chain conformations are dynamically disordered. These conformational defects seem to be kinks and end-*gauche*, because, if a successive *gauche* conformation were allowed, a wide space should be required in *ab*-plane of phase I; however, both *a*- and *b*-axes have nearly the same length in phase I and II. Since four consecutive C or N atoms are involved in the definition of a torsion angle, $n\text{-}C_5H_{11}NH_3^+$ chain has three independent possibilities to form either *trans* and *gauche* conformations. From the reported ΔS_t of 26 $J K^{-1} mol^{-1}$,[13] a conformational entropy per one C(or N)–C–C–C group is estimated to be 4.3 $J K^{-1} mol^{-1}$ suggesting that each C(or N)–C–C–C group can be interpreted as an independent pseudospin with two equivalent sites. This means that a rotation about –C–C– is not free and chain conformations are not completely melted.

A very large ΔS_t of 133 $J K^{-1} mol^{-1}$ was observed in $(n\text{-}C_{12}H_{25}NH_3)_2ZnCl_4$.[15] This transition is characterized by both the order-disorder of rigid alkylammonium cations about their molecular axes and cooperative conformational changes in the alkyl chains.[15] These results indicate that HTP in $(n\text{-}C_{12}H_{25}NH_3)_2ZnCl_4$ and phase I in $(n\text{-}C_5H_{11}NH_3)_2ZnCl_4$ are quite similar in dynamical state of cations. There are, however, some differences between the two phases: the X-ray powder diffraction pattern taken in $(n\text{-}C_{12}H_{25}NH_3)_2ZnCl_4$ showed only a few (00*l*) peaks, while that for $(n\text{-}C_5H_{11}NH_3)_2ZnCl_4$ showed some more peaks; a melting entropy ΔS_m of $(n\text{-}C_5H_{11}NH_3)_2ZnCl_4$ was 33 $J K^{-1} mol^{-1}$,[13] while that of $(n\text{-}C_{12}H_{25}NH_3)_2ZnCl_4$ was 17 $J K^{-1} mol^{-1}$.[15] These results show that HTP is more disordered than phase I. The positional order of both cations and anions seems to remain in both phases, judging from the X-ray powder patterns taken in phase I and HTP, suggesting that there are periodic arrangements in crystals. Moreover, the present NMR results suggest that the orientational and conformational order of the cations in phase I and HTP are almost the same. Accordingly, it is highly possible that the difference between phase I and HTP is caused by the orientational order of $ZnCl_4^{2-}$. In our previous study on $(n\text{-}C_nH_{2n+1}NH_3)_2ZnCl_4$ compounds,[13] we have estimated the contributions from the orientational order of the anions to ΔS_m to be 17 $J K^{-1} mol^{-1}$. Using these results, we see that the orientational order of rigid anions is almost lost in HTP but conserved in phase I, and hence we can conclude that the phase transition at 362 K in $(n\text{-}C_{12}H_{25}NH_3)_2ZnCl_4$ is accompanied by orientational disordering of cations about their molecular axes and of anions as a whole, and by the cooperative conformational melting of alkylammonium chains. From the observed ΔS_t of 133 $J K^{-1} mol^{-1}$, contributions from the orientational disorders of cations and anions should be subtracted for estimating only the conformational contribution to ΔS_t. Since a hindered rotation of cations about one axis has contribution of R to entropy and since the orientational entropy of $ZnCl_4$ is estimated to be 17 $J K^{-1} mol^{-1}$, the conformational contribution is evaluated to be about 100 $J K^{-1} mol^{-1}$. Accordingly, the conformational entropy per one C(or N)–C–C–C group becomes approximately 5 $J K^{-1} mol^{-1}$, suggesting disordering between two sites. The conformational defects, the majority of which seem to be kinks, move along the chain axis, so that chains are regarded to be melted. The chains are, however, not completey melted in HTP and some orders in chain conformations remain partly even in a liquid phase, at least just above the melting point.

Molecular Dynamics. From the present experimental results, it follows that phase I in $(n\text{-}C_5H_{11}NH_3)_2ZnCl_4$ and HTP in $(n\text{-}C_{12}H_{25}NH_3)_2ZnCl_4$ are the rotator phases, because the following motions characteristic in the rotator phase were observed. Namely, the uniaxial rotation accompanied by diffusion of conformational intrachain defects along the chain axis and two-dimensional cationic self-diffusion take place. On the other hand, we notice some differences in rotator phases of $(n\text{-}C_nH_{2n+1}NH_3)_2ZnCl_4$ and *n*-alkylammonium chlorides (abbreviated to C_nCl).[2–6] The temperature ranges of the rotator phases in $(n\text{-}C_5H_{11}NH_3)_2ZnCl_4$ and $(n\text{-}C_{12}H_{25}NH_3)_2ZnCl_4$ are 350—436 K and 362—438 K, respectively, narrower than those in C_nCl (C_5Cl: 256—503 K; $C_{12}Cl$: 345—475 K). In the ^1HNMR relaxation due to the cationic uniaxial reorientation, the non-linear $\log T_1$ vs. T^{-1} curve has been observed in C_nCl except for $C_{12}Cl$; however, $\log T_1$ vs. T^{-1} plots were linear in $(n\text{-}C_5H_{11}NH_3)_2ZnCl_4$ and $(n\text{-}C_{12}H_{25}NH_3)_2ZnCl_4$. The self-diffusion of the anions was not observed in phase I and HTP, while it was activated in C_nCl. E_a values of the cationic self-diffusion in $(n\text{-}C_5H_{11}NH_3)_2ZnCl_4$ and $(n\text{-}C_{12}H_{25}NH_3)_2ZnCl_4$ are nearly the same, while those in C_nCl depend on the length of the carbon chain. We need some more systematic experiments on $(n\text{-}C_nH_{2n+1}NH_3)_2ZnCl_4$ to conclude that these differences are generally observed between $(n\text{-}C_nH_{2n+1}NH_3)_2ZnCl_4$ and C_nCl. In what follows we discuss only the translational self-diffusion of alkylammonium ions.

It was reported that $(n\text{-}C_5H_{11}NH_3)_2ZnCl_4$ forms an orthorhombic lattice in phase I;[20] however, detailed structural data in phase I and HTP are unavailable. According to Refs. 10 and 20, the crystal structure of phase II is orthorhombic with space group *Pnma* and $a = 10.323$, $b = 7.406$, and $c = 25.171$ Å at 295 K; the cell parameters for phase I are: $a = 10.2$, $b = 7.1$, and $c = 27.9$ Å at 349 K. We see that the lengths of *a*- and *b*-axes are nearly the same in both phases, while *c*-axis in phase I increases by approximately 11%. This drastic change in *c*-axis at the transition can be interpreted as follows.[20] The all-*trans* and intercalated carbon chains in phase II transform to the non-intercalated chains that have shorter length and larger diameter due to kink and end-*gauche* structures in phase I, as is schematically depicted in Fig. 10. A phase transition from an intercalated to a non-intercalated bilayer structure was first reported in $C_{10}Cl$, which is reconstructive and not reversible.[28] The I–II and HTP–RTP transitions are however reversible. Such a cell expansion at a phase transition from the second highest-temperature to the highest-temperature phase was observed in $(n\text{-}C_{13}H_{27}NH_3)_2ZnCl_4$ and $(n\text{-}C_{14}H_{29}NH_3)_2ZnCl_4$ with 19[29] and 17.5%[30] increase in *c*-axis, respectively. Moreover, our

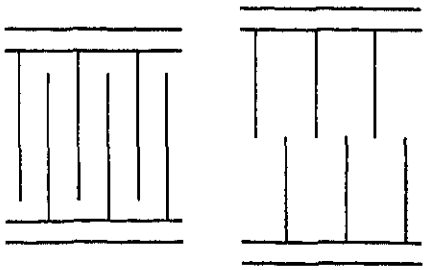

Fig. 10. The schematic representation of (a) intercalated and (b) non-intercalated layer structures.

X-ray powder diffraction gave $c = 51.7$ Å in HTP increased by 16.4%. Since it is clear that a non-intercalated structure is preferable for a diffusion of alkylammonium chains and in fact phase I and HTP showed a relatively high ionic conductivity of ca. $10^{-3}\ \Omega^{-1}\ m^{-1}$ comparable to that in C_nCl, it is most likely that phase I and HTP have the non-intercalated structure.

The ionic conductivities in phase I and HTP are expected to be anisotropic due to their layer structures. That is, the self-diffusion constant within the layer, $D_\perp$, is thought to be different from that along the c-axis, $D_\parallel$. In the present case, $D_\perp$ can be approximately related to the correlation time of the motion, τ_D, by the equation

$$D_\perp = \frac{d^2}{4\tau_D}, \tag{5}$$

where, d is the nearest jump distance. Assuming that ions jump to the nearest Schottky-type lattice defects, d in phase I can be estimated to be 6.0 and 6.7 Å based on the crystal structural data in phase II, because a- and b-lengths scarcely change at I–II transition. Since RTP has $a = 7.409$ and $b = 10.379$ Å and it is expected that HTP has nearly the same a- and b-lengths as in RTP,[26] d in HTP is also estimated to be 6—7 Å. These values are somewhat longer than 5.0—5.2 Å reported for C_nCl.[2–5] Using Eq. 5, we evaluated τ_D. Here the diffusional correlation time extrapolated to the melting point, $\tau_D(T_m)$, was calculated using $d = 6.4$ Å, leading to the order of 10^{-7} s for phase I and HTP. It has been reported that the same order of $\tau_D(T_m)$ is observed independent of compounds and melting points for plastic crystals and rotator phases in C_nCl.[5]

The activation energies of cationic self-diffusion, E_a, in phase I in $(n\text{-}C_5H_{11}NH_3)_2ZnCl_4$ and HTP in $(n\text{-}C_{12}H_{25}NH_3)_2ZnCl_4$ have similar values of 70—80 kJ mol^{-1}, while those of rotator phases in C_nCl depend on the chain length, i.e., E_a increases with increasing the chain length (C_5Cl: 50 kJ mol^{-1}; $C_{12}Cl$: 100 kJ mol^{-1}). This suggests that inter-chain interactions, i.e., van der Waals force, are very effective to the potential barrier for the diffusion in C_nCl. At least in $C_{12}Cl$, the interactions are seems to be dominant. The inter-chain interactions, however, seem to be less effective in $(n\text{-}C_nH_{2n+1}NH_3)_2ZnCl_4$, because their inter-chain distances are longer than those in C_nCl. Hence, it is expected that anion–cation interactions, mainly N–H···Cl hydrogen bonds, are more important in the potential energy for the diffusion in $(n\text{-}C_nH_{2n+1}NH_3)_2ZnCl_4$. As described previously, an orientational order of anions is preserved in phase I but is lost in HTP. It appears that this can also affect E_a of the diffusion, i.e., the disorder of anions can weaken the hydrogen bonds. Accordingly, it is concluded that the anion–cation interactions are more effective than inter-chain interactions especially in phase I and the orientational disordering of anions in HTP makes the barrier lower.

Conclusion

Phase I in $(n\text{-}C_5H_{11}NH_3)_2ZnCl_4$ and HTP in $(n\text{-}C_{12}H_{25}NH_3)_2ZnCl_4$ were found to be rotator phases where two distinct motions are excited. One is the uniaxial rotation of alkylammonium cations about their molecular long axes, accompanied by the conformational disorder in the chains such as kinks. Phase I and HTP are believed to be in such a high conformational disordered state that chains can be regarded as melting. The organic chains are however not completely melted and some orders in conformations remain, i.e., rotations about C–C axes are not free but reorientational jumps with two equivalent sites.

The other motion is the two-dimensional self-diffusion of the cations moving within the layer perpendicular to the c-axis. It is most likely that the alkyl chains are non-intercalated in phase I and HTP, so that the cationic diffusion is expected to be easily excited with the diffusional correlation time of the order of 10^{-7} s extrapolated to the melting point. The same order values were observed at the melting temperatures in plastic crystals and C_nCl compounds. N–H···Cl hydrogen bonds affect the diffusional activation energy more than inter-chain interactions, which are important in C_nCl compounds. It can be concluded that the rotator phases newly found here are quite analogous to those detected in C_nCl compounds, although there are some differences.

In a temperature range between ca. 120 K and the melting point, $(n\text{-}C_5H_{11}NH_3)_2ZnCl_4$ shows four first-order structural phase transitions; however, $(n\text{-}C_{12}H_{25}NH_3)_2ZnCl_4$ undergoes only a single transition. All of these transitions are regarded as order-disorder type. The I–II, II–III, and RTP–HTP transitions are related with disordering of alkylammonium ions. The II–III transition is an order–disorder one of the rigid pentylammonium ions with two equivalent sites about their molecular axes. In the I–II transition, the orientational order of cations about the axes is completely lost and a conformational melting takes place. The RTP–HTP transition can correspond to that between phase III and I in $(n\text{-}C_5H_{11}NH_3)_2ZnCl_4$, with a difference that the orientational order of $ZnCl_4^{2-}$ ions is lost in HTP but preserved in phase I.

This work was partly supported by a Grant-in-Aid for Scientific Research No. (B) 09440234 from the Ministry of Education, Science, Sports and Culture.

References

1 A. Mueller, *Proc. R. Soc. London, Ser. A*, 138, 514 (1932).

2 S. Fukada, H. Yamamoto, R. Ikeda, and D. Nakamura, *J. Chem. Soc., Faraday Trans. 1*, 83, 3207 (1987).

3 M. Hattori, S. Fukada, D. Nakamura, and R. Ikeda, *J. Chem. Soc., Faraday Trans.*, 86, 3777 (1990).

4 S. Iwai, R. Ikeda, and D. Nakamura, *Can. J. Chem.*, 66, 1961 (1988).

5 S. Iwai, M. Hattori, D. Nakamura, and R. Ikeda, *J. Chem. Soc., Faraday Trans.*, 89, 827 (1993).

6 S. Tanaka, N. Onoda-Yamamoto, S. Ishimaru, and R. Ikeda, *Bull. Chem. Soc. Jpn.*, 70, 2981 (1997).

7 J. Timmermans, *J. Phys. Chem. Solids*, 18, 1 (1961).

8 T. Shimizu, S. Tanaka, N. Onoda-Yamamoto, S. Ishimaru, and R. Ikeda, *J. Chem. Soc., Faraday Trans.*, 93, 321 (1997).

9 F. J. Zuniga, M. J. Tello, J. M. Perez-Mato, M. A. Perez-Jubindo, and G. Chapuis, *J. Chem. Phys.*, 76, 2610 (1982).

10 A. Gomez-Cuevas, M. J. Perez-Mato, M. J. Tello, G. Masariaga, J. Fernadez, A. Lopez-Echarri, F. J. Zuniga, and G. Chapuis, *Phys. Rev. B*, B29, 2655 (1984).

11 K. Horiuchi, *J. Phys. Soc. Jpn.*, 63, 363 (1994).

12 K. Horiuchi and Al. Weiss, *J. Mol. Struct.*, 345, 97 (1995).

13 Y. Sakiyama, K. Horiuchi, and R. Ikeda, *J. Phys.: Condens. Matter*, 8, 5345 (1996).

14 H. Ishihara, S.-q. Dou, K. Horiuchi, H. Paulus, H. Fuess, and Al. Weiss, *Z. Naturforsch., A*, 52a, 550 (1997).

15 C. Socias, M. A. Arriandiaga, M. J. Tello, L. Fernandez, and P. Gili, *Phys. Stat. Sol.(A)*, 57, 405 (1980).

16 Y. Kume, R. Ikeda, and D. Nakamura, *J. Magn. Reson.*, 33, 331 (1979).

17 T. Kobayashi, H. Ohki, and R. Ikeda, *Mol. Cryst. Liq. Cryst.*, 257, 279 (1994).

18 D. C. Look and I. J. Lowe, *J. Chem. Phys.*, 44, 2995 (1966).

19 J. G. Powles and J. H. Strange, *Proc. Phys. Soc.*, 82, 6 (1963).

20 A. Gomez Cuevas, M. J. Tell, and A. Lopez Echarri, *J. Phys. Chem. Solids*, 45, 1175 (1984).

21 N. Bloembergen, E. M. Purcell, and R. V. Pound, *Phys. Rev.*, 73, 679 (1948).

22 J. H. Van Vleck, *Phys. Rev.*, 74, 1168 (1948).

23 S. Fukada, R. Ikeda, and D. Nakamura, *Bull. Chem. Soc. Jpn.*, 57, 2802 (1984).

24 S. Fukada, R. Ikeda, and D. Nakamura, *Z. Naturforsch., A*, 40a, 347 (1984).

25 I. R. MacGillivray and C. A. Sholl, *J. Phys. C*, 18, 1691 (1985).

26 M. R. Ciajolo, P. Corradini, and V. Pavone, *Acta Crystallogr., Sect. B*, B33, 553 (1977).

27 Y. Ito, T. Asaji, R. Ikeda, and D. Nakamura, *Ber. Bunsenges. Phys. Chem.*, 92, 885 (1988).

28 R. Kind, R. Blinc, H. Arend, P. Muralt, J. Slak, G. Chapuis, K. J. Schenk, and B. Zeks, *Phys. Rev. A*, A26, 1816 (1982).

29 F. J. Zuniga and G. Chapuis, *Mol. Cryst. Liq. Cryst.*, 128, 349 (1985).

30 J. Fernandez, C. Socias, M. A. Arriandiaga, M. J. Tello, and A. Lopez Echarri, *J. Phys. C: Solid State Phys.*, 15, 1151 (1982).

Journal of the Physical Society of Japan
Vol. 69, No. 3, March, 2000, pp. 729-733

Studies on ^{133}Cs NMR Spectra and Spin-Lattice Relaxation Times in Incommensurate Cs_2HgCl_4

Koh-ichi SUZUKI, Shin'ichi ISHIMARU* and Ryuichi IKEDA

Department of Chemistry, University of Tsukuba, Tsukuba 305-8571

(Received September 13, 1999)

^{133}Cs NMR spectra and the spin-lattice relaxation times, T_1, in Cs_2HgCl_4 crystals were measured in the ranges of 160–361 K and 160–371 K, respectively. The central lines of the spectra show small splittings characteristic of the incommensurate (IC) phase. The splitting increases with decreasing temperature. The critical exponent ζ of T_1 at the phase transition from normal (N) to IC phase was determined to be 0.615±0.025 in the high-temperature side of the transition, which is in good agreement with the three-dimensional XY model predicting the one-dimensional modulation wave in the IC phase. The frequency dependence of T_1 in the IC phase can be explained by the fluctuations of phason with a small gap, 0–5 MHz, and amplitudon.

KEYWORDS: ^{133}Cs NMR, T_1, incommensurate, phase transition, critical phenomena, critical exponent

§1. Introduction

Many compounds belonging to the A_2BX_4 family with the pseudo-hexagonal β-K_2SO_4 type structure (*Pnma*) form incommensurate (IC) phases at low temperatures. We reported lattice dynamics in IC phases of Cs_2MBr_4 (M=Cd and Hg) studied by ^{133}Cs NMR.[1] The critical exponents obtained at the phase transitions from normal to incommensurate (N-IC) phase correspond to the three-dimensional XY and the mean field models for Cd and Hg compounds, respectively. This difference seems to be explained by the ionicities of cesium and halogen atom, but more practical examples are necessary to discuss details of dynamical interionic interactions in these compounds.

$HgCl_4^{2-}$ can be considered to be anionic more than $HgBr_4^{2-}$ because of the large electronegativity of chlorine. In the present study, to clarify details of interactions governing the appearance of the IC phase, we intend to measure ^{133}Cs NMR spectra and spin-lattice relaxation times in Cs_2HgCl_4, and compare its lattice dynamics around the IC phase with those in the bromo complexes reported previously.

Characteristic properties of phase transitions and the IC phase in Cs_2HgCl_4 have been extensively studied by X-ray diffraction,[2,3] birefringence,[4,5] calorimetric,[6,7] dielectric,[8-10] spontaneous polarization,[9,10] ^{35}Cl NQR frequency,[2,11,12] optical[4] and ultrasonic[4,5,13,14] measurements and lattice dynamics simulations.[15,16] According to the AC calorimetry measurement, Cs_2HgCl_4 undergoes seven phase transitions at T_{IC} = 219, T_C = 193, T_{C1} = 182.5, T_{C2} = 177, T_{C3} = 173.0, T_{C4} = 163.5 and T_{C5} = 120 K,[7] although the number and the temperatures of the phase transitions are not consistent necessarily with the other methods.[4,6,10] A crystallographic study[3] showed that the symmetry of the N phase above T_{IC} is centrosymmetric *Pnma* with displacement disorders in $HgCl_4^{2-}$ complex anions and one of the crystallographically inequivalent two Cs cations. It has been presumed that the ferroelectric commensurate (C) phase below T_C without centrosymmetry have a point symmetry $mm2$,[4] but detailed studies on structures below T_C have not been reported.

^{35}Cl NQR,[12] dielectric and Raman scattering[8] measurements revealed a different result that the IC phase appears between T_{IC} and T_{C1}.[12] From the optical polarization measurement, the low-temperature phase immediately below T_{C1} is anticipated to be a ferroelastic C phase analogous to that in Cs_2MBr_4 (M=Cd, Hg).

§2. Experimental

Cs_2HgCl_4 crystals were grown by cooling a molten mixture containing stoichiometric amounts of CsCl (purity 99.9%) and $HgCl_2$ (purity 99.9%) purchased from Wako Pure Chemical Industries, Ltd. The crystalline powder obtained was dried *in vacuo* and then sealed in glass tubes with nitrogen gas for differential thermal analysis (DTA) and NMR measurements.

DTA was measured between 120 and 300 K to confirm the phase transitions reported previously. The sample temperature was determined within ±0.2 K using a chromel-constantan thermocouple. The measurement of ^{133}Cs NMR T_1 was performed with a Bruker MSL-300 spectrometer at frequency of 39.4 MHz in the range 160–371 K and also with a Bruker MSL-400 spectrometer at 52.5 MHz in 196–215 K. ^{133}Cs NMR spectra were recorded by a Bruker MSL-300 using a saturated CsCl aqueous solution as a standard of frequency shift. The sample temperature was controlled within ±0.5 K by Bruker VT-1000 temperature controller and determined by a copper-constantan thermocouple with the same accuracy. The uncertainty in the T_1 measurement is estimated to be within 5%.

§3. Results

DTA thermograms on heating displayed endother-

* E-mail: ishimaru@staff.chem.tsukuba.ac.jp

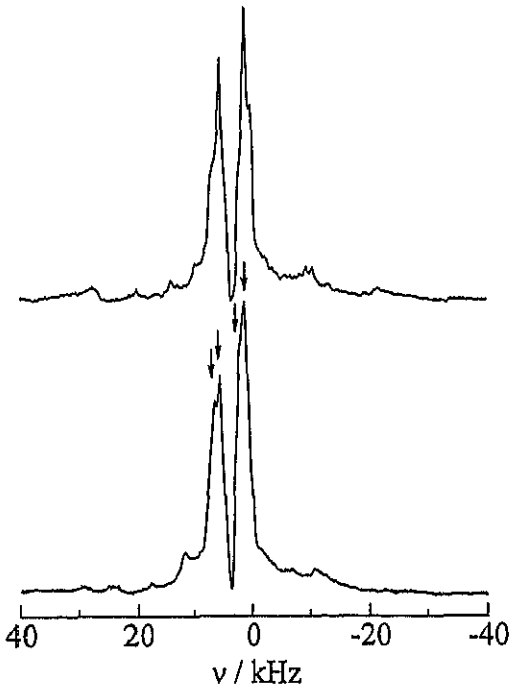

Fig. 1. ^{133}Cs NMR spectra observed at 295 K in the normal (N) phase (upper) and 184 K in the incommensurate (IC) phase (lower). Split peaks of central lines in the IC phase are marked by arrows.

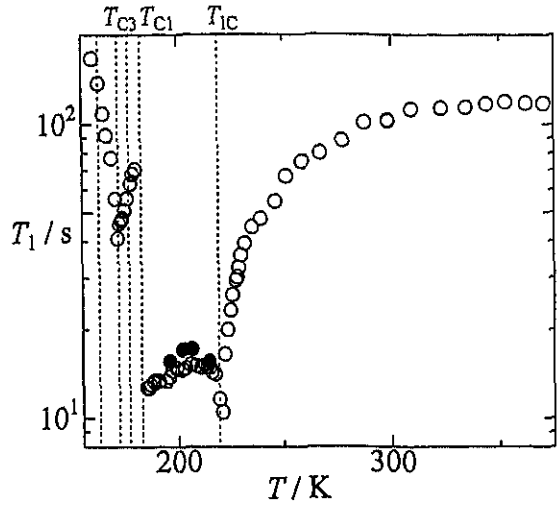

Fig. 2. Temperature dependences of ^{133}Cs NMR T_1 measured at 39.4 (○) and 52.5 (●) MHz. Vertical lines correspond to phase transition temperatures observed by DTA.

mic anomalies due to phase transitions at 163.0±0.6, 172.2±1.0, 177.3±0.9, 183.1±0.6 and 219.5±0.8 K in good agreement with the phase transition temperatures of T_{C4}, T_{C3}, T_{C2}, T_{C1} and T_{IC}, respectively, previously determined by the AC calorimetry measurement.[7] The anomaly reported at 193 K (T_C) was not detected, although a large thermal anomaly is usually observed at the IC-C transition. From these results, we assume in the following discussion that the IC phase is formed between T_{C1} and T_{IC} as shown in previous NQR,[12] dielectric and Raman scattering[8] studies.

Quadrupolar perturbed ^{133}Cs NMR spectra in the N and IC phases are shown in Fig. 1. The lineshapes obtained are explained by the superposition of two spectra with the 1st order perturbation. This result is consistent with the reported crystal structure containing two inequivalent Cs ions in a unit cell.[3] The respective quadrupole coupling constants e^2Qq/h and asymmetric parameters η are estimated to be 150±30 kHz and 0.1±0.1, and 230±80 kHz and 0.5±0.2 in the N phase by referring to the values of ^{133}Cs NMR of single crystals in an analogous compound Cs_2HgBr_4.[17] In the low-temperature range of the IC phase, the two central peaks show small splittings due to the IC modulation as shown by arrows in Fig. 1.

The temperature and frequency dependences of ^{133}Cs NMR T_1 are shown in Fig. 2. The T_1 shows a discontinuous jump at T_{C1} confirming the previous report of the 1st order phase transition.[10] The T_1 dips are observed around T_{IC} and T_{C3}, where 2nd order[6,8] and 1st order transitions[10] have been reported, respectively. No remarkable T_1 anomaly is observed at T_{C2} and T_{C4}. The T_1 values between T_{IC} and T_{C1} are shorter than those in the C phases as well as in the high-temperature region of the N phase. Such short T_1 values are characteristic of the IC phase.[18] A slight decrease of T_1 within the experimental error is observed at 193 K. This may correspond to the reported transition to the commensurate phase although T_1 changes at IC-C transitions more markedly in most cases.[18]

§4. Discussion

4.1 Normal (N) phase

The dip of ^{133}Cs NMR T_1 observed in the vicinity of T_{IC} can be explained by the critical fluctuation of the quadrupolar interaction due to the 2nd order phase transition. In the present case, T_1 in the N phase can be represented by the sum of contributions from normal lattice vibrations (T_{1l}) and critical fluctuation (T_{1c}) in the neighborhood of the phase transition as

$$T_1^{-1} = T_{1l}^{-1} + T_{1c}^{-1}. \quad (1)$$

Here, using a reduced temperature $\varepsilon = (T - T_{IC})/T_{IC}$, T_{1c} can be expressed as[19]

$$T_{1c}^{-1} \propto \varepsilon^{-\zeta}, \quad (2)$$

where the critical exponent ζ is given by $\zeta = \gamma - \nu(d - z)$, in which γ and ν are the critical exponents of the static susceptibility concerning with the critical lattice fluctuation and the correlation length, respectively, d is the dimensionality of the relevant interactions and z is the dynamical critical exponent.[19] ζ can be obtained from the slope of log T_1 vs. log ε plots in the vicinity of the transition point, because T_{1c} is expected to be the dominant mechanism in this temperature region. In fact, log T_1 vs. log ε plots gives an almost straight line in the vicinity of the transition temperature as shown in Fig. 3.

The critical exponent ζ was determined to be 0.615±0.025. This value agrees well with the value 0.62±0.02 reported previously in Cs_2CdBr_4[1] and is close to the theoretical value of $\zeta = 0.625$ for the three-dimensional XY model.[20-22] Cowley and Bruce predict that the three-dimensional XY model is acceptable for

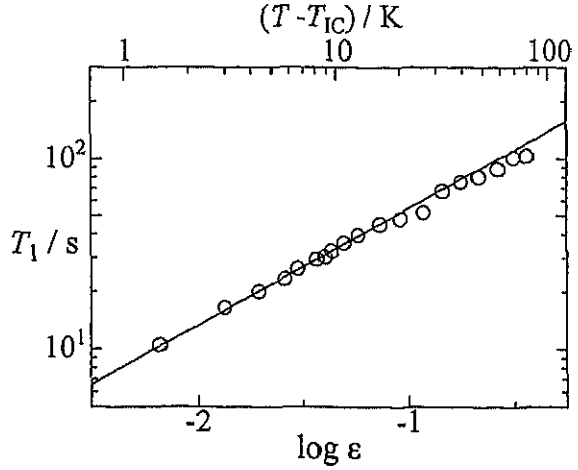

Fig. 3. Critical plots of ^{133}Cs NMR T_1 vs. the reduced temperature ($\varepsilon = (T - T_{IC})/T_{IC}$) observed above the normal-incommensurate (N-IC) phase transition temperature (T_{IC}). The solid line is the best-fitted curve in the range of $T - T_{IC} < 10$ K, see text.

the transition from the normal to the IC phase with the one-dimensional modulation because the order parameter of this system has two components, i.e., the amplitude and the phase of the incommensurate modulation.[23] The present result of T_1 in Cs_2HgCl_4 is different from that in Cs_2HgBr_4,[1] whose behavior could be explained by the classical mean field approximation due to the long-range interionic interaction.

4.2 Incommensurate (IC) phase

The short T_1 in the IC phase is characteristic compared with those in N and C phases. This type of NMR relaxation in the IC phase was discussed by Blinc in detail.[18] In the IC phase, the fluctuation of the incommensurate modulation wave can be expressed by two components with respect to amplitude and phase of the wave so called amplitudon and phason, respectively. The T_1 in the IC phase can be represented by the sum of the contributions from amplitudon and phason given by T_{1a} and $T_{1\phi}$, respectively, in addition to the usual lattice vibration as

$$T_1^{-1} = T_{1l}^{-1} + T_{1a}^{-1} + T_{1\phi}^{-1}. \quad (3)$$

Here T_{1a} is a mode which softens with approaching to T_{IC} and given by

$$T_{1a}^{-1} \propto (T_{IC} - T)^{-\zeta'}. \quad (4)$$

In most cases, T_{1a} shows no significant contribution except for the very close proximity to T_{IC} because the amplitudon frequency is much higher than the Larmor frequency ν_L.[18]

The phason behavior can be classified into two limiting cases: One is represented by the continuous plane wave and the other the multi-soliton model. According to Mischo *et al.*,[24] the contribution from the relaxatory phason in the former limit is represented as

$$T_{1\phi}^{-2} \propto T^2(\sqrt{1 + (\nu_L/\nu_\phi)^2} + 1)^{-1}, \quad (5)$$

where ν_ϕ is the phason gap frequency. On the other hand, in the multi-soliton limit, the IC phase is understood by the ensemble of commensurate domains separated by fluctuating domain walls so-called phase solitons with a steep phase change. Then the phason branch splits to acoustic and optical parts which correspond to phase oscillations in the commensurate domains and domain walls, respectively.[18] Thus $T_{1\phi}$ is represented as

$$T_{1\phi}^{-1} = (T_{1\phi})_{ac}^{-1} + (T_{1\phi})_{op}^{-1}, \quad (6)$$

where $(T_{1\phi})_{ac}$ and $(T_{1\phi})_{op}$ are the contribution from acoustic and optical phasons. For the damping oscillation phason in the multi-soliton limit in the limiting frequency region of $\nu_\phi \ll \nu_L$, the acoustic contribution can be written by[18]

$$(T_{1\phi})_{ac}^{-1} \propto [\nu_L(T - T_{C'})]^{-1/2}. \quad (7)$$

Equation (7) derived from the dispersion relation of the acoustic phason mode[18] indicates that this mode softens with approaching to some lower temperature $T_{C'}$. On the other hand, $(T_{1\phi})_{op}$ is also proportional to $\sqrt{\nu_L}$ but temperature independent.[18] In the opposite limiting case, $\nu_\phi \gg \nu_L$, $T_{1\phi}$ is independent of the frequency in both plane wave and multi-soliton models.

The frequency dependence of T_1 values obtained in the IC phase between 190 K and 210 K can be represented by a relation $T_1 \propto \nu_L^{0.45}$. Since the phason gap ν_ϕ can be estimated to be 0– 5 MHz from eq. (5) by the fitting assumed the above frequency dependence of T_1 in the plane wave limit, the phason gap is considered to fulfill the condition $\nu_\phi \ll \nu_L$. However, the behavior of T_1, which shows a decrease upon cooling in the low-temperature region of the IC phase, can not be explained by the plane wave model showing the opposite temperature dependence. This suggests that the multi-soliton model is more suitable than the plane wave model in this temperature region as predicted from the consideration of thermodynamic potential.[25]

The T_1 values observed in this phase are fitted by using eqs. (3)–(7), assuming $\zeta' = 0.5$ for the amplitudon (chain line) and the fitted values are shown in Fig. 4. In this calculation, temperature and frequency dependence are reproduced, but the absolute T_1 values which can not be obtained from eqs. (4), (5) and (7) were arbitrarily determined to fit the observed data. For the contribution from the phason, the plane wave limit, eq. (5), is employed above 210 K (bold broken lines) where T_1 increases with decreasing temperature, while eqs. (6) and (7) for the multi-soliton limit are used below 210 K. From the fitting, $T_{C'} \approx 172$ K was obtained, although the IC phase transforms into the C phase before reaching this temperature. Furthermore, the changing from the relaxatory phason to the damping oscillation phason in the IC phase of Cs_2HgCl_4 implies the occurrence of crossover from order-disorder to displacive behavior, which seems to be connected with the small size of the complex anion. Such a crossover was also reported by Raman scattering measurements in Rb_2ZnCl_4 and Rb_2ZnBr_4[26] but Cs_2CdBr_4 and Cs_2HgBr_4 did not show such behavior in our observation reported previously.[1]

Temperature dependences of frequencies of two central peaks in the N, IC and C phases are shown in Fig. 5. In

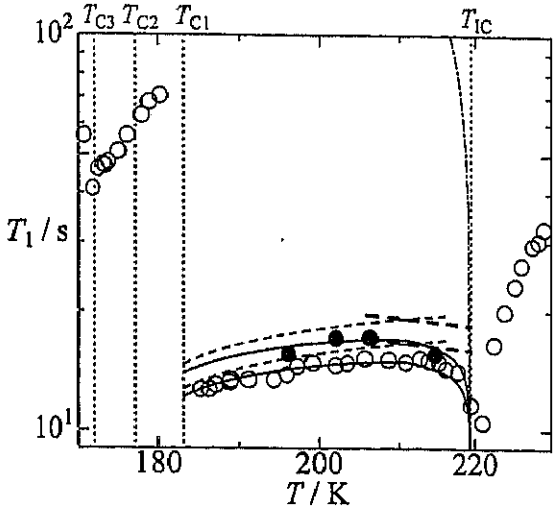

Fig. 4. Temperature and frequency dependences of ^{133}Cs NMR T_1 in the incommensurate (IC) phase measured at 39.4 (○) and 52.5 (●) MHz. Solid lines are calculated by introducing phason (broken lines) and amplitudon (chain line) contributions. Contributions from phasons assumed to be in the plane wave and multi-soliton limits in the temperature regions higher and lower than *ca.* 210 K in the IC phase are shown bold and fine broken lines, respectively. Vertical lines correspond to phase transition temperatures observed by DTA.

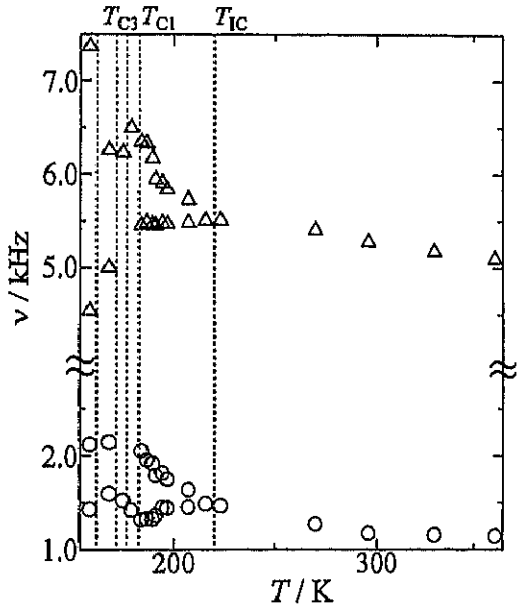

Fig. 5. Temperature dependences of splittings of two central peaks observed in ^{133}Cs NMR spectra. Vertical dotted lines correspond to phase transition temperatures observed by DTA.

the IC phase, the splittings of NMR lines are caused by the distribution of the electric field gradient at Cs nuclei owing to the IC modulation.[18,27] The splittings become clear in the high-frequency central peak below about 190 K. We roughly estimated frequencies of split peaks. These splittings are expected to be related to the amplitude of the IC modulation. The temperature dependences of the split of the peak frequencies are shown in Fig. 5. One splitting increases almost linearly with decreasing temperature and the other is inappreciably temperature dependent. Such temperature dependences of the split peaks were discussed well by Brinc *et al.*[27] According to their theoretical treatment, the critical exponent $\bar{\beta}$ given by $\Delta\nu \propto (T_{IC} - T)^{\bar{\beta}}$ can be estimated from the temperature dependence of the splitting width $\Delta\nu$ in the case of the plane wave limit.[28] The $\bar{\beta}$ value estimated to be *ca.* 2 is too large compared with $\bar{\beta} = 0.832$[28] expected for the XY model. This anomalous $\bar{\beta}$ value may be reduced to following condition: Reliable values of $\Delta\nu$ can be obtained only in low-temperature region of the IC phase where the IC modulation is not characterized by the plane wave limit but the multi-soliton limit as mentioned above.

4.3 Commensurate (C) phases

In this phase, we anticipate that the modulation can no more slide freely and the phason becomes a normal lattice mode resulting in long T_1 as shown in Fig. 2. The T_1 dip around $T_{C3} = 172.2$ K is attributable to the contribution from the phase transition.

4.4 Interionic interaction and transition mechanism

In the present study, we showed that the value of critical exponent of T_1 in the N phase near the N-IC phase transition and the T_1 behavior in the IC phase are quite analogous to those in Cs_2CdBr_4 reported previously.[1] We can reasonably expect that the interionic interaction between Cs cations and complex anions influences the critical dynamics near the phase transition and the behavior in the IC phase. The halogen ionicity can be estimated from e^2Qq/h using the Townes-Dailey relation:[29]

$$e^2Qq/h = (1-s)(1-i)(e^2Qq/h)_{\text{atom}}, \qquad (8)$$

where s is the contribution from s electrons in the chemical bond and assumed to be 0.15, i is the ionic character of the M-X bonds, i.e., $(1-i)$ affords the covalency, and $(e^2Qq/h)_{\text{atom}}$ is the e^2Qq/h in atomic halogen. Averaged ionicities of halogen in the complex anions are estimated from eq. (8) to be 0.699 for $HgBr_4^{2-}$, 0.783 for $CdBr_4^{2-}$ and 0.733 for $HgCl_4^{2-}$ from the previous results of the NQR frequencies[12,30] observed near room temperature by assuming $\eta = 0$. We can see that $CdBr_4^{2-}$ and $HgCl_4^{2-}$ have more ionic halogens than $HgBr_4^{2-}$. This difference in the halogen ionicity seems to induce the different behavior, i.e., the non-classical three-dimensional XY behavior near the N-IC phase transition in Cs_2CdBr_4 and Cs_2HgCl_4 crystals, whereas the classical mean field behavior in Cs_2HgBr_4. The origin of this difference seems to be difficult to decide only from the present data. More systematic measurements and analysis on various IC systems are required.

§5. Conclusion

The dip of ^{133}Cs NMR T_1 observed in Cs_2HgCl_4 at the N-IC phase transition is explained by the critical fluctuation driven by the three-dimensional XY type interaction. This result indicates that the distortion wave in the IC phase is one-dimensional modulation. In the IC phase, the frequency dependence is approximately given by $T_1 \propto \sqrt{\nu_L}$, and the absolute value of T_1 could be reproduced by the sum of two contributions of phason with a small gap, 0–5 MHz, and amplitudon. In the low-temperature range in the IC phase, the temperature de-

pendence of T_1 could be explained by the IC phase modulaton of the multi-soliton model rather than the plane wave.

^{133}Cs NMR spectra were reproduced as the superposition of two absorption lines with $e^2Qq/h = 150 \pm 30$ kHz, $\eta = 0.1 \pm 0.1$ and 230±80 kHz, 0.5±0.2. In the low-temperature region of the IC phase below about 190 K, splittings of central peaks could be detected and the splitting width ($\Delta\nu$) increases with decreasing temperature.

In our previous study, an analogous result in Cs_2CdBr_4 to the present data was explained by the XY model, while a different result in Cs_2HgBr_4 was attributed to the classical model. This difference can be explained by the negativity of halogen atoms.

Acknowledgments

We should like to thank Dr. Y. Onoda, Dr. M. Tansho and Dr. Y. Uchida of National Institute for Research in Inorganic Materials for their kind help in operating the MSL-400 NMR spectrometer. This work was partly supported by Grant-in-Aid for scientific research (B) No. 09440234 and (C) No. 10640554 from the Ministry of Education, Science, Sports and Culture and University of Tsukuba Research Projects.

1) K. Suzuki, S. Ishimaru and R. Ikeda: J. Phys. Soc. Jpn. **68** (1999) 1963.
2) V. I. Pakhomov, A. V. Goryunov, I. N. Ivanova-Korfini, A. A. Boguslavskii and R. Sh. Lotfullin: Russ. J. Inorg. Chem. **37** (1992) 259.
3) B. Bagautdinov, J. Luedecke, M. Schneider and S. van Smaalen: Acta Crystallogr. Sec. B **54** (1998) 626.
4) O. G. Vlokh, V. G. Gribik, A. V. Kityk, O. M. Mokryi, I. D. Olekseyuk and S. A. Piroga: Sov. Phys. Crystallogr. **35** (1990) 873.
5) A. V. Kityk, O. M. Mokry, V. P. Soprunyuk and O. G. Vlokh: J. Phys.: Condens. Matter **5** (1993) 5189.
6) V. V. Petrov, A. Yu. Khalakhan, V. G. Pitsyuga and V. E. Yachmenev: Sov. Phys. Solid State **30** (1988) 906.
7) S. N. Kallaev, A. M. Aliev, Sh. B. Abdulvagidov and A. B. Batdalov: Phys. Solid State **39** (1997) 153.
8) V. P. Dmitriev, Yu. I. Yuzyuk, A. V. Tregubchenko, E. S. Larin, V. V. Kirilenko and V. I. Pakhomov: Sov. Phys. Solid State **30** (1988) 704.
9) S. N. Kallaev, V. V. Gladkiĭ, V. A. Kirikov, V. I. Pakhomov, I. N. Ivanova-Korfini and A. V. Goryunov: Sov. Phys. Solid State **31** (1989) 1267.
10) S. N. Kallaev, V. V. Gladkiĭ, V. A. Kirikov and I. K. Kamilov: Ferroelectrics **106** (1990) 299.
11) V. V. Petrov, V. G. Pitsyuga, V. A. Gordeev, A. V. Bogdanova, M. A. Bagina and A. Yu. Khalakhan: Sov. Phys. Solid State **25** (1983) 1995.
12) A. A. Boguslavskiĭ, R. Sh. Lotfullin, M. V. Simonov, V. V. Kirilenko, V. I. Pakhomov and A. Ya. Mikhaĭlova: Sov. Phys. Solid State **27** (1985) 321.
13) A. V. Kityk, V. P. Soprunyuk, O. G. Vlokh, I. D. Olekseyuk and S. A. Piroga: Sov. Phys. Solid State **34** (1992) 1091.
14) A. V. Kityk, A. V. Zadorozhna, Ya. I. Shchur, I. Yu. Martynyuk-Lototska and O. G. Vlokh: Phys. Status Solidi B **210** (1998) 35.
15) A. V. Kityk Ya. I. Shchur, A. V. Zadorozhna, I. B. Trach, I. S. Girnyk, I. Yu. Martynyuk-Lototska and O. G. Vlokh: Phys. Rev. B **58** (1998) 2505.
16) A. V. Kityk, Ya. I. Shchur, A. V. Zadorozhna, I. B. Trach, I. S. Girnyk, I. Yu. Martynyuk-Lototska and O. G. Vlokh: Phys. Status Solidi B **211** (1999) 631.
17) A. A. Boguslavskii, Yu. N. Ivanov, A. I. Krieger, A. K. Moskalev, V. I. Pakhomov and R. Sh. Lotfullin: Phys. Status Solidi B **161** (1990) K49.
18) R. Blinc: Phys. Rep. **79** (1981) 331.
19) A. Rigamonti: Adv. Phys. **33** (1984) 115.
20) K.-P. Holzer, J. Petersson, D. Schüßler, R. Walish, U. Häcker and D. Michel: Europhys. Lett. **31** (1995) 213.
21) K.-P. Holzer, J. Petersson, D. Schüssler, R. Walish, U. Häcker and D. Michel: Phys. Rev. Lett. **71** (1993) 89.
22) C. Babnuls and C. Bervillier: Phys. Rev. B **32** (1985) 7209.
23) R. A. Cowley and A. D. Bruce: J. Phys. C: Solid State Phys. **11** (1978) 3577.
24) P. Mischo, F. Decker, U. Häcker, K.-P. Holzer and J. Petersson: Phys. Rev. Lett. **78** (1997) 2152.
25) A. P. Levanyuk: *Incommensurate Phases in Dielectrics 1. Fundamentals*, ed. R. Blinc and A. P. Levanyuk (North Holland, Amsterdam, 1986) Chap. 1.
26) M. Quilichini, J. P. Mathieu, M. Le Postollec and N. Toupry: J. Phys. **43** (1982) 787.
27) R. Blinc, P. Prelovšek, V. Rutar, J. Seliger and S. Žumer: *Incommensurate Phases in Dielectrics 1. Fundamentals*, ed. R. Blinc and A. P. Levanyuk (North Holland, Amsterdam, 1986) Chap. 4.
28) R. Walisch, J. M. Perez-Mato and J. Petersson: Phys. Rev. B **40** (1989) 10747.
29) C. H. Townes and B. P. Dailey: J. Chem. Phys. **23** (1955) 118.
30) S. Plesko, P. Kind and H. Arend: Phys. Status Solidi A **61** (1980) 87.

^{35}Cl NQR Studies of Hydrogen Transfer in Crystalline *p*-Chlorobenzoic Acid

Taka-aki Nihei, Shin'ichi Ishimaru, and Ryuichi Ikeda

Department of Chemistry, University of Tsukuba, Tsukuba 305-8571, Japan

Reprint requests to Prof. R. I.; Fax:+8 12 98 53 65 03; E-mail: ikeda@staff.chem.tsukuba.ac.jp.

Z. Naturforsch. **55a**, 355–358 (2000); received August 27, 1999

Presented at the XVth International Symposium on Nuclear Quadrupole Interactions, Leipzig, Germany, July 25–30, 1999.

^{35}Cl NQR frequencies and spin-lattice relaxation times T_{1Q} were measured in *p*-$ClC_6H_4CO_2H$(PCBA) and *p*-$ClC_6H_4CO_2D$(PCBA-d_1) at 77–333 K. T_{1Q} in PCBA gave a shallow minimum of 8.0 ms at ca. 110 K, which could be explained by a double proton transfer mechanism in the carboxylic acid dimer referring to ^{1}H NMR data giving a T_{1H} minimum at almost the same temperature. PCBA-d_1 showed temperature dependent NQR frequencies quite analogous to those in PCBA, whereas their T_{1Q} behaviour was quite different in its minimum value and its temperature as well as temperature gradient. These results were explained by suppressed deuteron tunnelling and the Ubbelohde effect.

Key words: Cl NQR; Hydrogen-Bond; Hydrogen-transfer; Tunneling.

Introduction

Intermolecular hydrogen bonds can be seen in many kinds of compounds which form molecular aggregates such as dimers, trimers, or 1,2 and 3-dimensional networks in solid, liquid and biological systems. Intermolecular hydrogen transfer through hydrogen bonds is an attractive phenomenon. As an example, the hydrogen exchange in solid dimerized benzoic acid has extensively been studied by ^{1}H NMR [1, 2]. The NMR measurement is, however, rather insensitive for this purpose owing to the small displacement of the H positions in the H-exchanging process, which usually requires the measurement of the relaxation times of the order of 10^2–10^3s [1, 2]. Here, we intend to detect this motion by the NQR measurement of chlorine introduced on the phenyl ring. This is because a subtle fluctuation of the electric field gradient throughout the π-electron system caused by a H-motion even in a remote position can be expected to be sensitively detected by the NQR technique. In the present study, the ^{35}Cl NQR frequencies and spin-lattice relaxation time were measured in *p*-chlorobenzoic acid and its partially deuterated analogue.

Experimental

Crystalline *p*-chlorobenzoic acid, *p*-$ClC_6H_4CO_2H$ (abbreviated to PCBA) was obtained by recrystallization of the commercial reagent from acetone. A partially deuterated analogue *p*-$ClC_6H_4CO_2D$(PCBA-d_1) was prepared by repeated crystallization of the protonated compound from CH_3OD.

The ^{35}Cl NQR frequencies and spin-lattice relaxation time (T_{1Q}) in both analogues were measured with a homemade pulsed spectrometer, described in [3], at 77–140 K. A 180°-τ-90° pulse sequence was used to determine T_{1Q}. The ^{1}H NMR spin-lattice relaxation time T_{1H} in PCBA was measured with a homemade spectrometer [4] at a Larmor frequency of 54.3 MHz at 30–300 K, using the saturation recovery pulse sequence.

Results

The temperature dependences of the ^{35}Cl NQR frequencies observed in PCBA and PCBA-d_1 are shown in Figure 1. The observed frequencies of 34.673±0.001 and 34.674±0.002 MHz in PCBA and PCBA-d_1, respectively, at 77 K agree well with 34.673 MHz reported for PCBA [5]. The resonance frequencies and their temperature dependences in both compounds were quite similar in the whole temperature range studied. The frequency difference at 130 K was 2.5 kHz. Upon heating, the resonance signals in both compounds gradually weakened and disappeared in the noise level at around 140 K.

The temperature dependences of ^{35}Cl NQR T_{1Q} observed in PCBA and PCBA-d_1 are shown in Figure 2.

0932-0784 / 2000 / 0100-0355 $ 06.00

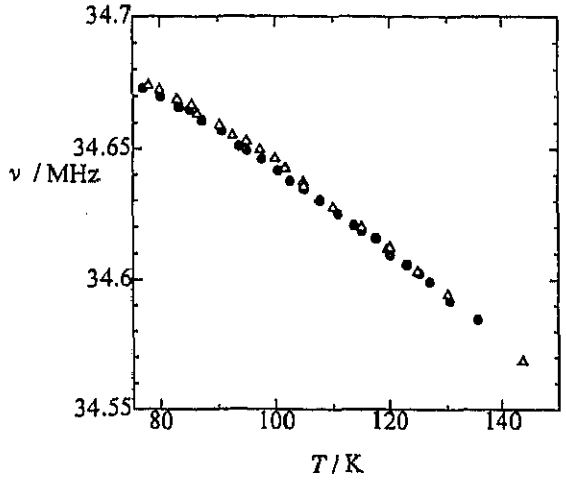

Fig. 1. Temperature dependences of ^{35}Cl NQR frequencies (ν) observed in *p*-$ClC_6H_4CO_2H$ (PCBA) (●), and *p*-$ClC_6H_4CO_2D$ (PCBA-d_1) (△).

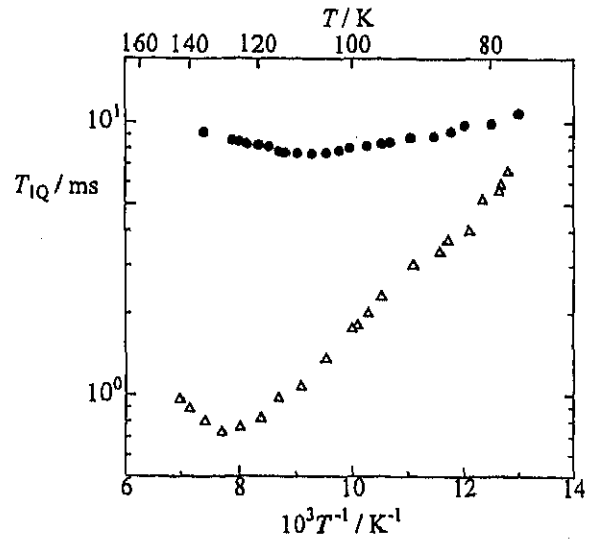

Fig. 2. Temperature dependences of the ^{35}Cl NQR spin-lattice relaxation times T_{1Q} observed in *p*-$ClC_6H_4CO_2H$ (PCBA) (●), and *p*-$ClC_6H_4CO_2D$ (PCBA-d_1) (△).

A shallow minimum of (8.0±1.0) ms was observed at ca. 110 K in PCBA, while a deep minimum of (0.80± 0.10) ms was obtained at ca. 130 K in PCBA-d_1.

The temperature dependence of ^{1}H NMR T_{1H}, observed in PCBA at 54.3 MHz, is shown in Figure 3. Our results agree well with data in the high-temperature range reported by Nagaoka et al. [1, 2]. An asymmetric T_{1H} curve with a minimum at ca. 105 K was clearly observed in the present work.

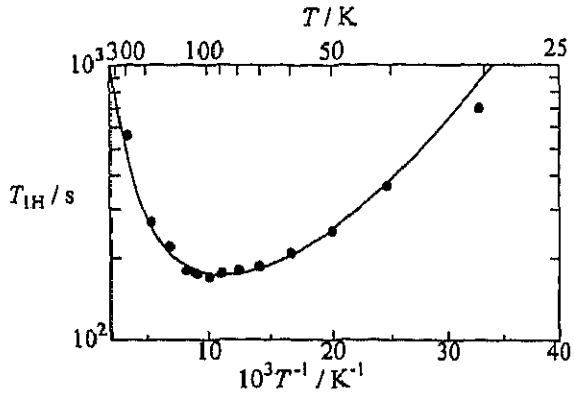

Fig. 3. A temperature dependence of the ^{1}H NMR spin-lattice relaxation time T_{1H} observed in *p*-$ClC_6H_4CO_2H$ (PCBA) at a Larmor frequency of 54.3 MHz. The solid curve is best-fitted (see text).

Discussion

^{1}H NMR Spin-Lattice Relaxation Time

The asymmetric temperature dependence of T_{1H} in PCBA, shown in Fig. 3, is quite analogous to T_{1H} data reported for crystalline benzoic acid (BA) [1, 2] in which the double proton transfer between the hydrogen bonded two molecules was shown to contribute to the relaxation. Referring to the analysis of T_{1H} in benzoic acid [6], the steep temperature dependence observed on the high-temperature side of the minimum can be explained by the BPP type relaxation [7] due to the classical random hydrogen jumps in an asymmetric double-well potential formed in the dimer structure. On the other hand, the relaxation on the low-temperature side is attributed to quantum mechanical proton tunnelling coupled to crystalline phonons. We analysed the obtained T_{1H} data using the theoretical treatment performed on benzoic acid given in [6]:

$$T_1^{-1} = C\frac{a}{(1+a)^2}\left[\frac{\tau_c}{1+(\omega\tau_c)^2}+\frac{4\tau_c}{1+4(\omega\tau_c)^2}\right], \tag{1}$$

$$a = \exp(A/RT), \tag{2}$$

$$\frac{1}{\tau_c} = k_{AB}+k_{BA}, \tag{3}$$

$$k_{AB} = k_{AB}^{L}+k_{AB}^{H}, \quad k_{BA} = k_{BA}^{L}+k_{BA}^{H}, \tag{4}$$

$$k_{AB}^{L} = k_0\, n(A), \quad k_{BA}^{L} = k_0\,[n(A)+1], \tag{5}$$

$$n(A) = \frac{1}{\exp(A/RT) - 1}, \tag{6}$$

$$k_{AB}^{H} = \frac{1}{\tau_0} \exp(-V/RT), \tag{7}$$

$$k_{BA}^{H} = \frac{1}{\tau_0} \exp[-(V-A)/RT],$$

where A, k_0 and V denote the potential energy difference, the tunnelling rate and the barrier height. The definitions of the other parameters are given in [6]. We fitted (1)–(7) to the data in Fig. 3, where C in (1), expressing the magnetic dipolar interaction modulated by this proton transfer, was estimated from the C value reported for benzoic acid, where we assumed that the ratio of C in the two compounds is roughly equal to that of the observed T_{1H} minima. This is because no data on H positions in crystals are available for PCBA. The derived best fitted T_{1H} curve and determined parameters are shown in Fig. 3 and Table 1, respectively.

The k_0 in PCBA (2.0×10^{10} s^{-1}) is larger than that in BA (4.5×10^{8} s^{-1}), indicating that tunnelling in PCBA is larger than in BA. This is explainable by a stronger H-bonding in PCBA which results in a short O–O distance of 2.615 Å [8] compared to 2.64 Å in BA [9]. This difference comes from the more acidic protons in PCBA due to the electron attracting effect of chlorine. The remarkable difference in T_{1H} minimum values in PCBA and BA, which gave ca. 6 s at 59.53 MHz [1, 2], implies that the H displacement in the double proton transfer process in PCBA is smaller than in BA. This can also be explained by the difference in the O–O separations or the strength of H-bonding in the two carboxylic acids.

^{35}Cl NQR Frequencies and T_{1Q}

The temperature dependence of the ^{35}Cl NQR frequencies above 77 K in both PCBA and PCBA-d_1, shown in Fig. 1, is normal and explainable by the Bayer theory [10]. At around 140 K the signals disappear. The two analogues showed almost the same frequencies in the whole temperature range, suggesting that the average electric field gradients at the Cl nuclei are almost unaffected by the deuteration in the carboxyl group.

The facts that T_{1Q} in PCBA has a minimum at almost the same temperature of ca. 105 K as T_{1H}, and also the slope of T_{1Q} of ca. (0.78±0.3) kJ mol^{-1} on the low-temperature side of the minimum is close to 0.98± 0.2 kJ mol^{-1} in T_{1H}, indicate that the relaxation mechanisms in T_{1Q} and T_{1H} are the same, i.e., a double proton transfer in the dimer. A marked difference for PCBA and PCBA-d_1 was observed in the T_{1Q} temperature dependences shown in Fig. 2, where a shallow minimum of ca. 8.0±1.0 ms was observed in PCBA around 110 K, while a deep minimum of 0.80±0.10 ms in PCBA-d_1 at ca. 130 K. This indicates that the observed T_{1Q} temperature dependence is closely connected with the hydrogen transfer process in carboxylic acid dimers. The markedly smaller T_{1Q} values obtained in NQR than in NMR imply that the H-transfer in these systems can be observed much more sensitively in NQR than in NMR studies.

Table 1. Motional parameters of the proton transfer in carboxylic acid dimers determined in *p*-chlorobenzoic acid from ^{1}H NMR relaxation data together with the reported values in benzoic acid.

	V/kJ · mol^{-1}	τ_0/s	A/kJ · mol^{-1}	k_0/s^{-1}	C/s^{-2}
p-chlorobenzoic acid (PCBA)	8±2	1.3×10^{-12}	0.98±0.2	2.0×10^{10}	2.40×10^{7}
benzoic acid (BA) [5]	5.5	3.3×10^{-12}	0.72	4.5×10^{8}	2.84×10^{8}

An interesting result in the T_{1Q} data is that the deuterated and undeuterated analogues exhibited a quite different T_{1Q} behaviour, even though they showed quite analogous resonance frequencies in a wide temperature range. An important characteristic of H-transfer in PCBA-d_1 is the much smaller tunnel interactions than that in PCBA because of the marked mass effect on tunnelling which results in quite small tunnelling probability in deuterated systems [11]. If we can ignore the contribution from the tunnelling to T_{1Q} in the deuterated analogue, the steep T_{1Q} slope observed on the low-temperature side of the minimum is mostly explainable by the classical H-jumps. The fact that the minimum temperature of T_{1Q} in PCBA-d_1 is higher than in PCBA can be understood by the shorter O–D, that is longer O–O distance in the deuterated dimer, the so-called Ubbelohde effect [12], resulting in a slower jumping rate of D than that of H.

A remarkable difference between the two analogues is that T_{1Q} in PCBA-d_1 is about ten times shorter than in PCBA. This can be explained by considering the tunnelling which enables quantum mechanical proton delocalization by overlapping two protonic wave functions implying that the tunnelling process is not a motion but a state giving no marked fluctuation of the electric field

gradient. Since, in PCBA, the efg fluctuation at Cl nuclei at high temperatures made by the exchange

is partly averaged by the tunnelling, the effective fluctuation in PCBA occurring around the T_{1Q} minimum is expected to be smaller than in the deuterated analogue with the markedly diminished tunnelling.

This work was partly supported by Grant-in Aid for scientific research No. (B) 09440234 from the Ministry of Education, Science, Sports and Culture.

[1] S. Nagaoka, T. Terao, F. Imashiro, A. Saika, and N. Hirota, J. Chem. Phys. **79**, 4694 (1983).
[2] S. Nagaoka, T. Terao, F. Imashiro, A. Saika, N. Hirota, and S. Hayashi, Chem. Phys. Lett. **80**, 580 (1981).
[3] H. Miyoshi, K. Horiuchi, N. Sakagami, K. Okamoto, and R. Ikeda, Z. Naturforsch. **53a**, 603 (1998).
[4] T. Kobayashi, H. Ohki, and R. Ikeda, Mol. Cryst. Liq. Cryst. **257**, 279 (1994).
[5] H. C. Meal, J. Amer. Chem. Soc. **74**, 6121 (1952).
[6] J. L. Skinner and H. P. Trommsdorff, J. Chem. Phys. **89**, 897 (1988).
[7] A. Abragam, The Principles of Nuclear Magnetism, Oxford University Press, New York 1986, Chapt. VIII.
[8] R. S. Miller, I. C. Paul, and D. Y. Curtin, J. Amer. Chem. Soc. **96**, 6334 (1974).
[9] G. A. Sim, J. M. Robertson, and T. H. Goodwin, Acta. Cryst. **8**, 157 (1955).
[10] H. Bayer, Z. Physik, **130**, 227 (1951).
[11] A. Stöckli, B. H. Meier, R. Kreis, R. Meyer, and R. R. Ernst, J. Chem. Phys. **93**, 1502 (1990).
[12] J. M. Robertson and A. R. Ubbelohde, Proc. Roy. Soc. A **170**, 222 (1939); J. M. Robertson and A. R. Ubbelohde, Proc. Roy. Soc. A **170**, 241 (1939); A. R. Ubbelohde, Proc. Roy. Soc. A **173**, 417 (1939); A. R. Ubbelohde and I. Woodware, Proc. Roy. Soc. A **179**, 399 (1942).

A ^{133}Cs NMR Spin-Lattice Relaxation Study in Incommensurate Cs_2CdI_4

Koh-ichi Suzuki, Shin'ichi Ishimaru, and Ryuichi Ikeda

Department of Chemistry, University of Tsukuba, Tsukuba 305-8571, Japan

Reprint requests to Dr. S. I.; Fax: 81-298-53-6503, E-mail: ishimaru@staff.chem.tsukuba.ac.jp

Z. Naturforsch. **55 a**, 339–342 (2000); received August 27, 1999

Presented at the XVth International Symposium on Nuclear Quadrupole Interactions, Leipzig, Germany, July 25 - 30, 1999.

^{133}Cs NMR spin-lattice relaxation times(T_1) in crystalline Cs_2CdI_4 were measured at 225 - 373 K. The critical exponent ζ of T_1 observed near the normal-incommensurate transition in the normal phase was determined to be 0.62 ± 0.03, in good agreement with the predicted value for three-dimensional XY-model. The frequency dependent T_1 in the incommensurate phase could be explained by the fluctuation of amplitudon and small gap phason.

Key words: ^{133}Cs NMR; T_1; Incommensurate; Phase Transition; Critical Exponent.

Introduction

Many compounds of the A_2BX_4 family with a pseudo-hexagonal β-K_2SO_4 structure (Pnma) have been reported to have a normal (N) to incommensurate (IC) phase transition at low temperatures [1]. The critical behaviour of most of these compounds around the N-IC phase transition can be described by the XY-model [2]. In [3] we have reported results of ^{133}Cs NMR observed in Cs_2HgBr_4 crystals and found a critical exponent ζ of the spin-lattice relaxation rate that is different from the expected value from the XY-model but rather close to the classical value. In this compound, the dynamics of the IC phase modulation wave could also be described by the classical plane-wave-approximation in all temperature range of the IC phase [3]. In the present study, we selected Cs_2CdI_4, reported to form an IC phase below 259.6 K [4], and intended to reveal the mechanism of the N-IC phase transition by comparing NMR results with those obtained for Cs_2CdBr_4 and Cs_2HgBr_4 [3].

Cs_2CdI_4 forms two modifications, A and B at room temperature, depending on the conditions of crystal growth. The modification A (orthorhombic Pnma) is obtained from a fused stoichiometric mixture of CsI and CdI_2, while the monoclinic modification B ($P2_1/m$) crystallizes from the aqueous solution [5]. B undergoes no phase transition below room temperature but transforms to A at *ca.* 420 K. On the other hand, A undergoes successive phase transitions [4]:

$$\begin{array}{ccccc} \text{commensurate(C')} & \xrightarrow{T_{C'}=183.4\,K} & \text{commensurate(C)} & & \\ P\bar{1};\ Z=1 & & P2_1/n;\ Z=4 & & \\ \xrightarrow{T_C=259.6\,K} & \text{incommensurate(IC)} & \xrightarrow{T_{IC}=332.3\,K} & \text{normal(N).} & \\ & P^{Pnma}_{1ss} & & Pnma;\ Z=4 & \end{array}$$

The N and C phases were shown to be isomorphous with corresponding phases in Cs_2HgBr_4 [6], while a modulation wave vector in the IC phase ($q_{IC} \simeq 0.26a^*$) [4] is different from that in the bromo compound ($q_{IC} \simeq 0.15a^*$) [7].

Experimental

Cs_2CdI_4 crystals were grown by slow evaporation of an aqueous solution containing stoichiometric amounts of CsI and CdI_2. The obtained crystalline powder was kept *in vacuo* at 450 K to be transformed to the modification A, then sealed in a glass tube with nitrogen gas for differential thermal analysis (DTA) and NMR measurements.

X-Ray powder diffraction and DTA were measured to confirm the complete transformation to the modification-A. The sample temperature was determined by a chromel-constantan thermocouple within ± 0.2 K. The ^{133}Cs NMR measurement was performed with a Bruker MSL-300 NMR system at a Larmor frequency of 39.4 MHz in the range 225 - 373 K. The ^{133}Cs NMR T_1 in IC phase was measured by a Bruker

0932–0784 / 00 / 0100–0339 $ 06.00

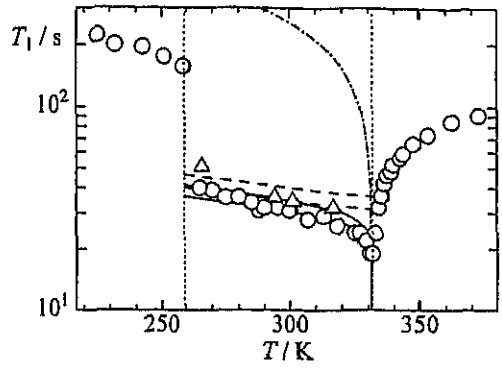

Fig. 1. Temperature and frequency dependences of ^{133}Cs NMR T_1 at 39.4 MHz (o) and 52.5 MHz (Δ). Solid lines are calculated values for the contributions from amplitudon (chain line) and phason (broken lines). The vertical dotted lines corresponds to phase transition temperatures observed by DTA measurement.

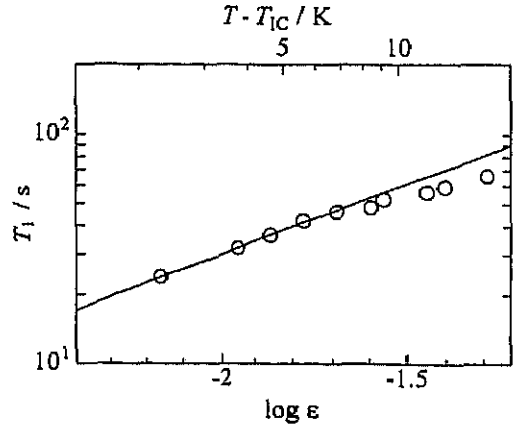

Fig. 2. A temperature dependence of critical ^{133}Cs NMR T_1 in the normal phase near the N-IC phase transition. The solid line represents calculated values for the critical exponent $\zeta = 0.62$.

MSL-400 system at 52.5 MHz in the range 266 - 317 K. The sample temperature was controlled within ±0.5 K by a Bruker VT-1000 temperature controller and determined by a copper-constantan thermocouple within ±0.5 K. The error in T_1 was estimated to be 5%.

Electric charges on isolated $HgBr_4^{2-}$, $CdBr_4^{2-}$ and CdI_4^{2-} were calculated by the semi-empirical method PM3 assuming a regular tetrahedral structure with the reported bond-length [8], without structural optimization.

Results

X-Ray Powder Diffraction and DTA

X-Ray powder diffraction peaks in neat crystals obtained from aqueous solution and after heat-treatment at 450 K were well explained by the reported structures [5, 9] of the modification B and A, respectively. In all following experiments, we used the heat-treated specimens.

DTA thermograms measured on heating displayed endothermic anomalies due to phase transitions at 183 ± 1, 259.3 ± 0.6 and 331.6 ± 0.7 K, in good agreement with the reported transition temperatures, $T_{C'}$, T_C and T_{IC} [4, 10, 11], respectively.

^{133}Cs NMR Spin-Lattice Relaxation Time T_1

The temperature dependence of ^{133}Cs T_1 is shown in Figure 1. The observed T_1 showed a sharp decrease and a jump near the N-IC and the IC-C phase transition point, respectively. T_1 revealed a weak frequency dependence, $T_1 \propto \omega^{0.45}$, on the high-temperature side of the IC phase.

Discussion

Normal (N) Phase

The T_1 dip observed near the phase transition temperature is attributable to the critical fluctuation of quadrupole interaction due to the second order phase transition. In this case, T_1 can be represented by the sum of two mechanisms as

$$T_1^{-1} = T_{1c}^{-1} + T_{1l}^{-1}, \quad (1)$$

where T_{1c} and T_{1l} are contributions from the critical fluctuation and non-critical lattice vibrations, respectively. Near the phase transition temperature, T_{1c}^{-1} shows an exponential divergence [12],

$$T_{1c}^{-1} \propto \epsilon^{-\zeta}, \quad (2)$$

where $\epsilon = (T - T_{IC})/T_{IC}$ and ζ are the reduced temperature and the critical exponent, respectively. T_{1l} is expected to be negligible in the total T_1 because $T_{1l} \geq 100$ s can be estimated from the observed T_1 at 370 K. ζ was obtained, from the slope of $\log T_1$ vs. $\log \epsilon$ plots, to be 0.62 ± 0.03 in a temperature range of 7 K above the transition (Figure 2). This

value coincides with that obtained in Cs_2CdBr_4 [3] and agrees well with the theoretical value of 0.625 [13] calculated for the three-dimensional XY-model with which the driving interaction of the N-IC phase transition is predicted [2]. The deviation of the observed T_1 values from the calculated ones at temperatures higher than 7 K above the phase transition is attributable to the contribution from $T_{1\parallel}$.

Incommensurate (IC) Phase

The T_1 values in this phase, smaller than in the N and C phases, sharply decreased around the N-IC transition point. This behaviour is explainable by considering two characteristic lattice modes, amplitudon and phason, which represent the fluctuations of IC modulation [14]. The total T_1 is then represented by,

$$T_1^{-1} = T_{1\parallel}^{-1} + T_{1a}^{-1} + T_{1\phi}^{-1}, \tag{3}$$

where T_{1a} and $T_{1\phi}$ are the contributions from the amplitudon and the phason, respectively. Since the T_1 values observed in the IC phase were one order shorter than those in the N and C phases (Fig. 1), the contribution from normal lattice modes $T_{1\parallel}^{-1}$ is assumed to be negligible.

In the plane wave limit, the contributions from amplitudon and phason are given by

$$T_{1a}^{-1} \propto (T_{IC} - T)^{-\zeta'}, \tag{4}$$

and

$$T_{1\phi}^{-2} \propto T^2 \left(\sqrt{1 + (\omega_L/\omega_\phi)^2} + 1 \right)^{-1}, \tag{5}$$

[15, 16], where ζ' is the critical exponent of T_1 on the low-temperature side of the phase transition point and ω_ϕ is the phason frequency or gap. In the frequency region $\omega_\phi \ll \omega_L$ the $T_{1\phi}$ is proportional to $\sqrt{\omega_L}$. The experimentally derived frequency dependence of T_1 in this phase, $T_1 \propto \omega^{0.45}$, approximately agrees with the predicted relation $T_1 \propto \sqrt{\omega_L}$. This implies that the phason gap is small enough compared with the Larmor frequency.

Based on the above discussion, we fitted the observed T_1 in the IC phase by a superposition of T_{1a}, and $T_{1\phi}$, as shown in Figure 1. In (4), we assumed the classical value $\zeta' = 0.5$ because the contribution from the amplitudon was shown to emerge only in the neighbourhood of T_{IC} [3] and could not be separated from the total T_1.

A small deviation of the calculated line from the observed T_1 in the low-temperature region of the IC phase is explainable by the breakdown of the plane-wave approximation for the IC modulation. This T_1 behaviour is analogous to the results obtained for Cs_2CdBr_4 [3].

Commensurate (C) Phase

In the C phase, ^{133} Cs T_1 is governed by normal lattice vibrations because the IC modulation wave is locked in a commensurate wave [1, 14]. The observed T_1 was longer than in the IC phase and the high-temperature region of the N phase, and showed a moderate dependence on temperature. No anomaly was observed near the first-order C-IC transition at 183 K.

Interionic Interaction and Transition Mechanism

In the present study we showed that the value of critical exponent of T_1 in the N-phase near the N-IC phase transition and T_1 behaviour in the IC phase are quite analogous to those in the previously reported Cs_2CdBr_4 [3]. We can reasonably expect that the interionic interaction between Cs cations and complex anions influences the critical dynamics near the phase transition and the behaviour of IC modulation wave. Here, we attempt to explain the relation of the dynamics around the transition and in the IC phase using interionic electrostatic interactions. The ionicity of halogen can be estimated from the observed e^2Qq/h using the Townes-Dailey relation [17]:

$$e^2Qq/h = (1 - s)(1 - i)(e^2Qq/h)_{atom}, \tag{6}$$

where s is the contribution of s electrons in the chemical bond and assumed to be 0.15, i is the ionicity of the halogen and $(e^2Qq/h)_{atom}$ is the e^2Qq/h of atomic halogen. The averaged electric charges per a halogen in the polyanions were calculated from (6) to be $-0.71 \sim -0.66$ for $HgBr_4^{2-}$, $-0.79 \sim -0.76$ for $CdBr_4^{2-}$ and $-0.74 \sim -0.71$ for CdI_4^{2-} from the reported NQR frequencies [6, 18] observed near room temperature by assuming $\eta = 0$. The ionicities of isolated polyanions, obtained by PM3 calculations,

were −0.676 for $HgBr_4^{2-}$, −0.836 for $CdBr_4^{2-}$ and −0.835 for CdI_4^{2-}. The NQR frequencies and PM3 calculations yield quite analogous results: $CdBr_4^{2-}$ and CdI_4^{2-} are more ionic than $HgBr_4^{2-}$. This difference of the halogen ionicity seems to induce the different behaviour, *i.e.*, the XY-interaction near the N-IC transition and the multi-soliton IC-modulation work in Cs_2CdI_4 and Cs_2CdBr_4 crystals, whereas the classical behaviour prevails in Cs_2HgBr_4 crystals.

Acknowledgements

We should like to thank Dr. Y. Onoda and Dr. M. Tansho of National Institute of Research in Inorganic Materials for their kind help in operating the MSL-400 NMR system. This work was partly supported by a Grant-in-aid for Scientific Research No. (B)0944023 and (C)10640554 from the Ministry of Education, Science, Sports and Culture, Japan.

[1] H. Z. Cummins, Phys. Rep. **185**, 211 (1990) and references therein.
[2] R. A. Cowley and A. D. Bruce, J. Phys. C: Solid State Phys. **11**, 3577 (1978).
[3] K. Suzuki, S. Ishimaru, and R. Ikeda, J. Phys. Soc. Japan **68**, 1963 (1999).
[4] K. S. Aleksandrov, S. V. Melnikova, I. N. Flerov, A. D. Vasilev, A. I. Kruglik, and I. T. Kokov, Phys. Status Solidi (a), **105**, 441 (1988).
[5] V. Touchard, M. Louër, J. P. Auffredic, and D. Louër, Rev. Chim. Min. **24**, 414 (1987).
[6] S. Plesko, P. Kind, and H. Arend, Phys. Status Solidi (a), **61**, 87 (1980).
[7] S. Plesko, V. Dvořák, P. Kind, and A. Treindl, Ferroelectrics **36**, 331 (1981).
[8] K. Friese, G. Madariaga, and T. Breczewski, Z. Kristallogr. **213**, 591 (1998).
[9] R. Sjövall, Acta Crystallogr. **C45**, 667 (1989).
[10] I. N. Flerov, M. V. Gorev, L. A. Kot, and V. A. Grankina, Sov. Phys. Solid State **30**, 1125 (1988).
[11] S. V. Melnikova and S. V. Primak, Phase Transition **36**, 191 (1991).
[12] A. Rigamonti, Adv. Phys. bf 33, 115(1984).
[13] K.-P. Holtzer, J. Petersson, D. Schüssler, R. Walisch, U. Häcker, and D. Michel, Europhys. Lett. **31**, 213 (1995).
[14] R. Blinc, P. Prelovšek, V. Rutar, J. Seliger, and S. Žumer, Incommensurate Phases in Dielectrics 1. Fandamentals, ed. R. Blinc and A. P. Levanyuk, North Holland, Amsterdam 1986.
[15] P. Mischo, F. Decker, U. Häcker, K.-P. Holtzer, and J. Petersson, Phys. Rev. Lett. **78**, 2152 (1997).
[16] R. Walisch, J. Petersson, D. Schüssler, U. Häcker, D. Michel, and J. M. Pérez-Mato, Phys. Rev. **B50**, 16192 (1994).
[17] C. H. Townes and B. P. Dailey, J. Chem. Phys. **23**, 118 (1955).
[18] E. V. Shemetov, K. S. Aleksandrov, I. P. Aleksandrova, and S. V. Primak, Phys. Stat. Sol. (a) **104**, K89 (1987).

PCCP

Dynamic behaviour of triethylamine molecules adsorbed in aluminophosphate ($AlPO_4$-5) and silicoaluminophosphate (SAPO-5) molecular sieves

Kazuma Gotoh, Shin'ichi Ishimaru and Ryuichi Ikeda*

Department of Chemistry, University of Tsukuba, Tsukuba 305-8571, Japan

Received 11th November 1999, Accepted 15th February 2000

^{1}H NMR spectra, second moments of line and spin–lattice relaxation times were measured for triethylamine (TEA) adsorbed in aluminophosphate ($AlPO_4$-5) and silicoaluminophosphate (SAPO-5) molecular sieves in the temperature range 90 K to room temperature. Two modes of motions, molecular reorientations about the pseudo-C_3 axis and the isotropic rotation were observed in both systems. The fact that the former motion in SAPO-5 is hindered more than in $AlPO_4$-5 was attributed to the hydrogen-bond formation between Brönsted acid sites and lone-pair electrons in TEA. This difference in interaction was shown to be the origin of the distribution of the motional correlation time (τ) in SAPO-5 less than in $AlPO_4$-5 in which the presence of molecular C_3 axes in micropores oriented more randomly than in SAPO-5 result in a marked τ distribution.

Introduction

$AlPO_4$-5, a typical aluminophosphate molecular sieve, forms microporous crystals having one-dimensional homogeneous channels with a pore diameter of 0.73 nm.[1–3] Because of its simple and cylindrical pore structure circumscribed by 12T(P, Al) as well as the moderate pore size, molecules adsorbed in micropores can form one-dimensional molecular arrays which are expected to exhibit new structural and dynamical properties different from two or three dimensionally aggregated molecular crystals.

In the present study, our interest is in one-dimensional molecules intercalated in $AlPO_4$-5, as well as in SAPO-5 (silicoaluminophosphate) in which some of the P (and Al) atoms are replaced by Si, and hence, Brönsted acid sites are created on the pore surface.[4,5] In preparation of these two molecular sieves, we employed triethylamine (TEA) molecules as a structure directing agent (SDA: template). Here, we intend to reveal dynamic properties and orientations of one-dimensionally arranged TEA molecules adsorbed in $AlPO_4$-5, and also to study the effect of Brönsted acid protons formed in SAPO-5 to molecular motions and arrangements in the one-dimensional channels by measuring temperature dependences of ^{1}H NMR spectra and spin–lattice relaxation. As an analogous system, dynamic properties of tetrapropylammonium cations occluded in the synthesis in a siliceous MFI-type (ZSM-5) zeolite were studied by NMR.[6] We try to compare differences in the effects of molecular sizes on mobilities, and also interactions with the pore surface expected in these two kinds of molecular sieves.

Experimental

$AlPO_4$-5 and SAPO-5 were synthesised by an analogous method reported previously[7–9] using TEA as the SDA by keeping gel mixtures of Al_2O_3, P_2O_5, SiO_2, TEA and H_2O with ratios of 1 : 1.03 : 0.0 : 1.5 : 600 for $AlPO_4$-5, and 1 : 1.03 : 0.1 : 1.5 : 600 for SAPO-5 at 450 K in a Teflon-lined stainless steel autoclave for 72 h. Fine crystals, *ca.* 100 μm long, were obtained and were dehydrated by heating to 413 K *in vacuo*.

X-Ray powder diffraction and metal microanalysis on calcined crystals were conducted for identifying the samples obtained with a Philips X'Pert PW3040/00 diffractometer and a JEOL JXA-8621 electron probe microanalyser (EPMA), respectively. ^{1}H MAS, ^{13}C CP-MAS, ^{1}H, ^{2}H and ^{14}N NMR spectra were recorded with a Bruker MSL-300 spectrometer at room temperature for ^{13}C, ^{14}N and ^{2}H, and in the range 125–295 K for the other nuclei. The second moment (M_2) of the ^{1}H NMR line was measured with a Bruker SXP-100 spectrometer by applying a solid echo pulse sequence[10] at 40 MHz in the range 90–295 K. The measurement of the spin–lattice relaxation time T_1 was carried out with a home-made pulsed spectrometer[11] using the inversion recovery method at Larmor frequencies of 21.0 and 42.0 MHz in the range 85–430 K for $AlPO_4$-5, and 40.1 and 68.6 MHz in the range 90–440 K for SAPO-5.

Results

X-Ray powder diffraction patterns recorded at room temperature were indexed well with tetragonal lattices with parameters $a = 1.372 \pm 0.005$, $c = 0.843 \pm 0.006$ nm for $AlPO_4$-5, and $a = 1.371 \pm 0.009$, $c = 0.852 \pm 0.005$ nm for SAPO-5 in agreement with the reported data.[1,3,12] It was shown from EPMA that *ca.* 9% of phosphorus in atomic ratio was replaced by silicon in SAPO-5. Combining this result and that of the elemental analysis, the number of Brönsted acid sites in SAPO-5 was estimated to be 1.0–1.2 times that of TEA molecules trapped in the capillaries. $AlPO_4$-5 prepared by using ^2H_2O as a starting material gave no ^{2}H NMR signal, but SAPO-5 analogously prepared showed a broad signal which is attributable to ^{2}H in Brönsted acid sites formed on the inside wall of capillaries. These results imply that the water content in capillaries is ignorable after keeping above 400 K *in vacuo*. A ^{13}C CP-MAS NMR spectrum on $AlPO_4$-5 shown in Fig. 1 gave two lines at 9.0 and 47.3 ppm assignable to CH_3 and CH_2 carbons, respectively, indicating the presence of triethylamine molecules in capillaries without decomposition after heating up to above 400 K.

Temperature dependences of ^{1}H NMR spectra in $AlPO_4$-5 and SAPO-5 are shown in Fig. 2. $AlPO_4$-5 gave an almost

DOI: 10.1039/a908962d

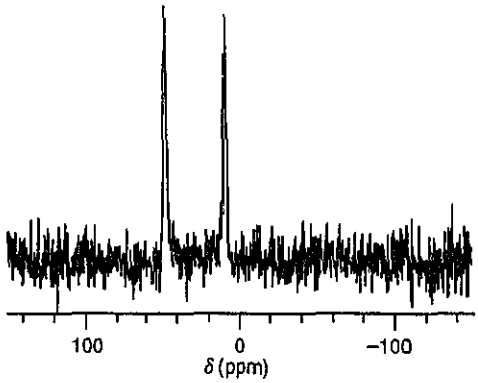

Fig. 1 A ^{13}C CP-MAS NMR spectrum observed at room temperature for TEA adsorbed in $AlPO_4$-5.

temperature independent half-height width of 3.4 ± 0.1 kHz at 295 K and 3.7 ± 0.1 kHz at 130 K, while SAPO-5 showed a marked temperature dependence: the width of 8.0 ± 0.2 kHz observed at 295 K increased to 14.5 ± 0.3 kHz at 150 K. Temperature dependences of M_2 of the ^1H NMR line measured on both samples are shown in Fig. 3. Upon heating, an M_2 of $(3.8 \pm 0.4) \times 10^{-2}$ mT^2 (Gauss^2) observed in $AlPO_4$-5 at 90 K gradually decreased to $(0.5 \pm 0.1) \times 10^{-2}$ mT^2 above 210 K, while, in SAPO-5, a wide line of $(8 \pm 1) \times 10^{-2}$ mT^2 observed around 100 K became $(1.2 \pm 0.2) \times 10^{-2}$ mT^2 above 220 K. ^1H T_1 temperature dependences in $AlPO_4$-5 and SAPO-5 are shown in Figs. 4 and 5, respectively. Two T_1 minima were observed in $AlPO_4$-5 at *ca.* 139 and 280 K, and at *ca.* 150 and

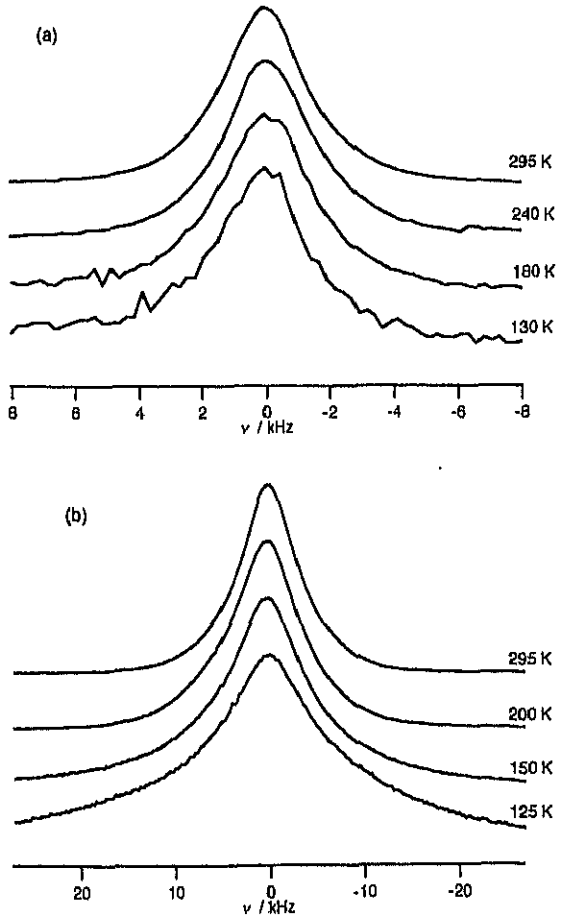

Fig. 2 Temperature dependences of ^1H NMR spectra observed for TEA adsorbed in $AlPO_4$-5 (a) and SAPO-5 (b).

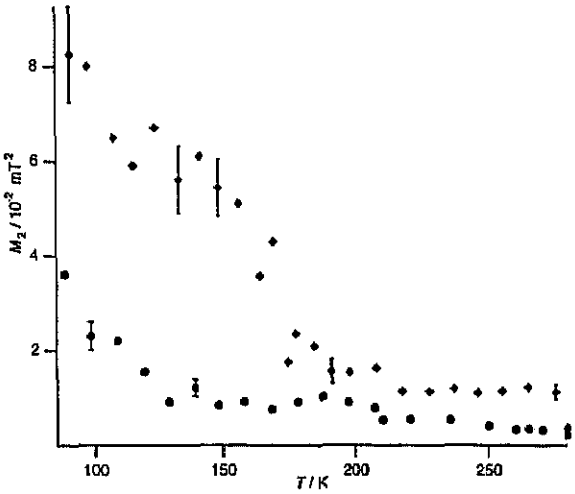

Fig. 3 Temperature dependences of the second moments (M_2) of the ^1H NMR line observed for TEA intercalated in $AlPO_4$-5 (●) and SAPO-5 (◆).

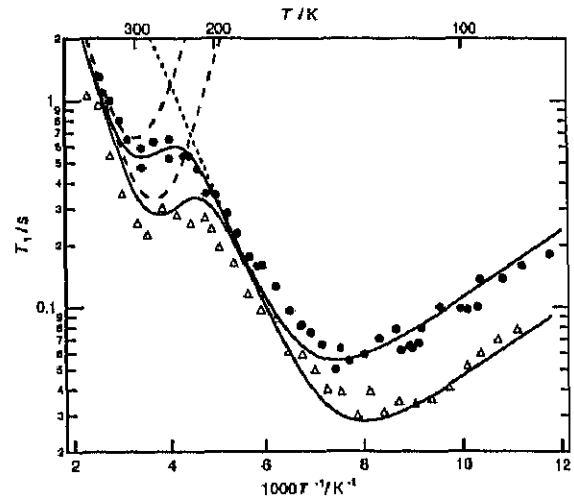

Fig. 4 Temperature dependences of the spin–lattice relaxation time (T_1) observed for TEA intercalated in $AlPO_4$-5 at 42.0 (●) and 21.0 MHz (△). The best fitted calculated curves expressed by solid lines are the sum of two T_1 components given by dotted lines.

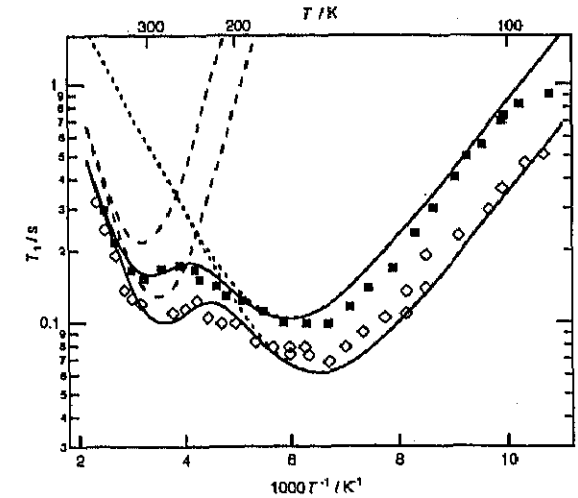

Fig. 5 Temperature dependences of the spin–lattice relaxation time (T_1) observed for TEA intercalated in SAPO-5 at 68.6 (■) and 40.1 MHz (◇). The best fitted calculated curves expressed by solid lines are the sum of two T_1 components given by dotted lines.

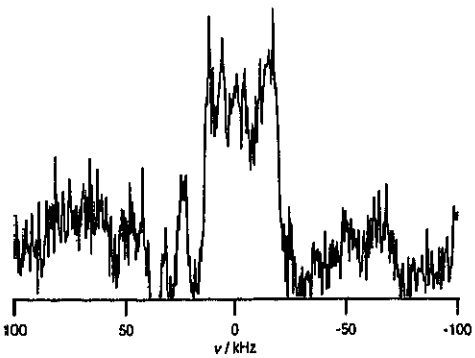

Fig. 6 A ^{14}N NMR spectrum observed at room temperature for TEA adsorbed in $AlPO_4$-5.

280 K in SAPO-5. ^{14}N NMR spectra observed at room temperature gave narrow lines with peak-to-peak widths of 40 ± 2 and 150 ± 4 kHz in $AlPO_4$-5 (Fig. 6) and SAPO-5 respectively. The ^1H MAS NMR spectrum of TEA in $AlPO_4$-5 observed at room temperature is shown in Fig. 7 (spinning rate = 3 kHz).

To get information of possible phase transitions in TEA-adsorbed $AlPO_4$-5, we performed the measurement of differential thermal analysis repeatedly in the range 120–290 K, but no thermal anomaly could be observed.

Discussion

Second moment (M_2) of ^1H NMR line

As the structure of a TEA molecule used as SDA, we assumed a molecular conformation of C_3 symmetry which was shown to be a stable form in the gaseous state.[13–15] A molecular structure projected along the C_3-axis is given in Fig. 8. This conformation was assumed because the pore diameter of *ca.* 0.73 nm in the present molecular sieves in close to 0.77 nm estimated for the long diameter of a TEA molecule in this conformation. We calculated ^1H M_2 values in four kinds of probable motional states of molecule using the above conformation; the results obtained are shown in Table 1. In this calculation, we tentatively ignored the contributions from intermolecular magnetic dipolar interactions because of small

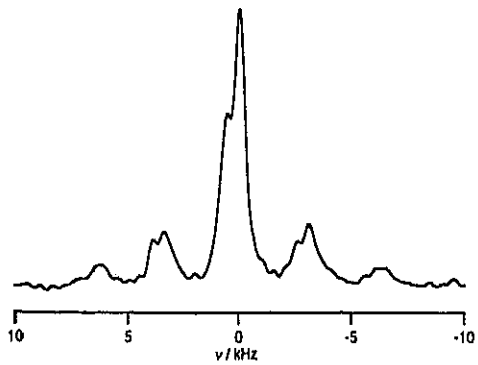

Fig. 7 A ^1H MAS NMR spectrum observed at room temperature for TEA adsorbed in $AlPO_4$-5 at a spinning rate of 3 kHz. Satellites on both sides of the central line are spinning side bands.

Table 1 Second moments (M_2) of the ^1H NMR line calculated for various motional states in triethylamine (TEA)

Motional mode	$M_2/10^{-2}$ mT^2
Rigid	22.7
Methyl rotation	11.9
Pseudo-C_3 rotation	1.3
Isotropic rotation	0.0

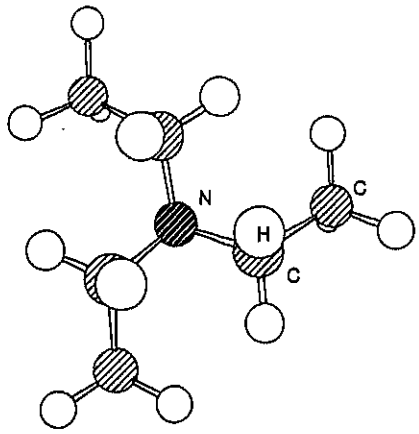

Fig. 8 A projection along the C_3-axis for a TEA molecule with the conformation of C_3 symmetry.

1-D interactions in capillaries. The comparison of observed and calculated M_2 values indicates that the CH_3 reorientation about C–C bonds contributes to M_2 in both systems even at 90 K. An M_2 of 0.3×10^{-2} mT^2 observed at room temperature can be explained by the isotropic reorientation, although this mode should give vanishing M_2 for intramolecular interactions. The observed finite value can be attributed to the contributions from ^{27}Al and ^{31}P nuclei in the wall of capillaries and neighbouring TEA molecules. Our rough calculation for these origins gave *ca.* 0.22×10^{-2} mT^2 at the centre of a capillary. The same motion is expected at room temperature in SAPO-5 which afforded a large M_2 of 1.2×10^{-2} mT^2 explainable by the theoretical value of 1.1×10^{-2} mT^2 including the contribution from protons in Brönsted acid sites on the wall. To get experimental support for the above explanation, we measured ^1H MAS NMR spectra of TEA-adsorbed $AlPO_4$-5 at room temperature. As shown in Fig. 7, the observed central line consists of two peaks assignable to CH_3 and CH_2 protons in TEA molecules. By comparing the ^1H spectrum in the same system observed without MAS at 295 K shown in Fig. 2(a), we can clearly see the spectrum narrowing by the MAS measurement indicating averaged dipolar interactions with Al and P nuclei in the wall.

The isotropic reorientation of TEA molecules at room temperature could be confirmed from ^{14}N NMR spectra observed at room temperature with widths of 40 ± 2 and 150 ± 4 kHz in $AlPO_4$-5 and SAPO-5, respectively. The quadrupole coupling constant (qcc) in a free TEA molecule was reported to be 4.8 MHz from the analysis of microwave rotation spectra.[16] Quite small qcc values of *ca.* 80 and 300 kHz in the present systems can be explained by the almost vanishing electric field gradient (efg) averaged only by the isotropic rotation of the whole molecule. The finite qcc values observed can be attributed to an efg made by electric charges of the capillary wall.

^1H NMR spin–lattice relaxation time T_1

The spin–lattice relaxation caused by averaging magnetic dipolar interactions due to molecular motions is usually expressed by the BPP equation:[17,18]

$$T_1^{-1} = \tfrac{2}{3}\gamma^2 \Delta M_2 \left(\frac{\tau_c}{1+\omega^2\tau_c^2} + \frac{4\tau_c}{1+4\omega^2\tau_c^2} \right) \quad (1)$$

where γ, ΔM_2, τ_c and ω are the magnetogyric ratio of a proton, the M_2 reduction through the motion, the correlation time of the motion, and the Larmor frequency, respectively. τ_c can be expressed by the Arrhenius equation given by

$$\tau_c = \tau_0 \exp \frac{E_a}{RT} \quad (2)$$

Here, τ_0 and E_a denote the correlation time in the limit of infinite temperature and the activation energy of the motion, respectively. The T_1 minimum observed at *ca.* 300 K in TEA-adsorbed $AlPO_4$-5 was analysed with eqns. (1) and (2) by assuming a symmetric BPP-type T_1 curve. The other T_1 minimum observed in the low-temperature range was unexplainable by the BPP equation given by eqn. (1) owing to the following three reasons: The first is that an asymmetric T_1 minimum in the plot of log T_1 *vs.* T^{-1} was observed. The second reason is that the frequency dependence of T_1 observed below *ca.* 150 K could not be expressed by the ω^2 rule given in eqn. (1) in the range $\omega\tau_c \gg 1$. The last is that the observed T_1 minimum value of 50 ms is much longer than 29 ms at 42 MHz calculated by the CH_3 reorientation model derived from the M_2 analysis given above. All of these disagreements can be explained by introducing the Cole–Davidson type τ_c distribution[19] which can be expected from the random orientations of TEA molecules in micropores. Conner has reported[20] that this type of asymmetric minimum can be explained by introducing distributed τ_c of the Cole–Davidson type given by

$$g(\tau) = \frac{\sin \beta\pi}{\pi}\left(\frac{\tau}{\tau_c - \tau}\right)^{\beta} \quad \tau \leqslant \tau_c$$
$$= 0 \quad \tau > \tau_c \qquad (3)$$

where β ($0 < \beta \leqslant 1$) shows the distribution amplitude. Using eqn. (3), T_1 is given by

$$T_1^{-1} = \tfrac{2}{3}\gamma^2 \Delta M_2 \left\{ \frac{\tau_c \sin(\beta \tan^{-1} \omega\tau_c)}{\omega\tau_c(1+\omega^2\tau_c^2)^{\beta/2}} + \frac{2\tau_c \sin(\beta \tan^{-1} 2\omega\tau_c)}{\omega\tau_c(1+4\omega^2\tau_c^2)^{\beta/2}} \right\} \qquad (4)$$

The minimum in the low-temperature side was fitted by eqns. (2)–(4), and the total T_1^{-1} was expressed by superimposed two T_1^{-1} values given by eqns. (1) and (4). The best fitted T_1 for $AlPO_4$-5 and the determined motional parameters are shown in Fig. 4 and Table 2, respectively. We assigned the minima observed at *ca.* 140 and 280 K to the molecular reorientations about the pseudo-C_3 axis and the isotropic rotation, respectively, because the M_2 of less than 4×10^{-2} mT^2 observed at 90 K indicates the onset of the C_3 reorientation, and the ^1H M_2 and ^{14}N spectrum at room temperature were explained well by the isotropic molecular rotation. The values obtained for β and ΔM_2 are discussed afterwards.

T_1 data obtained in SAPO-5 were analogously analysed to those in $AlPO_4$-5 given above. The high- and low-temperature minima were fitted by a BPP-type eqn. (1) and a Cole–Davidson-type eqn. (4) with a τ distribution, respectively. The fitted results are shown in Fig. 5 and Table 2. The low- and high-temperature minima were also assigned to the C_3 reorientation and the isotropic rotation, respectively.

The τ distribution applied for the TEA C_3 reorientation in both molecular sieves can be understood by the highly anisotropic crystal field where TEA molecules are located. It is also supported by the M_2 temperature dependence in SAPO-5 which showed a gradual decrease upon heating from *ca.* 90 to 220 K corresponding to the onset of the C_3 reorientation. A slow M_2 decrease over 100 K including the T_1 minimum temperature observed in SAPO-5 is unusual for the normal Arrhenius-type excitations and can be well explained by the τ distribution model. The same discussion seems to be applicable to M_2 of $AlPO_4$-5 for which low-temperature data are lacking.

The fact that the extent of the τ distribution $\beta = 0.3$ for the pseudo-C_3 reorientation in $AlPO_4$-5 is wider than $\beta = 0.7$ in SAPO-5 is attributable to the difference in the inner-wall structure of capillaries. In the low-temperature range, the lone-pair electrons in TEA molecules in SAPO-5 are expected to interact with Brönsted acid sites with a concentration higher than that of TEA in capillaries. This weak interaction restricts TEA molecules to rotation about the axis nearly perpendicular to the pore axis. On the other hand, molecules in $AlPO_4$-5 rotate in a homogeneous cylindrically symmetric field which enables molecular reorientations about axes with no specified orientations. This can afford a τ distribution in $AlPO_4$-5 wider than in SAPO-5.

We can see that the best fitted theoretical T_1 shown in Figs. 4 and 5 could not give a good fit in the high-temperature range of the respective T_1 minima for the C_3-rotation in $AlPO_4$-5 and SAPO-5, both showed a slight frequency dependent T_1 above the minimum, but no dependency in the calculated values. This implies that the Cole–Davidson model is incomplete for the present results, but we need a mixing of the other distribution model to some extent, for example, the Cole–Cole-type model[19,21] having a symmetric τ distribution.

ΔM_2 of 13.0×10^{-2} mT^2 reduced through the excitation of the pseudo-C_3 reorientation determined from the T_1 minimum value in $AlPO_4$-5 is much larger than 7.16×10^{-2} mT^2 for the same motion in SAPO-5, whereas $\Delta M_2 = 0.59 \times 10^{-2}$ mT^2 for the onset of the isotropic reorientation in $AlPO_4$-5 is much smaller than 2.94×10^{-2} mT^2 in SAPO-5. The observed ΔM_2 of 13.0×10^{-2} mT^2 in $AlPO_4$-5 larger than 10.8×10^{-2} mT^2 theoretically calculated for this motion can be explained by the onset of the tumbling of the pseudo-C_3 axis together with the molecular C_3-reorientation. The large motional freedom obtained in the low-temperature range in $AlPO_4$-5 results in a small ΔM_2 value for the isotropic rotation.

Comparison of motional states of tetrapropylammonium (TPA) cations in MFI-zeolite

In the present molecular sieves, we observed the overall isotropic rotation of TEA molecules above *ca.* 120 K in $AlPO_4$-5 and *ca.* 200 K in SAPO-5. On the other hand, such high mobilities were unobserved in TPA ions used as a SDA in the MFI-zeolite[6] where reorientations of propyl groups were reported to be the highest freedom motion observed up to *ca.* 450 K, although the motional freedom in the zeolite was shown to be larger than in bulk bromide salt below room temperature. The high mobility in the present systems are attributable to smaller molecular size and smaller electrostatic interactions with the pore surface. In the analysis of T_1

Table 2 Activation energies (E_a), reductions of ^1H NMR second moment (M_2), correlation times at infinite temperature (τ_0) and parameter expressing the distribution of correlation time (β) for molecular motions derived from ^1H NMR spin–lattice relaxation times observed in triethylamine (TEA) adsorbed in $AlPO_4$-5 and SAPO-5

	E_a/kJ mol^{-1}	$\Delta M_2/10^{-2}$ mT^2	$\tau_0/10^{-12}$ s	β	Motional mode
$AlPO_4$-5(TEA)	15.0 ± 0.5	0.59 ± 0.2	5.90	—	Isotropic rotation
	10.5 ± 0.4	13.0 ± 0.5	0.544	0.30	Pseudo-C_3 rotation
SAPO-5(TEA)	14.7 ± 0.5	2.94 ± 0.3	5.00	—	Isotropic rotation
	8.0 ± 0.4	7.16 ± 0.4	6.20	0.70	Pseudo-C_3 rotation

observed in all of these zeolites, the introduction of the distributed motional correlation time τ was required. Our data were explained by applying the Cole–Davidson-type distribution, while those in TPA–MFI zeolite were analysed by the Williams–Watts model. These results imply that molecules in these types of molecular sieves take generally distributed orientations in micropores. This tendency is more marked in systems with a homogeneous pore structure like $AlPO_4$-5 with many possible orientations with different potential energies to each other.

Conclusion

In the temperature range of 90 K to room temperature, the ^1H NMR spectra and T_1 of TEA molecules adsorbed in $AlPO_4$-5 and SAPO-5 could be explained by the same motional modes, *i.e.*, molecular C_3 and isotropic reorientations, but they showed different temperature dependences in the former mode. The fact that the C_3 reorientation in $AlPO_4$-5 is hindered less than in SAPO-5 is explained by the formation of a hydrogen bond between the lone-pair electrons in nitrogen and the Brönsted acid sites on the pore surface in SAPO-5. This interaction favouring TEA molecules with the orientation of the C_3 axis perpendicular to the pore axis results in the τ distribution for the C_3 reorientation being smaller (larger β) than in $AlPO_4$-5 in which the TEA molecules can take random orientations of the molecular C_3 axis in the pore more than in SAPO-5 giving a wide variety of the τ values (smaller β) in $AlPO_4$-5.

It is noted in the present molecular sieves that the template molecules showed high mobilities such as the isotropic molecular reorientation in micropores. On the other hand, we observed a remarkable characteristic that the template molecules are stable and stay in micropores even heated up to 450 K *in vacuo*. This result seems to be related with pore structures in a long range or conditions of crystal surfaces. To discuss this phenomenon in detail, we need analysis on more structural data for various adsorbed molecular sieves.

Acknowledgements

We are grateful to Dr Y. Kiyozumi at the National Institute of Materials and Chemical Research for his kind advice for the preparation of molecular sieves. This work was partly supported by Grant-in Aid for scientific research No. (B) 09440234 and No. (C) 10640554 from the Ministry of Education, Science, Sports and Culture.

References

1 J. M. Bennett, J. P. Cohen, E. M. Flanigen, J. J. Pluth and J. V. Smith, *ACS Symp. Ser.*, 1983, **218**, 109.
2 S. T. Wilson, B. M. Lok and E. M. Flanigen, *US Pat.*, 4310440, 1982.
3 S. T. Wilson, B. M. Lok, C. A. Messina, T. R. Cannan and E. M. Flanigen, *J. Am. Chem. Soc.*, 1982, **104**, 1146.
4 G. Sastre, D. W. Lewis and C. R. A. Catlow, *J. Phys. Chem.*, 1996, **100**, 6722.
5 B. M. Lok, C. A. Messina, R. L. Pattpm, T. R. Cannan and E. M. Flanigen, *J. Am. Chem. Soc.*, 1984, **106**, 6092.
6 R. Gougeon, J. M. Chezeau and B. Meurer, *Solid State Nucl. Magn. Reson.*, 1995, **6**, 281.
7 D. Demuth, G. D. Stucky, K. K. Unger and F. Schüth, *Microporous Mater.*, 1995, **3**, 473.
8 G. Finger, J. Richter-Mendau, M. Bülow and J. Kornatowski, *Zeolites*, 1991, **11**, 443.
9 G. Finger and J. Kornatowski, *Zeolites*, 1990, **10**, 615.
10 J. G. Powles and J. H. Strange, *Proc. Phys. Soc.*, 1963, **82**, 6.
11 T. Kobayashi, H. Ohki and R. Ikeda, *Mol. Cryst. Liq. Cryst.*, 1994, **257**, 279.
12 D. Zhao, W. Pang, L. Li and G. Yang, *Chem. J. Chin. Univ.*, 1992, **13**, 1165.
13 H. Takeuchi, T. Kojima, T. Egawa and S. Konaka, *J. Phys. Chem.*, 1992, **96**, 4389.
14 C. H. Bushweller, S. H. Fleischman, G. L. Grady, P. McGoff, C. D. Rithner, M. R. Whalon, J. G. Brennan, R. P. Marcantonio and R. P. Domingue, *J. Am. Chem. Soc.*, 1982, **104**, 6224.
15 C. Crocker and P. L. Goggin, *J. Chem. Soc., Dalton Trans.*, 1978, 388.
16 R. A. Bennett and H. O. Hooper, *Mol. Phys.*, 1970, **19**, 85.
17 N. Bloembergen, E. M. Purcell and R. V. Pound, *Phys. Rev.*, 1948, **73**, 679.
18 A. Abragam, *Principles of Nuclear Magnetism*, Oxford University Press, London, 1961, ch. 10.
19 D. W. Davidson and R. H. Cole, *J. Chem. Phys.*, 1951, **19**, 1484.
20 T. M. Conner, *Trans. Faraday Soc.*, 1964, **60**, 1574.
21 K. S. Cole and R. H. Cole, *J. Chem. Phys.*, 1941, **9**, 341.

Paper a908962d

Mol. Cryst. and Liq. Cryst., 2000, Vol. 341, pp. 309-314
Reprints available directly from the publisher
Photocopying permitted by license only.

Adsorption and Electronic Properties in Tetramethylbenzidine-Intercalated Tetrasilicicfluormica

SHINICHI ISHIMARU, HITOMI SAWATARI and RYUICHI IKEDA

Department of Chemistry, University of Tsukuba, Tsukuba 305–8571, Japan

(In final form June 24, 1999)

Adsorption and electronic properties in tetramethylbenzidine-intercalated tetrasilicicfluormica were investigated by powder X-ray diffraction, ESR, TG, and DC-electric conductivity measurements.

Keywords: tetrasilicicfluormica; tetramethylbenzidine; XRD; ESR; TG; conductivity

INTRODUCTION

Colour reactions of clay minerals with aromatic amines are known as amine oxidation in the interlayer space of clays[1]. 3,3',5,5'-Tetramethyl-benzidine (TMB) exhibiting this reaction shows the molecular arrangement dependence on the adsorption level in the interlayer space of hectorite[2]: A low adsorption level gives yellow free radicals whose molecular plane is parallel to the clay surface, while green π-π charge-transfer complexes with the molecular axis vertical on the surface are formed at high adsorption levels.

In mica, which is a higher charged clay than hectorite, the density of charge transfer complexes in the interlayer space increases, the overlapping of their π orbitals is expected to spread over many amine molecules. At the

same time, this system can be expected to be a development of new pillared clays[3-4] with characteristic adsorption and interlayer environment. In this study, we examined the adsorption and electronic properties of TMB-intercalated tetrasilicicfluormica (TSFM) by thermo-gravimetry (TG), and measurements of electron spin resonance (ESR) and DC electric conductivity.

Experimental

Synthetic tetrasilicicfluormica ($Na_{0.75}Si_4Mg_{2.7}F_{0.85}OH_{1.2}O_{10}$) was kindly gifted by CO-OP Chemical Co. Ltd. Dihydrochloride (TMB•2HCl) of TMB was recrystallized from an HCl solution of TMB (Tokyo Kasei Co. Ltd.). Intercalation compounds were obtained by following procedure: An aqueous solution of TMB•2HCl was poured to Na-TSFM suspensions in distilled water and stirred for 30 min. and another solution for 12 hours, where the final suspensions was shown to contain TMB^{2+} ions 0.45 times Na^+ ions in original TSFM. The suspensions were centrifuged and washed by distilled water. The apparent colour of dried precipitations is yellow in the specimen after the stirring of 30 min. and dark yellow after 12 hours stirring. The specimen stirred for 30 min. was stable for more than several weeks, while the colour in the latter was immediately changed to deep green in moist air. They are abbreviated to TMB-TSFM(y) and TMB-TSFM(g) in the same order in the following discussion.

TG curves were recorded on a Seiko EXSTAR6000 TG/DTA, ESR spectra on a Bruker EMX-T spectrometer, and DC conductivity was measured by using an ADVANTEST R6144 programmable DC voltage generator and an Iwatsu model 7411 digital multimeter. The crystal (001) spacing in intercalated compounds was measured with a Philips X'pert PW3040 diffractometer. All measurements were carried out on powdered samples.

RESULTS AND DISCUSSION

Elemental Analysis, X-Ray Powder Diffraction and TG

The results of elemental analysis are shown in Table 1. Calculated values were obtained on the assumption that all TMB^{2+} ions in the suspensions exchanged Na^+ ions in TSFM. From Table 1, it was found that both C and N contents are almost 90 % of calculated values in both TMB-TSFM(y) and TMB-TSFM(g) (the rest seems to be Na^+ ions), *i.e.*, the adsorption process was mostly completed within 30 min. An increase of H contents in TMB-TSFM(g) implies the existence of adsorbed or coordinated water.

TABLE1 Results of elemental analysis

specimens	C(%)	H(%)	N(%)
TMB-TSFM(y)	12.2	1.72	1.83
TMB-TSFM(g)	12.6	2.10	1.87
calc.	14.0	2.23	2.04

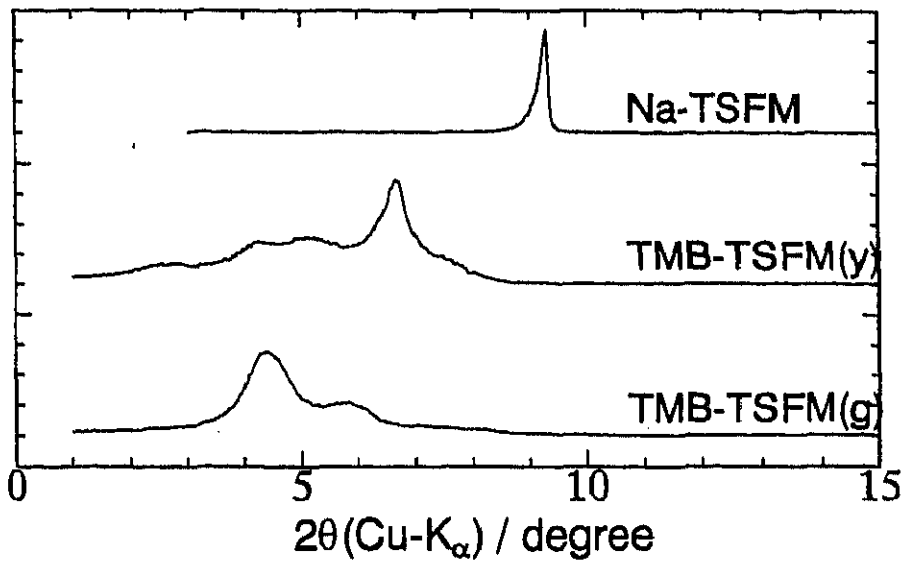

FIGURE 1 X-Ray reflections from (001) in powdered Na-TSFM, TMB-TSFM(y) and TMB-TSFM(g).

X-ray powder diffraction data revealed expansion of *d*-spacing for (001)

by intercalation. Broad and dispersed peaks imply inhomogeneity in the intercalation compounds. Observed several broad peaks suggest that the obtained samples contain some mixtures with different *d*-spacings, but they were used without farther purification in this study. The main peak corresponds to 13.3 Å spacing for (001) in TMB-TSFM(y) while 20.1 Å in TMB-TSFM(g). This suggests that TMB^{2+} ions were adsorbed as flat on the clay surface at first then they rearranged to vertically to the surface[2]. The TG measurement on TMB-TSFM(g) showed a weight-loss attributable to the desorption of water in a wide temperature range above room temperature, while TMB-TSFM(y) showed no considerable loss. The amount of water adsorbed on TMB-TSFM(g) was estimated from the weight-loss to be *ca.* 2.4 molecules per TMB^{+} ion. These facts imply that the water molecules adsorbed in micro- or mesopore in TMB-TSFM(g).

ESR spectra

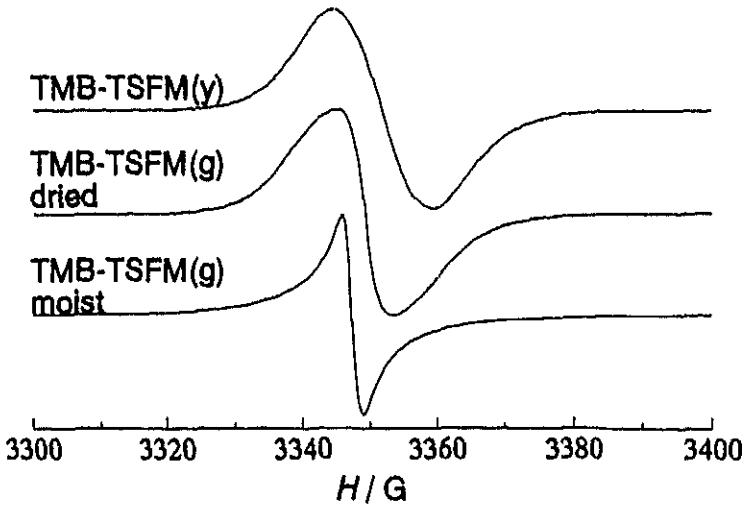

FIGURE 2 ESR spectra of TMB-TSFM complexes observed at room temperature.

ESR spectra were measured at room temperature in a specimen of TMB-TSFM(y) and two of TMB-TSFM(g): one of green specimen was dried *in*

vacuo and, in the other, water was adsorbed in moist air (Fig. 1). A broad

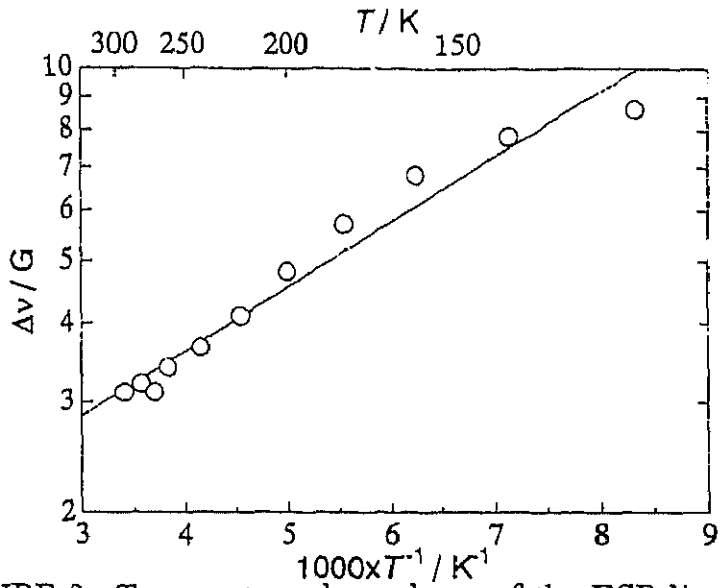

FIGURE 3 Temperature dependence of the ESR line-width ($\Delta\nu$) in moist TMB-TSFM(g). The solid line represents a best-fitted line.

ESR absorption line observed in TMB-TSFM(y) indicates that TMB ions are adsorbed as free radicals[2]. In desiccated TMB-TSFM(g) giving dark yellow colour, the absorption line was broad, whereas narrow in the moist green specimen. This implies that the charge transfer between TMB ions was assisted by adsorbed water molecules.

The ESR line-width of the moist TMB-TSFM(g) was increased with decreasing temperature (Fig. 3) and coincided at 120 K with that of the dried specimen at room temperature. This temperature dependence corresponds to an activation process of electron transfer and the activation energy of this process can be roughly estimated to be *ca.* 9±1 kJ mol^{-1} from the slope.

DC electric conductivity

It is expected in this system that the charge transfer occurs not only in pairs of

TMB ions but over many ions arranged vertically in the interlayer space. DC electric conductivity was measured at room temperature to confirm the delocalization of electrons. Because of the large resistance, conductivities could not be obtained in TMB-TSFM(y) and dried TMB-TSFM(g) where TMB is intercalated as free radical, for their large resistance. On the other hand, moist TMB-TSFM(g) showed a time dependent conductivity of *ca.* 10^{-6} S m^{-1} at immediately after starting the measurement, then it decreased continuously to a constant value of *ca.* 10^{-7} S m^{-1}, within *ca.* 10 min. The time dependent component is assignable to the polarization of ammonium protons in TMB^{2+} ions associated with the intercalated water, and the constant component is attributed to the electron conduction.

Because the electric conduction is limited in the 2-D interlayer space, the observed conductivity was low in our powder experiments. To get a higher conductivity, we need a measurement of oriented films.

Acknowledgements

This work was partly supported by Grant-in-aid for Scientific Research No. (B)0944023 and (C)10640554 from the Ministry of Education, Science, Sports and Culture, Japan.

The authors are grateful to Chemical Analysis Center, University of Tsukuba, for elemental analysis, TG and ESR measurements.

References

[1] D. T. B. Tennakoon, J. M. Thomas, M. J. Tricker, *J. Chem. Soc. Dalton Trans.*, **20,** 2211(1974).
[2] M. B. McBride, *Clays Clay Mineral.*, **33,** 510(1985).
[3] R. M. Barrer and D. M. MacLeod, *Trans. Faraday Soc.*, **51,** 1290(1955).
[4] *Pillared Clays,* edited by R. Burch, *Catal. Today,* **2,** 185(1988).

Mol. Cryst. and Liq. Cryst., 2000, Vol. 341, pp. 315-320
Reprints available directly from the publisher
Photocopying permitted by license only

Dynamics of n-Octylammonium Ions Intercalated in Saponite

MIHO YAMAUCHI, SHIN'ICHI ISHIMARU and RYUICHI IKEDA

Department of Chemistry, University of Tsukuba, Tsukuba 305–8571, Japan

(In final form June 25, 1999)

Dynamic behavior of n-octylammonium ions intercalated into saponite was investigated by ^{2}H and ^{1}H solid NMR method. Obtained data indicate distributions in the rate of cationic axial reorientations characterized by the heterogeneity of charge distribution in the saponite layer plane. Above ca. 400 K, in-plane random reorientations of cations were observed as a new kind of motion in the 2-D ionic system.

Keywords: solid state NMR; n-octylammonium; saponite; T_1; quadrupole coupling constant

INTODUCTION

It has been reported[1] that n-alkylammonium ions can be intercalated into layered clay minerals carrying negative charges in the wall, and, in clays with a low concentration of layer charges such as smectites, cations are arranged with their long axes parallel to the sheet. Since anionic sites in the wall are randomly located in clays, obtained alkylammonium systems can be regarded as two-dimensional cationic aggregates with randomly distributed positions as well as orientations. Our interest is the dynamic behavior in such two-dimensional systems and, in the present study, we intend to inv

EXPERIMENTAL

Intercalation of n-octylammonium ions into Na-saponite (a reference clay of the Clay Society of Japan, JCSS-3501) was performed by the ion exchange method. Obtained n-$C_8H_{17}NH_3$-saponite, and a deuterated analog, n-$C_8H_{17}ND_3$-saponite, are hereafter designated C8-SP and C8d_3-SP, respectively. Identification of C8-SP was carried out by elemental analysis and powder X-ray diffraction (XRD). ^{2}H NMR spectra in C8d_3-SP were observed at a Larmor frequency of 46.05 MHz with a Bruker MSL-300 NMR system. ^{1}H NMR spin-lattice relaxation times (T_1) in C8-SP and C8d_3-SP were determined with a home-made apparatus at 50.4 and 23.5 MHz, and 48.9 MHz, respectively.

RESULTS AND DISCUSSION

Sample Identification

The interlayer distance in C8-SP obtained by subtracting the layer thickness 0.96 nm[2] from *d*-spacing of the (001) peak of XRD patterns observed in C8-SP was 0.4±0.1 nm, indicating that n-octylammonium ions are intercalated into saponite and arranged their long axes parallel to the clay layers.

The elemental analysis in C8-SP showed that 58 % of Na in Na-SP was exchanged with n-octylammonium cations implying that the available area for a cation was ca. 0.75 nm^2. Since the area of a flat-lying n-octylammonium ion, ca. 0.60 nm^2 is close to 0.75 nm^2, we can presume that a two-dimensional phase of densely packed n-octylammonium ions was formed between the saponite layers.

NMR Measurements

^{2}H NMR spectra observed in a temperature range 116-480 K were shown to consist of superposed broad and sharp components. With increasing temperature, the broad component narrowed gradually and the proportion of the sharp one increased. This fact suggests the presence of several kinds of n-octylammonium ions in different motional states, namely, the sharp and broad components in the spectra originate from mobile and restricted ions,

respectively. Quadrupole coupling constants (QCC) determined from the linewidth of the broad component of ^2H spectra are shown in Fig. 2. The QCC of 50 ± 5 kHz obtained at 116 K was smaller than 58 kHz calculated for rotating ND_3^+ groups about the C_3 axis derived from 173 kHz observed in rigid $C_2H_5ND_3^+$[3], indicating that this motional mode has already been excited below 116 K. Over a wide range 116-400 K, QCC gradually decreased from 50 to 20 ± 10 kHz being smaller than 22 kHz calculated for the model of the cationic uniaxial rotation about its long axis. This unusually gradual reduction suggests that the reorientational correlation time of the uniaxial rotation is widely distributed. Above 400 K, it is expected that a large amplitude motion of the whole ion in the two dimensional interlayer space is excited together with the axial rotation because of the narrowed width of ca. 5 kHz observed in this temperature region.

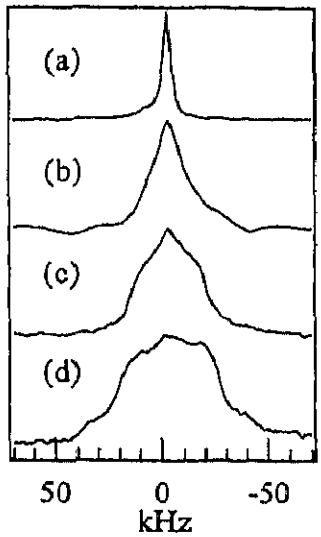

FIGURE 1 ^2H NMR spectra in C8-SP at 480 K(a), 380 K(b), 340 K(c) and 116 K(d).

The ^1H NMR spin-lattice relaxation times (T_1) measured in C8-SP and C8d_3-SP are shown in Fig. 3. We observed a broad and a sharp minimum around 150 and 450 K, respectively. The T_1 data in C8-SP and C8d_3-SP were nearly the same in the whole temperature range studied except for the range 160-300 K, where T_1 in C8d_3-SP was longer than those in C8-SP. This implies that the broad T_1 minimum consists of two minima: one in the high-

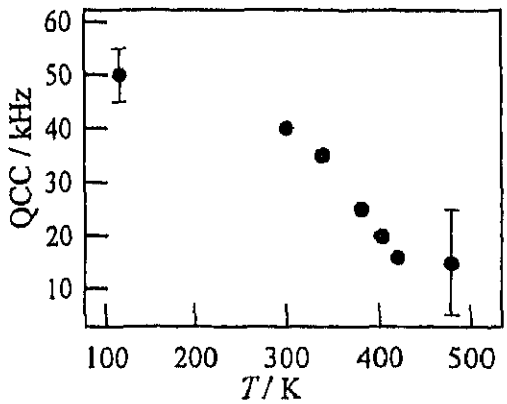

FIGURE 2 Temperature dependence of ^2H quadrupole coupling constant.

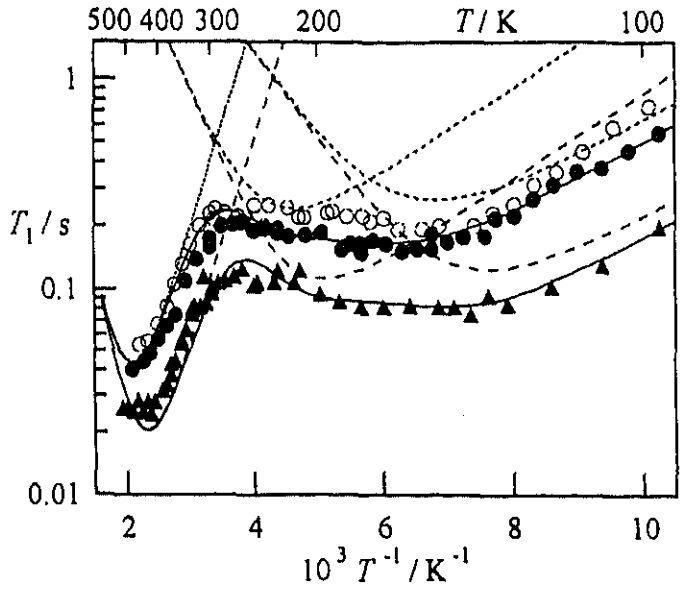

FIGURE 3 ^{1}H NMR spin-latticerelaxation times T_1 observed at 50.4 MHz(●) and 23.5 MHz (▲) in C8-SP, and at 48.9 MHz (○) in C8d_3-SP. The lines denote values calculated by introducing distributions in correlation times. See text.

temperature region, which was affected by the deuteration, is attributable to a motion of NH_3^+ groups, while the other in low-temperatures can be explained by the CH_3 rotation. Taking into consideration of the QCC decrease in the range 116-480 K, The T_1 minimum observed around 450 K was assigned to the uniaxial rotation of n-octylammonium ions about the long axis. In case T_1 relaxation is caused by a molecular motion, the BPP-type equation with a single correlation time τ has been shown to be an acceptable approximation[4]. It is noted, however, that observed T_1 values around the minima are longer than those estimated from the simple BPP theory: the T_1 minimum values observed around 160 and 400 K were ca. 0.17 and 0.075 s, while those calculated for NH_3^+- and uniaxial rotations are 0.13 and 0.021 s, respectively. Here, we introduce a distribution in the correlation time τ to explain these shallow minimum values and, at the same time, the gradual reduction of QCC. Assuming the Cole-Davidson type distribution[5] given by

$$g(\tau) = \frac{\sin\beta\pi}{\pi}\left(\frac{\tau}{\tau_0 - \tau}\right)^{\beta} \quad \tau \le \tau_0 \text{, or} \quad = 0 \quad \tau > \tau_0 \qquad (1),$$

where $\beta(0<\beta\leqq 1)$ is a measure of the distribution and τ_0 is the long limit of τ, we can obtain T_1 written as

$$\frac{1}{T_1'} = \frac{2}{3}\gamma^2 \Delta M_2 \left\{ \frac{\tau_0 \sin(\beta \tan^{-1}\omega\tau_0)}{\omega\tau_0(1+\omega^2\tau_0^2)^{\beta/2}} + \frac{2\tau_0 \sin(\beta \tan^{-1} 2\omega\tau_0)}{\omega\tau_0(1+4\omega^2\tau_0^2)^{\beta/2}} \right\} \qquad (2)$$

where γ, ΔM_2, and ω are the gyromagnetic ratio of a proton, the reduction in M_2 of the ^{1}H NMR line-width by the onset of the motion, and the angular Larmor frequency, respectively. Here, we assume an Arrhenius-type activation process given by

$$\tau = \tau_\infty \exp\left[\frac{E_a}{RT}\right] \qquad (3),$$

where E_a is the activation energy and τ_∞ is the correlation time in the limit of infinite temperature. The observed T_1 data in C8-SP were fitted by the superposition of three theoretical curves calculated by using Eqs. (1)-(3), as shown in Fig. 2, where dotted and broken lines are respective T_1 components calculated at 50.4 and 23.5 MHz and the sums are expressed by solid lines. The motional parameters determined by the fitting are shown in Table 1. It can be seen that T_1 calculated by introducing the τ distribution reproduces the experimental T_1 data, and ΔM_2 values obtained in this calculation agree well with those calculated for the CH_3-, NH_3^+- and uniaxial rotation as shown in Table 1. It is noted that the intramolecular motions as well as the overall uniaxial rotation are characterized by the distributed correlation times. E_a of 27 kJ mol^{-1} for the uniaxial rotation in C8-SP is much larger than 5-18 kJ mol^{-1} reported for rotator phases in n-alkylammonium salts[6, 7], where the axial rotation of the whole cations is excited. These results can be explained by the differences in space available for the cationic motion; i.e., the spacing between clay sheets is ca. 0.4 nm in C8-SP, while the spacing for the rotation in the rotator phase has been reported ca. 0.55 nm in n-dodecylammonium chloride[7].

The heterogeneity observed in n-octylammonium motions expected to be caused by the inhomogeneous charge distribution in clay layers. This result and the high E_a for cationic rotations imply that dynamic properties of n-

octylammonium ions in saponite are strongly influenced by clay's nature. On the other hand, the ^{2}H spectra observed above 400 K in C8d_3-SP are narrowed to ca. 5 kHz, being smaller than ca.15 kHz observed in the rotator phase of deuterated n-dodecylammonium chloride[7]. This implies that the order parameter giving the degree of dynamic distribution of the cationic axis orientation becomes ca. 0.23 in the present system much smaller than ca. 0.6 in the rotator phase of $C_{12}H_{25}NH_3Cl$. This in-plain cationic reorientation can be regarded as a characteristic new mode of motion in the layered clay minerals.

TABLE 1 The fitting parameters of ^{1}H NMR spin-lattice relaxation time. The values in parentheses show those calculated by BPP theory.

Motional Mode	E_a / kJ mol^{-1}	ΔM_2 / G^2	β
CH_3-rot	8.0±0.4	2.7±0.2(2.5)	0.4±0.2
NH_3^+-rot	13±0.5	3.6±0.4(3.7)	0.3±0.2
uniaxial-rot	27±2	12±1(10.5)	0.7±0.1

Acknowledgment

This work was partly supported by Grant-in-aid for Scientific Research No. (B)0944023 and (C)10640554 from the Ministry of Education, Science, Sports and Culture, Japan. The authors are grateful to Chemical Analysis Center, University of Tsukuba, for elemental analysis.

References

[1] G. Lagaly, *Clays Clay Minerals*, **27**, 1(1979).
[2] T. Endo, T. Sato and M. Shimad, *J. Phys. Chem. Solids*, **47**, 799(1986).
[3] M. J. Hunt and A. L. Mackay, *J. Magn. Reson.*, **15**, 402(1974).
[4] N. Bloembergen, E. M. Purcell and R. V. Pound, *Phys. Rev.*, **73**, 679 (1948).
[5] D. W. Davidson and R. H. Cole, *J. Chem. Phys*, **19**, 1484(1951).
[6] S. Fukuda, R. Ikeda and D. Nakamura, *Bull. Chem. Soc, Jpn.*, **57**, 2802 (1984).
[7] S. Tanaka, N. Onoda-Yamamuro, S. Ishimaru and R. Ikeda, *Bull. Chem. Soc. Jpn.*, **70**, 2981(1997).

PCCP

Ionic plastic phases in trimethylammonium trifluoroacetate studied by ^1H and ^{19}F NMR spectroscopy, X-ray diffraction and thermal measurements

Koji Kuchitsu,[a] Hiroshi Ono,[a] Shin'ichi Ishimaru,[a] Ryuichi Ikeda[a] and Hiroyuki Ishida*[b]

[a] *Department of Chemistry, University of Tsukuba, Tsukuba 305-8571, Japan*
[b] *Department of Chemistry, Faculty of Science, Okayama University, Okayama 700-8530, Japan*

Received 25th May 2000, Accepted 11th July 2000
Published on the Web 7th August 2000

^1H and ^{19}F NMR, differential scanning calorimetric and X-ray powder diffraction measurements were carried out in solid trimethylammonium trifluoroacetate, $(CH_3)_3NHCOOCF_3$. Two solid–solid phase transitions were observed at 307 and 330 K. The structures of the solid phases obtained above 330 K and between 307 and 330 K are CsCl-type cubic and tetragonal, respectively. In the two phases, both cations and anions perform self-diffusion and isotropic rotation. From the dynamic behaviour of the ions together with thermal data, both phases are assignable as ionic plastic phases.

Introduction

It is known that various methyl-substituted ammonium salts consisting of simple monovalent inorganic anions, such as ClO_4^-,[1–8] NO_3^-,[1,9] I^-,[10,11] Br^-,[12–14] SCN^-[15,16] and BF_4^-,[17,18] form a novel mesophase just below their melting or decomposition temperatures, the structure of which is CsCl- or NaCl-type cubic. In this phase, both cation and anion groups perform isotropic rotation, resulting in orientational disorder as in plastic phases of molecular crystals.[19,20] Further, the ionic self-diffusion of the ions was detected on the NMR time-scale. Recently, we have extended studies on the mesophase to salts containing bulky cations such as triethylammonium,[21] trimethylethylammonium,[22–24] piperidinium[25,26] and pyrrolidinium,[27] but counteranions have been limited to the small inorganic ions given above.

In this investigation, we undertook studies on trimethylammonium trifluoroacetate, $(CH_3)_3NHCOOCF_3$, with the expectation of obtaining the ionic plastic phase containing bulky organic anions. The detection of such a phase enables us to characterize more clearly the ionic plastic phase. For this purpose, we performed differential scanning calorimetry (DSC) and X-ray powder diffraction and measured ^1H and ^{19}F NMR spin–lattice relaxation time (T_1), spin–spin relaxation time (T_2) and second moment (M_2) of the ^1H and ^{19}F NMR linewidths.

Experimental

$(CH_3)_3NHCOOCF_3$ was prepared by neutralizing trimethylamine with trifluoroacetic acid. The crystals obtained were recrystallized twice from propan-1-ol. Anal. Calcd. for $(CH_3)_3NHCOOCF_3$ C, 34.69; H, 5.82; N, 8.09%. Found: C, 32.79; H, 6.01; N, 7.57%.

Before making DSC and NMR measurements, the samples were dried under dynamic vacuum (*ca.* 0.1 Pa) at room temperature for 24 h. DSC was carried out on a Seiko DSC 120 calorimeter with a heating rate of 1 K min^{-1} from 150 to 430 K. X-ray powder patterns were taken at *ca.* 300 and 380 K using a Philips X'Pert PW3050/00 diffractometer with Cu Kα radiation.

The second moments of the ^1H and ^{19}F NMR spectra were obtained with a Bruker SXP 100 spectrometer by applying the solid-echo method.[28] ^1H and ^{19}F NMR T_1 and T_2 values were measured on the same apparatus; the inversion-recovery method was used for the determination of T_1 and Hahn's spin-echo method[29] for T_2. The experimental uncertainty was estimated to be within 10% for T_1 and T_2. The sample temperature was controlled by the N_2 gas flow method with an accuracy of 1 K.

Results and discussion

Two solid–solid phase transitions and the melting temperature were recorded by DSC measurements at 307, 330 and 379 K, respectively. The solid phases revealed were designated Phases I to III in order of decreasing temperature. The X-ray powder patterns showed the crystal structures of Phase I and II to be CsCl-type cubic and tetragonal, respectively. The transition temperatures (T_{tra}), the associated enthalpy and entropy changes (ΔH and ΔS) and the structural parameters are presented in Table 1 together with the data for $(CH_3)_3NHClO_4$[7] and $(CH_3)_3NHBF_4$[17,30] for comparison; these salts are known to have three solid phases and to form a CsCl-type ionic plastic phase in the highest temperature solid phase. The cubic structure in Phase I implies that both the cation and anion are highly disordered and behave like spherical ions in the crystal. High disorder is also indicated by the observed melting entropy $\Delta_{fus}S$ of 17 J K^{-1} mol^{-1}, which, being less than 20 J K^{-1} mol^{-1}, meets the accepted criterion for the formation of the plastic phase in molecular crystals.[19,20] The radius of the rotating CF_3COO^- ion is estimated to be 2.62 Å using the radius of the rotating $(CH_3)_3NH^+$ ion of 2.71 Å, which is derived from the structural data for Phase I in $(CH_3)_3NHClO_4$ and $(CH_3)_3NHBF_4$, assuming the rotating radii of ClO_4^- and BF_4^- ions to be 2.36 and 2.28 Å, respectively.[31]

Although the structures of Phase II in the three salts are tetragonal, $(CH_3)_3NHCOOCF_3$ is not isomorphous with $(CH_3)_3NHClO_4$ and $(CH_3)_3NHBF_4$, as seen from Table 1. This difference in Phase II can be made clear by comparing the $\Delta_{tra}S$ values of $(CH_3)_3NHCOOCF_3$, $(CH_3)_3NHClO_4$ and

DOI: 10.1039/b004193i

Table 1 Structural parameters, transition temperatures (K), enthalpy changes (kJ mol^{-1}), and entropy changes (J K^{-1} mol^{-1}) for $(CH_3)_3NHX$ (X = CF_3COO^-, ClO_4^- and BF_4^-)

	CF_3COO^-	ClO_4^- [a]	BF_4^- [b]
Phase I (cubic)—			
a/Å	6.15(5)	5.845(1)	5.772(4)
V/Å^3	232(6)	199.7(2)	192.3(4)
D_x/Mg m^{-3}	1.24	1.327	1.269
Z	1	1	1
Phase II (tetragonal)—			
a/Å	8.54(5)	9.912(4)	9.815(5)
c/Å	5.31(5)	7.01(2)	6.895(5)
V/Å^3	387(9)	689(3)	664(2)
D_x/Mg m^{-3}	1.48	1.54	1.47
Z	2	4	4
Thermal data—			
T_{fus}	379(1)	~555	489(1)
$\Delta_{fus}H$	6.5(1)	(decomposition)	9.5(2)
$\Delta_{fus}S$	17(1)		19(1)
$T_{tra(II\rightarrow I)}$	330(1)	480(1)	453(1)
$\Delta_{tra}H_{(II\rightarrow I)}$	1.1(1)	3.96(5)	3.36(5)
$\Delta_{tra}S_{(II\rightarrow I)}$	3.2(3)	8.3(1)	7.4(1)
$T_{tra(III\rightarrow II)}$	307(1)	396(1)	384(1)
$\Delta_{tra}H_{(III\rightarrow II)}$	6.0(1)	1.0(2)	1.1(2)
$\Delta_{tra}S_{(III\rightarrow II)}$	20(1)	2.5(5)	2.9(5)

[a] Ref. 7. [b] Ref. 17 and 30.

$(CH_3)_3NHBF_4$. The large $\Delta_{tra}S_{(III\rightarrow II)}$ of 20 J K^{-1} mol^{-1} and the small $\Delta_{tra}S_{(II\rightarrow I)}$ of 3.2 J K^{-1} mol^{-1} in $(CH_3)_3NHCOOCF_3$ indicate that both the cation and anion have a large extent of orientational freedom in Phase II. The entropy change is approximated as $\Delta_{tra}S = R\ln(n_1/n_2)$, where n_1/n_2 is the ratio of the number of orientational freedoms of constituent molecules in the high and low temperature phases, respectively, assuming that the configurational entropy is the most dominant contribution.[32] A ratio of 11 is obtained for 20 J K^{-1} mol^{-1} and this value is believed to account for the change in the number of orientations of both ions at $T_{tra(III\rightarrow II)}$. On the other hand, the ions in $(CH_3)_3NHClO_4$ and $(CH_3)_3NHBF_4$ are considered to undergo little change in orientational freedom at $T_{tra(III\rightarrow II)}$ from $\Delta_{tra}S_{(III\rightarrow II)}$ of *ca.* 3 J K^{-1} mol^{-1}, much smaller than $\Delta_{tra}S_{(II\rightarrow I)}$ of *ca.* 8 J K^{-1} mol^{-1}.

Fig. 1 shows the temperature dependences of the ^{1}H and ^{19}F NMR M_2 values (abbreviated to M_{2H} and M_{2F}, respectively) observed in $(CH_3)_3NHCOOCF_3$ in the range 200–340 K. A sudden change in M_{2H} and M_{2F} was observed at $T_{tra(III\rightarrow II)}$ and they became less than 0.05 × 10^{-2} mT^2 in Phases I and II. This indicates that both ions change their motional modes from a hindered reorientation to the isotropic rotation at $T_{tra(III\rightarrow II)}$, in agreement with the above DSC results. Furthermore, the M_2 data imply the occurrence of translational self-diffusion of both ions, because M_2 calculated for the isotropically rotating cation and anion is 0.68 × 10^{-2} mT^2 for M_{2H} and 0.63 × 10^{-2} mT^2 for M_{2F}, hence the experimental values being smaller than these values can be explained only by the onset of self-diffusion. In the M_2 calculation, the ^{1}H and ^{19}F nuclei of the ions are assumed to be at the lattice point of the CsCl-type cubic lattice determined for Phase I. Hence, we can conclude that both Phases II and I of $(CH_3)_3NHCOOCF_3$ are plastic phases from the thermal data, *i.e.*, the small $\Delta_{fus}S$ and the large $\Delta_{tra}S_{(III\rightarrow II)}$, and the dynamic behaviour of the ions.

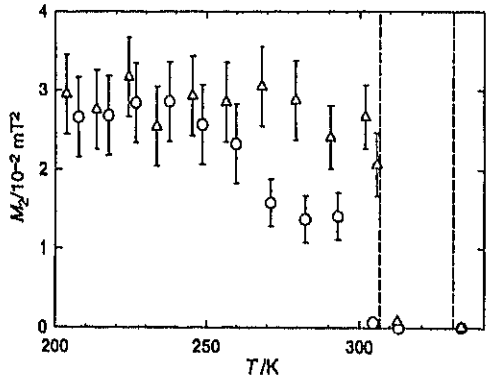

Fig. 1 Second moment (M_2) of ^{1}H (○) and ^{19}F (△) NMR linewidths observed in $(CH_3)_3NHCOOCF_3$. Broken lines show the phase transition temperatures determined by DSC.

Fig. 2 shows the temperature dependences of the ^{1}H NMR T_1 and T_2 values (abbreviated to T_{1H} and T_{2H}) observed at a Larmor frequency of 40.5 MHz, and the ^{19}F NMR T_1 and T_2 values (T_{1F} and T_{2F}) at 38.1 MHz in the range 250–380 K. From the M_2 results, we can assign the increase in T_{2H} and the decrease in T_{1F} with increasing temperature in Phase II to the cationic and anionic self-diffusion, respectively. Here the ionic rotation detected from M_2 measurement is assumed to be much faster than the self-diffusion; in other words, the correlation time of rotation ($\tau_{l,rot}$) and that of self-diffusion

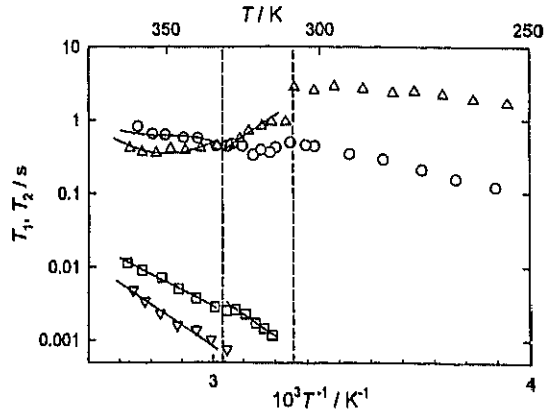

Fig. 2 ^{1}H and ^{19}F NMR spin–lattice (T_1) and spin–spin (T_2) relaxation times observed in $(CH_3)_3NHCOOCF_3$: T_{1H} at 40.5 MHz (○), T_{1F} at 38.1 MHz (△), T_{2H} at 40.5 MHz (□) and T_{2F} at 38.1 MHz (▽). Solid lines are the best-fitted values. Broken lines show the phase transition temperatures determined by DSC.

($\tau_{i,\,dif}$) of each ion (i = H and F for the cation and the anion, respectively) fulfill the conditions $\omega_i\tau_{i,\,rot} \ll 1$ and $\omega_i\tau_{i,\,dif} \gg 1$, where ω_H and ω_F are the Larmor frequencies of proton and fluorine nuclei, respectively. From the gradient of T_{2H} *vs.* T^{-1} plots, we evaluated the activation energy (E_a) of cationic self-diffusion as 56 ± 3 kJ mol^{-1}. For the anionic self-diffusion we obtained E_a of 58 ± 6 kJ mol^{-1} from the T_{1F} *vs.* T^{-1} plots.

In Phase I, T_{2H} and T_{2F} are longer than 1 ms and increases in T_{2H} and T_{2F} with temperature are attributable to the cationic and anionic self-diffusion, respectively. The E_a values of self-diffusion were evaluated to be 42 ± 2 and 55 ± 5 kJ mol^{-1} for the cation and the anion, respectively, from the slopes of T_{2H} and T_{2F}. The temperature dependence of T_{1H} and T_{1F} in Phase I can be explained from the anionic self-diffusion using the BPP-type equations:[33]

$$T_{1H}^{-1} = C_{HF}\{\tau/[1 + (\omega_H - \omega_F)^2\tau^2] + 3\tau/(1 + \omega_H^2\tau^2) + 6\tau/[1 + (\omega_H + \omega_F)^2\tau^2]\}$$

$$T_{1F}^{-1} = C_{FF}[\tau/(1 + \omega_F^2\tau^2) + 4\tau/(1 + 4\omega_F^2\tau^2)]$$

where ^{1}H–^{19}F and ^{19}F–^{19}F magnetic dipole interactions are taken into account for T_{1H} and T_{1F}, respectively, and C_{HF} and C_{FF} are the motional constants. The best fitted values using E_a obtained from T_{2H} and T_{2F} are shown in Fig. 2.

The E_a values obtained in Phases I and II show that the anionic self-diffusion is more hindered than the cationic diffusion, suggesting that the molecular weight has a greater effect than the molecular size on the self-diffusion. The same result was obtained in the ionic plastic phase of $(CH_3)_3NHClO_4$: the E_a of 55 kJ mol^{-1} for the cation is smaller than the 64 kJ mol^{-1} for the anion with a size much smaller than the cation.[6] Moreover, the influence of the molecular shape on the self-diffusion is derived from the fact that the E_a values of both ions in $(CH_3)_3NHCOOCF_3$ consisting of a heavy and bulky anion are smaller than those in $(CH_3)_3NHClO_4$. This can be explained by the non-spherical shape of the constituent ions, that is, in $(CH_3)_3NHCOOCF_3$ the rotating cation and anion can diffuse easily when each of the neighbouring ions has suitable orientations for ionic jumps.

Conclusion

We have found that $(CH_3)_3NHCOOCF_3$ crystallizes in a CsCl-type cubic lattice above 330 K and a tetragonal lattice between 309 and 330 K. Isotropic rotation and self-diffusion of the cation and the anion were observed in both phases. Since the dynamic properties of the ions in these phases are analogous to those in the plastic phase found in molecular crystals, these mesophases can be assigned to the ionic plastic phase. To our knowledge, this is the first example of an ionic plastic phase containing organic anions and also having a tetragonal structure. To obtain information on ionic rotations in Phases I and II, we are planning to perform neutron quasi-elastic scattering measurements.

Acknowledgements

This work was partly supported by Grants-in-Aid for Scientific Research, Nos. (B) 12440192 and (C) 10640554, from the Ministry of Education, Science, Sports and Culture.

References

1 H. Ishida, R. Ikeda and D. Nakamura, *Chem. Lett.*, 1982, 1943.
2 S. Jurga, *Phys. Status Solidi. A*, 1984, 81, 77.
3 S. Jurga and H. W. Spiess, *Z. Naturforsch. Teil A*, 1985, 40, 602.
4 S. Jurga and H. W. Spiess, *Ber. Bunsen-Ges. Phys. Chem.*, 1985, 89, 763.
5 S. Jurga, G. S. Harbison, B. Blümich, H. W. Spiess, F. Fujara and A. Olinger, *Ber. Bunsen-Ges. Phys. Chem.*, 1986, 90, 1153.
6 H. Ishida, R. Ikeda and D. Nakamura, *Bull. Chem. Soc. Jpn.*, 1987, 60, 467.
7 H. Ishida, Y. Kubozono, S. Kashino and R. Ikeda, *Z. Naturforsch., Teil A*, 1994, 49, 723.
8 Ishida and Y. Furukawa, *Z. Naturforsch Teil A*, 1996, 51, 83.
9 H. Ishida, R. Ikeda and D. Nakamura, *J. Chem. Soc., Faraday Trans. 2*, 1985, 81, 963.
10 H. Ishida, R. Ikeda and D. Nakamura, *Phys. Status Solidi. A*, 1982, 70, K151.
11 H. Ishida, R. Ikeda and D. Nakamura, *Bull. Chem. Soc. Jpn.*, 1986, 59, 915.
12 M. Tansho, D. Nakamura and R. Ikeda, *Z. Naturforsch. Teil A*, 1989, 44, 738.
13 M. Tansho, D. Nakamura and R. Ikeda, *J. Chem. Soc., Faraday Trans.*, 1991, 87, 3255.
14 M. Tansho, D. Nakamura and R. Ikeda, *Ber. Bunsen-Ges. Phys. Chem.*, 1991, 95, 1643.
15 T. Tanabe, R. Ikeda and D. Nakamura, *Phys. Status Solidi. A*, 1989, 114, K143.
16 T. Tanabe, R. Ikeda and D. Nakamura, *J. Chem. Soc., Faraday Trans.*, 1991, 87, 987.
17 H. Ishida, N. Hayama and R. Ikeda, *Chem. Lett.*, 1992, 1333.
18 H. Ishida. T. Iwachido and R. Ikeda, *Ber. Bunsen-Ges. Phys. Chem.*, 1992, 96, 1468.
19 *The Plastically Crystalline State*, J. N. Sherwood, Wiley, New York, 1979.
20 J. M. Chezeau and J. H. Strange, *Phys. Rev.*, 1979, 53, 1.
21 H. Ono, R. Seki, R. Ikeda and H. Ishida, *J. Mol. Struct.*, 1995, 345, 235.
22 H. Ishida, Y. Furukawa, S. Kashino, S. Sato and R. Ikeda, *Ber. Bunsen-Ges. Phys. Chem.*, 1996, 100, 433.
23 H. Ono, R. Ikeda and H. Ishida, *Ber. Bunsen-Ges. Phys. Chem.*, 1996, 100, 1833.
24 H. Ono, S. Ishimaru, R. Ikeda and H. Ishida, *Bull. Chem. Soc. Jpn.*, 1997, 70, 2963.
25 H. Ono, S. Ishimaru, R. Ikeda and H. Ishida, *Chem. Phys. Lett.*, 1997, 275, 485.
26 H. Ono, S. Ishimaru, R. Ikeda and H. Ishida, *Ber. Bunsen-Ges. Phys. Chem.*, 1998, 102, 650.
27 H. Ono, S. Ishimaru, R. Ikeda and H. Ishida, *Bull. Chem. Soc. Jpn.*, 1999, 72, 2049.
28 J. G. Powles and J. H. Strange, *Proc. Phys. Soc.*, 1963, 82, 6.
29 E. L. Hahn, *Phys. Rev.*, 1950, 80, 580.
30 H. Ishida, S. Kashino and R. Ikeda, to be published.
31 A. F. Kapustinski, *Q. Rev. Chem. Soc.*, 1956, 10, 283.
32 N. G. Parsonage and L. A. K. Staveley, *Disorder in Crystals*, Clarendon Press, Oxford, 1978.
33 A. Abragam, *The Principles of Nuclear Magnetism*, Oxford University Press, London, 1961.

13 October 2000

ELSEVIER

Chemical Physics Letters 329 (2000) 7–14

CHEMICAL PHYSICS LETTERS

www.elsevier.nl/locate/cplett

Hydrogen transfer in hydrogen-bonded chloranilic acid studied by ^{35}Cl NQR I – a 1:2 complex with 1,4-diazine

Taka-aki Nihei [a], Shin'ichi Ishimaru [a], Hiroyuki Ishida [b], Hideta Ishihara [c], Ryuichi Ikeda [a,*]

[a] *Department of Chemistry, University of Tsukuba, Tsukuba 305-8571, Japan*
[b] *Department of Chemistry, Faculty of Science, Okayama University, Okayama 700-8530, Japan*
[c] *Department of Chemistry, Faculty of Culture and Education, Saga University, Saga 840-8502, Japan*

Received 12 July 2000; received in final form 23 August 2000

Abstract

^{35}Cl NQR frequencies and spin-lattice relaxation time (T_{1Q}) and ^{1}H NMR relaxation times (T_{1H}) in a H-bonded three molecular system, chloranilic acid–1,4-diazine (1:2) were measured to reveal H-motions in a symmetric two H-bonds in solid. A single ^{35}Cl NQR frequency observed implies that the time-averaged structure of chloranilic acid is roughly monovalent in accordance with pK_a values in both acid and base. T_{1H} temperature dependence was explained by a single relaxation mechanism due to the correlated H-transfer in two H-bonds, while that of T_{1Q} yielded two relaxation processes. One of these undetected by ^{1}H NMR was explained by the uncorrelated H-transfer. © 2000 Elsevier Science B.V.

1. Introduction

Intermolecular H-bonding plays an important role in forming anisotropic interactions in condensed systems in which the hydrogen transfer through H-bonds between molecules enabling charge and energy transfers in solid and biological systems has been intensively studied in connection with ferro- and antiferro-electrics [1], dipolar glasses [2] and molecular solitons [3]. In our previous study [4], we reported for the first time that NQR can be used as a quite sensitive technique to detect the H-transfer by applying this method to *p*-chlorobenzoic acid forming a H-bonded dimer structure in crystals [5]. In that study, the ^{35}Cl NQR relaxation measurement even at a position remote from H-bonds can provide an effective probe much more sensitive than the familiar ^{1}H NMR technique. This is because a marked fluctuation of electric field gradient (efg) at resonant nuclei far from the hydrogen atoms can be made through π-electron systems in case the molecular charge is changed by H-transfer between molecules. On the other hand, ^{1}H NMR relaxation due to the fluctuation of magnetic dipolar interactions caused by hydrogen transfers can provide

* Corresponding author. Fax: +81-298-53-6503.
E-mail address: ikeda@chem.tsukuba.ac.jp (R. Ikeda).

0009-2614/00/$ - see front matter © 2000 Elsevier Science B.V.
PII: S0009-2614(00)00985-4

only a small contribution to the total relaxation because of a small displacement of H-atoms in jumping processes.

In the present study, we intend to detect new hydrogen transfer modes applying the NQR method to a H-bonded three molecular system, (chloranilic acid)–(1,4-diazine) 1:2 complex. In this system, three kinds of different ionic structures of chloranilic acid can be formed by H-transfers in two hydrogen bonds in this molecular system, where we can expect more complicated H-motions compared with the previous *p*-chlorobenzoic acid dimers [4].

2. Experimental

A molecular complex of chloranilic acid ($C_6O_2Cl_2(OH)_2$) with 1,4-diazine ($C_4H_4N_2$) with a ratio of 1:2 was prepared according to the literature [6] and obtained dark purple crystals were recrystallized from methanol. A partial deuterated analogue $C_6O_2Cl_2(OD)_2$–$(C_4H_4N_2)_2$ was obtained by repeated crystallizations of the protonated compound from CH_3OD.

^{35}Cl NQR frequencies were measured with a Dean-type external quenching superregenerative spectrometer with Zeeman modulation [7] in a temperature range 77 K to room temperature. The ^{35}Cl NQR spin-lattice relaxation time (T_{1Q}) was measured with a home-made pulsed spectrometer reported elsewhere [8] in the same temperature range for the protonated sample and 77–130 K for the deuterated analogues. A 180°–τ–90° pulse sequence was used for determining T_{1Q}. ^1H NMR spin-lattice relaxation time (T_{1H}) in the protonated sample was measured with a home-made pulsed spectrometer [9] at a Larmor frequency of 54.3 MHz in a range 85–300 K applying the saturation recovery method.

3. Results

Temperature dependences of ^{35}Cl NQR frequencies observed in $C_6O_2Cl_2(OH)_2$–$(C_4H_4N_2)_2$ and $C_6O_2Cl_2(OD)_2$–$(C_4H_4N_2)_2$ are shown in Fig. 1. A single resonance frequency was observed at

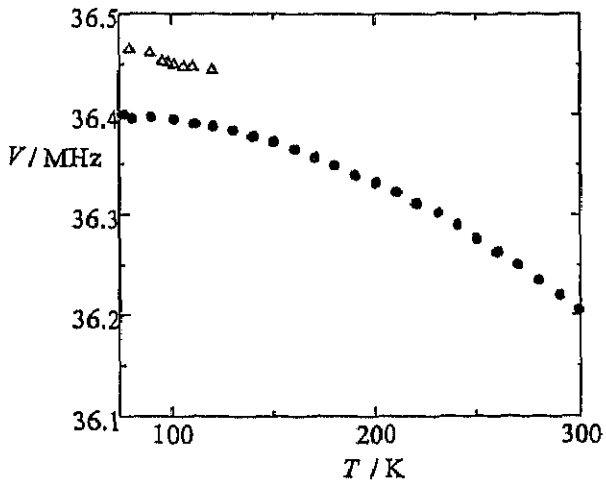

Fig. 1. Temperature dependences of ^{35}Cl NQR frequencies observed in $C_6O_2Cl_2(OH)_2$–$(C_4H_4N_2)_2$(•), and $C_6O_2Cl_2(OD)_2$–$(C_4H_4N_2)_2$(Δ).

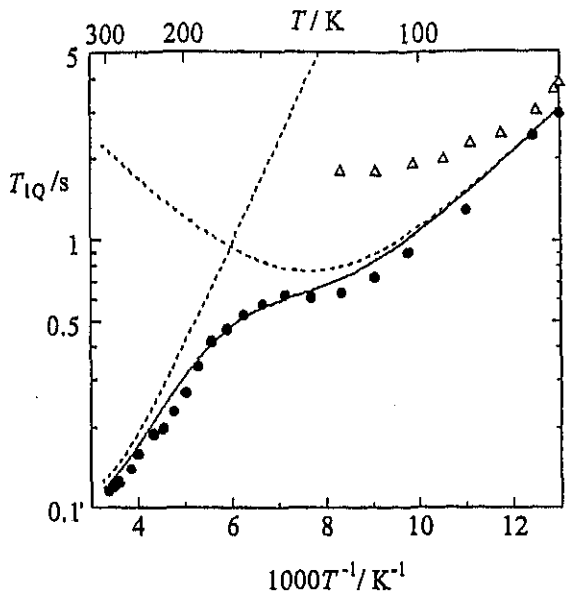

Fig. 2. Temperature dependences of the ^{35}Cl NQR spin-lattice relaxation times T_{1Q} observed in $C_6O_2Cl_2(OH)_2$–$(C_4H_4N_2)_2$(•), and $C_6O_2Cl_2(OD)_2$–$(C_4H_4N_2)_2$ (Δ). The filled curve is the best-fitted, calculated values expressed by the superposition of two components (dashed curves).

36.3997 ± 0.0005 and 36.466 ± 0.001 MHz at 77 ± 1 K for the protonated and deuterated analogues, respectively. These results agree with the crystal structure of the protonated complex that all chlorine atoms in crystals are equivalent at room temperature [6]. Upon heating, these resonance frequencies were gradually decreased and weakened, and disappeared in the noise level at ca. 300 and 120 K in protonated and deuterated analogues, respectively.

Temperature dependences of ^{35}Cl NQR spin-lattice relaxation time (T_{1Q}) observed in both analogues are shown in Fig. 2. On heating the protonated salt from 77 K, T_{1Q} was decreased, and showed a shallow minimum of ca. 600 ms at ca. 120 K. Upon further heating to room temperature, T_{1Q} again decreased down to ca. 100 ms. On the other hand, the deuterated salt showed T_{1Q} longer than in the protonated salt in the temperature range studied, where it decreased on heating and became almost temperature independent above ca. 110 K.

A temperature dependence of ^1H NMR spin-lattice relaxation time (T_{1H}) observed in the protonated salt at 54.3 MHz is shown in Fig. 3. A single long T_{1H} minimum of ca. 45 s was observed at 135 K.

4. Discussion

4.1. ^{35}Cl NQR frequencies

NQR frequencies gradually decreased upon heating from 77 K in both salts shown in Fig. 1 and can be explained by the normal Bayer-type lattice vibrations [10].

NQR frequencies in chloranilic acid ($C_6O_2Cl_2(OH)_2$) and its sodium salt ($C_6O_2Cl_2(ONa)_2$) observed at 77 K were reported to be 37.15, and 35.538 and 34.853 MHz [11], respectively. If we assume the formal charges on chloranilic acid and its sodium salt to be zero and −2, respectively, then we can see that the

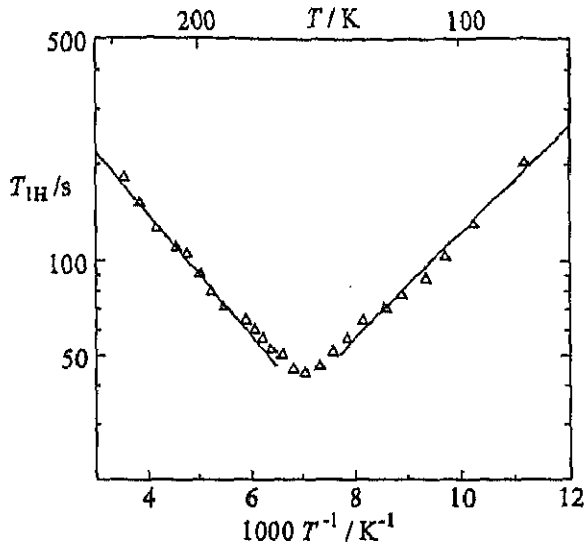

Fig. 3. A temperature dependence of the ^{1}H NMR spin-lattice relaxation time T_{1H} observed in $C_6O_2Cl_2(OH)_2$–$(C_4H_4N_2)_2$ at a Larmor frequency of 54.3 MHz. Solid lines are drawn to obtain activation energies.

frequency (36.4 MHz) observed in the present salt at 77 K comes to almost at the centre (36.2 MHz) of frequencies in the compounds with the two extreme structures. This result implies that chloranilic acid in the present system is partially ionized and its formal charge is close to −1. Since the presence of inversion symmetry in all chloranilic acid molecules in crystals was shown from X-ray diffraction at room temperature [6], we can expect that the equal contribution from the following formulas I and II are the most probable time-averaged structure at low temperatures:

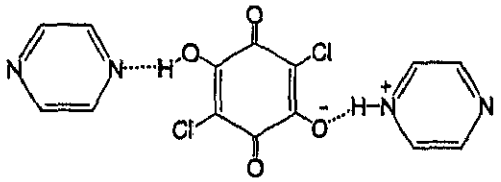

I

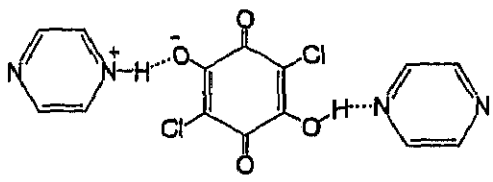

II

The formation of these ionic structures can be supported from the fact that chloranilic acid and 1,4-diazine act as moderately strong acid and base with pK_{a1} values of 0.76 and 0.57, respectively, in aqueous solution [12–14].

4.2. ^{1}H NMR relaxation time (T_{1H})

The long T_{1H} minimum of 45 s observed in the protonated salt at ca. 135 K was attributed to the averaging of magnetic dipolar interactions due to the H-transfer motion O–H---N ↔ O^----H–N^+ by the following reasons: first, ^{1}H NMR T_{1H} observed in the partially deuterated salt with OD groups around the

T_{1H} minimum temperature range gave T_{1H} values much longer than 500 s. This indicates that motions of protons in the hydrogen bond contributes to this relaxation. Second, we performed a rough calculation of the decrease in the second moment (ΔM_2) of ^{1}H NMR line which can be connected with T_{1H} by applying the BPP-type relaxation mechanism to be [15]

$$T_{1H}^{-1} = (2/3)\gamma^2 \Delta M_2 \left[\tau/(1+\omega_H^2\tau^2) + 4\tau/(1+4\omega_H^2\tau^2)\right], \quad (1)$$

where γ, τ and ω_H are the ^{1}H magnetogyric ratio, the motional correlation time and the Larmor frequency, respectively. Using the X-ray result [6] of the O–H distance (1.06 Å) and assuming the usually accepted N–H distance of 0.95 Å in aromatic N–H, we estimated intramolecular contributions to ΔM_2, which gave a T_{1H} minimum of ca. 20 s at the same Larmor frequency. This value is almost the same order of magnitude for the observed T_{1H} value of 45 s. Third, quite analogous long T_{1H} minimum values were reported in same temperature range in crystalline benzoic acid and its derivatives [4,16], which have been shown to perform the H-transfer in the H-bonded dimer structure in solid. As the motional mode of the H-transfer, we can expect the proton exchange between the two structures I and II shown above. This is because monovalent chloranilate ($C_6O_2Cl_2(OH)O^-$) is presumed to be the most populated structure from the foregoing NQR frequency analysis. The onset of this H-motion is consistent with the X-ray diffraction study [6] reporting large displacement parameters of H-atoms attributable to disorder of H-atoms in the H-bonds. The observed T_{1H} shown in Fig. 3 exhibits a little asymmetric temperature dependence different from the theoretically expected BPP-type temperature dependence given by Eq. (1). This asymmetry is attributable to the contribution from the tunnelling proton exchange in the low-temperature side of the minimum as already discussed in detail in solid benzoic acid [16] and *p*-chlorobenzoic acid [4]. The evaluated activation energies (E_a) from the high- and low-temperature sides of the minimum were 3.9 ± 0.5 and 3.2 ± 0.5 kJ mol^{-1}, respectively. The obtained E_a in the high-temperature side, which corresponds to the barrier for the classical jumping motion of protons between the two structures, is acceptable because it is comparable to 5.5 kJ mol^{-1} [16] obtained for the proton exchange in the H-bonded benzoic acid dimer in solid. These results are consistent with O–H---X (X: O or N) distances reported to be 2.633 Å (X:O) in benzoic acid [17] and 2.590 Å (X:N) in the present system [6] being close to each other.

4.3. ^{35}Cl NQR spin-lattice relaxation time (T_{1Q})

The temperature dependency of T_{1Q} shown in Fig. 2 is assumed to be expressed by the superposition of the following Debye-type relaxation and the Arrhenius-type activation equations [18]:

$$T_{1Q}^{-1} = C\left[\tau_c/\left(1+\omega_Q^2\tau_c^2\right)\right] \quad (2)$$

and

$$\tau_c = \tau_0 \exp(E_a/RT), \quad (3)$$

where C, τ_c, ω_Q, τ_0 and E_a denote the motional constant, the motional correlation time, the NQR angular frequency, the correlation time in the limit of infinite temperature and the activation energy, respectively. The observed T_{1Q} data were fitted by superimposed two relaxation mechanisms given by Eqs. (2) and (3) and the best-fitted curve is shown in Fig. 2. In this fitting calculation, we ignored the contribution from lattice vibrations which seems to be present in the background of the observed T_{1Q} temperature dependence. Since the T_{1Q} minimum observed around 120 K can be taken to correspond to the T_{1H} minimum at 135 K, by taking into account the difference in applied frequencies in these two measurements, we used the E_a determined in T_{1H} analysis as the fitting parameter for the low-temperature T_{1Q} minimum. The determined motional parameters are shown in Table 1. In accordance with T_{1H} analysis, the low-temperature minimum is attributed to the correlated hydrogen exchange between structures I and II.

Table 1
Motional parameters in H-transfers determined in (chloranilic acid)–(1,4-diazine) 1:2 complex $C_6O_2Cl_2(OH)_2$–$(C_4H_4N_2)_2$ from derived 35Cl NQR relaxation data

	Correlated H-transfer	Uncorrelated H-transfer
C (s^{-2})	$5.9 \pm 0.1 \times 10^8$	$\sim 4.0 \times 10^9$
τ_0 (s)	$2.2 \pm 0.1 \times 10^{-10}$	$\sim 4.0 \times 10^{-10}$
E_a (kJ mol^{-1})	3.2 ± 0.5^a	7.2 ± 2.0

[a] Determined from ^1H NMR T_{1H}.

Upon heating, the protons in two O–H groups in a chloranilic acid are expected to move independently between O and N sites. This motion enables the formation of divalent chloranilate ions ($C_6O_4Cl_2^{2-}$) and at the same time neutral chloranilic acid molecules. The structure changes in the correlated and uncorrelated H-transfer models are given by Fig. 4. The uncorrelated H-transfers of I(or II) ↔ III, and I(or II) ↔ IV shown in the figure yield the structure changes between mono- and divalent ions, and also between monovalent ions and neutral molecules, respectively, indicating marked changes in electronic structures which should results in the fluctuation of efg at resonant chlorine nuclei. The occurrence of these motions can be supported from T_{1H} data which showed no marked relaxation processes in the range of the high-temperature T_{1Q} decrease. This can be explained by considering that, once the magnetic dipolar interactions are averaged by the simultaneous H-exchange between the structures I and II, the further average from the

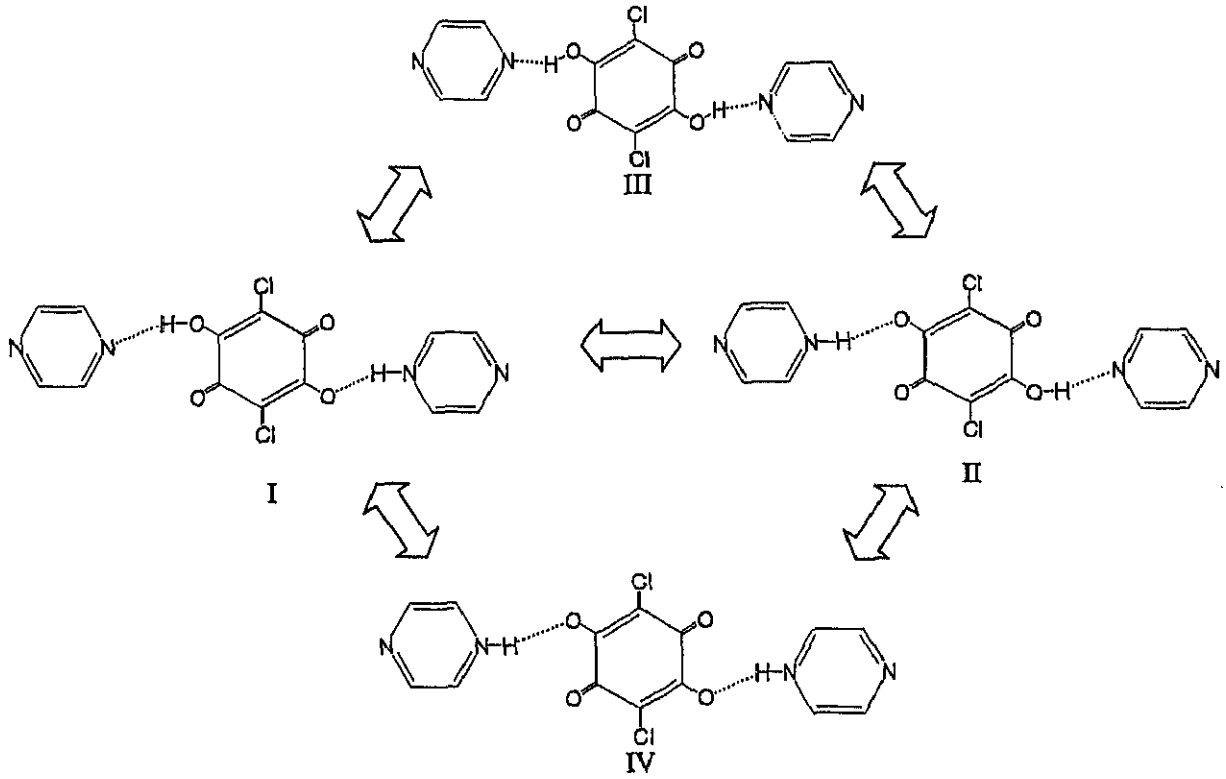

Fig. 4. H-transfer models. The correlated transfer model I ↔ II, where two hydrogen atoms jump simultaneously. The uncorrelated transfer model I(or II) ↔ II and I(or II) ↔ IV, where two hydrogen atoms move independently.

uncorrelated motions of almost the same displacements by the same hydrogen atoms is quite small and should give much longer T_{1H} values than those from the correlated motion. We roughly evaluated the ΔM_2 value caused by the uncorrelated H-transfers excited after being averaged by the correlated motions between I and II by assuming the same H-positions used in the foregoing section. The T_{1H} evaluated from ΔM_2 by the uncorrelated H-transfers became ca. 400 times longer than that from the correlated motion implying that T_{1H} from the uncorrelated motion is too long to be detected. On the other hand, the uncorrelated motions gave finite probabilities of the divalent and neutral structures in chloranilic acid which can markedly contribute to the NQR relaxation. From the present T_{1Q} data showing only a monotonous decrease on heating without any minima at high temperatures, we cannot identify the contributed relaxation mechanism possible to be H-exchanges I (and II) $\leftrightarrow$ III, I (and II) $\leftrightarrow$ IV, or both shown in Fig. 4.

The deuterated salt gave T_{1Q} values with a gradual decrease on heating from 77 K and a flat value of ca. 1.9 s around 120 K, where the T_{1Q} minimum in the protonated salt of ca. 800 ms was observed. The longer T_{1Q} in the deuterated salt indicates that the fluctuation of efg is decreased by the deuteration. This result is unexplainable by the general trend of the smaller tunnelling in deuterated compounds as observed in *p*-chlorobenzoic acid [4]. In the present stage, this increase of T_{1Q} is attributable to the Ubbelohde effect [19–22] resulting in a longer O–N distance, i.e., the larger crystalline unit cell caused by the deuteration. This effect can be expected to decrease the fluctuation of efg from intermolecular origins and give the shallower T_{1Q} minimum.

5. Summary

From the temperature dependences of ^{35}Cl NQR T_{1Q} in (chloranilic acid)–(1,4-diazine) 1:2 salt, we succeeded to obtain a new motional mode of the H-transfer which could not be detected by ^{1}H NMR. The observed T_{1Q} values were much shorter than T_{1H} in the whole temperature range studied indicating that the NQR method is a highly sensitive technique to detect subtle motions of H-bonded protons which result in formation of molecules with different electric charges.

Acknowledgements

This work was partly supported by Grants-in-Aid for scientific research Nos. (B)12440192 and (C)10640554 from the Ministry of Education, Science, Sports and Culture.

References

[1] F. Jona, G. Shirane, Ferroelectric Crystals, Dover Publ., New York, 1993.
[2] F.L. Howell, N.J. Pinto, V.H. Schmidt, Phys. Rev. B 46 (1992) 13762.
[3] A.S. Davydov, Solitons in Molecular Systems, Kluwer Academic Publ., Dordrecht, 1991 (English Translation).
[4] T. Nihei, S. Ishimaru, R. Ikeda, Z. Naturforsch. A 55a (2000) 355.
[5] R.S. Miller, I.C. Paul, D.Y. Curtin, J. Am. Chem. Soc. 96 (1974) 6334.
[6] H. Ishida, S. Kashino, Acta Cryst. C 55 (1999) 1714.
[7] T.P. Das, E.L. Hahn, in: F. Seitz, D. Turnbull (Eds.), Solid State Physics, (Suppl. 1) Nuclear Quadrupole Resonance Spectroscopy, Academic Press, New York, 1958, p. 90.
[8] H. Miyoshi, K. Horiuchi, N. Sakagami, K. Okamoto, R. Ikeda, Z. Naturforsch. A 53 (1998) 603.
[9] T. Kobayashi, H. Ohki, R. Ikeda, Mol. Cryst. Liq. Cryst. 257 (1994) 279.
[10] H. Bayer, Z. Phys. 130 (1951) 227.
[11] R.M. Hart, M.A. Whitehead, L. Krause, J. Chem. Phys. 56 (1972) 3038.
[12] J.I.G. Cadogan et al. (Eds.), Dictionary of Organic Compounds, 6th edn., vol. 3, Chapman and Hall, London, 1996, p. 2042.

[13] J.I.G. Cadogan et al. (Eds.), Dictionary of Organic Compounds, 6th edn., vol. 6, Chapman and Hall, London, 1996, p. 5482.
[14] M.M. Habeeb, H.A. Alwakil, A. El-Dissouky, H.A. Fattah, Pol. J. Chem. 69 (1995) 1428.
[15] A. Abragam, The Principles of Nuclear Magnetism, Oxford University Press, New York, 1986 (Chapter VIII).
[16] J.L. Skinner, H.P. Trommsdorff, J. Chem. Phys. 89 (1988) 897.
[17] G. Bruno, L. Randaccio, Acta Cryst. B 36 (1980) 1711.
[18] D.E. Woessner, H.S. Gutowsky, J. Chem. Phys. 39 (1963) 440.
[19] J.M. Robertson, A.R. Ubbelohde, Proc. Roy. Soc. A 170 (1939) 222.
[20] J.M. Robertson, A.R. Ubbelohde, Proc. Roy. Soc. A 170 (1939) 241.
[21] A.R. Ubbelohde, Proc. Roy. Soc. A 173 (1939) 417.
[22] A.R. Ubbelohde, I. Woodware, Proc. Roy. Soc. A 179 (1942) 399.

Hydrogen Transfer in a Hydrogen-Bonded 1:2 Complex of Chloranilic Acid with 1,2-Diazine Studied by ^{35}Cl NQR

Taka-aki Nihei, Shin'ichi Ishimaru, Hiroyuki Ishida,† Hideta Ishihara,†† and Ryuichi Ikeda
Department of Chemistry, University of Tsukuba, Tsukuba 305-8571
†Department of Chemistry, Faculty of Science, Okayama University, Okayama 700-8530
††Department of Chemistry, Faculty of Education, Saga University, Saga 840-8502

(Received September 18, 2000; CL-000858)

^{35}Cl NQR frequencies and spin–lattice relaxation time, and ^{1}H NMR spin–lattice relaxation time were measured on (chloranilic acid)-(1,2-diazine) 1:2 molecular complex to detect H-transfer motions in the H-bonded three molecular system. Only a single H-jump mode was observed by ^{1}H NMR, whereas three kinds of H-transfer modes were obtained in ^{35}Cl NQR in good agreement with the prediction.

We reported double H-transfer in solid *p*-chlorobenzoic acid[1] containing a dimer structure[2] by the ^{35}Cl NQR technique, and showed for the first time that the NQR relaxation can be a quite sensitive probe for detecting H-transfer in H-bonded systems compared with conventional ^{1}H NMR relaxation studies. As an application of this technique, we tried to find H-motions in a new three-molecular H-bonded system, (chloranilic acid)–(1,4-diazine) 1:2 complex[3] [$(C_6Cl_2O_2(OH)_2)$–$(C_4N_2H_4)_2$] (abbreviated to 1,4-complex) in the previous study,[4] and succeeded in observing two kinds of modes of H-transfer motion, one of which was a new kind of mode undetected by the ^{1}H NMR method. In the analysis of the H-bonded structure in 1,4-complex, we predicted three kinds of H-transfer modes, namely, H-jumps between two equivalent monovalent chloranilate(1–) ions, between (1–) and (2–) ions, and between (1–) ions and neutral chloranilic acid(0) molecules. We could detect the first mode by both NQR and NMR relaxation measurements in the low-temperature range, but nothing in NMR and only a single relaxation increase in NQR at high-temperatures. This disagreement could provide some doubt on the sensitivity of NQR and also the validity of our H-transfer models.

In the present study, we intend to solve this problem and measure NQR and NMR in a three-molecular H-bonded system, (chloranilic acid)–(1,2-diazine)1:2 complex [$(C_6Cl_2O_2(OH)_2)$–$(C_4N_2H_4)_2$][5] (abbreviated to 1,2-complex). Analogously to 1,4-complex, 1,2-complex crystals contain almost isolated three molecular units bonded by OH---N type H-bonding with a short O---N distance of 2.582 Å,[5] where a chloranilic acid molecule is located on an inversion center and only one of two N sites in a 1,2-diazine molecule takes part in the H-bonding. If we consider that pK_{a1} in 1,4-diazine is 0.57,[6] while 2.24 in 1,2-diazine,[6] and pK_{a1} and pK_{a2} in chloranilic acid are 0.76 and 2.72,[6] respectively, we can expect that the stability of chloranilate ions with high ionic charges increases in 1,2-complex compared with in 1,4-complex. This implies the easier formation of chloranilate(1–) and (2–) ions, suggesting that the above three kinds of H-transfer motions can be observed below room temperature.

^{35}Cl NQR frequencies observed in a range 77–265 K in 1,2-complex are shown in Figure 1. Its temperature dependence showed an anomalous positive temperature coefficient in the low-temperature range77–160 K, which is unexplainable by the conventional Bayer theory[7] taking into account of the influence from lattice and molecular vibrations. The origin of this unusual behavior will be discussed at the end of the paper. It should be noted that ^{35}Cl resonance frequency 34.940 ± 0.001 MHz observed at 77 K is much lower than 36.40 MHz obtained in the foregoing 1,4-complex.[4] It has been reported that ^{35}Cl NQR frequency in crystalline chloranilic acid($C_6O_2Cl_2(OH)_2$) is 37.15 MHz at 77 K,[8] while its divalent sodium salt containing $[C_6O_2Cl_2O_2]^{2-}$ ions gives an averaged frequency of ca. 35.20 MHz (two lines : 35.538 and 34.853 MHz) at 77 K.[8] From these frequencies, we can expect that the present 1,2-complex contains chloranilic acid with a formal charge close to 2– in crystal at 77 K. This contrasts with the result in the previous 1,4-complex[4] in which the monovalent chloranilate(1–) was shown to be the most populated species at low temperatues from the observed ^{35}Cl frequency. The present result in 1,2-complex can be supported by pK_a value in 1,2-diazine much larger than in 1,4-diazine favoring the formation of the H-transferred –N–H$^+$ structure in 1,2-complex.

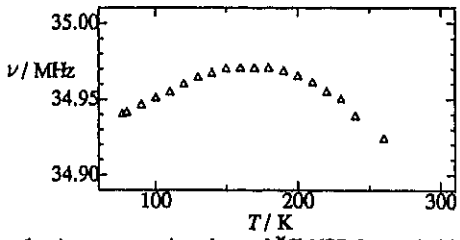

Figure 1. A temperature dependence of ^{35}Cl NQR frequencies(ν) observed in solid chloranilic acid-1,2-diazine (1:2) complex.

A temperature dependence of ^{1}H NMR spin–lattice relaxation time (T_{1H}) is shown in Figure 2. The very long T_{1H} observed in the whole temperature range studied and a single shallow minimum of 45 s around 110 K are quite analogous to reported results in 1,4-

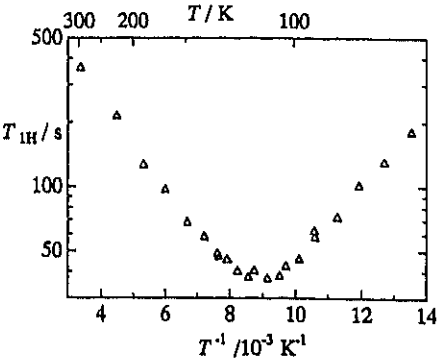

Figure 2. A temperature dependence of ^{1}H NMR spin-lattice relaxation time (T_{1H}) observed at a Larmore frequency of 54.3 MHz in solid chloranilic acid-1,2-diazine (1:2) complex.

complex.[4] Applying the same discussion as in 1,4-complex, we can reasonably assign this T_{1H} minimum observed in 1,2-complex to the fluctuations of the magnetic dipolar interactions caused by the H-transfer between chloranilic acid and two 1,2-diazine molecules H-bonded with each other. As an H-transfer model averaging H–H dipolar interactions, H-jumps between the divalent and monovalent chloranilate ions can be accepted, because H-motions should be excited from the most populated chloranilate(2–), and in this case, the next stable form is monovalent chloranilate(1–). Accordingly, starting from the chloranilate(2–) ion, H-jumps, I↔II and I↔III shown in Figure 3 are expected to take place with the same rate and contribute to the ^{1}H relaxation at low temperatures, where two stuctures, II and III; were assumed to be equivalent from the crystal symmety of 1,2-complex.[5]

A temperature dependence of ^{35}Cl NQR spin–lattice relaxation time(T_{1Q}) is shown in Figure 4. The observed T_{1Q} gave a complicated temperature dependence compared with that of T_{1H} and is explainable by the superposition of at least three T_{1Q} minima. Here, for simplicity, we assume the Debye type relaxation process as observed in ^{1}H NMR and the Arrhenius-type activation equation as used in the previous study on 1 ,4-complex.[4] We fitted superimposed three relaxation curves on T_{1Q} and the best fitted calculated values are shown in Figure 4. In the fitting for the lowest-temperature minimum, we used the T_{1H} slopes obtained in the T_{1H} curve and the minimum temperature after adjusting the frequency difference in the NQR and NMR measurements. In the present study, we could clearly observed separated three relaxation processes assignable to three kinds of H-transfer modes we predicted.[4] The lowest-temperature relaxation was explained by the two equivalent modes I↔II and I↔III shown in Figure 3 taking place with the same probability as derived from the above discussion of T_{1H}. As for the two other mechanisms expected in the high temperature range, one is the symmetric H-exchange keeping the chloranilate(1–) structure named the correlated motion in the previous study[4] given by II↔III in Figure 3. The other should be the H-transfer between chloranilate(1–) and (0) expressed by II↔IVand III↔IV in Figure 3. We can assign the former to the relaxation giving the minimum around 160 K, and the latter to that observed around room temperature. This indicates that the latter

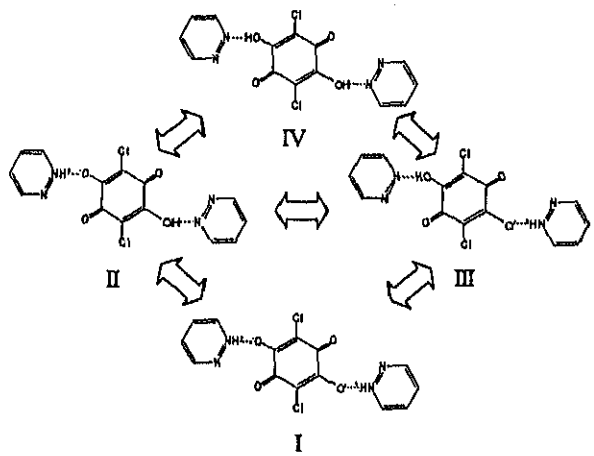

Figure 3. H-transfer models in crystalline chloranilic acid-1,2-diazine (1:2) complex. The most stable structure at low temperatures is given by I containing chloranilate(2-) ions. Structure II and III consisting of equivalent chloranilate(1-) ions are formed with thermal excitation of I. At high temperatures, the less stable chloranilic acid(0) molecules IV are made from II and III by H-transfer.

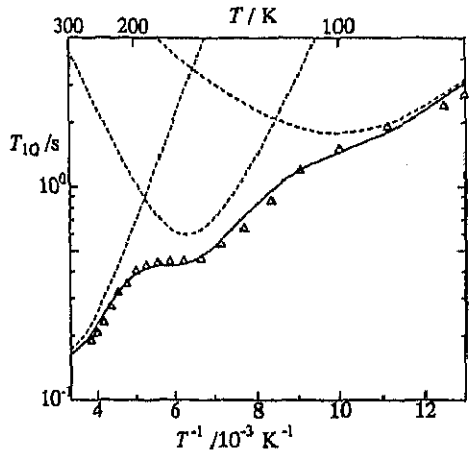

Figure 4. A temperature dependence of ^{35}Cl NQR spin-lattice relaxation time (T_{1Q}) observed in sold chloranilic acid-1,2-diazine (1:2) complex. Broken lines show three relaxation processes and the solid line is the best-fitted calculated values.

process has a higher barrier than the former, because, in the present 1,2-complex, the time averaged structure of chloranilic acid was shown to be close to 2– implying a high barrier for getting a neutral molecule. This can also be shown from the consideration of a marked difference in pK_{a1}(= 0.76) and pK_{a2}(= 2.72)[6] of chloranilic acid and also pK_{a1}(= 2.24)[6] of 1,2-diazine in solution.

The reason why the marked ^{35}Cl NQR relaxation, but no ^{1}H NMR T_{1H} change was observed in the high-temperature range is explained by the facts that H-transfer once excited affords a little further fluctuation of the magnetic field at ^{1}H nuclei, whereas remarkable changes in EFG at Cl nuclei are formed by the change of formal charges on chloranilic acid molecules.

The positive temperature coefficient of the NQR frequencies observed in a range 77–170 K unexplainable by the conventional Bayer-type lattice motions[7] can be attributable to the effect of H-transfer described above. Upon heating from 77 K,we can expect that the population of chloranilate(2–) ions decreases, while that of (1–) ions increases. Since the NQR frequency is determined by the time-averaged EFG at the resonance nuclei, the increase in the number of chloranilate(1–) ions which affords a higher frequency than (2–) ions can explain the increase of efg with increasing temperature. The frequency decrease observed on further heating can be explained by considering that contributions to the EFG decrease from lattice vibrations increase more than from the H-transfer.

This works was partly supported by Grant-in-Aid for scientific research No.(B) 12440192 and (C)10640554 from the Ministry of Education, Science, Sports and Culture.

References and Notes

1 T. Nihei, S. Ishimaru, and R. Ikeda, *Z. Naturforsch.*, **55a**, 355 (2000).
2 R. S. Miller, L C Paul, and D. Y Curtin, *J. Am. Chem. Soc.*, **96**, 6334 (1974).
3 H. Ishida and S. Kashino, *Acta Crystallogr., Sect. C*, **55**, 1714 (1999).
4 T. Nihei, S. Ishimaru, H Ishida, H. Ishihara, and R. Ikeda, *Chem. Phys. Lett.*, (2000) in press.
5 H. Ishida and S. Kashino, *Acta Crystallogr., Sect. C*, **55**, 1149 (1999).
6 "Dictionary of Organic Conpounds," 6th ed., ed. by J. I G. Cadogan, S. V Ley, G. Pattenden, and R A Raphael, C W. Ress, Chapman and Hall, London (1996), vol. 3.
7 H. Bayer, *Z. Physik*, 130, 227 (1951).
8 R. M. Hart, M. A. Whitehead, and L. Krause, *J. Chem. Phys.*, **56** 3038 (1972).

Molecular motions and phase transitions in halogen-bridged one-dimensional complexes $[Pt(en)_2][PtX_2(en)_2](ClO_4)_4$ (X: I, Br)

Noriyoshi Kimura,† Toru Hachisuka, Yukitaka Nakano and Ryuichi Ikeda*

Department of Chemistry, University of Tsukuba, Tsukuba 305-8571, Japan

Received 1st December 2000, Accepted 15th March 2001
First published as an Advance Article on the web 3rd April 2001

^1H and ^2H NMR and thermal measurements were performed on crystalline $[Pt(en)_2][PtI_2(en)_2](ClO_4)_4$ in which protonated and partially deuterated ethylenediamines $H_2N(CH_2)_2NH_2$, $D_2N(CH_2)_2ND_2$ and $H_2N(CD_2)_2NH_2$ were used as the ligand "en". A metastable crystalline phase of $[Pt(en)_2][PtBr_2(en)_2](ClO_4)_4$ with conformational disorder of the en chelate rings was shown to have a different phase transition at *ca.* 380 K to the stable crystalline form of the ordered structure. NMR spectra and relaxation times showed that the distribution of the en conformation is not static but dynamic in both I and Br complexes where a puckering motion of en chelate rings was shown to take place between asymmetric potential wells.

1. Introduction

Halogen-bridged mixed-valence complexes $[M^{II}(en)_2][M^{IV}X_2(en)_2](ClO_4)_4$ (en: ethylenediamine; M: Pt, Pd; X: Br, Cl, I) with a one-dimensional –X–M^{II}–X–M^{IV}–X– structure have been intensively studied from optical,[1] magnetic[2] and structural[3] points of view, and characteristic electronic excitations in mixed valence states[4] and charge and spin migrations along the 1-D chains[5] have been revealed. The above Cl and Br complexes were shown to have a structural phase transition in the range 269–298 K[6] where the conformations of en chelate rings having two possible conformations δ and λ in the $M(en)_2$ moieties are changed from δλ (λδ) in the low-temperature monoclinic phase ($P2_1/n$) to λλ (δδ) in the high-temperature orthorhombic phase (*I bam*).[6,7] Recently, a new modification of $[Pt(en)_2][PtBr_2(en)_2](ClO_4)_4$ was found, by crystallizing from aqueous solution at temperatures below the phase transition point (T_{tr}), and shown to be a monoclinic form (*C* 2/*m*) with disordered en conformations.[8] It is noted that this structure is isomorphous with the room-temperature phase of $[Pt(en)_2][PtI_2(en)_2](ClO_4)_4$[9] which was suggested to transform into the ordered form (*C* 2/*c*) in the range 150–160 K upon cooling, as shown by a neutron diffraction study of deuterated crystals.[10]

In the present study, we intend to reveal the phase diagram closely connected with en conformations and molecular motions at the transition in these crystals by measuring the thermal behaviour and ^1H and ^2H NMR spectra and spin–lattice relaxation.

2. Experimental

$[Pt(en)_2][PtI_2(en)_2](ClO_4)_4$ (abbreviated to PtI) was prepared according to a literature method[11] and recrystallized from water at room temperature. Partially deuterated analogues, $[Pt\{NH_2(CD_2)_2NH_2\}_2][PtX_2\{NH_2(CD_2)_2NH_2\}_2](ClO_4)_4$ (PtI-CD) and $[Pt\{ND_2(CH_2)_2ND_2\}_2][PtX_2\{ND_2(CH_2)_2ND_2\}_2](ClO_4)_4$ (PtI-ND) were obtained by using deuterated ethylenediamine, $(NH_2(CD_2)_2NH_2)$ as the starting material, and repeated crystallizations from D_2O, respectively. $[Pt(en)_2][PtBr_2(en)_2](ClO_4)_4$ (PtBr) synthesized analogously to PtI was recrystallized from water at *ca.* 10 °C to obtain the monoclinic crystalline form,[8] isomorphous with PtI.

Phase transition temperatures were determined with a homemade differential thermal analysis (DTA) apparatus and a Seiko differential scanning calorimetry (DSC) 120 calorimeter using sealed aluminium vessels. ^2H NMR spectra and spin–lattice relaxation times (T_{1D}) were observed with a Bruker MSL-300 spectrometer at a Larmor frequency of 46.051 MHz in the range 140–370 K using a VT-1000 temperature controller. The quadrupole pulse sequence[12] for observing an echo signal after two $\pi/2$ pulses with a $\pi/2$ phase difference, where a $\pi/2$ pulse width was 3.5–5.0 μs, was employed for the spectrum measurement and the inversion recovery method was used for the T_1 determination.

The ^1H NMR spin–lattice relaxation time T_{1H} and the second moments (M_2) of the resonance lines were determined with a home-made pulsed spectrometer[13] at 29.0 and 54.3 MHz using the inversion recovery method, and with a Bruker SXP-100 spectrometer at 54.3 MHz by employing the solid echo method,[14] respectively.

3. Results and discussion

Thermal measurements

In the DTA measurements with PtI, we observed a weak and broad anomaly with a peak at 157 ± 5 K accompanied by a long tail on the low temperature side. This temperature agrees well with the phase-transition temperature of 150–160 K estimated from the neutron diffraction study.[10]

DSC thermograms recorded on PtBr of a monoclinic structure reported to be *C* 2/*m*[8] are shown in Fig. 1. When crystals grown at *ca.* 283 K were cooled, no heat anomaly was recorded down to *ca.* 170 K. Upon heating this sample, an endothermic anomaly was observed at 381 ± 1 K with a transition enthalpy $\Delta_{tr}H = 8 \pm 1$ kJ mol^{-1}. Upon cooling from above the temperature, an exothermic anomaly was observed at 295 K with $\Delta_{tr}H = 10$ kJ mol^{-1} and, on heating the low-temperature phase again, an anomaly at 300 ± 1 K was obtained while no anomalies were observed around 380 K where the transition was observed in the virgin sample. Since

† Present address: Department of Chemistry, Faculty of Education, Wakayama University, Sakaedani 930, Wakayama 640-8510, Japan.

 DOI: 10.1039/b009646f

Table 1 Activation energies (E_a), potential energy differences (ΔE), jump angles (2θ), reductions in ^{1}H NMR second moments (ΔM_2) and correlation times at infinite temperature (τ_0) of the puckering motion of Pt(en) chelate rings in asymmetric potential wells in PtI and its partially deuterated analogues PtI-CD and PtI-ND, together with PtBr, determined by ^{1}H and ^{2}H NMR relaxation studies. Figures in parentheses are values obtained from ^{2}H spectrum analysis

Compound	E_a/kJ mol^{-1}	ΔE/kJ mol^{-1}	2θ/degrees	ΔM_2/mT^2	τ_0/10^{-14} s
PtI	31.0 ± 0.5	4.5 ± 1.0	—	0.12 ± 0.02	48 ± 0.5
PtI-CD	34.2 ± 0.5	2.9 ± 0.3(2.0 ± 1.0)	65 ± 2(68 ± 2)	—	8.0 ± 0.5
PtI-ND	34.8 ± 0.5	3.1 ± 0.5	28 ± 2(30 ± 4)	—	8.2 ± 1.0
PtBr	31.0 ± 0.5	5.2 ± 0.5	—	0.12 ± 0.02	44 ± 1.0

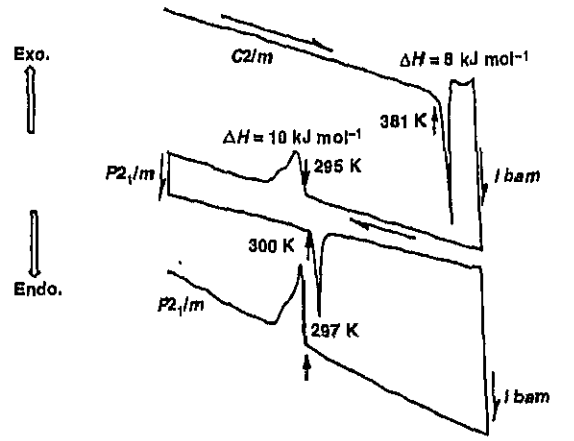

Fig. 1 Thermograms recorded in DSC measurements on PtBr. On heating the metastable monoclinic phase (*C* 2/*m*), the stable orthorhombic form (*I bam*) was obtained above the transition temperature at
381 K.

the transition temperature of 300 K agrees well with that in orthorhombic PtBr,[6] these thermal data imply that the monoclinic form, metastable at room temperature, transforms into the stable orthorhombic form at 381 K, and the first-order phase transition observed at 300 K is between two stable orthorhombic forms of *I bam* and $P2_1/m$ for the high and low temperature forms, respectively.

^{2}H NMR spectra

^{2}H NMR spectra observed in PtI-CD and PtI-ND are shown in Fig. 2. Below *ca.* 200 K, both complexes showed spectra with a small asymmetry parameter (η) for principal values of

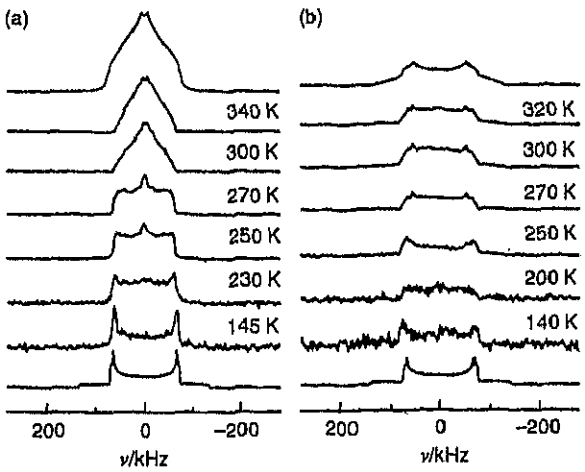

Fig. 2 Temperature dependences of ^{2}H NMR spectra observed in (a) PtI-CD and (b) PtI-ND. The top and bottom spectra shown in (a) and (b) are simulated for the highest and lowest temperature spectra observed, respectively.

the electric field gradient (efg) tensor. We evaluated $\eta = 0.05 \pm 0.02$ for both complexes below 200 K and quadrupole coupling constants (qcc) of 180 ± 5 kHz (145 K) and 190 ± 5 kHz (140 K) for PtI-CD and PtI-ND, respectively, by comparing with simulated spectra shown in Fig. 3. These results indicate the presence of the rigid CD_2 and ND_2 groups in crystals by reference to previously reported data.[15,16] Upon heating, the qcc values of both analogues gradually decreased, while η increased slowly. The increase in η implies the onset of two-site jumps of the C–D and N–D bond directions[17] being consistent with the X-ray diffraction study of PtI revealing the disordered orientations of ethylenediamine molecules in the high temperature phase,[9] if the dynamic disorder model is assumed. From the analysis of ^{1}H T_1 and M_2 of ^{1}H NMR absorptions described below, we can expect that this jump motion takes place between asymmetric potential wells. We simulated ^{2}H spectra for two-site jumping of C–D and N–D bonds between two directions at an angle of 2θ, and between two potential wells with an energy difference of ΔE by applying the static e^2Qq and η values determined from the low-temperature spectra. Here, we assumed that the jumping rate around 300 K is rapid compared with the observed linewidth because further increase in temperature above 300 K gave almost no spectrum change, as shown in Fig. 2. The simulated spectra are shown in Fig. 3. By comparing observed and simulated spectra, we obtained the best-fit values of 2θ and ΔE at 300 K to be 68 ± 2° and 2 ± 1 kJ mol^{-1}, respectively, for the C–D jumping and 2θ of 30 ± 4° for the N–D motion, as shown in Table 1. Here, it is noted that we could not determine ΔE for N–D, because almost no spectrum change was obtained even when scanning ΔE in a range 1–5 kJ mol^{-1}, probably because only a small spectrum change was caused by the motion.

These angles can be explained by the onset of the conformational change of the ethylenediamine chelate ring, because jump angles due to the conformational change between λ and δ were estimated to be *ca.* 60 and *ca.* 30° for the C–D and N–D bond directions, respectively, using the structural data.[9] This motional model is consistent with the results of X-ray and neutron diffraction studies[9,10] as well as the present DSC studies indicating the presence of an order–disorder phase transition at *ca.* 160 K associated with λ and δ conformations in ethylenediamine skeletons.

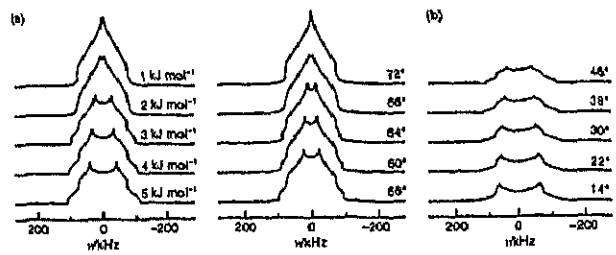

Fig. 3 ^{2}H NMR spectra simulated in (a) PtI-CD for various potential differences (ΔE) between two C–D jump directions (left) and various jump angles (2θ) (right), and (b) PtI-ND for changing jump angle 2θ values.

^{1}H and ^{2}H NMR absorptions and spin–lattice relaxation time

The temperature dependence of the second moment (M_2) of the ^{1}H NMR absorptions observed in PtI is shown in Fig. 4. Upon heating from *ca.* 170 up to 300 K, an unusually gradual decrease of M_2 from 0.22 to 0.15 mT^2 was observed. This M_2 decrease due to the onset of some motion can be compared to the narrowing of ^{2}H NMR spectra due to ethylenediamine motions observed in the same temperature range for the partially deuterated salts.

In Fig. 5, we show the temperature dependences of the ^{1}H NMR spin–lattice relaxation time (T_{1H}) observed in PtI and PtBr in the metastable monoclinic phase, and the ^{2}H NMR relaxation time (T_{1D}) in PtI-CD and PtI-ND. All the observed T_{1H} and T_{1D} values decreased with increasing temperature in the range 250–350 K, and gave a minimum around 350 K. These T_1 decreases are also attributable to the puckering motion of the ethylenediamine molecules. We should note that the frequency dependence of ^{1}H T_{1H} in PtI is unexplainable by the BPP (Bloembergen Purcell Pound) theory[18] requiring the ω^2 dependence of T_{1H} on the low-temperature side of the minimum, but the T_{1H} values observed are proportional roughly to $\omega^{1.5}$. These results together with the M_2 decrease observed over the quite wide temperature range of 100 K, can be explained well by introducing a model of jumping between asymmetric potential wells[19] for the two conformations of ethylenediamine molecules. Since the X-ray diffraction study of PtI[9] showed a crystal structure with disordered orientations of δ and λ conformations of ethylenediamine molecules in the high-temperature phase, we assume that these two orientations are not equivalent but have different energies. For the two-site jumps between the two unequal potential wells shown in Fig. 6, T_{1H} due to magnetic dipolar relaxation is expressed as[19]

$$T_{1H}^{-1} = \frac{2}{3}\gamma_H^2 \Delta M_2 \frac{4a}{(1+a)^2}\left[\frac{\tau}{1+\omega_0^2\tau^2} + \frac{4\tau}{1+4\omega_0^2\tau^2}\right] \quad (1)$$

where γ_H, ΔM_2 and ω_0 denote the proton magnetogyric ratio, the reduction of the M_2 value due to the onset of the motion and the angular Larmor frequency, respectively. a is the population parameter given by

$$a = \exp\left(\frac{\Delta E}{RT}\right) \quad (2)$$

where ΔE is the energy difference between the two unequal potential wells shown in Fig. 6. The correlation time τ is written as

$$\tau = \frac{1}{1+a}\tau_0 \exp\left(\frac{E_a}{RT}\right) \quad (3)$$

Here E_a is the activation energy shown in Fig. 6. Eqn. (1)–(3) were fitted to the observed T_{1H} data in Fig. 5, and the best-fit theoretical values and the determined parameters are shown in Fig. 5 and Table 1, respectively.

The theoretical ^{1}H NMR M_2 values before and after the onset of ethylenediamine puckering motions were evaluated with the Van Vleck equation[20] for the rigid ethylenediamine molecules, and the following equation for the M_2(mot) for the two-site jumps of the H–H vector directions[21] given by

$$M_2(\mathrm{mot})_{jk} = \frac{9}{20}\gamma_H^4\hbar^2\left[\frac{1}{r_{jkA}^6} + \frac{1}{r_{jkB}^6} + \frac{3\cos^2\alpha_l - 1}{r_{jkA}^3 r_{jkB}^3}\right] \quad (4)$$

where $M_2(\mathrm{mot})_{jk}$ and r_{jkA}, r_{jkB} and α_l are the motional M_2 contributed from the dipolar interaction between the jth and kth protons, the inter-proton distance in A and B conformations and the two-site jump angle of the vector between jth and kth protons, respectively. Using the crystal structure data[8,10] and the standard values of bond angles and distances, we obtained $M_2(\mathrm{rig}) = 0.228 \pm 0.01$ mT^2 and $M_2(\mathrm{mot}) = 0.108 \pm 0.005$ mT^2. The difference between these values $\Delta M_2 = 0.120$ mT^2 agrees well with the 0.12 ± 0.02 mT^2 evaluated from the T_{1H} fitting given above.

We also fitted ^{2}H NMR T_{1D} temperature dependences observed in PtI-CD and PtI-ND shown in Fig. 5 using the equation given in ref. 22:

$$T_{1D}^{-1} = \frac{1}{10}\frac{4a}{(1+a)^2}\left(\frac{3e^2Qq_{rlg}}{4\hbar}\right)^2 \times \sin^2 2\theta\left[\frac{\tau_D}{1+\omega_D^2\tau_D^2} + \frac{4\tau_D}{1+4\omega_D^2\tau_D^2}\right] \quad (5)$$

where e^2Qq_{rlg}, τ_D and ω_D are the quadrupole coupling constant in the rigid lattice given by the reported values of 180 and 190 kHz for rigid C–D[15] and N–D[16] groups, respectively, the motional correlation time assumed to be given by eqn. (3)

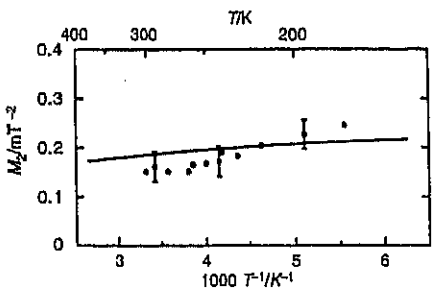

Fig. 4 Temperature dependence of the second moments (M_2) of ^{1}H NMR spectra observed in PtI. The solid curve is calculated by the model of two-site jumps in the asymmetric potential wells (see text).

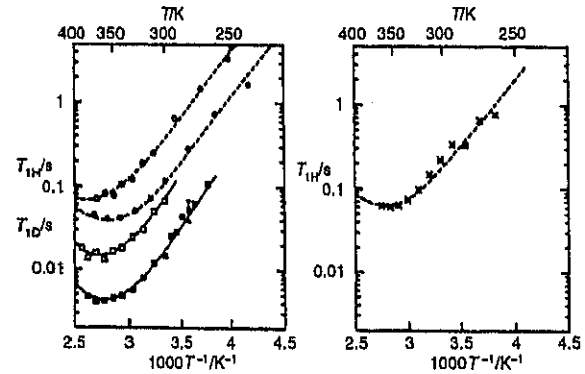

Fig. 5 ^{1}H NMR spin–lattice relaxation time (T_{1H}) observed in PtI at Larmor frequencies of 29.0 (●) and 54.3 MHz (○), PtBr (×) and ^{2}H NMR spin–lattice relaxation times (T_{1D}) in PtI-CD (■) and PtI-ND (□). Broken and solid lines are the best-fit theoretical data (see text).

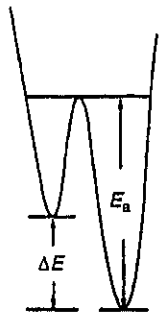

Fig. 6 Asymmetric potential curve used for the two-site jumps of C–D and N–D bonds.

and the angular NQR frequency, respectively. Applying eqn. (2), (3) and (5), we got the best-fit T_{1D} values given in Fig. 5, and the parameters in Table 1. The jump angles of $2\theta = 65°$ and 28° obtained for PtI-CD and PtI-ND, respectively, from the present ^2H T_1 data agree well with the 68° and 30° values obtained from the ^2H spectrum analysis given above, implying the adequacy of the present analyses. The obtained values of $E_a = 34.2$–34.8 and $\Delta E = 2.9$–3.1 kJ mol^{-1} are in good agreement with the values of 31.0 and 4.5 kJ mol^{-1}, respectively, determined by the T_{1H} fitting.

We also performed the same fitting calculation for the ^1H T_1 observed in PtBr in the metastable monoclinic phase shown in Fig. 5. The obtained best-fit T_1 curve and motional parameters are shown in Fig. 5 and Table 1, respectively. The large ΔE value obtained in PtBr compared with those in iodo complexes is attributable to the shorter Pt–Pt distance, *i.e.*, the interactions between neighbouring chelate rings in PtBr are stronger.

These results indicate that the disordered structure as for the ethylenediamine conformations revealed in the high-temperature phase in PtI by X-ray diffraction[10] is dynamic and the conformational change between λ and δ forms takes place in an asymmetric potential with a difference of *ca.* 3 kJ mol^{-1}. Using the determined values of activation parameters given in Table 1, we evaluated correlation times (τ) of the two-site jumps of C–D and N–D bond directions. At 300 K, τ values (the inverse of the jump rate) were 1.7×10^{-8} s for PtI evaluated from T_{1H} data, and 1.7×10^{-8} s for PtI-CD and 2.0×10^{-8} s for PtI-ND from T_{1D} data. These results support the hypothesis that the rapid motion limit assumed at 300 K in the ^2H spectrum analysis is acceptable.

The asymmetric potential model we used can be supported by the analysis of ^1H M_2 observed in PtI, shown in Fig. 4. The observed M_2 change over a wide-temperature range of over 100 K cannot be understood by the simple Arrhenius-type activation process but is explainable by the jumping between nonequivalent sites. Assuming the same asymmetric potential given above, the temperature dependence M_2(mot) is expressed as[21]

$$M_2(\text{mot}) = \sum M_2(\text{rig})_{jk} \frac{1}{(1+a)^2} \times [a^2 + a(3\cos^2 2\theta_{jk} - 1) + 1] \qquad (6)$$

where M_2(rig) is the rigid lattice M_2 value and θ_{jk} is the jump angle of the internuclear vector for two protons j and k. Substituting calculated jump angles θ_{jk} obtained from $2\theta = 65$ and 28°, $\Delta E = 3$ kJ mol^{-1} determined in the ^2H T_1 analysis and the calculated M_2(rig) into eqn. (2) and (6), we evaluated the M_2 temperature dependence shown in Fig. 4. We could not get a good agreement with experiment, but the qualitative feature of the gradual temperature dependence could be reproduced.

Summary

The monoclinic phase with the space group $C\,2/m$ obtained in Pt-Br was shown to be a metastable phase which transforms into the stable orthorhombic phase (*Ibam*) at 381 K.

From ^1H and ^2H NMR measurements, the puckering motion of Pt(en) chelate rings between δ and λ conformations was detected in $[Pt(en)_2][PtX_2(en)_2](ClO_4)_4$ (X: I, Br) in the monoclinic phase in which the presence of disordered conformations in chelate rings was known from X-ray and neutron diffraction studies. The obtained temperature dependences of ^1H and ^2H NMR spin-lattice relaxation and the second moments of ^1H NMR spectra were explained well by the model of two-site jumps between two asymmetric potential wells with energy differences of 3–5 kJ mol^{-1}, indicating that the disordered structure is dynamic between the nonequivalent lattice sites.

Acknowledgements

The authors are grateful to the Chemical Analysis Center, University of Tsukuba, for elemental analysis. N.K thanks JSPS Research Fellowships for Young scientists. This work was partly supported by Grant-in Aid for scientific research No. (B) 12440192 from the Ministry of Education, Science, Sports and Culture.

References

1 D. S. Martin, Jr., in *Extended Linear Chain Compounds*, ed. J. S. Miller, Plenum Press, New York, 1982, vol. 1, p. 409.
2 A. Kawamori, R. Aoki and M. Yamashita, *J. Phys. C*, 1985, **18**, 5487.
3 H. J. Keller, in *Extended Linear Chain Compounds*, ed. J. S. Miller, Plenum Press, New York, 1982, vol. 1, p. 357.
4 R. J. H. Clark, in *Infrared Spectroscopy*, ed. R. J. H. Clark and R. E. Hester, Wiley, New York, 1984, vol. 11, p. 95.
5 N. Kimura, S. Ishimaru, H. Okamoto, M. Yamashita and R. Ikeda, *Synth. Met.*, 1997, **86**, 2151; N. Kimura, S. Ishimaru, R. Ikeda and M. Yamashita, *J. Chem. Soc., Faraday Trans.*, 1998, **94**, 3659.
6 K. Toriumi, M. Yamashita, S. Kurita, I. Murase and T. Ito, *Acta Crystallogr., Sect. B*, 1993, **49**, 497.
7 S. C. Huckett, B. Scott, S. P. Love, R. J. Donohoe, C. J. Burns, E. Garcia, T. Frankcom and B. I. Swanson, *Inorg. Chem.*, 1993, **32**, 2137.
8 K. Toriumi, unpublished data.
9 H. Endres, H. J. Keller, R. Martin, H. N. Gung and U. Traeger, *Acta Crystallogr., Sect. B*, 1979, **35**, 1885.
10 J.-F. Bardeau, A. Bulou, W. T. Klooster, T. F. Koetzle, S. Johnson, B. Scott, B. I. Swanson and J. Eckert, *Acta Crystallogr., Sect. B*, 1996, **52**, 854.
11 N. Matsumoto, M. Yamashita and S. Kida, *Bull. Chem. Soc. Jpn.*, 1978, **51**, 2334.
12 J. H. Davis, K. P. Jeffrey, M. Bloom, M. I. Valic and T. P. Higgs, *Chem. Phys. Lett.*, 1976, **42**, 390.
13 T. Kobayashi, H. Ohki and R. Ikeda, *Mol. Cryst. Liq. Cryst.*, 1994, **257**, 279.
14 J. G. Powles and J. H. Strange, *Proc. Phys. Soc.*, 1963, **82**, 6.
15 J. Seelig, *Quart. Rev. Biophys.*, 1977, **10**, 353.
16 M. J. Hunt and A. L. MacKay, *J. Magn. Reson.*, 1974, **15**, 402.
17 R. Ikeda, A. Kubo and C. A. MacDowell, *J. Phys. Chem.*, 1989, **93**, 7315.
18 A. Abragam, *The Principles of Nuclear Magnetism*, Oxford University Press, Oxford, 1961, ch. VIII.
19 D. C. Look and I. J. Lowe, *J. Chem. Phys.*, 1966, **44**, 3437.
20 J. H. Van Vleck, *Phys. Rev.*, 1948, **74**, 1168.
21 E. R. Andrew and L. Latanowicz, *J. Magn. Reson.*, 1986, **68**, 232.
22 M. Mizuno, Y. Hamada, T. Kitahara and M. Suhara, *J. Phys. Chem.*, 1999, **103**, 4981.

ELSEVIER

Synthetic Metals 120 (2001) 777–778

SYNTHETIC METALS

www.elsevier.com/locate/synmet

Metal valence structures in 1-D mixed-metal complexes $[Ni_{1-x}Pd_xX(chxn)_2]X_2$ studied by solid NMR

Noriyoshi Kimura[1], Masataka Kano[1], Toshio Manabe[2], Masahiro Yamashita[2] and Ryuichi Ikeda[1]

[1]*Department of Chemistry, University of Tsukuba, Tsukuba, 305-8571, Japan*

[2]*Guraduate School of Science, Tokyo Metropolitan University, Hachioji, Tokyo 192-0397*

Abstract

^{13}C magic-angle-spinning NMR spectra in solid were measured in mixed-metal 1-D complexes $[Ni_{1-x}Pd_xX(chxn)_2]X_2$ (X: Cl, Br; $0.0 \leq x \leq 1.0$) where the antiferromagnetically coupled paramagnetic $-X-Ni^{3+}-X-Ni^{3+}-$ chains are formed at $x=0.0$, while the mixed-valence $-X-Pd^{2+}-X-Pd^{4+}-$ state is made at $x=1.0$. Upon increasing x from 0.0, ^{13}C spectra in the C_α position in the chxn ligand was broadened and shifted from original Pd^{2+} and Pd^{4+} positions indicating the fluctuation of Pd valency in mixed states. A marked spectrum broadening observed in C_β is also attributable to the effect from the partial mixing of paramagnetic Pd^{3+}sites in consistent with reported ESR results.

Keywords: Nuclear Magnetic Resonance Spectroscopy

1. Introduction

Halogen-bridged quasi-one-dimensional complexes $[MX(chxn)_2]X_2$ (chxn: 1*R*,2*R*-cyclohexanediamine, $C_6H_{10}(NH_2)_2$; X: Cl, Br) have been reported to form a mixed-valence diamagnetic $-X-M^{2+}-X-M^{4+}-$ structure for M=Pd [1], whereas an averaged paramagnetic $-X-M^{3+}-X-M^{3+}-$ structure for M= Ni[2]. Recently, crystals of mixed-metal complexes $[Ni_{1-x}Pd_xX(chxn)_2]X_2$ consisting of homogeneously mixed crystalline lattices of the two kinds of metal complexes with an isomorphous structure(I222) were prepared by applying the electrochemical oxidation technique[3]. The X-ray diffraction study on Br-bridged complexes showed continuously changing lattice constants from b=51.67(x=0.0) to 52.92 nm(x=1.0) corresponding to the M-M distances in the whole range $0.0 \leq x \leq 1.0$. On these series of complexes, the x dependence of ESR spectra was measured[4] and revealed a continuos change of spectrum-width with x. A marked result was that the evaluated spin susceptibility showed no linear relation with x, but almost constant up to $x \approx 0.6$. This suggests that most of diamagnetic Pd^{2+} and Pd^{4+} metal sites behave like paramagnetic at concentrations lower than $x = 0.5$. The change of the Pd valence was also observed in IR spectra[3] of the N-H stretching bands in both Pd^{2+} and Pd^{4+} units which showed a gradual shift to that in the Ni^{3+} unit. An analogous shift was also reported[3] in the measurement of the Pd-Br stretching band in Raman scattering with decreasing x.

*Corresponding author. Tel & fax:+81-298-53-4250;
E-mail:ikeda@chem.tsukuba.ac.jp

These studies imply the instability and fluctuation of the Pd valency in the present 1-D system where the energy difference between Pd^{2+} and Pd^{4+} is small compared with the other kinds of mixed-valence halogen-bridged complexes of Pd and Pt.

From ^{13}C NMR measurements, we can get local magnetic structures and magnetic field fluctuations on ligand carbons. In the present study, we intend to measure ^{13}C MAS NMR in $[Ni_{1-x}Pd_xX(chxn)_2]X_2$ (X: Cl, Br; $0.0 \leq x \leq 1.0$) and discuss the local electronic structure in this system.

2. Experimental

Crystals of mixed-metal complexes $[Ni_{1-x}Pd_xBr(chxn)_2]Br_2$($0.0 \leq x \leq 1.0$) were prepared by electrochemical oxidation of monomer complexes $[M(chxn)_2]Br_2$ (M: Ni, Pd) according to literature[3]. $[Ni_{1-x}Pd_xCl(chxn)_2]Cl_2$($0.0 \leq x \leq 1.0$) were synthesized analogously to Br complexes at ca. 320 K by flowing a dc current of ca. 15 μA for one month using tetramethylammonium chloride as a supporting electrolyte. The concentration of metals in measured specimens was determined by ICP emission spectrometry.

A Bruker MSL-300 spectrometer was used for the measurement of ^{13}C MAS-NMR spectra at a Larmor frequency of 75.468 MHz and sample spinning rate of 2-4 kHz at room temperature. TMS and solid adamantine were

0379-6779/01/$ - see front matter
PII: S0379-6779(00)00858-4

used as external standards of chemical shift. The ^{1}H NMR spin-lattice relaxation time was measured at 54.3 MHz by the inversion recovery method in a range of 100 - 300 K using a home-made spectrometer described elsewhere[5].

3. Results and Discussion

The x dependences of observed ^{13}C MAS NMR spectra at room temperature for $[Ni_{1-x}Pd_xCl(chxn)_2]Cl_2$ and $[Ni_{1-x}Pd_xBr(chxn)_2]Br_2$ are shown in Figs. 1 and 2, respectively. In both Figs. 1and 2, three kinds of carbons, C_α, C_β and C_γ in a

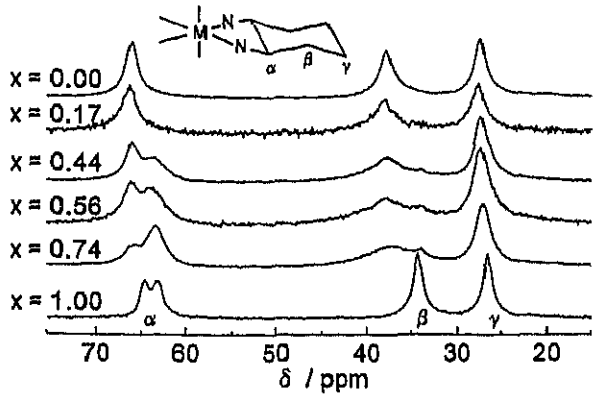

Fig. 1 ^{13}C MAS NMR spectra observed in $[Ni_{1-x}Pd_xCl(chxn)_2]Cl_2$ and carbon positions in a cyclohexanediamine ligand in a M(chxn) chelate ring(M: Pd,Ni).

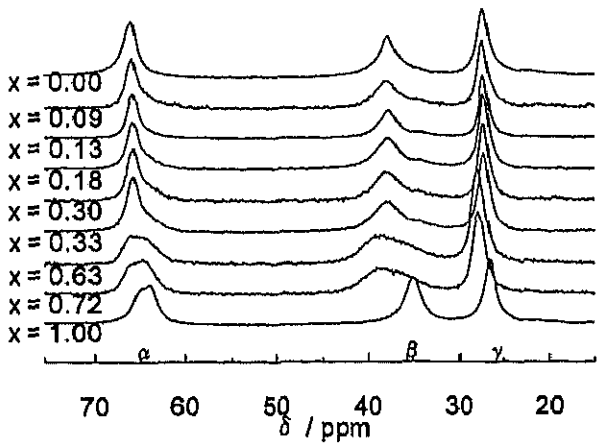

Fig. 2 ^{13}C MAS NMR spectra observed in $[Ni_{1-x}Pd_xBr(chxn)_2]Br_2$

cyclohexanediamine(chxn) ligand were observed as separated peaks. We can see that C_α and C_β signals showed marked metal and x dependences, while C_γ remote from metals gave almost independent shift values in both Cl and Br complexes. In x= 1.0, two C_α carbon signals observed are assignable to Pd^{2+} and Pd^{4+} sites, while a single C_α line in x =0.0 shows the formation of the averaged Ni^{3+} state[6]. With increasing x from 0.0, the C_α and C_β signals gradually decreased thier intensity at the same shift values. This implies that Ni atoms are always in the trivalent state regardless of Pd concentrations. On the other hand, C_α and C_β signals in Pd chelate rings observed in x= 1.0 were markedly weakened and broadened with decreasing x. This indicates that valency states of Pd^{2+} and Pd^{4+} become unstable in the presence Ni^{3+} sites in the neibourhood.

We tried to separate C_α signals observed in the Cl complex in the mixed metal range into two components corresponding to Ni and Pd sites. By this separation, we obtained small shifts and broadening of Pd carbons suggesting the fluctuation of Pd^{2+} and Pd^{4+} valences attributable to the mixing of the paramagnetic Pd^{3+} state. This explanation agrees well with the spin susceptibility data obtained from ESR measurement of Br complex[4] reporting the formation of paramagnetic Pd sites in the presence of Ni^{3+} in x>0.6.

We can expect that quite analogous discussion is possible in Br complex. In the Br complex of x= 1.0, since the energy difference between Pd^{2+} and Pd^{4+} is much smaller than in the Cl complex, the spectrum splitting between them is small implying the valence mixing in Pd easier than that in the Cl analogue. Similar results were reported from Raman spectra[3] showing a gradual intensity decrease in the Pd-Br stretching band with increasing x which was explained by the Pd valence fluctuation, i.e., the formation of Pd^{3+}.

We measured ^{1}H NMR spin-lattice relaxation time T_1 in some of this mixed metal system. At $x < 0.13$, T_1 values and its temperature dependence observed above *ca.* 100 K were almost independent of x. Since the T_1 temperature dependence at x= 0.0 was explainable by a strongly coupled antiferromagnetic 1-D chain model, this result suggests that this chain structure still retains in mixed crystals implying formation Pd^{3+}. At x=1.0, a gradual decrease T_1 observed upon heating from *ca.* 100 K was explained by the diffusion of spin solitons formed by the impurity order of Pd^{3+}[7]. With a little reduction of x from 1.0, T_1 showed marked changes that its value increased several times and its temperature dependency was reversed being close to that in x=0.0. This suggests the strong effect from paramagnetic spins which are present as Ni^{3+} even at low concentrations.

This work was partly supported by Grant-in Aid for scientific research No.(B) 12440192 from the Ministry of Education, Science, Sports and Culture.

References

[1] A. Hazell, Acta Crystallogr. C47 (1991) 962.
[2] H. Okamoto, K. Toriumi, T. Mitani and M. Yamashita, Phys. Rev. 42 (1990) 10381.
[3] M. Yamashita, T. Ishii, H. Matsuzaka, T. Manabe, T. Kawashima, H. Okamoto, H. Kitagawa, T. Mitani, K. Marumoto and S. Kuroda, Inorg. Chem. 38 (1999) 5124.
[4] K. Marumoto, T. Tanaka, S. Kuroda, T. Manabe and M. Yamashita, Phys. Rev. B 60 (1999) 7699.
[5] T. Kobayashi, H. Ohki and R. Ikeda, Mol. Cryst. Liq. Cryst. 257 (1994) 279.
[6] R. Ikeda, T. Tamura and M. Yamashita, Chem. Phys. Lett. 173 (1990) 466.
[7] R. Ikeda, M. Iida, T. Asaji, A. Ghosh and M. Yamashita, Chem. Phys. Lett. 210 (1993) 78.

ELSEVIER

Synthetic Metals 120 (2001) 779–780

SYNTHETIC METALS

www.elsevier.com/locate/synmet

Valence structure and magnetic interaction in MMX-type 1D complexes, $A_4[Pt_2I(P_2O_5H_2)_4]\cdot nH_2O$, studied by ^{31}P solid NMR

N. Kimura[a*], S. Ishimaru[a], T. Kawashima[b], S. Miya[b], T. Manabe[c], M. Yamashita[c] and R. Ikeda[a],

[a] *Department of Chemistry, University of Tsukuba, Tsukuba 305-8571, Japan*

[b] *Graduate School of Human Informatics, Nagoya University, Chikusa, Nagoya 464-8601, Japan*

[c] *Graduate School of Science, Tokyo Metropolitan University, Hachioji, Tokyo 192-0397, Japan*

Abstract

^{31}P MAS-NMR spectra and spin-lattice relaxation time T_1 in solid were measured on $A_4[Pt_2I(P_2O_5H_2)_4]\cdot nH_2O$ (A: Cs, Rb, K, Na and Li). Continuous spectrum changes in both line and splitting widths were observed with changing the cation size and the number of crystalline water. Complexes with A: Cs (n=0) and Rb (n=2) afforded two kinds of ^{31}P resonance lines with chemical shifts close to those in the Pt^{3+} and Pt^{2+} monomer complexes indicating a mixed valence structure. On the other hand, complexes with A: Na (n=2) and Li (n=4) yielded a broad single line suggesting the formation of paramagnetic Pt sites with an averaged valence of $Pt^{2.5+}$. An analogous continuous change was observed in ^{31}P T_1 in consistent with the above analysis. The observed spectra and T_1 depending on the cation size and the H_2O number suggest valence fluctuation due to spin jumps in and between Pt-Pt units sensitively influenced by crystal packings and hydrogen bonding.

Keywords: (Nuclear magnetic resonance spectroscopy)

1. Introduction

Halogen-bridged complexes with the quasi-one-dimensional chain structure of alternately arranged metal-halogen units have been shown to form the mixed valence state -M^{2+}-X-M^{4+}-X- in M: Pt, Pd; X: I, Br, Cl [1], and the averaged valence state -M^{3+}-X-M^{3+}-X- with a strong antiferro-magnetic spin structure in Ni complexes [2].

As a new type of halogen-bridged complexes, MMX type chains consisting of binuclear metal units in quasi-one-dimensional structures were reported [3-6]. In this system, following four possible oxidation states of the one-dimensional chain structure can be proposed:

(A) - M^{2+}- M^{2+}- X - M^{3+}- M^{3+}- X -

(B) - M^{2+}- M^{3+}- X - M^{2+}- M^{3+}- X -

(C) - M^{2+}- M^{3+}- X - M^{3+}- M^{2+}- X -

(D) - $M^{2.5+}$-$M^{2.5+}$- X - $M^{2.5+}$- $M^{2.5+}$- X -

So far, two types of MMX chains have been reported, i.e., $A_4[Pt_2X(P_2O_5H_2)_4]\cdot nH_2O$ (A: K, NH_4; X: I, Br, Cl) [3, 4] and $[M_2(CH_3CS_2)_4I]$ (M: Pt, Ni) [5, 6]. We have shown [7] that the valence structure in $(NH_4)_4[Pt_2X(P_2O_5H_2)_4]$ can be explained well by the model A from ^{31}P solid NMR measurement. Recently, the I-bridged complexes with various alkali metal ions A^+, $A_4[Pt_2I(P_2O_5H_2)_4]\cdot nH_2O$ (A: Cs, Rb, K, Na, Li) were prepared [8], and the valence structure on the chain has been discussed based on the studies of Raman and XP spectra [8]. We intend in the present study to measure ^{31}P MAS-NMR spectra and spin-lattice relaxation which can afford accurate information of Pt valences from the chemical shift and T_1 in ligand atoms.

2. Experimental

$A_4[Pt_2I(P_2O_5H_2)_4]\cdot nH_2O$ (A: Cs(n=0), Rb(n=2), K(n=2), Na(n=2) and Li(n=4)) were prepared according to literature [8]. A Bruker MSL-300 spectrometer was used for the measurement of ^{31}P MAS-NMR spectra at a Larmor frequency of 121.496 MHz and room temperature. A spinning rate of 3 - 8 kHz was employed and an 85 % aqueous solution of H_3PO_4 was used as the external standard of chemical shift. The spin-lattice relaxation time was measured by saturation recovery method in the temperature range of 200 - 300 K.

3. Results and Discussion

^{31}P MAS-NMR spectra observed at room temperature in $A_4[Pt_2I(P_2O_5H_2)_4]\cdot nH_2O$ (A: Cs(n=0), Rb(n=2), K(n=2), Na(n=2) and Li(n=4)) are shown in Fig. 1. In these spectra, we can see a continuous change of patterns with changing the cation size and also the number of H_2O molecules: A gradual broadening of spectrum width was observed with decreasing cation size and increasing water. At the same time, multiplet spectra were seen in complexes with large cations, while only a singlet was observed in small cation complexes and gradual increase in splitting was obtained with enlarging cations and reducing water.

*Corresponding author. Tel : +81-73-457-7365; fax: +81-73-457-7515; E-mail: nkimura@center.wakayama-u.ac.jp

0379-6779/01/$ – see front matter
PII: S0379-6779(00)00866-3

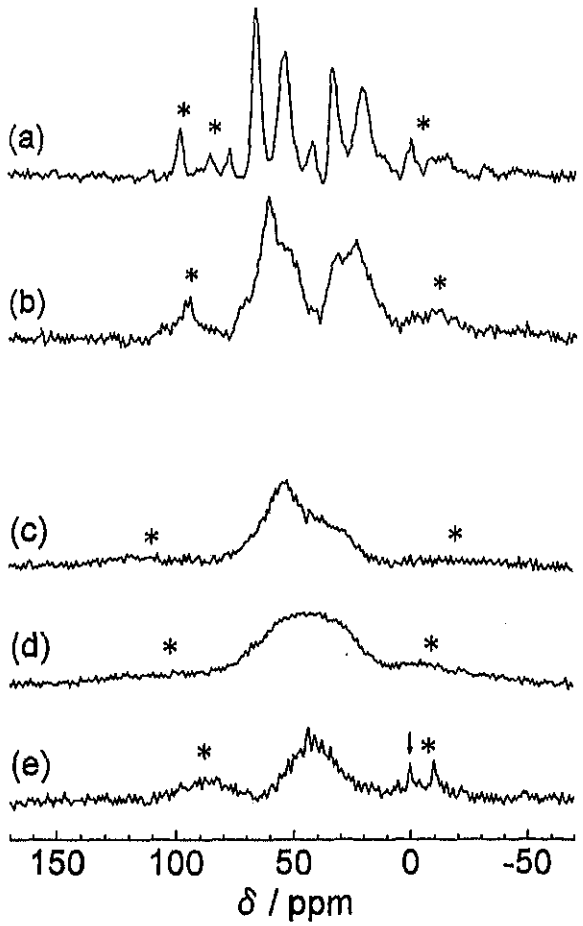

Fig.1 ^{31}P MAS-NMR spectra in (a) $Cs_4[Pt_2I(P_2O_5H_2)_4]$, (b) $Rb_4[Pt_2I(P_2O_5H_2)_4{\cdot}2H_2O$, (c) $K_4[Pt_2I(P_2O_5H_2)_4{\cdot}2H_2O$, (d) $Na_4[Pt_2I(P_2O_5H_2)_4{\cdot}2H_2O$ and (e) $Li_4[Pt_2I(P_2O_5H_2)_4{\cdot}4H_2O$. Peaks with asterisks are spinning sidebands. The arrow shows the signal of PO_4^{3-} impurity used as the internal standard.

In our previous study [7], we showed from ^{31}P MAS-NMR measurements on a polymer complex $(NH_4)_4[Pt_2I(P_2O_5H_2)_4]$ and corresponding Pt^{2+} and Pt^{3+} monomer complexes containing $[Pt_2(P_2O_5H_2)_4]^{4-}$ and $[Pt_2X_2(P_2O_5H_2)_4]^{4-}$ (X: I, Br, Cl) ions, that ^{31}P in $P_2O_5H_2$ ligands bonded to Pt^{2+} and Pt^{3+} sites afford chemical shifts of 65 ± 5 and 20 ± 5 ppm, respectively, and hence, the 1-D chain in the NH_4 salt has A structure. The centres of two doublet peaks in the present Cs and Rb salts being 60 and 26 ppm for Cs, and 58 and 26 ppm for Rb are explainable by Pt^{2+} and Pt^{3+}, respectively. These results imply that Cs and Rb salts consist of Pt^{2+} and Pt^{3+} mixed valence 1-D chains.

On the other hand, Li and Na salts gave only a broad singlet line at *ca.* 42 and *ca.* 45 ppm, respectively, being almost at the centre of shift values of ^{31}P on Pt^{2+} and Pt^{3+}sites. This result suggests that 1-D chains in Li and Na salts have the averaged D structure. Since NMR time scale is raher slow, it is possible that we observed a dynamically averaged structure, in case electron spins perform rapid jumps between Pt^{2+} and Pt^{3+} sites.

We also measured ^{31}P NMR spin-lattice relaxation times in these complexes. We can evaluate contributions from paramagnetic spins by the relaxation measurement, because the effect by magnetic field fluctuation from unpaired spins to NMR relaxation is expected in the preset system where the marked molecular motions contributing to relaxation are absent in the rigid 1-D molecular chains. ^{31}P spin-lattice relaxation times(T_1) observed at room temperature were *ca.* 0.7 s (Cs), 0.1-0.9 s (Rb), 0.1 s (K), 70 ms (Na), and 70 ms (Li). This order is also the same as that in spectrum width given above. The short T_1 of 70 ms in Li and Na salts implying contribution from electron spins is consistent with D model with an averaged valence state of $Pt^{2.5+}$. This model for Li salt can be supported from Raman and XP measurements[8] which showed the presence of a single Pt site in these measurements of the high frequencies unaveraged even with rapid spin motions.

As a possible valence structure for Cs and Rb salts, we may assign the diamagnetic structure A because of their rather long T_1 values. This explanation is consistent with the results of Raman and XP studies[8]. These T_1 are, however, not long enough compared with T_1 in Pt^{2+} and Pt^{3+} monomer complexes amounting to the order of 10 s. This suggests that the dynamical mixing of the other structures B-D with paramagnetic spins cannot be ignored in Cs and Rb salts. We can see this effect more markedly in K salt showing intermediate values in all of linewidth, splitting and T_1 that are explainable by the mixture of A-D. The continuous changes in spectrum widths and T_1 observed with the cationic size and the H_2O number seem to be associated with the onset of spin jumping in and between Pt-Pt units resulting in partial mixing of valence structures A-D. The observed clear dependency on the cation size and the H_2O number suggests that interactions between 1-D chains made by crystal packing and hydrogen bonding play important roles to determine the valence structure.

This work was partly supported by Grant-in Aid for scientific research No.(B) 12440192 from the Ministry of Education, Science, Sports and Culture.

References

[1] N. Matsumoto, M. Yamashita and S. Kida, Bull. Chem. Soc. Jpn., 51 (1978) 2334.
[2] K. Toriumi, Y. Wada, T. Mitani, S. Bandow, M. Yamashita and Y. Fujii, J.Am. Chem. Soc.,111(1989) 2341.
[3] C.-M. Che, F.H. Herbstein, W.P. Schaefer, R.E. Marsh and H.B. Gray, J. Am. Chem. Soc., 105 (1983) 4604.
[4] S. Jin, T. Ito, K. Toriumi and M. Yamashita, Acta Crystallogr., C45 (1989) 1415.
[5] C. Bellitto, A. Flamini, L. Gastaldi and L. Scaramuzza, Inorg. Chem., 22 (1983) 444.
[6] C. Bellitto, G. Dessy and V. Fares, Inorg. Chem., 24 (1985) 2815.
[7] N.Kimura, H.Ohki, R. Ikeda and M. Yamashita, Chem. Phys. Letters, 220 (1994) 40.
[8] M. Yamashita, S. Miya, T. Kawashima, T. Manabe, T. Sonoyama, H. Kitagawa, T. Mitani, H. Okamoto and R. Ikeda, J. Am. Chem. Soc., 121 (1999) 2321.

Proc. Int. Symposium on Advances in Neutron Scattering Research, Tokai, 2000
J. Phys. Soc. Jpn. 70 (2001) Suppl. A pp. 103–105

Magnetic Structure in a Halogen-Bridged 1-D $S = 1/2$ Heisenberg Antiferromagnet $[NiBr(chxn)_2]Br_2$

Shinya TAKAISHI, Shinichi ITOH[1] and Ryuichi IKEDA

Department of Chemistry, University of Tsukuba, Tsukuba 305-8571, Japan
[1]*Neutron Science Laboratory, Institute of Materials Structure Science, High Energy Accelerator Research Organization, Tsukuba 305-0801, Japan*

The presence of a strong one-dimentional(1-D) antiferromagnetic interaction was shown by the inelastic neutron scattering(INS) measurement on a polycrystalline sample of halogen-bridged complex $[NiBr(chxn)_2]Br_2$ (chxn:1R,2R-cyclohexanediamine), in which paramagnetic Ni(III) atoms were shown to form a -Br-Ni-Br-Ni-Br- type 1-D structure. The INS measurement was performed at 23 K with an inelastic neutron chopper spectrometer(INC) combined with the pulsed neutron source installed in Neutron Science Laboratory(KENS) with incident neutron energies, $E_i = 20.9$ and 31.4 meV. Scattering-angle dependences of the powder average spectra were observed at scattering angles from 5.5 to 30.6°. The intensity difference between scattering angles including and excluding the antiferromagnetic superlattice point was obtained. This result affords the first direct experimental proof of the presence of antiferromagnetic 1-D chains in this system.

KEYWORDS: inelastic neutron scattering, 1-D antiferromagnetic, halogen-bridged Ni complex

§1. Introduction

A series of halogen-bridged metal complexes having a one-dimentional(1-D) mixed-valence -X-M^{II}-X-M^{IV}-X- structure where M = Pt, Pd and X = Cl, Br, I have been extensively studied as a Peierls distorted linear chain system with a strong electron-lattice interaction resulting in the halogen position on the 1-D chain off-centered from the midpoint between neighboring metal atoms[1,2]. Recently, a new type of halogen-bridged complexes $[NiX(chxn)_2]X_2$ (chxn: 1*R*,2*R*-cyclohexanediamine, $C_6H_{10}(NH_2)_2$; X: Cl, Br) have been shown to crystallize in a quasi one-dimensional structure with -Br-Ni-Br-Ni-Br- in which all Ni atoms are crystallographically equivalent[3] implying the formation of $S = 1/2$ paramagnetic chains of Ni(III). The reported magnetic susceptibility and EPR measurements[4] suggested the presence of antiferromagnetic Heisenberg 1-D chains of a quite large exchange interaction amounting to $J = 3600$ K[4], but the accurate magnetic structure is not settled.

In the present study, we intend to measure scattering-angle dependences of INS at low-temperatures to confirm directly the presence of a strongly coupled 1-D antiferromagnetic interaction in the present complex by observing the magnetic excitation in the $S = 1/2$ Heisenberg system.

§2. Experimental

Crystals of polymer complex $[Ni^{III}Br(chxn)_2]Br_2$ were prepared by the slow diffusion of Br_2 gas into a solution of monomer complex $Ni^{II}Br_2(chxn)_2$ dissolved in 2-methoxyethanol. We used non-deuterated ligand, cyclohexanediamine because of complicated processes of the deuteration of this ligand containing two optical active carbon atoms. Prepared crystals were identified by the elemental analysis and X-ray diffraction patterns. Calcd for $[Ni^{III}Br(chxn)_2]Br_2$: C, 27.36; H, 5.37; N, 10.64 %. Found: C, 27.55; H, 5.56; N, 10.57 %. X-ray powder patterns recorded at room temperature were well indexed with the reported lattice constants: $a = 23.587$, $b = 5.161$, $c = 7.121$ Å[3]. About 8 g of polycrystalline sample was used for the present measurement.

The INS measurement was performed with an inelastic neutron chopper spectrometer(INC) combined with the pulsed neutron source installed in KENS of High Energy Accelerator Research Organization[5]. Pulsed polychromatic beams generated at the neutron source were monochromatized by a mechanical chopper synchronized with the repetition of neutron pulses(20 Hz). Scattering neutrons were received at the detector covering a wide-range of scattering angles form 5 to 130°. The energy transfer was determined from the time-of-flight method. In the present measurement, we applied incident neutron energies, $E_i = 20.9$ and 31.4 meV and all measurements were carried out at 23 K. The energy resolution in the scan with $E_i = 20.9$ and 31.4 meV was determined to be 1.0 and 1.6 meV at full width at half maximum(FWHM), respectively, by measuring the energy width of the incoherent elastic scattering.

§3. Result and Discussion

Figure 1 (a) shows the observed inelastic spectrum from $[Ni^{III}Br(chxn)_2]Br_2$ with $E_i = 31.4$ meV, where the sum of observed intensities at detectors located at scattering angles between 5.5° and 7.3° and that between 11.0° and 21.7° are plotted. We observed increase in the inelastic intensity at the high angles. The intensity of the inelastic neutron scattering is proportional to the dynamical structure factor $S(q, E)$, where q is

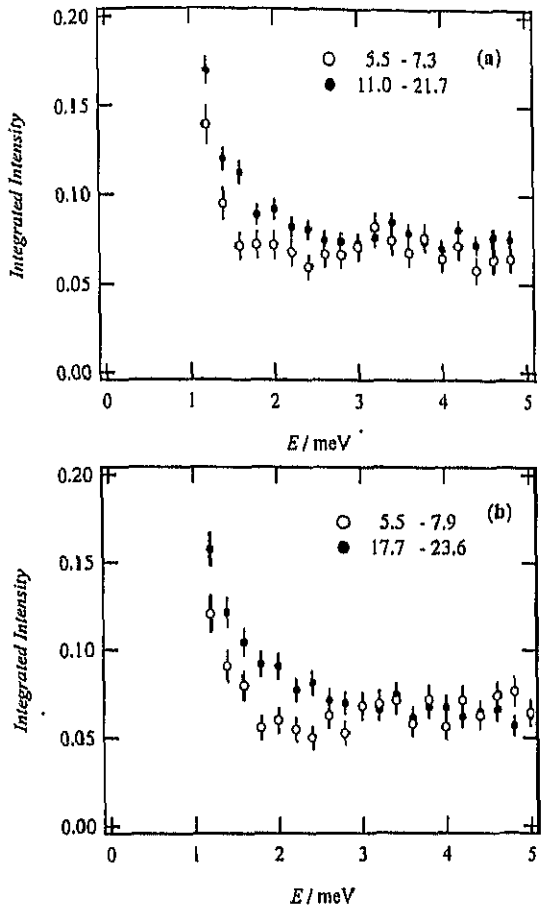

Fig. 1. The inelastic spectra observed in ranges of 11.0° - 21.7° (including the point) and 5.5° - 7.3° (excluding the point) for E_i = 31.4 meV(a) and 17.7° - 23.6° (including the superlattice point) and 5.5° - 7.9° (excluding the point) for E_i = 20.9 meV(b) in $[Ni^{III}Br(chxn)_2]Br_2$.

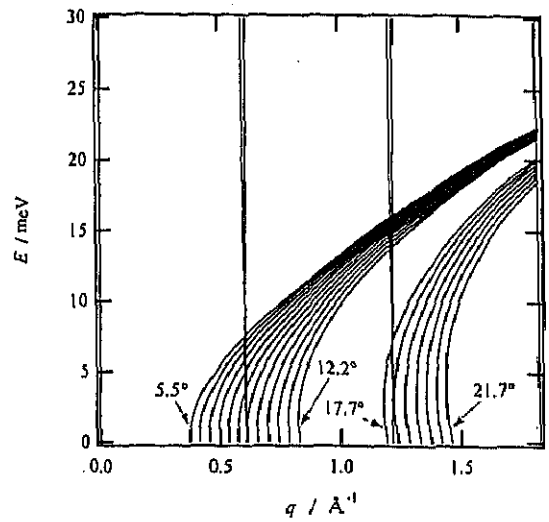

Fig. 2. The scan loci for detectors on the INC spectrometer for E_i = 31.4 meV with spin-wave dispersion in 1-D antiferromagnetic $[Ni^{III}Br(chxn)_2]Br_2$ with b = 5.16 Å and by assuming J=300 meV. $|q| < Q$ (left parts of curved solid lines) contribute to the energy transfer spectrum at respective scattering angles.

the component of the scattering vector (Q) parallel to the crystallographic 1-D direction (b-axis for the present complex) and E is the energy transfer given by E_i - E_f (the difference between the incident and the scattered neutron energies). For a polycrystalline sample of a 1-D magnetic system, the magnetic scattering intensity is an averaged $S(q, E)$ over q as follows[5]

$$I_{mag}(Q, E) = f(Q)^2 \frac{1}{2Q} \int_{-Q}^{Q} S(q, E)\, dq, \qquad (3.1)$$

where $f(Q)$ is the magnetic form factor of unpaired electrons. This shows that all (q, E) points with $|q| < Q$ will contribute in the energy spectrum. In a 1-D antiferromagnetic system, $S(q, E)$ exhibits a maximum at the superlattice point, $q = \pi/b$, while it vanishes at $q = 2n\pi/b$ with n being an integer. Therefore, a marked intensity can be expected at $Q > \pi/b$, while no intensity is expected at $Q < \pi/b$. In the present complex, the superlattice point is given by 0.61 Å^{-1}, and, in the scan with E_i = 31.4 meV, for instance, the scattering angle (ϕ) corresponding to the superlattice point is 8.9° at E = 0. Figure 2 shows the scan loci for detectors on the INC spectrometer around the superlattice point, with an antiferromagnetic dispersion curve. Since an intensity observed at Q is the integrated $S(q, E)$ over $|q| < Q$ as mentioned above, an intensity of the inelastic magnetic scattering should be observed at low energy transfers at detectors with $\phi > 8.9°$. The low angle data ($\phi = 5.5° - 7.3°$) at $E = 0$ exclude the superlattice point and the high angle data ($\phi = 11.0° - 21.7°$) include it. The observed intensity difference shown in Fig. 1 (a) suggests to be associated with the antiferromagnetic interaction. A similar intensity difference was observed with E_i = 20.9 meV as shown in Fig. 1 (b), in this condition, the superlattice point corresponds to $\phi = 11.0°$.

Next, in order to elucidate whether the origin of the observed intensity difference is the 1-D antiferromagnetic interaction, we plotted in Fig. 3 the integrated intensities in the energy transfers between 0.5 and 2 meV as a function of ϕ. In this energy range, the intensity difference was clearly observed as shown in Figure 1. Due to a coarse energy resolution of INC, a tail of a strong Bragg scattering at (200), of which scattering angle is expected to be 9.6° and 7.9° for E_i = 20.9 meV and 31.4 meV, respectively, was detected in this inelastic region. We assumed that the scattering function is given by

$$I(Q, E) = AI_{mag}(Q, E) + B\delta(Q - Q_0)\delta(E) + C, \quad (3.2)$$

where A, B and C are adjustable parameters. The second term in eq. (3.2) represents the Bragg scattering at (200) and thus Q_0 = 0.53 Å^{-1}, also, a constant background was assumed in the third term. We tried to fit the observed ϕ -dependence with the resolution-convoluted $I(Q, E)$ integrated over E between 0.5 meV and 2 meV on the scan locus for a given ϕ , where $S(q, E)$ in eq. (3.1) was assumed to be the following classical dynamical scattering function:

$$S(q, E) = (n(E) + 1)|\tan(bq/2)|\delta(E - E_q), \qquad (3.3)$$

where $(n(E)+1)$ is the temperature factor, $(\exp(E/kT) -$

$1)^{-1}+1$, and E_q is the dispersion relation of the magnetic excitations, $4SJ|\sin(bq)|$ (Hamiltonian: $2J\Sigma S_i S_{i+1}$)[6]. The magnetic form factor in eq. (3.1), $f(Q)$, was taken from the calculated value of the Ni^{III} free ion[7]. The resolution functions for E and Q were assumed to be Gaussian. The resolution width in E, ΔE, was measured as mentioned above, and that in Q, ΔQ, was taken from the calculated value from the angular resolution of the geometrical configuration of the spectrometer as well as ΔE[8]. In the present (Q, E) region, ΔQ (FWHM) was calculated to be 0.17 $Å^{-1}$ and 0.14 $Å^{-1}$ for E_i = 20.9 meV and 31.4 meV, respectively. The value of J was insensible to the present calculation, because it can be estimated to be several hundred meV from the susceptibility and EPR measurements[4] and this value is much larger than the present energy range, and therefore, J was fixed to be tentatively 300 meV in the present calculation. It is appropriate that the quantum dynamical structure factor is used because the present complex is expected to be an $S = 1/2$, 1-D system. The present energy range for the analysis is too small to discuss the functional form of $S(q, E)$ with a very large value of J. In fact, such an integrated quantity with very low energy ranges shown in Figs. 1 and 3 was insensible to the functional form of $S(q, E)$. The purpose of the present calculation is to show whether the observed inelastic scattering is of magnetic origin, and therefore, we used the simplest model for $S(q, E)$ in the present analysis. The solid line in Fig. 3 is the calculated curve, and the observed ϕ - dependence of the integrated intensity was in good agreement with the calculation. This indicates the existence of a 1-D antiferromagnetic interaction in the present complex.

§4. Conclusion

The increase of the scattered neutron intensity from excluding to including the superlattice point was observed. And the scattering angle dependence of the integrated intensity was well fitted by summation of component of 1-D magnetic excitations, Bragg scattering at (200) and a constant background. These results apparently indicate the presence of 1-D antiferromagnetic interaction along the paramagnetic -Ni-Br-Ni- chains.

This work affords the first direct experimental proof for the presence of the antiferromagnetic 1-D chains in the present complex. At the same time, we could provide an example of polycrystalline 1-D magnetic systems without deuteration of protons studied by INC in KENS.

To determine the quantitative J value, the measurement with single crystals is essential. Along this purpose, new methods for growing single crystals are now under developing.

This work was partly supported by Grant-in Aid for scientific research No.(B) 12440192 from the Ministry of Education, Science, Sports and Culture.

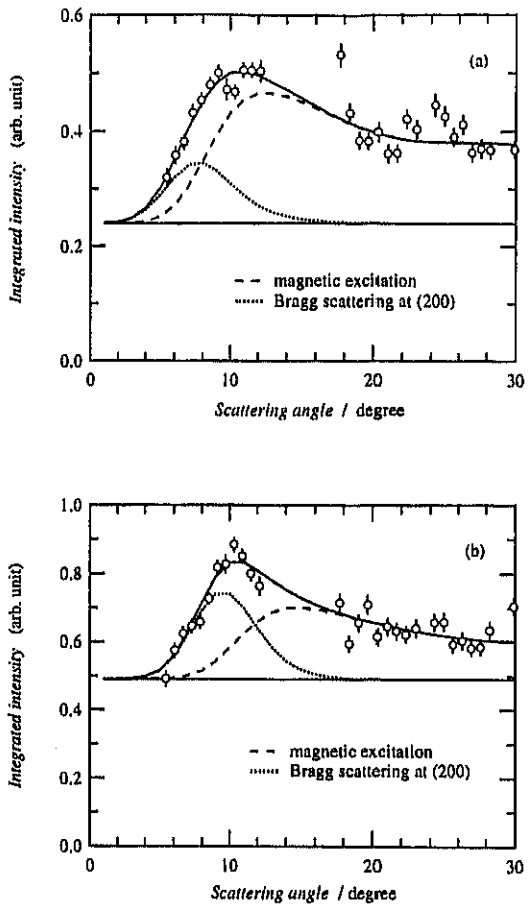

Fig. 3. Scattering-angle dependences of neutron intensity with E_i = 31.4 (a) and 20.9 meV(b) integrated in an energy transfer range, E = 0.5-2.0 meV. The dotted and broken lines show the calculated intensities due to the Bragg scattering at (200) and 1-D magnetic excitation, respectively. The solid straight line shows the constant background. The solid curved line shows the summation of components of 1-D magnetic excitations, Bragg scattering at (200) and a constant background.

1) H. J. Keller: *Extended Linear Chain Compounds*, ed. S. Miller (Plenum Press, New York, 1982)Vol.1, chap. 8.
2) D. S. Martin Jr.: *Extended Linear Chain Compounds*, ed. S. Miller (Plenum Press, New York, 1982)Vol.1, chap. 9.
3) K. Toriumi, Y. Wada, T. Mitani, S, Bandow, M. Yamashita and Y. Fujii: J. Am. Chem. Soc. **111**(1989)2341.
4) H. Okamoto, K. Toriumi, T. Mitani and M. Yamashita: Phys. Rev. **42**(1990)10381.
5) H. Mutka, C. Payen, P. Molinie, J. L Soubeyroux, P. Colombet and A. D. Taylor: Physica B **181&182**(1992)197.
6) See for instance, S. W. Lovesey: *Theory of Neutron Scattering from Condensed Matter* (Oxford University Press, Oxford, 1984).
7) R. E. Watson and A. J. Freeman: Acta. Cryst. 14(1961)27.
8) M. Arai, M. Kohgi, M. Itoh, H. Iwasa, N. Watanabe, S. Ikeda and Y. Endoh: *KENS REPORT-VII, KEK Progress Report 88-2*, (Nationbal Laboratory for High Enerhy Physics, Tsukuba, 1988)p.9.

CHEMCOMM Communication
www.rsc.org/chemcomm

An unusual six-co-ordinate platinum(II) complex containing a neutral I_2 ligand

Rie Makiura,[b] Isoroku Nagasawa,*[a] Noriyoshi Kimura,[c] Shin'ichi Ishimaru,[b] Hiroshi Kitagawa[b] and Ryuichi Ikeda[b]

[a] *Department of Chemistry, Fukuoka University of Education, Akama 729-1, Munakata, Fukuoka 811-4192, Japan. E-mail: isoroku@fukuoka-edu.ac.jp*
[b] *Department of Chemistry, University of Tsukuba, Tennodai 1-1-1, Tsukuba, Ibaraki 305-8571, Japan. E-mail: ikeda@staff.chem.tsukuba.ac.jp*
[c] *Department of Chemistry, Faculty of Education, Wakayama University, Sakaedani 930, Wakayama 640-8510, Japan. E-mail: nkimura@center.wakayama-u.ac.jp*

Received (in Cambridge, UK) 24th April 2001, Accepted 20th July 2001
First published as an Advance Article on the web 7th August 2001

The present paper deals with a rare platinum(II) complex containing the κ-I_2 ligand, which is an unusual example of a six-co-ordinated octahedral platinum(II) complex.

Platinum(II) strongly demands a square-planar co-ordination geometry and very few six-co-ordinate complexes have so far been characterized.[1] *Trans*-[PtI_2(diars)$_2$] (diars = *o*-phenylenebis(dimethylarsine)) has been the only example of a six-co-ordinate platinum(II) complex determined by X-ray study.[1b] However, Pt–I bonds in this complex seem to be weak because of long Pt–I distances of 3.50 Å. Here, we present a novel octahedral platinum(II) complex, [PtI(dmpe)$_2$(κ-I_2)]I_3 (dmpe = 1,2-bis(dimethylphosphino)ethane) in which the neutral molecular iodine co-ordinates to the platinum(II) ion. This is a quite rare example of the platinum(II) complex having clearly short Pt–I bond distances.

Treatment of [Pt(dmpe)$_2$](SCN)$_2$ 1[2] with a 3 molar amount of iodine gave black needle crystals formulated as [PtI(dmpe)$_2$(κ-I_2)]I_3 **2** (Scheme 1, yield 21%).†

The molecular structure of complex **2** is displayed in Fig. 1, with partial labeling.‡ Complex **2** is a mononuclear complex with Pt1, I1, I2, and I3 atoms located on a crystallographic mirror plane that is coincident with mirror symmetry of the complex. The I4, I5 and I6 atoms of I_3^- anion are located on a crystallographic mirror. The co-ordination geometry around the platinum atom is octahedral with 4P and 2I donor atoms, with two iodine atoms having *trans* geometry. The bond distances between platinum and iodine atoms are 2.811(1) and 2.817(1) Å for Pt1–I1 and Pt1–I2, respectively. These values are considerably shorter than those in the complex *trans*-[PtI_2(diars)$_2$] **3** (here the bond length of Pt–I is 3.50 Å).[1b] Compared to **3**, complex **2** can be undoubtedly considered to be a six-co-ordinate octahedral platinum(II) complex. Furthermore, it is worthy of note that the neutral molecular iodine co-ordinates to the platinum(II) ion by end-on type (Pt1–I2–I3 = 171.58(3)°), and the I2–I3 bond distance of 3.061(1) Å is much longer than that of 2.715(6) Å in free diiodine molecules.[3] This means that the electrons on the central platinum(II) flow into the κ-I_2 ligand, which is attributable to a d_{z^2} (Pt) to σ* (I_2) donation.[4]

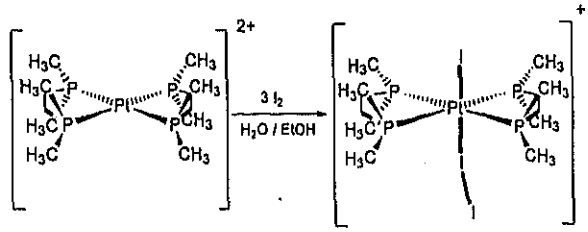

Scheme 1

Van Koten and coworkers have reported five-co-ordinate platinum(II) complexes containing the κ-I_2 ligand, [PtI{C_6H_3(CH_2NMe_2)$_2$-2,6}(κ-I_2)] **4a** and [Pt(κ-I_3)(κ-I_2){C_6H_3(CH_2N(*t*-Bu)Me)$_2$-2,6}] **4b**.[5] The Pt–I_2 bond distances of 2.895(1) and 2.906(2) Å in **4a** and **4b**, respectively,[5d] are longer than 2.817(1) Å in **2**, showing that a stronger platinum–molecular iodine bond is realised in **2**. The I–I bond distances in these complexes show a marked difference: the I2–I3 distance of 3.061(1) Å in **2** is much longer than that of 2.822(1) and 2.793(1) Å in **4a** and **4b**, respectively. This elongation is attributable to the existence of the ligand on a *trans* position of the κ-I_2 ligand. The bond distances between platinum and co-ordinated phosphorus in **2** are 2.369(2) and 2.374(2) Å for Pt1–P1 and Pt1–P2, respectively. These values are longer than that of starting square-planar complex **1** with a Pt–P of 2.317(1) Å.[6]

The formal oxidation state of the platinum ion in **2** is expected to be +2. To confirm this, X-ray photoelectron spectroscopy (XPS) measurements were performed.§ Binding energies of the Pt 4f region given in Table 1 were determined by a conventional deconvolution procedure. The XPS spectrum of **2** shows a doublet, whose binding energies are coincident with the values of Pt(II) binding energies.[5c,7] From XPS measurements, the platinum ion in complex **2** was found to have the +2 oxidation state.

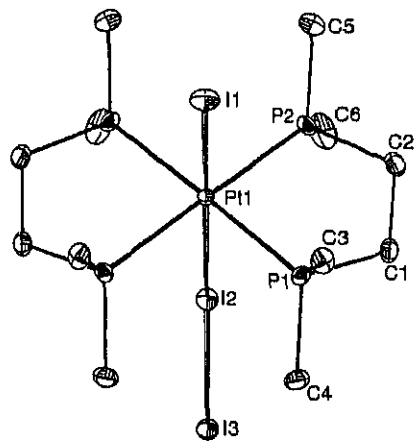

Fig. 1 The structure of **2**. Selected bond distances (Å) and angles (°): Pt1–I1 2.811(1), Pt1–I2 2.817(1), Pt1–P1 2.369(2), Pt1–P2 2.374(2), I2–I3 3.061(1), P1–C1 1.82(1), P1–C3 1.80(1), P1–C4 1.80(1), P2–C2 1.82(1), P2–C5 1.82(1), P2–C6 1.80(1), C1–C2 1.52(1); I1–Pt1–I2 177.75(3), I1–Pt1–P1 89.73(5), I1–Pt1–P2 92.45(5), I2–Pt1–P1 91.78(5), I2–Pt1–P2 86.04(5), P1–Pt1–P2 84.46(6), Pt1–I2–I3 171.58(3).

DOI: 10.1039/b103648n

Table 1 Binding energies (eV) for the 4f region of platinum

Compound	$4f_{5/2}$	$4f_{7/2}$
1	76.0	72.7
2	76.0	72.6

The ^{31}P MAS NMR spectral data for **1** and **2** in the solid state and in CD_3CN or D_2O solution are given in Table 2. In the ^{31}P MAS NMR spectrum of **2**, a signal appeared at δ 11.9 ppm with satellites due to the coupling with ^{195}Pt (1758 Hz). The smaller coupling constant $^1J_{Pt-P}$ in **2** compared with 2173 Hz in **1**, is explained by the difference in the co-ordination number.[8] $^1J_{Pt-P}$ of 2173 Hz in **1** is a normal value compared with analogous platinum(II) square-planar co-ordinate complexes.[9] On the other hand, in CD_3CN solution, the observed $^1J_{Pt-P}$ of 2172 Hz in **2** was very close to 2162 Hz observed in D_2O solution for **1**. This result indicates that complex **2** has a square-planar geometry caused by the dissociation of iodine in CD_3CN solution.

Table 2 ^{31}P NMR spectroscopic data

Compound	$\delta_{^{31}P}$/ppm	$^1J(^{195}Pt-^{31}P)$/Hz
1	32.75[a]	21 273[a]
	33.06[b]	2162[b]
2	11.85[a]	1758[a]
	28.95[c]	2172[c]

[a] MAS NMR spectrum in the solid state with a spinning rate of 4–5 kHz. [b] In D_2O. [c] In CD_3CN solution.

This work was partly supported by Grant-in Aid for Scientific Research No.(B) 12440192 from the Ministry of Education, Science, Sports and Culture. The authors are grateful to Dr Y. Yokoyama and Mr H. Nakazono, the Chemical Analysis Center, University of Tsukuba, for JEOL EX-270 NMR spectral and elemental analysis measurements. We thank Dr H. Kuma and Dr T. Kawamoto, Osaka University, for discussion of X-ray data.

Notes and references

† In this reaction, two electrons are gained, but the fully balanced equation was not understood. The authors consider that the reaction is related to the redox systems of Pt(II) with Pt(IV) and of $2I^-$ with I_2.

‡ *Crystal data* for **2**: $C_{12}H_{32}I_6P_4Pt$, M = 1256.8, orthorhombic, *Pnma*, a = 8.6718(4), b = 10.7317(5), c = 30.9849(3) Å, U = 2883.6(3) Å^3, D_c = 2.89 g cm^{-3}, Z = 4, $F(000)$ = 2240, μ(Mo-Kα) = 11.51 mm^{-1}, graphite monochromator, room temperature, 4933 reflections measured, 2734 observed [$I > 3\sigma(I)$], 115 parameters. Empirical absorption corrections (ψ-scan) were applied. Final R factor = 0.033, R_w = 0.040. Hydrogen atoms were included in fixed positions with isotropic thermal parameters, while all other atoms were refined by anisotropic thermal parameters.

CCDC reference number 155325. See http://www.rsc.org/suppdata/cc/b1/b103648n/ for crystallographic data in CIF or other electronic format.

§ XPS spectra were carried out on an Ulvac Phi 5600ci with monochromated Al-Kα X-rays (1487 eV). Binding energies were measured relative to the Au $4f_{7/2}$ peak of the gold fine powder mixed with the sample.

1 (*a*) C. M. Harris, R. S. Nyholm and D. J. Phillips, *J. Chem. Soc.*, 1960, 4379; (*b*) N. C. Stephenson, *J. Inorg. Nucl. Chem.*, 1962, **24**, 791.
2 D. J. Gulliver, W. Levason and K. G. Smith, *J. Chem. Soc., Dalton Trans.*, 1981, 2153.
3 F. van Bolhuis, P. B. Koster and T. Migchelsen, *Acta Crystallogr.*, 1967, **23**, 90.
4 F. M. Bickehaupt, E. J. Baerends and W. Ravenek, *Inorg. Chem.*, 1990, **29**, 350.
5 (*a*) J. A. M. van Beek, G. van Koten, W. J. J. Smeets and A. L. Spek, *J. Am. Chem. Soc.*, 1986, **108**, 5010; (*b*) J. A. M. van Beek, G. van Koten, G. P. C. M. Dekker, E. Wissing, M. C. Zontberg and C. H. Stam, *J. Organomet. Chem.*, 1990, **394**, 659; (*c*) J. C. Muijsers, J. W. Niemantsverdriet, I. C. M. Wehman-Ooyevaar, D. M. Grove and G. van Koten, *Inorg. Chem.*, 1992, **31**, 2655; (*d*) R. A. Gossage, A. D. Ryabov, A. L. Spek, D. J. Stufkens, J. A. M. van Beek, R. van Eldik and G. van Koten, *J. Am. Chem. Soc.*, 1999, **121**, 2488.
6 I. Nagasawa and R. Ikeda, unpublished work.
7 J. Moulder, W. F. Stickle, P. E. Sobel and K. D. Bomben, *Handbook of X-Ray Photoelectron Spectroscopy*, ed. J. Chastain, Perkin-Elmer Co., 1992, pp.180, 234.
8 J. F. Nixon and A. Pidcock, *Annual Review of NMR Spectroscopy*, ed. E. F. Mooney, Academic Press, London, 1969, vol. 2, p 374.
9 E. G. Hope, W. Levason and N. A. Powell, *Inorg. Chim. Acta*, 1986, **115**, 187; V. S. Reddy, K. V. Katti and C. L. Barnes, *Inorg. Chim. Acta*, 1995, **240**, 367.

Dynamics of Water Molecules in Micropores of $AlPO_4$-5 and SAPO-5 Studied by ^1H NMR

Kazuma Gotoh, Shin'ichi Ishimaru, and Ryuichi Ikeda
Department of Chemistry, University of Tsukuba, Tsukuba 305-8571

(Received August 20, 2001; CL-010808)

Dynamics of water molecules in one-dimensional micropores $AlPO_4$-5 and SAPO-5 frameworks was studied by measuring ^1H NMR spectra, second moment M_2 of line-width and spin-lattice relaxation time T_1. Although the presence of two kinds of water molecules free and bound on the capillary wall were reported in $AlPO_4$-5, our NMR T_1 results imply the absence of two kinds of H_2O motions, but the motional rate distributes from slow to fast jumps in both $AlPO_4$-5 and SAPO-5.

$AlPO_4$-5, one of typical aluminophosphate microporous crystals forms a one-dimensional homogeneous channel structure with a pore diameter of 0.73 nm. SAPO-5 has an analogous structure to that in $AlPO_4$-5, but a part of P (and Al) atoms in channel walls are replaced by Si, and hence, Brönsted acid sites are created on the pore surface. Molecules adsorbed in $AlPO_4$-5 and SAPO-5 can form one-dimensional molecular arrays which are expected to exhibit new structural and dynamical properties different from two or three dimensionally aggregated molecular systems.

From the measurement of ^2H NMR spectra of ^2H_2O in $AlPO_4$-5,[1,2] Goldfarb et al. reported the presence of two kinds of water molecules in pores: one is free and the other is fixed on the wall. To study dynamics of H_2O motions affected by the wall structures in $AlPO_4$-5 and SAPO-5, we measured ^1H NMR spin-lattice relaxation times (T_1), second moments of resonance lines (M_2) and spectra of H_2O adsorbed in $AlPO_4$-5 and SAPO-5.

$AlPO_4$-5 and SAPO-5 were synthesized according to the reported method.[3] Obtained fine crystals of ca. 100 μm long were calcined at ca. 990 K for 48 h and kept in vacuo at 393 K for 2 days, then exposed to saturated H_2O vapor. These specimens abbreviated to $AlPO_4$-5(H_2O) and SAPO-5(H_2O) were used for measurements.

X-Ray powder diffraction on calcined crystals were conducted for identifying the obtained samples. The Si/P atomic ratio in SAPO-5 was determined by a JEOL JXA-8621 electron probe microanalyser(EPMA) to be 9 ± 1 / 91 ± 1. The water content in $AlPO_4$-5(H_2O) was obtained by thermo-gravimetry affording a weight loss of 22% at 360–370 K corresponding to the water desorption. Comparing this value with 21.96%[4] reported, micropores in $AlPO_4$-5 are presumed to be almost filled with water molecules.

As shown in Figure 1, ^1H NMR spectra in $AlPO_4$-5(H_2O) and SAPO-5(H_2O) observed by a Bruker MSL-300 spectrometer exhibited a single peak with a width of 2.0 ± 0.1 kHz above room temperature. This implies that water molecules in both systems perform mostly the isotropic rotation in this temperature range. This result seems to be inconsistent with the reported ^2H NMR spectra[2] showing a doublet structure even at 353 K. An almost temperature independent small splitting also observed in our ^2H NMR measurement is attributable to the electric field gradient formed by charges on the pore wall. Our

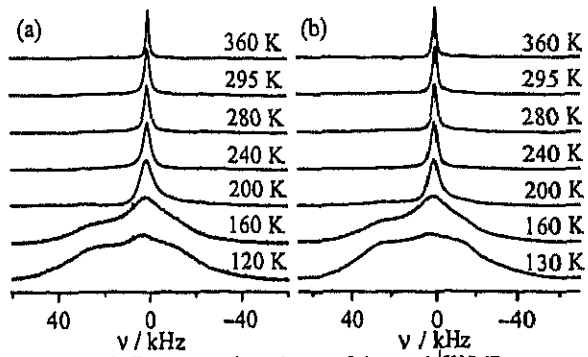

Figure 1. Temperature dependences of observed ^1H NMR spectra in H_2O adsorbed in (a) $AlPO_4$-5 and (b) SAPO-5.

rough calculation based on the point charge model supported this explanation. Upon cooling, a gradually growing broad component with a width of ca. 60 kHz appeared accompanied by a slowly broadening narrow peak suggesting two kinds of water molecules as reported.[1]

Figure 2 shows M_2 observed by the solid echo method with a Bruker SXP-100 spectrometer in $AlPO_4$-5(H_2O) and SAPO-5(H_2O). M_2 of ca. $(30 \pm 5) \times 10^{-2}$ mT^2 observed at ca. 100 K agreed with 33.7×10^{-2} mT^2 calculated for the rigid water molecule. Above ca. 200 K, the echo signals in both systems showed barely separable two components in consistent with the foregoing ^1H spectra showing the superimposed broad and narrow signals. We could determine large M_2 components in both specimens and the small component of SAPO-5(H_2O). A small M_2 of $(0.5 \pm 0.1) \times 10^{-2}$ mT^2 in SAPO-5 above 220 K implies the onset of the H_2O isotropic rotation, and the large component showing a width of ca. 2.5×10^{-2} mT^2 in both systems at room temperature is attributed to the restricted water. It is noted that the gradual M_2 change over 150 K observed in both systems is unexplainable by the usual thermal activation process of molecular motions.

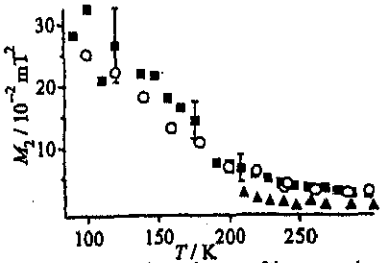

Figure 2. Temperature dependences of the second moment (M_2) of observed ^1H NMR absorptions in H_2O adsorbed in $AlPO_4$-5 (broad [○] component) and SAPO-5 (broad [■] and sharp [▲] components).

The small and the large M_2 observed below room temperature in both systems can correspond to the observed two ^1H spectrum components together with the reported narrow and

broad ^{2}H spectra.[1] These results imply the presence of free and fixed two kinds of H_2O molecules in micropores in accordance with the result reported by Goldfarb et al.[1]

The recovery of ^{1}H magnetization in ^{1}H NMR T_1 measurement with a Bruker SXP-100 spectrometer showed nonexponential decay in the T_1 measurement. We divided this decay curve into two T_1 components, where the ratio of the short component vs the whole T_1 was ca. 1/10. Figure 3 shows the temperature and frequency dependences of only the long T_1. The long T_1 component was assigned to H_2O adsorbed in micropores, while the short is attributable to H_2O located near trace of amounts of paramagnetic impurities formed in the wall which was observed by ESR.

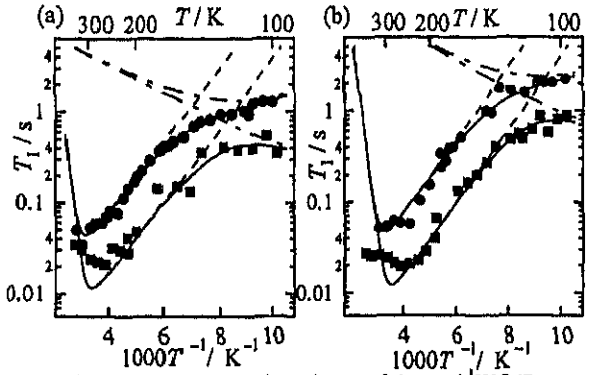

Figure 3. Temperature dependences of observed ^{1}H NMR spin-lattice relaxation times (T_1) of H_2O adsorbed in (a) $AlPO_4$-5 (b) SAPO-5, at 54.1 MHz [●] and at 14.1 MHz [■]. Solid lines are the best-fitted calculated values superposed by two T_1 components expressed as dotted and chain lines.

We tried to fit the observed long T_1 data by superposed two BPP-type minima originating from reported two kinds of H_2O molecules in pores, but could not obtain satisfactory fit. T_1 observed in both systems below room temperature could not be expressed by the ω^2 rule expected from the conventional BPP theory[5] in the range $\omega\tau_c >> 1$. Moreover, the T_1 minimum of 21 ms observed at 14 MHz was much longer than 3.9 ms calculated for the isotropic rotation model derived from the above M_2 analysis. These results together with the gradual M_2 decrease observed over 150 K as noted above, can be explained by assuming the Cole–Davidson type τ_c distribution[6] which can be expected from the presence of several kinds of water molecules with different environments in micropores. Conner has reported[7] a distributed τ_c given by

$$g(\tau) = \frac{\sin\beta\pi}{\pi}\left(\frac{\tau}{\tau_c - \tau}\right)^{\beta} \quad \tau \le \tau_c \qquad (1)$$
$$= 0 \quad \tau > \tau_c$$

where τ is the correlation time of the motion and β ($0 < \beta \le 1$) shows the distribution amplitude. Substituting eq 1 into the BPP equation, T_1 is given by

$$T_1^{-1} = \frac{2}{3}\gamma^2\Delta M_2\left\{\frac{\tau_c \sin\left(\beta\tan^{-1}\omega\tau_c\right)}{\omega\tau_c\left(1+\omega^2\tau_c^2\right)^{\beta/2}} + \frac{2\tau_c \sin\left(\beta\tan^{-1}2\omega\tau_c\right)}{\omega\tau_c\left(1+4\omega^2\tau_c^2\right)^{\beta/2}}\right\} \qquad (2)$$

where γ, ΔM_2 and ω are the protonic magnetogyric ratio, the M_2 reduction by the motion, and the Larmor frequency, respectively. The Arrhenius equation for the cut-off time τ_c is assumed by

$$\tau_c = \tau_0 \exp\frac{E_a}{RT} \qquad (3)$$

Here, E_a denotes the activation energy of the motion.

The observed values were fitted by superimposed two motional modes: the high-temperature mode 1 was assumed to have a τ_c distribution given by eq 1, while the low-temperature mode 2 is expressed by the BPP-type relaxation for simplicity. We assigned mode 1 to the H_2O isotropic rotation because M_2 less than 3×10^{-2} mT^2 above 250 K in $AlPO_4$-5(H_2O) was explained by this motion. Mode 2 was assigned to the 180°-flip because of the small ΔM_2 of 0.38×10^{-2} and 0.2×10^{-2} mT^2 observed in $AlPO_4$-5(H_2O) and SAPO-5(H_2O), respectively. This model is consistent with the reported ^{2}H spectrum at 148 K[1] with a narrow component explainable by this motion of a part of H_2O in pores. The best fitted T_1 and determined motional parameters are shown in Figure 3 and Table 1, respectively.

Table 1. Motional parameters of water molecules derived from T_1 data.

Sample	Mode	E_a / kJ mol^{-1}	ΔM_2 / 10^{-2} mT^2	τ_0 / s	β
$AlPO_4$-5 (H_2O)	1	50 ± 4	33.5 ± 2	4.0×10^{-17}	0.15 ± 0.03
	2	3.0 ± 0.5	0.38 ± 0.1	8.0×10^{-11}	1 (BPP)
SAPO-5 (H_2O)	1	40 ± 3	29.3 ± 2	4.0×10^{-16}	0.17 ± 0.03
	2	3.0 ± 0.5	0.21 ± 0.1	6.5×10^{-11}	1 (BPP)

It is noted that we obtained small β values of 0.15 ± 0.03 and 0.17 ± 0.03 in $AlPO_4$-5(H_2O) and SAPO-5(H_2O), respectively, indicating the presence of quite a wide τ_c distribution of the isotropic reorientation. This implies that the barrier for water rotation, i.e., the rotational jump rate is widely spread in capillaries. This conclusion is consistent with temperature dependences of M_2 in the present study and also reported ^{2}H spectra[1] exhibiting a gradual change in a wide temperature range. We showed from the ^{1}H NMR spectra the presence of two kinds of water, free one in the central part in capillaries and the other fixed on the wall. Here, we have to say, however, that H_2O in micropores above ca. 200 K cannot be divided into the two groups, but they distribute between these two extreme states, namely, freely rotating and fixed in both molecular sieves.

Any detectable difference on H_2O dynamics in SAPO-5 from in $AlPO_4$-5 was not observed in all NMR measurements despite of the existence of acid sites on the surface of micropores. The number of water molecules much larger than the acid site seems to smear out the effect of the site.

References
1 I. Kustanvich and D. Goldfarb, *J. Phys. Chem.*, **95**, 8818 (1991).
2 D. Goldfarb, Hong-Xin Li, and M. E. Davis, *J. Am. Chem. Soc.*, **114**, 3690 (1992).
3 D. Demuth, G. D. Stucky, K. K. Unger, and F. Schüth, *Microporous Mater.*, **3**, 473 (1995).
4 B. L. Newalker, R. V. Jasra, V. Kamath, and S. G. T. Bhat, *Microporous and Mesoporous Mater.*, **20**, 129 (1998).
5 N. Bloembergen, E. M. Purcell, and R. V. Pound, *Phys. Rev.*, **73**, 679 (1948).
6 D. W. Davidson and R. H. Cole, *J. Chem. Phys.*, **19**, 1484 (1951).
7 T. M. Conner, *Trans. Faraday Soc.*, **60**, 1574 (1964).

ELSEVIER

Microporous and Mesoporous Materials 51 (2002) 17–22

MICROPOROUS AND MESOPOROUS MATERIALS

www.elsevier.com/locate/micromeso

Dynamic behavior of acetonitrile molecules adsorbed in $AlPO_4$-5 and SAPO-5 studied by ^1H and ^2H NMR

Shin'ichi Ishimaru, Kazuma Gotoh, Mio Ichikawa, Ryuichi Ikeda *

Department of Chemistry, University of Tsukuba, Tsukuba 305-8571, Japan

Received 6 July 2001; received in revised form 20 October 2001; accepted 24 October 2001

Abstract

We studied dynamic behavior of acetonitrile molecules adsorbed in molecular sieves $AlPO_4$-5 and SAPO-5 by ^1H and ^2H solid state NMR methods and compared the result with that in bulk acetonitrile. The isotropic rotation of molecules is observed in $AlPO_4$-5 above 200 K but they are bound to Brønsted acid sites on the wall in SAPO-5 even at room temperature. An anomalous frequency dependency of ^1H NMR T_1 observed in acetonitrile in SAPO-5 implies a large distribution of the environment around the molecules. This distribution of environment is attributable to the random arrangement in positions of acid sites and acetonitrile molecules. It was shown that molecules in $AlPO_4$-5 are movable compared with those in bulk although the interaction with the pore wall seems to hinder motions.

Keywords: Aluminophosphate; Molecular sieves; Acetonitrile; Solid state NMR; Molecular dynamics; Spin–lattice relaxation

1. Introduction

$AlPO_4$-5 and SAPO-5 are molecular sieves having one-dimensional micropores with an effective diameter of 0.73 nm [1]. They crystallize in an isomorphic structure *P6/mcc* in which SAPO-5 [2] is formed by substituting some P or Al atoms in $AlPO_4$-5 by Si resulting in the formation of –OH groups on the wall. Previously, we reported NMR observations of triethylamine molecules included in $AlPO_4$-5 and SAPO-5 as template in the process of crystal formation [3]. It was implied that amine molecules are pinned to acid sites in SAPO-5, while those in $AlPO_4$-5 orientate more randomly than in SAPO-5.

In the present study, we intend to investigate dynamic behavior of acetonitrile molecules adsorbed in $AlPO_4$-5 and SAPO-5 to characterize molecular orientations and motions in micropores in connection with those in bulk crystals by the measurements of ^2H NMR spectra, second moment (M_2) of ^1H NMR lines, and spin–lattice (T_1) and spin–spin (T_2) relaxation times. Acetonitrile which has often been used to evaluate the acidity of zeolite compounds [4,5], is expected to be a better probe than triethylamine to investigate catalytic properties of molecular sieves. This is because the molecular size is comparable with actual reactants, and the simple and polar structure of the molecule is suitable to clarify the interactions with the host wall.

* Corresponding author. Tel.: +81-298-53-4250; fax: +81-298-53-6503.

E-mail address: ikeda@chem.tsukuba.ac.jp (R. Ikeda).

1387-1811/02/$ - see front matter
PII: S1387-1811(01)00463-2

2. Experimental

$AlPO_4$-5 and SAPO-5 were synthesized by an analogous method to that reported by Demuth et al. [6]. Gel mixtures containing Al_2O_3, P_2O_5, SiO_2, triethylamine and H_2O with ratios of 1.0:1.03:0.0: 1.5:600 for $AlPO_4$-5 and 1.0:1.03:0.1:1.5:600 for SAPO-5 were kept at 450 K in Teflon-lined stainless steal autoclaves for 72 h. Obtained fine colorless crystals of ≈100 μm long were calcined at 1000 K for 24 h under an oxygen flow to remove triethylamine included as the template. Measurements of X-ray powder diffraction and electron probe microanalysis (EPMA) were conducted for confirmation of samples by a Philips X'pert PW3040/00 diffractometer and a JEOL JXA-8621 microanalyzer, respectively. Air and water included in the pores were removed by keeping the sample in vacuo at 400 K for 24 h, and then, acetonitrile with the saturated vapor pressure was loaded to a glass tube containing the sample at room temperature. Deuterated acetonitrile (CD_3CN) was also adsorbed by an analogous procedure. These specimens were sealed with a normal pressure of He gas for NMR measurements. Amounts of adsorbed acetonitrile were determined by a thermogravimeter (Seiko EXSTAR6000 TG/DTA in Chemical Analysis Center, University of Tsukuba) as 1.3 ± 0.1 and 1.6 ± 0.1 molecules per unit cell of $AlPO_4$-5 and SAPO-5, respectively.

^2H NMR spectra were recorded with a Bruker MSL-300 system at a Larmor frequency of 46.1 MHz below room temperature. The ^1H NMR measurement was performed by a Bruker SXP-100 spectrometer at Larmor frequencies of 27 and 39 MHz for both systems in a temperature range 4.2–295 K. ^1H NMR T_2 and M_2 were measured in the $AlPO_4$-5 system by spin-echo and solid-echo methods, respectively, at 54 MHz in a range 107–295 K.

3. Results and discussion

X-Ray powder diffraction patterns recorded at room temperature were indexed well with hexagonal lattices with $a = 1.372 \pm 0.005$, $c = 0.843 \pm 0.006$ nm for $AlPO_4$-5, and $a = 1.371 \pm 0.005$, $c = 0.852 \pm 0.005$ nm for SAPO-5 in agreement with the reported data [1,2]. It was shown from EPMA that ≈9% of P in atomic ratio were replaced by Si in SAPO-5.

Temperature dependences of ^2H NMR spectra of CD_3CN included in $AlPO_4$-5 and SAPO-5 abbreviated to $AlPO_4$-5(CD_3CN) and SAPO-5(CD_3CN), respectively, are shown in Fig. 1. The spectra showed a typical Pake-pattern with quadrupole coupling constants (QCC) and asymmetric parameters (η) of 50 ± 1 kHz and nearly 0.0, respectively, for $AlPO_4$-5(CD_3CN) at 130 K and 53 ± 1 kHz and ~0.0 for SAPO-5(CD_3CN) at 150 K. These QCC values agree well with 53.2 kHz at 77 K reported for bulk crystalline acetonitrile [7] containing molecules rapidly rotating about the molecular axis (CH_3 rotation). At these temperatures, acetonitrile in pores of both systems can, accordingly, be described as a solid-like state, being analogous to that in bulk crystals observed in the same temperature range where the same motion was observed [7]. With the temperature increase in $AlPO_4$-5(CD_3CN), the line shape became vague and the line width rapidly decreased. In a range 230–293 K, the spectrum showed again a Pake-pattern with a very narrow line width of 1.8 kHz attributable to the onset of the isotropic rotation. The observed small doublet pattern corresponding to QCC ~ 2 kHz can be attributed to the axially symmetric electric field gradient along the pore axis made by charges in the wall, and molecules in the pore always feel this field gradient even they perform the isotropic rotation.

On the other hand, the ^2H NMR line width in SAPO-5(CD_3CN) showed a gradual decrease in a wide temperature range 130–293 K on heating, but its value remained at about 10 kHz even at 293 K. This reduced line width is too large to attribute to the overall reorientation. This difference between $AlPO_4$-5 and SAPO-5 systems suggests that the hydrogen bond between adsorbed molecules and –OH groups on the channel wall markedly affects the molecular motion. The decrease of QCC in SAPO-5(CD_3CN) is probably attributed to the activation of the fluctuation motion of the molecular axis pinned to the wall by the hydrogen bond between the –CN group and an –OH group.

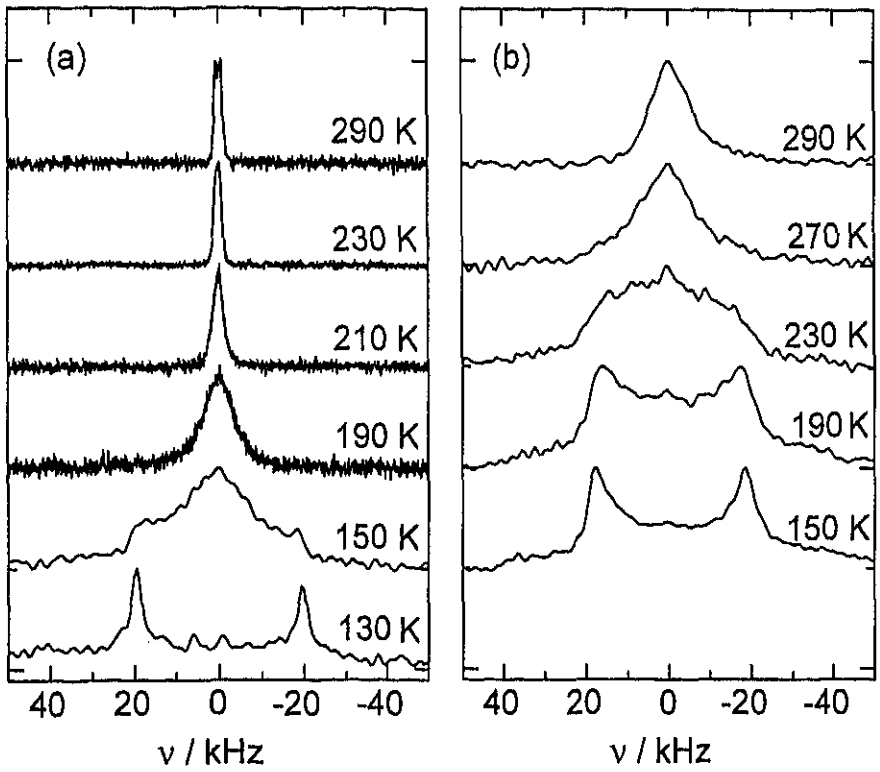

Fig. 1. Temperature dependences of ^{2}H NMR spectra of acetonitrile-d_3 in (a) $AlPO_4$-5 and (b) SAPO-5.

The gradual reduction of QCC can be explained by a distribution of the hindrance barrier for the motion. The fact that the number of –OH groups and acetonitrile molecules per host unit cell is 1.1 and 1.6, respectively, implies that not all molecules can form the hydrogen bond, but it is probable that the excess acetonitrile molecules are mobile more than those fixed on the wall. Furthermore, –OH groups distribute randomly on the pore wall. From these facts, we can expect that the distributed potential barrier for molecular motions in the pores.

Information of molecular motions can also be derived from ^{1}H NMR M_2. A temperature dependence of M_2 observed in $AlPO_4$-5(CH_3CN) is shown in Fig. 2. A M_2 of $\approx(3.9 \pm 0.1) \times 10^{-2}$ mT^2 observed at 100–120 K smaller than 5.2×10^{-2} mT^2 calculated for a molecule with the axial rotation indicates the onset of this motion. M_2 decreased rapidly with the temperature increase and almost vanished above 200 K implying that molecules obtain both rotational and diffusional freedoms. These facts imply that the acetonitrile molecules already undergo the axial rotational

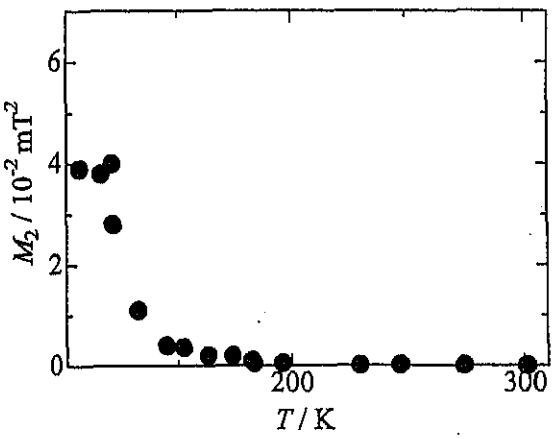

Fig. 2. Temperature dependence of the second moment (M_2) of ^{1}H NMR absorption lines.

motion at about 100 K and the isotropic reorientation and the local diffusion above 200 K. From these results, we can say that molecules obtain motional freedom as in liquid above 200 K. This expectation is in consistent with the ^{2}H NMR spectra analysis.

Dynamic behavior of adsorbed molecules more in detail could be obtained from data of ^{1}H NMR T_1 and T_2. Two T_1 components were observed in all temperature range for both systems. We assigned the long major T_1 component to acetonitrile adsorbed in the pores. The origin of the short T_1 component is not clear. Because of its small magnetization of 10–20% of the long one, one may attribute to molecules outside micropores or effect from paramagnetic impurities formed on the wall which was observed in H_2O adsorbed $AlPO_4$-5. Figs. 3 and 4 show temperature dependences of the long T_1 component observed in $AlPO_4$-5(CH_3CN) and SAPO-5(CH_3CN), respectively. Observed T_2 values in $AlPO_4$-5 system are also shown in Fig. 3.

In case the relaxation is governed by the fluctuation of magnetic dipolar interactions between ^{1}H nuclei caused by molecular motions, it obeys BPP-type relations [8]:

$$T_1^{-1} = C\left\{\frac{\tau}{1+\omega^2\tau^2} + \frac{4\tau}{1+4\omega^2\tau^2}\right\} \tag{1}$$

and

$$T_2^{-1} = \frac{1}{2}C\left\{3\tau + \frac{\tau}{1+\omega^2\tau^2} + \frac{2\tau}{1+4\omega^2\tau^2}\right\}, \tag{2}$$

where C, ω and τ are the motional constant, the ^{1}H angular Larmor frequency and the correlation time of the motion, respectively. τ can be expressed by the Arrhenius equation given by

$$\tau = \tau_0 \exp\left(\frac{E_a}{RT}\right). \tag{3}$$

Here τ_0 and E_a denote the correlation time in the limit of infinite temperature and the activation energy of the motion, respectively. These equations imply that a T_1 minimum is observed at $\omega\tau \sim 1$ and T_1 values are proportional to ω^2 in the low-temperature range fulfilling $\omega\tau \gg 1$. The T_1 observed in both systems given in Figs. 3a and 4a showed a shallow minimum near room temperature but their frequency dependences observed at low temperatures were unexplainable by the above ω^2 law. This kind of anomalous frequency dependence has often been observed in inhomogeneous systems such as intercalation compounds [9,10] and explained by introducing some distribution in τ caused by inhomogeneous environment around the adsorbed molecules as described in the foregoing ^{2}H NMR analysis. The T_1 behavior observed in our systems can be explained by introducing the Cole–Davidson type τ distribution [11] given by

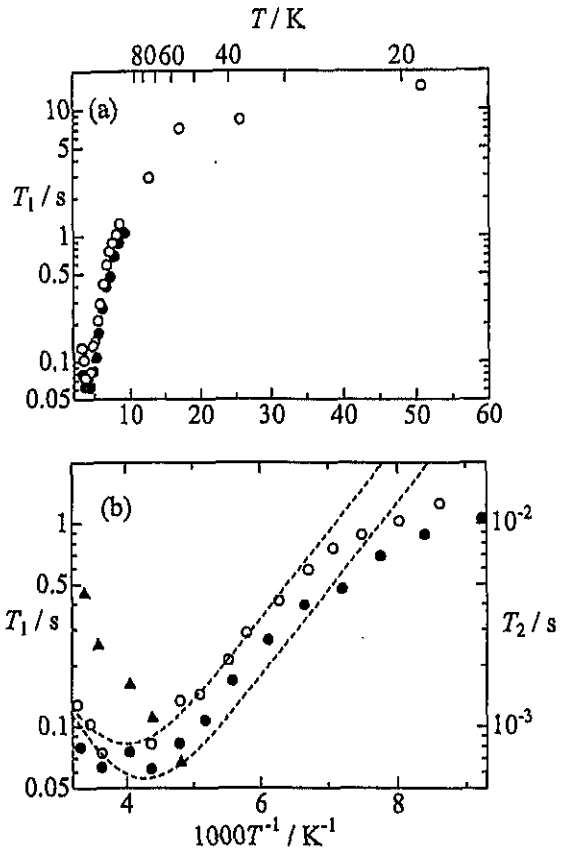

Fig. 3. (a) Temperature dependences of T_1 in $AlPO_4$-5(CH_3CN) observed at 27 (●) and 39 MHz (○) and T_2 at 54.3 MHz (▲), (b) T_1 data in the high-temperature region. Dashed lines represent best-fitted curves using Eqs. (3)–(5) in text.

$$g(\tau) = \begin{cases} \frac{\sin\beta\pi}{\pi}\left(\frac{\tau}{\tau_c-\tau}\right)^{\beta} & \tau \leqslant \tau_c \\ 0 & \tau > \tau_c. \end{cases} \tag{4}$$

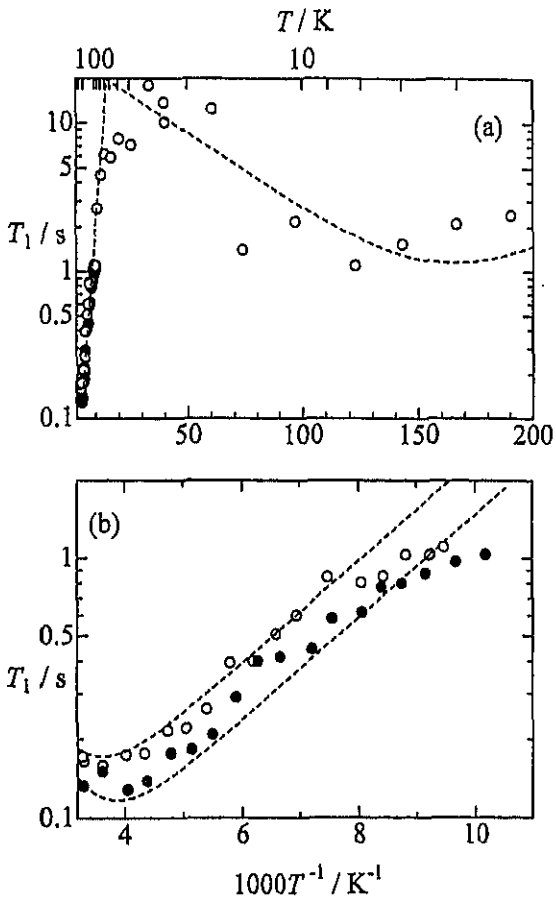

Fig. 4. (a) Temperature dependences of T_1 in SAPO-5(CH_3CN) observed at 27 (●) and 39 MHz (○), (b) T_1 data in the high-temperature region. Dashed lines represent best-fitted curves using Eqs. (3)–(5) in text.

The limit of $\beta = 1$ corresponds to a single τ in all over the sample and the distribution amplitude increases with β decrease. Using Eq. (4), the modified BPP equation is written by [12]

$$T_1^{-1} = C\left\{\frac{\tau_c \sin(\beta \tan^{-1}\omega\tau_c)}{\omega\tau_c(1+\omega^2\tau_c^2)^{\beta/2}} + \frac{2\tau_c \sin(\beta \tan^{-1} 2\omega\tau_c)}{\omega\tau_c(1+4\omega^2\tau_c^2)^{\beta/2}}\right\}. \quad (5)$$

The observed T_1 data given in Figs. 3 and 4 were fitted by Eqs. (3)–(5). The obtained best-fitted curves are plotted in these figures and the fitting parameters are listed in Table 1.

Table 1
Motional constants (C), activation energies (E_a) and parameters expressing the degree of distribution of correlation times (β) derived from ^{1}H NMR T_1 and T_2 of acetonitrile adsorbed in $AlPO_4$-5 and SAPO-5

	C (10^9 s^{-2})	E_a (kJ mol^{-1})	β	Motional mode
CH_3CN in $AlPO_4$-5	2.5 ± 0.2	12 ± 1 (T_1)	0.7	
	–	11 ± 1 (T_2)	–	Isotropic rotation
CH_3CN in SAPO-5	–	0.2 ± 0.05	–	Axial rotation
	1.9 ± 0.2	13 ± 2	0.3	Fluctuation motion

Referring to the analyses of ^{2}H NMR spectra and ^{1}H M_2 the gentle T_1 change observed below 80 K in $AlPO_4$-5(CH_3CN) shown in Fig. 3a and a minimum near 6 K in SAPO-5(CH_3CN) given in Fig. 4a were attributed to the axial rotation of the acetonitrile molecules. The motional parameters are not clear except for the E_a for SAPO-5(CH_3CN) because tunneling rotation cannot be ignored in this temperature region. The other minima observed at 200–250 K in respective systems seen in Figs. 3b and 4b were attributed to the isotropic rotation of acetonitrile molecules for $AlPO_4$-5(CH_3CN) and the fluctuation of the molecular axis in SAPO-5(CH_3CN), respectively. The C of 2.5×10^9 s^{-2} determined for $AlPO_4$-5(CH_3CN) coincides well with the calculated value 2.51×10^9 s^{-2} for the isotropic rotation of a single acetonitrile molecule using $r_{H\text{-}H} = 1.800 \times 10^{-1}$ nm determined in the crystalline phase [13]. The E_a of this motion was also estimated from the temperature dependence of T_2 shown as 11 ± 1 kJ mol^{-1} which agrees well with 12 ± 1 kJ mol^{-1} obtained from T_1 analysis shown in Table 1. The small β value 0.3 observed in SAPO-5 system indicates a large distribution of environment of molecules as discussed in the above ^{2}H NMR analysis.

It is noted that, in bulk crystals, only the molecular axial rotation (CH_3 rotation) was observed in the T_1 measurement [14] and no relaxation due to the overall rotation or the fluctuation of molecular axes observed in the present systems was detected up to ≈180 K. Moreover, the activation

energy for the axial rotation in bulk reported to be 8.8 kJ mol^{-1} seems to be much higher than those in the present systems. These results imply that acetonitrile molecules in the micropores are much free to move, that is, they packed in the pores more loosely than in bulk.

The difference of the averaged number of molecules per unit cell of $AlPO_4$-5 and SAPO-5 given by 1.3 and 1.6, respectively, can be also explained by the pinning effect. The excluded volume of acetonitrile molecules is reduced by pinning in SAPO-5 and more molecules can be adsorbed than $AlPO_4$-5.

Jacobs et al. discussed the orientation of acetonitrile molecules in SAPO-5 from polarized IR spectra [15]. They reported that the CN axis, i.e., the corresponding transition moment of acetonitrile molecules adsorbed on acid sites is perpendicular to the pore axis. This result agrees well with the present NMR analysis that the direction of molecular axis fluctuates with the CN group fixed on the Brønsted acid site.

4. Conclusion

From ^{2}H and ^{1}H NMR observations, acetonitrile adsorbed in one-dimensional pores of $AlPO_4$-5 and SAPO-5 is expected to show solid-like behavior at ≈130 K. With increasing temperature, the isotropic rotation is activated and become liquid-like around 200 K in $AlPO_4$-5. Acetonitrile molecules in the micropores in $AlPO_4$-5 were shown to be much movable compared with those in bulk crystals, but the interactions with atoms on the pore wall seem to prevent the overall and self-diffusional motions at low temperatures.

Molecular motions in SAPO-5, on the other hand, are restricted even at room temperature. This difference is attributable to the –OH groups, forming the hydrogen bond with acetonitrile in SAPO-5. Small E_a values of 11 and 12 kJ mol^{-1} evaluated from ^{1}H T_1 and T_2 data, respectively, for the isotropic rotation of acetonitrile in $AlPO_4$-5 are attributable to the fact that only a few molecules interact with each other in the narrow one-dimensional pore. A large distribution of τ ($\beta = 0.3$) observed in acetonitrile in SAPO-5 is explained by random mutual arrangements of –OH groups on the crystal wall and adsorbed molecules.

Acknowledgement

This work was supported by Grant-in Aid for scientific research no. (B) 12440192 from the Ministry of Education, Culture, Sports, Science and Technology.

References

[1] J.M. Bennett, J.P. Cohen, E.M. Flanigen, J.J. Pluth, J.V. smith, ACS Symp. Ser. 218 (1983) 109.
[2] G. Sastre, D.W. Lewis, C.R.A. Catlow, J. Phys. Chem. 100 (1996) 6722.
[3] K. Gotoh, S. Ishimaru, R. Ikeda, Phys. Chem. Chem. Phys. 2 (2000) 1865.
[4] A.G. Pelmenschikov, R.A. van Santen, J. Jänchen, E. Meijer, J. Phys. Chem. 97 (1993) 11071.
[5] J. Kotrla, L. Kubelkova, C.-C. Lee, R.J. Gorte, J. Phys. Chem. B 102 (1998) 1437.
[6] D. Demuth, G.D. Stucky, K.K. Unger, F. Schüth, Micropor. Mater. 3 (1995) 473.
[7] R.G. Barnes, Adv. Nucl. Quadrupole Reson. 1 (1974) 357; J.W. Enesley, J.C. Lindon, J. Tabony, Mol. Phys. 26 (1973) 1499.
[8] A. Abragam, Principles of Nuclear Magnetism, Oxford University Press, London, 1961, chapter 8.
[9] W. Müller-Warmuth, R. Schöllhorn (Eds.), Progress in intercalation research, Physics and Chemistry of Materials with Low-Dimensional Structures, vol. 17, Kluwer, Dordrecht, 1994.
[10] M. Molitor, W. Müller-Warmuth, H.W. Spiess, R. Schöllhorn, Z. Naturforsch. 38a (1983) 237.
[11] D.W. Davidson, R.H. Cole, J. Chem. Phys. 19 (1951) 1484.
[12] T.M. Connor, Trans. Faraday Soc. 60 (1964) 1574.
[13] C.C. Costain, J. Phys. Chem. 29 (1958) 864.
[14] E.O. Stejskal, D.E. Woessner, T.C. Farrar, H.S. Gutowsky, J. Chem. Phys. 31 (1959) 55.
[15] W.P.J.H. Jacobs, D.G. Demuth, S.A. Schunk, F. Schüth, Micropor. Mater. 10 (1997) 95.

Mol. Cryst. Liq. Cryst., Vol. 379, pp. 89-94

1058-725X/02 $12.00+.00
DOI: 10.1080/10587250290090318

Complex-Plane Impedance Study on a Hydrogen-Doped Copper Coordination Polymer: *N,N'*-bis-(2-hydroxyethyl)dithiooxamidato-copper(II)

YUKI NAGAO[a], RYUICHI IKEDA[a], SEIICHI KANDA[b], YOSHIHIRO KUBOZONO[c] and HIROSHI KITAGAWA[a,d,e]

[a]*Department of Chemistry, University of Tsukuba, Ibaraki 305-8571, Japan,*
[b]*Department of Chemistry, The University of Tokushima, Tokushima 770-8506, Japan,*
[c]*Institute for Molecular Science, Okazaki 444-8585, Japan,*
[d]*School of Materials Science, Japan Advanced Institute of Science and Technology, Ishikawa 923-1292, Japan and*
[e]*PRESTO, JST, Saitama 332-0012, Japan*

AC conductivity measurements with an impedance analyzer were carried out for a hydrogen-doped coordination polymer, *N,N'*-bis-(2-hydroxyethyl)dithiooxamidatocopper(II), in order to estimate the protonic conductivity (σ_p). The log σ_p was linearly increased from 2.6×10^{-9} to 2.2×10^{-6} S cm^{-1} with relative humidity (RH) from 45 to 100 % at 300 K. A slight hysteresis of protonic conductivity was observed upon increasing and decreasing RH, which implies that H_3O^+ is generated by a reaction between water molecule and acid-base polymer near RH ~ 100 %.

Keywords: protonic conduction; coordination polymer; AC conductivity measurement; hydrogen doping; electronic conduction; inorganic-organic hybrids

INTRODUCTION

Inorganic-organic hybrids are one of the most promising materials

because they possess a wide variety of inorganic and organic functionalities[1]. Protonic conduction is one of the unexplored and most attractive functionalities in inorganic-organic hybrids.

N,N'-bis-(2-hydroxyethyl)dithiooxamidatocopper(II), $(HOC_2H_4)_2$-*dtoa*Cu, is a two-dimensional coordination polymer (Figure 1)[2,3]. In the previous work, this polymer was revealed to be a protonic conductor[4]. The electronic conductivity of $(HOC_2H_4)_2$*dtoa*Cu is increased by about nine orders of magnitude as the hydrogen doping proceeds[5]. The hydrogen is doped to $(HOC_2H_4)_2$*dtoa*Cu according to the proton-coupled redox property, as shown in Figure 2. The hydrogen doped to the coordination polymer reduces Cu(II) to Cu(I), and bonds the nitrogen sites of the ligands as a proton. The protonic conductivity of hydrogen-doped $(HOC_2H_4)_2$*dtoa*Cu is expected to be higher than that of the non-doped one. In this paper, we report on proton transport properties of the hydrogen-doped polymer by AC conductivity measurements.

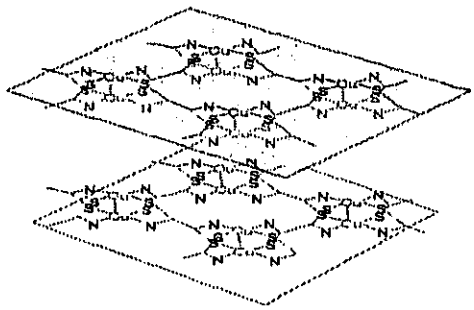

FIGURE 1 Proposed structure of $(HOC_2H_4)_2$*dtoa*Cu[2,3].

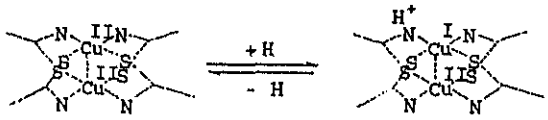

FIGURE 2 Proton-coupled redox property of $(HOC_2H_4)_2$*dtoa*Cu.

EXPERIMENTAL

The title coordination polymer was prepared by a simple stoichiometric mixing of 5 % C_2H_5OH*aq* solution of $(HOC_2H_4)_2$*dtoa* and $CuSO_4$*aq*. Hydrogen doping was electrochemically performed by generated hydrogen gas on the cathode's surface with a KCl solution of 0.1 mol/l under vigorous stirring for 3 hours. The qualities of samples were checked by powder X-ray diffraction measurements. The X-ray diffraction patterns were measured with synchrotron radiation at the BL-1B in the Photon Factory of High Energy Accelerator Research Organization (KEK-PF). The X-ray wavelength λ used was 0.8500(4) Å.

For AC conductivity measurements, the powdered sample was processed into pellets of 0.57 mm thickness and 2.5 mm ϕ under pressure (~ 1 GPa) and vacuous condition. The impedance measurements were carried out by a conventional quasi-four-probe method using gold paste and gold wires (25 μm ϕ) with an Agilent Technologies 4294A impedance analyzer in the frequency range of 40 Hz – 4 MHz at 300 K. Relative humidity (RH) was changed in the range of 45 – 100 % by using water and saturated solution of salts, generating an atmosphere of a defined RH[6]. The measurements were carried out with decreasing RH from 100 to 45 % (the first series), and then with increasing it from 45 to 100 % (the second series).

RESULTS AND DISCUSSION

Figure 3 shows the X-ray diffraction patterns of hydrogen-doped $(HOC_2H_4)_2$*dtoa*Cu and non-doped one. The two-dimensional framework of the coordination polymer is maintained during hydrogen doping because main intense peaks are unchanged. The lattice of non-doped $(HOC_2H_4)_2$*dtoa*Cu is tetragonal with constants of a = 8.54 and c = 9.85 Å.

The protonic conductivity was obtained by the complex-plane impedance plots. Figure 4 shows the real (Z') versus imaginary (Z") parts of the complex-impedance data for the hydrogen-doped $(HOC_2H_4)_2$*dtoa*Cu under RH of 100 % in the first series. The plots consist of a depressed semicircular arc followed by a low frequency tail. The bulk resistance of this polymer is directly given by the intersection of depressed semicircle with the real axis. The conductivity estimated in

this manner is 2.2×10^{-6} S cm^{-1}, which is in principle the sum of the protonic (σ_p) and electronic (σ_e) contributions. The σ_e is 2.0×10^{-10} S cm^{-1} measured by DC electrical conductivity, which is negligible compared to the σ_p. So the protonic conductivity is determined to be 2.2×10^{-6} S cm^{-1}.

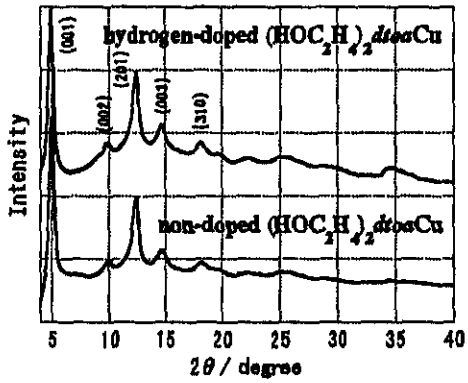

FIGURE 3 X-ray diffraction patterns of the hydrogen-doped and non-doped $(HOC_2H_4)_2$*dtoa*Cu.

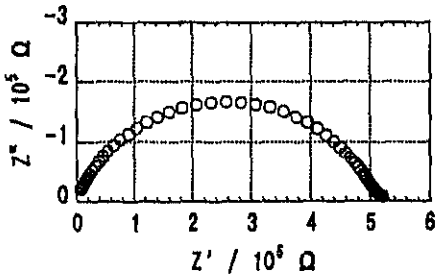

FIGURE 4 Complex-plane impedance plots of hydrogen-doped $(HOC_2H_4)_2$*dtoa*Cu under RH of 100 % and 300 K.

Figure 5 shows the RH dependence of protonic conductivity for the hydrogen-doped $(HOC_2H_4)_2dtoa$Cu. The log σ_p are linearly decreased from 2.2×10^{-6} to 2.6×10^{-9} S cm^{-1} with decreasing RH from 100 to 45 % (the first series). The conductivities in the second series are a little lower although the conductivity is almost equal to that in the first one under RH of 100 %. This implies that H_3O^+ is generated near RH ~ 100 % by a reaction between water molecule and the hydrogen at NH bonds of the acid-base polymer. The protonic conductivity of hydrogen-doped $(HOC_2H_4)_2dtoa$Cu is lower by about two orders of magnitude than that of non-doped one under RH of 83 %[4], which is due to the larger pK_a of hydrogen-doped $(HOC_2H_4)_2dtoa$Cu than non-doped one.

The concentration of water molecules included in the non-doped $(HOC_2H_4)_2dtoa$Cu was also found to increase with RH[4]. This fact implies that the protonic conductivity depends on the quantity of water molecules containing in the polymer. The lattice constant c of $(HOC_2H_4)_2dtoa$Cu was found by the X-ray diffraction measurements to become slightly longer with RH[7]. It is reported that the proton conductor "Nafion®", which is used as solid electrolyte in the fuel cell, also contains much water clusters and these make pathway of the protonic conduction[8,9]. This coordination polymer is supposed to have the same mechanism. Detailed investigation on the mechanism of the protonic conduction of this polymer is in progress.

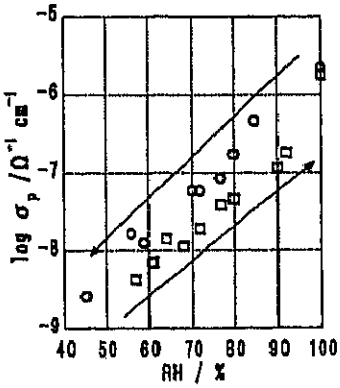

FIGURE 5 Log (protonic conductivity) vs. RH plots of hydrogen-doped $(HOC_2H_4)_2dtoa$Cu at 300 K. ○: the first series; □: the second series (See EXPERIMENTAL).

CONCLUSION

In this work, AC conductivity measurements were carried out for the hydrogen-doped coordination polymer, *N,N'*-bis-(2-hydroxyethyl)-dithiooxamidatocopper(II). The protonic conductivity was found to increase from 2.6×10^{-9} to 2.2×10^{-6} S cm^{-1} with RH (45 - 100 %). A slight hysteresis was observed, which implies that H_3O^+ is generated by the reaction between water molecule and acid-base polymer near RH ~ 100 %.

Acknowledgments
X-ray-diffraction study was performed under proposals of KEK-PF (01G058) and (01G262). This work was partly supported by Grants-in-Aid for Scientific Researches, Nos. 12440192 of (B), 11640559 of (C), 10149104 (401: Metal-Assembled Complexes) and 11135211 (299: New Protium Function) of Priority Areas (A) from the Ministry of Education, Culture, Sports, Science and Technology of Japan, and by the grant program of The Saneyoshi Scholarship Foundation.

References

[1.] A. K. Cheetham, *et al.*, *Angew. Chem. Int. Ed. Engl.*, **38** 3268 (1999).
[2.] S. Kanda, *et al.*, *Bull. Chem. Soc. Jpn.*, **52(11)** 3296 (1979).
[3.] M. Fujishima, *et al.*, *Synth. Met.*, **119** 485 (2001).
[4.] Y. Nagao, *et al.*, submitted to *Synth. Met.*.
[5.] M. Fujishima, *et al.*, to be submitted.
[6.] F. Opekar and D. Svozil, *J. Electroanal. Chem.*, **385** 269 (1995).
[7.] Y. Nagao, *et al.*, to be submitted.
[8.] K. D. Kreuer, *Chem. Mater.*, **8** 610 (1996).
[9.] J. J. Sumner, *et al.*, *J. Electrochem. Soc.*, **145(1)** 107 (1998).

Mol. Cryst. Liq. Cryst., Vol. 379, pp. 223-228

1058-725X/02 $12.00 + .00
DOI: 10.1080/10587250290090516

Electronic State of A Hydrogen-Doped Copper Coordination Polymer: *N,N'*-bis-(hydroxyethyl)dithiooxamidatocopper(II), $(HOC_2H_4)_2$*dtoa*Cu

MUSASHI FUJISHIMA[a], RYUICHI IKEDA[a], SEIICHI KANDA[b] and HIROSHI KITAGAWA[a,c,d]

[a]*Department of Chemistry, University of Tsukuba, Ibaraki 305-8571, Japan,*
[b]*Department of Chemistry, The University of Tokushima, Tokushima 770-8506, Japan,*
[c]*School of Materials Science, Japan Advanced Institute of Science and Technology, Ishikawa 923-1292, Japan and*
[d]*PRESTO, JST, Saitama 332-0012, Japan*

Hydrogen doping was electrochemically performed on the title coordination polymer, catena-μ-*N,N'*-bis-(hydroxyethyl)dithiooxamidatocopper(II), $(HOC_2H_4)_2$*dtoa*Cu. From X-ray photoelectron spectroscopy, the oxidation state of Cu(II) in $(HOC_2H_4)_2$*dtoa*Cu was revealed to be reduced to the Cu(I,II) mixed-valence state on hydrogen doping. While the spin susceptibility increases during initial hydrogen doping, it decreases and then shows no temperature dependence as the hydrogen doping proceeds. The temperature-independent behavior is supposed to be derived from Pauli paramagnetism.

Keywords: Coordination polymer; Hydrogen doping; Spin susceptibility; X-ray photoelectron spectroscopy.

INTRODUCTION

Recently, carrier doping into molecular materials has received a renaissance through its physical properties such as conductivity, magnetic property and dielectlic property. In particular, some of the alkali metal-doped fullerenes indicates superconductivity, in which the alkali

metal acts as an electron donor to the fullerene. Taking into account the doping effect on the physical property, it is able to create novel functional materials such as switching device, capacitor and sensor by means of carrier doping.

The copper(II) complex, catena-μ-*N,N'*-bis-(hydroxyethyl)dithiooxamidatocopper(II), $(HOC_2H_4)_2$*dtoa*Cu (Figure 1), is an amorphous two-dimensional coordination polymer with Cu-dimeric units[1,2]. The electrical conductivity of $(HOC_2H_4)_2$*dtoa*Cu is increased by about nine orders of magnitude during hydrogen doping[3,4]. This polymer also indicates proton conduction[5-7]. Electron and proton conductive properties are derived from a dibasic-acid character of the ligand (Figure 2)[8] and a proton-coupled redox property. The electron-proton coupling like this plays an important role of energy metabolism in biological system. By the use of these properties induced by the hydrogen doping, a new type of functional material would be developed. In this work, X-ray photoelectron spectroscopy (XPS) and magnetic susceptibility measurements were carried out in order to reveal the electronic state of hydrogen-doped $(HOC_2H_4)_2$*dtoa*Cu.

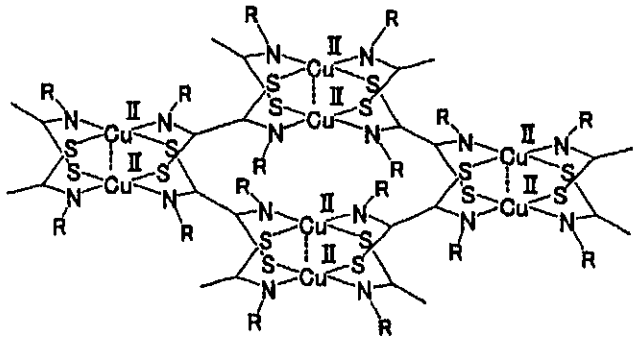

FIGURE 1 Two-dimensional coordination polymer (R = C_2H_4OH).

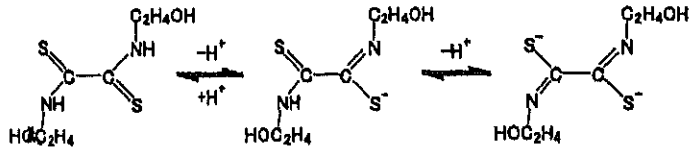

FIGURE 2 Dibasic-acid character of the ligand.

EXPERIMENTAL

Synthesis

The title coordination polymer was prepared by a simple stoichiometric mixing of ethanol solution of $(HOC_2H_4)_2$*dtoa* with aqueous solution of copper(II) sulfate[1,2]. The synthesized sol was washed with water and ethanol several times and separated from the supernatant fraction with the centrifuge. The qualities of obtained samples were checked by the elemental analysis and powder X-ray diffraction measurement.

Hydrogen doping

Hydrogen doping was performed by electrolysis of water with a conventional electrochemical cell. The 0.1 mol/l KCl solution was used as electrolyte. A Pt working electrode, a spiral of Pt-black wire as a counter electrode and a saturated calomel reference electrode were employed. The electrolyte was purged with Ar prior to use and blanket of Ar was maintained over the solution during the experiment. The applied potential to cathode was between –1.0 to –0.7 V. The colloidal $(HOC_2H_4)_2$-*dtoa*Cu dispersed into the electrolyte was exposed to generated hydrogen gas on the cathode's surface under stirring at room temperature. Hydrogen-doped samples were taken out of the cell at hourly intervals.

Measurement

X-ray photoelectron spectroscopy (XPS) measurement was performed using an Ulvac Phi 5600ci photoelectron spectrometer with a monochromated Al-Kα X-ray ($h\nu$=1487 eV) as an excitation light source at room temperature. Magnetic susceptibility measurements were performed with samples dried in an evacuated desiccator. The samples were wrapped with diamagnetic materials. The temperature dependences were measured in the temperature range 2 – 300 K on a Quantum Design MPMS-5 SQUID magnetometer. The total diamagnetic contributions were subtracted after the measurement.

RESULTS AND DISCUSSION

XPS measurements

XPS measurements were made on $(HOC_2H_4)_2$*dtoa*Cu to examine the oxidation state of Cu during hydrogen doping. Figure 3 shows the XPS spectra of Cu $2p_{3/2}$ region for $(HOC_2H_4)_2$*dtoa*Cu. In the spectrum of the hydrogen-undoped sample, a peak centered at 934.2 eV was observed, which is a typical binding energy of Cu(II). As the hydrogen doping

proceeds, a new shoulder peak centered at 932.2 eV appears, which is derived from a signal of Cu(I). The hydrogen doped coordination polymer, therefore, is considered to reduce the Cu(II) into the Cu(I,II) mixed-valence state. The broad peak centered at 943-945 eV is a satellite peak derived from Cu(II).

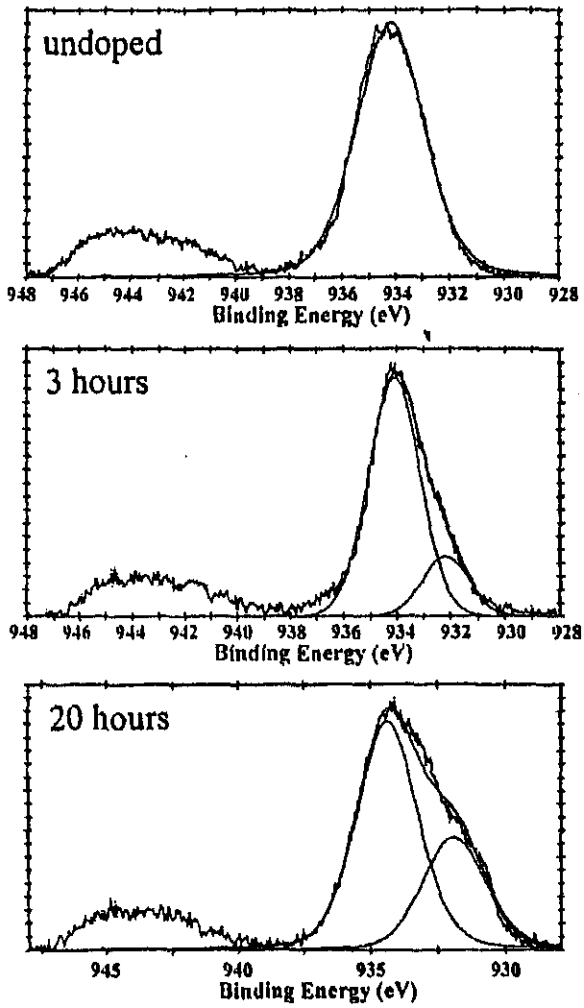

FIGURE 3 Hydrogen-doping time dependence of XPS spectra.

Magnetic susceptibility measurements

In order to confirm the reduction of Cu(II) into the Cu(I,II) mixed-valence state by hydrogen doping, the temperature dependences of molar spin susceptibilities per dimer unit of the coordination polymer were measured, as shown in Figure 4. From the theoretical consideration of spin susceptibility of hydrogen-undoped sample[9], the observed antiferromagnetic susceptibility, in which the estimated J value is -594 K, is considered to be due to the intradimer superexchange interaction between Cu(II) ions *via* ligands. The spin susceptibility for the three-hours hydrogen-doped sample increases compared to the undoped one in the whole temperature region. This can be explained as follows. As the Cu(II) ions proceed to be reduced to Cu(I), the cancelled spins by a large negative J become revived on losing the opposite spin. The spin susceptibility for the twenty-hours hydrogen-doped sample decreases from that for the three-hours one, which indicates no temperature dependence. This temperature-independent behaviour is supposed to be derived from Pauli paramagnetism.

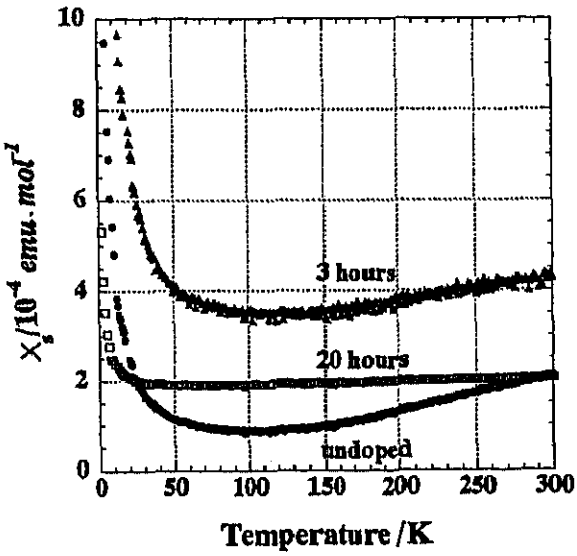

FIGURE 4 Temperature dependences of spin susceptibility of $(HOC_2H_4)_2$*dtoa*Cu, (hydrogen doping time ●:undoped, ▲:3 hours, □:20 hours).

CONCLUSION

The hydrogen doping was electrochemically performed on $(HOC_2H_4)_2$-*dtoa*Cu. The oxidation state of Cu(II) in $(HOC_2H_4)_2$*dtoa*Cu was revealed from XPS measurement to be reduced to the Cu(I,II) mixed-valence state on hydrogen doping. While the spin susceptibility increases during initial hydrogen doping, it decreases and then showed no temperature dependence as the hydrogen doping proceeds. The temperature-independent behavior is supposed to be derived from Pauli paramagnetism. In this coordination polymer, it is possible to control physical properties continuously by hydrogen doping, which is achieved by the proton- coupled redox property of this system.

Acknowledgements

This work was partly supported by Grants-in-Aid for Scientific Researches, No. 11640559 of (C), 10149104 (401: Metal-Assembled Complexes) and 11135211 (299: New Protium Function) of Priority Areas (A) from the Ministry of Education, Culture, Sports, Science and Technology of Japan, and by the grant program of The Iwatani Naoji Foundation's Research Grant.

References

[1.] S. Kanda, A. Suzuki, K. Ohkawa, *Ind. Engin. Chem., Prod. Res. Develop.*, **12**, 88 (1973).
[2.] M. Fujishima, S. Kanda, T. Mitani, H. Kitagawa, *Synth. Met.*, **119**, 485 (2001).
[3.] S. Kanda, *Bul. Chem. Soc. Jpn.*, **83**, 560 (1962).
[4.] M. Fujishima et al., to be published.
[5.] S. Kanda, K. Yamashita, K. Ohkawa, *Bul. Chem. Soc. Jpn.*, **52**, 3296 (1979).
[6.] S. Kanda, F. Yamamoto, *Bul. Chem. Soc. Jpn.*, **69**, 477 (1996).
[7.] Y. Nagao et al., submitted to *Synthetic Metals.*
[8.] P. Geboes, H. Hofmans, H. O. Desseyn, R. Dommisse, A.T.H.Lenstra, S.Bamidele.Sanni, J. M.M. Smits, and P.T.Beurskens, *Spectrochim. Acta.*, **43A**, 35 (1987).
[9.] M. Fujishima et al., submitted to *Synthetic Metals.*

Mol. Cryst. Liq. Cryst., Vol. 379, pp. 279-284

1058-725X/02 $12.00+.00
DOI: 10.1080/10587250290090606

Relaxation Process of CT Exciton State in a One-Dimensional MX-Chain Compound $[NiBr(chxn)_2]Br_2$

SHINYA TAKAISHI[a], HIROSHI KITAGAWA[a,b] and RYUICHI IKEDA[a]

[a]*Department of Chemistry, University of Tsukuba, Tsukuba, Ibaraki 305-8571, Japan and*
[b]*School of Materials Science, Japan Advanced Institute of Science & Technology, Tatsunokuchi, Ishikawa 923-1292, Japan*

Luminescence spectroscopy measurements were performed in a one-dimensional halogen-bridged transition-metal compound $[NiBr(chxn)_2]Br_2$ (*chxn*: 1*R*,2*R*-cyclohexanediamine) and its mixed-metal compound $[Ni_{1-x}Pd_xBr(chxn)_2]Br_2$ with x = 0.005, 0.05, 0.33. The broad peaks were observed at 1.3 and 1.4 eV for $[NiBr(chxn)_2]Br_2$, which are attributed to a relaxation of LMCT exciton state and a hot luminescence, respectively. No Stokes shift of the luminescence at 1.3 eV was observed, which shows the electron-lattice interaction (*S*) is weak in this system. From the temperature dependence of luminescence spectra, it was clarified that the relaxation process is continuously changed from luminescence to thermal relaxation. The luminescence peak at 1.3 eV is remarkably quenched with increase of x for $[Ni_{1-x}Pd_xBr(chxn)_2]Br_2$, implying that the LMCT exciton is trapped to in-gap states caused by doped Pd^{3+}.

Keywords MX chain; luminescence; charge-transfer exciton; mixed valence

INTRODUCTION

A series of one-dimensional halogen-bridged(X) transition-metal(M) complexes (MX-chains) have been studied as a Peierls distorted system

with a strong electron-lattice interaction resulting in mixed-valence state. Recently, a new type of MX-chain complexes $[NiX(chxn)_2]X_2$ (*chxn*: 1*R*,2*R*-cyclohexanediamine; X: Cl, Br) have been shown to crystallize with no Peierls distortion implying the formation of $S = 1/2$ spin chain of Ni^{III}. From an optical conductivity for $[NiBr(chxn)_2]Br_2$, an energy gap of this complex was measured to be about 1.3 eV[1], and the on-site Coulomb repulsion (U) was determined to be 5 eV from X-ray photoelectron and Auger spectroscopies[2]. Since the optical energy gap was much smaller than U, this material is recognized as a charge-transfer insulator. Thus, the peak at 1.3 eV is attributed to a charge-transfer transition from bridging-halogen to metal (LMCT) [2]. Although relaxation processes in Peierls-distorted (mixed-valence) MX-chain compounds have been extensively studied[3-8], the processes in $[NiX(chxn)_2]X_2$ are not clarified. In this paper, we report on luminescence properties of the non-Peierls MX-chain system $[NiBr(chxn)_2]Br_2$.

EXPERIMENTAL

Single crystals of $[NiBr(chxn)_2]Br_2$ were prepared by a slow diffusion of Br_2 vapor into a solution $[Ni(chxn)_2]Br_2$ dissolved in methanol. Single crystals of a mixed-metal MX-chain system $[Ni_{1-x}Pd_xBr(chxn)_2]Br_2$ were prepared by an electrochemical oxidation method described elsewhere[9]. The concentration of metals in measured specimens was determined by ICP emission spectrometry. The luminescence spectroscopy measurements were performed using a DIOLOR-JOBINYVON-SPEX spectrometer with He-Ne (1.96 eV) and Ar ion (2.41 eV) lasers as excitation light sources. Incident laser was polarized parallel to the chain axis ($E // b$).

RESULTS AND DISCUSSION

Figure 1 shows the luminescence spectra of $[NiBr(chxn)_2]Br_2$ at 2 K for the excitation energy of 1.96 and 2.41 eV. Large and small broad peaks were observed at 1.3 and 1.4 eV, respectively. It is reported that an intense band was observed at 1.3 eV in the optical conductivity spectrum[2], being accounted to be a LMCT transition (Br^-, $Ni^{3+} \rightarrow Br^0$, Ni^{2+}). The

luminescence peak observed at 1.3 eV is, therefore, considered to be a relaxation of LMCT exciton state (Br^0, Ni^{2+} → Br^-, Ni^{3+}). This luminescence exhibits no or little Stokes shift, showing that the LMCT exciton is not easy to be relaxed into a self-trapped state. This is a good contrast to a relaxation process of the CT exciton state (M^{3+}, M^{3+} → M^{4+}, M^{2+}) in Peierls-distorted MX-chain system of M = Pd, Pt. These materials show large Stokes shifts due to the strong electron-lattice interaction because bridging halogen ion X^- are quite sensitive to the charge of metal ions. On the other hand in [NiBr(*chxn*)$_2$]Br$_2$, the bridging bromine, which is neutral (Br^0) when the LMCT occurs, is insensitive to the charge at Ni ions, so that the electron-lattice interaction(S) of this system is small. The very small S in [NiBr(*chxn*)$_2$]Br$_2$ supports the validity of description of electron state in this system with extended-Hubburd model[10]. The small broad peak at 1.4 eV would be attributed to a hot luminescence.

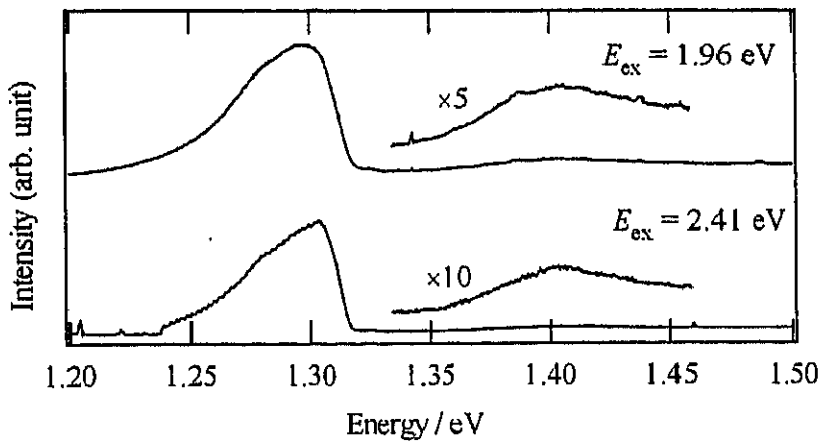

FIGURE 1. Luminescence spectra of [NiBr(chxn)$_2$]Br$_2$ at 2 K for the excitation energy of 1.96 and 2.41 eV.

Figure 2 shows the temperature dependence of luminescence spectra with excitation energy E_{ex} = 1.96 eV. The peaks at 1.3 and 1.4 eV are gradually disappeared with temperature. This shows that the deactivation process is continuously changed from luminescence to thermal relaxation. The peak at 1.3 eV slightly shifts to low energy with temperature. This slight shift might be accounted as follows. The Ni-Br distance is expected to become longer with temperature, resulting in a decrease of the separation of Br^-

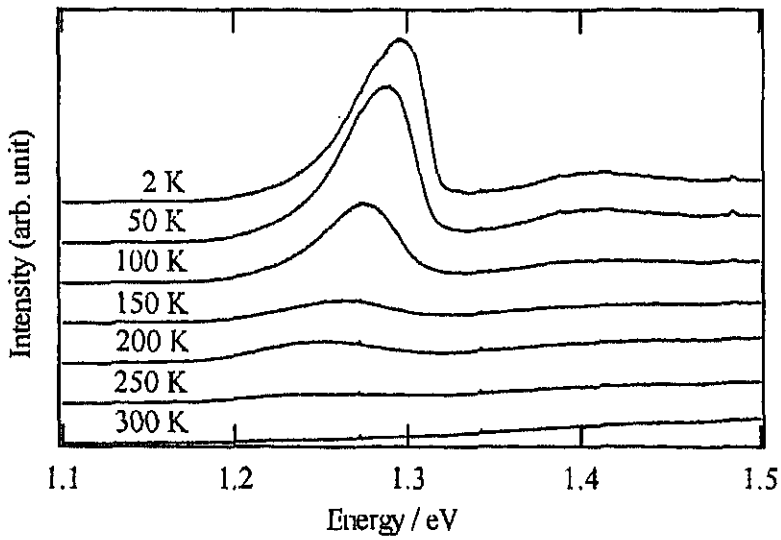

FIGURE 2 Temperature dependence of luminescence spectra in $[NiBr(chxn)_2]Br_2$ with excitation energy E_{ex} = 1.96 eV.

$3p_z$ and Ni^{3+} $3d_{z^2}$ orbitals.

The luminescence spectra of mixed-metal complexes $[Ni_{1-x}Pd_xBr(chxn)_2]Br_2$ (x = 0.005, 0.05, 0.33) at 2 K for the excitation energy of 1.96 eV are shown in Figure 3. The luminescence at 1.3 eV is remarkably quenched with increase of x. It is reported that the Pd ion in $[Ni_{1-x}Pd_xBr(chxn)_2]Br_2$ exists as Pd^{3+} in the range of $0 < x < 0.6$ [11,12].

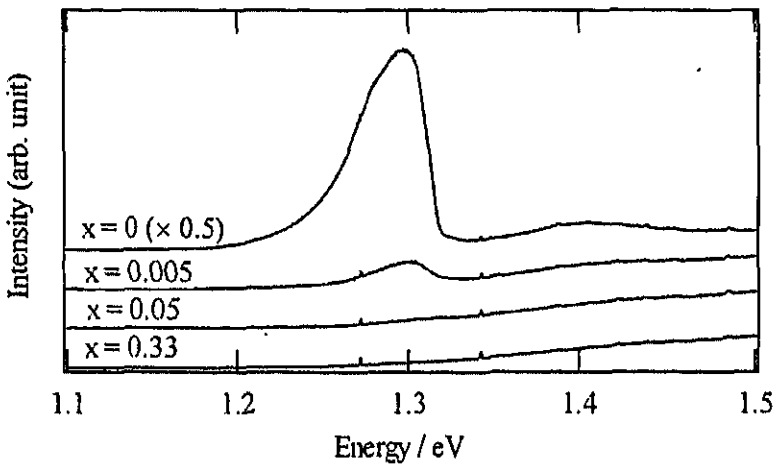

FIGURE 3 Luminescence spectra in $[Ni_{1-x}Pd_xBr(chxn)_2]Br_2$ with x = 0, 0.005, 0.05, 0.33 for the excitation energy of 1.96 eV at 2 K.

Therefore, the impurity level of Pd^{3+} is considered to quench the luminescence at 1.3 eV. From optical conductivity measurements in $[Ni_{1-x}Pd_xBr(chxn)_2]Br_2$[13], broad LMCT band shifts to the low-energy side with increasing x. This result implies that the energy level of d_{z^2} orbital of Pd^{3+} is located between the $3p_z$ band of Br^- and upper Hubbard band (UHB) of Ni^{3+}. An expected schematic electronic structure is shown in Figure 4. The disappearance of luminescence can be accounted as follows. The LMCT exciton is trapped to the in-gap states, formed by $4d_{z^2}$ orbitals of Pd^{3+}.

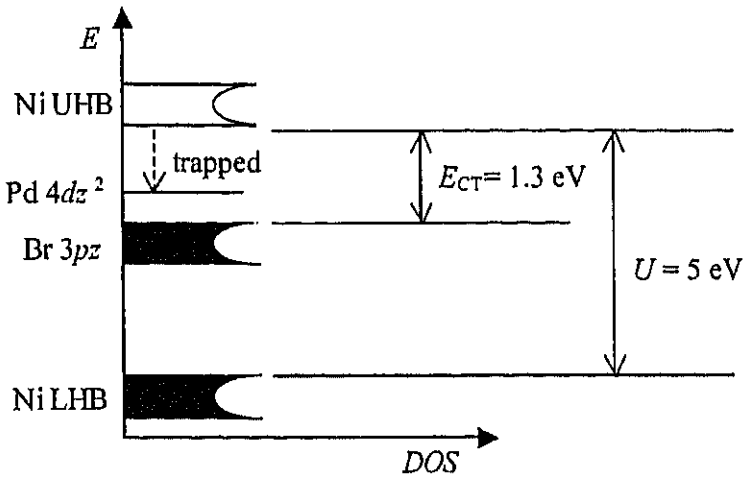

FIGURE 4 Schematic electronic structure for $[Ni_{1-x}Pd_xBr(chxn)_2]Br_2$ (x ál).

CONCLUSION

We have investigated the relaxation process of $[NiBr(chxn)_2]Br_2$ and $[Ni_{1-x}Pd_xBr(chxn)_2]Br_2$ by means of luminescence spectroscopy. In $[NiBr(chxn)_2]Br_2$, LMCT exciton state is not deactivate *via* self-trap exciton state, and this process is changed from luminescence to thermal relaxation with temperature. On the other hand in $[Ni_{1-x}Pd_xBr(chxn)_2]Br_2$ (x = 0.005, 0.05, 0.33), the luminescence is almost quenched even at 2 K, because the LMCT exciton state is trapped to the in-gap states, which is formed by $4d_{z^2}$ orbitals of Pd^{3+}.

Acknowledgements
This work was partly supported by Grants-in-Aid for Scientific Researches Nos. 12440192 of (B), 11640559 of (C), 10149104 (401: Metal-Assembled Complexes) and 12046235 (407: Transition Metal Oxides) of Priority Area (A) from the Ministry of Education, Culture, Sports, Science and Technology of Japan, and by The Iwatani Naoji Foundation's Research Grant.

References
[1.] H. Okamoto, K. Toriumi, T. Mitani, and M. Yamashita, *Phys. Rev.* **B42**, 10381(1990).
[2.] H. Okamoto, Y. Shimada, Y. Oka, A. Chainani, T. Takahashi, H. Kitagawa, T. Mitani, K. Toriumi, K. Inoue, T. Manabe, and M. Yamashita, *Phys. Rev.* **B54**, 8438(1996).
[3.] Y. Wada, T. Mitani, M. Yamashita, and T. Koda, *J. Phys. Soc. Jpn.*, **54**, 3143(1985).
[4.] Y. Wada, N. Matsushita, and M. Yamashita, *Mol. Cryst. Liq. Cryst.*, **216**, 175(1992).
[5.] H. Okamoto, T. Mitani, *Prog. Theor. Phys. Supp.*, **113**, 191(1993).
[6.] H. Okamoto, Y. Oka, T. Mitani, K. Toriumi, M. Yamashita, *Mol. Cryst. Liq. Cryst.*, **256**, 161(1994).
[7.] H. Okamoto, Y. Kaga, Y. Shimada, Y. Oka, Y. Iwasa, T. Mitani, and Yamashita, *Phys. Rev. Lett.*, **80**, 861(1998).
[8.] H. Okamoto, M. Yamashita, *Bull. Chem. Soc. Jpn.*, **71**, 2023(1998).
[9.] T. Manabe, M. Yamashita, T. Kawashima, H. Okamoto, H. Kitagawa, T. Mitani, K. Toriumi, H. Miyamae, K. Inoue, and K. Yakushi, *Proc. SPIE*, **3145**, 106(1998).
[10.] N. Tomita, K. Nasu, *Phys. Rev.* **B56**, 3779(1997).
[11.] K. Marumoto, H. Tanaka, S. Kuroda, T. Manabe, and M. Yamashita,*Phys. Rev.* **B60**, 7699(1999).
[12.] N. Kimura, M. Kano, T. Manabe, M. Yamashita, and R. Ikeda, *Synth. Met.*, **120**, 777(2001).
[13.] M. Yamashita, T. Ishii, H. Matsuzaka, T. Manabe, T. Kawashima, H. Okamoto, H. Kitagawa, T. Mitani, K. Marumoto, and S. Kuroda, *Inorg. Chem.*, **38**, 5124(1999).

Mol. Cryst. Liq. Cryst., Vol. 379, pp. 309-314

1058-725X/02 $12.00+.00
DOI: 10.1080/10587250290090651

Electronic State of a Halogen-Bridged Mixed-Valence Binuclear Complex, $Ni_2(dta)_4I$

RIE MAKIURA[a], HIROSHI KITAGAWA[a,b] and RYUICHI IKEDA[a]

[a]*Department of Chemistry, University of Tsukuba, Tennodai 1-1-1, Tsukuba, Ibaraki 305-8571, Japan and*
[b]*Japan Advanced Institute of Science & Technology, Tatsunokuchi, Ishikawa 923-1292, Japan*

The electronic state of a halogen-bridged mixed-valence binuclear nickel complex, $Ni_2(dta)_4I$ (dta = $CH_3CS_2^-$), has been investigated by optical and magnetic measurements. The X-ray photoelectron spectrum of Ni $2p_{3/2}$ region is reasonably fitted with two components. Under the time scale of X-ray photoelectron spectroscopy (10^{-16} s), the charges of nickel ions in $Ni_2(dta)_4I$ were detected as Ni^{2+} and Ni^{3+}. The strong absorption band was observed at 0.65 eV, which is attributable to an interdimer ($d_{\sigma^*} \rightarrow d_{\sigma^*}$) transition. This band was clearly split below 100 K, implying a charge ordering in the one-dimensional -Ni-Ni-I- chains, such as $\cdots Ni^{2+}$-Ni^{3+}–I–Ni^{3+}-$Ni^{2+}\cdots I\cdots Ni^{2.5+}$-$Ni^{2.5+}\cdots I\cdots$. This distortion is also suggested by the spin concentration ~1/3, the splitting of υ(Ni-Ni) mode, and the activation of υ(Ni-I) mode in Raman spectra at low temperature.

Keywords: 1-D chain compound; Mixed-Valence; MX chain; MMX chain; Interdimer transition; Raman spectra

INTRODUCTION

Halogen-bridged(X) one-dimensional(1-D) transition-metal(M) complexes, the so-called MX chains show unique physical properties relating to a 1-D electronic system[1-3]. One of the most important features

of MX-chain materials is that their electronic states can be controlled by varying their constituents of the metal ions, the bridging halogen ions, the ligands, the counter ions and also by the external field of light or pressure.

Recently, attention has been directed to MMX chains in which 1-D –M-M–X–M-M–X– chains are formed[4-10]. According to our recent works[11-14], the $Pt_2(dta)_4I$ (*dta* = $CH_3CS_2^-$) was found to exhibit metallic conduction around room temperature, which is the first observation of a metallic halogen-bridged 1-D transition-metal complex. Such a 1-D mixed-valence polynuclear unit-assembled conductor is expected to a spin-charge-lattice coupled system. In addition, novel electronic phases were found, such as $-X\cdots M^{2+}\text{-}M^{3+}-X\cdots M^{2+}\text{-}M^{3+}-X\cdots$ (charge-polarization state) and $\cdots X\cdots M^{2+}\text{-}M^{3+}-X-M^{3+}\text{-}M^{2+}\cdots X\cdots$ (alternate charge-polarization state). On the other hand in the Ni analogue, the physical properties have not been enough investigated except a few reports[6-10]. A strong on-site Coulomb repulsion (U) is expected to interact between the Ni spins (S = 1/2), different from the Pt system.

From these interests, the electronic state of $Ni_2(dta)_4I$ was investigated by X-ray photoelectron spectroscopy (XPS), optical absorption spectroscopy, polarized Raman spectroscopy, and SQUID magnetometry measurements.

EXPERIMENTAL

This complex was prepared by the method previously reported[6]. The single crystals were grown by the diffusion technique in CS_2 solution which contained $Ni_2(dta)_4$ and I_2. The qualities of obtained crystals were checked by elemental analysis and X-ray diffraction.

The XPS measurements were carried out on an Ulvac Phi 5600ci with a monochromated Al-Kα X-ray source (1487 eV) at rt.

For optical absorption spectra, powdered samples ground down from single crystals were diluted with KBr and then the mixtures were processed into pellets. The UV-VIS-NIR absorption spectra were recorded in the temperature region 4.0–302 K by a Jasco-V570 spectrometer with an Oxford Optistat^{CF}. IR spectra were measured in the temperature region 4.0–302 K by a ThermoNicolet NEXUS 670 FT-IR spectrometer with an Oxford Microstat^{CF}.

The polarized Raman spectra of single crystals were measured in the temperature region 3.2–300 K by a Jasco NR-1800 subtrac-

tive-dispersion triple polychromator using a microscope with an Oxford Microstat^{CF}. A Spectra-Physics model 2017 Ar^+ laser provided the exciting line (514.5 nm). Wavenumber calibration was effected by reference to the emission of Ne lamp.

The magnetic susceptibility measurement of unoriented single crystals was performed in the temperature range of 2-300 K using a Quantum Design MPMS-5 SQUID magnetometer.

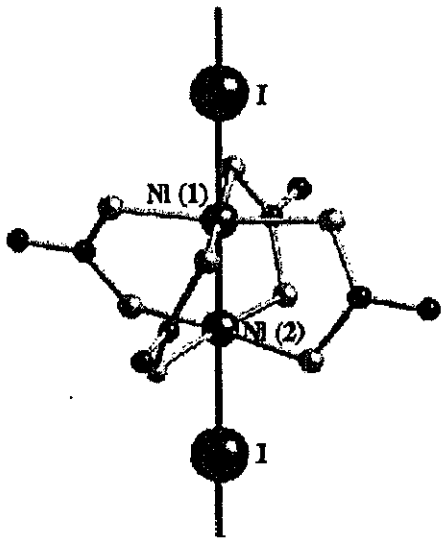

FIGURE 1 Crystal structure of $Ni_2(dta)_4I$.

RESULT AND DISSUCUSSION

The crystal structures of $Ni_2(dta)_4I$ was reported[6,8] as shown in Figure 1, in which each metal-dimer unit $[Ni_2(dta)_4]$ is uniform.

The oxidation state of nickel ions has been investigated from XPS. Figure 2 shows the XPS spectra of Ni $2p_{3/2}$ region for $Ni_2(dta)_4I$ and Ni(II) complex $Ni_2(dta)_4$. As shown Figure 2b, $Ni_2(dta)_4$ was fitted with one component of Ni^{2+}. On the other hand, for the iodine–bridged $Ni_2(dta)_4I$, the spectrum was reasonably fitted with two components of Ni^{2+} and Ni^{3+} (Figure 1a). Binding energies and full widths at half maximum (fwhm) of the components were given in Table 1. Under the time scale of XPS (10^{-16} s), the charges of nickel ions in $Ni_2(dta)_4I$ are detected as Ni^{2+} and Ni^{3+}.

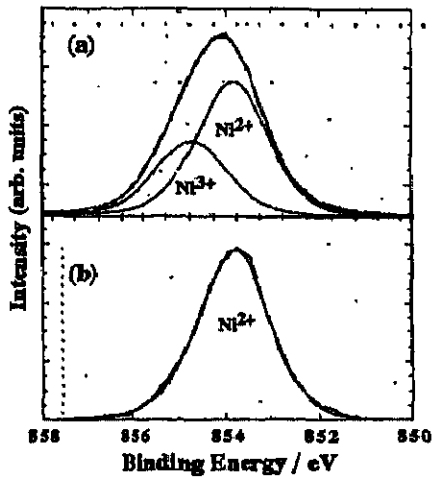

FIGURE 2 XPS spectra of Ni $2p_{3/2}$ region at rt; (a) a fit for the observed spectrum of $Ni_2(dta)_4I$, (b) the Ni(II) complex $Ni_2(dta)_4$.

TABLE 1 Binding energies (eV) for the Ni $2p_{3/2}$ region.

complex	$2p_{3/2}$ Ni^{2+} (fwhm)	Ni^{3+} (fwhm)
$Ni_2(dta)_4$	853.8 (1.8)	
$Ni_2(dta)_4I$	854.0 (1.8)	855.0 (1.8)

Optical absorption spectra are shown in Figure 3. One of the most important features in $Ni_2(dta)_4I$ is a strong absorption with a maximum centered at 0.65 eV, which is absent in the Ni(II) complex $Ni_2(dta)_4$. This strong band is considered to be attributable to an interdimer ($d_{\sigma^*} \rightarrow d_{\sigma^*}$) transition. The transition energy is roughly equal to the U of d_{σ^*} in the $[Ni_2(dta)_4]$ dimer units. The splitting of this band was clearly observed below 100 K as shown in Figure 4, which implies some distortion occurring in the 1-D -Ni-Ni-I- chains.

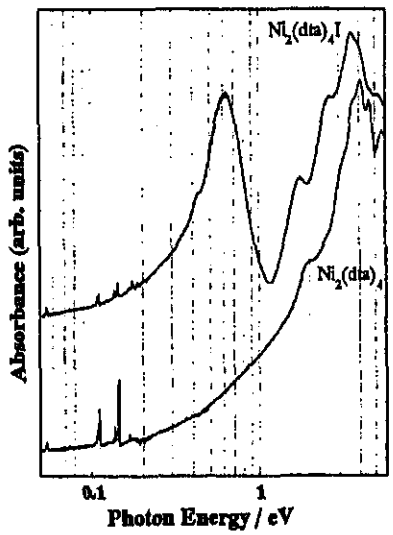

FIGURE 3 Absorption spectra of $Ni_2(dta)_4I$ and $Ni_2(dta)_4$.

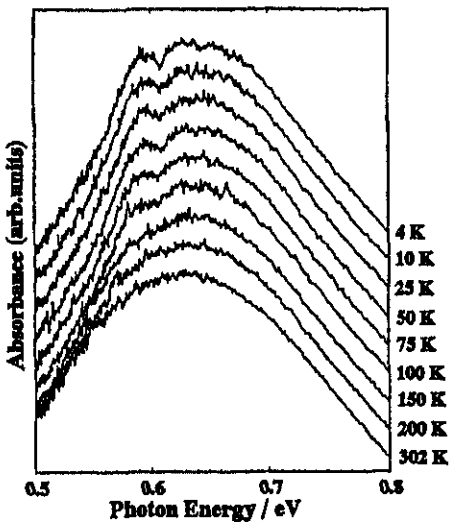

FIGURE 4 Temperature dependence of the interdimer charge-transfer band.

Raman spectroscopy has been widely used to study the vibrational and structural properties, since Raman modes are very sensitive to the symmetry of metal complexes[15]. Temperature dependence of Raman spectra in the low-frequency region for $Ni_2(dta)_4I$ is shown in Figure 5. The stretching mode of υ(Ni-Ni) around 90 cm^{-1} shows a shoulder at the higher wavenumber side at 300 K, although it was reported that $[Ni_2(dta)_4]$ units were uniform[6,8]. This υ(Ni-Ni) mode was clearly split into a doublet and shifted slightly to the high-frequency side at low temperatures. In addition, the Ni-I stretching mode υ(Ni-I) around 125 cm^{-1} was gradually activated below 100 K, which would be Raman-inactive if the iodine ions were centrally placed between $[Ni_2(dta)_4]$ dimer units. The splitting of the υ(Ni-Ni) mode and the appearance of the υ(Ni-I) mode also imply a distortion of the 1-D chains.

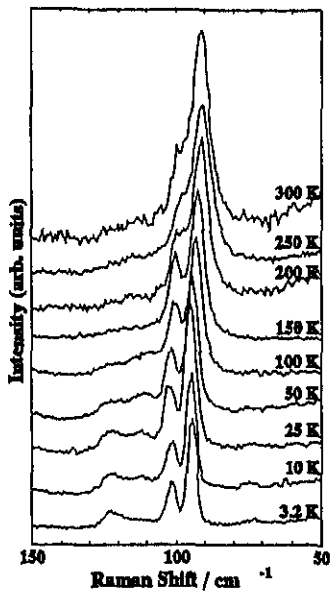

FIGURE 5 Temperature dependence of Raman spectra (E // Chain) of the Ni-Ni stretching mode in $Ni_2(dta)_4I$.

To clarify the spin state of $Ni_2(dta)_4I$, the temperature dependence of magnetic susceptibility was measured. The spin concentration of $Ni_2(dta)_4I$ was estimated to be ~ 1/3 from Curie constant or Bonner-Fisher equation. From the optical and magnetic measurements, a model for the distorted 1-D chain can be led as shown in Figure 6. Two structurally independent sites of $[Ni_2(dta)_4]$ units should exist in 1-D chain. Considering the spin concentration ~ 1/3, two thirds $[Ni_2(dta)_4]$ units must be dimerized, resulting in spin-singlet being formed and one

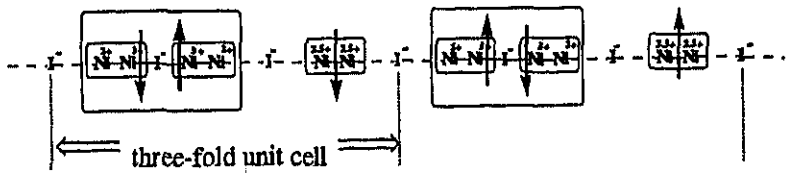

FIGURE 6 A proposed model for 1-D charge-ordering state of $Ni_2(dta)_4I$.

third spins surviving. In the present model, the unit cell would be three-fold. To examine this model, X-ray diffuse scattering measurements are underway.

Acknowledgments
This work was partly supported by Grants-in-Aid for Scientific Researches Nos. 12440192 of (B), 11640559 of (C), 10149104 (401: Metal-Assembled Complexes) and 12046235 (407: Transition Metal Oxides) of Priority Area (A) from the Ministry of Education, Culture, Sports, Science and Technology of Japan, and by The Iwatani Naoji Foundation's Research Grant.

References

[1.]J. Keller, in *Extended linear Chain Compounds*, edited by J. S. H. Miller, (Plenum, New York, 1982), **Vol. 1**, p. 357.
[2.] P. Day, in *Low-Dimensional Cooperative Phenomena*, edited by H. J. Keller, (Plenum, New York, 1974), p. 191.
[3.] R. J. H. Clark, in *Mixed Valence Compounds*, edited by D. E. Brown, (Reidel, Dordrecht, 1982), p. 271.
[4.] K. Toriumi, Y. Wada, T. Mitani, S. Bandow, M. Yamashita, Y. Fujii, *J. Am. Chem. Soc.*, **111**, 2341 (1989).
[5.] M. Whangbo, M. Foshee, *Inorg. Chem.*, **113**, 20 (1981)
[6.] C. Bellito, G. Dssey, V. Fares, *Inorg. Chem.*, **24**, 2815 (1985).
[7.] R. J. H. Clark, J. R. Walton, *Inorg. Chem. Acta*, **129**, 163 (1987)
[8.] M. Yamashita, Y. Wada, K. Toriumi, T. Mitani, *Mol. Cryst. Liq. Cryst.*, **216**,207 (1992).
[9.] R. Ikeda, N. Kimura, H. Ohki, T. Furuta, M. Yamashita, *Synthetic Metals*, **71**, 1907 (1995).
[10.]K. Kanoda, private communications.
[11.]H. Kitagawa, N. Onodera, J. –S. Ahn, T. Mitani, K. Toriumi, M. Yamashita, *Mol. Cryst. Liq. Cryst.*, **285**, 311 (1996).
[12.]H. Kitagawa, N. Onodera, T. Mitani, K. Toriumi, M. Yamashita, *Synthetic Metals*, **86**,193 (1997).
[13.]H. Kitagawa, T. Mitani, *Coord. Chem. Rev.*, **190-192**, 1169-1184 (1999).
[14.]H. Kitagawa, N. Onodera, T. Sonoyama, M. Yamashita, T. Fukawa, T. Mitani, M. Seto, Y. Maeda, *J. Am. Chem. Soc.*, **121**, 10068-10080 (1999).
[15.]R. J. H. Clark, *Infrared Raman Spectrosc.*, **11**, 95 (1984).

Mol. Cryst. Liq. Cryst., Vol. 379, pp. 315-320

1058-725X/02 $12.00+.00
DOI: 10.1080/10587250290090660

Structural and Optical Properties of $Pt_2(dtp)_4Br_2$ (dtp = dithiopropionato) and its Halogen-Replacement Effect

ATSUSHI KOBAYASHI[a], HIROSHI KITAGAWA[a,b] and RYUICHI IKEDA[a]

[a]*Department of Chemistry, University of Tsukuba, Tsukuba 305-8571, Japan and*
[b]*School of Materials Science, Japan Advanced Institute of Science & Technology, Tatsunokuchi, Ishikawa 923-1292, Japan*

A novel binuclear Pt(III) complex, $Pt_2(dtp)_4Br_2$ (dtp = $CH_3CH_2CS_2^-$, dithiopropionato), was synthesized by a reaction of $Pt_2(dtp)_4$ and Br_2 in refluxing toluene, which could be used as starting material for a new MMX-chain system such as a possible mixed-valence $Pt_2(dtp)_4Br$. The title complex has been characterized by X-ray single-crystal structure analysis, UV-Visible-NearIR, IR, and polarized Raman spectroscopies. The $Pt_2(dtp)_4Br_2$ crystallized in monoclinic $P2_1/a$ and this structure is almost same as $Pt_2(dtp)_4I_2$. Halogen-replacement effect from X = I to Br on $Pt_2(dtp)_4X_2$ has been examined. The Pt-Pt distance in X = Br is slightly shorter than that in X = I. Raman peak of the ν(Pt-Pt) mode is slightly shifted to higher wavenumber from X = I to Br. These changes are considered to be mainly caused by the difference of electron densities of antibonding d_{σ^*} orbitals.

Keywords MMX chain; mixed valence; diplatinum(III) complex; binuclear complex

INTRODUCTION

Halogen-bridged (X) one-dimensional (1-D) binuclear-metal (MM) complexes (MMX-chain complexes) have drawn much attention because of their interesting physical properties such as metallic

conduction, metal-insulator transition with 1-D charge ordering, and so on [1]. MMX-chain complexes are classified to two systems with the terminal ligand, the *dta* (*dta* = dithioacetato; $CH_3CS_2^-$) and the *pop* (*pop* = $H_2P_2O_5^{2-}$; diphosphonato) systems [2]. In the *dta* system, there are three main structural components, centric metal, terminal ligand, and bridging halogen. Until now, there have been several reports on the *dta* system with X = I of which alkyl-chain of terminal ligand is lengthened [3], but no report on this system using bromide or chloride as a bridging halide ion. The halogen replacements from X = I to Br or Cl in MMX-chain would bring significant change of physical properties, because the bridging halogen plays an important role in the superexchange or supertransfer interaction between the metal dimers. From these reasons, we have synthesized a Pt(III) complex, $Pt_2(dtp)_4Br_2$ (*dtp* = dithiopropionato; $CH_3CH_2CS_2^-$) which could be used as starting material to obtain a new MMX-chain complex with X = Br. In this paper, we report on the structural and optical properties of $Pt_2(dtp)_4Br_2$ and the halogen-replacement effect from X = I to Br by X-ray single-crystal structure analysis, UV-Visible-NearIR, IR, and polarized Raman spectroscopies.

EXPERIMENTAL

SYNTHESES

$Pt_2(dtp)_4Br_2$ (1): Tetra-dithiopropionato-diplatinum(II), $Pt_2(dtp)_4$ [4] , (170.1 mg, 0.213 mmol) was dissolved in 50 ml of toluene under reflux in argon atmosphere. To this strong reddish orange solution was added a solution of bromine (0.43 g, 2.7 mmol) in 10 ml of toluene. The mixture was refluxed for 30 min. with stirring. On cooling, bright red needle crystals with metallic luster separated from the resulting light red solution were collected by suction filtration, washed with toluene, and dried in *vaccuo* (yield 102.2 mg, 50 %). IR (KBr, cm^{-1}): 2970(s), 2922(m), 2864(m), 1450(s), 1373(m), 1326(vw), 1263(w), 1159(s), 1087(m), 1038(m), 972(s), 936(m), 763(vw), 543(vw). Anal. Caled for $C_{12}H_{20}S_8Pt_2Br_2$: C, 14.85; H, 2.08. Found: C, 14.88: H, 2.05.

$Pt_2(dtp)_4I_2$ (2): The $Pt_2(dtp)_4I_2$ was prepared according to the procedure reported [3].

X-RAY CRYSTAL STRUCTURE DETERMINATION

Intensity data of **(1)** were collected on an Enraf Nonius CAD4 diffractometer with graphite-monochromated Mo Kα radiation (λ = 0.71069 Å) at 293 K. The structure was solved and refined by using the Crystal Structure software package [5]. Crystal data; crystal dimensions $1.20 \times 0.20 \times 0.10$ mm^3, $C_{12}H_{20}Br_2Pt_2S_8$, fw = 970.76, monoclinic, $P2_1/a$, $Z = 4$, $T = 293$ K, $a = 9.755(7)$, $b = 15.67(1)$, c = 15.87(2) Å, $\beta = 85.03(9)°$, $V = 2417.3(33)$ Å^3, μ(Mo Kα) = 155.19 cm^{-1}, $F(000) = 1784.00$, 10372 reflections measured ($2\theta_{max} = 52.7°$), of which 10163 were independent and 2202 were observed with $I > 3\sigma(I)$, 239 refined parameters, $R = 0.073$, $Rw = 0.078$.

ELEMENTAL ANALYSIS

Elemental analysis was performed by a Perkin-Elmer 2400 series II CHNS/O analyzer at the Chemical analysis Center, University of Tsukuba.

OPTICAL MEASUREMENTS

UV-Visible-NearIR spectra of the complexes as KBr pressed disks and toluene solution were recorded on a Jasco V-570 spectrometer. IR spectra were recorded as KBr pressed disks on ThermoNicolet NEXUS 670 FT-IR spectrometer. Polarized Raman spectra were recorded with a Jasco NR-1800 subtractive-dispersion triple (filter single) polychromator using a microscope. A Spectra Physics model 2017 Ar^+ laser provided the exciting line (514.5 nm). Detection of the scattered radiation was made by a cooled Photometrics CC200 CCD camera system with operating temperature of 153 K. Wavenumber calibration was made based on the emission lines of Ne lamp.

RESULT AND DISCUSSION

The ORTEP and packing diagrams of **(1)** are shown in FIGURE 1. The complex **(1)** crystallized in the monoclinic $P2_1/a$. Two platinum atoms of the complex are bridged by four *dtp* ligands. Each platinum atom is six coordinated in a tetragonally distorted octahedral geometry and being surrounded by four sulfur atoms in an approximately square-planar arrangement and a bromide and the other platinum atom in apical positions. The two PtS_4 planes are twisted by the angle of ca. 25.6° from the eclipsed D_{4h} structure. The structure of **(1)** is almost equal to that of **(2)** [3]. The Pt-Pt distance of 2.572(4) Å in **(1)** is slightly shorter than that in **(2)** (2.582(1) Å) [3]. This is due to the difference in the electron densities of antibonding d_{σ^*} orbital, that is the difference in the σ-donations from axial halide p_z orbital. The Br-Pt-Pt-Br sequence is almost linear. The two Pt-Br distances (2.573(5) and 2.578(5) Å) are the same within standard deviations.

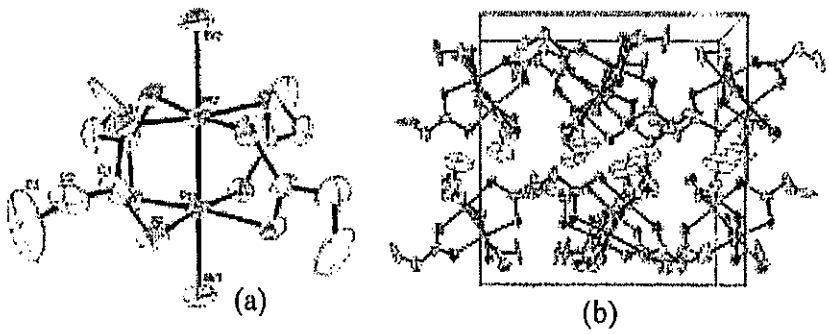

FIGURE 1 (a) ORTEP diagram of **(1)** with 50% thermal ellipsoids. (b) Packing diagram projected along the *a* axis for **(1)**.

Electronic spectra of **(1)** and **(2)** are shown in FIGURE 2. The spectra of two complexes are very similar both in solid and solution state. An important feature of the absorption spectra is the intense band at ca. 2.5 eV. These bands are assigned to LMCT (Ligant-to-Metal Charge Transfer) transition, $p_\sigma(X) \rightarrow d_{\sigma^*}(M)$. The energy of LMCT band is higher in **(1)** than that in **(2)**, because the energy level of $p_\sigma(X)$ is shifted to lower energy with changing X from I to Br.

The observed bands around at 3.5 and 4.2 eV are also assigned to d_{π^*}(M) → d_{σ^*}(M) and d_{π^*}(M) → p_σ(M) transitions, respectively.

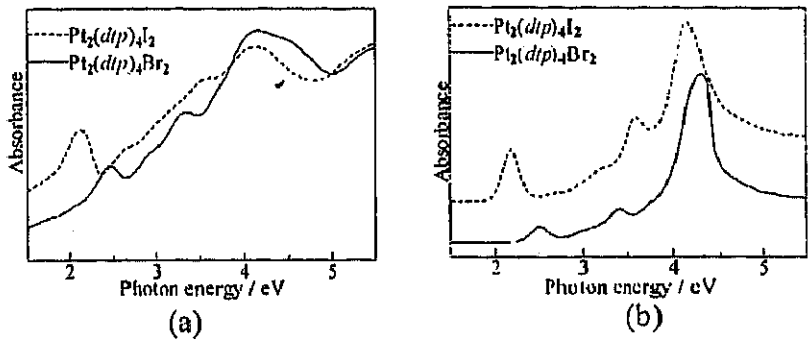

FIGURE 2 Electronic spectra of **(1)** and **(2)** in KBr disk (a) and in toluene solution (b).

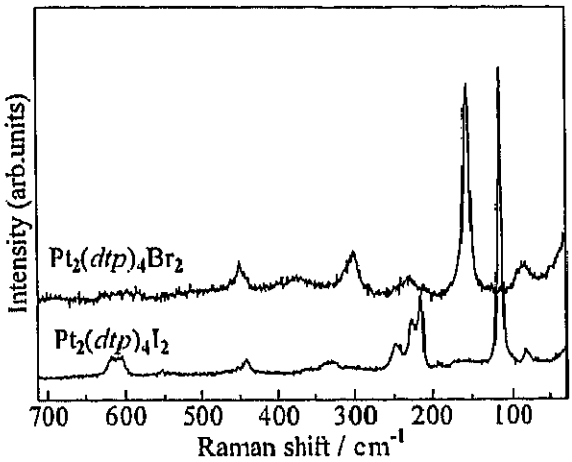

FIGURE 3 Polarized Raman spectra of **(1)** and **(2)**.

Polarized Raman spectra of **(1)** and **(2)** are shown in FIGURE 3. The peaks at 154 and 300 cm^{-1} in **(1)** are assigned to ν(Pt-X) mode and its overtone. The strong peak at 114 and 226 cm^{-1} in **(2)** is also assigned as well, which is shifted to lower wavenumber than that in **(1)**. The weak peaks at 86 cm^{-1} in **(1)** and 81 cm^{-1} in **(2)** are assigned to the ν(Pt-Pt) modes. This slight shift is due to the difference in the electron densities of antibonding d_{σ^*} orbitals of **(1)** and **(2)**.

Acknowledgements

The authors thank Dr. M. Mitsumi and Prof. K. Toriumi at Himeji Institute of Technology for stimulus discussions. This work was partly supported by Grants-in-Aid Scientific Researches Nos. 11640559 of (C), 12440192 of (B), 10149104 (401: Metal-Assembled Complexes) and 12046235 (407: Transition Metal Oxides) of Priority Area (A) from the Ministry of Education, Culture, Sports, Science and Technology of Japan, and by the grant program of The Yazaki Memorial Foundation, for Science & Technology.

References

[1] (a) H. Kitagawa, N. Onodera, T. Sonoyama, M. Yamamoto, T. Fukawa, T. Mitani, M. Seto, and Y. Maeda, *J. Am. Chem. Soc.* **121**, 10068 (1999).
(b) C. Bellito, A. Flamini, L. Gastaldi, and L. Scaramuzza, *Inorg. Chem.*, **22**, 444 (1983).

[2] M. Yamashita, S. Miya, T. Kawashima, T. Manabe, T. Sonoyama, H. Kitagawa, T. Mitani, H. Okamoto, and R. Ikeda, *J. Am. Chem. Soc.* **121**, 2321 (1999).

[3] M. Mitsumi, T. Murase, H. Kishida, T. Yoshinari, Y. Ozawa, K. Toriumi, T. Sonoyama, H. Kitagawa, and T. Mitani, *J. Am. Chem. Soc.* **123**, 11179 (2001).

[4] M. Mitsumi, T. Yoshinari, Y. Ozawa, and K. Toriumi, *Mol. Cryst. Liq. Cryst.* **342**, 127 (2000).

[5] CrystalStructure 2.00:Crystal Structure Analysis Package, Rigaku and MSC (2001).

Mol. Cryst. Liq. Cryst., Vol. 379, pp. 321-326

1058-725X/02 $12.00+.00
DOI: 10.1080/10587250290090679

Spin Polarization in Infinite Zigzag Chains of $[Rh_2(HNCOCH_3)_4Cl]_n$

MIHO YAMAUCHI[a], ANDREI B. KOUDRIAVTSEV[a], RYUICHI IKEDA[a], ZHIONG YANG[b] and TAKASHI KAWAMURA[b]

[a]*Department of Chemistry, University of Tsukuba, Tsukuba 305-8571, Japan and*
[b]*Department of Chemistry, Faculty of Engineering, Gifu University, Yanagido, Gifu 501-1193, Japan*

A temperature dependence of ^{13}C CPMAS NMR was measured for revealing the local electron spin structure in $[Rh_2(acam)_4Cl]_n$ (Hacam=acetamide). Observed two sharp peaks were assigned to carbons of crystallographycally nonequivalent CH_3 groups and a broad one to C in the C=O group. A large high-field shift of -125 ppm was observed in C (C=O), indicating a negative spin polarization on this carbon. From the temperature dependence of Fermi contact shifts, the hyperfine coupling constant of each carbon was determined. By considering hyperfine coupling constants, it is found that a marked amount of electron spins are distributed on C (C=O) with the negative polarization, and a small positive spin exists even on the terminal carbons in methyl groups. ^1H MAS NMR spectra can be explained by the superposition of different shift lines, implying that spin polarization is also generated on hydrogen atoms.

Keywords: Rhodium complex; Acetamidato complex; Dinuclear complex; Electron spin polarization; ^{13}C CPMAS NMR; Hyperfine coupling constant

INTRODUCTION

Halide bridged tetrakis(acetamidato)dirhodium cation radicals

$[Rh_2(HNCOCH_3)_4X]_n$ (X=Cl, Br, I) have a 1D zigzag chain structure supported by hydrogen bonds between ligands in neighboring dimers as illustrated in Figure 1[1]. These complexes have unique features: (1)an odd spin exists on a Rh_2^{5+} unit dimer, and SOMO (singly occupied molecular orbital) is supposed to be the d_{δ^*} molecular orbital in a metal dimer[1], (2) the zigzag alignment of dimers gives rise to an overlap between SOMO's[2], (3) the d_{δ^*} SOMO is symmetry-allowed to delocalize onto the π system of the bridging ligand[2]. By comparison with 1D metal complexes with local d_σ HOMO, it can be presumed that interdimer magnetic interaction is small, in other words, variable by a slight change of their chain structures. It is also likely that the distribution of electron spin on the ligands is relatively large. From these reasons, their magnetic property is expected to be sensitively changed with temperature, and governed not only by the metal-metal interactions but also by the interaction through ligands.

In this study, to understand the structure of electronic spin in these rhodium complexes in detail, the distribution of electron spin on the ligand were investigated by the measurements of temperature dependence of ^{13}C CPMAS NMR and ^1H MAS NMR spectra in $[Rh_2(HNCOCH_3)_4Cl]_n$.

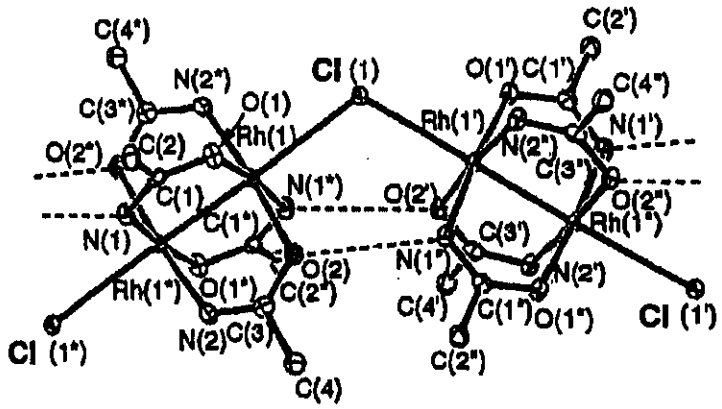

FIGURE 1 Zigzag chain structure in $[Rh_2(HNCOCH_3)_4Cl]_n$[1].

EXPERIMENTAL

$[Rh_2(HNCOCH_3)_4Cl]_n$ was obtained by the method previously

reported[1]. The ^{13}C CPMAS NMR spectra were measured at 75.6 MHz with a BRUKER MSL 300 NMR spectrometer with a $\pi/2$ pulse of 5 μs long and a contact time of 1 ms. The magic angle spinning rate was set between 5 and 7 kHz in a temperature range 175-330 K. ^1H NMR spectrum was measured in the same NMR system as mentioned above at a frequency of 300.13 MHz with a spinning rate of 6 kHz at 300 K.

RESULTS AND DISCUSSION

^{13}C CPMAS NMR Spectrum

A temperature dependence of ^{13}C CPMAS NMR spectra is shown in Figure 2. In the spectrum at 300 K, two relatively sharp and a broad peaks were observed. Two sharp peaks observed at 91 and 46 ppm are attributed to two crystallographically nonequivalent methyl groups in the ligand, but one-to-one correspondence between them cannot be determined at present stage. The broad peak of -125 ppm can be attributed to the carbon in C=O group, which is located close to Rh. The broad width comes from the effect of much fast paramagnetic relaxation of an electron spin on the Rh dimer. The most remarkable result is that a quite large high-field shift of -125 ppm was observed in the C=O carbon. This value differs by several hundred ppm from the common shift of +200 ppm in diamagnetic compounds. From the comparison of electronic structures with various dirhodium complexes,

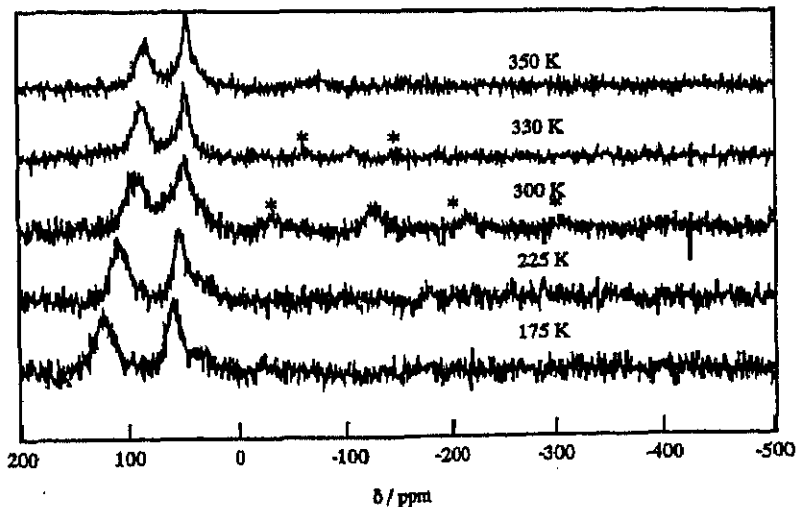

FIGURE 2 Temperature dependence of ^{13}C CPMAS NMR spectrum. The peaks marked with * are spinning side bands.

it was proposed that the matal-ligand bond contains π overlap between the Rh d_{δ^*} and the ligand p_π orbitals[1]. Taking into consideration of these facts mentioned above, it is likely that a considerable amount of electron spins is distributed on the C (C=O), and its spin is negatively polarized.

The observed shifts δ is descried by a sum of the temperature-dependent Fermi contact δ_{Fermi}[3] and pseudo contact δ_{pseudo} shift[4], and temperature independent diamagnetic shift δ_{dia} ;

$$\delta = \delta_{Fermi} + \delta_{pseudo} + \delta_{dia},$$

$$\delta_{Fermi} = \frac{g_{iso}\mu_B}{\gamma/2\pi} \cdot \frac{A}{3k_BT},$$

$$\delta_{pseudo} = (g^2_{para} - g^2_{perp})\frac{\mu_B^2}{12kT} \cdot (3\cos^2\theta - 1)/r^3,$$

where A and γ are the hyperfine coupling constant and the gyromagnetic ratio of ^{13}C, g_{para}, g_{perp}, and g_{iso} are parallel, perpendicular, and isotropic value of g-tensor. The magnitude of A is directly related to the spin polarization. At first, δ_{pseudo} shifts of respective ^{13}C were determined by the method reported in [3]. In this estimation, experimentally determined g_{para} and g_{perp} in the frozen solution of $[Rh_2(acam)_4Cl_2]^+$ were used[1]. Then, $\delta_{Fermi} + \delta_{dia}$ values were obtained by subtracting δ_{pseudo} from δ, and $\delta_{Fermi} + \delta_{dia}$ values were plotted versus reciprocal temperature in Figure 3. Here, one peak of methyl carbon with a higher shift than the other was related to the carbon with larger

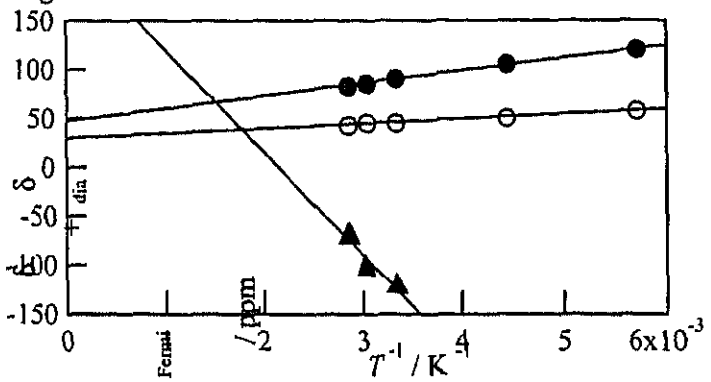

FIGURE 3 Temperature dependencies of Fermi contact shifts of the peaks assigned to carbons in CH_3 (● ,○) and C=O (▲). The solid lines are fitted by $\delta_{Fermi} \propto T^{-1}$.

δ_{pseudo} value, and the average δ_{pseudo} value for two kinds of C (C=O) was used as δ_{pseudo} for C (C=O). The δ_{Fermi} values of carbons (CH_3) increased linearly with T^{-1}, while that of C (C=O) decreased, implying that spin polarization on C (CH_3) is positive, on the other hand, that on C (C=O) is negative. The negative and rather small value of A of the C atom (C=O) is consistent with the model that the odd electron on d_{δ^*} is delocalized onto the HOMO of the acam ligand. Finally, A and δ_{dia} values were determined from the slopes and the y intercepts of δ_{fermi} variations, respectively. Obtained values are tabulated in Table 1. The presumed spin polarization on the ligands is given in Figure 4.

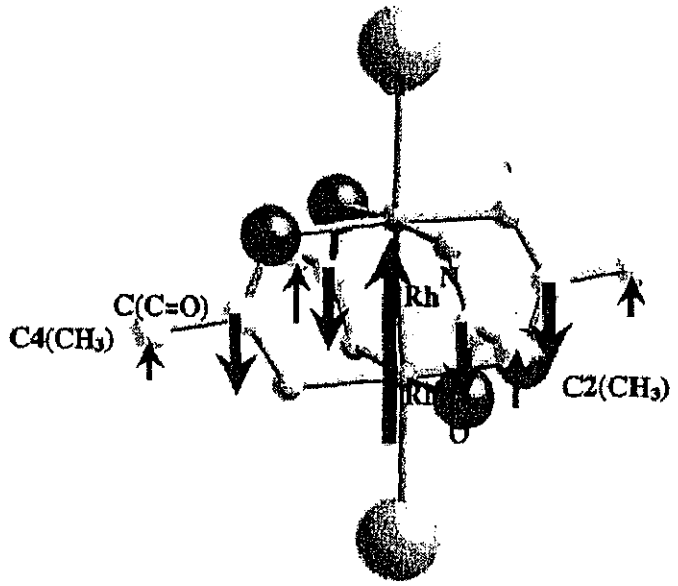

FIGURE 4 Spin polarization presumed from hyperfine coupling constants.

TABLE 1 Hyperfine coupling constants (A) , and diamagnetic shifts (δ_{dia}). C2 and C4 follow the notation in Figure 1.

	A / MHz	δ_{dia} / ppm
C2 (CH_3)	0.41	45
C4 (CH_3)	0.15	29
C (C=O)	-3.2	220

The estimated d_{dia} values are in the common range of values reported in diamagnetic compounds.

^{1}H MAS NMR Spectrum

A ^{1}H MAS NMR spectrum observed at 300 K is shown in Figure 5. The spectral shape is asymmetric and expanding to the high-field, indicating that there is several kinds of ^{1}H with different shift. This result implies the presence of spin polarization on hydrogen atoms.

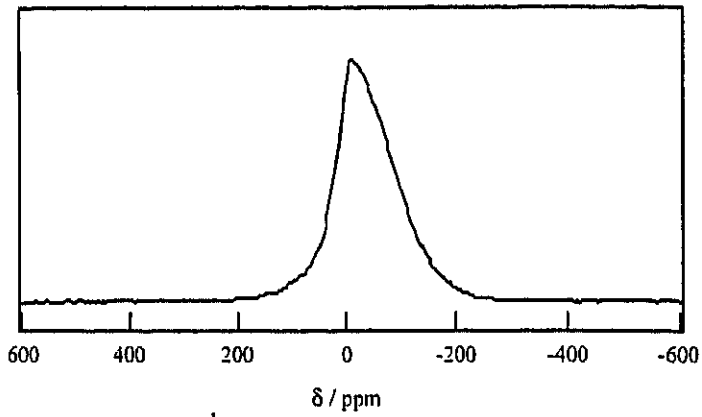

FIGURE 5 ^{1}H MAS NMR spectrum at 300 K.

Acknowledgement

This work was partially supported by Grants-in-Aid for Scientific Researches No.12440192 of (B) and No. 10149105 (401:Metal-Assembled Complex) of Priority Areas (A) from the Ministry of Education, Culture, Sports, Science and Technology of Japan.

References

[1.] Z. Yang, M. Ebihara, T. Kawamura, T. Okubo, and T. Mitani, *Inorg. Chim. Acta*, **321**, 97(2001).

[2.] T. Kawamura, H. Katayama, N. Nishikawa, T. Yamabe, *J. Am. Chem. Soc.*, **111**, 8156(1989).

[3.] T. Kawamura, H. Kachi, H. Fujii, C. Kachi-terajima, Y. Kawamura, N. Kanematsu, N. Ebihara, K. Sugimoto, T. Kuroda-Sowa, and M. Munakata, *Bull. Chem. Soc. Jpn.*, **73**, 657(2000).

[4.] G. Maruta, S. Takeda, R. Imachi, T. Ishida, T. Nogami, and K. Yamaguchi, *J. Am. Chem. Soc.*, **121**, 424(1999).

Spin Structure and Dynamics in a Spin 1/2 One Dimensional Antiferromagnet, $[NiBr(chxn)_2]Br_2$ (chxn: 1*R*, 2*R*-cyclohexanediamine)

Shinya Takaishi, Masataka Kano, Hiroshi Kitagawa, Yuji Furukawa,† Ken-ichi Kumagai,† and Ryuichi Ikeda*
Department of Chemistry, University of Tsukuba, Tsukuba 305-8571
†*Division of Physics, Graduate School of Science, Hokkaido University, Sapporo 060-0810*

(Received May 27, 2002; CL-020457)

The ^{1}H NMR spin-lattice relaxation time T_1 in a spin 1/2 1-D antiferromagnetic complex $[NiBr(chxn)_2]Br_2$ was observed down to 1.8 K. The observed T_1 temperature dependence was well reproduced by the Sachdev's treatment giving an exchange interaction energy (J) of ca. 2500 K. 1-D spin migration assignable to paramagnetic electrons in impurity amounts of Ni^{II} sites was observed at low temperatures.

Halogen-bridged one-dimensional (1-D) metal complexes with a chain structure of -X-M^{II}-X-M^{IV}-X- (M: Pt, Pd; X: Cl, Br, I) have been shown to form an almost isolated 1-D structure in which mixed valence states of metals M(II) and M(IV) are formed owing to strong electron phonon interactions characteristic in this system. Recently, new halogen-bridged 1-D complexes $[NiX(chxn)_2]X_2$ (chxn: 1*R*, 2*R*-cyclohexanediamine; X: Cl, Br) were prepared[1] and shown that bridging halogen atoms are located at the center between two neighboring Ni atoms suggesting the formation of an averaged valence structure (Mott-Hubbard system) consisting of 1-D chains of paramagnetic Ni(III) expressed as -X-Ni^{III}-X-Ni^{III}-X-. To reveal its magnetic structure, the magnetic susceptibility measurement on the Br complex has been performed[2] and obtained results were tried to explain with the Bonner-Fisher model[3] of an antiferromagnetically coupled 1-D system. It is noteworthy that the analyzed result suggested a quite large exchange interaction energy (J) amounting to ca. 3600 K.[2] However, this result is not clear because such a large J value is difficult to be determined from data observed in the low-temperature range up to 300 K. If this reported J value is acceptable, this system would be the 1-D system having the strongest antiferromagnetic interaction so far reported.

It has been shown that 1-D systems consisting of $S = 1/2$ paramagnetic spins with antiferromagnetic interactions cannot form an ordered state at low temperatures, but it has a fluctuated spin state of quantum mechanical origin. From this effect, we can anticipate the non-vanishing NMR spin-lattice relaxation rate in the limit of the low temperature. By assuming the Heisenberg-type interaction, Sachdev proposed[4] that the spin-lattice relaxation time T_1 in the range of $T/J < 0.5$ is expressed as

$$T_1^{-1} \propto \ln^{1/2}(2J/T) \quad (1)$$

where J is defined by $H_{ex} = 2J\Sigma S_l \cdot S_{l+1}$ giving finite T_1 at low temperatures. We confirmed this prediction in the low-temperature range by measuring ^{1}H T_1 in $[CuBr_2(AdH^+)_2]Br_2$ (Ad: adenine)[5] which has been shown to be an antiferromagnetically coupled $S = 1/2$ 1-D system with $J = 52.6$ K.[6]

In the present study, we intend to reveal the magnetic structure and dynamic electron-spin behavior of 1-D chains in $[NiBr(chxn)_2]Br_2$ and obtain the information of magnetic interactions expected to be quite strong by measuring the temperature dependence of the ^{1}H NMR spin-lattice relaxation time at low temperature range and discussing the obtained data in connection with the above relaxation theory.

We prepared crystalline samples of $[NiBr(chxn)_2]Br_2$ for the NMR measurement by two methods which gave quite different results. Starting from a monomer complex $[Ni(chxn)_2]Br_2$ containing Ni^{II} prepared according to literature,[1] the polymer complex $[NiBr(chxn)_2]Br_2$ was obtained in the first method by the oxidation of the monomer complex dissolved in methoxyethanol by slowly diffusing Br_2 gas. Fine plate like crystals were obtained in a week. The second method was performed by the recently developed electrochemical oxidation technique.[7] Using a methanol solution of the monomer complex containing tetra-*n*-butylammonium salt as a supporting electrolyte, several mm size single crystals were appeared on the Pt electrode in 2–3 months with a current of ca. 10 μA. The crystals obtained by 1st and 2nd methods are hereafter named Sample 1 and 2, respectively. We confirmed that both Sample 1 and 2 have the same crystal structure.

The ^{1}H NMR spin-lattice relaxation time T_1 was measured by a Bruker SXP100 pulsed NMR spectrometer using the inversion recovery method with a homemade temperature controller in a range 100–300 K. A home made pulsed spectrometer applying the same pulse sequence was used in a range 4.2–100 K using an Oxford CF1200 cryostat. For the measurement below 4.2 K, an NMR spectrometer and a cryostat made in Hokkaido University was used. The sample temperature was controlled and determined within ± 1 and ± 0.1 K, above and below 100 K, respectively. For detecting possible phase transitions taking place at low temperatures, we carried out single crystal X-ray diffraction measurements on Sample 1 using a low-temperature X-ray imaging-plate (IP) system (DIP320V, Mac Science Co., Ltd.) with a graphite monochromated Mo Kα radiation and a continuous He gas-flow cryostat. The crystal structure determined at ca. 20 K ($I222$, $a = 23.469(3)$, $b = 5.138(1)$, $c = 7.071(2)$ Å, $Z = 2$) showed the same isomorphous nondistorted 1-D chains as determined at room temperature[1] and no diffused scattering pattern was observed. These results imply that no spin Peierls type transition is expected down to ca. 20 K.

In the NMR relaxation measurement, the ^{1}H magnetization observed after a $\pi/2$ pulse plotted against the pulse interval τ showed a nonexponential decay in both samples. We roughly evaluated T_1 from the initial linear part of the decay. This short T_1 component was ca. 90% of the ^{1}H magnetization in the whole temperature range studied. At first, we measured ^{1}H T_1 in Sample 1 and obtained data shown in Figure 1 exhibiting a T_1 expansion upon cooling to 1.8 K. This result was inconsistent with the above theoretical prediction by Sachdev.[4] The recently prepared Sample

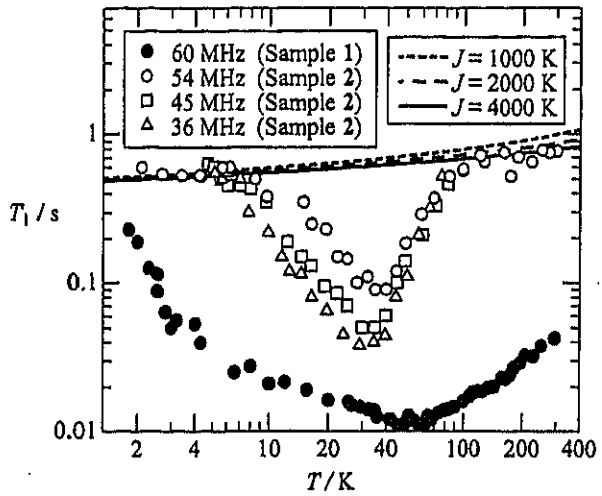

Figure 1. ^{1}H NMR spin-lattice relaxation time T_1 observed in $[NiBr(chxn)_2]Br_2$ prepared by Br_2 diffusion method (Sample 1) and electrochemical oxidation (Sample 2). Solid and broken lines are theoretically calculated by Sachdev's treatment.

2, however, showed a quite different relaxation from in Sample 1 as given in Figure 1, where no T_1 expansion was observed below 4.2 K. The observed T_1 in 2 was ca. 10 times longer than in 1 and gave almost temperature independent values in both high- and low-temperature ranges except for a minimum observed ca. 30 K. Quite different relaxation behavior observed in Sample 1 and 2 suggests marked influences from chain ends, impurities and other lattice imperfections being expected more in Sample 1. The T_1 temperature dependence observed in Sample 2 can be divided into two components: the almost temperature-independent flat part and the minimum at ca. 30 K affording a marked Larmor frequency dependency as shown in Figure 2. The temperature independent part of T_1 tending to a finite value in the low-temperature limit is now consistent with the theoretical expectation and its temperature dependency could be fitted by Equation (1) and fitted curves are shown in Figure 1. From the fitting, we could evaluate the exchange interaction energy $J = 2500 \pm 1{,}000$ K. This value is comparable to 2700 ± 500 K estimated from the spin susceptibility data obtained by ESR measurements[8] and also a recently reported value of 1700 K derived from the Bonner-Fisher fitting of the magnetic susceptibility.[9] It is noteworthy that these J values are almost the same as 2200 K in Sr_2CuO_3[10] that has been reported to be the antiferromagnetically coupled 1-D system having the highest J value so far reported.

Figure 2 shows Arrhenius plots of T_1 having a marked Larmor frequency (ω) dependence. This indicates the presence of time-dependent relaxation mechanisms different from the fluctuation of antiferromagnetically coupled 1-D electron spins in Ni^{III} sites that gives the flat part of T_1. The fact that a T_1 minimum was observed at ca. 30 K indicates the presence of another relaxation with a fluctuation rate close to the Larmor frequency at ca. 30 K by considering the T_1 minimum condition of $\omega\tau \approx 1.0$ where τ is the correlation time given by the reciprocal of the jumping rate. We assigned the origin of this mechanism to some spin motions associated with impurities formed along 1-D chains, because Sample 1 containing more impurities gave a more remarkable relaxation than in 2. The most probable impurity expected in the present system is paramagnetic Ni^{II} sites having

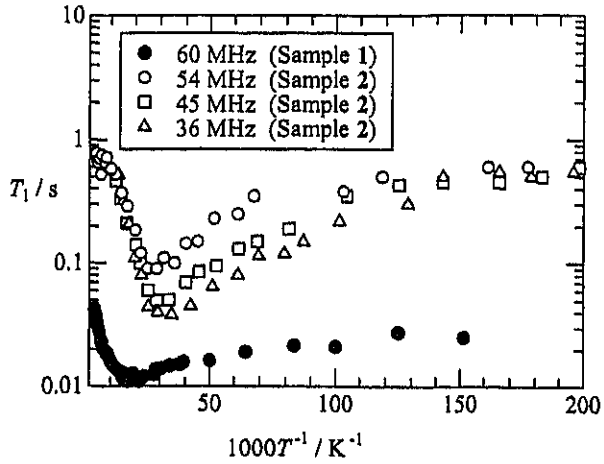

Figure 2. Arrhenius plots of temperature and Larmor frequency dependences of ^{1}H NMR T_1 in $[NiBr(chxn)_2]Br_2$.

an extra electron movable to neighboring normal Ni^{III} sites through Br $4p_z$ orbitals. This model can be supported by the reported high electrical conductivity of 7×10^{-2} S m^{-1} at room temperature,[9] which was also explained by the effect of Ni^{II} impurities.[2] From the present NMR results, we could determine the rate of random jumping of electrons in Ni^{II} sites along the chain to be 10^8/s at ca. 30 K.

The observed temperature and Larmor frequency dependences of T_1 given in Figure 2 were both unexplainable by the conventional BPP theory.[11] Since expected Ni^{II} impurities could be formed not only near cationic impurities, but at chain ends, several kinds of Ni^{II} sites with various concentrations and jumping activation energies seem to be possible. The observed asymmetric T_1 data are attributable to the superimposed effects from these impurities on the relaxation.

This work was partly supported by Grant-in Aid for Scientific Research No. (B) 12440192 from the Ministry of Education, Culture, Sports, Science and Technology of Japan.

References

1 K. Toriumi, Y. Wada, T. Mitani, and S. Bandow, *J. Am. Chem. Soc.*, 111, 2341 (1989).
2 H. Okamoto, K. Toriumi, T. Mitani, and M. Yamashita, *Phys. Rev.*, **B42**, 10381 (1990).
3 J. Bonner and M. Fisher, *Phys. Rev.*, **135**, A640 (1964).
4 S. Sachdev, *Phys. Rev.*, **B50**, 13006 (1994).
5 S. Takaishi, H. Kitagawa, Y. Furukawa, K. Kumagai, and R. Ikeda, to be published.
6 D. Brown, J. Hall, H. Helis, E. Walton, D. Hodgson, and W. Hatfield, *Inorg. Chem.*, **16**, 2675 (1977).
7 M. Yamashita, T. Ishii, H. Matsuzaka, T. Manabe, T. Kawashima, H. Okamoto, H. Kitagawa, T. Mitani, K. Marumoto, and S. Kuroda, *Inorg. Chem.*, **38**, 5124 (1999).
8 K. Marumoto, H. Tanaka, S. Kuroda, T. Manabe, and M. Yamashita, *Phys. Rev.*, **B60**, 7699 (1999).
9 M. Yamashita, T. Manabe, K. Inoue, T. Kawashima, H. Okamoto, H. Kitagawa, T. Mitani, K. Toriumi, H. Miyamae, and R. Ikeda, *Inorg. Chem.*, **38**, 1894 (1999).
10 N. Motoyama, H. Eisaki, and S. Uchida, *Phys. Rev. Lett.*, **76**, 3212 (1996).
11 N. Bloembergen, E. Purcell, and R. Pound, *Phys. Rev.*, **73**, 679 (1948).

INSTITUTE OF PHYSICS PUBLISHING JOURNAL OF PHYSICS: CONDENSED MATTER
J. Phys.: Condens. Matter 14 (2002) 1085–1090 PII: S0953-8984(02)27279-3

Nuclear quadrupole resonance studies on weak exchange interactions between paramagnetic ions in $M(II)(H_2O)_6SnCl_6$ (M(II) = Mn, Co, and Ni)

Hiroshi Miyoshi[1], Ryuichi Ikeda[1], Akira Koshio[1] and Keizo Horiuchi[2,3]

[1] Department of Chemistry, University of Tsukuba, Tsukuba 305-8571, Japan
[2] Faculty of Science, University of the Ryukyus, Nishihara-cho, Okinawa 903-0213, Japan

Received 27 July 2001, in final form 23 November 2001
Published 25 January 2002
Online at stacks.iop.org/JPhysCM/14/1085

Abstract
The ^{35}Cl NQR spin–lattice relaxation times T_{1Q} in paramagnetic $Mn(H_2O)_6SnCl_6$ and $Co(H_2O)_6SnCl_6$ crystals were measured as a function of temperature. Using the T_{1Q} values observed, the correlation times τ_f of electron-spin flip-flops and exchange parameters J were estimated. The J value in Mn salt was found to be smaller than those found for Co and Ni salts. It is inferred from the J values that the indirect interaction where some chemical bonds (including OH···Cl hydrogen bonds) intervene is dominant in the exchange interactions between the paramagnetic ions in $M(II)(H_2O)_6SnCl_6$ (M(II) = Mn, Co and Ni).

1. Introduction

Measurements of nuclear spin–lattice relaxation times in paramagnetic insulators can give dynamical information of unpaired electrons through the magnetic hyperfine interactions. When an atom of the resonant nucleus is not directly bonded to any paramagnetic atoms, it is an excellent approximation for nuclear spin relaxation to take into account only magnetic dipole–dipole interactions between the nucleus and unpaired electrons. Since it is easy to estimate magnetic dipolar interactions as long as the exact geometrical information is available, values of electron correlation times obtained from nuclear-relaxation measurements are quite reliable.

In our previous papers [1, 2], we measured the temperature dependence of the ^{35}Cl nuclear quadrupole resonance (NQR) and ^{1}H nuclear magnetic resonance (NMR) spin–lattice relaxation times in paramagnetic $Ni(H_2O)_6SnCl_6$ crystals, and estimated the correlation time for electron-spin flips and exchange interactions between the paramagnetic ions. These investigations showed that in measuring electron-spin dynamics an NQR method can afford some advantages: a resonance signal can be observed even in nuclei close to paramagnetic

[3] Author to whom any correspondence should be addressed.

0953-8984/02/051085+06$30.00

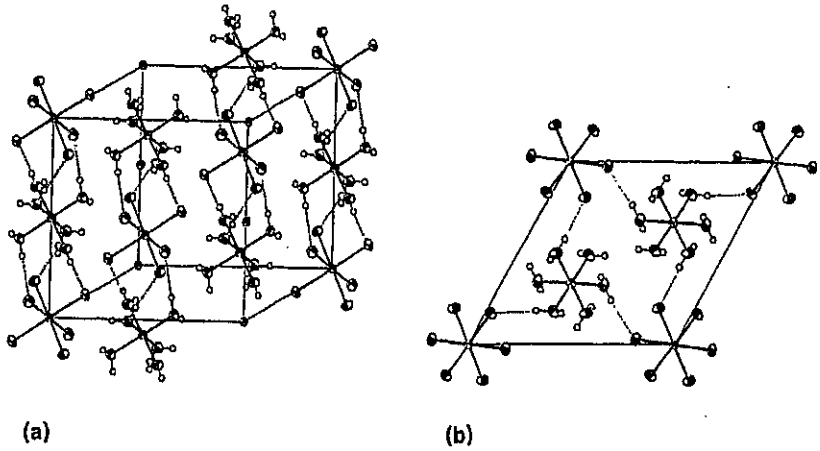

Figure 1. The crystal structure of $Ni(H_2O)_6SnCl_6$ drawn by ORTEP with 50%-probability-displacement ellipsoids [6]. (a) Trigonal unit cell (b) projection of the unit cell onto the *ab*-plane. Double and single dotted lines indicate OH···Cl hydrogen bonds along the *c*-axis and on the *ab*-plane, respectively.

atoms, and resonance signals can be one-to-one corresponded to nonequivalent lattice sites in crystals. As a result of these benefits we were able to measure precisely the electron correlation times in paramagentic crystals. The NQR method has another advantage. A very small exchange parameter of around 10^{-2} K can be estimated without measuring at very low temperatures. In our former studies [1, 2], all relaxation-time measurements were carried out only above 77 K and an exchange parameter of 0.019 K was obtained.

In the present investigation we measure the ^{35}Cl NQR spin–lattice relaxation time T_{1Q} in isomorphous $Mn(H_2O)_6SnCl_6$ and $Co(H_2O)_6SnCl_6$ crystals, and discuss weak exchange interactions in $M(II)(H_2O)_6SnCl_6$ (M(II) = Mn, Co and Ni).

2. Experimental

The polycrystalline samples were prepared by the same method as described in [1]. The temperature variation of the ^{35}Cl NQR T_{1Q} was measured with a homemade pulsed NQR spectrometer described in [3]. The sample temperature was controlled and determined within ± 1 K. T_{1Q} was measured by a $180° - \tau - 90° - \tau' - 180°$ pulse sequence with a fixed τ' of 110–150 μs through the whole T_{1Q} measurement.

3. Results and analysis

$Mn(H_2O)_6SnCl_6$ and $Co(H_2O)_6SnCl_6$ have been shown to be isomorphous with $Ni(H_2O)_6SnCl_6$ [4], which forms a trigonal crystal with space group $R\bar{3}$ and a slightly distorted CsCl-type structure with $\alpha = 96°45'$ consisting of $[Ni(H_2O)_6]^{2+}$ and $[SnCl_6]^{2-}$ octahedra [5]. The unit cell of $Ni(H_2O)_6SnCl_6$ is shown in figure 1 [6]. Each chlorine atom is surrounded by five H_2O molecules, while each $[Ni(H_2O)_6]^{2+}$ ion is in contact with 12 chlorine atoms at 4.2–4.4 Å.

A single ^{35}Cl NQR signal has been detected for the both compounds [7] in agreement with the above crystal structure. The temperature dependences of the ^{35}Cl NQR T_{1Q} in Mn and Co salts are shown in figure 2. We find marked differences in the magnitude and temperature

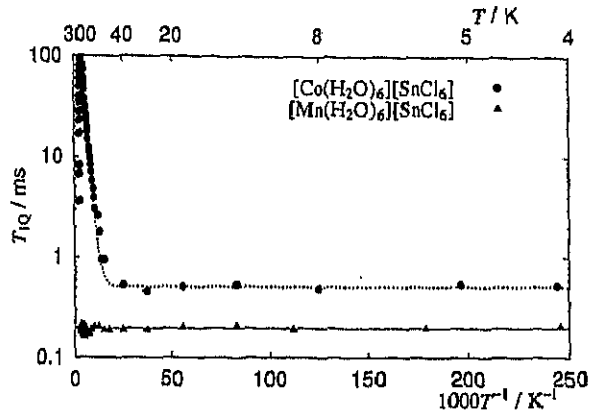

Figure 2. Temperature dependence of ^{35}Cl NQR T_{1Q} in $Mn(H_2O)_6SnCl_6$ and $Co(H_2O)_6SnCl_6$ crystals.

dependence in T_{1Q} between the two salts. That is, T_{1Q} in Mn salt is almost constant over the whole temperature region investigated, whereas in Co salt it increases rapidly on heating. We shall see, however, that both of them are governed by electron-spin dynamics, except for the rapid decrease above room temperature observed in Co salt, which is attributed to electric-field-gradient (EFG) fluctuation at the chlorine sites caused by the $[SnCl_6]^{2-}$ reorientations with an activation energy of 69 ± 10 kJ mol^{-1} [8]. Although the same relaxation mechanism must exist in the Mn salt, it is masked by the paramagnetic relaxation.

When a resonant quadrupolar nucleus with $I = 3/2$ experiences a fluctuation in the magnetic field caused by the motion of electron spins S, T_{1Q} is expressed as [9]

$$T_{1Q}^{-1} = 9\gamma_I^2 g^2 \mu_B^2 S(S+1) \sum_i \Lambda_i \frac{\tau_e}{1+\omega_Q^2 \tau_e^2}. \tag{1}$$

Here γ_I, g and μ_B indicate the gyromagnetic ratio of ^{35}Cl nucleus, the g factor and the Bohr magneton, respectively. ω_Q and τ_e are the resonance frequency of the NQR line measured and the electron-spin correlation time, respectively. The geometrical factor Λ_i is given by

$$\Lambda_i = \tfrac{1}{18}|F_i^{(0)}|^2 + |F_i^{(1)}|^2 + \tfrac{1}{2}|F_i^{(2)}|^2. \tag{2}$$

Here $F_i^{(q)}(q = 0, 1, 2)$ are the spatial parts of the dipolar Hamiltonian between the nucleus and the ith electron spin and are given by

$$\begin{aligned} |F_i^{(0)}|^2 &= (1 - 3\cos^2\theta_i)^2 / r_i^6 \\ |F_i^{(1)}|^2 &= \sin^2\theta_i \cos^2\theta_i / r_i^6 \\ |F_i^{(2)}|^2 &= \sin^4\theta_i / r_i^6. \end{aligned} \tag{3}$$

Here θ_i represents the angle between the principal axis of EFG at the resonant nucleus and the interspin vector r_i. Since ^{35}Cl NQR frequencies in Mn and Co salts were observed around 16 MHz, the condition $\omega_Q^2 \tau_e^2 \ll 1$ is fulfilled and hence we have

$$T_{1Q}^{-1} = 9\gamma_I^2 g^2 \mu_B^2 S(S+1) \sum_i \Lambda_i \tau_e. \tag{4}$$

We see that the relaxation rate T_{1Q}^{-1} is proportional to τ_e.

The electron-spin correlation time τ_e is given by the electron-spin–lattice relaxation time T_{1e} and the correlation time τ_f of electron-spin flip-flops as follows [10]

$$\tau_e^{-1} = T_{1e}^{-1} + \tau_f^{-1}. \tag{5}$$

Since the electron-spin flips are caused by the exchange interaction between neighbouring electron spins, τ_f is independent of temperature. On the other hand, T_{1e} is ascribed to spin–phonon interactions and depends on temperature T as follows [11]:

$$T_{1e}^{-1} = \beta \coth\left(\frac{h\nu_e}{2kT}\right) + \gamma T^n + \frac{\zeta}{\exp(\Delta/kT) - 1}. \tag{6}$$

The first term represents the direct process where ν_e is a Larmor frequency of the magnetic ion. The second term corresponds to the Raman process and the exponent n can take numerical values depending on the electronic states of the magnetic ion. The last term describes the Orbach process where transitions between two low-lying states of the magnetic ion occur via an excited state whose energy is less than the maximum phonon energy and also higher by Δ than energies of the two ground states.

3.1. $Mn(H_2O)_6SnCl_6$

The T_{1Q} values observed in Mn salt shown in figure 2 were almost temperature-independent, suggesting that T_{1Q} is governed by electron-spin flip-flops. The correlation time τ_f can be evaluated from the observed T_{1Q} value using (4) and (5). Since the effective Bohr magneton value μ_{eff} and detailed data on the crystal structure are unavailable for Mn salt, we used the μ_{eff} value for Mn^{2+} in $(NH_4)_2[Mn(H_2O)_6](SO_4)_2$ for the former [12], the lattice parameters in table 2 [4] and assumed the chlorine positions for the latter to estimate τ_f. We finally obtained $\tau_f = 1.1 \times 10^{-10}$ s by substituting $\mu_{eff} = 5.88\ \mu_B$ and $\sum \Lambda_l = 2.42 \times 10^{44}\ cm^{-6}$, where contributions from the paramagentic ions within 11^3 primitive cells around the resonant nucleus were summed up.

On the basis of Kubo and Tomita [13], Moriya [14] derived the following equation for the exchange frequency ω_{ex} on the assumption of the nearest-neighbour interaction:

$$\omega_{ex}^2 = \frac{2}{3}\frac{J^2}{\hbar^2} z S(S+1) \tag{7}$$

where z is the number of nearest neighbours of the paramagnetic ion and J is the exchange parameter that appears in the following Hamiltonian of the isotropic exchange interaction

$$H_{ex} = \sum_{i<j} J_{ij} S_i \cdot S_j. \tag{8}$$

Using the relation [13]

$$\omega_{ex}^2 = \frac{\pi}{2\tau_f^2} \tag{9}$$

the exchange parameter J can be evaluated from τ_f. Moreover, since the paramagnetic Curie temperature Θ is given by

$$\Theta = \frac{z}{3}\frac{J}{k} S(S+1) \tag{10}$$

in the mean-field approximation [15] Θ can also be evaluated from τ_f.

The values of J and Θ obtained from τ_f are listed in table 1. Since J and/or Θ values determined experimentally for Mn salt by no other methods have been reported, the paramagnetic Curie temperature Θ_{obs} determined from the adiabatic magnetization curves observed in the isomorphous complex $Mn(H_2O)_6SiF_6$ is listed for comparison [16].

Table 1. Observed T_{1Q} values, the correlation time τ_f of electron-spin flip-flops, exchange parameter J values between nearest neighbours and the paramagnetic Curie temperature values Θ for $Mn(H_2O)_6SnCl_6$ and $Co(H_2O)_6SnCl_6$.

Compound	T_{1Q} (μs)	τ_f (10^{-10} s)	J (10^{-2} cm^{-1})	Θ (K)	Θ_{obs} (K)[a]
$Mn(H_2O)_6SnCl_6$	196 ± 7	1.1	0.84	0.28	0.11–0.12[b]
$Co(H_2O)_6SnCl_6$	510 ± 30	0.97	1.6	0.22	0.15–0.19[c]

[a] Θ_{obs} is the absolute value of the paramagnetic Curie temperature determined in the isomorphous $Mn(H_2O)_6SiF_6$ and $Co(H_2O)_6SiF_6$ crystals.
[b] $Mn(H_2O)_6SiF_6$ [16].
[c] $Co(H_2O)_6SiF_6$ [16].

Table 2. Exchange parameter J values between the nearest neighbours, the lengths of the a- and c-axes of the unit cell [4] and electronegativities [22] for M(II)$(H_2O)_6SnCl_6$.

Compound	J (10^{-2} cm^{-1})	a (Å)	c (Å)	Electronegativity
$Mn(H_2O)_6SnCl_6$	0.84	9.87	10.25	1.5
$Co(H_2O)_6SnCl_6$	1.6	10.69	10.91	1.8
$Ni(H_2O)_6SnCl_6$	1.3	10.60	10.74	1.8

3.2. $Co(H_2O)_6SnCl_6$

Figure 2 shows that T_{1Q} observed in Co salt below room temperature decreased gradually on cooling and at temperatures below 40 K it became constant as in the Mn salt. This temperature dependence seems to be explained by the fact that τ_c is dominated by T_{1e} below room temperature and by τ_f at lower temperatures. Using the assumption that the Orbach process is most effective in T_{1e}, the best-fit calculation leads to the energy difference $\Delta = 550$ K (350 cm^{-1}) between the ground and the first-excited states of Co^{2+}, with this value being comparable to reported values in several compounds [10, 17–20]. According to [11], the parameter ζ in (6) is estimated to be $10^4\Delta^3$ in K units for the rare-earth group. Using this value, T_{1e}^{-1} is calculated to be 1.5×10^8 s^{-1} for 50 K, 3.7×10^{10} s^{-1} for 100 K, and 1.5×10^{12} s^{-1} for 300 K, which are very reasonable values compared with the τ_f value given below.

From the temperature-independent part of T_{1Q}, we estimated τ_f using (4) and (5). By substituting $\mu_{eff} = 4.61\mu_B$ observed for Co^{2+} in $CoCl_2 \cdot 6H_2O$ [12], and $\sum \Lambda_l = 1.57 \times 10^{44}$ cm^{-6} calculated with lattice parameters in table 2 [4] and assuming chlorine positions in the equation, we obtained $\tau_f = 0.97 \times 10^{-10}$ s. The values of J and Θ obtained from τ_f using (7), (9) and (10) are listed in table 1 along with Θ_{obs} determined from the adiabatic magnetization curves in isomorphous complex $Co(H_2O)_6SiF_6$ [16].

4. Discussion and conclusion

The J value decreases in the order of Co, Ni and Mn, as does the unit-cell volume. Since the calculation of the J value includes some approximations and/or hypotheses, it is difficult to discuss the differences in the J values between the Co and Ni salts. However, the J value in Mn salt is certainly smaller than the values in the other two salts. Hence it is concluded that the exchange interaction between the paramagnetic ions in Mn salt is weaker than that in the others and the J value has no correlation with the lattice size in the present system. This suggests that the exchange interactions in the three salts are made indirectly through some chemical bonds in such a path, M(II)–OH···Cl–Sn–Cl···HO–M(II), rather than directly. This path has two M(II)–O bonds and two O–H···Cl hydrogen bonds. The order of J values in the three compounds seems to be explained by differences in these bond characters.

The frequencies of M(II)-O stretching and M(II)–OH_2 wagging vibrations are reported to be 405 and 645 cm^{-1}, respectively in $Ni(H_2O)_6SiF_6$, while those in $Mn(H_2O)_6SiF_6$ are 395 and 560 cm^{-1}, respectively [21]. If the Ni–O bond in the present system is stronger than the Mn–O bond, Ni salt can have a larger J than Mn salt. Electronegativities of Mn, Co and Ni are listed in table 2 [22]. Since Co and Ni are more electronegative than Mn, the O–H···Cl hydrogen bonds in Co and Ni salts are stronger than those in Mn salt, leading to J values in the former being larger than those in the latter. Therefore it is concluded that the direct exchange interactions between the paramagentic ions have a minor effect compared with the indirect interactions in $M(II)(H_2O)_6SnCl_6$ (M(II) = Mn, Co and Ni), and the small J value in Mn salt can be explained by a relatively weak Mn–O bond and a small Mn electronegativity making the O–H···Cl bonds weak.

References

[1] Horiuchi K, Asaji T and Ikeda R 1994 *Phys. Rev.* B **50** 6169
[2] Horiuchi K 1994 *Phys. Status Solidi* b **186** 519
[3] Miyoshi H, Horiuchi K, Sakagami N, Okamoto K and Ikeda R 1998 *Z. Naturforsch.* a **53** 603
[4] US Dept of Commerce, NBS, and the Joint Committee on Powder Diffraction Standards, USA 1973 *Crystal Data Determinative Tables* vol 2, 3rd edn Inorganic Compounds
[5] Pauling L 1930 *Z. Kristallogr.* **72** 482
[6] Sakihara A 1999 *Master Thesis* University of the Ryukyus
[7] Horiuchi K, Sasane A, Mori Y, Asaji T and Nakamura D 1986 *Bull. Chem. Soc. Japan* **59** 2639
[8] Horiuchi K 1994 *Z. Naturforsch.* a **49** 286
[9] Mizuno M, Asaji T, Nakamura D and Horiuchi K 1990 *Z. Naturforsch.* a **45** 527
[10] Birkeland A and Svare I 1978 *Phys. Scr.* **18** 154
[11] Abragam A and Bleany B 1970 *Electron Paramagnetic Resonance of Transition Ions* (Oxford: Clarendon)
[12] Koenig E 1966 *Landolt–Boernstein New Series Group II: Atomic and Molecular Physics* vol 2, ed K H Hellwege and A M Hellwege (Berlin: Springer) p 69
[13] Kubo R and Tomita K 1954 *J. Phys. Soc. Japan* **9** 888
[14] Moriya T 1956 *Prog. Theor. Phys. (Kyoto)* **16** 23
Moriya T 1956 *Prog. Theor. Phys. (Kyoto)* **16** 641
[15] Stanley H E 1971 *Introduction to Phase Transitions and Critical Phenomena* (Oxford: Clarendon)
[16] Ohtsubo A 1965 *J. Phys. Soc. Japan* **20** 82
[17] Zverev G M and Petelina N G 1962 *Sov. Phys.–JETP* **15** 820
[18] Pryce M H L 1965 *Proc. R. Soc.* A **283** 433
[19] Rager H 1984 *Z. Naturforsch.* a **39** 111
[20] Mizuno M, Asaji T, Tachikawa A and Nakamura D 1991 *Z. Naturforsch.* a **46** 1103
[21] Nakagawa I and Shimanouchi T 1964 *Spectrochim. Acta* **20** 429
[22] Pauling L 1960 *The Nature of the Chemical Bond* 3rd edn (Ithaca, NY: Cornell University Press)

ELSEVIER

Journal of Molecular Structure 608 (2002) 63–69

Journal of
MOLECULAR
STRUCTURE

www.elsevier.com/locate/molstruc

Thermochromism in nickel(II) complexes: thermal, solid state ^{1}H NMR and single crystal X-ray analysis of bis-(*N*,*N*-dimethyl-1,2-ethanediamine) nickel(II) perchlorate

Subratanath Koner[a,b,*], Masaru Tsutake[a], Isoroku Nagasawa[a], Ryuichi Ikeda[a], Pratap K. Saha[b], Alok K. Mukherjee[c], Surajit Banerjee[c]

[a]*Department of Chemistry, University of Tsukuba, Tsukuba, Ibaraki 305-8573, Japan*
[b]*Department of Chemistry, Jadavpur University, Jadavpur, Calcutta 700 032, India*
[c]*Department of Physics, Jadavpur University, Jadavpur, Calcutta 700 032, India*

Received 31 July 2001; revised 24 October 2001; accepted 24 October 2001

Abstract

The complex bis-(*N*,*N*-dimethyl-1,2-ethanediamine) nickel(II) perchlorate undergoes a first-order thermochromic phase transition at ca. 476 K, changing its color from orange to red. The room temperature X-ray crystal structure determination showed that the nickel ion possesses a square-planar geometry with two five membered chelate rings, in the $\delta\lambda$ conformation, forming the NiN_4 chromophore. The broad-line ^{1}H NMR indicates the onset of a dynamic disorder of diamine chelate rings at the phase transition temperature region, while T_1 measurement of ^{1}H affords the activation energy of the puckering metal chelate rings to be 26 kJ mol^{-1}. The electronic spectrum revealed that a weakening of ligand field around the nickel is associated with the phase transition.

Keywords: Thermochromism; Nickel(II) complex; Solid state ^{1}H NMR; Crystal structure

1. Introduction

Thermochromic materials, i.e. the materials which change their color with change of temperature, are one of the interesting classes of materials that bear the promise for application [1–4]. They may be purely organic [5,6] or inorganic [7,8], organometallic [9,10] or metal complexes [1,11–16]. Several applications have been envisioned to use the thermochromic materials for the fabrication of special devices [1–4,17]. Amongst these materials a series of metal complexes containing diamine based ligand have been studied by using several techniques, for example, X-ray single crystal, solid state NMR, IR, EPR and calorimetric measurements, etc. in the last few decades [11–16,18–21]. These complexes showed abrupt color change on heating in the solid state. We and the others have proposed on the basis of X-ray single crystal analysis and ^{1}H NMR second moment (M_2) measurements that the sudden change of color which occurs on heating is due to a weakening of the ligand field strength resulting from onset of dynamic disorder of chelate rings [19,22–24]. In some cases different mechanisms for color change have been proposed for the same species of these

* Corresponding author. Address: Department of Chemistry, Jadavpur University, Jadavpur, Calcutta 700 032, India. Fax: +91-33473-1484.
E-mail address: skoner55@hotmail.com (S. Koner).

0022-2860/02/$ - see front matter
PII: S0022-2860(01)00930-9

types of thermochromic complexes [13,24–26]. For example, Fukuda et al. [13] have claimed that thermochromism of the $[Cu(daco)_2](NO_3)_2$ (daco = 1,4-diazacyclooctane) complex has a large part of its origin in the thermal motion of anion/ligand hydrogen bond system. This motion actually causing the weakening of ligand field strength and hence the color change is observed. Conversely, we have proposed on the basis of solid state ^{1}H NMR study that weakening of ligand field is occurring due to the dynamic conformational interconversion of the daco ligand [24]. Latter heat capacity measurements of this complex showed that the mechanism proposed by us is appeared to be operative in $[Cu(daco)_2](NO_3)_2$ case [25]. Therefore, further studies in this area are in demand to unravel the mechanism of the color change of these types of thermochromic complexes. Moreover, it is well known that the measurement of second moment (M_2) ^{1}H NMR absorption and spin lattice relaxation times (T_1) of ^{1}H are useful to elucidate the mechanism of different types of molecular motion in the crystalline state [27,28]. These techniques have been successfully employed in the case of thermochromic materials recently [14,24]. In an earlier communication we have reported the thermochromism of several nickel diamine complexes containing *N,N*-dimethyl-1,2-ethanediamine ligand [29]. Almost all those complexes showed color change due to the *cis–trans* isomerization except for the present one. This actually necessitates to study the $[Ni(dmen)_2](ClO_4)_2$ complex in details to understand the mechanism of the color change in solid state on heating of this complex. In this paper we report the studies on thermal, solid state ^{1}H NMR and single crystal X-ray analysis in detail of the $[Ni(dmen)_2](ClO_4)_2$ (dmen = *N,N*-dimethyl-1,2-ethanediamine) complex in the following sections.

2. Experimental

2.1. Preparation of the complex

The complex was prepared by mixing the methanolic solution of $Ni(ClO_4)_2{\cdot}6H_2O$ and the *N,N*-dimethyl-1,2-ethanediamine in required stoichiometry. The orange colored crystalline product thus obtained was filtered and washed with little methanol and dried in a desiccator. This complex $[Ni(dmen)_2](ClO_4)_2$ is known to react with CO_2 present in the air to produce CO_3^- bridged complexes [30]. Therefore, an inert (Argon) atmosphere was used to grow single crystals of the title complex from methanol.

2.2. Physical measurements

Differential scanning calorimetry (DSC) measurement was carried out using a Seiko Instruments SSC 5200 calorimeter between room temperature and ca. 510 K with a heating rate of ca. 5 K min^{-1}. Electronic spectra in nujol mull were measured on a Hitachi U 3400 spectrophotometer. The effective magnetic moment (μ_{eff}) of the complexes was measured as reported earlier [29].

2.3. Solid state NMR measurements

The ^{1}H NMR absorptions were measured by a Varian WL-15 wide line NMR spectrometer at a Larmor frequency 14.5 MHz equipped with a temperature controller. A copper-constantan thermocouple was used to measure the sample temperature within an accuracy of ±2 K. The M_2 also measured by solid echo method [31] with the help a Bruker SXP100 Pulse NMR spectrometer at a Larmor frequency 40.8 MHz. The echo amplitude $F(t)$ after time t from the top of the echo can be written as:

$$F(t) = 1 - M_2t^2/2! + M_4t^4/4! \quad (1)$$

where M_4 is the fourth moment of ^{1}H NMR absorption. To obtain M_2, this equation was used for least squares fitting of the echo amplitude versus t plot. In this measurements a $90°_x–\tau–90°_y$ pulse sequence was used [31].

The spin–lattice relaxation times (T_1) of ^{1}H of this complex were measured on a home made NMR instrument operated at a Larmor frequency 40.8 MHz equipped with a temperature controller within an accuracy of ±1 K.

2.4. Crystal data

$C_8H_{24}N_4O_8Cl_2Ni$, $M = 433.92$, monoclinic, $a = 6.049(1)$, $b = 16.242(3)$, $c = 8.705(2)$ Å, $\beta = 87.22(1)°$ $V = 854.2(3)$ Å^3 (by least squares refinement of diffractometer setting angles for 25 automatically

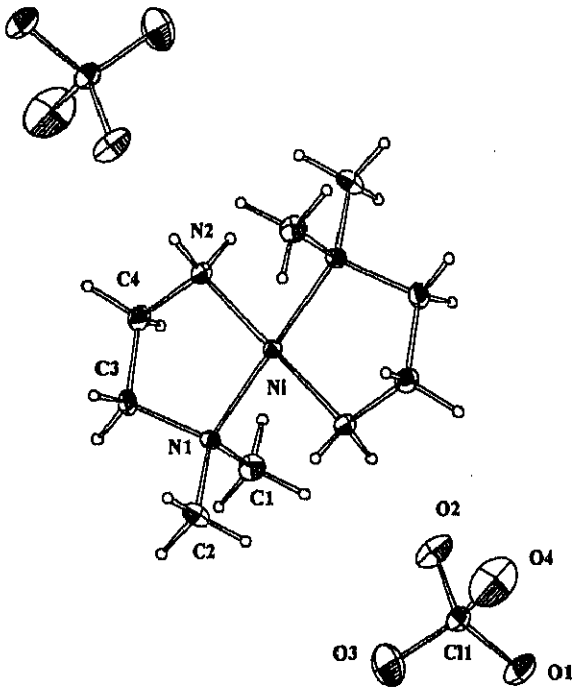

Fig. 1. ORTEP plot with atom numbering scheme of $[Ni(dmen)_2](ClO_4)_2$.

centered reflections, $\lambda = 0.71073$), space group $P2_1/c$, $Z = 2$, $D_c = 1.687\ g\ cm^{-3}$, $F(000) = 452$, $\mu(Mo\ K_\alpha) = 1.492\ mm^{-1}$, orange crystals, dimensions $0.35 \times 0.25 \times 0.20\ mm^3$, $T = 293$ K.

2.5. Structure determination

Intensities of 5296 reflections ($3.6 < \theta < 30.5$) were collected using an Enraf Nonius CAD 4 diffractometer in $\omega - 2\theta$ scan mode with graphite monochromated Mo K_α radiation. Data were corrected for Lorentz, polarization and an empirical absorption based on ψ scan ($T_{min}/T_{max} = 0.645/0.743$) was obtained. Out of 2481 unique reflections ($R_{int} = 0.1396$) 1861 reflections with $I > 2\sigma(I)$ were considered observed. The structure was solved by heavy atom method and refined by full-matrix least-squares using SHELXL 97 [32,33]. Final refinement with all non-hydrogen atoms anisotropic and hydrogen atoms (placed at geometrical positions) held fixed with isotropic temperature factors converged to $R_1 = 0.0569$, $wR_2 = 0.1154$ for 1861 observed reflections ($R_1 = 0.0903$, $wR_2 = 0.1290$ for all reflections). The weighting scheme $w = 1/[\sigma^2(F_0)^2 + (0.0779P)^2 + 0.04P]$ where $P = (F_0^2 + 2F_c^2)/3$, gave satisfactory agreement analyses.

3. Results and discussion

3.1. Thermal analysis and thermochromism

The DSC measurement was carried out between room temperature and ca. 510 K. The complex undergoes an endothermic phase transition at ca. 476 ± 2 K. The transition is associated with a visual color change from orange to red. The sample does not show any exothermic peak on cooling in DSC measurement but on keeping in dry atmosphere for several days eventually it reverts to the original form. This shows that the transition is actually a reversible one with very long hysteresis. It has been observed that the rate of reversion increases with increase in % of relative humidity of the atmosphere, which means H_2O molecules present in the atmosphere accelerates the reversion. It has been observed in an earlier study that H_2O molecule present in the atmosphere acts as heterogeneous catalyst in the reversion [34]. Therefore, it can be concluded that in this case also H_2O molecules act as heterogeneous catalyst in the reversion. The enthalpy change for this thermochromic phase transition (ΔH) is calculated to be $5.7 \pm 1\ kJ\ mol^{-1}$. As the red species is stable for several days after the transition we were able to measure the electronic spectra and magnetic moment of both the species at room temperature. The magnetic moment measurement showed both the species are diamagnetic. The λ_{max} in the electronic spectra, which can be assigned for the d–d transition for a square planar nickel(II) complex, shifted from 455 to 478 nm on phase transition. This red shift in d–d transition band in electronic spectra clearly shows a weakening of ligand field around the Ni ion is associated with the phase transition [16]. Nevertheless complex retains its square planar geometry (hence diamagnetism) after the phase transition.

3.2. Description of the structure

An ORTEP [35] view of the complex with an atom numbering scheme is shown in Fig. 1. With the Ni

Table 1
Selected bond distances (Å) and angles (°) with e.s.d.s in parentheses for $[Ni(dmen)_2](ClO_4)_2$

Ni–N1	1.948(2)	N2–C4	1.478(3)
Ni–N2	1.923(2)	Cl–O1	1.383(4)
N1–C3	1.498(3)	C3–C4	1.502(4)
N1–Ni–N2	86.20(7)	Ni–N1–C3	105.86(1)
N1–C3–C4	108.60(2)	Ni–N2–C4	112.72(1)

atom lying at the center of inversion the crystallographic asymmetric unit of the title complex consists of half of $[Ni(dmen)_2]$ cation and one ClO_4 anion. The geometry around the nickel center is distorted square planar with an in-plane distortion introduced by the ligand bite angle N1–Ni–N2 = 86.2°(1). The two five-membered chelate rings are in the $\delta\lambda$ conformations. Out of the oxygen atoms [O(2)] of the perchlorate ion is hydrogen bonded to one of amino nitrogen atoms [N(2)] of the cation: N2···O2···3.072(4) Å; N2–HN2–O2 173.4 Å. The Ni–N, C–C and C–N distances are comparable to those observed in the similar systems [36–40]. The selected bond distances and angles of this complex are given in Table 1. The single crystallinity of the complex is observed to loose on phase transition. Therefore, we could not collect the intensity data of the red variety of the complex.

3.3. Solid state ^1H NMR measurements

The temperature dependence of the second moment (M_2) of ^1H NMR absorption of the title complex measured from 297 to 489 K is shown in Fig. 2. The

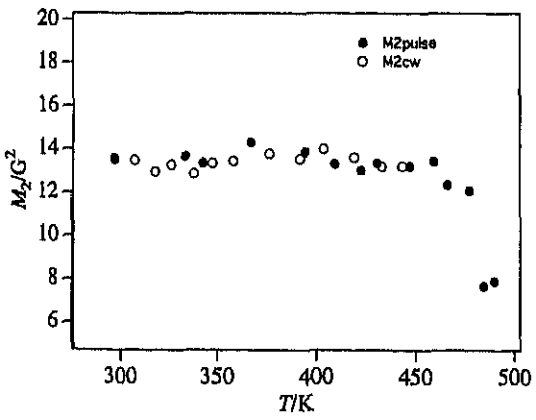

Fig. 2. The plot of M_2 (second moment) versus temperature for $[Ni(dmen)_2](ClO_4)_2$.

M_2values were measured by two different techniques viz. solid echo and continuous wave (cw) method. The two sets of data match each other very closely. The M_2 values remain almost constant up to ca. 460 K then suddenly dropped from 13 ± 1 G^2 to 7.7 ± 0.5 G^2 around 475 K, where the complex is observed to undergo thermochromic phase transition (vide supra). The abrupt drop in M_2values around 475 K of the complex with the thermochromic phase transition convincingly demonstrates that some kind of molecular motion is associated with the phase transition. It is also noteworthy that around this temperature the complex changes its color from orange to red. The similar type of behavior is also observed in some other thermochromic complexes [12,14,24]. The most probable motion may be the conformational change of the metal chelate rings. As it is well known that five member rings can have either of the two ring conformations δ or λ [41], the ligand molecules while coordinated to the metal in this case can possess one of the following conformations, $\delta\delta$, $\delta\lambda$ or $\lambda\lambda$. The single crystal X-ray analysis showed the conformation of the $[Ni(dmen)_2]^{2+}$ moiety is $\delta\lambda$. For molecular solids with known crystal structure, experimental values of M_2 may be compared with values obtained using the theory of Van Vleck [42] for rigid structure and for various possible motional model in order to identify the molecular motion at before and after transition temperature ranges. The M_2 value calculations in this study for a powder sample was performed using Van Vleck equations: [42,43]

$$M_2(\text{rigid})_{jk} = (9/10)h^2\gamma_H^2 N^{-1}\sum \mathrm{r}_{jk}^{-6} \quad (2)$$

$$M_2(\text{motional})_{jk} = M_2(\text{rigid})_{jk}\{(3\cos^2\gamma_{jk} - 1)/2\}^2 \quad (3)$$

for interacting protons j and k, where γ_H, N, r_{jk} and γ_{jk} denote the proton gyromagnetic ratio, the number of the interacting protons considered for calculation, the distance between the protons and the angle between the rotation axis and interproton vector r_{jk}, respectively. In the post phase temperature range, the motion is approximated as the jumps between two equivalent orientations of chelate rings according to the assumption (b) (vide infra).

In this case the values of rigid and motional lattices are calculated with the following assumptions: (a) before the phase transition the only allowed motion

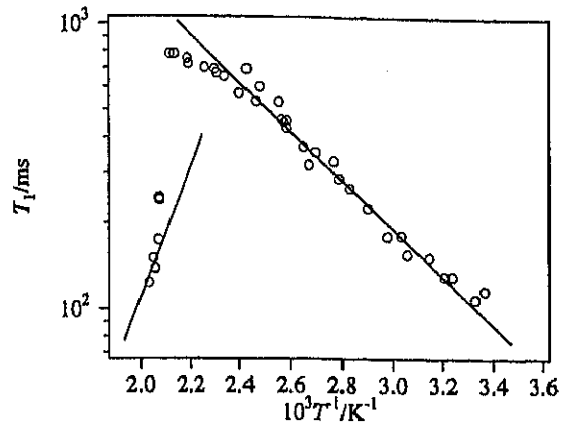

Fig. 3. The temperature dependence of the ^{1}H spin–lattice relaxation time (T_1) for $[Ni(dmen)_2](ClO_4)_2$. The solid line was the best fitted line in the manner described in the text.

is the reorientation of CH_3 groups about the C–C bonds and rest of complex cation is considered to be rigid; (b) in motional lattices the ligand is undergoing dynamic two fold rotation about the axis goes through the mid point of C–C bond of ethylene substructure of the diamine and the central metal ion to give rise the $\delta \leftrightarrow \lambda$ interconversion of chelate rings. Since the position of the protons could not be well resolved by X-ray analysis, their coordinates are not reliable for the calculation. Therefore, the proton coordinates were simulated by using the CHEM 3D program [44] feeding the heavy atom coordinates to the said program and allowing the protons to take the standard C–H and N–H distances and the standard angles. The proton coordinates of the motional lattices of the complex were also simulated by using CHEM 3D program. The theoretical values of the rigid and motional lattices calculated by this method were 12.6 and 7.6 G^2, respectively, which were in good agreement with the experimental values for rigid and motional lattices of 13.1 and 7.7 G^2, respectively. The small difference between the theoretical and experimental results can be attributable due to the intermolecular contributions to M_2 values that were not included in the calculation. However, the reduction factor (R_{cal}) given by the equation: [45]

$$R_{cal} = M_2(\text{motional})_{jk}/M_2(\text{rigid})_{jk} \quad (4)$$

is roughly calculated to be 0.60, which is very close to the experimental value ($R_{exp} = 0.59$). This shows the adequacy of our assumption for the calculation of M_2 values. The temperature dependence of the proton spin–lattice relaxation times (T_1) for complex are displayed on a logarithmic scale against inverse temperature in Fig. 3. The observed temperature dependence of T_1 is explicable by the averaging of magnetic dipolar interactions due to molecular motions of protons can be expressed by the BPP (after Bloembergen, Purcell and Pound) equation [46,47] given by:

$$1/T_1 = C_M[\tau/(1 + \omega^2\tau^2) + 4\tau/(1 + 4\omega^2\tau^2)] \quad (5)$$

and the Arrhenius equation written as:

$$\tau = \tau_0 \exp(E_a/RT) \quad (6)$$

here C_M, τ, ω and E_a are the motional constant, the correlation time of the motion, the Larmor frequency and the activation energy, respectively. Since we could observe no T_1 minimum in this temperature range, we apply Eqs. (5) and (6) for the slow motion limit $\omega\tau \gg 1$ below the transition temperature, while for the rapid limit, $\omega\tau \ll 1$, above the transition temperature.

So we have $\log T_1 = -E_a/RT + C$ for above the transition temperature region and $\log T_1 = E_a/RT + C$ for below the transition temperature region, we can get E_a value in these regions from the slope of $\log T_1$ versus $1/T$ plot (Fig. 3). For the complex $[Ni(dmen)_2](ClO_4)_2$ E_a in the low temperature region is calculated to be 7.2 ± 0.4 kJ mol^{-1} and in the high temperature region E_a is 26 ± 3 kJ mol^{-1}. These two values are for the activation energy of CH_3 rotation and C–C bond puckering, respectively. So far our knowledge goes no studies have been reported to date regarding the evaluation of the activation energy for chelate ring puckering of this type of complexes in the condensed phase. But it is noteworthy that the energy barrier between two or several possible conformations of the five membered carbon ring systems has been determined by several methods, these values are found to be very close to the activation energy obtained in the present study for the puckering of metal chelate rings [48–50].

4. Conclusions

It is evident from the above-mentioned studies that

the thermochromic phase transition at ca 476 K of the complex $[Ni(dmen)_2](ClO_4)_2$ is associated with the conformational inter-conversion of the metal chelate rings and the said molecular motion is dynamic in nature. The room temperature crystal structure analysis of the complex shows that one of the oxygen atoms of the ClO_4 ion is H-bonded with the amine hydrogen of diamine ligand. Therefore, it can be postulated that as the temperature increases the reorientational motion of ClO_4^- ion also increases and at around phase transition temperature region the H-bond network in the complex completely breaks down and the conformation of the chelate rings become free for interconversion. This molecular motion is causing hindrance for optimal overlap between the donor atom orbital of the ligand and metal orbitals. As a result, a weakening of ligand field around the central metal cation is occurring on phase transition. Hence, we observe the color change.

5. Supplementary materials

Tables of fractional coordinates and anisotropic thermal parameters, complete list of bond distances and angles, calculated and observed structure factors have been deposited with CCDC. The CCDC deposition number for this material is 153395.

References

[1] Y. Fukuda, K. Sone, Inorganic Thermochromism, Springer, New York, 1987.
[2] G. Schopf, G. Kossmehl, Adv. Polym. Sci. 127 (1997) 1.
[3] S.M. Burkinshaw, J. Griffiths, A.D. Towns, J. Mater. Chem. (1998) 2677.
[4] A. Seeboth, J. Kriwanek, R. Vetter, J. Mater. Chem. (1999) 2277.
[5] N. Dicésare, M. Belletête, M. Leclere, G. Durocher, Chem. Phys. Lett. 291 (1998) 487.
[6] L.S. Li, S.I. Strupp, Macromolecules 30 (1997) 5733.
[7] Z. Halmos, W.W. Wendtlandt, Thermochim. Acta 7 (1973) 113.
[8] A.F. Well, Structural Inorganic Chemistry, Third ed, Oxford University Press, New York, 1967 p. 267.
[9] A.J. Ashe III, F.J. Drone, Organometallics 3 (1984) 495.
[10] A.J. Ashe III, W. Butler, T.R. Diephouse, J. Am. Chem. Soc. 103 (1981) 207.
[11] D.R. Bloomquist, R.D. Willett, Coord. Chem. Rev. 47 (1982) 125.
[12] L. Menabue, G.C. Pellacani, L.P. Battaglia, A.B. Corradi, F. Sandrolini, A. Motori, R.J. Pylkki, R.D. Willett, J. Chem. Soc., Dalton Trans. (1984) 2187.
[13] N. Hoshino, Y. Fukuda, K. Sone, K. Tanaka, F. Marumo, Bull. Chem. Soc. Jpn 62 (1989) 1822.
[14] S. Koner, A. Ghosh, N. Ray Chaudhuri, A.K. Mukherjee, M. Mukherjee, R. Ikeda, Polyhedron 12 (1993) 1311.
[15] S. Koner, A. Ghosh, C. Pariya, D. Das, H. Kikuchi, K. Okamoto, R. Ikeda, J. Mol. Struct. 345 (1995) 265.
[16] L. Febbrizzi, M. Micheloni, P. Paoletti, Inorg. Chem. 13 (1974) 3019.
[17] M. Suzuki, M. Kimura, K. Hanabusa, H. Shirai, Chem. Commun. (1997) 2061.
[18] D.R. Bloomquist, M.R. Pressprich, R.D. Willett, J. Am. Chem. Soc. 110 (1988) 1563.
[19] I. Grenthe, P. Paoletti, M. Sandstrom, S. Glikberg, Inorg. Chem. 18 (1979) 2687.
[20] A. Nishimori, E.A. Schmitt, D.N. Hendrickson, M. Sorai, J. Phys. Chem. Solids 55 (1994) 99.
[21] A. Nishimori, M. Sorai, E.A. Schmitt, D.N. Hendrickson, J. Coord. Chem. 37 (1996) 327.
[22] M.M. Andino, J.D. Curet, M.M. Muir, Acta Crystallogr. B 32 (1976) 3185.
[23] R.J. Pylkki, R.D. Willett, H.W. Dodgen, Inorg. Chem. 23 (1984) 594.
[24] S. Koner, H. Ohki, H. Kikuchi, R. Ikeda, Ber. Bunsen-Ges. Phys. Chem. 98 (1994) 734.
[25] H. Hara, M. Sorai, J. Phys. Chem. Solids 56 (1995) 223.
[26] A.B.P. Lever, E. Mantovani, J.C. Donini, Inorg. Chem. 10 (1971) 2424.
[27] C.P. Slichter, Principles of Magnetic Resonance, Springer, New York, 1990.
[28] A. Carrington, A.D. McLachlan, Introduction to Magnetic Resonance, Harper and Row, New York, 1967.
[29] S. Koner, A. Ghosh, N. Ray Chaudhuri, Bull. Chem. Soc., Jpn 63 (1990) 2387.
[30] T. Tanase, S. Nitta, S. Yoshikawa, K. Kobayashi, T. Sakurai, S. Yano, Inorg. Chem. 31 (1992) 1058.
[31] G. Powels, J.H. Stranger, Proc. Phys. Soc. London 82 (1963) 6.
[32] G.M. Sheldrick, SHELXS 97, Program for Crystal Structure Determination, University of Göttingen, 1997.
[33] G.M. Sheldrick, SHELX 76, System of Crystallographic Computing Programs, University of Cambridge, 1976.
[34] G. De, P.K. Biswas, N. Ray Chaudhuri, J. Chem. Soc., Dalton Trans. (1984) 2591.
[35] C.K. Johnson, ORTEP, Report ORNL-5138, Oak Ridge National Laboratory, Oak Ridge, TN, 1976.
[36] A.K. Mukherjee, M. Mukherjee, S. Ray, A. Ghosh, N. Ray Chaudhuri, J. Chem. Soc., Dalton Trans. (1990) 2347.
[37] D.J. Royer, V.H. Schievelbein, A.R. Kalyanaraman, J.A. Bertrand, Inorg. Chim. Acta 6 (1972) 307.
[38] M.S. Hussain, Inorg. Chim. Acta 69 (1983) 227.
[39] M.S. Hussain, J. Chem. Soc., Dalton Trans. (1982) 2545.
[40] A.K. Mukherjee, S. Koner, A. Ghosh, N. Ray Chaudhuri, A.J. Welch, J. Chem. Soc., Dalton Trans. (1994) 2367.
[41] Y. Saito, Inorganic Molecular Dissymmetry, Springer, New York, 1979.
[42] J.H. Van Vleck, Phys. Rev. 74 (1948) 1168.

[43] H.S. Gutowsky, G.E. Pake, J. Chem. Phys. 18 (1950) 162.
[44] CHEM 3D, A Computer Program for Molecular Modeling, Cambridge Scientific Computing, Cambridge, USA, 1986.
[45] J.C. Crowly, H.W. Dodgen, R.D. Willett, J. Phys. Chem. 86 (1982) 4046.
[46] N. Bloembergen, E.M. Purcell, R.V. Pound, Phys. Rev. 73 (1948) 679.
[47] R. Kubo, K. Tomita, J. Phys. Soc. Jpn 9 (1954) 888.
[48] J. March, Advanced Organic Chemistry, Fourth ed, Wiley, New York, 1992 pp. 142–149.
[49] D. Nasipuri, Stereochemistry of Organic Compounds, Second ed, Wiley Eastern Ltd, Calcutta, 1995 pp. 273–286.
[50] L. Luz, I. Zimmerman, J. Am. Chem. Soc. 104 (1982) 5307.

INSTITUTE OF PHYSICS PUBLISHING JOURNAL OF PHYSICS: CONDENSED MATTER

J. Phys.: Condens. Matter 14 (2002) 6815–6822 PII: S0953-8984(02)34056-6

Cationic motions studied by ^{1}H and ^{2}H nuclear magnetic resonance, x-ray powder diffraction and thermal measurements in solid $CH_3(CH_2)_2NH_3X$, $CH_3(CH_2)_2ND_3X$ and $CD_3(CH_2)_2NH_3X$ (X = F, Cl, Br and I)

Shin'ichi Ishimaru[1], Tae Ishitomi and Ryuichi Ikeda

Department of Chemistry, University of Tsukuba, Tsukuba 305-8571, Japan

E-mail: ishimaru@chem.tsukuba.ac.jp

Received 20 February 2002
Published 28 June 2002
Online at stacks.iop.org/JPhysCM/14/6815

Abstract

Dynamic behaviour of cations in propylammonium fluoride, chloride, bromide and iodide has been investigated by x-ray powder diffraction, thermal and ^{1}H and ^{2}H nuclear magnetic resonance measurements. The mobilities of the cations at room temperature were shown to be in the order iodide > bromide > chloride ≫ fluoride corresponding to the order of anion size. It was found that propylammonium fluoride has no rotator phase. In the highest-temperature phase in chloride, a highly disordered cationic state was obtained and the fluctuation angle of the cationic axis was estimated to be about 30°.

1. Introduction

The highest-temperature solid phases in *n*-alkylammonium chloride, bromide and iodide with alkyl chains longer than C_3 form a tetragonal crystal, $P4/nmm$, with a bilayer lamellar-type structure (α'-form) [1] as shown in figure 1. In propylammonium halides, only chloride was reported to take this structure. The highest-temperature phase in propylammonium bromide and iodide and also the room temperature phase of the chloride were shown to have the structure (α-form) [2, 3] shown in figure 1, which has the same space group as the α'-form with about a halved *c*-length. In both crystals, the alkylammonium cations are expected to be dynamically disordered about their long axes: the so-called rotator phase.

Cationic motions in α- and α'-phases in propylammonium chloride and bromide have been studied by ^{1}H nuclear magnetic resonance (NMR) and electrical conductivity [4] measurement, and the axial rotation and self-diffusion of the cations in the rotator phases have

[1] Author to whom any correspondence should be addressed.

0953-8984/02/276815+08$30.00

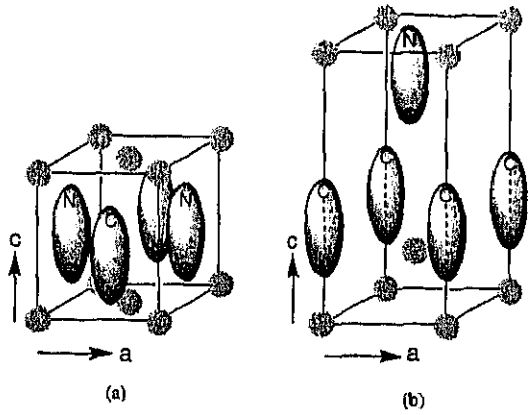

Figure 1. Schematic models of two tetragonal crystal structures in alkylammonium halides, (a) the α-form and (b) the α′-form. The two structures belong to the same space group, $P4/nmm$. Alkylammonium and halide ions occupy sites on fourfold axes.

been reported. There has, however, been no detailed discussion of the bromide because of the instability of the highest-temperature phase. For iodide and fluoride, no studies on the dynamics in crystals have been reported.

In this study, we investigated the detailed dynamics of propylammonium cations in these halides by means of differential thermal analysis (DTA), differential scanning calorimetry (DSC), x-ray powder diffraction and ^1H and ^2H NMR measurements, especially for the highest-temperature phases, and tried to clarify differences in dynamics of the crystals among these halides.

2. Experimental details

$CH_3(CH_2)_2NH_3X$ (X = F, Cl, Br and I, abbreviated to C_3X) and $CD_3(CH_2)_2NH_3X$ (X = Cl and Br, abbreviated to Cd_3X) were prepared by neutralizing propylamine and propylamine-d_3 (CDN, 99.4 at.%), respectively, with corresponding acid solutions of hydrogen halides. The specimens obtained, except for the fluoride, were recrystallized from ethanol. Prepared fluoride crystals were used for measurements without further purification. $CH_3(CH_2)_2ND_3X$ (X = Cl, Br and I, abbreviated to Nd_3X) were obtained by recrystallizing $CH_3(CH_2)_2NH_3X$ three times from heavy water (Isotec, 99.96 at.%).

DSC and DTA measurements were carried out with a Seiko DSC 120 calorimeter and a home-built apparatus, respectively. X-ray powder diffraction patterns were taken by a Philips X'Pert PW3040/00 diffractometer with Cu Kα radiation.

Second moments M_2 of the ^1H NMR line were obtained with a Bruker SXP-100 spectrometer and a Bruker MSL-300 system by applying the solid-echo method [5]. ^2H NMR spectra were measured by the MSL-300 system. The ^1H NMR T_1 was determined with the Bruker SXP-100 spectrometer by applying the inversion–recovery method. The experimental error in T_1 was estimated to be within 10%. The sample temperature was controlled by the N_2 gas flow method with an accuracy of 1 K.

3. Results and discussion

3.1. Thermal measurements and x-ray diffraction

Phase transition temperatures T_{tr} and enthalpy and entropy changes ($\Delta_{tr}H$, $\Delta_{tr}S$) obtained from DTA and DSC measurements are listed in table 1. We call the solid phases obtained I, II

Table 1. Phase transition temperatures T_{tr}, enthalpies $\Delta_{tr}H$ and entropies $\Delta_{tr}S$ obtained by DTA and DSC measurements. Melting is shown in parentheses.

	T_{tr} (K)			
	DTA	DSC	$\Delta_{tr}H$ (kJ mol^{-1})	$\Delta_{tr}S$ (J K^{-1} mol^{-1})
$C_3H_7NH_3F$	219.5 ± 0.5	—		
	225.0 ± 0.5	—		
		(402.8 ± 1.5)	(19.7 ± 1.2)	(48.8 ± 3.0)
$C_3H_7NH_3Cl$	186.7 ± 0.5	188[a]	1.15[a]	6.14[a]
	405.7 ± 0.5	408[a]	4.15[a]	10.22[a]
	(437.5 ± 0.5)	(439)[a]	(5.90)	(13.4)[a]
$C_3H_7NH_3Br$	161.5 ± 1.0	163 ± 1.0	1.69 ± 0.02	10.4 ± 0.1
	(456.7 ± 0.2)	(458.3 ± 1.0)	(10.1 ± 0.1)	(22.1 ± 0.5)
$C_3H_7NH_3I$	179.0 ± 5.0	188.3 ± 5.0	0.36 ± 0.05	1.9 ± 0.3
	244.5 ± 5.0	246.6 ± 2.0	6.17 ± 0.7	25.0 ± 3.0
		(461.0 ± 4.0)	(9.86 ± 1.3)	(21.0 ± 3.0)

and so on in the order of temperature decrease. T_{tr}-values obtained from DTA measurements on chloride and bromide agree with the DTA data reported by Fukada *et al* [4] within experimental errors. The fact that the $\Delta_{tr}S$ values at transitions from phase II to III observed in chloride and from phase II to I in chloride, bromide and iodide were of the same order as their melting entropies imply that phase I in these three compounds and phase II in chloride are highly disordered. On the other hand, the transition entropies at the solid–solid phase transitions in fluoride were small and hardly observed in DSC.

X-ray diffraction patterns obtained at room temperature for phase II of chloride and phase I of bromide and iodide could be reproduced by assuming the structure with space group $P4/nmm$ reported for these phases [1]. The pattern obtained for phase I of fluoride at room temperature could not be explained by this space group, suggesting that this phase in fluoride has a symmetry lower than tetragonal.

3.2. *Second-moment M_2 for the ^1H NMR line in C_3F and C_3I*

Motional states of propylammonium ions in C_3Cl and C_3Br had been studied by means of M_2-measurements [4]. To determine the motional states in C_3F and C_3I, we conducted ^1H NMR M_2-measurements. The temperature dependences of M_2 measured for fluoride and iodide are shown in figures 2 and 3, respectively. M_2 for fluoride decreased gradually from about 35 G^2 for phase III to about 25 G^2 for phase I. In iodide, steep decreases of M_2 from 16 G^2 for phase III to 7 G^2 for phase II and to 4 G^2 for phase I were observed.

To explain these data, we calculate M_2-values for various motional states of the cation by Van Vleck's method [6] and show the results in table 2. Inter-cationic contributions to M_2 were roughly estimated to be about 20% of the intra-cationic contribution [4] although they depend on the crystal structure. M_2-values for fluoride should be larger than these estimates because of contributions from ^{19}F nuclei with a large magnetic moment.

We can see from table 2 that no cationic motion other than the methyl rotation is activated in fluoride even at 350 K, indicating that fluoride has no rotator phase. In iodide, on the other hand, methyl and ammonium rotations are activated even at 100 K and the axial rotation of the cation as a whole was observed in phase I. Intermediate M_2-values observed in phase II can be understood on the basis of reorientation of the cation around its long axis in an asymmetric potential made by a lower symmetry of crystal field than C_4 where the averaging by this

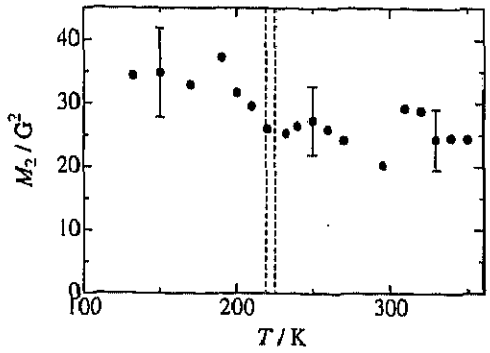

Figure 2. The temperature dependence of the second moment (M_2) of ^{1}H NMR lines observed for propylammonium fluoride. The vertical lines show transition temperatures obtained by DTA.

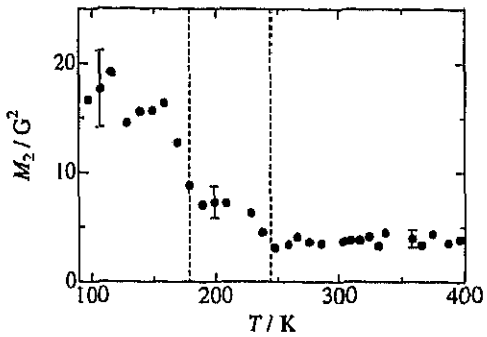

Figure 3. The temperature dependence of the second moment (M_2) of ^{1}H NMR lines observed for propylammonium iodide. Vertical lines show transition temperatures obtained by DTA.

Table 2. M_2-values calculated for possible motional states in a propylammonium cation. The values contain a rough estimate of inter-cationic contributions of 20% of the intra-cationic contributions (shown in the parentheses) assuming the all-trans-conformation.

Motional mode	Rigid	CH_3 rotation	(CH_3 + NH_3) rotation	(CH_3 + NH_3) rotation + chain rotation
M_2/G^2	30.7	24.8	16.8	5.0
	(25.6)	(20.7)	(14.0)	(4.2)

motion is imperfect. It can be concluded that phase I in iodide isomorphous with the room temperature phases in chloride and bromide is a rotator phase and phase II in iodide is also expected to be a rotator phase. M_2-values in the room temperature α-phase in chloride (phase II), bromide (phase I) [4] and iodide (phase I), isomorphous with each other, were of the order of chloride(5.1 G^2) < bromide(4.8 G^2) < iodide(3.8 G^2). This implies that the fluctuation amplitude of the cationic motion becomes large with the increase of the anion size.

3.3. ^{1}H NMR T_1 in C_3F and C_3I

We measured the ^{1}H T_1 to reveal cationic motions in detail. In the case where the relaxation is caused by the fluctuation of magnetic dipole–dipole interactions from molecular motions, the relaxation rate T_1^{-1} can be assumed to be given by the superposition of respective contributions

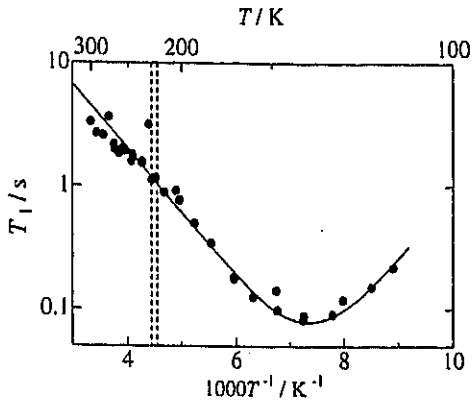

Figure 4. The temperature dependence of the ^1H NMR spin–lattice relaxation time (T_1) observed at 33.8 MHz in propylammonium fluoride. Vertical lines show transition temperatures obtained by DTA and the solid curve is the best-fitted curve calculated by applying equations (2) and (3) in the text.

Table 3. Motional constants C and activation energies E_a derived by curve fitting of the temperature dependences of T_1 observed in $CH_3(CH_2)_2NH_3F$ and $CH_3(CH_2)_2NH_3I$.

	C (10^9 s^{-2})	E_a (kJ mol^{-1})	Motional mode
$CH_3(CH_2)_2NH_3F$ $CH_3(CH_2)_2NH_3I$	1.9	10 ± 1	CH_3 rotation
Phases II and III	2.3	10 ± 1	CH_3 rotation
	1.6	10.5 ± 1	NH_3 rotation
	1.2	23 ± 2	Anisotropic chain rotation
Phase I	—	10 ± 1	Chain rotation

expressed as

$$T_{1total}^{-1} = \sum T_1^{-1} \tag{1}$$

where each T_1 is given by a BPP-type function [7]:

$$T_1^{-1} = C\left\{\frac{\tau}{1+\omega^2\tau^2} + \frac{4\tau}{1+4\omega^2\tau^2}\right\} \tag{2}$$

where C is the motional constant, ω is the ^1H Larmor frequency and τ is the correlation time of the motion obeying the Arrhenius equation:

$$\tau = \tau_0 \exp(E_a/RT). \tag{3}$$

Here τ_0 and E_a denote the correlation time at infinite temperature and the activation energy of the motion, respectively.

Temperature dependences of ^1H NMR T_1 for fluoride and iodide are shown in figures 4 and 5, respectively. A single T_1-minimum was observed in fluoride around 140 K. T_1 in fluoride could be fitted by a single BPP function (figure 3). A possible motion for this relaxation is the terminal methyl rotation relating to the analysis of M_2 given above. The best-fitted motional parameters are listed in table 3. A small deviation of the fitted curve from the experimental data in phase I is attributable to the influence of phase transitions.

In iodide, since marked influences of the phase transition from III to II on the ^1H relaxation could not observed, the experimental data were fitted by the superposition of three BPP

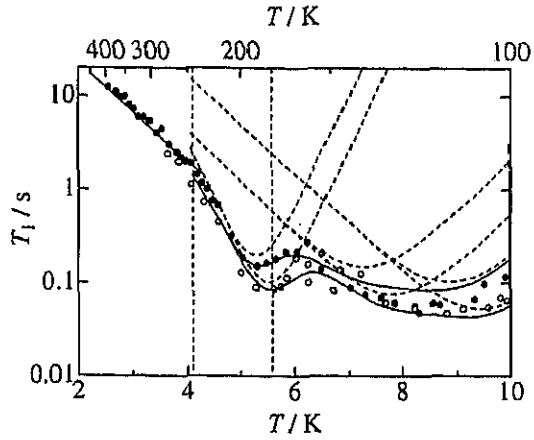

Figure 5. Temperature dependences of the ^{1}H NMR T_1 observed at 54.0 (●) and 27.7 MHz (○) in propylammonium iodide. Vertical lines show transition temperatures obtained by DTA. Solid curves are the best-fitted curves calculated by the superposition of the broken curves derived from equations (1)–(3) in the text.

curves. Three motional modes corresponding to these relaxations are attributed to methyl and ammonium rotations, and the anisotropic axial reorientation as a whole, as discussed in the M_2-analysis. The T_1-slope changed obviously at the transition point (II to I) and above that temperature the T_1-value can be considered to be governed mainly by the cationic axial rotation.

3.4. ^{2}H NMR spectra in Nd_3X (X = Cl, Br, I) and Cd_3X (X = Cl, Br)

The ^{2}H NMR linewidth is expected to be a sensitive probe for detecting slight changes in molecular motions. When a rotational motion takes place, the ^{2}H quadrupole coupling constant $\overline{\nu_Q}$ is reduced to [8]

$$\overline{\nu_Q} = \left|\frac{3\cos^2\theta - 1}{2}\right|\nu_Q \tag{4}$$

where θ is the angle between the principal axis of the electric field gradient tensor and the rotation axis.

All ^{2}H NMR spectra observed for ND_3^+ and CD_3 groups showed typical Pake patterns. Figures 6 and 7 show the temperature dependences of ν_Q estimated from spectra observed for the rotator phase for Nd_3Cl, Nd_3Br, Nd_3I and Cd_3Cl, Cd_3Br, respectively, by assuming the asymmetry parameter $\eta = 0$. The three Nd_3X gave almost the same ν_Q-values of 41 ± 2 kHz, almost independent of temperature in the α-phase. At 410 K (α'-phase) Nd_3Cl showed a much small ν_Q of about 13 kHz. In Cd_3X, chloride gave a constant ν_Q of 38 kHz in the α-phase, while, for bromide, it decreased gradually from 39 to 31 kHz with the temperature increase. The value for chloride decreased drastically at the transition to the α'-phase to less than 10 kHz.

These ν_Q-values observed for the α-phase in these compounds were much smaller than 58 and 55 kHz calculated for $-ND_3^+$ and $-CD_3$ rotations, respectively, by using reported values 173 kHz for $C_2H_5ND_3Cl$ [9] and 165 kHz for $(CD_3)_2NH_2Cl$ [10], respectively, for rigid cations, where we used equation (4) with the tetrahedral angle $\theta = 70.5°$ for calculation. This further reduction in ν_Q-values implies that some motions in chain skeletons have been activated in this phase. The experimental values of 41 ± 2 kHz observed for the α-phase of

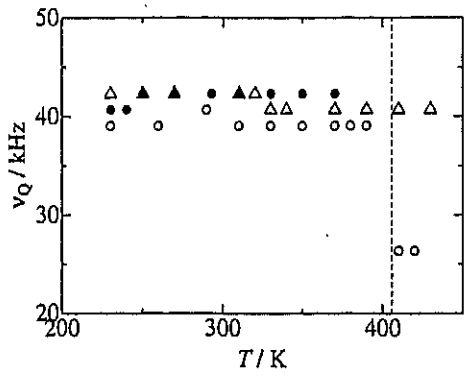

Figure 6. Temperature dependences of quadrupole coupling constants (ν_Q) determined from ^{2}H NMR spectra observed for $CH_3(CH_2)_2ND_3X$, X = Cl (○), Br (●) and I (△). The vertical line shows the phase transition temperature obtained for $CH_3(CH_2)_2NH_3Cl$ by DTA.

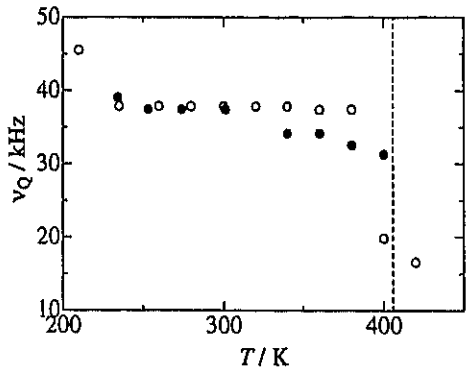

Figure 7. Temperature dependences of quadrupole coupling constants (ν_Q) determined from ^{2}H NMR spectra observed in $CD_3(CH_2)_2NH_3X$, X = Cl (○) and Br (●). The vertical line shows the phase transition temperature obtained for $CH_3(CH_2)_2NH_3Cl$ by DTA.

Nd_3X (X = Cl, Br and I) and 38 ± 1 kHz for the same phase of Cd_3X (X = Cl and Br) are roughly explainable on the basis of the calculated values 47 and 44 kHz, respectively, if one assumes axial rotation of the cation as a whole around the axis through the terminal C and N atoms, assuming the angle $\theta_b = 21°$ (figure 8(a)). The slight ν_Q-reduction observed in the α-phase of Cd_3Br implies that the N end is fixed by surrounding anions while the C end is expected to move more freely than in chloride.

In the α'-phase of chloride, the large reduction in ν_Q is attributable to the fluctuation of the rotational axis (figure 8(b)). Under an assumption of a random fluctuation of the axis within a cone in which the N atom is at the apex, the vertical angle θ_V of the cone was estimated to be 33 ± 1° from the ν_Q of 26 kHz observed for Nd_3Cl at 410 K. This large θ_V is attributable to the packing in the α'-form being looser than that in the α-form. On the other hand, the ν_Q of 12 kHz obtained at 420 K for the α'-phase of Cd_3Cl is much smaller than the 24 kHz calculated by using the above θ_V. This implies a large fluctuation of the C end enabled by the non-rigidity of a propylammonium ion.

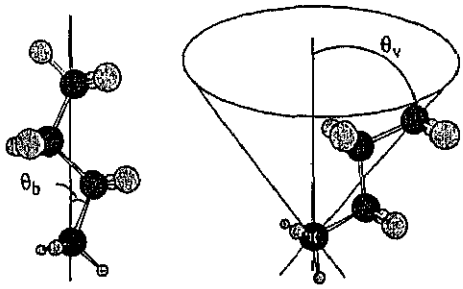

Figure 8. Schematic models of (a) axial rotation of the propylammonium cation as a whole and (b) random fluctuation of the cationic axis in a cone.

4. Conclusions

The axial rotation of the cation as a whole was newly observed by ^1H and ^2H NMR methods in phases I (α-phase) and II of propylammonium iodide. It can be concluded from these results that the α-phase in propylammonium iodide, as well as those in chloride and bromide, and the low-temperature phase II with a symmetry lower than tetragonal are rotator phases. It was shown that the amplitude of the fluctuation at the C end of a cation in the α-phase is increased in the order chloride < bromide < iodide while those at the N end are almost the same for these three compounds. This is because the N end is tightly bound to surrounding anions by hydrogen bonds while the C end feels only weak van der Waals force.

It was found that the α'-phase (phase I) in chloride is a highly disordered state. The highest-temperature solid phase in *n*-alkylammonium halides with chains longer than C_3 takes the α'-phase, but only chloride forms this phase in propylammonium halides. This result can be explained by considering that weak van der Waals forces among short chain alkyl groups in propylammonium ions cannot maintain the crystal with the loose structure of the α'-phase. Only in chloride can the electrostatic force between cations and anions be expected to be strong enough to maintain the α'-phase. On the other hand, in propylammonium fluoride, the inter-ionic force is implied to be too strong for formation of a rotator phase.

Acknowledgments

This work was partly supported by Grant-in-Aid for scientific research (B) no 12440192 from the Ministry of Education, Culture, Sports, Science and Technology. The authors are grateful to the Chemical Analysis Centre, University of Tsukuba, for elemental analysis.

References

[1] Hendricks S B 1928 Z. *Kristallogr.* **68** 189
[2] Hendricks S B 1928 Z. *Kristallogr.* **67** 465
[3] King M V and Lipscomb W N 1950 *Acta Crystallogr.* **3** 222
[4] Fukada S, Yamamoto H, Ikeda R and Nakamura D 1987 *J. Chem. Soc. Faraday Trans.* I **83** 3207
[5] Powles J G and Strange J H 1963 *Proc. Phys. Soc.* **82** 6
[6] Van Vleck J H 1948 *Phys. Rev.* **74** 1168
[7] Abragam A 1961 *The Principle of Nuclear Magnetism* (Oxford: Clarendon)
[8] Slichter C P 1990 *Principles of Magnetic Resonance* 3rd edn (Berlin: Springer)
[9] Hunt M J and Mackay A L 1975 *J. Magn. Reson.* **15** 402
[10] Ratcliffe C I 1990 *J. Phys. Chem.* **94** 152

A ^{35}Cl NQR Study on Exchange Interactions between Paramagnetic $[IrCl_6]^{2-}$ Ions

Hiroshi Miyoshi, Keizo Horiuchi[a], and Ryuichi Ikeda

Department of Chemistry, University of Tsukuba, Tsukuba 305-8571, Japan
[a] Faculty of Science, University of the Ryukyus, Nishihara, Okinawa 903-0213, Japan

Reprint requests to Prof. R. I.; Fax: +81 298 53 6503, E-mail: ikeda@staff.chem.tsukuba.ac.jp

Z. Naturforsch. 57 a, 431–434 (2002); received January 23, 2002

Presented at the XVIth International Symposium on Nuclear Quadrupole Interactions, Hiroshima, Japan, September 9-14, 2001.

The ^{35}Cl and ^{37}Cl NQR frequencies and spin-lattice relaxation times T_{1Q} in paramagnetic M_2IrCl_6 (M = NH_4, Cs) were measured at 4 - 350 K. The observed temperature dependences were attributed to EFG fluctuations caused by lattice vibrations and magnetic field fluctuations caused by paramagnetic ions. The exchange parameters J in the NH_4 and Cs salts were calculated from ^{35}Cl NQR T_{1Q} to be 8.6 K and 1.8 K respectively. ^{37}Cl data yielded 9.1 K and 2.1 K respectively. The obtained lattice constant dependence of J values was explained by considering Ir-Cl. . . Cl-Ir superexchange interaction.

Key words: Cl NQR;Superexchange Interaction; Paramagnetic Salt; Spin-lattice Relaxation.

1. Introduction

Electron spin dynamics in paramagnetic solids has been intensively studied by measurements of magnetic resonance, magnetic susceptibility, *etc.* Information on the microscopic structure and dynamics of electron spins can be effectively obtained by magnetic resonance techniques such as ESR, NMR and NQR. Among these, the ^{35}Cl NQR method, although having experimental limitations, has the following advantages:

1. Resonance signals can be observed even from nuclei located close to paramagnetic atoms. This seems to originate from the small gyromagnetic ratio of ^{35}Cl compared with NMR nuclei such as ^{1}H.

2. Different resonance signals correspond to different lattice sites in crystals. This is due to the narrow resonance linewidths and the high sensitivity of the frequency measurements. Applying these benefits, we have studied spin dynamics in solid paramagnetic systems in which we measured NQR relaxation in ^{35}Cl nuclei in counter ions [1].

In the present study, we selected paramagnetic $[IrCl_6]^{2-}$ ions as a target in which the monitoring Cl atoms are directly bonded to the paramagnetic metal ion. We employed ammonium and cesium salts having different inter-spin distances but the same antifluorite structure and intended to compare the obtained results with those reported on K_2IrCl_6 [2]. From ^{35}Cl and ^{37}Cl NQR measurements we expected to obtain reliable information on electron spin dynamics such as exchange interactions.

2. Experimental

Cs_2IrCl_6 was prepared by passing chlorine gas through a mixture of equivalent amounts of Ir metal powder and CsCl, and heating up to 970 K in a quartz tube. $(NH_4)_2IrCl_6$ was prepared by adding an NH_4Cl aqueous solution to an Na_2IrCl_6 hydrochloric acid solution. $(NH_4)_2IrCl_6$ was recrystallized from 3 N hydrochloric acid containing approximately 1 percent of nitric acid to avoid reduction. This solvent was used in all preparation processes described above for the same purpose.

The ^{37}Cl and ^{35}Cl NQR frequency and spin-lattice relaxation time(T_{1Q}) measurements were made with a home-made pulsed spectrometer [3] at 4 - 350 K by use of a conventional π-τ-$\pi/2$ pulse sequence with a $\pi/2$ pulse-width of 14 - 23 μs. The sample tempera-

0932–0784 / 02 / 0600–0431 $ 06.00

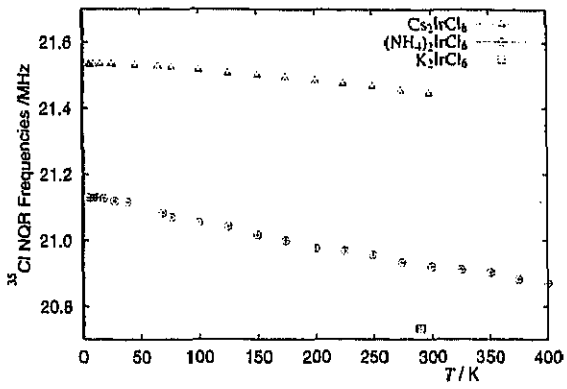

Fig. 1. Temperature dependences of ^{35}Cl NQR frequencies observed in $(NH_4)_2IrCl_6$ and Cs_2IrCl_6.

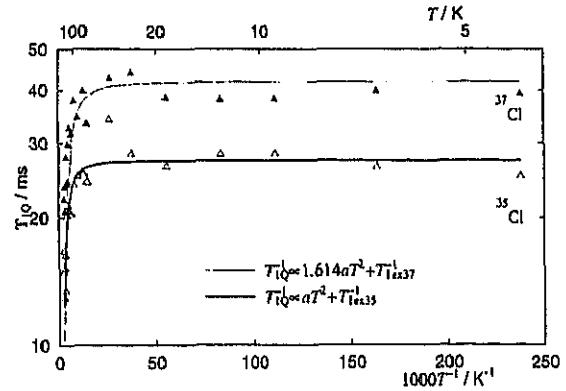

Fig. 2. Temperature dependences of ^{35}Cl and ^{37}Cl T_{1Q} observed in $(NH_4)_2IrCl_6$ and fitted theoretical curves.

ture was controlled and determined within ±0.1 K and ±3 K bellow and above 30 K, respectively.

3. Results and Discussion

The observed temperature dependences of the ^{35}Cl NQR frequencies in $(NH_4)_2IrCl_6$ and Cs_2IrCl_6 are shown in Figure 1. The ratio of the ^{35}Cl and ^{37}Cl NQR frequencies was 1.269 ± 0.001 at all temperatures studied, in agreement with the theoretical ratio within experimental errors.

From the observed NQR frequencies one can see that the electric field gradient (EFG) at the Cl nuclei in Cs_2IrCl_6 is by 3.4% larger than that in K_2IrCl_6 at room temperature.

The temperature dependences of ^{35}Cl and ^{37}Cl T_{1Q} measured in $(NH_4)_2IrCl_6$ and Cs_2IrCl_6 are shown in Figs. 2 and 3, respectively. Since T_{1Q}^{-1} in the present

Table 1. Relaxation times T_{1ex} due to electron spin exchange interactions derived from observed relaxation times.

	T_{1ex} (^{35}Cl) /ms	T_{1ex} (^{37}Cl) /ms
$(NH_4)_2IrCl_6$	27.3	41.9
Cs_2IrCl_6	5.72	9.55
K_2IrCl_6 [2]	35.1	–

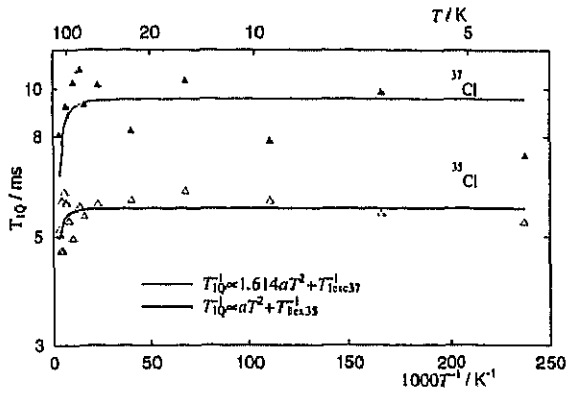

Fig. 3. Temperature dependences of ^{35}Cl and ^{37}Cl T_{1Q} observed in Cs_2IrCl_6 and fitted theoretical curves.

systems is expected to both on lattice vibrations ($\propto T^2$) and exchange interactions between electron spins (T_{1ex}^{-1}), we fitted the observed results by superimposing two contributions with an open coefficient A:

$$T_{1Q}^{-1} = \frac{T^2}{A} + T_{1ex}^{-1}. \tag{1}$$

Since the measurement was made in the low-temperature region, the present fitting was carried out without the term of the $[IrCl_6]^{2-}$ reorientation, which is expected to become important above room temperature. $A = 3.7 \times 10^6$ K^{2}s in $(NH_4)_2IrCl_6$ and $A = 3.6 \times 10^6$ K^{2}s in Cs_2IrCl_6 were obtained from the ^{35}Cl data. For ^{37}Cl, we used $1.614A$ because lattice vibrations affect T_1 by a factor of the squared quadrupole moment. The obtained values of T_{1ex} are listed in Table 1.

T_{1ex} can be expressed by use of the exchange frequency ω_e as [2]

$$T_{1ex}^{-1} = \frac{2S(S+1)}{\omega_e}\sqrt{\frac{\pi}{2}}\left(\frac{B}{\hbar}\right)^2, \tag{2}$$

$$B = -\frac{\gamma\hbar g\beta}{R^3}, \tag{3}$$

Table 2. Electron spin exchange parameters J derived from T_{1ex} together with values obtained from magnetic susceptibility.

	^{35}Cl NQR /K	^{37}Cl NQR /K	magnetic susceptibility [4] / K
$(NH_4)_2IrCl_6$	8.6 ±2	9.1 ±3	6.7
Cs_2IrCl_6	1.8 ±0.3	2.1 ±0.8	–
K_2IrCl_6	11.0 (fixed)	–	11.0±1.5

$$\omega_e^2 = \frac{8S(S+1)J^2}{\hbar^2}, \tag{4}$$

$$H_{ex} = \sum_{i<j} J_{ij} S_i \cdot S_j. \tag{5}$$

Here J, γ, β, g, S_i, H_{ex}, and R are the exchange parameter, the gyromagnetic ratio of resonant nuclei, Bohr magneton, g-factor, ith spin, the Hamiltonian that describes the electron system and the distance between resonant nuclei and an electron spin, respectively. In the present study we assumed R, which is the Ir-Cl distance, to be constant and independent of the counter cations. Under this assumption we can express T_{1ex} with a constant C as

$$T_{1ex} = CJ, \tag{6}$$

The values J, derived from the obtained values of T_{1ex}, are showed in Table 2.

The relation between the evaluated J values and the cubic lattice constant a obtained at room temperature is shown in Figure 4. The relation between J and a is nearly linear. No marked change in the NH_4 salt, in which the superexchange path by way of Cl... H-N hydrogen bonding is expected, is found. On the other hand, since J showed a strong dependency on a and can not be expressed by $\exp(-R)$, this result can not be explained by any ordinary direct spatial interactions between Ir atoms. This suggests that paths of exchange interactions in these compounds are indirect through some chemical interaction, rather than direct. Hence we can assume an Ir-Cl... Cl-Ir path by taking into account the relatively large size of the anions.

A superexchange interaction between $[IrCl_6]^{2-}$ ions by way of Ir-Cl bonds has been proposed by Griffiths, Owen, Park, and Partridge in their ESR

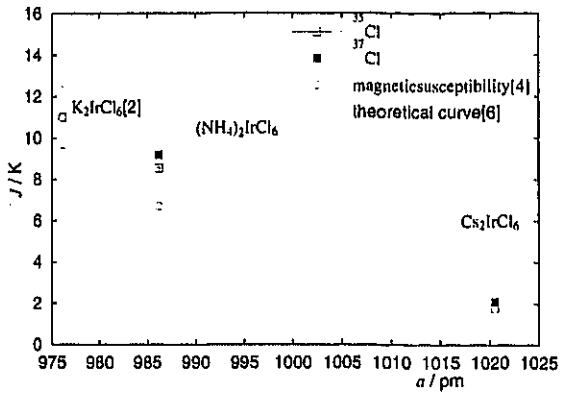

Fig. 4. Calculated and reported [2] J values, vs. lattice contant a [5]. The line represents a theoretical curve by Griffiths et al. [6].

study [6]. They expressed J through such a path as

$$J \approx 2p^2 D[1 - [1 - \exp\{-\beta(r - r_e)\}]^2], \tag{7}$$

where D (≈ 20000 cm^{-1}), β (= 2.04), r_e (= 199 pm), p(= 0.05) and r is the Cl-Cl separation in a free Cl_2 molecule, a reduction factor corresponding to the probability of finding the spins on Cl atoms, and the Cl... Cl distance between nearest neighbors, respectively. This dependence of J is shown in Figure 4. Although this assumption was intended primarily as a simple illustration of the superexchange mechanism, the obtained result showed the order-of-magnitude agreement with the present data.

4. Conclusions

1) It was shown that ^{35}Cl and ^{37}Cl NQR relaxation data can give reliable information on electron spin dynamics, especially exchange interactions.

2) The J values showed a strong dependence on the lattice constant a. This J dependence on a can roughly be understood by introducing an Ir-Cl... Cl-Ir superexchange path proposed by Griffiths et al. No marked influence from Cl... H-N hydrogen bonds in the NH_4 salt was observed.

Acknowledgement

This work was partly supported by Grant-in Aid for scientific research No. (B)12440192 from Ministry of Education, Culture, Sports, Science, and Technology.

[1] K. Horiuchi, T. Asaji, and R. Ikeda, Phys. Rev. **B50**, 6169 (1994).
[2] K. R. Jeffrey, R. L. Armstrong, and K. E. Kisman, Phys. Rev. **B1**, 3770 (1970).
[3] H. Miyoshi, K. Horiuchi, N. Sakagami, K. Okamoto, and R. Ikeda, Z. Naturforsch. **53a**, 603 (1998).
[4] E. Koenig, Landolt-Boernstein New Series Group II: Atomic and Molecular Physics, Vol. 2, ed, A. M. Hellwege, Spinger-Verlag Berlin 1966, p. 69.
[5] U. S. Dept. of Commerce, N. B. S. and the Joint Committee on Powder Diffraction Standards, Cryatal Data Determinative Tables 3rd ed., Vol. 2 Inorganic Compds., USA 1973.
[6] J. Griffiths, J. Owen, G. Park, and F. Partridge, Proc. Roy. Soc. London **A250**, 84 (1958).

^1H, ^2H and ^{13}C NMR Studies of Cation Dynamics in a Layered Perovskite-Type Incommensurate Compound $(n\text{-}C_3H_7NH_3)_2CdCl_4$

Koh-ichi Suzuki, Hiroki Fujimori, Tetsuo Asaji, Shin'ichi Ishimaru[a], and Ryuichi Ikeda[a]

Department of Chemistry, College of Humanities and Sciences, Nihon University, Sakurajosui, Setagaya-ku, Tokyo 156-8550, Japan

[a] Department of Chemistry, University of Tsukuba, Tsukuba 305-8571, Japan

Reprint requests to Dr. K. S.; Fax: +81-3-5317-9433, E-mail: suzuki_k@chs.nihon-u.ac.jp

Z. Naturforsch. **57 a**, 451–455 (2002); received December 17, 2001

Presented at the XVIth International Symposium on Nuclear Quadrupole Interactions, Hiroshima, Japan, September 9-14, 2001.

Cation dynamics in $(n\text{-}C_3H_7NH_3)_2CdCl_4$ and $(n\text{-}C_3H_7ND_3)_2CdCl_4$ were investigated by ^1H, ^2H, and ^{13}C NMR measurements. An overall motion of the cation being associated with the fluctuation of the molecular axis is suggested to be activated with increasing temperature. The cationic motion is enhanced at the counter side of the $-NH_3^+$ group probably because the group is bound with the inorganic layer through the N-H...Cl hydrogen bonds.

Key words: ^1H NMR T_1; ^2H NMR Spectra; ^{13}C MAS NMR T_1; Cation Dynamics; Phase Transition.

1. Introduction

Layered perovskite-type compounds with the general formula $(C_nH_{2n+1}NH_3)_2MX_4$, where M and X express divalent metals and halogen ions, respectively, have interesting electronic properties as nonlinear optical materials [1 - 3], and the dynamics of their cations in the two-dimensional structure are useful as model of lipid membranes [4, 5]. These compounds consist of inorganic layers of corner-sharing MX_6 octahedra and organic layers of alkylammonium ions. The $-NH_3^+$ polar heads of the alkylammonium, forming NH...X hydrogen bonds with halogen atoms, occupy cavities among the octahedra. Some of propylammonium salts with this structure have been reported to undergo a transition to the incommensurate (IC) phase [6 - 9]. The cation dynamics and interionic interactions through hydrogen bonds are expected to be closely related with the physical properties and mechanisms of structural phase transitions in these materials.

Bis(*n*-propylammonium) tetrachlorocadmate $(n\text{-}C_3H_7NH_3)_2CdCl_4$ (abbreviated to PACC), belonging to this group of layered compounds have been reported to undergo phase transitions at 178.7, 156.8 and 105.5 K [10] and show a normal (N) - IC - commensurate (C) - commensurate (C') phase transition sequence with decreasing temperature [7]. In the N phase, which has an orthorhombic lattice with space group Abma ($Z = 4$), the propylammonium ions are disordered between two equivalent orientations, related by a mirror plane perpendicular to the *b*-axis [11]. In the IC phase with the superspace group $P^{Abma}_{s\,1\,1}$, the modulation vector $q = 0.418\,b^*$ was reported to be independent of temperature [12]. The IC modulation of the $CdCl_6$ octahedra is related to rotation around the *a*-axis and translation along the *c*-axis. Thus, the position of the nitrogen atoms in the propylammonium chains gets modulated through hydrogen bonds to halogens [12]. In the C phase with space group Pbca ($Z = 4$), the angular fluctuation of octahedra about the *a*-axis is locked-in, and the orientation of the propylammonium ions is ordered [12].

In the present study, temperature dependences of the ^1H NMR spin-lattice relaxation time T_1 in PACC and in a partially deuterated analogue $(n\text{-}C_3H_7ND_3)_2CdCl_4$ (PACC-d_3), ^2H NMR spectra in each phase of PACC-d_3, and ^{13}C MAS NMR spectra and T_1 in PACC at room temperature were measured in order to clarify the cation dynamics.

0932–0784 / 02 / 0600–0451 $ 06.00

2. Experimental

PACC crystals were obtained by slow cooling from about 350 K to room temperature of an aqueous solution containing stoichiometric amounts of cadmium chloride and propylammonium chloride with an additional small amount of hydrochloric acid. Chemical analysis, found: C = 19.26, H = 5.48, N = 7.38(%); calcd.: C = 19.24, H = 5.38, N = 7.48(%). PACC-d_3 was prepared by crystallizing PACC three times from heavy water. The obtained powdered crystals were put in glass tubes, dried *in vacuo* and then sealed with nitrogen gas for differential thermal analysis (DTA) and NMR measurements. In the DTA measurements the sample temperature was determined within ±0.2 K with a chromel-constantan thermocouple.

The ^{1}H NMR spin-lattice relaxation times T_1 were measured with home made pulsed NMR spectrometers at a Larmor frequency of 41.6 MHz using the 180°-τ-90° pulse sequence in temperature ranges 92 - 360 K and 92 - 350 K for PACC and PACC-d_3, respectively. The accuracy of the temperature measurement was ±0.2 K and the uncertainty in ^{1}H T_1 was estimated within 10%. ^{2}H NMR spectra in PACC-d_3 were measured with a Bruker MSL-300 NMR system at 46.1 MHz in a temperature-range 131 - 356 K. The sample temperature was controlled within ±1 K with a VT-1000 temperature controller and determined by a copper-constantan thermocouple with the same accuracy. A ^{13}C MAS NMR spectrum in PACC at room temperature (ca. 295 K) was taken at 67.9 MHz using a JEOL EX-270 spectrometer. The sample was rotated at 4 kHz. The spectrum was obtained by Fourier transform of free induction decay accumulated under ^{1}H decoupled condition. The inversion recovery method was used in the ^{13}C T_1 measurements. For the standard of ^{13}C NMR chemical shift, adamantane was used, in which the two kinds of carbons denote 29.5 and 38.6 ppm. The uncertainty in ^{13}C T_1 was estimated to be within 20%.

3. Results and Discussion

3.1. Phase Transition Temperatures Observed by DTA

DTA thermograms measured on heating showed endothermic anomalies due to phase transitions at 101.4±1, 155.4±0.5, and 178.8±1 K in PACC. They agree well with the reported phase transition temperatures $T_{C'}$ = 105.5, T_C = 156.8 and T_{IC} = 178.7 K in PACC [10], respectively, and at 101.2±1, 158.4±0.5, and 178.0±1 K in PACC-d_3. The difference in T_C observed in PACC and PACC-d_3 suggests that the mechanism of the C-IC phase transition concerns the hydrogen-bond.

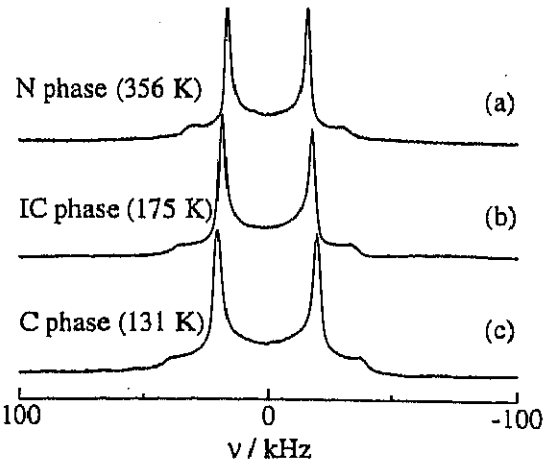

Fig. 1. ^{2}H NMR spectra in PACC-d_3 observed at 356 K in N phase (a), at 175 K in IC phase (b), and at 131 K in C phase (c).

3.2. ^{2}H NMR Spectra in PACC-d_3

^{2}H NMR spectra in PACC-d_3 showed line-shapes with an asymmetry parameter of the electric field gradient $\eta \sim 0$ in the whole temperature range studied, as shown in Figure 1. From the X-ray structural analysis, a disorder of the cation has been expected in the N phase [11]. We have examined whether the NMR line-shape can be explained by assuming a 2-site jump of the cation in the N phase. Using the jumping angle of about 21° which was estimated from the reported structure [11], η = 0.05 was evaluated for the motionally averaged EFG tensor of the deuterium [13]. With this value of η the line-shape is almost indiscriminable with η = 0, so that the 2-site jump does not conflict with the observed line-shape. The quadrupole coupling constant e^2Qqh^{-1} was calculated from the line-shape by assuming η = 0 in the C phase, where the cation is expected in ordered state, and η = 0.05 in the IC and N phases. The temperature dependence of e^2Qqh^{-1} is shown in Figure 2. The e^2Qqh^{-1} value of 52 kHz at 131 K in the C phase is already smaller than $e^2Qqh^{-1}{}_{ND_3}$ = 57 kHz calculated

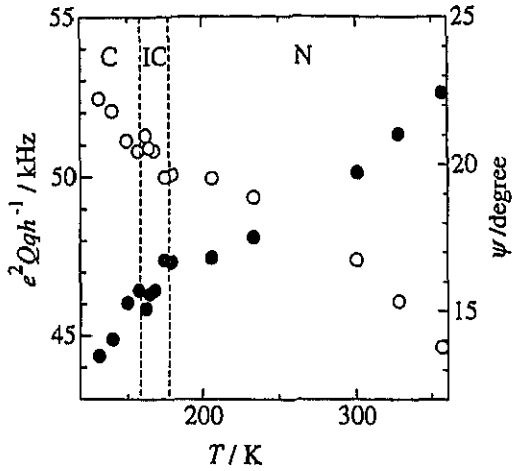

Fig. 2. Temperature dependence of the quadrupole coupling constant e^2Qqh^{-1} (o) determined from ^{2}H NMR lineshapes observed in PACC-d_3 assuming $\eta = 0$ in the C phase and $\eta = 0.05$ (2-site jump with the angle $2\theta = 21.25°$) in the N and IC phases. The vertical lines show the transition temperatures observed by DTA. The angle ψ (•) which was calculated from (1) and (2) in the text is also shown.

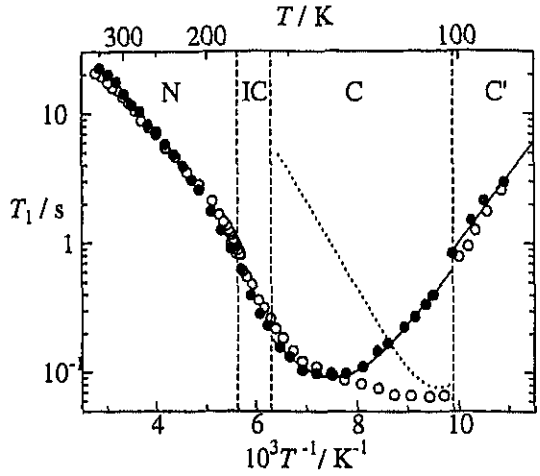

Fig. 3. Temperature dependences of the ^{1}H NMR T_1 observed at 41.6 MHz in PACC (o) and PACC-d_3 (•). The vertical lines show the transition temperatures observed by DTA for PACC-d_3, and the solid lines in the C and C' phases are best-fitted curves for PACC-d_3, applying (3) and (4) in the text. The broken line in the C phase indicates the contribution from the NH_3^+ rotation in PACC.

for rotating -ND_3^+ assuming a tetrahedral geometry and $(e^2Qqh^{-1})_{\text{Rigid}} = 173$ kHz, which was reported for rigid -ND_3^+ in ethylammonium chloride [14]. The value decreased gradually with increasing temperature, although the values are still larger than 38 kHz, the value which was calculated for the axial rotation of the cation as a whole about the principal axis of the moment of inertia assuming that the EFG principal axis of the rotating -ND_3^+ makes 27° with it. This behaviour seems to be similar with the temperature dependence of the second moment of ^{1}H NMR line reported by Blinc et al. [15]. This gradual decrease of e^2Qqh^{-1} is often observed in long chain compounds such as smectic liquid crystals and is explained by a random fluctuation of the molecular axis [16].

The e^2Qqh^{-1} value, reduced by the fluctuation, can be written as

$$e^2Qqh^{-1} = (e^2Qqh^{-1})_{ND_3}S \qquad (1)$$

and

$$S = \frac{\langle 3\cos^2\phi - 1\rangle}{2} = \frac{3\cos^2\psi - 1}{2}. \qquad (2)$$

Here S is an order parameter which describes the degree of fluctuation [17], ϕ is the angle between a principal axis of the EFG tensor and the fluctuation axis of the molecule, and the brackets denote the statistical average. The angle ψ is defined as $\cos\psi$ giving the root mean square of $\cos\phi$. The temperature dependence of ψ is also shown in Figure 2.

3.3. ^1H NMR T_1 Measurements

The recovery of ^{1}H magnetization could be explained by a single T_1 value in the whole temperature region including the IC phase. This result differs from the previous report by Blinc et al., where the recovery was described by a sum of two exponential terms in the IC phase. In the case of the relaxation caused by the fluctuation of magnetic dipole-dipole interaction due to molecular motions, the relaxation rate T_1^{-1} can be represented by superposition of the BPP-type functions [18] for each motional mode,

$$T_1^{-1} = \sum C\left(\frac{\tau_c}{1+\omega^2\tau_c^2} + \frac{4\tau_c}{1+4\omega^2\tau_c^2}\right) \qquad (3)$$

where C, ω, τ_c denote the motional constant, the ^{1}H Larmor frequency, and the correlation time of the motion, respectively. Assuming an Arrhenius-type relation, τ_c is represented by the activation energy E_a of the motional process as follows,

$$\tau_c = \tau_0 \exp(E_a/RT). \qquad (4)$$

Table 1. Motional constants C and activation energies E_a derived by curve fitting of the temperature dependence of ^1H T_1 observed in PACC and PACC-d_3.

	$C/10^9 s^{-2}$	E_a/kJ mol^{-1}	Motional mode
PACC			
N phase ($T > 280$ K)	–	8.0 ± 1	
C phase	2.0	10 ± 1	-CH_3 rotation
	2.4	13 ± 1	-NH_3^+ rotation
C' phase	–	12 ± 1	-CH_3 rotation
PACC-d_3			
N phase ($T > 280$ K)	–	8.5 ± 1	
C phase	2.0	9.6 ± 1	-CH_3 rotation
C' phase	–	10 ± 1	-CH_3 rotation

Here τ_0 denotes the correlation time at infinite temperature.

Temperature dependences of ^{1}H NMR T_1 on PACC and PACC-d_3 seem to be similar except for the low temperature region in the C phase, as shown in Figure 3. In the C phases of PACC-d_3 and PACC, the T_1 curve can be reproduced by one and two BPP-curves, respectively. The BPP-curve of PACC, showing a minimum at higher temperature, is almost the same as that of PACC-d_3. This implies that these curves are from the -CH_3 rotation, and the other curve in PACC, showing a minimum at lower temperature, is from the -NH_3^+ rotation. In the N phase, the temperature dependence of T_1 becomes gentle gradually with increasing temperature, as shown in Figure 3. This may be explained by taking the 2-site jump and / or the molecular axis fluctuation into account. The best-fitted motional parameters in the C and C' phases of PACC and PACC-d_3, and the activation energies in the high temperature region in the N phase of each compound are listed in Table 1.

3.4. A ^{13}C MAS NMR Spectrum and T_1 Measurements

As shown in Fig. 4, the ^{13}C MAS NMR spectrum observed in PACC gave three peaks at 12.6 ± 0.2, 21.5 ± 0.2, and 43.7 ± 0.2 ppm, which can be assigned to carbons in methyl, the middle methylene, and the end methylene groups, respectively. ^{13}C NMR T_1 values are 7 ± 1, 17 ± 5, and 20 ± 6 s for the 12.6, 21.5, and 43.7 ppm lines, respectively. ^{13}C T_1 is dominated

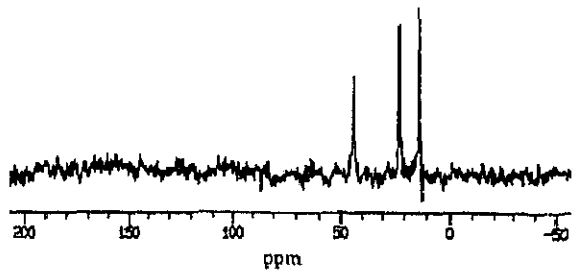

Fig. 4. ^{13}C MAS NMR spectrum observed at room temperature in PACC.

usually by the fluctuation of the anisotropic chemical shift, and the T_1 becomes short with larger amplitude of molecular motions [19]. This implies that the amplitude of the cationic motion is enhanced at the C-end, that is, the N-end of the organic cation is fixed on the inorganic layer through N-H... Cl hydrogen bonds.

4. Conclusion

Phase transition temperatures in PACC-d_3 were determined by DTA. The difference in the C-IC phase transition temperature observed in PACC and PACC-d_3 suggests that the mechanism of the phase transition concerns a change of hydrogen-bond. The cationic motion as a whole, being associated with the fluctuation of the molecular axis is expected to be gradually excited with increasing temperature. The fact that the ^{13}C MAS NMR T_1 decreased with increasing distance from the -NH_3^+ group implies that the amplitude of the cationic motion is enhanced at the counter side of the -NH_3^+ group due to the N-H...Cl hydrogen bonds.

Acknowledgements

The authors are grateful to the Chemical Analysis Centre, University of Tsukuba, for elemental analysis. This work was partly supported by Grant-in-Aid for scientific research (B) No. 12440192 from the Ministry of Education, Science, Sports and Culture, by Nihon University Research Grant for Assistants, and by Grant from the Ministry of Education, Science, Sports and Culture to promote advanced scientific research.

[1] C. Q. Qu, T. Kondo, H. Sakakura, K. Kumata, Y. Takahashi, and R. Ito, Solid State Commun. **79**, 245 (1991).
[2] G. C. Papavassiliou, Prog. Solid State Chem. **25**, 125 (1997).
[3] D. B. Mitzi, Prog. Inorg. Chem. **48**, 1 (1999).
[4] R. Blinc, M. Kozelj, V. Rutar, I. Zupanicic, B. Žecš, H. Arend, R. Kind, and G. Chapuis, Faraday Discuss. Chem. Soc. **69**, 58 (1980).
[5] R. Kind, Ber. Bunsenges. Phys. Chem. **87**, 248 (1983).
[6] W. Depmeier, Acta Crystallogr. **B37**, 330 (1981).
[7] R. Mokhlisse, M. Couzi, N. B. Chanh, Y. Haget, C. Hauw, and A. Meresse, J. Phys. Chem. Solids **46**, 187 (1985).
[8] J. Etxebarria, I. Ruiz-Larrea, M. J. Tello, and A. López-Echarri, J. Phys. C: Solid State Phys. **21**, 1717 (1988).
[9] Y. Abid, M. Kamoun, A. Daoud, F. Romain, and A. Lautie, Phase Transitions **40**, 239 (1992).
[10] M. A. White, N. W. Granville, N. J. Davies, and L. A. K. Staveley, J. Phys. Chem. Solids **42**, 953 (1981).
[11] G. Chapuis, Acta Crystallogr. **B34**, 1506 (1978).
[12] B. Doudin and G. Chapuis, Acta Crystallogr. **B44**, 495 (1988).
[13] R. Ikeda, A. Kubo, and C. A. McDowell, J. Phys. Chem. **93**, 7315 (1989).
[14] M. J. Hunt and A. L. Mackay, J. Magn. Reson. **15**, 402 (1974).
[15] R. Blinc, M. Burgar, B. Lozar, J. Seliger, J. Slak, and V. Rutar, J. Chem. Phys. **66**, 278 (1977).
[16] J. W. Doane, in F. J. Owens et al. (eds), Magnetic Resonance of Phase Transitions, Academic Press, New York 1979.
[17] A. Saupe and W. Maier, Z. Naturforsch. **16a**, 816 (1961).
[18] A. Abragam, The Principles of Nuclear Magnetism, Oxford University Press, London 1961.
[19] B. C. Gerstein and C. R. Dybowski, Transient Techniques in NMR of Solids, Academic Press Inc., London 1985.

^{133}Cs NMR Spin-Lattice Relaxation Time and Chemical Shift Studies on Cs_2MX_4 Crystals with Sr_2GeS_4 and β-K_2SO_4 Structures Performing no Low Temperature Phase Transition

Koh-ichi Suzuki*, Shin'ichi Ishimaru, and Ryuichi Ikeda

Department of Chemistry, University of Tsukuba, Tsukuba 305-8571, Japan

* Present address: Department of Chemistry, College of Humanities and Sciences, Nihon University, Sakurajosui, Setagaya-ku, Tokyo 156-8550, Japan

Reprint requests to Dr. K. S.; Fax: +81-3-5317-9433, E-mail: suzuki_k@chs.nihon-u.ac.jp

Z. Naturforsch. **57 a**, 461–464 (2002); received December 17, 2001

Presented at the XVIth International Symposium on Nuclear Quadrupole Interactions, Hiroshima, Japan, September 9-14, 2001.

^{133}Cs NMR spectra and spin-lattice relaxation times T_1 in crystalline Cs_2ZnCl_4 and Cs_2ZnBr_4 with β-K_2SO_4 structure, and Cs_2CdI_4 and Cs_2HgI_4 with Sr_2GeS_4 structure, which have no phase transition in the lower temperature regions, were measured to clarify the relation between the interionic covalency and crystal structures. Two central lines corresponding to two crystallographically inequivalent Cs sites were observed in all compounds. One of the two peaks in β-K_2SO_4-type compounds appears below 40 ppm, but another peak in those compounts and the both lines in Sr_2GeS_4-type compounds show larger shifts, 130 - 200 ppm. The temperature dependences of T_1 observed in Sr_2GeS_4-type compounds were close to the theoretical behaviour, calculated by considering contributions from normal lattice vibrations. Deviations from the calculation obtained for β-K_2SO_4-type systems are attributable to the difference in interionic interactions, i. e., partial covalency, in the crystals.

Key words: ^{133}Cs NMR; Chemical Shift; T_1; Partial Covalency.

1. Introduction

A_2BX_4 compounds containing isolated tetrahedral BX_4^{2-} ions form a modification of (A) the orthorhombic β-K_2SO_4-type (Pnma, Z=4) or (B) the monoclinic Sr_2GeS_4-type ($P2_1/m$, Z = 2) structure. Many of the (A) compounds undergo phase transitions to incommensurate (IC) phases at low temperatures [1], but all (B) compounds have no IC phase. Some of (B) compounds transform to (A), called α-β transition, at a temperature $T_{\alpha\text{-}\beta}$ [2 - 4]. Below $T_{\alpha\text{-}\beta}$, (B) is more stable than (A), but often (A) can exist as a metastable state [5].

Recently, we reported ^{133}Cs NMR results on Cs_2CdBr_4, Cs_2HgBr_4 [6], Cs_2CdI_4 [7], and Cs_2HgCl_4 [8], which form modification (A) with phase transitions, and discussed the lattice dynamics in IC phases and the mechanism of phase transitions caused by differences in interionic interactions. To clarify the relations between interionic interactions and crystal structures, we measured ^{133}Cs NMR spectra and spin-lattice relaxation times T_1 of β-K_2SO_4-type Cs_2ZnCl_4 [9] and Cs_2ZnBr_4 [10], and Sr_2GeS_4-type Cs_2CdI_4 [3] and Cs_2HgI_4 [4]. All perform no phase transitions below room temperature. These compounds were suitable to investigate lattice motions because we can exclude influences from phase transitions.

2. Experimental

Crystals of Cs_2ZnCl_4, Cs_2ZnBr_4, and Cs_2HgI_4 were grown by cooling a molten mixture containing stoichiometric amounts of corresponding CsX and MX_2 (purity of 99.9% for all). Cs_2CdI_4 crystals of modification (B) were obtained by slow evaporation of an aqueous solution containing stoichiometric amounts of CsI and CdI_2. The obtained fine crystals were dried *in vacuo* and then sealed in glass tubes with nitrogen gas for differential thermal analysis (DTA) and NMR measurements. DTA was carried out to

0932–0784 / 02 / 0600–0461 $ 06.00

confirm the absence of phase transitions in the the range 100 - 360 K. The sample temperature was determined within ±0.2 K by using a chromel-constantan thermocouple. ^{133}Cs NMR spectra and spin-lattice relaxation times T_1 were measured with a Bruker MSL-300 NMR system at a Larmor frequency of 39.4 MHz in the ranges 211 - 364 K, 173 - 373 K, 220 - 360 K and 214 - 359 K for Cs_2ZnCl_4, Cs_2ZnBr_4, Cs_2CdI_4, and Cs_2HgI_4, respectively. Chemical shifts of observed lines were recorded relative to a saturated CsCl aqueous solution. The sample temperature was controlled within ±1 K with a VT-1000 temperature controller and determined by a copper-constantan thermocouple with the same accuracy. The uncertainty in the T_1 measurement was estimated to be within 5%.

3. *Results*

No thermal anomaly was detected by DTA measurement between 100 and 360 K for all compounds studied.

Quadrupolar perturbed ^{133}Cs NMR spectra are shown in Figure 1. The width of the 90° pulse tuned for the measurement of all powdered samples was close to that of a saturated CsCl aqueous solution used as standard. This suggests that a single quantum transition in ^{133}Cs NMR was excited in all observations, i. e., ^{133}Cs nuclei have small quadrupole coupling constants (e^2Qq/h) compared with the Zeeman interaction in all compounds. The observed line-shapes were explained by the superposition of two 1st order perturbed spectra. This is consistent with the reported crystal structure containing crystallographically in-

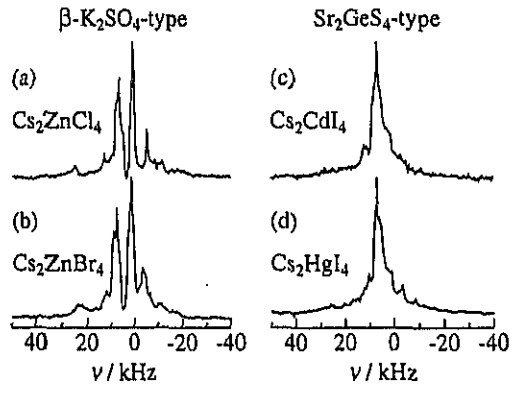

Fig. 1. Quadrupolar perturbed ^{133}Cs NMR spectra at 39.4 MHz at room temperature in Cs_2ZnCl_4 (a) and Cs_2ZnBr_4 (b) with β-K_2SO_4 structure, and Cs_2CdI_4 (c) and Cs_2HgI_4 (d) with Sr_2GeS_4 structure.

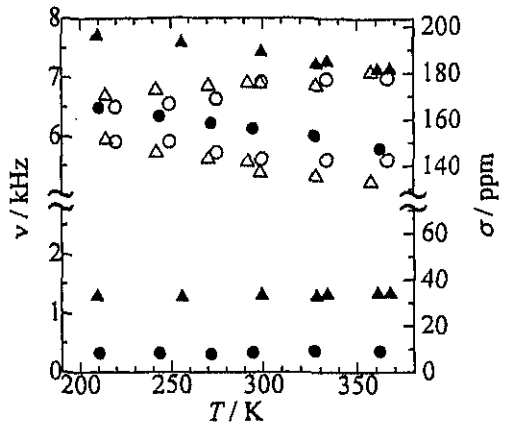

Fig. 2. Temperature dependences of central peak frequencies ν and their chemical shifts σ in ^{133}Cs NMR spectra for Cs_2ZnCl_4 (•) and Cs_2ZnBr_4 (▲) with β-K_2SO_4 structure, and Cs_2CdI_4 (o) and Cs_2HgI_4 (△) with Sr_2GeS_4 structure.

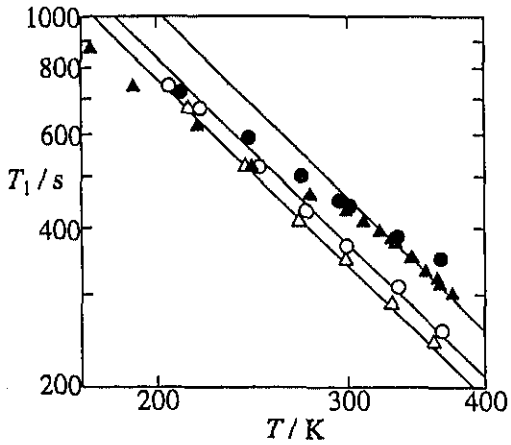

Fig. 3. Temperature dependences of ^{133}Cs NMR T_1 in Cs_2ZnCl_4 (•) and Cs_2ZnBr_4 (▲) with β-K_2SO_4 structure, and Cs_2CdI_4 (o) and Cs_2HgI_4 (△) with Sr_2GeS_4 structure. Solid lines are theoretical curves calculated by using (3).

equivalent two Cs ions [11 - 15]. Temperature dependences of the peak position of central lines observed in ^{133}Cs NMR are shown in Figure 2. In Cs_2ZnCl_4 and Cs_2ZnBr_4 with the β-K_2SO_4 structure, we observed two kinds of central lines at room temperature, one has a small chemical shift of ca. 10 and 30 ppm and the other has a large shift ca. 150 and 190 ppm. In Cs_2CdI_4 and Cs_2HgI_4 with the Sr_2GeS_4 structure, observed two lines gave large chemical shifts in a range of 140 - 180 ppm at room temperature.

The magnetization recovery in ^{133}Cs nuclei observed after saturation pulses could be reproduced by

a single exponential curve in the whole temperature range studied, and a unique T_1 value could be determined. Temperature dependences of ^{133}Cs NMR T_1 are shown in Figure 3. T_1 increased with decreasing temperature.

4. Discussion

4.1. Relations between NMR Chemical Shifts and Interionic Interactions

The NMR shielding tensor was formulated by Ramsey in the first approximation [16] as

$$\tilde{\sigma} = \tilde{\sigma}_D + \tilde{\sigma}_P . \tag{1}$$

Here, $\tilde{\sigma}$ represents the diagonalized tensor with diagonal components σ_{XX}, σ_{YY} and σ_{ZZ}. $\tilde{\sigma}_D$, called the diamagnetic term, is related only to the electron density around the nucleus in question. The paramagnetic term $\tilde{\sigma}_P$, is related to the local field induced by electron transfer from the ground to excited states. Taking into account relative chemical shift values from that of the reference sample, it was shown that the paramagnetic term in the heavy atoms is by about two orders of magnitude larger than the diamagnetic one [17]. In the following interpretation of ^{133}Cs NMR chemical shifts we only consider the paramagnetic terms. Moreover, we use the isotropic shielding constant $\sigma = (\sigma_{XX} + \sigma_{YY} + \sigma_{ZZ})/3$ as an approximation because isotropic shielding can be assumed in alkali metal ions in first order approximation. Since it was reported that the chemical shift is influenced by the degree of partial covalency in interionic bonds [18, 19], we take into account the covalency in this study. When the covalency of the chemical bond is small enough to approximate a cation in the bonding as an isolated system, the isotropic shielding constant σ_M in an alkaline metal nucleus relative to the ideal ion is given by [19]

$$\sigma_M = \lambda \frac{2e^2\hbar^2}{3m^2c^2} a_p^2 \frac{1}{\Delta E} \left\langle \frac{1}{r^3} \right\rangle_p , \tag{2}$$

where λ, e and m are the total bond covalency in Cs-X bonds (conversely, $(1 - \lambda)$ is the bond ionicity), the charge and the static mass of an electron, respectively, a_p is a fraction of p-orbitals related to hybrid orbitals in the partial-covalent bond, ΔE is the mean energy of all excited states contributing to the probability, and $\langle 1/r^3 \rangle_p$ is the mean $1/r^3$ value of a valence p-electron causing partial covalency in a Cs-X ionic bond. In the case of heavy atoms such as Cs, d-orbital electrons also contribute to the chemical shift which can be analogously expressed [19]. This shift is, accordingly, getting larger with the increase of the total degree of covalency. Thus, we can see from Fig. 2 that one of the two crytallographically nonequivalent Cs ions in Cs_2MX_4 crystals with the β-K_2SO_4-type structure has a lower covalency than in the other Cs ion of the β-K_2SO_4-type, and both ions in the Sr_2GeS_4-type structures.

4.2. Relations between NMR Relaxation Times and Interionic Interactions

The ^{133}Cs NMR T_1, which increased with temperature decrease, can be explained by the fluctuation of the quadrupole interaction due to normal lattice vibrations because of the absence of phase transitions in all four compounds. Since the frequencies of lattice vibrations are much higher than the NMR Larmor frequency $\nu_L = \omega_L/2\pi$, it can be assumed that the two-phonon Raman process is much more effective than the one-phonon direct process. In the high-temperature limit, i.e., $T \geq \theta_D$ where θ_D is the Debye temperature, the quadrupolar relaxation rate contributed from thermal lattice vibrations via the two-phonon Raman process is represented approximately as [20]

$$T_1^{-1} = AT^2. \tag{3}$$

The constant A is determined by the amplitude of the quadrupole coupling fluctuation $\Delta e^2Qq/h$ caused by lattice vibrations [20].

We tried to fit the experimental data by (3). Temperature dependences of T_1 in Cs_2CdI_4 and Cs_2HgI_4 with the Sr_2GeS_4-type structure could well be fitted with the constants $A = 3.0\times10^{-8}$ and 3.3×10^{-8} $s^{-1}K^{-2}$ for Cs_2CdI_4 and Cs_2HgI_4, respectively, as shown in Fig. 3, but those in Cs_2ZnCl_4 and Cs_2ZnBr_4 with the β-K_2SO_4-type structure were unexplainable by a simple theoretical treatment of lattice mode with $A = 2.4 \times 10^{-8}$ $s^{-1}K^{-2}$. The deviations in the calculation from experimental data were getting large with decreasing temperature. This result suggests that A is not a constant but a function of temperature in Cs_2ZnCl_4 and Cs_2ZnBr_4, i.e., the fluctuation of the electric field gradient $\Delta e^2Qq/h$ relating to the relaxation is increased upon cooling. A temperature depen-

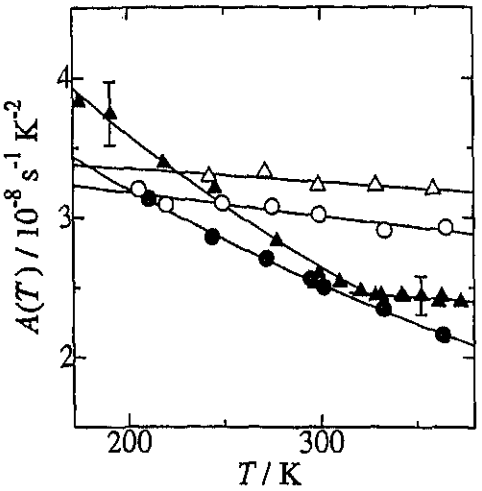

Fig. 4. Temperature dependences of $A(T)$ values in (3) obtained by substitution of ^{133}Cs NMR T_1 for Cs_2ZnCl_4 (•) and Cs_2ZnBr_4 (▲) with β-K_2SO_4 structure, and Cs_2CdI_4 (○) and Cs_2HgI_4 (△) with Sr_2GeS_4 structure. Solid lines are fitting curves assumed exponentially temperature dependenct functions.

dent A given by the relation $A(T) = T_1^{-1}T^{-2}$ derived from (3) was plotted in Figure 4. The value of the $A(T)$'s for Cs_2ZnCl_4 and Cs_2ZnBr_4 increased exponentially with increasing temperature. This anomaly in β-K_2SO_4-type compounds can be understood by considering the change of the covalency λ related to the interionic distance, and it maybe cause the anharmonicity of lattice vibrations. This temperature variation of the covalency may be related to the anomalously small ^{133}Cs chemical shift in one of the two lines observed in β-K_2SO_4-type crystals. This difference of the potential harmonicity in the β-K_2SO_4-type from that in Sr_2GeS_4-type crystals derived from crystal structures seems to be one of the reasons for the appearance of IC phase only in Cs_2MX_4 compounds with the β-K_2SO_4-type structure.

Acknowledgements

This work was partly supported by Grant-in-Aid for scientific research (B) No. 12440192 from the Ministry of Education, Science, Sports, and Culture.

[1] H. Z. Cummins, Phys. Rep. **185**, 211 (1990).
[2] F. Shimizu, T. Yamaguchi, H. Suzuki, M. Takashige, and S. Sawada, J. Phys. Soc. Japan **59**, 1936 (1990).
[3] K. S. Aleksandrov, I. N. Flerov, I. T. Kokov, A. I. Kruglik, S. V. Melnikova, and E. V. Shemetov, Ferroelectrics **79**, 137 (1988).
[4] A. A. Boguslavskii, D. L. Zagorskii, R. Sh. Lotfulin, V. I. Pakhomov, V. V. Kirilenko, and G. K. Semin, Russ. J. Inorg. Chem. **34**, 1023 (1989).
[5] E. V. Shemetov, K. S. Aleksandrov, I. P. Aleksandrova, and S. V. Primak, Phys. Status Solidi (a) **104**, K89 (1987).
[6] K. Suzuki, S. Ishimaru, and R. Ikeda, J. Phys. Soc. Japan **68**, 1963 (1999).
[7] K. Suzuki, S. Ishimaru, and R. Ikeda, Z. Naturforsch. **55a**, 339 (2000).
[8] K. Suzuki, S. Ishimaru, and R. Ikeda, J. Phys. Soc. Japan **69**, 729 (2000).
[9] O. P. Lamba and S. K. Sinha, Solid State Commun. **57**, 365 (1986).
[10] S. Plesko, P. Kind, and H. Arend, Phys. Status. Solidi (a) **61**, 87 (1980).
[11] J. A. Mcginnety, Inorg. Chem. **13**, 1057 (1974).
[12] B. Morosin and E. C. Lingafelter, Acta Crystallogr. **12**, 744 (1959).
[13] S. V. Mel'nikova and S. V. Primak, Sov. Phys. Solid State **34**, 1161 (1992).
[14] V. Touchard, M. Louër, J. P. Auffredic, and D. Louër, Rev. Chim. Min. **24**, 414 (1987).
[15] R. Sjövall and C. Svensson, Acta Crystallogr. **C44**, 207 (1988).
[16] N. F. Ramsey, Phys. Rev. **78**, 699 (1950).
[17] C. P. Slichter, Principles of Magnetic Resonance, 3rd ed., Springer-Verlag, New York 1990.
[18] T. Kanda, J. Phys. Soc. Japan **10**, 85 (1955).
[19] K. Yoshida and T. Moriya, J. Phys. Soc. Japan **11**, 33 (1956).
[20] A. Abragam, The Principles of Nuclear Magnetism, Oxford University Press, Oxford 1961.

Molecular Motions in Halogen-Bridged One-Dimensional Pt Complexes, $[Pt^{II}(en)_2][Pt^{IV}X_2(en)_2](ClO_4)_4$ (X = Cl, Br) Studied by ^2H and ^1H NMR

Noriyoshi Kimura[a], Toru Hachisuka, Yukitaka Nakano, and Ryuichi Ikeda

Department of Chemistry, University of Tsukuba, Tsukuba 305-8571, Japan

[a] Present address: Department of Chemistry, Faculty of Education, Wakayama University, Sakaedani 930, Wakayama 640-8510, Japan

Reprint requests to Dr. N. K.; Fax: 81-73-457-7515; E-mail: nkimura@center.wakayama-u.ac.jp

Z. Naturforsch. **57** a, 413–418 (2002); received February 26, 2002

Presented at the XVIth International Symposium on Nuclear Quadrupole Interactions, Hiroshima, Japan, September 9-14, 2001.

^2H and ^1H NMR measurements were performed on crystalline $[Pt(en)_2][PtX_2(en)_2](ClO_4)_4$ (X = Cl, Br), where the protonated and partially deuterated ethylenediamines (en's), $NH_2(CH_2)_2NH_2$, $NH_2(CD_2)_2NH_2$ and $ND_2(CH_2)_2ND_2$ were used as ligands. Measurements of ^2H and ^1H NMR spin-lattice relaxation times showed the presence of motions of en chelate rings at the temperatures near the phase transitions, whereas broad ^2H NMR spectra and the reported X-ray diffraction data showed no marked motions. These results were consistently explained by introducing the en puckering motion between highly asymmetric potential wells with an energy difference of 10 - 13 kJ mol^{-1}. This difference was shown to be much larger than 2 - 5 kJ mol^{-1}, reported for the iodo-complex, $[Pt(en)_2][PtI_2(en)_2](ClO_4)_4$.

Key words: Phase Transition; NMR; Spin-lattice Relaxation; Molecular Motion.

1. Introduction

Halogen-bridged mixed-valence complexes $[Pt(en)_2][PtX_2(en)_2](ClO_4)_4$ (en = ethylenediamine; X = Cl, Br, I) with a one-dimensional -X-Pt^{II}-X-Pt^{IV}-X- structure have been intensively studied because of optical [1], magnetic [2] and structural interests [3]. Characteristic electronic excitations in mixed valence states [4], and charge and spin migrations along the one-dimensional chains have been revealed. $[Pt(en)_2][PtI_2(en)_2](ClO_4)_4$ was shown to have a structural phase transition with an order-disorder type as for the conformation of "en" chelate rings at 150 - 160 K [5]. We showed from studies of ^1H and ^2H NMR spectra and spin-lattice relaxation times T_1 that the disorder of the en conformation in the high-temperature phase is not static but dynamic, where the puckering motion of Pt(en) chelate rings between δ and λ conformations was well explained by the model of two-site jumps between two asymmetric potential wells with an energy difference of 2 - 5 kJ mol^{-1} [6]. On the other hand, the above complexes with X = Cl or Br were shown to have structural phase transitions at 293.2 [7] and 297.8 K [7] for Cl and Br, respectively, where the conformations of en-chelate rings having two possible conformations δ and λ in the $Pt(en)_2$ moieties are changed from $\delta\lambda$ or $\lambda\delta$ in the low-temperature monoclinic phase ($P2_1/m$) [7] to $\lambda\lambda$ or $\delta\delta$ in the high-temperature orthorhombic phase (Ibam) [7]. This structural change, resulting in no disordered structure for the conformation of en chelate rings in the high-temperature phase, is different from that in the iodo-complex. We reported [8] ^1H NMR T_1 results in the present chloro- and bromo-complexes, and an observed T_1 decrease upon heating from *ca.* 200 K to phase transition temperatures was attributed to thermal motions. In the present study, we performed ^2H and ^1H NMR measurements on these complexes and we discuss the dynamics of the chelate rings in the neighborhood of the phase transitions in order to reveal the mechanism of the phase transition by comparing the new results with those obtained for the previous iodo-complex.

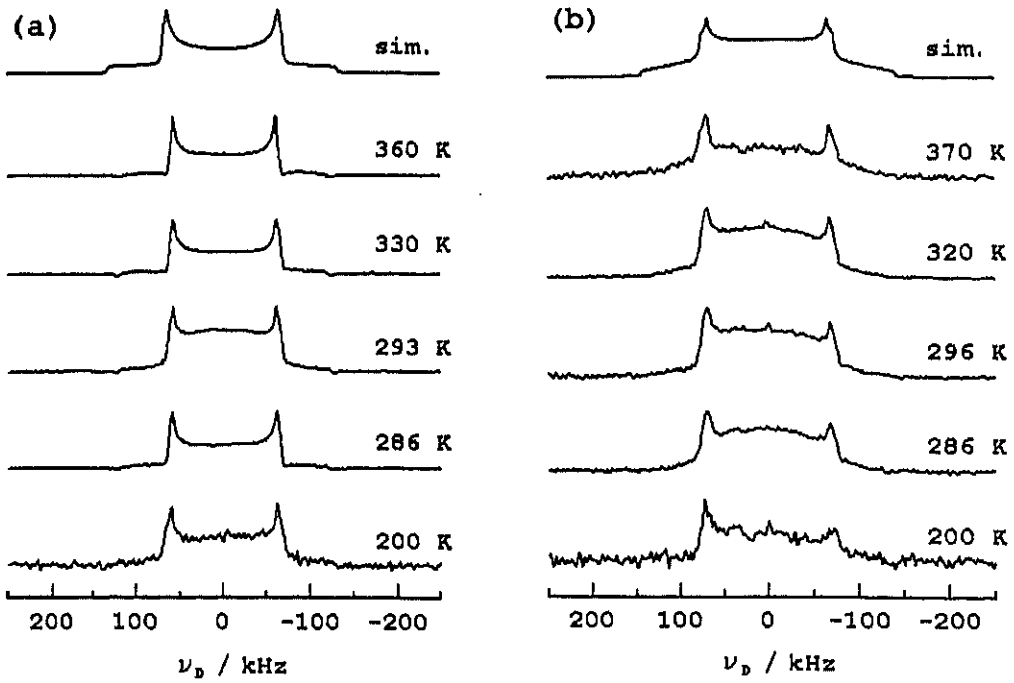

Fig. 1. Temperature dependences of ^2H NMR spectra observed in (a) $[Pt(NH_2(CD_2)_2NH_2)_2][PtCl_2(NH_2(CD_2)_2NH_2)_2](ClO_4)_4$ (**PtCl-CD**) and (b) $[Pt(ND_2(CH_2)_2ND_2)_2][PtCl_2(ND_2(CH_2)_2ND_2)_2](ClO_4)_4$ (**PtCl-ND**). The top spectra shown in (a) and (b) are simulated for the highest temperature spectra observed.

2. Experimental

$[Pt(en)_2][PtCl_2(en)_2](ClO_4)_4$ (abbreviated to **PtCl**) was prepared according to [9] and recrystallized from water at room temperature. The partially deuterated analogs, $[Pt(NH_2(CD_2)_2NH_2)_2][PtCl_2(NH_2(CD_2)_2NH_2)_2](ClO_4)_4$ (**PtCl-CD**) and $[Pt(ND_2(CH_2)_2ND_2)_2][PtCl_2(ND_2(CH_2)_2ND_2)_2](ClO_4)_4$ (**PtCl-ND**) were obtained by using ethylenediamines, $NH_2(CD_2)_2NH_2$ and $NH_2(CH_2)_2NH_2$, respectively, as the starting materials, and **PtCl-ND** repeated crystallizations from D_2O. $[Pt(en)_2][PtBr_2(en)_2](ClO_4)_4$ (**PtBr**) synthesized [9] analogously to **PtCl** was recrystallized from water.

The phase transition temperatures (T_{tr}) were determined with a Seiko Instrument DSC 120 calorimeter using sealed aluminum vessels.

The ^2H NMR spectra and spin-lattice relaxation times (T_{1D}) were observed with a Bruker MSL-300 spectrometer at a Larmor frequency of 46.051 MHz at 200 - 370 K using a VT-1000 temperature controller. The quadrupole pulse sequence [10] with a $\pi/2$ pulse width of 3.5 - 5.0 μs was employed for the spectrum measurement, and the inversion recovery method was used for the T_{1D} determination.

The ^1H NMR T_{1H} was determined with a home-made pulsed spectrometer [11] at 54.3 and 21.3 MHz, using the inversion recovery method.

3. Results and Discussion

Differential Scanning Calorimetry (DSC)

The DSC measurements revealed phase transitions at (295 ± 4), (293 ± 5) and (298 ± 3) K with transition enthalpies ΔH_{tr} of (8.8 ± 1.0), (11 ± 1.0) and (9.0 ± 1.0) kJ mol^{-1} in **PtCl**, **PtCl-CD** and **PtCl-ND**, respectively. The phase transition temperature (T_{tr}) of **PtBr** was observed at (303 ± 4) K with a ΔH_{tr} of 12 kJ mol^{-1}. The T_{tr}'s of **PtCl** and **PtBr** agree well with 293.2 [7] and 297.8 K [7], respectively, determined by measurements of the temperature dependence of lattice parameters [7].

^2H NMR in $[Pt(en)_2][PtCl_2(en)_2](ClO_4)_4$

The temperature dependences of the ^2H NMR spectra of **PtCl-CD** and **PtCl-ND** are shown in Figs. 1(a)

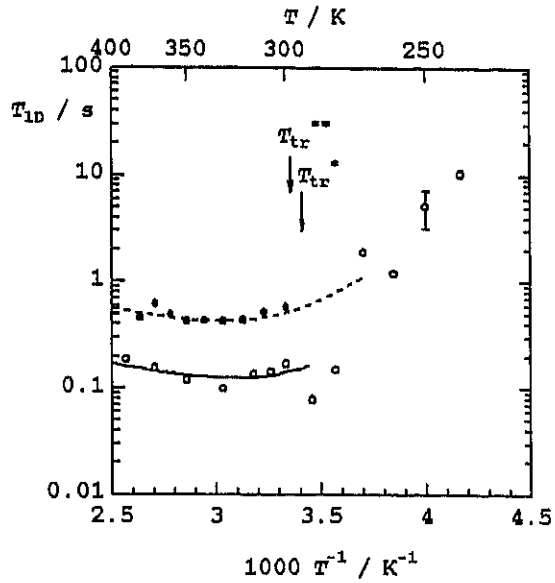

Fig. 2. ^{2}H NMR spin-lattice relaxation times (T_{1D}) in $[Pt(NH_2CD_2)_2NH_2)_2][PtCl_2(NH_2(CD_2)_2NH_2)_2](ClO_4)_4$ (**PtCl-CD**) (o) and $[Pt(ND_2(CH_2)_2ND_2)_2][PtCl_2(ND_2(CH_2)_2ND_2)_2](ClO_4)_4$ (**PtCl-ND**) (•). Broken and solid lines are the best-fitted theoretical values. T_{tr}^{*} and T_{tr}^{**} are phase transition temperatures for **PtCl-CD** and **PtCl-ND**, respectively, determined by DSC.

and (b), respectively. At 200 - 370 K both complexes yielded spectra with a small η (< 0.05) and e^2Qqh^{-1} values of (180 ± 5) and (190 ± 10) kHz for **PtCl-CD** and **PtCl-ND**, respectively. The reported data [12, 13] imply that the CD_2 and ND_2 groups are almost rigid.

The temperature dependences of ^{2}H T_{1D} in **PtCl-CD** and **PtCl-ND** are shown in Figure 2. Upon heating from *ca.* 200 K to T_{tr}, T_{1D} in **PtCl-CD** decreased. After a sudden increase at T_{tr}, T_{1D} in both **PtCl-CD** and **PtCl-ND** showed a minimum at *ca.* 320 K. This T_{1D}-minimum is expected to be connected with motions of Pt-en chelate rings, as observed in $[Pt(en)_2][PtI_2(en)_2](ClO_4)_4$ [6]. Since X-ray diffraction [7] of **PtCl** showed a change in the ethylenediamine conformations in the $Pt(en)_2$ moieties from the δ-λ or λ-δ form in the low-temperature phase to λ-λ or δ-δ in the high-temperature phase, one can assume that the δ and λ conformations have different energies. If the energy difference is much larger than the thermal energy, the above T_{1D} data are consistent with the results of ^{2}H NMR spectra with e^2Qqh^{-1} of the almost rigid CD_2 and ND_2 groups. Here, it is expected that T_{1D} is dominated by the fluctuation of the EFG caused by the puckering motion in the asymmetric double minimum potential shown in Figure 3. Using the rigid quadrupole interaction parameters of $e^2Qq_{rigid}h^{-1}$ and η_{rigid}, T_{1D} is written by assuming $\eta_{rigid} = 0$ as [14]

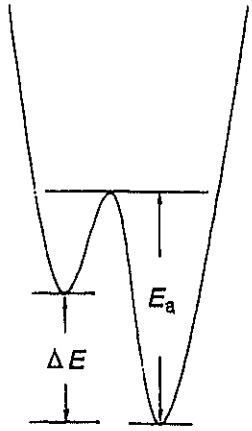

Fig. 3. The model of asymmetric potential wells used for the two-site jumps of C-D and N-D bonds.

$$\frac{1}{T_{1D}} = C_D \frac{4a}{(1+a)^2}\left[\frac{\tau_D}{1+\omega_D^2\tau_D^2} + \frac{4\tau_D}{1+4\omega_D^2\tau_D^2}\right], \quad (1)$$

$$C_D = \frac{1}{10}\left(\frac{3e^2Qq_{rigid}}{4\hbar}\right)^2 \sin^2 2\theta, \quad (2)$$

where ω_D and τ_D are the angular NMR frequency of ^{2}H and the correlation time, respectively. θ is the angle between the C-D or N-D bond and the flipping axis. The population parameter a is defined for the unequal-two-well potential in Fig. 3 as

$$a = \exp\left(\frac{\Delta E}{RT}\right). \quad (3)$$

Here ΔE is the difference between the deep and the shallow well. τ_D is written as

$$\tau_D = \frac{1}{1+a}\tau_0 \exp\left(\frac{E_a}{RT}\right), \quad (4)$$

where E_a and τ_0 are the activation energy for jumps from the deep to the shallow minimum and the correlation time at infinite temperature. The best fitted broken and solid lines in Fig. 2 were obtained using (1), (3) and (4) with C_D, ΔE, τ_0 and E_a as parameters. The determined parameters are shown in Table 1 for **PtCl-CD** and **PtCl-ND**. The 2θ values were estimated

Table 1. Motional constants (C), reductions of ^{1}H NMR second moments (ΔM_2), potential energy differences (ΔE), correlation times at the infinite temperature (τ_0) and activation energies (E_a) of the puckering motion of Pt(en) chelate rings in asymmetric potential wells in $[Pt(en)_2][PtX_2(en)_2](ClO_4)_4$ determined for ^{2}H and ^{1}H NMR relaxation times obtained in the high-temperature phase.

Compound	$C/10^9 s^{-2}$	$\Delta M_2/mT^2$	ΔE/kJ mol^{-1}	$\tau_0/10^{-13}$ s	E_a/kJ mol^{-1}
$[Pt(NH_2(CD_2)_2NH_2)_2][PtCl_2(NH_2(CD_2)_2NH_2)_2](ClO_4)_4$	62.0 ± 5	—	12.8 ± 0.5	6.6 ± 2.0	32.4 ± 1.0
$[Pt(ND_2(CH_2)_2ND_2)_2][PtCl_2(ND_2(CH_2)_2ND_2)_2](ClO_4)_4$	18.3 ± 5	—	13.0 ± 0.5	7.0 ± 1.0	32.7 ± 0.5
$[Pt(NH_2(CH_2)_2NH_2)_2][PtCl_2(NH_2(CH_2)_2NH_2)_2](ClO_4)_4$	6.1 ± 0.5	0.13 ± 0.04	13.0 ± 1.0	6.6 ± 1.0	31.7 ± 1.0
$[Pt(NH_2(CH_2)_2NH_2)_2][PtBr_2(NH_2(CH_2)_2NH_2)_2](ClO_4)_4$	6.1 ± 0.5	0.13 ± 0.04	13.0 ± 1.0	6.6 ± 1.0	31.0 ± 1.0
$[Pt(NH_2(CH_2)_2NH_2)_2][PtCl_2(NH_2(CH_2)_2NH_2)_2](ClO_4)_4$*	5.6 ± 0.5	0.12 ± 0.04	10.2 ± 1.0	1.4 ± 4.0	34.1 ± 1.0

* Low-temperature phase

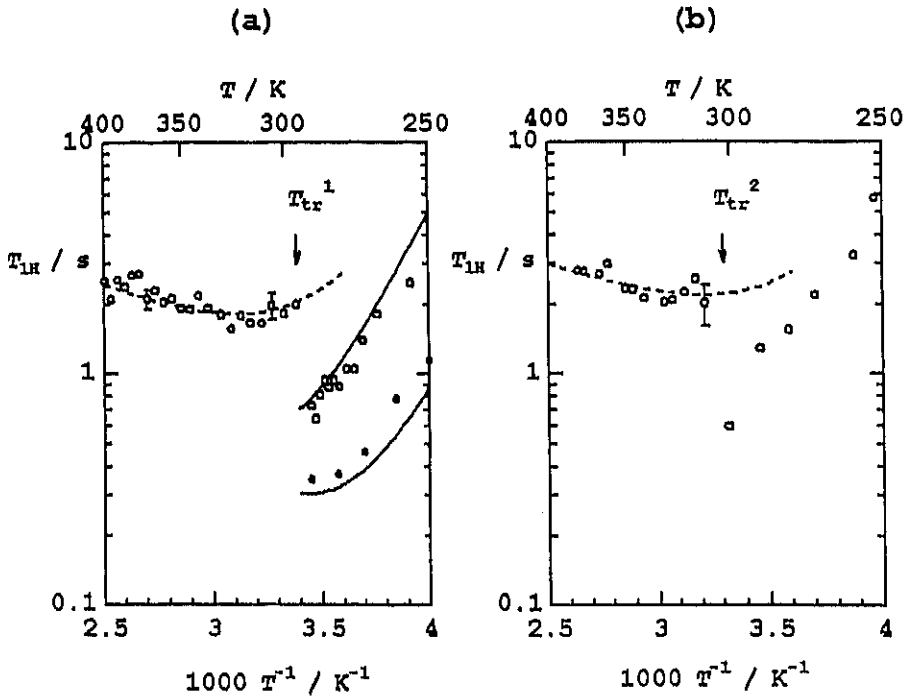

Fig. 4. ^{1}H NMR spin-lattice relaxation times (T_{1H}) observed in (a) $[Pt(en)_2][PtCl_2(en)_2](ClO_4)_4$ (**PtCl**) at Larmor frequencies of 54.3 (o) and 21.3 (•) MHz and (b) $[Pt(en)_2][PtBr_2(en)_2](ClO_4)_4$ (**PtBr**) at 54.3 MHz. Broken and solid lines are the best-fitted theoretical values. T_{tr}^1 and T_{tr}^2 are phase transition temperatures in **PtCl** and **PtBr**, respectively, determined by DSC.

to be 68 and 28.5° for **PtCl-CD** and **PtCl-ND**, respectively, from (2), using $e^2Qq_{rigid}h^{-1}$ of (180 ± 10) and (190 ± 10) kHz for **PtCl-CD** and **PtCl-ND**, respectively, given in [12] and [13]. These angles can be explained by the onset of the conformational change of en-chelate rings, because the jump angles by the conformational change between λ and δ were estimated to be *ca.* 60 and 30° for the C-D and N-D bond directions, respectively, by use of the structural data [7]. The ΔE values obtained for chloro-complexes in the present study are larger than 2 - 5 kJ mol^{-1}, determined for the iodo-complex [6]. This difference can be explained by the loose crystal packing of the iodo-complex [5, 15], which is favorable for the puckering motion. In fact, it is concluded from X-ray and neutron diffraction measurements [5, 7, 15] that the steric hindrance for the motion around en-ligands in intra-chain for iodo-complex [5, 15] is smaller than that for the chloro-complex [7]. From these reports and the present studies of ^{2}H NMR spectra and T_{1D} measure-

ments, most of the en-ligands in the chloro-complex have stable δ-λ or λ-δ and δ-δ or λ-λ conformations in the low and high-temperature phases, respectively, and the puckering motion of the en-skeleton takes place in the large asymmetric double minimum potential, but the lifetime, *i.e.*, the population of the excited state is quite low because of the high ΔE value. This asymmetric motional model is supported by the results of the ^{2}H NMR simulation spectra in **PtCl-CD** and **PtCl-ND** shown in Figure 1. We simulated the spectra in **PtCl-CD** and **PtCl-ND** for two-site jumping C-D and N-D bonds, respectively, taking place between two directions with angles of 68 and 28.5° in the same order, and between two potential wells with an energy differences of ΔE = 12.8 and 13.0 kJ mol^{-1} by applying the $e^2Qq_{\text{rigid}}h^{-1}$ = 180 and 190 kHz and the η_{rigid} = 0.05 values given above. Here, we assumed that the jumping rate at 350 K is rapid enough compared with the observed linewidth. We see that the spectra observed above room temperature are mostly reproduced by the simulation.

^{1}H NMR in $[Pt(en)_2][PtX_2(en)_2](ClO_4)_4$ (X = Cl, Br)

The temperature dependences of ^{1}H T_{1H} in **PtCl** and **PtBr** are shown in Figs. 4(a) and (b), respectively. Upon heating, T_{1H} decreased to T_{tr}, and T_{1H} showed a minimum at *ca.* 320 K in both complexes. Using the asymmetric potential model, the relaxations in the high-temperature phase can be expressed by [16]

$$\frac{1}{T_{1H}} = C_H \frac{4a}{(1+a)^2}\left[\frac{\tau_H}{1+\omega_H^2\tau_H^2} + \frac{4\tau_H}{1+4\omega_H^2\tau_H^2}\right], \quad (5)$$

$$C_H = \frac{2}{3}\gamma_H^2 \Delta M_2, \quad (6)$$

where γ_H and ΔM_2 denote the protonic gyromagnetic ratio and the reduction of M_2 by the onset of the motion in question, respectively.

The fitting calculation was performed above T_{tr}, using (3 - 6) with ΔE, τ_0, E_a and ΔM_2 as parameters. The best fitted T_1 curves are shown in Fig. 4, and the determined parameters for **PtCl** and **PtBr** are listed in Table 1.

The theoretical ^{1}H NMR M_2 values before and after the onset of ethylenediamine puckering motions were, respectively, estimated with the Van Vleck equation [17] for the rigid ethylenediamine molecules, and the following equation for the M_2(mot.) for the two-site jumps of the proton-proton vector directions [18]:

$$M_2(\text{mot.})_{ij} = \frac{9}{40}\gamma_H^2\hbar^2\left[\frac{1}{r_{jkA}^6} + \frac{1}{r_{jkB}^6} + \frac{3\cos^2\alpha - 1}{r_{jkA}^3 r_{jkB}^3}\right]. \quad (7)$$

$M_2(\text{mot.})_{jk}$, r_{jkA}, r_{jkB} and α are the motional M_2 contributed from the dipolar interaction between j-th and k-th protons, the inter-proton distance in the A and B conformations and the two-site jump angle of the vector between the j-th and k-th protons, respectively. Using the crystal structure data [7] and the standard values of bond angles and distances, we obtained M_2(rig.) = (0.228 ± 0.01) mT^2 and M_2(mot.) = (0.108 ± 0.005) mT^2. The difference between these values ΔM_2 = 0.120 mT^2 agrees well with ΔM_2 = (0.13 ± 0.04) mT^2 shown in Table 1.

Temperature dependences of ^{1}H T_{1H} of **PtCl** observed below T_{tr} are shown in Figure 4(a). We should note that the frequency dependence of T_{1H} in the low-temperature phase of **PtCl** is unexplainable by the BPP theory [19] requiring the ω^2 dependence for the low-temperature side of the minimum, but the observed T_{1H} was roughly proportional to ω. This result can be explained by introducing a jumping model between asymmetric potential wells for the two conformations of the ethylenediamine molecules. We fitted (3 - 6) to the observed data. The best fitted T_1 curves and the determined values of parameters are shown in Fig. 4(a) and Table 1, respectively. These results imply that the decrease of T_{1H} in the temperature range below T_{tr} can be attributed to the motion of the en-chelate ring.

4. Summary

From ^{2}H and ^{1}H NMR measurements, the puckering motion of Pt(en) chelate rings between the δ and λ conformations was detected in $[Pt(en)_2][PtX_2(en)_2](ClO_4)_4$ (X = Cl, Br) in the range of 250 - 400 K. The obtained temperature dependences of ^{2}H and ^{1}H NMR T_1 were explained by two-site jumps between two asymmetric potential wells with energy differences of 10 - 13 kJ mol^{-1}. These large energy differences are consistent with the observed ^{2}H spectra and the X-ray diffraction study [7] requiring ordered conformations of en-chelate rings.

Acknowledgements

The authors are grateful to the Chemical Analysis Center, University of Tsukuba, for elemental analysis. The author N. K. thanks for a JSPS Research Fellowships for Young scientists. This work was partly supported by the Grant-in Aid for scientific research No. (B) 12440192 from the Ministry of Education, Culture, Sports, Science and Technology.

[1] D. S. Martin Jr., in: Extended Linear Chain Compounds, Vol. 1, ed. J. S. Miller, Plenum Press, New York 1982, p. 409.
[2] A. Kawamori, R. Aoki, and M. Yamashita, J. Phys. C, **18**, 5487 (1985).
[3] H. J. Keller, in: Extended Linear Chain Compounds, Vol. 1, ed. J. S. Miller, Plenum Press, New York 1982, p. 357.
[4] R. J. H. Clark, in: Infrared Spectroscopy, Vol. 11, eds. R. J. H. Clark and R. E. Hester, John Wiley, New York 1984, p. 95.
[5] J.-F. Bardeau, A. Bulou, W. T. Klooster, T. F. Koetzle, S. Johnson, B. Scott, B. I. Swanson, and J. Eckert, Acta Crystallogr. **B52**, 854 (1996).
[6] N. Kimura, T. Hachisuka, Y. Nakano, and R. Ikeda, Phys. Chem. Chem. Phys. **3**, 1778 (2001).
[7] K. Toriumi, M. Yamashita, S. Kurita, I. Murase, and T. Ito, Acta Crystallogr. **B49**, 497 (1993); S. C. Huckett, B. Scott, S. P. Love, R. J. Donohoe, C. J. Burns, E. Garcia, T. Frankcom, and B. I. Swanson, Inorg. Chem. **32**, 2137 (1993).
[8] R. Ikeda, A. Ghosh, L. S. Prabhumirashi, D. Nakamura, and M. Yamashita, Mol. Cryst. Liq. Cryst. **216**, 181 (1992); N. Kimura, S. Ishimaru, H. Okamoto, M. Yamashita, and R. Ikeda, Synth. Metals **86**, 2151 (1997); N. Kimura, S. Ishimaru, R. Ikeda, and M. Yamashita, J. Chem. Soc. Faraday Trans. **94**, 3659 (1998).
[9] N. Matsumoto, M. Yamashita, and S. Kida, Bull. Chem. Soc. Japan **51**, 2334 (1978).
[10] J. H. Davis, K. R. Jeffrey, M. Bloom, M. I. Valic, and T. P. Higgs, Chem. Phys. Lett. **42**, 390 (1976).
[11] T. Kobayashi, H. Ohki, and R. Ikeda, Mol. Cryst. Liq. Cryst. **257**, 279 (1994).
[12] J. Seelig, Quart. Rev. Biophys. **10**, 353 (1977).
[13] M. J. Hunt and A. L. MacKay, J. Mag. Reson. **15**, 402 (1974).
[14] M. Mizuno, Y. Hamada, T. Kitahara, and M. Suhara, J. Phys. Chem. **103**, 4981 (1999).
[15] N. Matsumoto, M. Yamashita, S. Kida, and I. Ueda, Acta Crystallogr. **B35**, 1458 (1979); H. Endres, H. J. Keller, R. Martin, H. N. Gung, and U. Traeger, Acta Crystallogr. **B35**, 1885 (1979).
[16] D. C. Look and I. J. Lowe, J. Chem. Phys. **44**, 3437 (1966).
[17] J. H. Van Vleck, Phys. Rev. **74**, 1168 (1948).
[18] E. R. Andrew and L. Latanowicz, J. Mag. Reson. **68**, 232 (1986).
[19] A. Abragam, The Principle of Nuclear Magnetism, Oxford University Press, Oxford 1961, Chapt. VIII.

^{35}Cl Quadrupole Relaxation Study on $Cs_2[Au(I)Cl_2][Au(III)Cl_4]$ and $Cs_2[Ag(I)Cl_2][Au(III)Cl_4]$

A. Ishikawa, M. Kurasawa, K. Kurasawa, A. Sasane, R. Ikeda[a], and N. Kojima[b]

Department of Chemistry, Faculty of Science, Shinshu University, Matsumoto 390-8621, Japan
[a] Department of Chemistry, University of Tsukuba, Tsukuba 305-8751, Japan
[b] Department of Basic Science, Graduate School of Arts and Sciences, The University of Tokyo, Tokyo 153-8902, Japan

Reprint requests to Dr. A. I.; Fax: +81-263-37-2559, E-mail: ishikawa@ripms.shinshu-u.ac.jp

Z. Naturforsch. **57 a**, 348–352 (2002); received January 23, 2002

Presented at the XVIth International Symposium on Nuclear Quadrupole Interactions, Hiroshima, Japan, September 9-14, 2001.

Two ^{35}Cl NQR spin echo signals, ν_{Q1} = 17.28 MHz (Au(I)-Cl) and ν_{Q2} = 27.10 MHz (Au(III)-Cl), have been observed at 77 K from two samples of $Cs_2[Au(I)Cl_2][Au(III)Cl_4]$ prepared differently. The resonances resulted at the same frequencies but with different line widths. $Cs_2[Ag(I)Cl_2]$-$[Au(III)Cl_4]$ yielded a singlet, ν_{Q2} = 27.96 MHz, at 77 K. The three samples gave rise to ESR signals indicating the presence of paramagnetic Au(II) or Ag(II) sites with low concentration. ^{35}Cl NQR spin-lattice relaxation time T_{1Q} measurements revealed that only the reorientational motions of the anions $[Au(III)Cl_4]^-$ are exited at high temperatures.

Key words: ^{35}Cl NQR Spin-lattice Relaxation; Mixed-valence Complex; Reorientational Motion; Lattice Vibration; ESR.

Introduction

The mixed-valence complexes $M_2[Au(I)X_2]$-$[Au(III)X_4]$ (M = Rb and Cs; X = Cl, Br, and I) have attracted many workers, cf. [1]. In a previous paper [2], we reported that tetragonally distorted perovskite type $Cs_2[Au(I)Cl_2][Au(III)Cl_4]$ polycrystals yielded two ^{35}Cl NQR lines, ν_{Q1} = 17.28 and ν_{Q2} = 27.10 MHz at 77 K, in accordance with the crystal structure, I4/mmm [3 - 5]. These signals were assigned to the two kinds of Cl atoms in the crystal: ν_{Q1} to Cl-Au(I) and ν_{Q2} to Cl-Au(III). The estimate of the charge distribution in the complex anions clarified that the charge transfer interactions between the anions are weak in this mixed-valence complex.

However, there were two experimental evidences [2], possibly caused by the charge transfer effect: 1. the NQR lines ν_{1Q} and ν_{2Q} showed ten times larger width than those usually observed in the single valence Au(III) complexes [6]. 2. ESR spectra confirmed the presence of paramagnetic Au(II) sites in the crystal with an abundance of ca. 5×10^{20}/mol.

Preliminary results of ^{35}Cl quadrupole relaxation time T_{1Q} measurements indicated that the T_{1Q} of both ν_{Q1} and ν_{Q2} were governed by the lattice vibration at low temperatures. However, the T_{1Q} behavior at high temperatures remained uncertain.

The concentration of paramagnetic sites can considerably affect the NQR line width $\Delta\nu$ and T_{1Q} behavior. Therefore we have undertaken further $\Delta\nu$ and T_{1Q} measurements on the same compound, but prepared in a different manner [2], because the Au(II) concentration is expected to depend on the method of preparation. $Cs_2[Ag(I)Cl_2][Au(III)Cl_4]$ has been also prepared for NQR and ESR measurements, because the Ag(I) complex is isostructural with Cs_2-$[Au(I)Cl_2][Au(III)Cl_4]$ and is expected to have more clearly a different Au(II) site concentration.

Experimental

The NQR, ESR, and X-ray diffraction studies were performed on polycrystalline $Cs_2[M(I)Cl_2]$-$[Au(III)Cl_4]$ (M = Ag, Au). A home made pulsed

0932–0784 / 02 / 0600–0348 $ 06.00

Table 1. Lattice constants and interatomic distances of Cs_2-[M(I)Cl_2][Au(III)Cl_4] (M = Au and Ag).

Compound	*a*/pm	*c*/pm	Cl-Au(III) *L*/pm	M(I)··· ClAu(III) *L*/pm	Ref.
Sample I	748(4)	1084(8)	229.5(5)*	299(3)	
Sample II	748(5)	1084(15)	229.5(5)*	300(4)	
Sample III	737(5)	1086(10)	228.5(5)*	293(4)	
Cs_2[$AuCl_2$][$AuCl_4$]	749(2)	1087(2)	242	298	[3]
Cs_2 [$AuCl_2$][$AuCl_4$]	749.5(1)	1088.0(2)	229.5	300.5	[4, 5]
Cs_2[$AgCl_2$][$AuCl_4$]	738(2)	1101(2)	230	292	[3]

* The value is estimated from ^{35}Cl NQR frequency vs. bond length plot [2].

spectrometer [7] was used for the observation of ^{35}Cl NQR. The line shape of the resonances was determined by monitoring the spin echo amplitude dependence on the rf frequencies. The pulse sequence $\pi/2$–τ–$\pi/2$–τ_e–π was employed for the measurements of the spin-lattice relaxation time T_{1Q}, in which τ_e was set to ca. 400 μs throughout the experiments. The ESR spectra were recorded on a JEOL JES-FE1XP X-band spectrometer. The X-ray powder patterns were recorded on a model 2012 diffractometer from Rigaku Denki Co., equipped with a copper anticathode.

Two kinds of samples of Cs_2[Au(I)Cl_2]-[Au(III)Cl_4] [2] were employed for the measurements. One (**I**) was prepared by the Bridgman method [8] and recrystallized by the thermal diffusion method. The other (**II**) was prepared in a similar way as described in [9] and purified by sublimation. Cs_2[Ag(I)Cl_2][Au(III)Cl_4] (**III**) was also prepared as in [9] and used without further purification.

Results and Discussion

X-ray Diffraction and ESR

The diffraction patterns, strongly resembling each other, were observed for the samples **I**, **II**, and **III**. No impurity peaks were observed.

The one-to-one correspondence of the diffraction lines indicated that the crystals of the three samples were isostructural with the space group I4/mmm.

The determined tetragonal lattice constants *a* and *c* are given in Table 1. These values are in good agreement with those already reported [3 - 5], except the *c*-axis length of Cs_2[Ag(I)Cl_2][Au(III)Cl_4].

All the samples showed ESR. The appearance of the ESR signals evidences the presence of a small amount of d^9 paramagnetic sites in the sample crystals. Sample **I** showed a single resonance line arising from Au(II) sites with abundance of ca. 5×10^{20} mol^{-1} [2]. A similar but much weaker resonance line was observed for **II**, showing a one order of magnitude lower Au(II) concentration. The sample **III** exhibited two peaks with nearly the same intensity on the ESR spectrum. That the spectrum consists of a doublet is attributable to the existence of Ag(II) and Au(II) sites in the crystal. The paramagnetic concentration was nearly the same in **II**.

NQR Frequency and Line Width

The sample **I** showed the ^{35}Cl resonance ν_{Q1} = 17.28 MHz for Au(I)-Cl and ν_{Q2} = 27.10 MHz for Au(III)-Cl at 77 K [2]. The sample **II** yielded the same resonance frequencies as **I**, whereas **III** showed a singlet frequency ν_{Q2} = 27.96 MHz at 77 K attributable to Au(III)-Cl. Experiments to detect the ^{35}Cl NQR of Cl-Ag(I) for **III** have been unsuccessful.

Comprehensive studies have revealed the existence of strong correlations between the ^{35}Cl NQR frequency and the bond lengths C-Cl and Sn-Cl [10]. The NQR frequency vs. bond length plot in various [Au(III)Cl_4]$^-$ [2] reasonably suggests that the Au(III)-Cl bond length in **III** is 228.5 pm, which is shorter by ca. 1 pm than that in Cs_2[Au(I)Cl_2]-[Au(III)Cl_4] (Table 1). A reduction on the *a*-axis occurs when Au(I) is substituted by Ag(I). This is likely caused by the smaller ionic radius of Ag(I) resulting in a shorter inter-atomic distance Ag(I)···Cl-Au(III).

The resonance line shapes determined from ^{35}Cl spin echo intensity measurements were Lorentzian [11]. Gaussian fits to the experimental data showed clear deviations. The normalized lines are shown in Figure 1. The lines were temperature independent and much broader than $\Delta\nu_Q \sim$ 10 kHz observed for the single valence compound Cs[$AuCl_4$] [6]. The sample **I**, **II** and **III** showed full line widths of 60, 155 and 60 kHz, respectively, at half height. The line width of the sample **I** annealed at 673 K, just below the melting point, was unchanged. The thermal treatment removes adsorbed solvent molecules such as H_2O and HCl from the crystal and releases the crystal from strain. An effect of crystal imperfection, unconnected with the presence of Au(II), was not discernible in the line width of **I**. The presence of Au(II) should be an essential factor for the line broadening because such a broad

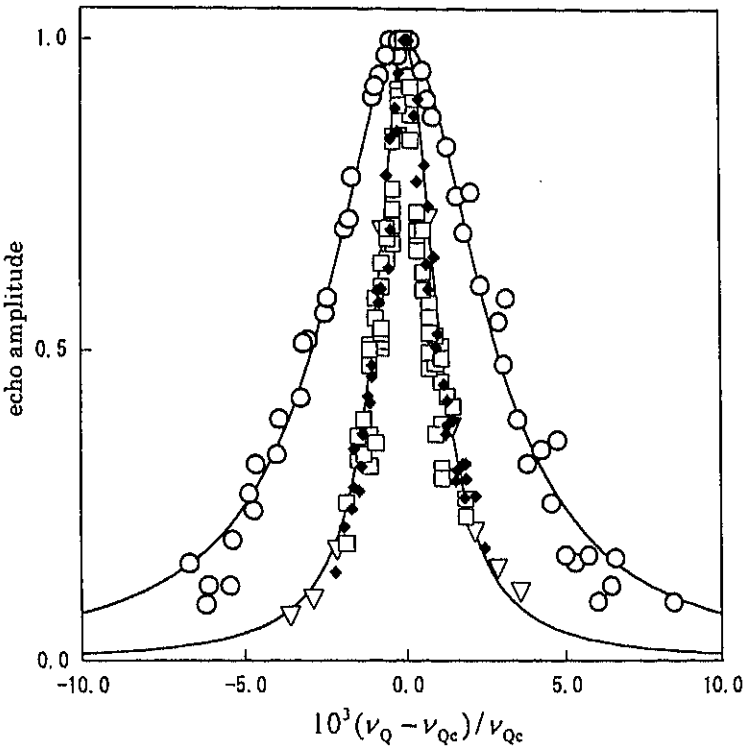

Fig. 1. Echo spectra of ^{35}Cl NQR in $Cs_2[Au(I)Cl_2][Au(III)Cl_4]$ and $Cs_2[Ag(I)Cl_2][Au(III)Cl_4]$. Solid lines represent the best fitted Lorentzian curves. ν_{Qc} is the center frequency of each resonance. ◆: ν_{Q1} for smaple I; □: ν_{Q2} for sample I, ○: ν_{Q2} for sample II, ▽: ν_{Q2} for sample III.

width has not been observed in single valence Au(III) complexes. The sample **II** yielded the widest line in spite of its lowest Au(II) site concentration of the tree samples. The problem about the origin of the line broadening has not been yet settled. At least the experimental results suggest that even a small amount of paramagnetic sites, such as ca. 5×10^{19} mol^{-1}, can contribute to the broadening effect, and the excess contents of the sites is irrelevant for this effect.

Librational Motion

The temperature dependence of the ^{35}Cl resonance frequencies is shown in Figure 2. The frequency decrease is attributable to the EFG averaging at Cl due to the librational motion of the complex anions. Since the temperature dependence of ν_Q is almost linear, we can apply the Bayer-Kushida equation in the high temperature limit [12]:

$$[\nu_Q(T) - \nu_{Q0}]/\nu_{Q0} = -\frac{3k}{2I_{eff}\omega_{eff}^2}T = -AT, \quad (1)$$

where ν_{Q0} denotes the NQR frequency at a fictitious vibrationless state. The temperature coefficient A is a librational amplitude factor which consists of the Boltzmann constant k, an effective moment of inertia I_{eff} and an effective librational frequency ω_{eff}. The values of A and ν_{Q0} which fit (1) best are summarized in Table 2. The small difference of A between **I** and **II** for ν_{Q2} falls within the experimental errors due to the broadness of the resonance lines. The large A for ν_{Q1} results from the large librational amplitude of $[Au(I)Cl_2]^-$, which has a smaller I_{eff} than $[Au(III)Cl_4]^-$. It is worth to note that ν_{Q1} showed an about four times larger A than ν_{Q2} despite the maximum moment of inertia of $[Au(III)Cl_4]^-$ is roughly two times larger than that of $[Au(I)Cl_2]^-$, when we consider the motion of the isolated complex anions. Possibly the repulsive force between the Au(I)-Cl chlorine and d_{z^2} electrons on Au(III) contributes to

Table 2. ^{35}Cl NQR frequency and librational amplitude factor A in $Cs_2[M(I)Cl_2][Au(III)Cl_4]$ (M = Au and Ag) at a fictitious vibrationless state ν_{Q0} which fit best with the Bayer-Kushida equation (1).

Sample		ν_{Q0} / MHz	$10^3 A$ / K^{-1}
I	ν_{Q1}	17.45	11.7
I	ν_{Q2}	27.16	2.82
II	ν_{Q2}	27.16	2.74
III	ν_{Q2}	28.07	5.23

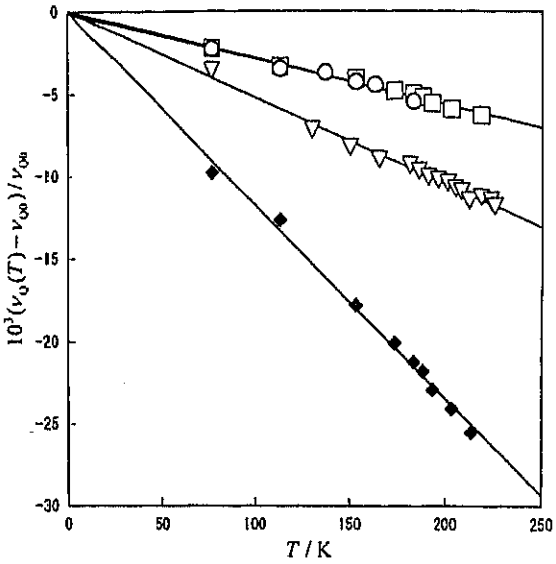

Fig. 2. Temperature dependence of ^{35}Cl NQR frequencies of $Cs_2[Au(I)Cl_2][Au(III)Cl_4]$ and $Cs_2[Ag(I)Cl_2][Au(III)Cl_4]$. The solid lines are least-squares fits of the data with the Bayer-Kushida equation (1). The resonance frequencies are normalized by the frequency ν_{Q0} at a fictitious rigid state of the lattice vibration. ◆: ν_{Q1} for sample **I**; □: ν_{Q2} for sample **I**, ○: ν_{Q2} for sample **II**, ▽: ν_{Q2} for sample **III**.

this effect through ω_{eff}. Sample **III** yielded larger A of ν_{Q2} than **I** and **II**. The $d_{x^2-y^2}$ electrons on Ag(I) will repel more strongly the Cl in $[Au(III)Cl_4]^-$ than the electrons on Au(I).

Spin-lattice Relaxation

The temperature dependence of the ^{35}Cl NQR spin-lattice relaxation times T_{1Q} is displayed in Figure 3. The T_{1Q} of ν_{Q2} for the three samples behaved similarly against temperature variation. At 77 - 180 K the T_{1Q} values were nearly proportional to T^{-2}. At 180 - 220 K, the log T_{1Q} values were proportional to $1/T$. The temperature dependence of T_{1Q} is expressed [13 - 15] by

$$T_{1Q}^{-1} = aT^n + b\exp(-E_a/RT), \qquad (2)$$

where a, n, and b are the parameters relating to the molecular motions including Cl. The first term concerns the lattice vibration and the second term the molecular reorientation over the potential barrier E_a. The motional parameters and E_a which fit best with the experimental data are listed in Table 3. The temperature dependence of T_{1Q} for ν_{Q1} also showed the

Table 3. Motional parameters a, n, b, and E_a for $Cs_2[M(I)Cl_2][Au(III)Cl_4]$ (M = Au and Ag).

Sample		$10^4 a/(s^{-1}K^{-n})$	n	$10^{-11}b/s^{-1}$	$E_a/(kJ\ mol^{-1})$
I	ν_{Q1}	1.2	2.1		
I	ν_{Q2}	1.3	2.2	1.4	34
II	ν_{Q2}	1.8	2.7	1.6	34
III	ν_{Q2}	4.0	2.1	2.4	37

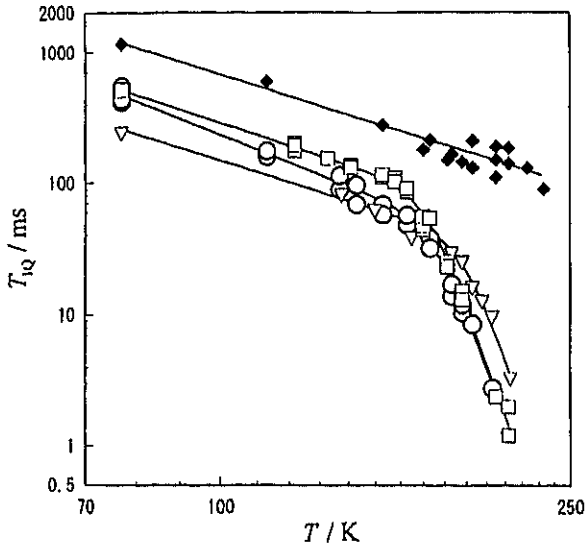

Fig. 3. Temperature dependence of the ^{35}Cl NQR spin-lattice relaxation times T_{1Q} of $Cs_2[Au(I)Cl_2][Au(III)Cl_4]$ and $Cs_2[Ag(I)Cl_2][Au(III)Cl_4]$. The solid lines represent the best fitted theoretical curve (2). ◆: ν_{Q1} for sample **I**; □: ν_{Q2} for sample **I**, ○: ν_{Q2} for sample **II**, ▽: ν_{Q2} for sample **III**.

T^{-2} behavior at lower temperatures. However, no further activation process was observed even at higher temperatures.

Relaxation Mechanism and Conservation of Gold Valence

The concentration of Au(II) for **I** was ten times larger than that for **II**. However, a similar temperature dependence of T_{1Q} was observed on both samples for ν_{2Q}. The small T_{1Q} difference arises mainly from the different values of the parameters a and n, both of which depend directly on the lattice vibration. The presence of the Au(II) site in the crystal may affect the lattice vibration, but the magnitude of the effect is unknown. In the high temperature region 180 - 220 K, the T_{1Q} values of ν_{Q1} and ν_{Q2} were fairly different. This indicates that the ^{35}Cl NQR spin-lattice relax-

ation takes place respectively within a single anion $[Au(I)Cl_2]^-$ or $[Au(III)Cl_4]^-$. The Au(II) diffusion process is not observable in the T_{1Q} behavior. The diffusion causes the jumping of electrons between $[Au(I)Cl_2]^-$ and $[Au(III)Cl_4]^-$, which will equalize the T_{1Q} of both ν_{Q1} and ν_{Q2}. As an independent relaxation mechanism, reorientation of $[Au(III)Cl_4]^-$ around the C_4 axis is responsible for the T_{1Q} of ν_{Q2} in the high temperature range. The samples I and II yielded the same E_a for the reorientation. The sample III showed a close value to those of I and II. For ν_{Q1} the lattice vibrations govern the relaxation in the whole temperature range. The temperature dependence of T_{1Q} for the three samples is well described by (2), in which only the effects of the lattice vibration and reorientational motion of the complex anions are taken into account. Furthermore, samples having different paramagnetic concentrations yielded the similar motional parameters for ν_{Q2}. Therefore it is concluded that the charge transfer interaction between the anions is unchanged and no additional formation of paramagnetic sites is allowed for these mixed-valence complexes in the temperature range studied. This conclusion is also supported by the fact that the temperature dependence of the signal intensity of the ESR signals obeyed Curie's law for I [2].

Acknowledgement

We appreciate the experimental assistance of Mr. M. Kano in recording the ESR spectra.

[1] N. Kojima, Bull. Chem. Soc. Japan **73**, 1445 (2000).
[2] A. Ishikawa, M. Kurasawa, S. Kitahara, A. Sasane, N. Kojima, and R. Ikeda, Z. Naturforsch. **53a**, 590 (1998).
[3] N. Elliot and L. Pauling, J. Amer. Chem. Soc. **60**, 1846 (1938).
[4] J. C. M. Tindemans-v. Eijndhoven and G. C. Verschoor, Mater. Res. Bull. **9**, 1667 (1974).
[5] D. Denner, H. Schulz, and H. d'Amour, Acta Cryst. **35A**, 360 (1979).
[6] A. Ishikawa, T. Asaji, D. Nakamura, and R. Ikeda, Z. Naturforsch. **44a**, 125 (1989).
[7] A. Sasane, M. Shinha, Y. Hirakawa, and A. Ishikawa, J. Mol. Struct. **345**, 205 (1995).
[8] H. Kitagawa, N. Kojima, N. Matsushita, T. Ban, and I. Tsujikawa, J. Chem. Soc. Dalton Trans. **1991**, 3115.
[9] H. L. Wells, Amer. J. Sci. **3**, 315 (1922).
[10] Al. Weiss and S. Wigand, Z. Naturforsch. **45a**, 195 (1990).
[11] K. Horiuchi, R. Ikeda, and D. Nakamura, Ber. Bunsenges. Phys. Chem. **91**, 1351 (1987).
[12] T. Kushida, G. B. Benedek, and N. Bloembergen, Phys. Rev. **104**, 1364 (1956).
[13] S. Alexander and A. Tzalmona, Phys. Rev. **A138**, 845 (1965).
[14] K. R. Jeffrey and R. L. Armstrong, Phys. Rev. **174**, 359 (1968).
[15] H. Chihara and N. Nakamura, Adv. Nucl. Quadrupole Reson. **4**, 1 (1980).

Yamada Conference LVI, the Fourth International Symposium on Crystalline Organic Metals, Superconductors and Ferromagnets
ISCOM 2001 – Abstract Number F13Mon

Substituent effect on the magnetic properties of copper coordination polymers with dithiooxamide and *N,N'*-bis-(hydroxyethyl)dithiooxamide

M. Fujishima[a*], Y. Nagao[a], R. Ikeda[a], S. Kanda[b], H. Kitagawa[a, c, d]

[a] University of Tsukuba, Department of Chemistry, Ibaraki 305-8571, Japan
[b] The University of Tokushima, Department of Chemistry, Tokushima 770-8506, Japan
[c] Japan Advanced Institute of Science and Technology, Ishikawa 923-1292, Japan
[d] PRESTO, JST, Saitama 332-0012, Japan

Tel: +81 298 53 4487; Fax: +81 298 53 4487; E-mail: mu-fuji@dmb.chem.tsukuba.ac.jp

Abstract

The magnetic properties of copper coordination polymers with dithiooxamide [H_2dtoaCu] and its substituent *N,N'*-bis-(hydroxyethyl)dithiooxamide [$(HOC_2H_4)_2$dtoaCu] have been investigated. They indicate different temperature dependence, which was analyzed by Bleaney-Bowers equation. The estimated *J* values of H_2dtoaCu and $(HOC_2H_4)_2$dtoaCu are -861 K and -594 K, respectively. The large negative *J* values are derived from intradimer antiferromagnetic coupling through the ligands. The absolute *J* value of H_2dtoaCu is larger than that of $(HOC_2H_4)_2$dtoaCu, which is considered to be due to the difference of the superexchange interaction between Cu(II) ions *via* ligands. The electronic structure of the coordination polymer is supposed to depend on the substituent groups.

Keywords: coordination polymer, magnetic susceptivility, substituent effect.

1. Introduction

These ten years many molecular scientists have explored novel functional materials using both of organic and inorganic molecules, ie., molecular photocatalyst, organic electroluminescence device, electronic conductor, ionic conductor, porous materials for gas storage and nano-sized chemical reaction. One of the merits of organic-inorganic hybrid molecular system is that it provides us with wide varieties of materials, structures, and functionalities.

Copper(II) complexes with organic ligand dithiooxamide [H_2dtoaCu] and its substituent *N,N'*-bis-(hydroxyethyl)dithiooxamide [$(HOC_2H_4)_2$dtoaCu] (Fig. 1) are amorphous two-

dimensional coordination polymers with Cu-dimeric units [1, 2]. The electrical conductivity of $(HOC_2H_4)_2$dtoaCu is increased by about nine orders of magnitude during hydrogen doping [3] and this polymer also indicates proton conduction [4]. These properties are derived from the dibasic-acid character of the ligand (Fig. 2) and the proton-coupled redox property. The electron-proton coupling like this plays an important role of energy metabolism in biological system. By the use of these properties, the new type of functional materials would be realized.

In this paper the magnetic properties of H_2dtoaCu and $(HOC_2H_4)_2$dtoaCu have been investigated in order to reveal the substituent effect of R = H to C_2H_4OH.

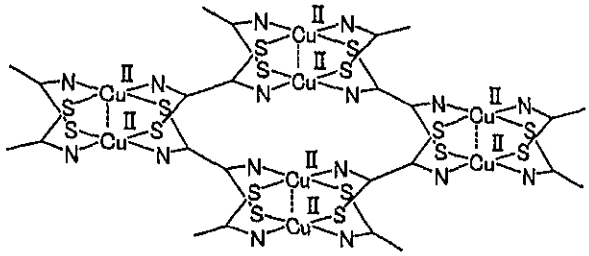

Fig. 1. Two-dimensional coordination polymer (R = H, C_2H_4OH).

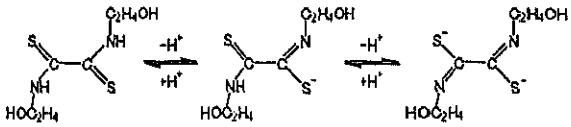

Fig. 2. Dibasic-acid character of the ligand.

2. Experimental

2.1 Synthesis

The title coordination polymers were prepared by simple mixing of ethanol solution of H_2dtoa or $(HOC_2H_4)_2$dtoa with aqueous solution of copper(II) sulfate [1, 2]. The synthesized sol was washed with water and ethanol several times and separated from the supernatant fraction with the centrifuge. The qualities of samples obtained were checked by elemental analysis and powder X-ray diffraction measurement.

2.2 Measurement

Magnetic susceptivility measurements were performed with samples dried in an evacuated desiccator. The samples were wrapped with diamagnetic materials. The temperature dependences were measured in the temperature range 2 – 300 K on a Quantum Design MPMS-5 SQUID magnetometer. The total diamagnetic contributions were subtracted after the measurement.

3. Results and Discussions

The observed molar magnetic susceptivilities per dimer unit for coordination polymers and their fitting curves are shown in Figs. 3, 4. The equation used in fitting is Eqn. (1) which consists of three terms, the first term is Bleaney-Bowers equation [5] which means a singlet-

triplet spin system, the second term, Curie-Weiss equation originated from paramagnetic impurity, and the third term, Van Vleck paramagnetism (T.I.P: Temperature Independent Paramagnetism). The abbreviations used are as follows ; N_A : Avogadro's constant, g : g-factor, μ_B : Bohr magneton, k_B : Boltzmann constant, T : temperature, J : exchange integral, N_{imp} : molecular number of impurity, S : spin angular momentum, θ : Weiss constant, $N_A\alpha$: T.I.P per mole.

$$\chi_{calc} = \frac{N_A g^2 \mu_B^2}{3k_B T}\left[1+\frac{1}{3}\exp\left(\frac{-2J}{k_B T}\right)\right]^{-1} + \frac{N_{imp} S(S+1) g^2 \mu_B^2}{3k_B (T+\theta)} + N_A\alpha \qquad (1)$$

Although the coordination forms around Cu(II) of coordination polymers are almost same [2], different temperature dependences were observed. The estimated J values of H_2dtoaCu and $(HOC_2H_4)_2$dtoaCu are -861 K and -594 K, respectively. The large negative J value is derived from intradimer antiferromagnetic coupling through the ligands. The absolute J value of H_2dtoaCu is larger than that of $(HOC_2H_4)_2$dtoaCu, which is considered to be due to the difference of the superexchange interaction between the d_{x2-y2} orbitals of Cu(II) *via* ligands. The contribution of the ligand molecular orbitals to the superexchange interaction seems to depend on the substituent groups.

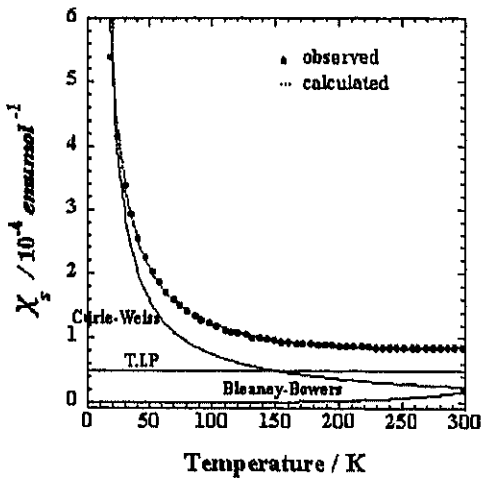

Fig. 3. Temperature dependence of the magnetic susceptivility: $[H_2dtoa]_2Cu_2$.

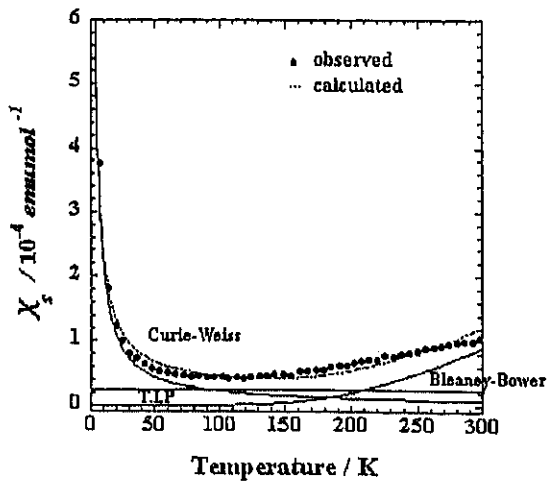

Fig. 4. Temperature dependence of the magnetic susceptivility: $[(HOC_2H_4)_2dtoa]_2Cu_2$.

The impurity concentration for H_2dtoaCu is 1.8% and that for $(HOC_2H_4)_2$dtoaCu is 0.59% from the estimation of Curie-Weiss equation. This implies that H_2dtoaCu is less crystalline than $(HOC_2H_4)_2$dtoaCu, which is consistent with the result of powder X-ray works [6].

4. Conclusion

The temperature dependences of the magnetic susceptibilities of H_2dtoaCu and $(HOC_2H_4)_2$dtoaCu were measured and the substituent effect has been discussed. Although the coordination forms around Cu(II) are almost same, the difference in J values between H_2dtoaCu and $(HOC_2H_4)_2$dtoaCu was observed. This difference is considered to be due to the difference of the superexchange interaction between Cu(II) ions *via* ligands. It may be possible to control the physical properties of the two-dimensional coordination polymer by changing substituent and to construct novel functional materials, which is under way.

5. Acknowledgements

This work was partly supported by Grant-in-Aid Scientific Researches Nos.11135211 (299: New Protium Function), 10149104 (401: Metal-Assembled Complexes), and 12046235 (407: Transition-Metal Oxides) of Priority Areas (A) from the Ministry of Education, Culture, Sports, Science and Technology of Japan, and by the Research Foundation for Materials Science.

6. References

[1] S. Kanda, K. Yamashita, K. Ohkawa, Bul. Chem. Soc. Jpn., 52 (1979) 3296.
[2] M. Fujishima, S. Kanda, T. Mitani, H. Kitagawa, Synth. Met., 119 (2001) 485.
[3] M. Fujishima et al., to be published.
[4] Y. Nagao et al., to be unpublished.
[5] Bleaney, B., Bowers, and K.D: Proc. Roy. Soc. (London) A214 (1952) 451.
[6] M. Fujishima et al., to be published.
[7] S. Kanda, A. Suzuki, K. Ohkawa, Ind. Eng. Chem. Prod. Res. Develop., 1 (1973) 12.
[8] R. D. Hartman, S. Kanda, H. A. Pohl, Proc. Okla. Acad. Sci., 47 (1968) 246.
[9] A. Suzuki, K. Ohkawa, S.Kanda, M. Emoto, S. Watari, Bul. Chem. Soc. Jpn., 48 (1975) 2634.
[10] S. Kanda, H. Mizobuchi, R. Sioda, Electroanal. Chem., 243 (1994) 375.
[11] S. Kanda, A. Son, K. Ohkawa, Chem. Soc. Jpn.,11 (1987) 2144.
[12] S. Kanda, N. Munemori, Electroanal. Chem., 1 (1989) 274.
[13] S. Kanda, Bul. Chem. Soc. Jpn., 83 (1962) 560.
[14] J. J. Girerd, S. Jeannin, Y. Jeannin, and O. Kahn, Inorg. Chem., 17 (1978) 3034.
[15] C. Chauvel, J. J. Grerd, Y. Jeannin, O. Kahn, G. Lavigne, Inorg.Chem., 18 (1979) 3015.
[16] P. Geboes, H. Hofmans, H. O. Desseyn, R. Dommisse, A.T.H.Lenstra, S.Bamidele.Sanni, J. M.M. Smits, and P.T.Beurskens, Spectrochim. Acta 43A (1987) 35.

Ab initio calculations of copper coordination polymers: H_2*dtoa*Cu and $(HOC_2H_4)_2$*dtoa*Cu (*dtoa* = dithiooxamide)

M. Fujishima[a*], R. Ikeda[a], T. Kawamura[b], H. Kitagawa[a, c]

[a]*Department of Chemistry, University of Tsukuba, Tennodai 1-1-1, Tsukuba, Ibaraki 305-8571, Japan*
[b]*Faculty of Engineering, Gifu University, Yanagido 1-1, Gifu, Gifu 501-1193, Japan*
[c]*PRESTO, JST, Honcho 4-1-8, Kawaguchi, Saitama 332-0012, Japan*

Abstract

The ab initio molecular orbital calculations were carried out to clarify the electronic states of copper coordination polymers: $(HOC_2H_4)_2$*dtoa*Cu and H_2*dtoa*Cu. The intradimer Cu-Cu distance of H_2*dtoa*Cu has been predicted to be longer than that of $(HOC_2H_4)_2$*dtoa*Cu. Lowest unoccupied and highest occupied molecular orbitals, which are composed of copper $3d_{x2-y2}$ and ligand p_σ orbitals, are considered to contribute to electrical conduction and superexchange interaction between Cu(II) ions, respectively.

Keywords: Ab initio quantum chemical method and calculations, Coordination polymer, Electrical conductivity, Magnetic susceptibility

1.Introduction

The title copper(II) complexes are two-dimensional coordination polymers which are cross-linked by organic ligands *N,N'*-bis-(hydroxyethyl)dithiooxamide $(HOC_2H_4)_2$*dtoa* [1] and dithiooxamide H_2*dtoa*, respectively (Fig. 1) [2, 3]. We have performed hydrogen doping to them by means of electrochemical method [3] and hydrogen induced properties have been investigated. As the results, it was found for $(HOC_2H_4)_2$*dtoa*Cu that the Cu(II) are reduced into the Cu(I, II) mixed-valence state during hydrogen doping [4] and the doped hydrogen atom bonds to nitrogen atom of the ligand [3]. Moreover, electrical conductivities of the polymers are much increased by nine orders of magnitude [5]. These behaviours are considered to be due to a dibasic-acid character of the ligands and a proton-coupled redox property, which is consistent with proton conduction [6-8]. From the spin susceptibilities, large negative J values were observed, which are derived from the superexchange interaction between the Cu(II) *via* ligands [9]. Since the estimated absolute J value of $(HOC_2H_4)_2$*dtoa*Cu (- 594 K) is larger than that of H_2*dtoa*Cu (- 861 K), the contribution of the ligand molecular orbitals to the superexchange interaction seems to depend on the substituent groups. In this study, to clarify the origins of electrical conduction and the superexchange interaction between the Cu(II) of these polymers, the electronic states have been investigated by ab initio MO calculations.

*M.Fujishima. Tel & fax: +81-298-53-4487;
E-mail: mufuji@dmb.chem.tsukuba.ac.jp

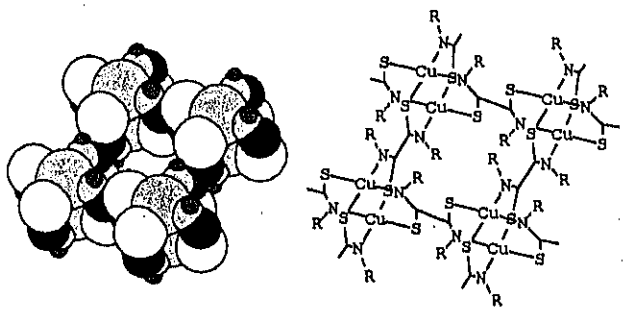

Fig. 1. Two-dimensional coordination polymer (R= C_2H_4OH or H).

2. Computational details

Since the title polymers are amorphous, the computational models were assumed as shown in Fig. 2 (i), Fig. 3 (i) which are termed respectively as follows: *cis*-$(HOC_2H_4)_2$-*dtoa*Cu; *cis*-H_2*dtoa*Cu. Their symmetry point group is C_{2h} in which sulfur and nitrogen atoms face across Cu atom. The initial geometrical parameters are taken from the EXAFS data as shown in Table 1 [5]. The optimized geometrical parameters of $(HOC_2H_4)_2$*dtoa* were used for *cis*-$(HOC_2H_4)_2$*dtoa*Cu, and typical values of analogous copper complex are used for other parameters [10, 11].

Ab initio MO calculations of the singlet basis states for these models were carried out by using one of the DFT method, hybrid B3LYP with basis sets: LANL2DZ for copper atoms, 6-31G for other atoms. The geometries of studied models were fully optimized with tight convergence criteria. All calculations were performed with the Gaussian 98 program package [12].

3. Results and discussion

The initial and optimized geometrical parameters of the polymers are summarized in Table 1. The calculations have predicted that the intradimer Cu-Cu distance of *cis*-H_2*dtoa*Cu is longer than that of *cis*-$(HOC_2H_4)_2$*dtoa*Cu. Moreover, contributions of ligand molecular orbitals to HOMOs are large as shown in Fig. 2 (ii) and Fig. 3 (ii). These would indicate that Cu atoms do not interact directly, but are coupled through the ligands. That is to say, the superexchange interaction occurs between the Cu(II) $3d_{x2-y2}$ orbitals *via* ligand p_σ orbitals, in which the substituent groups of ligands seem to effect the contribution of the ligand molecular orbitals to the superexchange interaction [9].

Table 1 Initial and optimized geometrical parameters of *cis*-$(HOC_2H_4)_2$*dtoa*Cu and *cis*-H_2*dtoa*Cu

	cis-$(HOC_2H_4)_2$*dtoa*Cu		*cis*-H_2*dtoa*Cu	
/ Å	initial	optimized	initial	optimized
r(Cu-Cu)	2.61	2.61	2.60	2.70
r(Cu-S)	2.21	2.47	2.21	2.44
r(Cu-N)	1.99	2.07	1.98	2.04

The LUMOs of the polymers composed of Cu(II) $3d_{x2-y2}$ and ligand p_σ orbitals are shown in Fig. 2 (iii) and Fig. 3 (iii). The increase of electrical conductivity on hydrogen doping [5] is considered to be due to these LUMOs' electronic state, *i.e.*, electronic conduction bands composed of these LUMOs become to be filled on hydrogen doping.

HOMO-LUMO energy separation for *cis*-$(HOC_2H_4)_2$-*dtoa*Cu is predicted to be smaller than that for *cis*-H_2*dtoa*Cu as shown in Fig. 4. (a), (b). Furthermore, d_{x2-y2}-d_{x2-y2} orbitals of HOMO and LUMO for *cis*-$(HOC_2H_4)_2$*dtoa*Cu_2 are symmetric and antisymmetric, respectively, in contrast to those for *cis*-H_2*dtoa*Cu are antisymmetric and symmetric. These might cause differences of electrical conductivity and magnetic susceptibility between polymers.

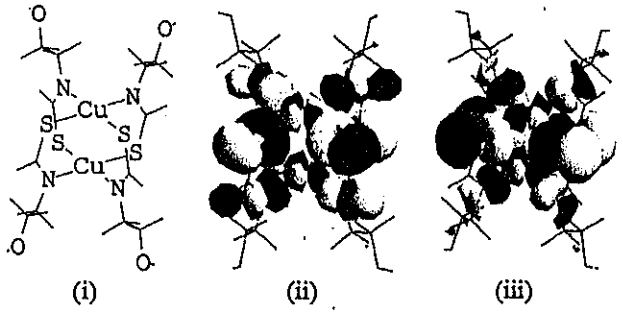

Fig. 2. (i) Computational model, (ii) HOMO and (iii) LUMO of *cis*-$(HOC_2H_4)_2$*dtoa*Cu.

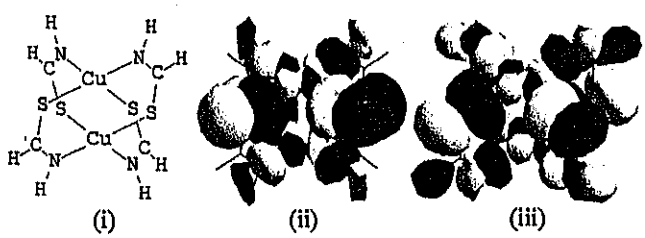

Fig. 3. (i) Computational model, (ii) HOMO and (iii) LUMO of *cis*-H_2*dtoa*Cu.

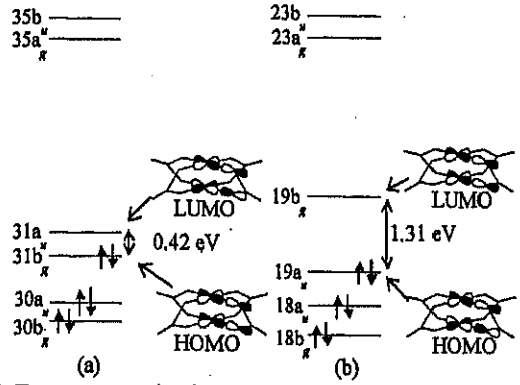

Fig. 4. Energy separation between HOMO and LUMO, and several upper and lower orbitals for (a) *cis*-$(HOC_2H_4)_2$*dtoa*Cu and (b) *cis*-H_2*dtoa*Cu.

4. Conclusion

The ab initio MO calculations were carried out to clarify the electronic states of $(HOC_2H_4)_2$*dtoa*Cu and H_2*dtoa*Cu. The intradimer Cu-Cu distance of H_2*dtoa*Cu has been predicted to be longer than that of $(HOC_2H_4)_2$*dtoa*Cu. The electrical conduction and the superexchange interaction between Cu(II) ions are considered to be derived from HOMOs and LUMOs, which are composed of copper $3d_{x2-y2}$ and ligand p_σ orbitals.

5. Acknowledgements

This work was partly supported by Grant-in-Aid Scientific Researches No. 13874081 of Exploratory Research, No. 11640559 of (C), and No. 10149104 (401: Metal-Assembled Complexes) of Priority Areas (A) from the Ministry of Education, Culture, Sports, Science and Technology of Japan, and by the grant program of Yazaki Memorial Foundation for Science & Technology.

6. References

[1] P. Geboes, H. Hofmans, H. O. Desseyn, R. Dommisse, A.T.H.Lenstra, S.Bamidele.Sanni, J. M.M. Smits, and P.T.Beurskens, *Spectrochim. Acta.* 43A (1987) 35.
[2] S. Kanda, A. Suzuki, K. Ohkawa, *Ind. Engin. Chem. Prod. Res. Develop.* 12 (1973) 88.
[3] M. Fujishima, S. Kanda, T. Mitani, H. Kitagawa, *Synth. Met.* 119 (2001) 485.
[4] M. Fujishima et al., *Mol. Cryst. & Liq. Cryst.* in press.
[5] M. Fujishima et al. to be published.
[6] S. Kanda, F. Yamamoto, *Bul. Chem. Soc. Jpn.* 69 (1996) 477.
[7] Y. Nagao et al., *Synth. Met.* in press.
[8] Y. Nagao et al., *Mol. Cryst. & Liq. Cryst.* in press.
[9] M. Fujishima et al., *Synth. Met.* in press.
[10] J. J. Girerd, S. Jeannin, Y. Jeannin, and O. Kahn, *Inorg. Chem.* 17 (1978) 3034.
[11] C. Chauvel, J. J. Grerd, Y. Jeannin, O. Kahn, G. Lavigne, *Inorg.Chem.* 18 (1979) 3015.
[12] M. J. Frisch, G. W. Trucks, H. B. Schlegel, G. E. Scuseria, M. A. Robb, J. R. Cheeseman, V. G. Zakrzewski, J. A. Montgomery, Jr., R. E. Stratmann, J. C. Burant, S. Dapprich, J. M. Millam, A. D. Daniels, K. N. Kudin, M. C. Strain, O. Farkas, J. Tomasi, V. Barone, M. Cossi, R. Cammi, B. Mennucci, C. Pomelli, C. Adamo, S. Clifford, J. Ochterski, G. A. Petersson, P. Y. Ayala, Q. Cui, K. Morokuma, P. Salvador, J. J. Dannenberg, D. K. Malick, A. D. Rabuck, K. Raghavachari, J. B. Foresman, J. Cioslowski, J. V. Ortiz, A. G. Baboul, B. B. Stefanov, G. Liu, A. Liashenko, P. Piskorz, I. Komaromi, R. Gomperts, R. L. Martin, D. J. Fox, T. Keith, M. A. Al-Laham, C. Y. Peng, A. Nanayakkara, M. Challacombe, P. M. W. Gill, B. Johnson, W. Chen, M. W. Wong, J. L. Andres, C. Gonzalez, M. Head-Gordon, E. S. Replogle, and J. A. Pople, Gaussian, Inc., Pittsburgh PA, 2001.

A study on hydrogen adsorption of polymer protected Pt nanoparticles

Yuko Isobe[a], Miho Yamauchi[a*], Hiroshi Kitagawa[a], and Ryuichi Ikeda[a]

[a] *Department of Chemistry, University of Tsukuba, Tennodai 1-1-1, Tsukuba 305-8571, Japan*

Received 2002; accepted 2002

Abstract

Monodispersed Pt nanoparticles protected with poly(*N*-vinyl-2-pyrrolidon) were synthesized from H_2PtCl_6 by the methanol reduction. The structure of obtained nanoparticles was shown to be analogous to that in bulk crystals, and the particle size was determined to be 3.2±0.7 nm from the observation of TEM images. Hydrogen adsorption into particles was investigated by observing PCT curves repeatedly measured at 303 K. From the result of PCT measurements, the amount of absorbed hydrogen in the present size-controlled nanoparticles was found to be more than that in Pt black.

Keywords : Pt nanoparticles, hydrogen absorption, PCT curve,

1. Introduction

Size-controlled metal nanoparticles are one of excellent candidates for wide ranges of applications such as hydrogen cells, the preparation of high-purity hydrogen, practical hydrogen adsorbents, etc. Since the proportion of activated atoms on the surface increases with decreasing the size of particles, the more absorption of hydrogen is expected with decreasing the particle size from in bulk metal. It is also possible that their physical properties are continuously changed according to their diameter[1], because the electronic state and amounts of absorbed hydrogen should depend on their size. No systematic works have, however, been reported on hydrogen uptakes into metal nanoparticles with diameters of several nm and not attached to any substances such as zeolite.

In the present study, we intended to synthesize monodispersed Pt nanoparticles and evaluate hydrogen absorption behavior from measurements of TEM images, X-ray diffraction, and PCT curves.

2. Experimental

According to the literature[2,3], Pt nanoparticles protected with poly(*N*-vinyl-2-pyrrolidon) (abbreviated to PVP) were prepared from $H_2PtCl_6 \cdot 6H_2O$ by the methanol reduction in ultrapure water. Using a Hitachi H-7100 electron microscope, transmission microscopy (TEM) images of prepared nanoparticles were observed with an acceleration voltage of 125 keV and 400,000 magnification, and their average diameter and distribution were determined.

X-ray diffraction patterns were observed at KEK with an 84.949 pm radiation from SOR. Samples for measurements were made by putting Pt nanoparticles into glass capillaries under H_2 gas pressures of 0, 200, 500 and 760 torr and sealed. PCT curves were measured at 303 K with a Belsorp 18 gas adsorption system from Japan.Bel.Co.

3. Results and Discussions

3.1.TEM image

A TEM image of prepared PVP protected Pt nanoparticles is shown in Fig. 1. It was shown that almost the constant size of particles was obtained. As shown in Fig. 2, the obtained size distribution of particles was seen to be

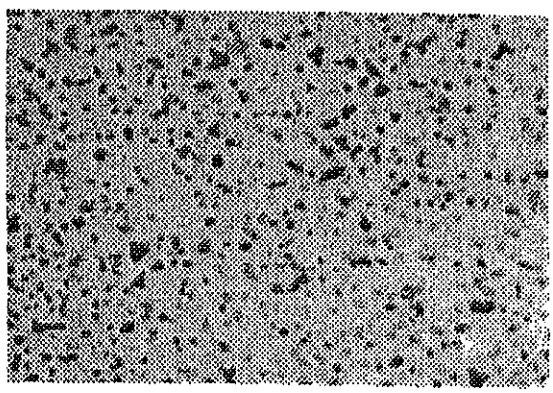

Fig. 1. TEM image of PVP protected Pt nanoparticles (×400,000).

* Corresponding author. Tel: +81(Japan)-298-53-4487; fax: +81(Japan)-298-53-4487; E-mail: yamauchi@chem.tsukuba.ac.jp

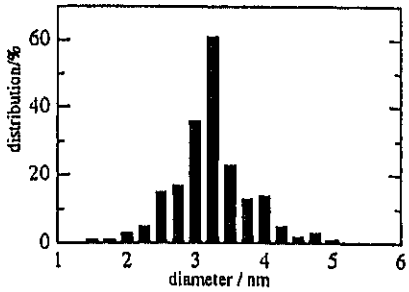

Fig.2 Size distribution obtained from TEM photographs of PVP protected Pt nanoparticles

narrow, and this indicates that monodispered nanoparticles were properly synthesized. The averaged size of particles was determined to be 3.2±0.6 nm from the figure.

3.2 Xray-diffraction

The dependence of diffraction peaks from (220) in PVP protected nanoparticles upon the H_2 pressure is shown in Fig. 3. Since the obtained Pt nanoparticles with and without H_2 gas showed an analogous X-ray diffraction patterns as in bulk Pt. This implies that Pt nanoparticles with an averaged diameter of 3.2 nm have the same fcc structure as in bulk Pt. However, the peak of the nanoparticles with H_2 gas was shown to be shifted to lower angles compared with that of bulk Pt. This result suggests that the crystalline lattice of nanoparticles is expanded compared with in bulk Pt. The peak in particles exposed to 500 torr H_2 pressure is shifted to an angle lower than that of 0 torr H_2 pressure. The top with 760 torr H_2 gas was shifted more to a lower angle than peakes in the other samples. These results imply that hydrogen is not only adsorbed on the surface of Pt nanoparticles but also absorbed into inside of the particles.

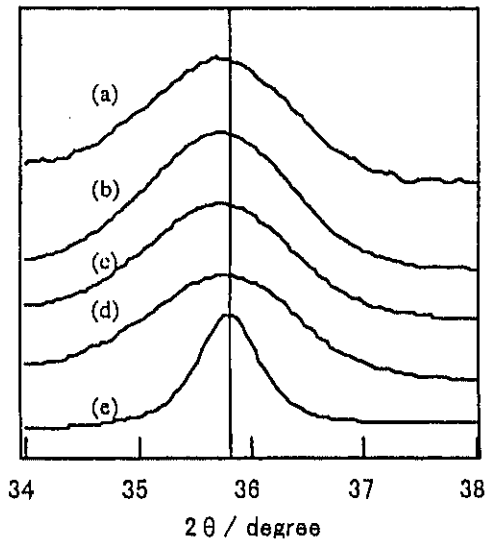

Fig 3. H_2-pressure dependence of X-ray diffraction patterns. Observed peaks indicate (220) diffractions obtained at (a) PVP protected Pt nanoparticles under H_2 gas of 760 torr, (b)500 torr, (c)200 torr, (d) PVP protected Pt nanoparticles without H_2 gas and (e)Pt black without H_2 gas. The central vertical line indicates the center of the peak of Pt black.

3.3 PCT curve

The H_2 pressure-composition isotherms (PCT curves) of PVP protected Pt nanoparticles repeatedly measured are shown in Fig. 4. The result of the mearsurement on Pt black is also indicated by a bold curve. In the first measurement of nanoparticles, its hydrogen uptake was larger than that in Pt black. This indicates that the present mono-dispersed Pt nanoparticles with a diameter of 3.2 nm can absorb a larger amount of hydrogen than bulk Pt.

Below ca. 75 torr, the hydrogen composition increased rapidly in the first and repeated PCT measurements on nanoparticles. Similar behavior was also observed in the Pt black. Above ca. 75 torr, the hydrogen composition increased linearly in curve (a), while this increase was never observed in Pt black, *i.e.*, the hydrogen composition in the Pt black was nearly constant above 100 torr. As seen from curves (b) and (c), this linear increase of composite was maintained in the repeated scanning. Since Pt black is known to adsorb hydrogen only on its surface, the behavior under ca. 75 torr observed in nanoparticles can be regarded as the surface adsorption of hydrogen. However, the linearly increasing parts in nanoparticles cannot be observed in PCT curves on Pt black. Accordingly, this increase observed in nanoparticles implies the existence of the other absorbing positions or mechanisms different from that in Pt black. Considering the result of XRD, PCT data suggest that hydrogen can be adsorbed inside of nanoparticle, but this absorbing sites are not determined in the present stage.

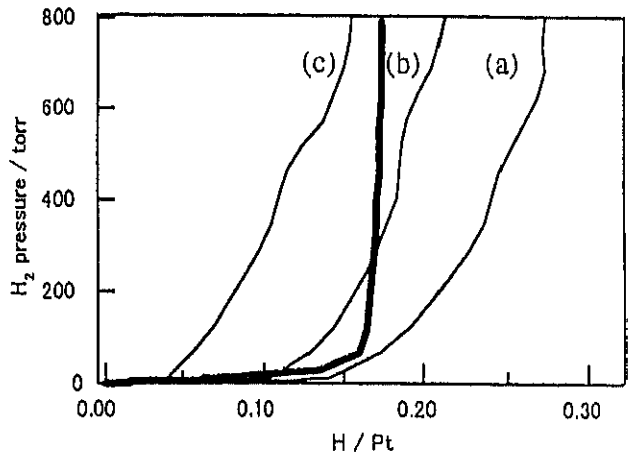

Fig. 4. Hydrogen pressure-composition isotherms (PCT curves) of PVP protected Pt nanoparticles measured (a)first, (b)second, and (c)third runs of scanning. The bold curve indicates data on Pt black.

References

[1] T. Teranishi, H. Hori, and M. Miyake, *J. Phys. Chem.* **B101** (1997)5774.
[2] T. Teranishi, M. Hosoe, T. Tanaka, and M. Miyake, *J. Phys. Chem.* B103 (1999) 388.
[3] T. Teranishi, and M. Miyake, *Hyomen*, 35 (1997) 439.

Electron Spin Dynamics in a Spin 1/2 One-Dimensional Heisenberg Antiferromagnet $[CuX_2(AdH^+)_2]X_2$

Shinya Takaishi[a*], Yuji Furukawa[b], Ken-ichi Kumagai[b], and Ryuichi Ikeda[a]

[a]*Department of Chemistry, University of Tsukuba, Tsukuba 305-8571, Japan*

[b]*Division of Physics, Graduate School of Science, Hokkaido University, Sapporo 060-0810, Japan*

Abstract

Electron spin dynamics on a spin 1/2 one-dimensional Heisenberg antiferromagnet, $[CuX_2(AdH^+)_2]X_2$ (X : Cl, Br ; Ad : adenine) was studied by ^1H NMR spin-lattice relaxation measurement. ^1H T_1 of $[CuBr_2(AdH^+)_2]Br_2$ (J = 52.6 K) in the low-temperature region below 25 K was well described by the spin fluctuation relaxation theory proposed by Sachdev.

Keywords: nuclear magnetic resonance, one-dimensional, Heisenberg antiferromagnet,

1. Introduction

It has been shown that one-dimensional (1-D) systems consisting of paramagnetic spins of small spin quantum numbers with antiferromagnetic interactions can form no ordered state at finite temperatures, but a fluctuated spin state of quantum mechanical origin. In recent years, theoretical studies of quantum spin dynamics have been extensively made on an S=1/2 1-D Heisenberg antiferromagnetic system that will be expected to show a strong quantum effect. The theoretical temperature dependence NMR spin-lattice relaxation time (T_1) on this system at low temperatures was proposed by Sachdev[1], who proposed an analytical expression of its temperature dependence.

In the present study, we measured ^1H NMR T_1 on a 1-D antiferromagnetic spin system $[CuBr_2(AdH^+)_2]Br_2$ (Ad : Adenine) with a large exchange interaction: J = 52.6 K and a corresponding chloro-complex with J = 10.9 K[2] in order to confirm the validity of Sachdev's treatment.

2. Experimental

Polycrystalline samples of $[CuX_2(AdH^+)_2]X_2$ were prepared as described in literature[2]. Prepared crystals were identified by the elemental analysis and SQUID susceptibility measurement.

The ^1H NMR spin-lattice relaxation time T_1 was measured by a Bruker SXP100 pulsed NMR spectrometer using the inversion recovery method with a homemade temperature controller in a range 100-300 K. A homemade pulsed spectrometer applying the same pulse sequence was used in a range 4.2-100 K using an Oxford CF1200 cryostat. For the measurement below 4.2 K, an NMR spectrometer and a cryostat made in Hokkaido University was used. The sample temperature was controlled and determined within ±1 and ±0.1 K, above and below 100 K, respectively. All T_1 measurements were made at a Larmor frequency of 50.4 MHz.

3. Results and Discussions

The temperature dependence of ^1H NMR T_1 observed in $[CuBr_2(AdH^+)_2]Br_2$ is shown in Fig. 1. In the

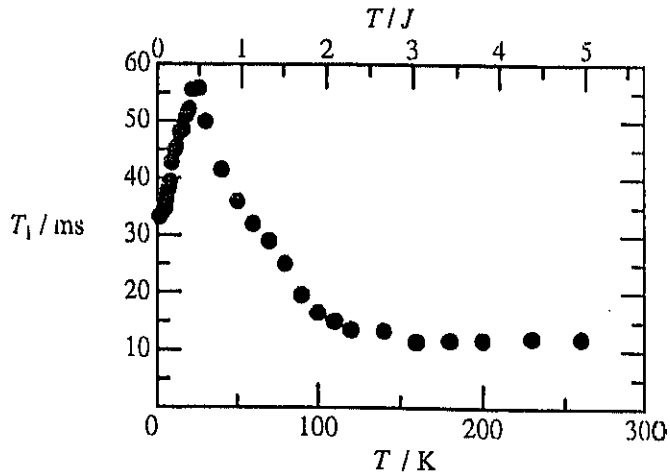

Fig. 1 Temperature dependence of ^1H NMR spin - lattice relaxation time T_1 observed in $[CuBr_2(AdH^+)_2]Br_2$

*Corresponding author. Tel & Fax: +81-298-53-4487;
E-mail: takaishi@ipchemgw.chem.tsukuba.ac.jp

NMR relaxation measurement, the ^{1}H magnetization observed after a $\pi/2$ pulse plotted against the pulse interval τ showed a single-exponential and non-exponential decay above and below *ca.* 100K ($\approx 2J$), respectively. We roughly evaluated T_1 from the initial linear portion of the decay. This short T_1 component was the main part of the ^{1}H magnetization in the whole temperature range where the non-exponential decay was observed.

Above 150 K, ^{1}H T_1 of $[CuBr_2(AdH^+)_2]Br_2$ gave temperature independent values. In this temperature range, almost free paramagnetic spins of Cu^{2+} are responsible for the proton spin-lattice relaxation. By assuming the dipolar relaxation process, powder averaged relaxation rate is presented as follows[3][4]:

$$J = \frac{T_1\hbar}{Z}\sum\frac{20}{15}\frac{1}{r^6}\gamma_H{}^2\mu_B{}^2 g^2 S(S+1), \qquad (1)$$

where γ_H is the gyromagnetic ratio of the ^{1}H spin, μ_B is the Bohr magneton, g is the spectroscopic splitting factor, r is the distance from a paramagnetic site to respective proton sites, and Z is the number of the nearest neighbors of a paramagnetic ion (1-D system, $Z = 2$). We substituted the observed temperature independent T_1 value (=12 ms) and respective r values evaluated from the structural data[5], and we obtained J in the order of 10K, being consistent with the evaluated value from the susceptibility measurement.

In the temperature range $25 < T < 150$ K, it is noted that T_1 increased with decreasing temperature. In this intermediate range where the exchange interaction becomes comparable to the thermal energy, we can expect the occurring of partial ordering of antiferromagnetically coupled spins.

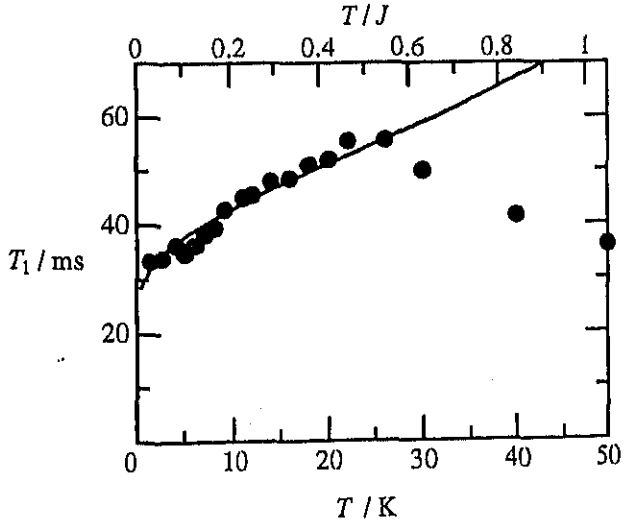

Fig. 2 Temperature dependence of ^{1}H NMR spin - lattice relaxation time T_1 observed in $[CuBr_2(AdH^+)_2]Br_2$. Solid line is theoretically calculated by the Sachdev's treatment

Fig. 2 shows a temperature dependence of ^{1}H NMR T_1 in $[CuBr_2(AdH^+)_2]Br_2$ observed below 50 K. T_1 became short with decreasing temperature below 25 K. Sachdev proposed[1] that T_1 in the range $T < 0.5J$ is expressed as

$$T_1 \propto \ln^{1/2}(2J/T), \qquad (2)$$

where J is defined by $H = 2J\,\Sigma S_i S_{i+1}$ giving finite T_1 values at low temperatures. Using the reported $J = 52.6$ K[2], we evaluated a theoretical temperature dependent T_1 curve as shown in Fig. 2, which could well reproduce the experimental result.

Fig. 3 shows a temperature dependence of ^{1}H NMR T_1 observed in $[CuCl_2(AdH^+)_2]Cl_2$. T_1 showed the maximum at $0.5J$ and became constant at temperatures above $3\sim4J$. This result can be understood analogously to those in the bromo-complex by applying a small J value of 10.9 K implying the validity of the above T_1 analysis.

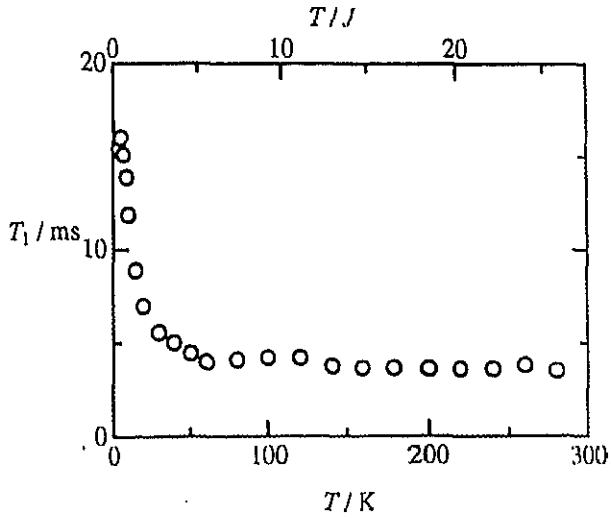

Fig. 3 Temperature dependence of ^{1}H NMR spin - lattice relaxation time T_1 observed in $[CuCl_2(AdH^+)_2]Cl_2$

Acknowledgement

This work was partly supported by Grant-in Aid for Scientific Research No.(B) 12440192 from the Ministry of Education, Culture, Sports, Science and Technology of Japan.

References

[1] S. Sachdev, *Phys. Rev.*, B50, 13(1984).

[2] D. B. Brown, J. W. Hall, H. M. Helis, E. G. Walton, D. J. Hodgson, and W. E. Hatfield, *Inorg. Chem.*, 16, 11(1977).

[3] H. Rager, Z. *Naturforsch*, 36a, 637(1981).

[4] A. Birkeland and I. Svare, *Physica Scripta*, 18, 154(1978).

[5] P. de Masser and A. C. Seapski, *J. C. S. Dalton*, 424(1973).

^{129}I Mössbauer spectroscopic study of a one-dimensional halogen-bridged binuclear complex, $Pt_2(dtp)_4I$ ($dtp = C_2H_5CS_2^-$)

Atsushi Kobayashi [a], Hiroshi Kitagawa [a], Ryuichi Ikeda [a], Shinji Kitao [b] and Makoto Seto [b]

[a] *Department of Chemistry, University of Tsukuba, 1-1-1 Tennodai, Tsukuba 305-8571, Japan*

[b] *Research Reactor Institute, Kyoto University, Kumatori, Sennan, Osaka 590-0494, Japan*

Abstract

^{129}I Mössbauer spectroscopic measurement was made for the title complex to investigate the insulating phase below a metal-insulator transition (T_{MI} = 205 K). Two chemically independent sites of iodine were observed, suggesting that the insulating phase is in alternate charge-polarization state of $-Pt^{2+}$-Pt^{3+}-I-Pt^{3+}-$Pt^{2+}-I-Pt^{2+}$-Pt^{3+}-I-Pt^{3+}-$Pt^{2+}-I-$.

Keywords: Mössbauer spectroscopy, Metal-insulator transition, MMX-Chain

1. Introduction

One-dimensional halogen-bridged binuclear-metal complexes, the so-called MMX-Chains, have drawn much attention as a dynamical electronic system [1-3]. The MMX-Chain possesses the charge degree of freedom in dimer-unit and therefore four possible charge-ordering states are expected as follows:

(1) Averaged-valence state: -$\boxed{M^{2.5+}\text{-}M^{2.5+}}$-X-$\boxed{M^{2.5+}\text{-}M^{2.5+}}$-X-

(2) Charge-density-wave state: -$\boxed{M^{2+}\text{-}M^{2+}}$-X-$\boxed{M^{3+}\text{-}M^{3+}}$-X-

(3) Charge-polarization state: -$\boxed{M^{2+}\text{-}M^{3+}}$-X-$\boxed{M^{2+}\text{-}M^{3+}}$-X -

(4) Alternate charge-polarization state:

-$\boxed{M^{2+}\text{-}M^{3+}}$-X-$\boxed{M^{3+}\text{-}M^{2+}}$-X-

The title complex exhibits many interesting properties such as metallic transport with effectively half-filled d_σ^* (i.e $(5dz^2\text{-}5dz^2)^*$) conduction band, metal-insulator transition (T_{MI} = 205 K) keeping the spin degree of freedom, and so on [4]. While the metallic phase above T_{MI} is found to be in the averaged-valence state (1) with $2k_F$ fluctuation of (2) or (4) [4], the low-temperature insulating phase has not yet been made clear. ^{129}I Mössbauer spectroscopy is very sensitive to the charge distribution around iodine, so that we could obtain information on the Pt charge state through ^{129}I. In this paper, we discuss the charge-ordering mode in $Pt_2(dtp)_4I$ from ^{129}I Mössbauer spectroscopy.

Tel: +81-298-53-4487; Fax: +81-298-53-4487;

E-mail: akobayas@dmb.chem.tsukuba.ac.jp

2. Experimental

The sample for Mössbauer spectroscopy with iodine was synthesized as a black-violet luster powder using radioisotope ^{129}I (19.9 mg) in a draft chamber of KUR by the following chemical reactions;

$$2Na^{129}I + NaSO_3 + 2H_2O_2 + H_2SO_4 \rightarrow 2Na_2SO_4 + 3H_2O + {}^{129}I_2$$

$$Pt_2(dtp)_4 + {}^{129}I_2 \rightarrow Pt_2(dtp)_4{}^{129}I_2$$

$$Pt_2(dtp)_4 + Pt_2(dtp)_4{}^{129}I_2 \rightarrow Pt_2(dtp)_4{}^{129}I$$

Mössbauer spectroscopic measurement of a 27.7 keV γ-ray transition in ^{129}I was carried out with both source and absorber cooled down to 11 K by using a constant-acceleration spectrometer with a NaI(Tl) scintillation counter and a DAIKIN CryoKelvin closed-cycle refrigerator system employing helium gas as a working medium. A ^{129}Te source was obtained by neutron irradiation of enriched $Mg_3{}^{128}TeO_6$ due to the nuclear reaction ^{128}Te[n, γ]^{129m}Te in the Kyoto University Reactor (KUR). The half-life time of the precursor ^{129m}Te isotope is 33 days. The observed spectrum was analyzed by use of a computer program including folding and least-squares fitting with Lorentzian lines.

3. Results and Discussion

The observed ^{129}I Mössbauer spectrum at 11 K is shown in Fig. 1. The ^{129}I nuclear spin states in ground and excited states are 7/2 and 5/2 respectively, so that quadrupole-split spectrum consists of a minimum of eight lines. The best fit was obtained by two octuplets of I_a and I_b, indicating that two chemically independent sites of iodine exist in $Pt_2(dtp)_4I$. In the four possible charge-ordering modes mentioned above, only the alternate charge-polarization state (4) has two chemically independent iodine sites, which should be responsible for the low-temperature insulating phase.

The linear relation between the ^{129}I Mössbauer parameters, isomer shift (IS) and quadrupole coupling constant (QCC) has been well known for the series of I^-, I^0, and I^+ [5]. The linear IS-QCC relation is explained as follows: IS value, which is proportional to the electron density at the nucleus (i.e. *s* electron's density), increases in the order of $I^- < I^0 < I^+$, because of a decrease in the occupation of *p* orbitals as a result of less screening the valence and core *s* orbitals from nucleus. QCC value, on the other hand, which reflects an asymmetric charge distribution of valence electrons, also increases in this order, because of a deviation from the closed-shell configuration along the series. The I_b site has larger IS (4.01 mm/s) and QCC (1448 MHz) than the I_a site (IS = 3.86 mm/s, QCC = 1211 MHz), which shows that I_b is more oxidized than I_a.

For iodide ion having $5s^25p^6$ electron configuration, the IS value is known to be given by the following empirical equation [5]:

$$IS = -9.2\,h_s + 1.5\,h_p - 0.54$$

where the IS value (mm/s) are referenced to ZnTe, and h_s and h_p are the number of hole in *s* and *p* orbitals, respectively. From this equation, the oxidation state of I_a and I_b can be estimated to be -0.4, and -0.3, respectively. The observed spectrum is very similar to that of the isostructural, $Pt_2(dta)_4I$ (*dta* = $CH_3CS_2^-$) [6], so that the two iodine atoms of I_a and I_b are assigned below, as well as those for $Pt_2(dta)_4I$.

$\cdots$[Pt^{2+}-Pt^{3+}]-$I_a^{0.4-}$-[Pt^{3+}-Pt^{2+}]$-I_b^{0.3-}-$[Pt^{2+}-Pt^{3+}]-$I_a^{0.4-}$-[Pt^{3+}-Pt^{2+}]$-I_b^{0.3-}\cdots$

Coulomb interaction between the Pt_2 cation and I anion plays a key role in the charge order of this 1-D system.

From Mössbauer spectroscopic study, charge-ordering

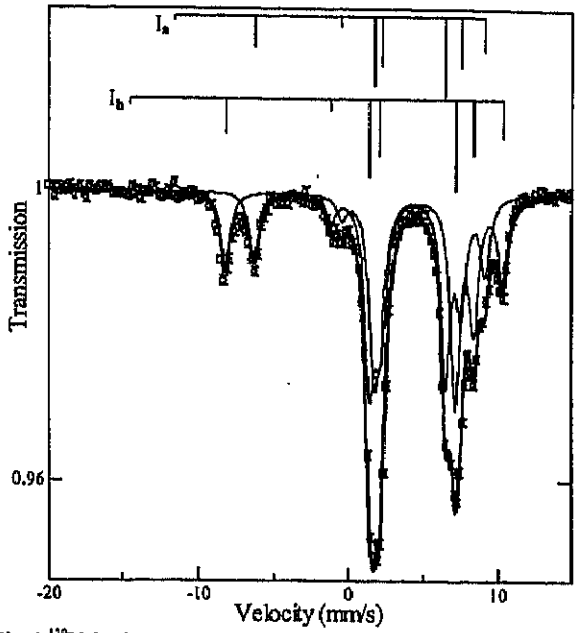

Fig. 1 ^{129}I Mössbauer spectrum at 11 K. The velocity scale is referenced to Mg_3TeO_6. In order to refer this scale to iodine in ZnTe, 3.49 (mm/s) have to be subtracted from the scale.

mode in the low-temperature insulating phase is in the alternate charge-polarization state (4), which is consistent with the recent result of X-ray crystallographic analysis at 48 K [7]. Coulomb interaction is dominant factor in the charge order of MMX-Chain.

Acknowledgement

This work was partly supported by Grant-in-Aid Scientific Researches No. 14340215 of (B) and No. 14038208 (407: Transition Metal Oxides) of Priority Areas (A) from the Ministry of Education, Culture, Sports, Science, and Technology of Japan, and by the grant program of the Thermal & Electric Energy Technology Foundation.

Reference

[1] H. Kitagawa *et al.*, J. Am. Chem. Soc.121 (1999) 10068

[2] A. Kobayashi *et al.*, Mol. Cryst. Liq. Cryst. in press.

[3] A. Kobayashi *et al.*, Inorg. Chem. to be submitted.

[4] M. Mitsumi *et al.*, J. Am. Chem. Soc. 123 (2001) 11179.

[5] R. V. Parish, in *Mössbauer Spectroscopy Applied to Inorganic Chemistry*, G. J. Long (ed), Plenum, New York, Vol. 2 (1984) 391.

[6] H. Kitagawa *et al.*, Synth. Met. 103 (1999) 2159.

[7] M. Mitsumi *et al.*, Angew. Chem. Int. ed. in press.

A new semiconducting organic-inorganic nanocomposite, 1,5-diaminonphthalene-saponite intercalation compound

Shin'ichi Ishimaru*, Miho Yamauchi and Ryuichi Ikeda

Department of Chemistry, University of Tsukuba, Tsukuba 305-8571, Japan
Received

Abstract

We synthesized a new intercalation compound, 1,5-diaminonaphathalene(DAN)- saponite where intercalated DAN molecules were shown to have a formal charge of +0.67. The measurement of optical diffuse reflectance spectra revealed the formation of electronic bands with a gap of ca. 1 eV suggesting semiconducting behaviour of this system. From ESR measurements, the radical formation in DAN-saponite was confirmed and the spin concentration was determined to be 1 spin per 200 and 300 DAN-molecules at 290 K and 7.9 K, respectively. This temperature dependence of the spin density also implies the semiconductive nature of DAN-saponite.

PACS: 72.80Tm; 78.40Fy

Keywords: semiconductor; intercalation compound; saponite; 1,5-diaminonaphthalene

*Corresponding Author. Tel & fax: +81-298-53-4487.
E-mail address: ishimaru@chem.tsukuba.ac.jp

1. Introduction

As a noticeable approach to produce new organic conductors, several intercalation-compounds of TTF and its derivatives with clay minerals have been synthesized [1-3]. Advantages of the intercalation method we can point out are: (1) the preparation of stacked structures separated donor and acceptor molecules, which is an important condition to form a conduction band, is possible, and (2) since clay minerals are good insulators, we can prepare isolated low-dimensional conductors in the interlayer space in clay minerals. In the above reported works, the partial oxidation of TTF molecules attended on the intercalation was obtained, whereas no obvious electrical conduction was observed.

It has been reported that many aromatic compounds such as benzidine, perylene, phenothiazine, etc., are also oxidized by intercalation in clay minerals [4]. These intercalated compounds are expected to suitable candidates for exhibiting the electrical conductivity. Previously, we reported electronic and ionic conduction in a intercalation compound of saponite with 3,3',5,5'-tetramethylbenzidine [5], of which oxidizing process in the solution [6] and on the surface of hectorite [7] has been clarified. But the benzidine derivatives have a disadvantage for stacking of the molecules because of its most stable conformation twisted around the central C-C bond. Planar conjugated systems such as naphthalene derivatives are expected to form a conducting material easier than benzidine derivatives. In this work, we selected 1,5-diaminonaphthalene for the starting material, because planar conjugated systems are expected to form a conducting material easier than benzidine derivatives, and report electronic properties in a new conducing intercalation-compound with saponite.

2. Experimental

Synthetic Na-saponite (Kunimine Industry Co. Ltd.), accepted as a reference clay (JCSS-3501) of the Clay Science Society of Japan, was employed as the starting material. Dihydrochloride of 1,5-diaminonaphthalene (abbreviated to DAN) was crystallized from a solution of DAN (Tokyo Kasei Kogyo Co. Ltd.) dissolved in conc. HCl. A pale yellow aqueous solution of DAN·2HCl showed strong acidity implying that the monocation, $C_{10}H_6(NH_2)(NH_3)^+$ is the main species in the solution. An intercalation compound was obtained as follows: The aqueous solution of DAN·2HCl was poured to a colloidal solution of Na-saponite. The dispersed saponite was coagulated immediately and the colour of this suspension was gradually changed from pale yellow to black with stirring for three days. The suspension was centrifuged and washed by distilled water repeatedly. Finally, glossy black powder was obtained by drying the precipitation in a desiccator over $CaCl_2$.

The substance obtained was characterized by the organic elemental analysis and the electron microprobe analysis (EPMA) with a JEOL JAX-8621 analyzer at Chemical Analysis Center, University of Tsukuba. Powder X-ray diffraction patterns were collected by a Philips PW3040/00 diffractometer using Cu K_α radiation. ESR spectra in solid state were recorded on a JEOL FE1XG spectrometer with a 100 kHz field modulation at 7.9 and 290 K, and the spin concentration was determined by use a standard sample (crystalline $CuSO_4 \cdot 5H_2O$) sealed together in a sample tube. UV-VIS-NIR absorption spectra were obtained by the K-M conversion of diffuse reflectance spectra recorded on a JASCO V-570 spectrometer at room temperature.

3. Results and Discussion

3.1 Elemental analysis and Powder X-ray diffraction

A chemical formula of the prepared specimen was expected to be written as

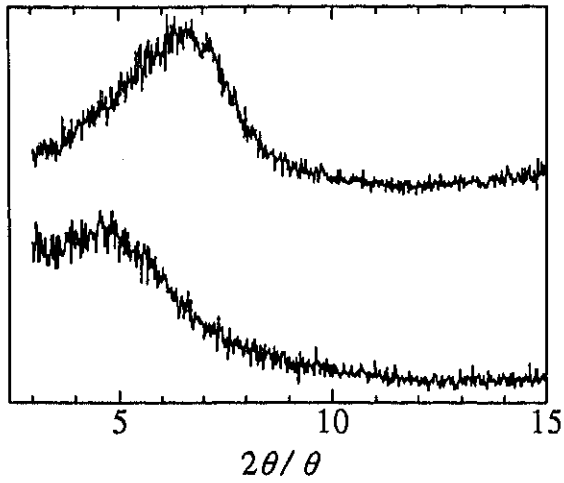

Fig. 1 X-ray powder diffraction peaks from (001)-plane in Na-saponite (upper) and DAN-saponite (lower).

$\{C_{10}H_6(NH_2)_2\}_x(SAP)\cdot nH_2O$ (SAP: $[Si_{3.6}Al_{0.4}Mg_3(OH)_2O_{10}]^{0.4-}$ determined in Kunimine Industry Co. Ltd.) by ignoring additional protons in ammonium groups. The elemental analysis in this compound gave C: 14.35, H: 2.46 and N: 2.86 wt% corresponding to $x = 0.6$ and $n = 3$. This x value is larger than 0.4 predicted from the chemical formula of the starting Na-saponite. No chloride anion, which is possible to be intercalated in the stage of neutralization of DAN, was detected by the EPMA measurement with a pellet specimen.

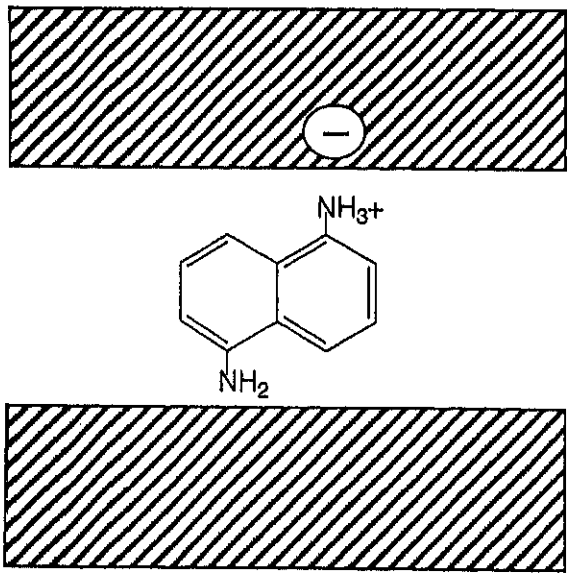

Fig. 2 A schematic model of DAN-cationic arrangement in saponite.

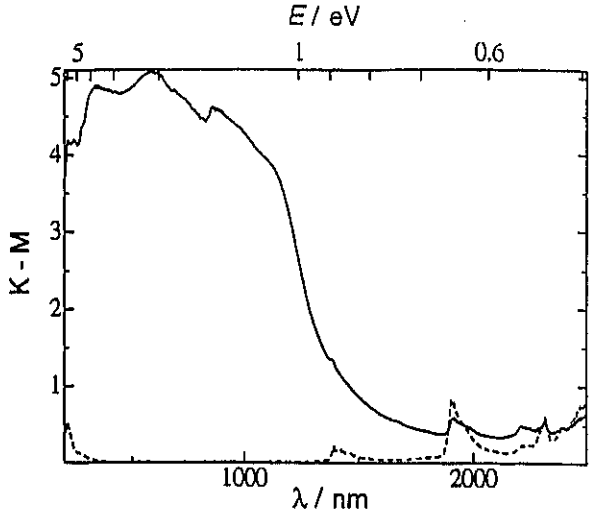

Fig. 3 UV-VIS-NIR absorption spectra obtained by K-M conversion of diffuse reflectance observed in Na-saponite (broken line) and DAN-saponite (solid line).

These facts indicate the formal charge of DAN is +0.67 in DAN-saponite.

Fig. 1 shows powder XRD peaks from (001) planes in DAN-saponite and Na-saponite. The *d*-spacing of (001) plane in DAN-saponite was determined to be 18.5 ± 0.1 nm from the peak of $2\theta = 4.7°$. The interlayer spacing was estimated to be *ca.* 0.9 nm from the spacing by subtracting the layer thickness of 0.96 nm [8]. This interlayer spacing implies that DAN molecules are vertically arranged to the saponite surface as shown in Fig. 2.

3.2 UV-VIS-NIR absorption spectra

Fig. 3 shows UV-VIS-NIR absorption spectra of Na-saponite and DAN-saponite. The starting Na-saponite showed no obvious absorption in the visible range, while DAN-saponite exhibited a strong continuous absorption above *ca.* 1 eV. This means the formation of electronic bands with a gap of *ca.* 1 eV in DAN-saponite. The fact that this band gap is nearly equal to 1.1 eV reported in crystalline silicon implies the formation of a new semiconductor in the interlayer space of the saponite.

3.3 ESR spectra

An ESR spectrum in DAN-saponite observed at 290 K is shown in Fig. 4. A sharp signal with a width of 9.3 gauss was observed at g~2.0 suggesting the radical formation in DAN-saponite. The spin-concentration in DAN-saponite was estimated to be 1 spin per 200 DAN-molecules. At 7.9 K the line-width was slightly broadened to 12.5 gauss and the spin-concentration was reduced to 1 spin per 300 DAN molecules at 7.9 K. The band-gap roughly estimated from the temperature dependence of the spin-concentration became 0.3 eV being in the same order as 1 eV estimated from UV-VIS-NIR spectrum described above.

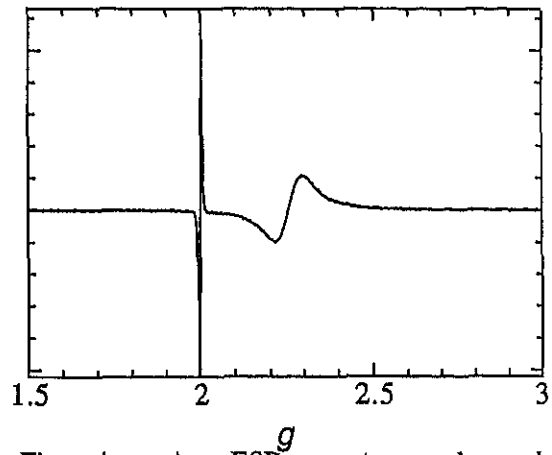

Fig. 4 An ESR spectrum observed in DAN-saponite. A broad signal is from a single crystal of $CuSO_4 \cdot 5H_2O$ appearing at $g = 2.3$.

This work was partly supported by Grant-in Aid for Scientific Research No. (B) 12440192 from the Ministry of Education, Culture, Sports, Science and Technology of Japan.

References

[1] H. Van Damme, F. Obrecht, M. Lettelier, Nouv. J. Chim. 8 (1984) 681.
[2] A. S. Mandair, W. R. Mcwhinnie, P. M. Mirzai, Inorg. Chim. Acta 134 (1987) 99.
[3] M. Soma, Y. Soma, Chem. Lett. (1988) 405.
[4] Y. Matsunaga, Bull. Chem. Soc. Jpn. 45 (1972) 770.
[5] S. Ishimaru, R. Ikeda, Mol. Cryst. Liq. Cryst. 341 (2000) 309.
[6] P. D. Josephy, T. Eling, R. P. Mason, J. Biol. Chem. 257 (1982) 3669.
[7] M. B. McBride, Clay. Clay Miner. 33 (1985) 510.
[8] T. Endo, T. Sato, M. Shimada, J. Phys. Chem. Solids 47 (1986) 799.

Dynamic Structure of Molecules Included in Porous Solids Studied by Solid State NMR

Shin'ichi Ishimaru and Ryuichi Ikeda
Department of Chemistry, University of Tsukuba, Tsukuba 305-8571, Japan

ABSTRACT

Recent NMR works on dynamic properties of acetonitrile, water and triethylamine molecules included in 1-D nanospaces existing in zeolite-like aluminophosphate ($AlPO_4$-5 and SAPO-5) and alkali and alkylammonium ions in 2-D spaces in layered clay minerals (smectites and tetrasilicicfluormica) are summerized.

I. INTRODUCTION

Molecules and ions enclosed in zero-, one- (1-D) or two-dimensional (2-D) nanospaces are expected to exhibit novel properties associated with low-dimensional structures of molecular assemblies different from those in bulk. Highly anisotropic spaces formed in solids have been expected to be excellent fields for new material design. For example, *p*-nitroaniline in zeolite shows strong nonlinear optical effects of second order [1]. This can be obtained by realizing the one-dimensional alignment of polar molecules unavailable in bulk crystal.

As another characteristic in these porous systems, included polar molecules strongly interact with acid sites on the host wall and form complexes. This host-guest interaction plays an important role for understanding of catalytic behaviour of porous materials.

In these unique features obtainable in inclusion compounds, dynamic structures of included molecules in pores are expected to be closely connected with physical properties and chemical reactions in adsorbed molecular systems. In this article we intend to review dynamic structures observed by solid-state NMR methods on various molecules and ions loaded in 1-D channel of zeolite-like aluminophosphate ($AlPO_4$-5) and silicoaluminophosphate (SAPO-5) and 2-D spaces of layered clay minerals (cation-exchanged smectites and tetrasilicicfluormicas).

1-D porous aluminophosphate, $AlPO_4$-5 and silicoaluminophosphate SAPO-5

More than hundred kinds of porous aluminosilicates, so called zeolites, have been found in nature and artificially synthesized [2]. Recently, new zeolitic materials other than zeolites, such as silicates [3-5], metallophosphates [6-9], carbon nanotubes [10,11], *etc.*, have been synthesized and drawn much attentions about their new possibilities for catalysis and functions.

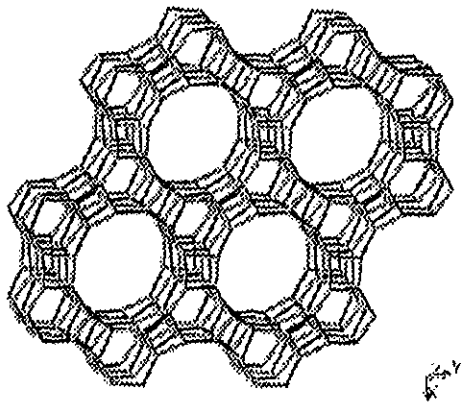

Fig. 1 A skeleton of crystal lattices in $AlPO_4$-5 and SAPO-5. A view down along the crystalline *c*-axis.

$AlPO_4$-5 (chemical formula: $AlPO_4$) is the first synthesized zeolitic aluminophosphate which has hydrophobic and highly symmetric straight 1-D channels constructed by twelve-membered oxygen rings [12] (fig. 1). Such a straight channel structure had not been found in zeolites. Another characteristic is that $AlPO_4$-5 is a neutral material in contrast with zeolites with anionic lattices in which the existence of cations in channels is essential. SAPO-5 (chemical formula: $Al_{1-x}Si_xPO_4(OH)_x$) is a silicoaluminophosphate which is isomorphous with $AlPO_4$-5. A marked difference between two materials is the existence of Brønsted's acid sites on the channel-wall in SAPO-5 [13]. It is expected that the comparison of dynamic behaviour of molecules in the pores of these two materials reveals interactions between acid sites and adsorbed molecules.

Layered clay minerals

It is an important feature of layered compounds that a two-dimensionally extended space is formed between sheets in which many kinds of chemical species can be intercalated. The interlayer distance in these 2D compounds can be expanded according to sizes and shapes of guest molecules. Because of this structure, layered compounds are able to intercalate macromolecules as well as small molecules in contrast to zeolites used for "molecular sieves". This flexibility of the host lattice is a great advantage for the material design. Although many kinds of layered

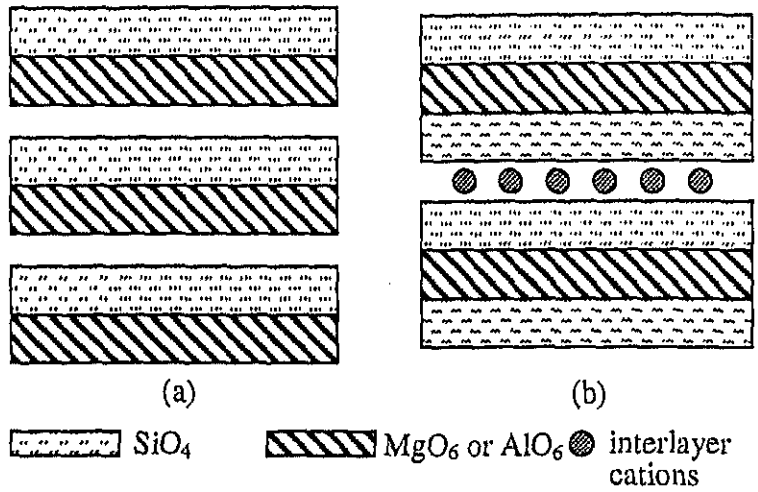

Fig. 2 Schematic models of (a) 1:1-type and (b) 2:1-type layered clay minerals.

compounds have been known, layered clay minerals are widely used for preparing intercalation compounds because they are quite stable, safe and low-cost.

Most of clay minerals constructed from stacked polyoxo-acid sheets easy to be abraded. In most of these minerals, each sheet consists of sub-layers formed from SiO_4 and MgO_6 or AlO_6 as minimal units, and classified by the stacking manner of these sub-layers (fig. 2), such as 1:1 (general formula: $Al_4Si_4O_{10}(OH)_8$) and 2:1-types ($A^{n+}_{x/n}Al_{2-x}Mg_xSi_4O_{10}(OH)_2$ or $A^{n+}_{x/n}Mg_{3-x}Li_xSi_4(OH)_{10}$, A=cation) [14]. Isomorphous replacements of Si and metal ions with lower charged ions generating negative charges are often seen in 2:1-type minerals, *i.e.*, Si^{4+} with Al^{3+}, Al^{3+} with Mg^{2+}, Mg^{2+} with Li^+, *etc.* 2:1-type layered clay minerals are further classified into subgroups: smectites ($0.2< x <0.6$), vermiculites ($0.6< x <0.9$), and micas ($x \sim 1$) according to the negative charge density [14] in a sheet.

Various cations are included in the interlayer space of these compounds for cancelling charges. In smectites and vermiculites, water molecules surround the interlayer-cations and these minerals are swelled well by moisture. Structures of water and ionic dynamics different from bulk solutions are expected in these systems.

NMR Application for Studying on Molecular Environment

Observation of molecular motions can give important information for the evaluation of molecular environment because motions as a whole directly reflect the potential formed by surroundings. The wide-line NMR has

been used as one of useful methods for observing molecular motions in solid [15,16]. Applying this method, we can measure magnetic dipole-dipole interactions between ^{1}H nuclei as well as electric quadrupole interactions between ^{2}H nuclei and electric field gradients (EFG) made by surrounding charges. These interactions are averaged by the onset of molecular motions upon heating. In NMR measurements, the averaged interactions can be studied by two different approaches, *i.e.*, the spectrum analysis and the relaxation measurement. Both spectrum and relaxation show characteristic changes when the rate of molecular motions is close to time scales of magnetic interactions with surroundings and the external field, respectively, *i.e.*, ~10^4 Hz in the spectral and 10^6-10^8 Hz in the relaxation measurements.

Dynamic properties of molecules adsorbed in porous materials can be effectively investigated by the NMR method, because this method enables us to observe selectively particular nuclei in a certain chemical species in complex systems.

In many cases, the ^{1}H NMR relaxation is caused by fluctuations of magnetic dipolar interactions caused by molecular motions. This relaxation process is expressed as the following BPP equation [17,18] as a good approximation:

$$T_1^{-1} = C\left\{\frac{\tau}{1+\omega^2\tau^2} + \frac{4\tau}{1+4\omega^2\tau^2}\right\} \qquad (1),$$

where C, ω and τ are the motional constant, the angular Larmor frequency of ^{1}H and the motional correlation time, respectively. τ is varied with temperature and expressed as the Arrhenius activation process:

$$\tau = \tau_0 \exp(-E_a / kT) \qquad (2).$$

Here E_a is the activation energy of the motion. In this treatment, T_1 shows a minimum where $\omega\tau$ = 0.616 is fulfilled (fig. 3). The symmetric temperature dependent T_1 curve is obtained by plotting log T_1 against T^{-1} or τ. The relation $T_1 \propto \omega^2$ is expected in the low-temperature range of the T_1 minimum, while no frequency dependency is seen in the high-temperature side.

It has, however, been reported that ^{1}H T_1 in molecules included in porous materials often give different temperature dependences from the

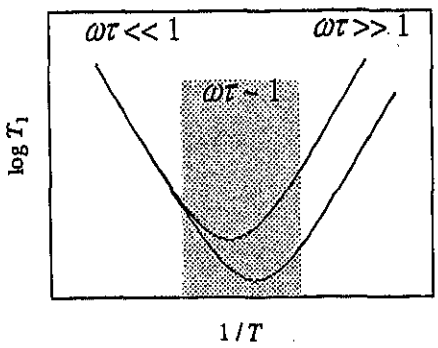

Fig. 3 T_1 curves predicted by the BPP-theory at two different Larmor frequencies.

above relation and shows asymmetric T_1 curves with weak frequency dependencies in the low-temperature side. This T_1 behaviour is explain-able by introducing the distribution in τ [19] which has also been successfully used in the data analysis in the dielectric studies [20] on water dynamics in clay systems. τ Distribution is mostly caused by the inhomogeneity of molecular environ-ments, *i.e.*, widely spread potentials surrounding molecules.

As for guest molecules in porous systems, observed T_1 data are often reproduced well by introducing the Cole-Davidson type τ distribution function [21] given by

$$g(\tau) = \frac{\sin \beta\pi}{\pi}\left(\frac{\tau}{\tau_C - \tau}\right)^{\beta} \qquad \tau \le \tau_C$$
$$= 0 \qquad \tau > \tau_C \tag{3}$$

where β $(0 < \beta \le 1)$ shows the distribution amplitude (fig. 4). Here, the limit of $\beta = 1$ corresponds to the homogeneous environment. Under this τ distribution, eq. (1) is modified as [19],

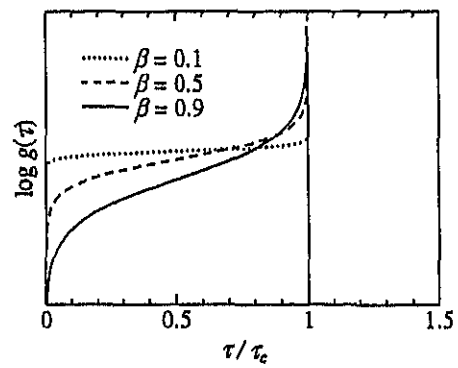

Fig. 4 Cole-Davidson type distribution functions.

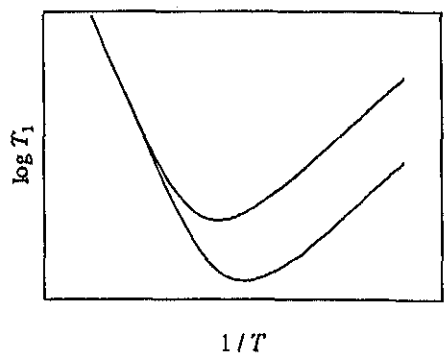

Fig. 5 T_1 curves predicted by the BPP-theory at two different Larmor frequencies under Cole-Davidson type τ distribution.

$$T_1^{-1} = C\left\{\frac{\tau_C \sin(\beta \tan^{-1} \omega\tau_C)}{\omega\tau_C(1+\omega^2\tau_C{}^2)^{\beta/2}} + \frac{2\tau_C \sin(\beta \tan^{-1} 2\omega\tau_C)}{\omega\tau_C(1+4\omega^2\tau_C{}^2)^{\beta/2}}\right\} \quad (4).$$

This gives a frequency dependency less than eq. (1). The critical correlation time τ_c is assumed to obey the Arrhenius-type activation:

$$\tau_C = \tau_0 \exp(-E_a / kT) \quad (5).$$

Temperature dependences of T_1 predicted by eqs. (4) and (5) are shown in fig. 5.

II. Dynamic behaviour of molecules in one-dimensional channels of $AlPO_4$-5 and SAPO-5

a) Triethylamine molecules included in $AlPO_4$-5 and SAPO-5

Zeolitic materials with large channels have successfully been synthesized by the hydrothermal method using alkylamines, quaternary ammonium salts or other organic compounds as structure-directing agents (SDA) [22]. Studies on dynamics of SDA molecules as well as van der Waals and Coulombic interactions between SDA molecules and the framework is considered to be important to direct the channel structure during the hydrothermal reaction [23-25].

Triethylamine (TEA) is a typical SDA for the synthesis of a typical aluminophosphate molecular sieve $AlPO_4$-5 and its isomorphous silicoaluminophosphate SAPO-5 [26]. Two orientation-models for the TEA molecules in $AlPO_4$-5 have been reported from the polarised IR spectrum measurement [27] and the neutron powder diffraction [28] study. The molecular orientation proposed in the former work is that the pseudo C_3 axes of TEA molecules are perpendicular to the channel axis. On the other hand, the latter has suggested the head-to-tail arrangement of TEA molecules in the channel.

Gotoh *et al.* [29] studied motions of TEA in $AlPO_4$-5 and SAPO-5 and discussed the influence of Brønsted's acid sites on the molecular orientation by use of NMR data. The isotropic rotation of TEA molecules in both $AlPO_4$-5 and SAPO-5 at room temperature was shown by the reduction of ^{14}N quadrupole coupling constants from the static value of 4800 kHz [30] to 80 kHz and 300 kHz, respectively, implying the onset of the almost isotropic reorientation of TEA molecules. These results do not necessarily

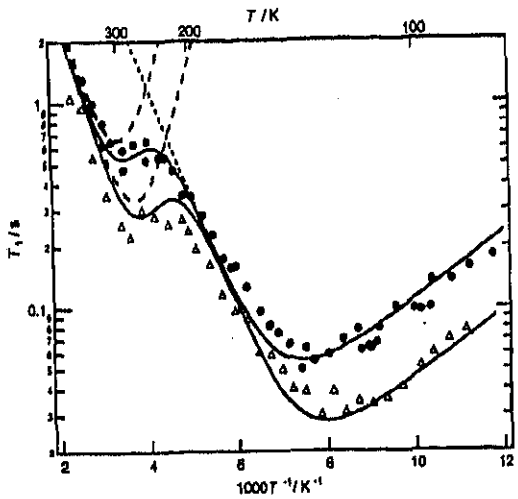

Fig. 6 Temperature dependences of ^{1}H NMR T_1 observed for triethylamine included in $AlPO_4$-5 at 42.0 (closed circle) and 21.0 MHz (triangle). The best fitted calculated curves expressed by solid lines are the sum of two T_1 components given by dotted lines. (Reproduced from ref. 29 by permission of The Royal Society of Chemistry on behalf of the PCCP Owner Societies.)

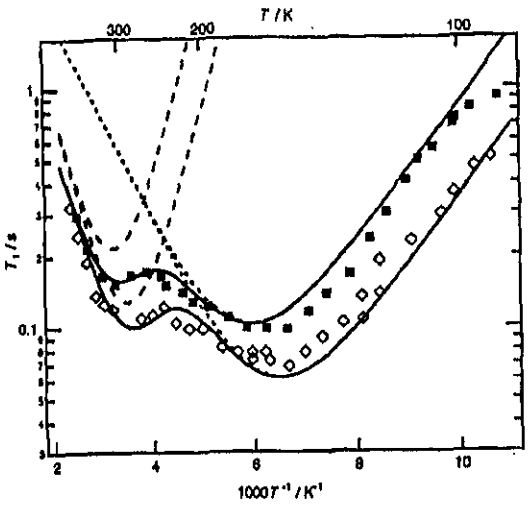

Fig. 7 Temperature dependences of ^{1}H NMR T_1 observed for triethylamine included in SAPO-5 at 68.6 (closed square) and 21.0 MHz (open diamond). The best fitted calculated curves expressed by solid lines are the sum of two T_1 components given by dotted lines. (Reproduced from ref. 29 by permission of The Royal Society of Chemistry on behalf of the PCCP Owner Societies.)

conflict with the stable molecular orientations suggested by the IR and the neutron diffraction studies, because the NMR observes the molecular motions much slower than in IR and neutron diffraction in which the most preferential orientation of molecules can be detected in case molecules in channels have a stable orientation.

Details of molecular motions were clarified by ^{1}H T_1 measurements [29] on TEA in $AlPO_4$-5 and SAPO-5's with various Si concentrations. Figs. 6 and 7 show temperature and frequency dependences of ^{1}H T_1 of TEA in $AlPO_4$-5 and SAPO-5 (Si/Al=0.09), respectively. They were reproduced well by a superposition of two relaxation components represented by eqs. (4) and (5). These two relaxation mechanisms attributed to the isotropic rotation as a whole and the pseudo C_3 rotation. The latter mode showed a quite large distribution of τ, *i.e.*, a small β of 0.3 in $AlPO_4$-5 while a large value of 0.7 in SAPO-5. This implies that the hindrance barrier for the C_3 rotation in a TEA molecule in the molecular sieves becomes homogeneous by the existence of acid sites. Gotoh *et al.*, explained this fact by the pinning effect of molecules to acid sites as shown in fig. 8. By forming

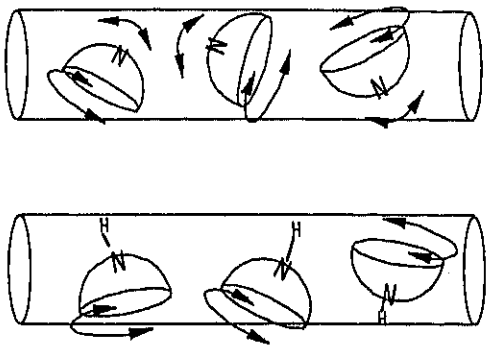

Fig. 8 Schematic two limiting models for orientations of triethyl-amine molecules in $AlPO_4$-5 (upper) with no acid site and highly silicated SAPO-5 (lower) in which respective amine molecules are attracted to nearest acid sites.

hydrogen bonds between N atoms in TEA molecules and Brønsted's acid sites on the wall, the C_3 axes of TEA molecules are likely to orient to perpendicular to the channel axis. However, TEA molecules free from pinning in $AlPO_4$-5 can rotate about axes with arbitrary directions resulting in widely spread barriers for rotation.

b) Acetonitrile molecules absorbed in $AlPO_4$-5 and SAPO-5

Acetonitrile molecules with a length of 6.2 Å for the longest axis in $AlPO_4$-5 and SAPO-5 with an effective diameter of 7.3 Å are regarded as free from steric hindrance for the isotropic molecular reorientation. The electrostatic interaction between acetonitrile molecules with a dipole moment of 3.9 D are considered to be important to determine the molecular behaviour in $AlPO_4$-5 because the interaction between molecules and the hydrophobic host wall is expected to be weaker than that between molecules. On the other hand in SAPO-5, a strong interaction between acetonitrile molecules and Brønsted's acid sites

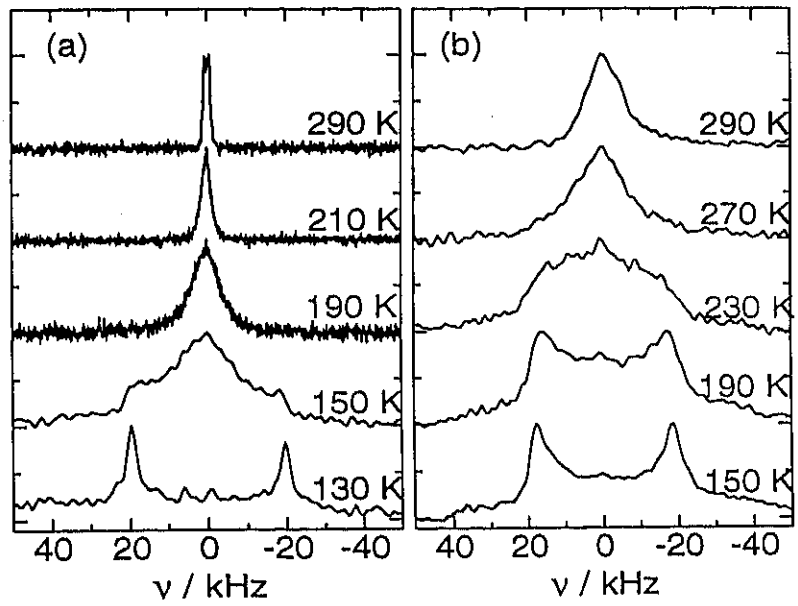

Fig. 9 Temperature dependence of ^2H NMR spectra of acetonitrile-d_3 in (a)$AlPO_4$-5 and (b)SAPO-5.

was reported from the IR study [31].

Ishimaru *et al.* measured ^{1}H NMR spectra and T_1 of CH_3CN in $AlPO_4$-5 and SAPO-5, and also ^{2}H spectra of adsorbed CD_3CN to evaluate effects of the acid sites on adsorbed molecules [32]. The ^{2}H NMR spectra of CD_3CN showed an absorption line at 130 K with a width of 36-39 kHz (fig. 9) explainable by the CD_3 rotation. The line-width was steeply decreased with the temperature increase from 150 K and became 1.8 kHz at 290 K in $AlPO_4$-5 implying the isotropic rotation as a whole. This suggests that acetonitrile in $AlPO_4$-5 behaves like in liquid above 150 K. This temperature is much lower than the melting point (229 K) in bulk. A small splitting in the spectrum observed at 290 K is attributable to the electric field gradient made by partial charges on the atoms in the host-wall [33].

On the other hand, the ^{2}H NMR line-width in the SAPO-5 system gradually decreased over a wide range 130-293 K on heating and it remained about 10 kHz even at 293 K. This implies that the isotropic rotation observed in $AlPO_4$-5 is unexcited in SAPO-5 at room temperature. This is attributable to the pinning effect of Brønsted's acid sites. The gradual decrease in line-width observed for CD_3CN in SAPO-5 (fig. 9) was explained by the tumbling motion of molecular axes fixed on acid sites as shown in fig. 10. This model is consistent with the IR study [31] reporting the presence of hydrogen-bonded acetonitrile molecules even at 500 K.

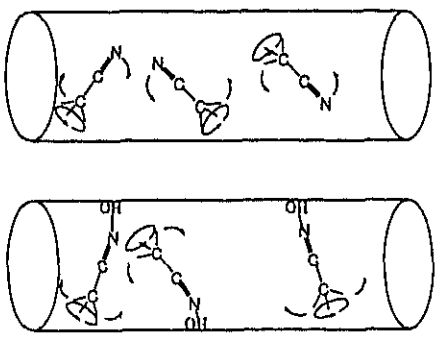

Fig. 10 Schematic models of acetonitrile motions in $AlPO_4$-5 and SAPO-5.

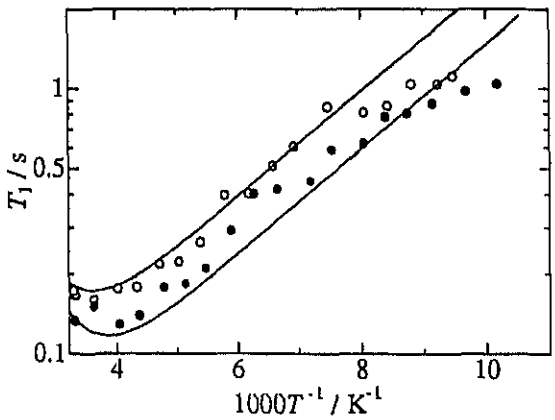

Fig. 11 Temperature dependences of ^{1}H NMR T_1 in acetonitrile in SAPO-5 observed at 27 MHz (closed circle) and 39 MHz (open circle). Solid lines represent best-fitted curves using eqs. (4) and (5).

A large τ distribution (small β value) of the tumbling motion was obtained from the curve fitting of ^{1}H T_1 for acetonitrile in SAPO-5 (fig. 11) using eqs. (4) and (5). This is attributable to inhomogeneous distributions of acid sites on the wall and also distributed distances between acetonitrile molecules and acid sites. The latter reason can be derived from the fact that the number of adsorbed acetonitrile molecules is about 1.5 times larger than that of acid sites.

III. Molecular orientations and dynamics in two-dimensional silicate-layers

a) Water molecules in interlayer space of clay minerals

From studies on thermal behaviour, motions and structures of intercalated water [20,34], it was shown that its microscopic properties depend on the kind of clays and its adsorption level.

NMR techniques have been applied to clarify the dynamic structure of intercalated water molecules [35-38]. An unavoidable problem in these studies [35-38] is the presence of paramagnetic impurities contained in natural minerals which complicate the analysis of results. Ishimaru *et al.* conducted ^{2}H NMR measurements in D_2O molecules intercalated into synthetic clays, such as Na-tetrasilicicfluormica (TSFM), Na-fluorhectorite (Hec) and several cation-exchanged saponites (Sap) including ignorable amounts of paramagnetic impurities, and also Na-montmorillonite as a natural clay [39-41], all except for TSFM being classified to smectites.

Table 1. D_2O contents determined by thermogravimetry in clays exposed to D_2O at saturated vapour pressure at room temperature.

Clay	D_2O molecules / cation
Li-saponite	35±1
Na-saponite	15.8±0.2
Cs-saponite	26.0±0.2
TMA-saponite	14.0±0.2
Na-hectorite	14.9±0.2
Na-montmorillonite	19.4±0.2
Na-tetrasilicicfluormica	6.7±0.1

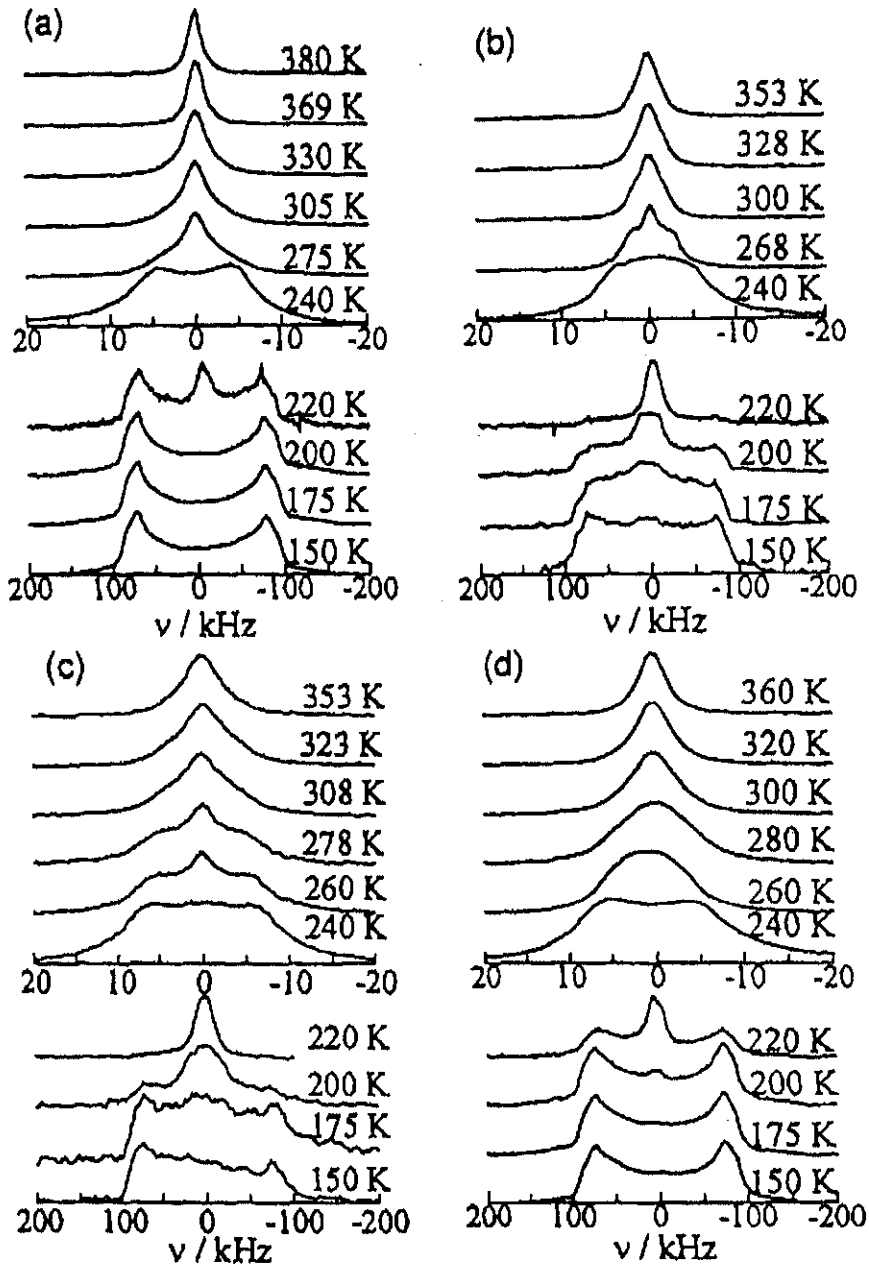

Fig. 12 Temperature dependences of ^{2}H NMR spectra in D_2O saturated Na-saponite (a), Cs-saponite (b), TMA-saponite (c) and Na-hectorite (d). (Reprinted from ref. 41. Copyright 1999 Verlag der Zeitschrift für Naturforschung.)

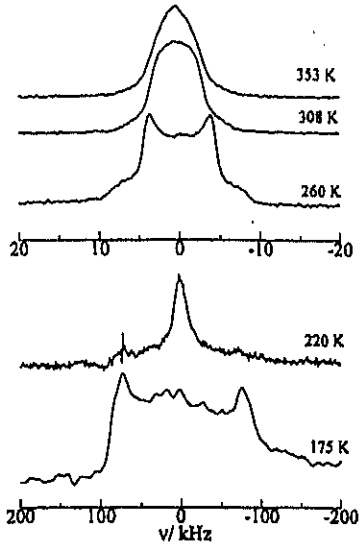

Fig. 13 A temperature dependence of ^2H NMR spectra in D_2O saturated Li-saponite. (Reprinted from ref. 39. Copyright 1997 Verlag der Zeitschrift für Naturforschung.)

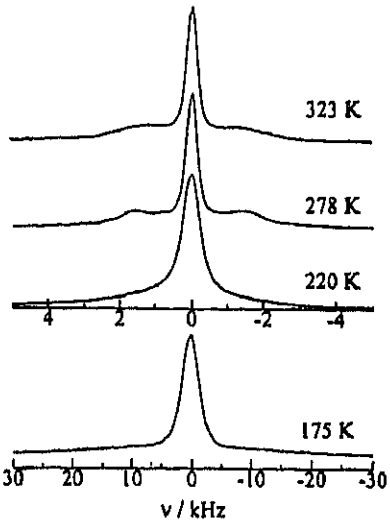

Fig. 14 Temperature dependence of ^7Li NMR spectrum in D_2O saturated Li-saponite. (Reprinted from ref. 39. Copyright 1997 Verlag der Zeitschrift für Naturforschung.)

Contents of D_2O adsorbed in clays after the contact with the saturated vapour at room temperature were determined by the thermogravimetry as shown in table 1. Obtained D_2O contents except for Na-TSFM were high compared with the accepted hydration numbers of 6~10 for an Na^+ ion in aqueous solution. This implies the existence of non-hydrated water molecules in the interstitial space of clay layers. On the other hand, Na-TSFM, known as a highly charged mineral (micas) with a small amount of interstitial sites, showed a hydration number of 6.7, corresponding to the normal number of 6.

Figs. 12 and 13 show temperature dependences of ^2H NMR spectra of D_2O in synthetic smectites, *i.e.*, cation-replaced Saps and Na-Hec. On the other hand, montmorillonite as a natural smectite, showed distorted spectra attributable to the influence from paramagnetic impurities, but no detailed analysis has been reported. Water in all clays given in these figures showed a similar ^2H line-shape with each other in spite of differences in D_2O contents. These compounds showed broad spectra with a peak-to-peak width of 165 kHz around 150 K indicating that the most water molecules are rigid in this temperature. A narrow component appeared upon heating and a single component with a peak-to-peak width of 10~20 kHz was observed at *c.a.* 240 K. This line-shape and width are explainable by the C_2 rotation of D_2O molecules. A further reduction in

line-width implying the D_2O isotropic rotation was observed above 240 K. A surprising result was that all smectites showed a single ^2H NMR spectrum around 240 K, although the presence of more than two kinds of water molecules, free and hydrated to cations, are expected from a large amount of D_2O contents. This implies the fast exchange between D_2O sites in clays.

Structures and motions of hydrated water in Li-Sap were also studied by ^7Li NMR spectrum measurements [39]. Observed spectra showed a central peak with symmetric satellites at *ca.* ±10 kHz above 278 K (fig. 14). This line shape is typical for I=3/2 nuclei coupled with a symmetric electric field gradient (EFG) made by surrounding charges. A small ^7Li quadrupole coupling constant of 6.5±0.5 kHz estimated at 278 K from the observed separation of satellites implies that the EFG at Li nuclei is almost averaged by the isotropic motion of hydration spheres. In low temperatures, spectra were broadened and the fine structure was smeared out. This change of spectra was interpreted by inhomogeneous charge distribution in clay layers.

In contrast to the results in smectites, a temperature independent ^2H NMR absorption-line with a peak-to-peak width of 45 kHz was observed in Na-TSFM (fig. 15) [41]. This line-shape was explained by the C_3 rotation

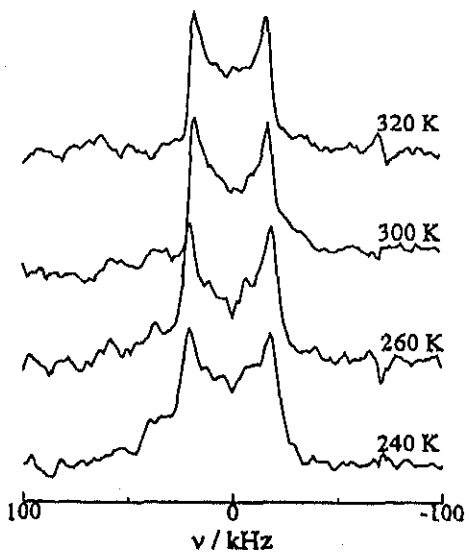

Fig. 15 Temperature dependence of ^2H NMR spectrum in D_2O saturated Na-tetrasilicicfluormica. (Reprinted from ref. 41. Copyright 1999 Verlag der Zeitschrift für Naturforschung.)

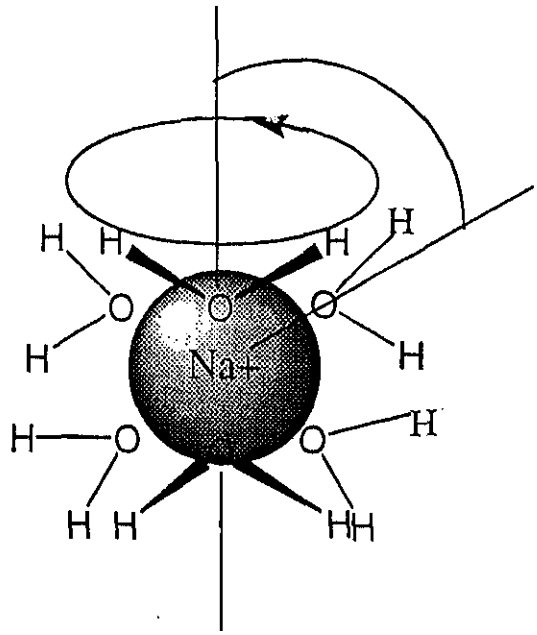

Fig. 16 A schematic model of structure and motions of water molecules hydrated to an Na^+ ion.

of octahedral $[Na(D_2O)_6]^+$ ions accompanied by the D_2O 180°-flip about the molecular C_2 axis as shown in fig. 16. The obtained tilt-angle of 61° between the C_3 axis of the cation and the D_2O C_2 axis agrees well with 65° proposed by Hougardy *et al.* [36] in Na-vermiculite from the ^1H NMR measurement of oriented specimens.

b) Alkylammonium ions in interlayer space of clay minerals

Alkylammonium ions in clay minerals have been reported to form a characteristic layer structure depending on their lengths and cation exchange capacities (CEC) of clays [42]. In clays with a large CEC, *e.g.*, vermiculite, densely packed alkylammonium ions form mono- or bi-layers in which the long-axis of ions has an inclination of 50-60° to the clay sheet [43]. On the other hand, in smectites with small CEC values, alkylammonium ions are arranged with their long axes parallel to the clay layer, forming mono- to tri-layers according to their chain lengths [44].

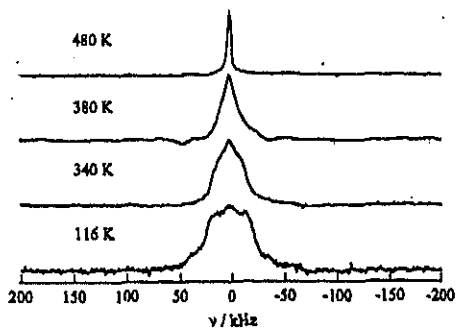

Fig. 17 Temperature dependence of ^4H NMR spectra in n-$C_8H_{17}ND_3$-saponite.

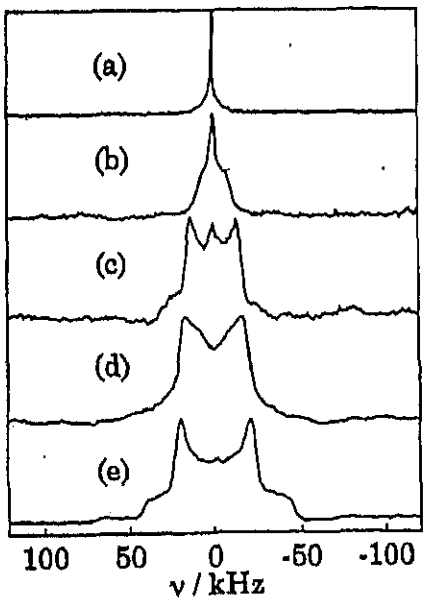

Fig. 18 ^4H NMR spectra in n-$C_8H_{17}ND_3$-tetrasilicicfluormica at 480 (a), 460 (b), 430 (c), 300 (d) and 108 K (e). (Reprinted from ref. 46. Copyright 1999 Verlag der Zeitschrift für Naturforschung.)

Yamauchi *et al.* conducted ^1H and ^2H NMR measurements on n-octylammonium (OA) ions inter-calated into Sap [45] and TSFM [46] and spherical tetramethyl-ammonium (TMA) ions in Sap [40] to clarify dynamic structures of the cations in 2-D interlayer spaces of clay minerals.

The powder X-ray diffraction implied a parallel arrangement of OA cations in TSFM as well as Sap. The onset of the $-ND_3$ rotation was shown in OA-Nd_3 intercalated into

both Sap and TSFM below 120 K by ^2H NMR spectral analyses (figs. 17 and 18). A reduction in the ^2H line-width from *ca.* 50 kHz at 120 K to *ca.* 20 kHz at 400 K was interpreted by the onset of the cationic axial rotation. Further decrease in line-width observed at higher temperatures was attributed to a novel 2-D motion absent in bulk crystal, *i.e.*, a large amplitude tumbling of cationic long axes in the interlayer space fixing $-ND_3^+$ groups on the anionic centre of the host layer. The environment around the cations was shown to be more homogeneous in OA-TSFM than in OA-Sap because ^2H spectra showed structures with determinable quadrupole coupling constants in the TSFM system, while it was vague in the Sap system.

In contrast to the OA systems, spherical TMA-d_{12} cations intercalated into Sap showed a narrow ^2H NMR line with a width of *ca.* 1 kHz even at 120 K [40]. This result indicates that the cations undergo the isotropic rotation as a whole at this temperature. The line-width was further reduced around 250 K implying the onset of the cationic self-diffusion. It can be concluded that spherical TMA ions are highly mobile comparing with bulk TMA-salts, such as TMA-thiocianate [47].

IV. CONCLUSION

NMR studies on dynamic structures of molecules and ions included in 1-D and 2-D nanospaces in porous crystals have been reviewed. It has been revealed that arrangements and dynamic properties of guest molecules and ions depend markedly on guest-guest and host-guest interactions. In zeolitic silicoaluminophosphate SAPO-5, which has Brønsted's acid sites on the inner surface, the molecules orient to the acid sites because of strong interactions between molecules and acid sites. On the other hand, the host-guest interaction is weak in aluminophosphate $AlPO_4$-5 and molecules in the pores orient arbitrary.

Behaviour of water molecules loaded in layered clay minerals could be understood as dynamics of hydration spheres around interlayer cations even in the presence of large excess amount of water comparing with hydration numbers of cations.

Alkylammonium ions in two kinds of layered clay minerals, saponite and tetrasilicicfluormica were shown to be packed with their long axes parallel to the 2-D layers and perform the tumbling motion of the long axes which

has not been observed in bulk crystals.

References

[1] F. Marlow, J. Kornatowski, B. Reck, I. Leike, K. Hoffmann and J. Caro, *Mol. Cryst. Liq. Cryst. Sci. Tech. A*, **276**, 295 (1996).
[2] H. Robson, *Zeolites*, **13**, 399 (1993).
[3] F. Liebau, H. Gies, R. P. Gunawaradane and B. Marler, *Zeolites*, **6**, 373 (1986).
[4] F. Liebau, *Strucrural Chemistry of Silicates - Structure, Bonding, nd Classification*, Springer-Verlag, Berlin, Heiderberg (1985).
[5] B. Marler, N. Dehnbostel, H.-H. Eulert, H. Gies and F. Liebau, *J. Incl. Phenom.*, **4**, 339 (1986).
[6] S. T. Wilson, B. M. Lok, C. A. Messina, T. R. Cannan and E. M. Flanigen, *J. Am. Chem. Soc.*, **104**, 1146 (1982).
[7] S. T. Wilson, B. M. Lok, C. A. Messina, T. R. Cannan and E. M. Flanigen, *Intrazeolite Chemistry*, Am. Chem. Soc., Washington, D. C. (1983) pp. 79.
[8] B. M. Lok, T. R. Cannan and C. A. Messina, *Zeolites*, **3**, 282 (1983).
[9] E. M. Flanigen, B. M. Lok, R. L. Patton and S. T. Wilson, *New Developments in Zeolite Science and Technology*, Y. Murakami, A. Iijima and J. W. Ward (eds.), Tokyo (1986), pp. 103.
[10] S. Iijima and T. Ichihashi, *Nature*, **363**, 603 (1993).
[11] D. S. Bethune, C. H. Kiang, M. S. de Vries, G. Gorman, R. Savoy, J. Vazquez and R. Beyers, *Nature*, **363**, 605 (1993).
[12] J. M. Bennet, J. P. Cohen, E. M. Flanigen, J. J. Pluth and J. V. Smith, *ACS Sym. Ser.*, **218**, 109 (1983).
[13] E. M. Flanigen, B. M. Lok, R. L. Patton and S. T. Wilson, *Pure Appl. Chem.*, **58**, 1351 (1986).
[14]A. C. D. Newman and G. Brown, *Chemistry of Clays and Clay Minerals*, ed. A. C. D. Newman, Mineralogical Society Monograph No.6, ch. 1, Weily, New York, 1987.
[15] Abragam, *Principles of Nuclear magnetism*, Oxford University Press, London, 1961.
[16] C. P. Slichter, *Principles of Magnetic Resonance*, 3rd ed., Springer-Verlag, Berlin, 1990.
[17] N. Bloembergen, E. M. Purcell and R. V. Pound, *Phys. Rev.*, **73**, 679

(1948).
[18] R. Kubo and K. Tomita, *J. Phys. Soc. Jpn.*, **9**, 888 (1954).
[19] T. M. Connor, *Trans. Faraday Soc.*, **60**, 1574(1964).
[20] G. Sposito and R. Prost, *Chem. Rev.*, **82**, 553 (1982).
[21] D. W. Davidson and R. H. Cole, *J. Chem. Phys.*, 19, 1484 (1951).
[22] S. T. Wilson, *Verified Syntheses of Zeolitic Materials*, ed. by H. Robson, Elsevier, Amsterdam, 2001, pp. 27-31.
[23] T. V. Harris, Y. Nakagawa, D. S. Santilli and S. I. Zones, *Book of Abstracts, 211th ACS National Meeting*, New Orleans, La, USA, 1996.
[24] T. V. Harris and S. I. Zones, *Stud. Surf. Sci. Catal.* **84**, J. Weitkamp, H. G. Karge, H. Pfeifer and W. Hölderich (eds.), Elsevier, Amsterdam, 1994.
[25] D. W. Lewis, C. M. Freeman and C. R. A. Catlow, *J. Phys. Chem.*, 99, 11194 (1995).
[26] D. Young and M. E. Davis, *Zeolites*, **11**, 277 (1991).
[27] S. C. Popescu, S. Thomson and R. F. Howe, *Phys. Chem. Chem. Phys.*, **3**, 111 (2001).
[28] T. Ikeda, K. Miyazawa, F. Izumi, Q. Huang and A. Santoro, *J. Phys. Chem. Solids*, **60**, 1531 (1999).
[29] K. Gotoh, S. Ishiamru and R. Ikeda, *Phys. Chem. Chem. Phys.*, **2**, 1865 (2000).
[30] J. P. Lucas and L. Guibe, *Mol. Phys.*, **19**, 85 (1970).
[31] W. P. J. H. Jacobs, D. G. Demuth, S. A. Schunk and F. Schüth, *Microporous Mater.*, **10**, 95 (1997).
[32] S. Ishimaru, K. Gotoh, M. Ichikawa and R. Ikeda, *Microporous Mesoporous Mater.*, **51**, 17 (2002).
[33] Y. Millot, P. P. Man, M.-A. Springuel-Huet and J. Fraissard, *Zeolites and Mesoporous Matterials at the Dawn of the 21th Century*, 14-P-27, Studies in Surface Science and Catalysis **135**, A. Galarneau, F. Di Renzo, F. Faujula and J. Vedrine (eds.), Elsevier, Amsterdam (2001).
[34] A. C. D. Newman, *Chemistry of Clays and Clay Minerals*, ed. A. C. D. Newman, Mineralogical Society Monograph No.6, ch. 5, Weily, New York, 1987.
[35] R. F. Giese and J. J. Fripiat, *J. Colloid Interface Sci.*, 71, 441(1979).
[36] J. Hougardy, W. E. E. Stone and J. J. Fripiat, J. Chem. Phys., 64, 3840 (1976).
[37] J. Hougardy, W. E. E. Stone and J. J. Fripiat, J. Magn. Reson., 25, 563

(1977).
[38] W. E. Stone, Advanced Techniques for Clay Mineral Analysis, ed. J. J. Fripiat, pp. 77-112, Elsevier, Amsterdam, 1981.
[39] S. Ishiamru and R. Ikeda, Z. Naturforsch., 52a, 863(1997).
[40] S. Ishimaru, M. Yamauchi and R. Ikeda, Z. Naturforsch., 53a, 903(1998).
[41] S. Ishimaru and R. Ikeda, Z. Naturforsch., 54a, 431(1999).
[42] Al. Weiss, Angew. Chem., 75, 113 (1963).
[43] G. F. Walker, Clay Miner., 7, 129 (1967).
[44] G. Lagaly, Clay Miner., 16, 1 (1981).
[45] M. Yamauchi, S. Ishimaru and R. Ikeda, Mol. Cryst. Liq. Cryst., 341, 315 (2000).
[46] M. Yamauchi, S. Ishimaru and R. Ikeda, Z. Naturforsch., 54a, 755 (1999).
[47] T. Tanabe and D. Nakamura, *J. Chem. Soc. Faraday Trans.*, **87**, 987 (1991).

Highly proton-conductive copper coordination polymer, H_2dtoaCu (H_2dtoa = dithiooxamide anion)

Hiroshi Kitagawa [a, b, *], Yuki Nagao[a], Musashi Fujishima [a], Ryuichi Ikeda [a], Seiichi Kanda[c]

[a] *Department of Chemistry, University of Tsukuba, Tennodai 1-1-1, Tsukuba, Ibaraki 305-8571, Japan*
[b] *PRESTO21, Japan Science and Technology Corporation, Honcho 4-1-8, Kawaguchi, Saitama 332-0012, Japan*
[c] *Department of Chemistry, The University of Tokushima, Minamijosanjima 2-1, Tokushima 770-8506, Japan*

Received 2002; accepted 2002

Abstract

Room-temperature proton conductivity, coordination geometry, and pore-diameter distribution of the title Cu(II) coordination polymer have been investigated by AC conductivity, EXAFS, and N_2 adsorption isotherm measurements. The AC proton conductivity (σ_p) obtained from Cole-Cole plot analysis under relative humidity of 75 % and 300 K exhibits a considerable high value of 10^{-6} S cm^{-1} as a room-temperature σ_p. The mechanism of proton conduction seems to be similar to that of a proton-exchange membrane, Nafion, which contains much cluster of water molecules in the porous space of the polymer. The present Cu coordination polymer was revealed to possess porous space of about 6 Å, which includes much water molecules more than $10H_2O$ per unit cell. The dimeric Cu(II) square-planar coordination geometry was confirmed by EXAFS analysis using synchrotron radiation source at SPring-8.

1. Introduction

Solid state ionics is a new research field attracting much current attention. One of the most urgent subjects in this field is to create a novel proton conductor, from the viewpoint of developing new energy and energy conservation technologies, including photovoltaic, hydrogen storage and fuel cell technologies. In this paper, we report on a highly proton-conductive property of an inorganic-organic hybrid system, which is a 2-D coordination polymer [1 - 10] composed of Cu(II) dimers and bridging ligands H_2dtoa^{2-} (H_2dtoa^{2-} = dithiooxamide anion), as shown in Figure 1. Such a metal-dimer system with multi-redox property has a large potentiality for the creation of new-functional and high-performance materials in metal-complex solids [11 - 13].

2. Experimental

The title copper coordination polymer was prepared by a simple mixing of aqueous solution of H_2dtoaH_2 and $CuSO_4$ [1 - 3]. The qualities of samples were checked by powder X-ray diffraction, elemental analysis, and IR spectroscopy. EXAFS measurements were performed at JASRI SPring-8 (BL01B1). The distribution of pore diameters were estimated from the result of N_2 adsorption isotherm carried out at liquid nitrogen temperature with a Bell Japan Inc. BELSORP 18. The proton conductivities of H_2dtoaCu were measured by a conventional quasi-four-probe method with an Agilent Technologies 4294A impedance analyzer in the frequency range of 40 Hz - 4 MHz under relative

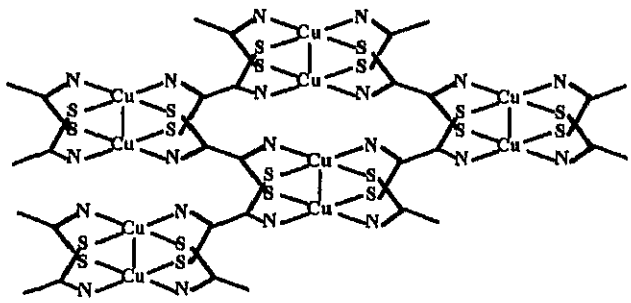

Fig. 1. Structure of H_2dtoaCu (H is omitted for the sake of clarity) [1-3].

* Corresponding author. Tel: +81(Japan)-298-53-6922; fax: +81(Japan)-298-53-6922;
E-mail: hiroshi@staff.chem.tsukuba.ac.jp

humidity (RH) of 75 % and 300 K. The RH of 75 % was maintained using saturated solution of NaCl.

3. Results and Discussions

The H_2*dtoa*Cu complex exhibits a proton-coupled redox property [4], as shown in Figure 2. According to this property, hydrogen atom (H•) can be doped to the coordination polymer, in which the hydrogen transfers an electron to the Cu(II) ion and bonds to the lone pair of electrons at the nitrogen site as a proton (H^+).

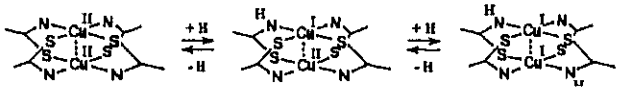

Fig. 2. Proton-coupled redox property in H_2*dtoa*Cu.

As shown in Figure 3, the Fourier-filtered $k^3\chi(k)$ vs. k EXAFS spectrum was well reproduced on the assumption that Cu(II) ion was surrounded by two S, two N, and one Cu atoms, in which obtained interatomic distances are

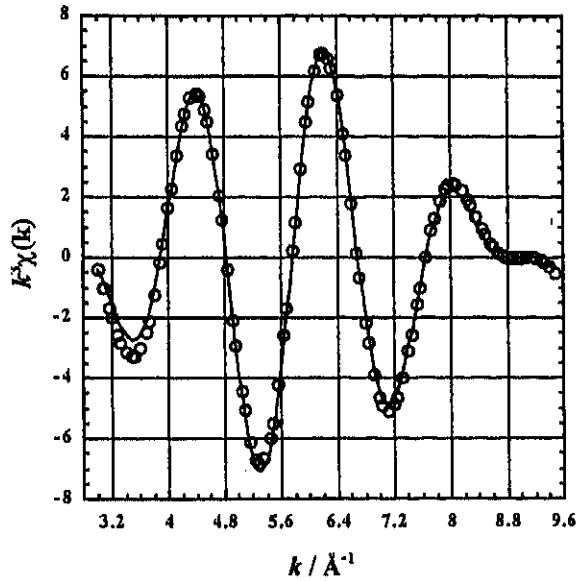

Fig. 3. Fourier-filtered $k^3\chi(k)$ vs. k EXAFS spectrum for H_2*dtoa*Cu.

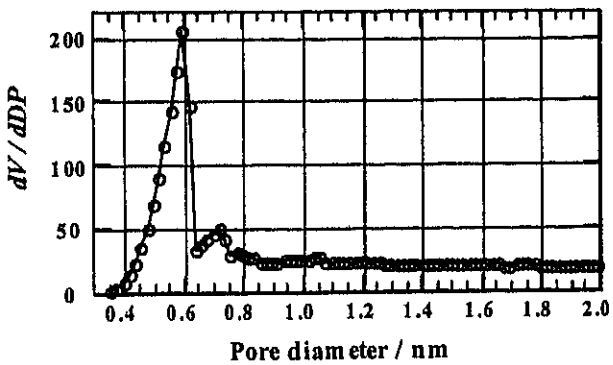

Fig. 4. Distribution curve of pore diameter for H_2*dtoa*Cu.

typical values (C-N: 1.98, C-S: 2.21, Cu-Cu: 2.60 Å). This result is consistent with the dimeric Cu(II) square-planar coordination geometry.

Figure 4 shows the distribution curve of pore diameter calculated by the HK method for the N_2 adsorption isotherm of H_2*dtoa*Cu. This indicates a sharp maximum around 0.6 nm in good agreement with the tetragonal unit cell of a = 7.04, c = 5.69 Å [9].

Figure 5 shows the real (Z') versus imaginary (Z") parts of complex-plane impedance data for H_2*dtoa*Cu under RH = 75 % and 300 K. From the plots, this coordination polymer was found to exhibit a high proton conduction of $\sigma_p = 10^{-6}$ S cm^{-1}. This value is considerable high as a room-temperature proton conductivity. The mechanism of proton conduction in H_2*dtoa*Cu is considered to be similar to that in Nafion proton-exchange membrane [14], which is well known for a solid electrolyte of fuel cell. This coordination polymer contains much water molecules more than $10H_2O$ per the unit cell under RH = 100 % [9], as well as Nafion. This is derived from the porous space of about 6 Å in H_2*dtoa*Cu, estimated from the N_2 adsorption isotherm. The proton conduction of R_2*dtoa*Cu (R = C_2H_4OH) increases by several orders of magnitude with RH [8]. The clusters of water molecules included in the polymer could make pathways of proton carriers.

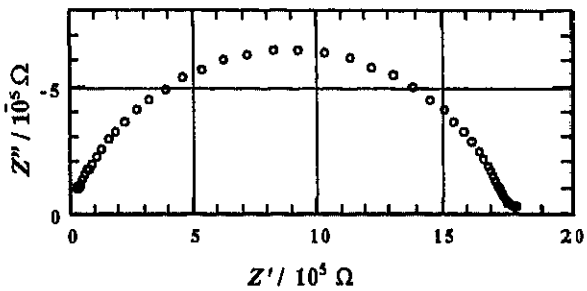

Fig. 5. Complex-plane impedance plots for H_2*dtoa*Cu.

4. Conclusion

The title Cu coordination polymer is revealed to be a proton conductor with $\sigma_p = 10^{-6}$ S cm^{-1} under RH = 75 % and 300 K from AC conductivity measurements. This kind of inorganic-organic hybrid polymers possessing proton-coupled multi-redox property could open a new field of *Molecular Solid State Ionics*.

Acknowledgments

The authors express their gratitude to Dr. Y. Kubozono of Institute for Molecular Science for his help to measure EXAFS spectra. EXAFS work was performed under the proposal of SPring-8 (2000A0194-NX). This study was partly supported by Grant-in-Aid for Exploratory Research No. 13874081 from the Japan Society for the Promotion of Science (JSPS), and by the Iwatani Naoji Foundation.

References

[1] S. Kanda, S. Kawaguchi, J. Chem. Phys. 34 (1961) 1070.
[2] S. Kanda, K. Ito, T. Nogaito, J. Poly. Sci. C 17 (1967) 151.
[3] S. Kanda, K. Yamashita, K. Ohkawa, Bull. Chem. Soc. Jpn. 52 (1979) 3296.
[4] M. Fujishima, S. Kanda, T. Mitani, H. Kitagawa, Synth. Met. 119 (2001) 485.
[5] Y. Nagao, M. Fujishima, R. Ikeda, S. Kanda, H. Kitagawa, Synth. Met. in press.
[6] M. Fujishima, Y. Nagao, R. Ikeda, S. Kanda, H. Kitagawa, Synth. Met. in press.
[7] M. Fujishima, R. Ikeda, S. Kanda, H. Kitagawa, Mol. Cryst. & Liq. Cryst. in press.
[8] Y. Nagao, R. Ikeda, S. Kanda, Y. Kubozono, H. Kitagawa, Mol. Cryst. & Liq. Cryst. in press.
[9] Y. Nagao, R. Ikeda, K. Iijima, T. Kubo, K. Nakasuji, H. Kitagawa, submitted to Synth. Met.
[10] M. Fujishima, R. Ikeda, T. Kawamura, H. Kitagawa, submitted to Synth. Met.
[11] H. Kitagawa, N. Onodera, T. Sonoyama, M. Yamamoto, T. Fukawa, T. Mitani, M. Seto, and Y. Maeda, J. Am. Chem. Soc. 121 (1999) 10068.
[12] M. Mitsumi, T. Murase, H. Kishida, T. Yoshinari, Y. Ozawa, K. Toriumi, T. Sonoyama, H. Kitagawa, T. Mitani, J. Am. Chem. Soc. 123 (2001) 11179.
[13] M. Mitsumi, K. Kitamura, A. Morinaga, Y. Ozawa, M. Kobayashi, K. Toriumi, Y. Iso, H. Kitagawa, T. Mitani, Angew. Chem. Int. Ed. in press.
[14] K.D. Kreuer, Chem. Mater., 8 (1996) 610.

* Corresponding author. Tel: +81(Japan)-298-53-6922; fax: +81(Japan)-298-53-6922; E-mail: hiroshi@staff.chem.tsukuba.ac.jp

Synthetic Metals, in preparation for ICSM2002

A new proton-conductive copper coordination polymer, $(HOC_3H_6)_2$*dtoa*Cu (*dtoa* = dithiooxamide)

Y. Nagao[a], R. Ikeda[a], K. Iijima[b], T. Kubo[b], K. Nakasuji[b], and H. Kitagawa[a, c]

[a] *Department of Chemistry, University of Tsukuba, Tsukuba, Ibaraki 305-8571, Japan*
[b] *Department of Chemistry, Osaka University, Toyonaka, Osaka 560-0043, Japan*
[c] *PRESTO, JST, Saitama 332-0012, Japan*

Abstract

A new copper coordination polymer, $(HOC_3H_6)_2$*dtoa*Cu (*dtoa* = dithiooxamide), was synthesized. The crystal structure is considered to be similar to that of a two-dimensional (2-D) coordination polymer $(HOC_2H_4)_2$*dtoa*Cu. The concentration of water molecules included in this polymer was found by thermogravimetric (TG) analysis to increase with relative humidity (RH) upon the sample preservation. The a.c. conductivity measurements with an impedance analyzer were carried out for $(HOC_3H_6)_2$*dtoa*Cu in order to estimate the proton conductivity (σ_p). The log σ_p was linearly increased from 3.3×10^{-9} to 2.0×10^{-6} S cm^{-1} with RH from 58 to 100 % at 300 K. These facts imply that the proton conduction depends on the quantity of water molecules contained in the polymer.

Keywords: proton conduction, coordination polymer, a.c. conductivity measurements, transport measurements, proton exchange membrane

1. Introduction

Proton conduction plays an important role in the solid electrolytes of a hydrogen fuel cell [1, 2], most of which are sulfonic-acid-based perfluorinated organic polymers such as the so-called Nafion®. As a novel proton-conductive system, we have investigated a series of the inorganic-organic hybrid polymers, R_2*dtoa*Cu (R= -H, $-C_2H_4OH$, etc.). *N,N'*-bis(2-hydroxyethyl)dithiooxamidato-copper(II), $(HOC_2H_4)_2$*dtoa*Cu, is a proton-conductive 2-D coordination polymer with Cu-dimeric units (Fig. 1) [3 - 5]. The proton conductivity of $(HOC_2H_4)_2$*dtoa*Cu is ~10^{-4} S cm^{-1} under relative humidity (RH) of 100 % and 300 K. The proton conductivity depends on the quantity of water molecules contained in the polymer.

As an extension of this system, we have investigated a new derivative $(HOC_3H_6)_2$*dtoa*Cu, which could contain more water molecules since the interplanar spacing is expected to be longer in R= $-C_3H_6OH$ than R= $-C_2H_4OH$.

2. Experimental

N,N'-bis(3-hydroxypropyl)dithiooxamide was prepared by a reaction of dithiooxamide with 3-aminopropanol [6] and identified by ^{1}H and ^{13}C NMR, IR, and EI-MS spectroscopies. The title coordination polymer was prepared by a simple stoichiometric mixing of 5 % C_2H_5OH(aq) solution of $(HOC_3H_6)_2$*dtoa* and $CuSO_4$(aq). The quality of sample was checked by elemental analysis, powder X-ray diffraction (XRD), and IR spectra. Thermogravimetric (TG) analysis with SII TG/DTA 6300 was made in the temperature range of 298 – 453 K for the samples preserved under the constant RHs (0, 75, 100 %) for 1 day. For a.c. conductivity measurements, the powdered sample was processed into pellets of 0.96 mm thickness and 2.5 mm ϕ under pressure (~ 1 GPa). The impedance measurements were carried out by a conventional quasi-four-probe method using gold paste and gold wires (25 μm ϕ) with an Agilent Technologies 4294A impedance analyzer in the frequency range of 40 Hz – 4 MHz at 300 K. RH was controlled in the range of 58 –

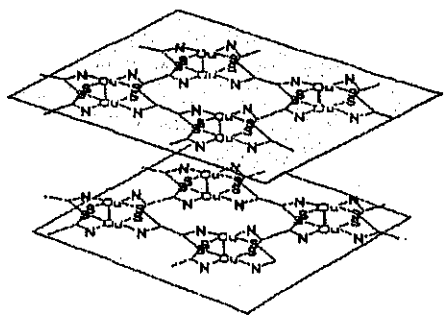

Fig. 1. Crystal structure of $(HOC_2H_4)_2$*dtoa*Cu. (R = $-C_2H_4OH$ is omitted for the sake of clarity). [3 - 5]

* Tel; +81-298-53-4487; fax: +81-298-53-4487; E-mail: ynagao@dmb.chem.tsukuba.ac.jp

100 % by using water and saturated solution of salts, generating an atmosphere of a defined RH [7].

3. Results and discussion

The crystal structure of $(HOC_3H_6)_2$*dtoa*Cu is confirmed by XRD to be similar to that of 2-D coordination polymer $(HOC_2H_4)_2$*dtoa*Cu, as shown in Fig. 1. The interplanar spacing is increased in the order of $(HOC_2H_4)_2$*dtoa*Cu (9.95 Å) < $(HOC_3H_6)_2$*dtoa*Cu (11.9 Å). The results of elemental analysis (Found: C, 29.0; H, 4.70; N, 8.51; S, 20.3) was calculated with two models. Anal. Calcd for $(HOC_3H_6)_2$*dtoa*Cu·0.25H_2O (0.25H_2O was determined by TG): C, 31.7; H, 4.63; N, 9.26; S, 21.2. Anal. Calcd for $[(HOC_3H_6)_2dtoa]_{1-x}4x(H_2O)\cdot y(H_2O)$Cu ($x$ = 0.11, y = 0.81) ($4x(H_2O)$ is coordinated water, $y(H_2O)$ is crystal water forming hydrogen bonds): C, 29.0; H, 5.08; N, 8.47; S, 19.4. The latter model seems more reasonable, because of the followings; the weight loss up to ca. 420 K is due to the crystal water, while that above it to the coordinated water. The crystal structure was maintained up to 473 K, which was checked by XRD.

Fig. 2 shows the results of TG analysis for $(HOC_3H_6)_2$*dtoa*Cu. The concentration of water molecules was found to increase with RH upon the sample preservation was increased. Although the $(HOC_3H_6)_2$*dtoa*Cu was expected to contain more water molecules because of the increased interplanar spacing, each of $(HOC_3H_6)_2$*dtoa*Cu and $(HOC_2H_4)_2$*dtoa*Cu was found to contain the same number (3.3) of water molecules per dimeric units under RH of 100 %.

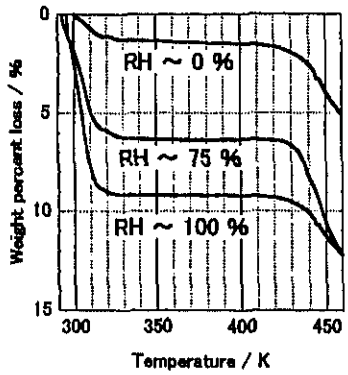

Fig. 2. TG analysis for $(HOC_3H_6)_2$*dtoa*Cu.

The proton conductivity (σ_p) was obtained by the complex-plane impedance plots. The d.c. electron conductivity is found to be negligible ($\sigma_e \sim 5.8 \times 10^{-11}$ S cm^{-1}) compared to the proton conductivity under RH of 58 – 100 %. Fig. 3 shows the RH dependence of log σ_p for $(HOC_3H_6)_2$*dtoa*Cu. The log σ_p is linearly increased from 3.3×10^{-9} to 2.0×10^{-6} S cm^{-1} with RH from 58 to 100 %. The concentration of water molecules included in the polymer was also found to increase with RH (Fig. 2). These facts imply the proton conduction depends on the quantity of water molecules contained in the polymer.

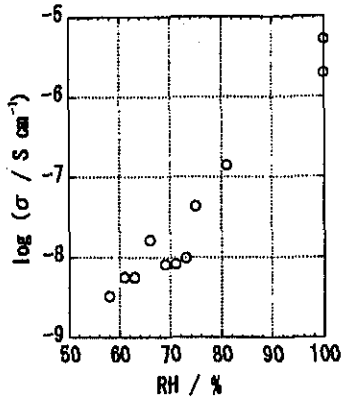

Fig. 3. Log (proton conductivity) vs. RH plots for $(HOC_3H_6)_2$*dtoa*Cu at 300 K.

It is well known that the proton conductor "Nafion®", which is used as solid electrolyte in the fuel cell, also contains much water clusters and these make pathway of the proton conduction [1, 2]. This coordination polymer is considered to have the same mechanism.

4. Conclusion

A new derivative copper coordination polymer, $(HOC_3H_6)_2$*dtoa*Cu, was revealed to be a proton conductor by a.c. conductivity measurements. The proton conductivity depends on the quantity of water molecules contained in the polymer.

5. Acknowledgment

This work was partly supported by Grant-in-Aid Scientific Researches No. 13874081 of Exploratory Research, No. 11640559 of (C), and No. 10149104 (401: Metal-Assembled Complexes) of Priority Areas (A) from the Ministry of Education, Culture, Sports, Science, and Technology of Japan, and by the grant program of Yazaki Memorial Foundation for Science & Technology.

References

[1] P. Colomban, (ed.), Proton Conductors: Solids, membranes and gels – materials and devices, Cambridge University Press, Cambridge, 1992.
[2] K.D. Kreuer, Chem. Mater. 8 (1996) 610.
[3] S. Kanda, K. Yamashita, K. Ohkawa, Bull. Chem. Soc. Jpn. 52(11) (1979) 3296.
[4] M. Fujishima, S. Kanda, T. Mitani, H. Kitagawa, Synth. Met. 119 (2001) 485.
[5] Y. Nagao, M. Fujishima, S. Kanda, R. Ikeda, H. Kitagawa, Synth. Met. in press.
[6] H.M.Woodburn, M. Platek, E.L. Graminski, J. Org. Chem. 23 (1958) 319.
[7] F. Opekar, D. Svozil, J. Electroanal. Chem. 385 (1995) 269.

Highly proton-conductive copper coordination polymer, H_2dtoaCu (H_2dtoa = dithiooxamide anion)

Hiroshi Kitagawa [a, b, *], Yuki Nagao [a], Musashi Fujishima [a], Ryuichi Ikeda [a], Seiichi Kanda [c]

[a] *Department of Chemistry, University of Tsukuba, Tennodai 1-1-1, Tsukuba, Ibaraki 305-8571, Japan*
[b] *PRESTO21, Japan Science and Technology Corporation, Honcho 4-1-8, Kawaguchi, Saitama 332-0012, Japan*
[c] *Department of Chemistry, The University of Tokushima, Minamijosanjima 2-1, Tokushima 770-8506, Japan*

Received 2002; accepted 2002

Abstract

Room-temperature proton conductivity, coordination geometry, and pore-diameter distribution of the title Cu(II) coordination polymer have been investigated by AC conductivity, EXAFS, and N_2 adsorption isotherm measurements. The AC proton conductivity (σ_p) obtained from Cole-Cole plot analysis under relative humidity of 75 % and 300 K exhibits a considerable high value of 10^{-6} S cm^{-1} as a room-temperature σ_p. The mechanism of proton conduction seems to be similar to that of a proton-exchange membrane, Nafion, which contains much cluster of water molecules in the porous space of the polymer. The present Cu coordination polymer was revealed to possess porous space of about 6 Å, which includes much water molecules more than $10H_2O$ per unit cell. The dimeric Cu(II) square-planar coordination geometry was confirmed by EXAFS analysis using synchrotron radiation source at SPring-8.

Keywords: Solid state ionics, Proton conduction, Hydrogen storage, Proton-exchange membrane, EXAFS, Coordination polymer

1. Introduction

Solid state ionics is a new research field attracting much current attention. One of the most urgent subjects in this field is to create a novel proton conductor, from the viewpoint of developing new energy and energy conservation technologies, including photovoltaic, hydrogen storage and fuel cell technologies. In this paper, we report on a highly proton-conductive property of an inorganic-organic hybrid system, which is a 2-D coordination polymer [1 - 10] composed of Cu(II) dimers and bridging ligands H_2dtoa^{2-} (H_2dtoa^{2-} = dithiooxamide anion), as shown in Figure 1. Such a metal-dimer system with multi-redox property has a large potentiality for the creation of new-functional and high-performance materials in metal-complex solids [11 - 13].

2. Experimental

The title copper coordination polymer was prepared by a simple mixing of aqueous solution of H_2dtoaH_2 and $CuSO_4$ [1 - 3]. The qualities of samples were checked by powder X-ray diffraction, elemental analysis, and IR spectroscopy. EXAFS measurements were performed at JASRI SPring-8 (BL01B1). The distribution of pore diameters were estimated from the result of N_2 adsorption isotherm

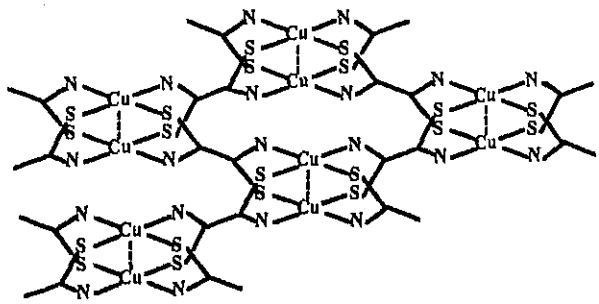

Fig. 1. Structure of H_2dtoaCu (H is omitted for the sake of clarity) [1-3].

* Corresponding author. Tel: +81(Japan)-298-53-6922; fax: +81(Japan)-298-53-6922;
E-mail: hiroshi@staff.chem.tsukuba.ac.jp

carried out at liquid nitrogen temperature with a Bell Japan Inc. BELSORP 18. The proton conductivities of H_2*dtoa*Cu were measured by a conventional quasi-four-probe method with an Agilent Technologies 4294A impedance analyzer in the frequency range of 40 Hz - 4 MHz under relative humidity (RH) of 75 % and 300 K. The RH of 75 % was maintained using saturated solution of NaCl.

3. Results and Discussions

The H_2*dtoa*Cu complex exhibits a proton-coupled redox property [4], as shown in Figure 2. According to this property, hydrogen atom (H•) can be doped to the coordination polymer, in which the hydrogen transfers an electron to the Cu(II) ion and bonds to the lone pair of electrons at the nitrogen site as a proton (H^+).

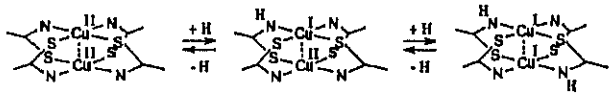

Fig. 2. Proton-coupled redox property in H_2*dtoa*Cu.

As shown in Figure 3, the Fourier-filtered $k^3\chi(k)$ vs. k EXAFS spectrum was well reproduced on the assumption that Cu(II) ion was surrounded by two S, two N, and one Cu atoms, in which obtained interatomic distances are typical values (C-N: 1.98, C-S: 2.21, Cu-Cu: 2.60 Å). This result is consistent with the dimeric Cu(II) square-planar coordination geometry.

Figure 4 shows the distribution curve of pore diameter calculated by the HK method for the N_2 adsorption isotherm of H_2*dtoa*Cu. This indicates a sharp maximum around 0.6 nm in good agreement with the tetragonal unit cell of $a = 7.04$, $c = 5.69$ Å [9].

Figure 5 shows the real (Z') versus imaginary (Z") parts of complex-plane impedance data for H_2*dtoa*Cu under RH = 75 % and 300 K. From the plots, this coordination polymer was found to exhibit a high proton conduction of $\sigma_p = 10^{-6}$ S cm^{-1}. This value is considerable high as a room-temperature proton conductivity. The mechanism of proton conduction in H_2*dtoa*Cu is considered to be similar to that in Nafion proton-exchange membrane [14], which is well known for a solid electrolyte of fuel cell. This coordination polymer contains much water molecules more than $10H_2O$ per the unit cell under RH = 100 % [9], as well as Nafion. This is derived from the porous space of about 6 Å in H_2*dtoa*Cu, estimated from the N_2 adsorption isotherm. The proton conduction of R_2*dtoa*Cu (R = C_2H_4OH) increases by several orders of magnitude with RH [8]. The clusters of water molecules included in the polymer could make pathways of proton carriers.

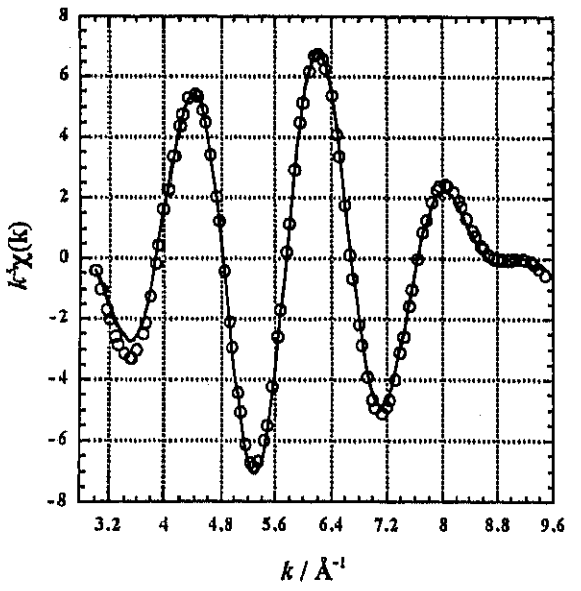

Fig. 3. Fourier-filtered $k^3\chi(k)$ vs. k EXAFS spectrum for H_2*dtoa*Cu.

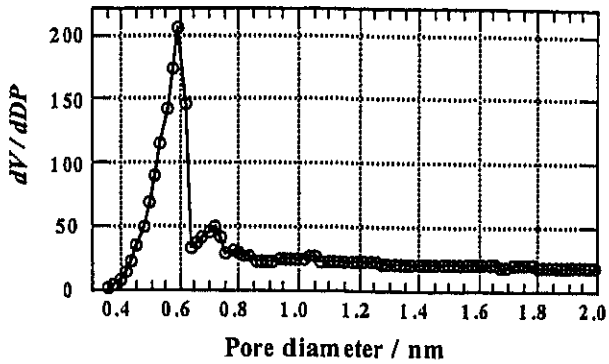

Fig. 4. Distribution curve of pore diameter for H_2*dtoa*Cu.

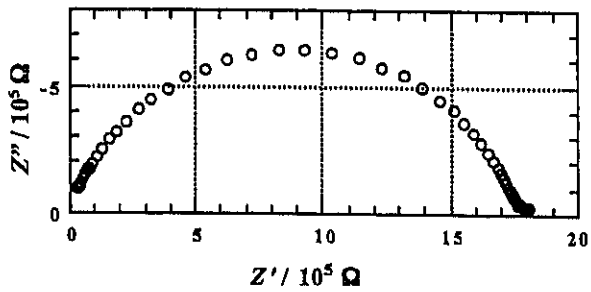

Fig. 5. Complex-plane impedance plots for H_2*dtoa*Cu.

4. Conclusion

The title Cu coordination polymer is revealed to be a proton conductor with $\sigma_p = 10^{-6}$ S cm^{-1} under RH = 75 % and 300 K from AC conductivity measurements. This kind of inorganic-organic hybrid polymers possessing proton-coupled multi-redox property could open a new field of *Molecular Solid State Ionics*.

Acknowledgments

The authors express their gratitude to Dr. Y. Kubozono of Institute for Molecular Science for his help to measure EXAFS spectra. EXAFS work was performed under the proposal of SPring-8 (2000A0194-NX). This study was partly supported by Grant-in-Aid for Exploratory Research

No. 13874081 from the Japan Society for the Promotion of Science (JSPS), and by the Iwatani Naoji Foundation.

References

[1] S. Kanda, S. Kawaguchi, J. Chem. Phys. 34 (1961) 1070.
[2] S. Kanda, K. Ito, T. Nogaito, J. Poly. Sci. C 17 (1967) 151.
[3] S. Kanda, K. Yamashita, K. Ohkawa, Bull. Chem. Soc. Jpn. 52 (1979) 3296.
[4] M. Fujishima, S. Kanda, T. Mitani, H. Kitagawa, Synth. Met. 119 (2001) 485.
[5] Y. Nagao, M. Fujishima, R. Ikeda, S. Kanda, H. Kitagawa, Synth. Met. in press.
[6] M. Fujishima, Y. Nagao, R. Ikeda, S. Kanda, H. Kitagawa, Synth. Met. in press.
[7] M. Fujishima, R. Ikeda, S. Kanda, H. Kitagawa, Mol. Cryst. & Liq. Cryst. in press.
[8] Y. Nagao, R. Ikeda, S. Kanda, Y. Kubozono, H. Kitagawa, Mol. Cryst. & Liq. Cryst. in press.
[9] Y. Nagao, R. Ikeda, K. Iijima, T. Kubo, K. Nakasuji, H. Kitagawa, submitted to Synth. Met.
[10] M. Fujishima, R. Ikeda, T. Kawamura, H. Kitagawa, submitted to Synth. Met.
[11] H. Kitagawa, N. Onodera, T. Sonoyama, M. Yamamoto, T. Fukawa, T. Mitani, M. Seto, and Y. Maeda, J. Am. Chem. Soc. 121 (1999) 10068.
[12] M. *Mitsumi*, T. *Murase*, *H. Kishida*, T. *Yoshinari*, Y. Ozawa, K. Toriumi, T. Sonoyama, H. Kitagawa, T. Mitani, J. Am. Chem. Soc. 123 (2001) 11179.
[13] M. Mitsumi, K. Kitamura, A. Morinaga, Y. Ozawa, M. Kobayashi, K. *Toriumi*, Y. Iso, H. Kitagawa, T. Mitani, Angew. Chem. Int. Ed. in press.
[14] K.D. Kreuer, Chem. Mater., 8 (1996) 610.

* Corresponding author. Tel: +81(Japan)-298-53-6922; fax: +81(Japan)-298-53-6922; E-mail: hiroshi@staff.chem.tsukuba.ac.jp

^{13}C NMR Spectra, ^{1}H NMR Relaxation and ESR Measurements of Br_2 Doped $\{[Pt(en)_2][PtBr_2(en)_2]\}_3(CuBr_4)_4 \cdot 12H_2O$

N. Kimura[a,*], H. Aso[b], K. Takizawa[b], T. Ishii[b], H. Miyasaka[b], K. Sugiura[b], M. Yamashita[b] and R. Ikeda[c]

[a] *Department of Chemistry, Faculty of Education, Wakayama University, Wakayama 640-8510, Japan*
[b] *Graduate School of Science, Tokyo Metropolitan University, Hachioji 192-0397, Japan*
[c] *Department of Chemistry, University of Tsukuba, Tsukuba 305-8571, Japan*

Received; accepted

Abstract

We measured NMR and ESR in solid state of a Br_2 doped halogen-bridged one-dimensional mixed-valence complex, $\{[Pt(en)_2][PtBr_2(en)_2]\}_3(CuBr_4)_4 \cdot 12H_2O$, which forms a double chain structure consisting of -Pt(II)-Br-Pt(IV)-Br- and -Cu(I)-Br-Cu(I)-Br-. ^{13}C NMR measurements gave broad spectra explainable by marked effects from paramagnetic sites assignable to Pt(III) and/ or Cu(II) in the chain oxidized by bromine. Pt(III) sites are considered to form neutral solitons by referring to the electrical conductivity result.

Keywords: (Nuclear magnetic resonance spectroscopy, Electron spin resonance)

1. Introduction

Halogen-bridged one-dimensional mixed-valence complexes with a chain structure, -M(II)-X-M(IV)-X- (M: Pt, Pd; X: Cl, Br, I) have attracted attention interests among chemists and physicists because of their marked optical [1], structural [2] and magnetic properties [3]. In this system, the neutral soliton is expected to be formed by inserting a paramagnetic M(III) site as -X-M(II)-X-M(IV)-X-M(III)-X-M(II)-X-M(IV)-X-, by noting a twofold degeneracy of the electronic ground state in this chain structure.

Recently, UV-Vis-NIR absorption and ESR studies [4] have been reported on Br_2 doped $\{[Pt(en)_2][PtBr_2(en)_2]\}_3(CuBr_4)_4 \cdot 12H_2O$ (en: ethylenediamine), which consists of double chains of -Pt(II)-Br-Pt(IV)-Br- and -Cu(I)-Br-Cu(I)-Br-. It was shown that the concentration of paramagnetic sites in the doped sample is one order of magnitude higher than in the pure crystals. In the present study, we investigate the paramagnetic spin behavior on the chain by measuring ^{13}C and ^{1}H NMR, and ESR.

2. Experimental

$\{[Pt(en)_2][PtBr_2(en)_2]\}_3(CuBr_4)_4 \cdot 12H_2O$ was prepared by the reported method [5]. Doped sample was synthesized by exposing Br_2 vapor to crystalline samples of the compound in a dessicator for 30 min.

A Bruker MSL-300 spectrometer was used for the measurement of ^{13}C CP/ MAS NMR spectra at a Larmor frequency of 75.468 MHz and a sample-spinning rate of *ca.* 4kHz at room temperature. TMS and solid adamantane were used as external standards of chemical shift. The ^{1}H NMR spin-lattice relaxation time (T_1) was measured at 54.3 MHz by the inversion recovery method in a range 100-300 K using a homemade spectrometer [6]. ESR spectra were observed with a Bruker EMX-T spectrometer.

*Corresponding author. Tel: +81-73-457-7365; fax: +81-73-457-7515;
E-mail: nkimura@center.wakayama-u.ac.jp

3. Results and Discussion

^{13}C CP/ MAS NMR spectra at room temperature for doped and pure samples are shown in Figs. 1 (a) and (b), respectively.

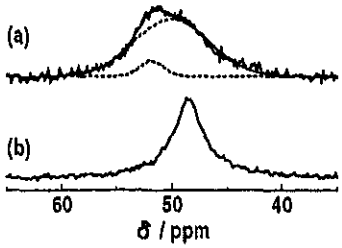

Fig. 1 ^{13}C CP / MAS NMR spectra observed at room temperature for Br_2 doped (a) and pure samples (b). The best-fitted solid line in Fig. 1(a) shows spectra obtained by the combination of two broken lines.

We can see that ^{13}C in the doped sample gave a signal broader than in the pure sample, and consists of separated two peaks shown by two broken lines in Fig. 1(a). The strong peak with a smaller chemical shift is assignable to carbons in ethylenediamine coordinated to Pt(II) and Pt(IV), because the shift value of this peak can be corresponded to that in pure sample. On the other hand, the observed weak signal at a low field is attributable to carbons in the fluctuated magnetic field made by paramagnetic Pt(III) and Cu(II) sites. This shift could not be attributed to the Knight shift because no increase of the electrical conductivity upon doping was reported [4]. The intensity ratio obtained for these two peaks nearly corresponds to the spin concentration (*ca.* 0.05 in molar ratio to the total Pt and Cu concentration) observed in ESR measurement shown in Fig. 2(a). The ESR spectrum (Fig.2 (b)) for the pure sample was estimated to be *ca.* 10^{-4} molar ratio, and we can assume that these paramagnetic sites were formed as impurities in the stage of crystallization.

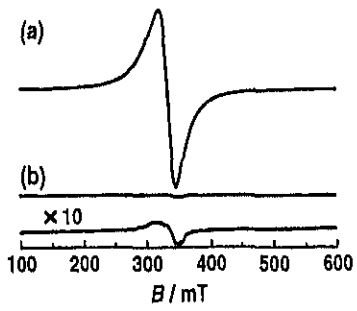

Fig. 2 ESR spectra at room temperature observed in Br_2 doped (a) and the pure samples (b). Samples of *ca.* 0.1 g were used for measurements.

We also measured temperature dependences of ^1H spin-lattice relaxation times T_1 in Br_2 doped and the pure samples, and the magnetization recovery expresses as $\log(M_0-M_\tau)$ after a $\pi/2$ pulse observed at 114 K in the doped sample is shown in Fig. 3.

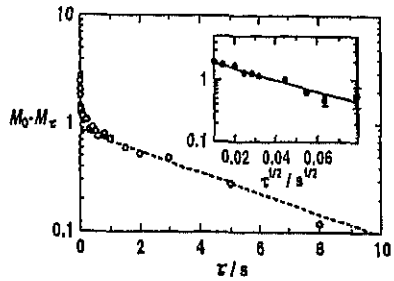

Fig. 3 ^1H magnetization recoveries after a π-τ-$\pi/2$ pulse sequence observed at 114 K and a Larmor frequency of 54.3 MHz in Br_2 doped $\{[Pt(en)_2][PtBr_2(en)_2]\}_3(CuBr_4)_2 \cdot 12H_2O$. The slope of the broken line affords T_1 of 4.4 s. Solid line is fitted the magnetization proportional to the square root of the duration time τ.

This curve can be roughly divided into two components exhibiting fast and slow relaxations. The origin of the fast and main relaxation component can be assigned to trapped or fixed paramagnetic sites on the chain. This is because proton spins located near fixed paramagnetic sites feel a strong fluctuating of magnetic field made by the electron spins, and, since the magnitude of the fluctuation field depends upon the electron-proton distance, distributed T_1 values are observed. In such cases, the recovery of $\log(M_0-M_\tau)$ at short duration times τ shows a linear relation with the square root of τ when spin diffusion among protons is slow enough [7]. In fact, the fast component roughly satisfied this relationship as shown in Fig. 3, supporting this interpretation of the paramagnetic relaxation mechanism. These trapped paramagnetic sites are expected to be Pt(III) and/ or Cu(II) species oxidized in the chain, and the Pt(III) sites are considered to form neutral solitons by referring to the conductivity result [4].

Acknowledgements

The ESR spectra were recorded with a Bruker EMX-T ESR spectrometer at Chemical Analysis Center, University of Tsukuba.

This work was partly supported by Grant-in Aid for scientific research No.(B) 12440192 from the Ministry of Education, Culture, Sports Science and Technology.

References

[1] D. S. Martin, Jr., in J. S. Miller, (ed.), Extended Linear Chain Compounds, Plenum Press, New York, vol. 1, 1982, p. 409.

[2] H. J. Keller, in J. S. Miller, (ed.), Extended Linear Chain Compounds, Plenum Press, New York, vol. 1, 1982, p. 357.

[3] A. Kawamori, R. Aoki, M. Yamashita, J. Phys. C 18 (1985) 5487; N. Kimura, S. Ishimaru, R. Ikeda, M. Yamashita, J. Chem. Soc. Faraday Trans. 94 (1998) 3659.

[4] H. Aso, T. Manabe, T. Kawashima, T. Ishii, H. Matsuzaka, M. Yamashita, N. Kuroda, Synth. Met. 120 (2001) 775.

[5] H. Endres, H. J. Keller, R. Martin, U. Traeger, Acta Crystallogr. B35 (1979) 2880.

[6] T. Kobayashi, H. Ohki, R. Ikeda, Mol. Cryst. Liq. Cryst. 257 (1994) 279.

[7] W. E. Blumberg, Phys. Rev. 119 (1960) 79.

METAL VALENCE STRUCTURES IN 1-D MIXED-METAL COMPLEXES $[Ni_{1-x}Pd_xX(chxn)_2]X_2$ STUDIED BY SOLID NMR

Noriyoshi Kimura[1], Masataka Kano[1], Toshio Manabe[2], Masahiro Yamashita[2] and Ryuichi Ikeda[1*]

[1]*Department of Chemistry, University of Tsukuba, Tsukuba, 305-8571, Japan*

[2]*Graduate School of Science, Tokyo Metropolitan University, Hachioji, Tokyo 192-0397*

Abstract

^{13}C magic-angle-spinning NMR spectra in solid were measured in mixed-metal 1-D complexes $[Ni_{1-x}Pd_xX(chxn)_2]X_2$ (X: Cl, Br; $0.0 \leq x \leq 1.0$) where the antiferromagnetically coupled paramagnetic $-X-Ni^{3+}-X-Ni^{3+}-$ chains are formed at $x=0.0$, while the mixed-valence $-X-Pd^{2+}-X-Pd^{4+}-$ state is made at $x=1.0$. Upon increasing x from 0.0, ^{13}C spectra in the C_α position in the chxn ligand was broadened and shifted from original Pd^{2+} and Pd^{4+} positions indicating the fluctuation of Pd valency in mixed states. A marked spectrum broadening observed in C_β is also attributable to the effect from the partial mixing of paramagnetic Pd^{3+}sites in consistent with reported ESR results.

Keywords: Nuclear Magnetic Resonance Spectroscopy

1. Introduction

Halogen-bridged quasi-one-dimensional complexes $[MX(chxn)_2]X_2$ (chxn: 1*R*,2*R*-cyclohexanediamine, $C_6H_{10}(NH_2)_2$; X: Cl, Br) have been reported to form a mixed-valence diamagnetic $-X-M^{2+}-X-M^{4+}-$ structure for M=Pd [1], whereas an averaged paramagnetic $-X-M^{3+}-X-M^{3+}-$ structure for M= Ni[2]. Recently, crystals of mixed-metal complexes $[Ni_{1-x}Pd_xX(chxn)_2]X_2$ consisting of homogeneously mixed crystalline lattices of the two kinds of metal complexes with an isomorphous structure(I222) were prepared by applying the electrochemical oxidation technique[3]. The X-ray diffraction study on Br-bridged complexes showed continuously changing lattice constants from b=51.67(x=0.0) to 52.92 nm(x=1.0) corresponding to the M-M distances in the whole range $0.0 \leq x \leq 1.0$. On these series of complexes, the x dependence of ESR spectra was measured[4] and revealed a continuos change of spectrum-width with x. A marked result was that the evaluated spin susceptibility showed no linear relation with x, but almost constant up to $x \approx 0.6$. This suggests that most of diamagnetic Pd^{2+} and Pd^{4+} metal sites behave like paramagnetic at concentrations lower than $x = 0.5$. The change of the Pd valence was also observed in IR spectra[3] of the N-H stretching bands in both Pd^{2+} and Pd^{4+} units which showed a gradual shift to that in the Ni^{3+} unit. An analogous shift was also reported[3] in the measurement of the Pd-Br stretching band in Raman scattering with decreasing x.

These studies imply the instability and fluctuation of the Pd valency in the present 1-D system where the energy difference between Pd^{2+} and Pd^{4+} is small compared with the other kinds of mixed-valence halogen-bridged complexes of Pd and Pt.

From ^{13}C NMR measurements, we can get local magnetic structures and magnetic field fluctuations on ligand carbons. In the present study, we intend to measure ^{13}C MAS NMR in $[Ni_{1-x}Pd_xX(chxn)_2]X_2$ (X: Cl, Br; $0.0 \leq x \leq 1.0$) and discuss the local electronic structure in this system.

2. Experimental

Crystals of mixed-metal complexes $[Ni_{1-x}Pd_xBr(chxn)_2]Br_2$ ($0.0 \leq x \leq 1.0$) were prepared by electrochemical oxidation of monomer complexes $[M(chxn)_2]Br_2$ (M: Ni, Pd) according to literature[3]. $[Ni_{1-x}Pd_xCl(chxn)_2]Cl_2$ ($0.0 \leq x \leq 1.0$) were synthesized analogously to Br complexes at ca. 320 K by flowing a dc current of ca. 15 μA for one month using tetramethylammonium chloride as a supporting electrolyte. The concentration of metals in measured specimens was determined by ICP emission spectrometry.

A Bruker MSL-300 spectrometer was used for the measurement of ^{13}C MAS-NMR spectra at a Larmor frequency of 75.468 MHz and sample spinning rate of 2-4 kHz at room temperature. TMS and solid adamantine were

*Corresponding author. Tel & fax:+81-298-53-4250;
E-mail:ikeda@chem.tsukuba.ac.jp

used as external standards of chemical shift. The ^{1}H NMR spin-lattice relaxation time was measured at 54.3 MHz by the inversion recovery method in a range of 100 - 300 K using a home-made spectrometer described elsewhere[5].

3. Results and Discussion

The x dependences of observed ^{13}C MAS NMR spectra at room temperature for $[Ni_{1-x}Pd_xCl(chxn)_2]Cl_2$ and $[Ni_{1-x}Pd_xBr(chxn)_2]Br_2$ are shown in Figs. 1 and 2, respectively. In both Figs. 1and 2, three kinds of carbons, C_α, C_β and C_γ in a

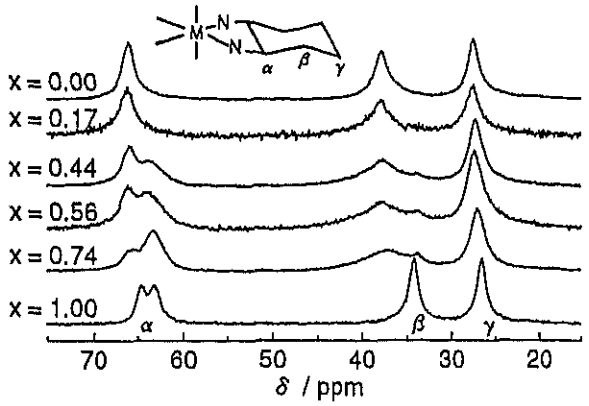

Fig. 1 ^{13}C MAS NMR spectra observed in $[Ni_{1-x}Pd_xCl(chxn)_2]Cl_2$ and carbon positions in a cyclohexanediamine ligand in a M(chxn) chelate ring(M: Pd,Ni).

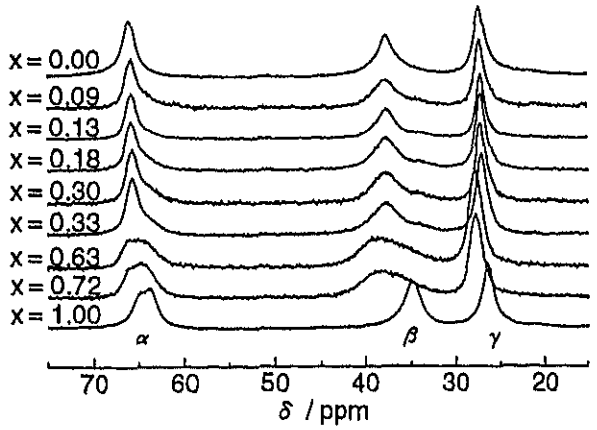

Fig. 2 ^{13}C MAS NMR spectra observed in $[Ni_{1-x}Pd_xBr(chxn)_2]Br_2$

cyclohexanediamine(chxn) ligand were observed as separated peaks. We can see that C_α and C_β signals showed marked metal and x dependences, while C_γ remote from metals gave almost independent shift values in both Cl and Br complexes. In x= 1.0, two C_α carbon signals observed are assignable to Pd^{2+} and Pd^{4+} sites, while a single C_α line in x =0.0 shows the formation of the averaged Ni^{3+} state[6]. With increasing x from 0.0, the C_α and C_β signals gradually decreased thier intensity at the same shift values. This implies that Ni atoms are always in the trivalent state regardless of Pd concentrations. On the other hand, C_α and C_β signals in Pd chelate rings observed in x= 1.0 were markedly weakened and broadened with decreasing x. This indicates that valency states of Pd^{2+} and Pd^{4+} become unstable in the presence Ni^{3+} sites in the neibourhood.

We tried to separate C_α signals observed in the Cl complex in the mixed metal range into two components corresponding to Ni and Pd sites. By this separation, we obtained small shifts and broadening of Pd carbons suggesting the fluctuation of Pd^{2+} and Pd^{4+} valences attributable to the mixing of the paramagnetic Pd^{3+} state. This explanation agrees well with the spin susceptibility data obtained from ESR measurement of Br complex[4] reporting the formation of paramagnetic Pd sites in the presence of Ni^{3+} in x>0.6.

We can expect that quite analogous discussion is possible in Br complex. In the Br complex of x= 1.0, since the energy difference between Pd^{2+} and Pd^{4+} is much smaller than in the Cl complex, the spectrum splitting between them is small implying the valence mixing in Pd easier than that in the Cl analogue. Similar results were reported from Raman spectra[3] showing a gradual intensity decrease in the Pd-Br stretching band with increasing x which was explained by the Pd valence fluctuation, i.e., the formation of Pd^{3+}.

We measured ^{1}H NMR spin-lattice relaxation time T_1 in some of this mixed metal system. At $x < 0.13$, T_1 values and its temperature dependence observed above *ca.* 100 K were almost independent of x. Since the T_1 temperature dependence at x= 0.0 was explainable by a strongly coupled antiferromagnetic 1-D chain model, this result suggests that this chain structure still retains in mixed crystals implying formation Pd^{3+}. At x=1.0, a gradual decrease T_1 observed upon heating from *ca.* 100 K was explained by the diffusion of spin solitons formed by the impurity order of Pd^{3+}[7]. With a little reduction of x from 1.0, T_1 showed marked changes that its value increased several times and its temperature dependency was reversed being close to that in x=0.0. This suggests the strong effect from paramagnetic spins which are present as Ni^{3+} even at low concentrations.

This work was partly supported by Grant-in Aid for scientific research No.(B) 12440192 from the Ministry of Education, Science, Sports and Culture.

References

[1] A. Hazell, Acta Crystallogr. C47 (1991) 962.
[2] H. Okamoto, K. Toriumi, T. Mitani and M. Yamashita, Phys. Rev. 42 (1990) 10381.
[3] M. Yamashita, T. Ishii, H. Matsuzaka, T. Manabe, T. Kawashima, H. Okamoto, H. Kitagawa, T. Mitani, K. Marumoto and S. Kuroda, Inorg. Chem. 38 (1999) 5124.
[4] K. Marumoto, T. Tanaka, S. Kuroda, T. Manabe and M. Yamashita, Phys. Rev. B 60 (1999) 7699.
[5] T. Kobayashi, H. Ohki and R. Ikeda, Mol. Cryst. Liq. Cryst. 257 (1994) 279.
[6] R. Ikeda, T. Tamura and M. Yamashita, Chem. Phys. Lett. 173 (1990) 466.
[7] R. Ikeda, M. Iida, T. Asaji, A. Ghosh and M. Yamashita, Chem. Phys. Lett. 210 (1993) 78.

Electrical conductivity of a conductive mixed-valence MMX-chain $Pt_2(CH_3CS_2)_4I$ under high pressure

Hiroshi Kitagawa [a, *], Tomohiko Suto [a], Rie Makiura [a], Ryuichi Ikeda [a], and Nao Takeshita [b], Nobuo Môri [b, §]

[a] *Department of Chemistry, University of Tsukuba, Tennodai 1-1-1, Tsukuba, Ibaraki 305-8571, Japan*
[b] *Institute for Solid State Physics, University of Tokyo, Kashiwanoha, Kashiwa, Chiba 277-8581, Japan*
[§] *Present address; Department of Physics, Saitama University, Shimo-okubo 255, Saitama 338-8570, Japan*

Received 2002; accepted 2002

Abstract

The effect of hydrostatic pressure on the electrical conductivity of a halogen-bridged one-dimensional mixed-valence binuclear transition-metal complex (the so-called MMX chain), $Pt_2(CH_3CS_2)_4I$ has been investigated using a clamp-cell-type apparatus. Charge-polarization state of $-Pt^{2+}$-Pt^{3+}-I—Pt^{2+}-Pt^{3+}-I—, which is a Mott-Hubbard insulator, was found to be stabilized at high pressures. The stabilization of this charge order is considered to be due to the Coulomb repulsion of the nearest-neighbor pairs of electrons.

Keywords: MMX Chain, Mixed Valence, High Pressure, Electrical Conductivity, Metal-Insulator Transition, Charge Ordering

1. Introduction

The search for high-temperature superconductivity and novel superconducting mechanisms is one of the most challenging tasks of condensed-matter physicists and materials research scientists. Bednorz and Müller considered mixed-valent effect of Cu ions in the $La_{1-x}Ba_xCuO_4$ system as a mechanism for strong electron-phonon interactions allowing a high T_c. To our interest, a possibility of an unusual superconducting state, which results from condensation of bipolarons, is postulated under a strongly coupled electron-phonon system [1]. According to this model, Cooper-pair formation due to the condensation of bipolarons occurs under some electron-phonon coupling constant λ, while in the large λ limit bipolarons' formation occurs at real space.

On the other hand, insulating MX chain of $-M^{II}$-X-M^{IV}-X- is regarded as on-site bipolaronic state where bipolarons form a one-dimensional (1-D) lattice and localize at M^{II} sites, so that it has been investigated as "a model material" for searching for high-T_c.

Recently attention as alternative model material has been focused on a wide variety of 1-D electronic states in halogen-bridged 1-D mixed-valence binuclear transition-metal complexes (the so-called MMX chains) from both chemical and physical points of view [2 - 4]. Lots of kinds of physical properties, derived from their one dimensionality, have been observed; examples including charge orders, metallic transport, charge-density-wave (CDW) state, Mott-Hubbard state, spin-Peierls state. Some of the possible 1-D charge modes for the MMX chain are shown below.

(1) ····$M^{2.5+}$-$M^{2.5+}$—X—$M^{2.5+}$-$M^{2.5+}$—X—$M^{2.5+}$-$M^{2.5+}$—X····
(2) ····M^{2+}-M^{2+}—X-M^{3+}-M^{3+}-X—M^{2+}-M^{2+}—X-M^{3+}-M^{3+}-X····
(3) ····M^{2+}-M^{3+}-X—M^{2+}-M^{3+}-X—M^{2+}-M^{3+}-X—M^{2+}-M^{3+}-X····
(4) ····M^{2+}-M^{3+}-X-M^{3+}-M^{2+}—X—M^{2+}-M^{3+}-X-M^{3+}-M^{2+}—X····

The title MMX chain has a neutral-chain structure of -I-$Pt_2(CH_3CS_2)_4$-I-$Pt_2(CH_3CS_2)_4$-I-, as shown in Fig. 1. According to our recent work [2], this complex was found to exhibit a metal-insulator transition at 300 K (=T_{M-I}), which relates to a Mott-Hubbard transition associated with 1-D charge ordering like mode (3) keeping the spin degree of freedom down to 100 K, below which a spin-Peierls-like transition occurs, resulting a formation of mode (4). In this work, we report on transport properties under high pressure for $Pt_2(CH_3CS_2)_4I$, in which an effectively half-filled conduction band of d_σ* [i.e. ($5d_{z^2}$-$5d_{z^2}$)*] is formed (each Pt_2-dimer unit originally has three $5d_{z^2}$ electrons, but actually has one spin because of the strong Pt-Pt intermetallic bond).

2. Experimental

Single crystals of the title complex were obtained by a slow diffusion in toluene solutions of $Pt_2(CH_3CS_2)_4$ and I_2.

* Corresponding author. Tel: +81(Japan)-298-53-6922; fax: +81(Japan)-298-53-6922;
E-mail: hiroshi@staff.chem.tsukuba.ac.jp

The electrical resistivity of single crystal was measured by a standard *dc* four-probe technique using a clamp-cell-type high-pressure apparatus. A mixture of Fluorinert FC70 and FC77 was used as fluid pressure transmitting medium. In this way, the high-pressure apparatus works at pressures up to 15 kbar and at low temperatures down to 50 K under high-static-pressure conditions and without any damages in the single crystals.

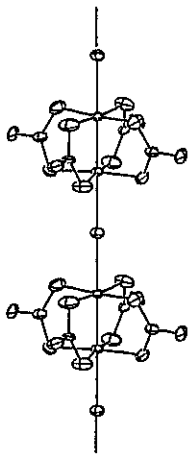

Fig. 1. 1-D structure of $Pt_2(CH_3CS_2)_4I$ at 297 K [2].

3. Results and Discussions

As shown in Fig. 2, a metal-insulator transition was observed at 300 K under ambient pressure for $Pt_2(CH_3CS_2)_4I$, which relates to a crossover-type Mott-Hubbard transition from phase (1) to phase (3) [2]. Pressure dependence of the resistivity ($\rho//$) parallel to the *b*-axis at 310 K is shown in Fig. 3. As pressure is increased, the resistivity linearly decreases but deviates from the line above 2.5 kbar, which is due to a pressure-induced phase transition from (3) to (1), mentioned afterward.

Fig. 4 shows the Arrhenius plots for $\rho//$ of $Pt_2(CH_3CS_2)_4I$ under high pressures of 2.0, 5.5, 11.2, and 15.5 kbar. The transitions from the Mott-insulator phase (3) to the spin-Peierls phase (4) are appreciated between 80 and 100 K. The transition temperature is decreased with pressure. Elastic energy, in general, increases at high pressure, so that spin-Peierls transition could be suppressed

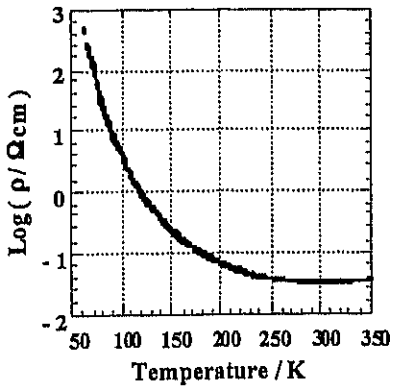

Fig. 2. Temperature dependence of Log (ρ / Ω cm) at ambient pressure [2].

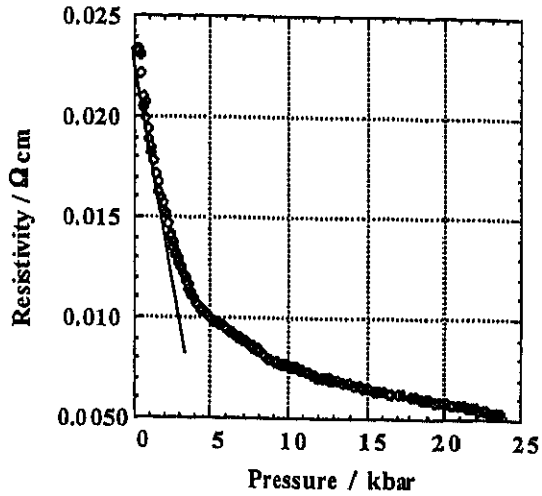

Fig. 3. Pressure dependence of $\rho//$ at 310 K.

under high pressure. On the other hand, the metal-insulator transition was revealed to shift to higher temperature, which is consistent with the transition observed at 2.5 kbar upon applying pressure at 310 K. This indicates that the Mott-insulator phase, that is charge-polarization state (3), is stabilized at high pressure. The stabilization of this charge order is considered to be due to the Coulomb repulsion of the nearest-neighbor pairs of electrons.

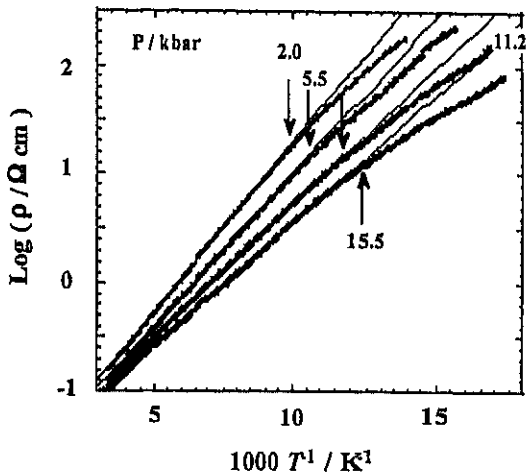

Fig. 4. Arrhenius plots of $\rho//$ under high pressures. Arrows indicate the transition point.

References

[1] B.K. Chakraverty, J. Phys. Lett. 40 (1979) L99.

[2] H. Kitagawa, N. Onodera, T. Sonoyama, M. Yamamoto, T. Fukawa, T. Mitani, M. Seto, Y. Maeda, J. Am. Chem. Soc. 121 (1999) 10068.

[3] C. Bellitto, A. Flamini, L. Gastaldi, L. Scaramuzza, Inorg. Chem. 22 (1983) 444.

[4] M. Mitsumi, T. Murase, H. Kishida, T. Yoshinari, Y. Ozawa, K. Toriumi, T. Sonoyama, H. Kitagawa, T. Mitani, J. Am. Chem. Soc. 123 (2001) 11179.